Uranium geochemistry, mineralogy, geology, exploration and resources

Uranium geochemistry, mineralogy, geology, exploration and resources

Edited by
B. De Vivo, F. Ippolito, G. Capaldi and P. R. Simpson

The Institution of Mining and Metallurgy

ISBN-13: 978-94-009-6062-6 e-ISBN-13: 978-94-009-6060-2
DOI: 10.1007/978-94-009-6060-2

UDC 550.4:553.495.2

Published at the offices of the Institution of Mining and Metallurgy
44 Portland Place
London W1
England

Introduction

The uranium minerals that today are at the centre of worldwide attention were unknown until 1780, when Wagsfort found a pitchblende sample in Johanngeorgenstadt. This discovery passed unnoticed, however, since Wagsfort thought that it contained a black species of a zinc mineral—hence the name 'pitchblende' (= pitch-like blende). Seven years later, Klaproth, while examining the mineral, noted that it contained an oxide of an unknown metal, which he called 'uranium' in honour of the planet Uranus, recently discovered by Herschel. Klaproth also believed that he had separated the metal, but, in fact, the attempt failed, and uranium, given its strong affinity with oxygen, was not separated until several years later. In 1833 Arfwedson attempted the separation and, in so doing, reduced the pitchblende. His attempt was not successful and only UO_2 was obtained. It was Peligot, in 1840, who was finally successful. He managed the reduction of the metal working with metallic potassium. It should be remembered that twelve years earlier Berzelius had isolated thorium.

This successful outcome of the experiment, however, was not given much importance in uranium history because, initially, there was little interest among scientists in this metal and in the industrial-technical field the many attempts to use it in the form of metal had scarcely proved successful. Attempts were made to use it for making Auer mantles in gas-lighting; filaments in electric light-bulbs were also tried, but both experiments failed. Only U_3O_8, some uranates and some uranium salts were utilized as dyes in ceramics and in the glass industry, and also for special photographic preparations. As a result of such a limited utilization, the demand for uranium remained so low that, at the end of the last century, the only mineral deposit to be exploited was that in Joachimsthal, Bohemia—the same formation in which, in 1780, Wagsfort had found the first pitchblende sample. The other known mineral deposits at that time—those in Portugal, Cornwall, Colorado, etc.—were practically untouched. Even thorium found no practical application until 1885, when Auer used the oxide for constructing the mantles that had been patented by him.

The year 1895 marks the beginning of a new chapter in the history of uranium minerals. Becquerel discovered the radioactive property of pitchblende and the Curies isolated radium. Suddenly scientists everywhere became interested in uranium minerals, which assumed a new importance in the mining industry. The extraction of radium from uranium salts led to the development of significant mining exploitation at St. Ives in Cornwall, in the Paradox Valley in Colorado and in Portugal. The first discoveries of uranium minerals in Katanga go back to 1915 and in 1921 exploitation was begun. The wealth of these mines was such as to put into difficulty all the others, including the Joachimsthal deposits.

Since then the uranium market has been subject to two other turning points that, in the course of a few years, have made this metal an essential raw material.

First, the destructive property of fission reactions made uranium a metal of fundamental strategic importance, increasing research in some nations, but the revolution came with the plan for the real possibility of utilizing chain reactions for energy production in place of conventional fuels.

Since that time a 'uranium race' has been in progress in many countries—often justified by the well-founded hope of becoming self-sufficient with regard to energy, or at least of paying off a part of the financial deficit due to increasing fuel imports.

The importance of electro-nuclear energy should, however, be considered on the world rather than the national scale, especially when the following points are taken into account: the very marked increase in the demand for energy, the increasing cost of classic fuels and the need to use the latter more and more for specialized purposes (chemical, iron and steel industries, motor-vehicle traction, etc.).

Thus, exploiting radioactive material is a very urgent national and world problem and the many aspects of the geochemistry and geology of uranium and thorium ore deposits are of extreme value in both theoretical and practical terms.

With these points in mind, in 1960 one of the editors (F.I.) presented *Lezioni di Geologia dell'Uranio* (lessons on the geology of uranium), which summarized a course held for a decade at the School of specialization in applied nuclear physics at Milan Polytechnic. Owing to the novelty of the subject and the particular interest that it holds for the development of the nuclear industry, these lessons quickly became obsolete, and it was felt that a new publication was necessary for both students and practising exploration geologists. Because of the complexity of the subject, which, if it is to be treated thoroughly, should be considered as an interdisciplinary field of research, with the help of our co-editors we decided to promote this volume in which various specialists treat the problems that are presented by the geology of uranium in the widest sense. We hope that the presentation of these complex problems—from the mineralogy of uranium to the search for it and its practical utilization—from different aspects and as completely as possible has been successful.

We wish to thank all our collaborators and the Institution of Mining and Metallurgy, which has assumed responsibility for publishing this volume.

Benedetto De Vivo
Felice Ippolito
January, 1984

Contents

Introduction
Benedetto De Vivo and Felice Ippolito v

History of radioactivity
Paolo Gasparini 1

Uranium in mantle processes
Massimo Cortini 4

Transport and deposition of uranium in hydrothermal systems at temperatures up to 300°C: geological implications
Samuel B. Romberger 12

Geochemical behaviour of uranium in the supergene environment
Gaetano Dongarra 18

Uranium exploration techniques
Chester E. Nichols 23

Uranium mineralogy
Deane K. Smith Jr. 43

Time, crustal evolution and generation of uranium deposits
R. W. Hutchinson and J. D. Blackwell 89

Uranium exploration
Richard H. De Voto 101

Geochemistry of uranium in the hydrographic network
Bernard Soyer 109

Uranium deposits of the world, excluding Europe
Robert G. Young 117

Uranium deposits in Europe
Valery Ziegler and Jacques Dardel 140

Uranium in the economics of energy
B. De Vivo and F. Ippolito 162

Role of high heat production granites in uranium province formation
P. R. Simpson and Jane A. Plant 167

Uranium deposits in Italy
Claudio Tedesco 179

Name index 189

Subject index 194

History of radioactivity

Paolo Gasparini
Istituto di Geologia e Geofisica, University of Naples, Italy

Our understanding of the evolution of the earth and the solar system had its beginning in radioactivity. Radioactivity provided a tool for absolute geochronology, it was found to be an important heat source within the planets and it produced small changes in the isotopic composition of some elements, which enabled us to trace geochemical processes back to the earth's past. Moreover, radioactive processes are a source of energy for human beings.

The history of radioactivity as a science is full of surprises and the outstanding quality of those prominent in this field was a mind that was open to the unexpected rather than possessing the capability of foresight and research planning.

In 1896, shortly after Röntgen had shocked the scientific world by announcing the discovery of X-rays, Henri Becquerel, stimulated by Röntgen's results, hoped to produce X-rays from fluorescent minerals. Becquerel had the idea, perfectly plausible at that time, that X-ray emission and fluorescence had the same cause. The concept later proved to be completely false, but Becquerel had the good fortune to choose a fluorescent mineral of uranium to test his idea. Thus, he observed penetrating radiations emitted from the mineral and reported his findings to the Académie des Sciences de Paris in a paper entitled 'Sur les radiations émises par phosphorescence' on 24 February, 1896. Shortly afterwards, Becquerel began to observe some strange things, the most curious being that the uranium mineral emitted penetrating radiations even when it was not hit by light. Becquerel reported the results of his observations in a series of eight papers that give a comprehensive insight into a growing awareness that uranium atoms were unexpectedly emitting penetrating radiations. This conclusion, reached only two and half months after the presentation of the first paper, was a triumph of observation over reason; it was more remarkable in that Becquerel knew that some researchers claimed to have succeeded where he had failed, reporting observations of X-rays from fluorescent minerals in evidently careless experiments.

That same year at Cambridge University J. J. Thomson was starting to check experimentally the theory of the ionization mechanism of air by X-rays that he had just put forward. To obtain help with his experiments he asked Ernest Rutherford, a brilliant student of physics, to join him. Rutherford started working on the electrification produced by X-rays and, in 1898, recalling that Becquerel had shown that the mysterious radiations emitted from uranium could also ionize gases, began the study of the ionization produced by these radiations to check how much that process depended on the nature of the rays and how much on the specific gas involved. Unexpectedly, Rutherford found the uranium rays to be a mixture of two different types. One, which he called alpha, had quite a strong ionizing power, but it had so little penetrating power that it could be stopped by a sheet of paper; the other, which he called beta, had weaker ionizing power, but its penetrating power was similar to that of X-rays. That same year G. C. Schmidt in Erlagen and Maria Skłodowska Curie in Paris discovered that thorium also emitted ionizing, penetrating radiations. In 1899 Rutherford moved to McGill University in Montreal, where he made the acquaintance of R. B. Owens, professor of electrical engineering. He persuaded Owens to work on the ionizing radiations emitted by thorium, himself working on those emitted by uranium. The radiations from thorium proved more difficult to deal with because the ionization seemed to fluctuate widely. Owens proposed air current as the possible cause of the problem and, just before leaving for England for his summer vacation, succeeded in stabilizing the ionization by sealing his thorium oxide specimen in an airtight box. Rutherford was left alone to explain the puzzle, rapidly reaching the conclusion that the fluctuations in ionization were due to the 'emanation' of a radioactive substance from thorium. One year later, in London, Sir William Crookes was trying to purify uranium nitrate. In doing so he was astonished to discover that he had almost completely eliminated the radioactivity from uranium. He began a series of chemical tests that separated uranium from a totally different, highly radioactive substance, which he called 'Uranium X'. Additionally, a new emanation was discovered from radium.

Rutherford realized that any further progress would be difficult without the help of a chemist and persuaded Frederick Soddy to join him in his work. He and Soddy proposed to (1) ascertain whether the emanation came from thorium or from something that was also mixed with it, (2) discover what kind of gas the emanation might be, (3) weigh the emanation and (4) ascertain what chemical properties of thorium made the emanation possible. They found definite answers to the first two questions: the emanation came from a highly radioactive substance, which they called 'Thorium X', and the emanation had the chemical behaviour of an inert gas of the argon series.

Meanwhile, Becquerel had observed that although uranium lost almost all its radioactivity when uranium X was removed, after a short time it recovered the lost radioactivity. Rutherford and Soddy also found that thorium, after having been separated from thorium X, generated in time both its radioactivity and its power to produce emanations. Realizing that thorium X was chemically different from thorium, and yet there was nothing but the thorium to produce it, they proposed the new revolutionary theory of transmutation whereby thorium was transformed into thorium X by emitting ionizing radiations. In their paper, published in 1902 (only six years after the discovery of radioactivity), they also stated the exponential nature of the laws of radioactive decay and growth.

In 1900 Becquerel had discovered that beta-rays were streams of swiftly moving, negatively charged electrons. Rutherford, in 1902, investigated alpha-rays and discovered that they were also particles, though they carried positive charges and were enormously larger than electrons. Because of their size it was quite clear to Rutherford that alpha particles carried practically all of the energy contained in the process of radioactivity. With remarkable intuition, in a paper published in 1903, Rutherford suggested that helium must be a stable product of radioactive decay of uranium and thorium, because it often accompanies radioactive minerals, where it accumulated in such quantities as to be measurable. Soddy and Rutherford tried to estimate the energy that is released in the alpha decay of radium, obtaining the amazing figure of 15 000 calories per gramme. While that calculation was still awaiting publication, Pierre Curie and Albert Laborde in Paris published the results of experimental measurements carried out on radium and barium bromide. They obtained the far greater figure of 880 000 cal/g of radium. These figures were, however, far larger than the energy released by ordinary chemical reactions. The process had to involve not elements but some other entities, which Rutherford called 'metabolons'.

In the same year Soddy moved to the laboratory of Sir William Ramsey in London (Ramsey was the discoverer of helium and he had also isolated the rare gases neon, krypton, xenon and argon). Soddy hoped to identify the spectrum of the emanation from a pure radium bromide. The experiment failed because they did not see the expected spectrum but the familiar

lines of helium. Since helium entered in no chemical combination there was no way in which the radium bromide could have picked it up. It must have formed inside the crystals of radium bromide from the decay of radium. Since both radium and helium were acknowledged elements, this was direct evidence in favour of the theory of transmutation.

That autumn, in Montreal, Rutherford began to make experimental measurements of the heat released by radioactive processes. From studies of the details of alpha emission he succeeded in identifying all the chain of decays through which U transmuted into a stable substance. He published his results in 1905 and, with that paper, the transmutation theory became a solid working hypothesis. It took account of what was known, explaining every variation in radioactivity that experiments could create. It established the new principle that a radioactive element could be identified by its half-life.

Only nine years had elapsed from Becquerel's announcement of strange radiations from uranium, but the basic concepts of radioactivity were already established. Subsequent work would account for the details of the process.

The possibility of the application of radioactivity to the earth sciences had already been pointed out by Rutherford and Soddy when they had suggested that the age of minerals could be determined by measurement of the helium/uranium ratio.

Appendix

Tables 1–3* give the members, half-lives, decay constants and modes of decay of the natural radioactive decay series of ^{238}U, ^{235}U and ^{232}Th, respectively.

Table 1 ^{238}U series

Isotope	Classical name	$T_{1/2}$	$\lambda(sec^{-1})$	Primary decay mode	Remarks
$^{238}_{92}U$	Uranium I	$4.51 \cdot 10^9$ yr	$4.88 \cdot 10^{-18}$	α	
$^{234}_{90}Th$	Uranium X_1	24.10 days	$3.33 \cdot 10^{-7}$	β^-	
$^{234m}_{91}Pa$	Uranium X_2	1.175 min	$9.83 \cdot 10^{-3}$	β^-	Isomeric transition to ^{234}Pa (0.13%)
$^{234}_{91}Pa$	Uranium Z	6.75 h	$2.85 \cdot 10^{-5}$	β^-	
$^{234}_{92}U$	Uranium II	$2.47 \cdot 10^5$ yr	$8.91 \cdot 10^{-14}$	α	
$^{230}_{90}Th$	Ionium	$8.0 \cdot 10^4$ yr	$2.75 \cdot 10^{-13}$	α	
$^{226}_{88}Ra$	Radium	1602 yr	$1.37 \cdot 10^{-11}$	α	
$^{222}_{86}Rn$	Radon	3.8223 days	$2.10 \cdot 10^{-6}$	α	
$^{218}_{84}Po$	Radium A	3.05 min	$3.79 \cdot 10^{-3}$	α, β^-	Branched decay: α to ^{214}Pb (99.98%); β^- to ^{218}At (0.02%)
$^{214}_{82}Pb$	Radium B	26.8 min	$4.31 \cdot 10^{-4}$	β^-	
$^{218}_{85}At$	Astatine-218	~2 sec	~0.35	α	
$^{214}_{83}Bi$	Radium C	19.7 min	$5.86 \cdot 10^{-4}$	α, β^-	Branched decay: α to ^{210}Tl (0.04%); β^- to ^{214}Po (99.96%)
$^{214}_{84}Po$	Radium C′	$1.64 \cdot 10^{-4}$ sec	$4.23 \cdot 10^3$	α	
$^{210}_{81}Tl$	Radium C″	1.32 min	$8.75 \cdot 10^{-2}$	β^-	
$^{210}_{82}Pb$	Radium D	22.0 yr	$1 \cdot 10^{-9}$	β^-	Branched decay: α to ^{206}Hg ($1.8 \cdot 10^{-6}$%); β^- to ^{210}Bi (~100%)
$^{210}_{83}Bi$	Radium E	5.013 days	$1.60 \cdot 10^{-6}$	β^-	Branched decay: α to ^{206}Tl ($\sim 10^{-5}$%); β^- to ^{210}Po (~100%)
$^{210}_{84}Po$	Radium F	138.4 days	$5.78 \cdot 10^{-8}$	α	
$^{206}_{82}Pb$	Radium G	Stable			

*Adams J. A. S. and Gasparini P. *Gamma-ray spectroscopy of rocks* (Amsterdam, etc.: Elsevier, 1970), 295 p.

Table 2 ^{235}U series

Isotope	Classical name	$T_{1/2}$	$\lambda(sec^{-1})$	Primary decay mode	Remarks
$^{235}_{92}U$	Actiniouranium	$7.1 \cdot 10^{8}$ yr	$3.09 \cdot 10^{-17}$	α	
$^{231}_{90}Th$	Uranium Y	25.52 h	$3.70 \cdot 10^{-4}$	β^-	
$^{231}_{91}Pa$	Protoactinium	$3.48 \cdot 10^{4}$ yr*	$6.32 \cdot 10^{-13}$	α	
$^{227}_{89}Ac$	Actinium	21.6 yr	$1 \cdot 10^{-9}$	α, β^-	Branched decay: 98.8% β^- to ^{227}Th, 1.2% α to $^{223}F_2$
$^{227}_{90}Th$	Radioactinium	18.2 days	$4.41 \cdot 10^{-7}$	α	
$^{223}_{87}Fr$	Actinium K	22 min	$5.25 \cdot 10^{-4}$	β^-	
$^{223}_{88}Ra$	Actinium X	11.435 days	$7.88 \cdot 10^{-6}$	α	
$^{219}_{86}Rn$	Actinon	4.00 sec	0.173	α	
$^{215}_{84}Po$	Actinium A	$1.778 \cdot 10^{-3}$ sec	$3.90 \cdot 10^{2}$	α	
$^{211}_{82}Pb$	Actinium B	36.1 min	$3.20 \cdot 10^{-4}$	β^-	
$^{211}_{83}Bi$	Actinium C	2.16 min	$5.33 \cdot 10^{-3}$	α, β^-	Branched decay: 0.32% β^- to ^{211}Po, 99.68% α to ^{207}Tl
$^{211}_{84}Po$	Actinium C′	0.52 sec	0.13	α	
$^{207}_{81}Tl$	Actinium C″	4.79 min	$2.41 \cdot 10^{-3}$	β^-	
$^{207}_{82}Pb$	Actinium D	Stable			

$^{223}_{87}Fr$ also undergoes $4 \cdot 10^{-3}$% α decay to 0.9 min $^{219}_{85}At$, which, in turn, undergoes branched decay: 3% β^- to ^{219}Rn and 97% α to 8 min ^{215}Bi, which β^- decays to ^{215}Po.

* After Hyde E. K. *et al. The nuclear properties of the heavy elements* (Englewood Cliffs, N.J.: Prentice-Hall, 1964), 3 vols.

Table 3 ^{232}Th series

Isotope	Classical name	$T_{1/2}$	$\lambda(sec^{-1})$	Primary decay mode	Remarks
$^{232}_{90}Th$	Thorium	$1.41 \cdot 10^{10}$ yr	$1.56 \cdot 10^{-18}$	α	
$^{228}_{88}Ra$	Mesothorium 1	6.7 yr	$3.28 \cdot 10^{-9}$	β^-	
$^{228}_{89}Ac$	Mesothorium 2	6.13 h	$3.14 \cdot 10^{-5}$	β^-	
$^{228}_{90}Th$	Radiothorium	1.910 yr	$1.15 \cdot 10^{-8}$	α	
$^{224}_{88}Ra$	Thorium X	3.64 days	$2.21 \cdot 10^{-6}$	α	
$^{220}_{86}Rn$	Thoron	55.3 sec	$1.25 \cdot 10^{-2}$	α	
$^{216}_{84}Po$	Thorium A	0.145 sec	4.78	α	
$^{212}_{82}Pb$	Thorium B	10.64 h	$1.81 \cdot 10^{-5}$	β^-	
$^{212}_{83}Bi$	Thorium C	60.60 min	$1.91 \cdot 10^{-4}$	α, β^-	Branched decay: β^- (66.3%) to ^{212}Po α (33.7%) to ^{208}Tl
$^{212}_{84}Po$	Thorium C′	$3.04 \cdot 10^{-7}$ sec	$2.28 \cdot 10^{6}$	α	
$^{208}_{81}Tl$	Thorium C″	3.10 min	$3.73 \cdot 10^{-3}$	β^-	
$^{208}_{82}Pb$	Thorium D	Stable			

Uranium in mantle processes

Massimo Cortini
Istituto di Geologia e Geofisica, University of Naples, Italy

Uranium is a large ion lithophile (LIL) element that occurs in the tetravalent (U^{+4}), pentavalent (U^{+5}) and in the hexavalent (U^{+6}) states, the U^{+6} form being stable under highly oxidizing conditions.[1] It does not enter the lattices of most rock-forming minerals, but may be strongly concentrated in accessory minerals.[2] A large fraction of U in volcanic rocks is concentrated along inter-crystal boundaries, where it is loosely bound, and from where it can be easily leached by dilute acids.[3,4,5]

Uranium is strongly concentrated in the crust (1.26–1.8 ppm[6]) with respect to the mantle. Estimates of U concentrations in the mantle range from 0.013 ppm for the undepleted mantle[7] to 0.032 ppm for the present mantle.[8]

The redistribution of U within the earth's mantle is mostly controlled by mantle metasomatism.

Mantle metasomatism

'Metasomatism is a chemical change, whereby a pre-existing mineral or rock is converted to another composition. It usually refers to a solid-state transformation, with material transfer through a vapour or fluid, without melting'.[9] In this paper the term metasomatism is used in a slightly broader sense to enable the inclusion of the processes that form glass veinlets in mantle rocks and glass films coating mantle rock-forming minerals. Evidence that metasomatism is an effective process within the mantle is now overwhelming, especially in continental sites of alkaline volcanism, where this concept was first proposed (see Bailey[9] and references cited therein).

Direct evidence for metasomatism is derived from petrochemical studies of mantle nodules. Lloyd and Bailey[10] reported on ultramafic nodules from the West Eifel and Southwest Uganda volcanic provinces, and described a series of primary (i.e. unaffected by low-pressure environment) features that include pockets or veins of hydrated minerals (amphibole, mica) or, sometimes, vesicular glass. Based on the textures and on the chemical sequence of the metasomatized nodules they concluded that the mantle portion represented by the nodules was subjected to extensive infiltration of elements, such as K, Na, Fe, Rb, etc. Metasomatic enrichment of mantle rocks was also reported by Boettcher *et al.*,[11] Erlank *et al.*,[12,13] Sutherland and Hollis[14] and many others (see Table 3 in Menzies and Murthy[15] and Menzies[16]).

Studies of Sr, Pb and Nd isotopes, coupled with trace-element geochemical studies, have shown that the source regions of many continental alkaline volcanics have been enriched in LIL elements, generally some hundreds of million years prior to the beginning of volcanism, and enrichment has been interpreted as due to mantle metasomatism.[15,17–20] It has been suggested that mantle metasomatism is a necessary precursor to alkaline continental volcanism.[11,21,22] Alkaline rocks erupted in oceanic environments, and even ridge tholeiites, sometimes bear evidence of source enrichment, which has been interpreted as a result of mantle metasomatism.[23,24,25]

Mantle metasomatism will be considered as a fact throughout this paper. Moreover, somewhat arbitrarily, it will be assumed that LIL element enrichment in the mantle, as detected by trace-element and isotopic studies of lavas, is essentially produced by mantle metasomatism.

Because of their large ionic radii U, Th and Pb are loosely bound in mantle rocks[4,26,27] and can be easily mobilized and redistributed by metasomatizing fluids. For Nyiragongo Vollmer and Norry[20] have shown that the source region of the nephelinites was enriched very strongly in U—also with respect to other LIL elements, such as Rb. In all the cases where enrichment due to metasomatism has been invoked, high enrichment factors were consistently derived for U. It has been suggested that in some areas LIL elements were enriched by mantle metasomatism as a direct function of their ionic radii.[17,24] If this is so, the effective ionic radius of U should probably be larger than that of Rb (1.47 Å).

Evidence for metasomatism holds in spite of the uncertainty about the origin, and partly about the nature, of the metasomatizing fluids. Wyllie[28] proposed that mantle metasomatism is a two-stage process. He emphasized that 'Although the evidence is clear for the existence of components CO_2 and H_2O in magmas reaching the crust, and although the involvement of carbonate and CO_2 appears to be required for generation of magmas of kimberlite composition, the fact that kimberlites and their xenoliths contain diamond and graphite confirms that the oxygen fugacity at depth is not high enough to oxidize all carbon'. Accordingly, he suggested that there is a deep-seated metasomatism, mainly governed by CO_2; the flux of CO_2 may trigger partial melting (as was also suggested by Spera[29]). Kimberlitic melts that do not reach the crust would solidify at depth and release aqueous solutions that would be responsible for metasomatism in the upper mantle. Church and Tatsumoto[30] suggested another interesting possibility, which was also favoured by Schilling and co-workers.[24] If convection within the mantle crosses the lower boundary of the stability field of pyroxene (about 350-km depth), the transformation of pyroxene into garnet structure, together with the reduction of grain size, should result in strong exclusion of LIL elements. This process would produce a relatively mobile interstitial phase, strongly enriched in LIL elements.

Partial melting and radioactive disequilibria

Partial melting of a mantle fraction, and the eventual uprise and eruption of the magma, is the process by which U, along with many other LIL elements, is transferred from the earth's mantle to the crust. The behaviour of LIL elements during partial melting was quantitatively modelled by Gast[31] in a very important paper that was based on the concept of mineral/melt partition coefficients. The work of Gast,[31] however, and the very concept of partition coefficient were based on the implicit assumption that magma formation is a closed-system process, i.e. that the portion of the mantle that produces a magma can be considered as a closed chemical system. The writer believes that such an assumption is no longer tenable, though perhaps for the very reason that it is generally unstated it represents a commonly held opinion.

That partial melting is *not* an isochemical process has been suggested based both on general[9] and specific considerations[32–35] (the two last works[34,35] are disequilibria studies). Radioactive disequilibria represent an ideal tool for the study and modelling of magma-forming processes[36] and are dealt with in some detail here.

The long-lived members of the ^{238}U and ^{232}Th radioactive series (those of interest in disequilibria studies) and their half-lives are listed in Table 1. In any rock that has remained as a closed chemical system for a sufficient amount of time (about 50 years for the ^{232}Th series; about 5×10^5 years for the ^{238}U series) radioactive (or secular) equilibrium condition is attained. Radioactive equilibrium means that, for every nuclide of a radioactive series, the following relationship is valid:

$$\lambda_1 N_1 = \lambda_2 N_2 = \cdots = \lambda_n N_n$$

where N and λ indicate the number of atoms and the decay constant for every member of a radioactive series. This is

Table 1 ^{238}U and ^{232}Th series long-lived radionuclides

Nuclide	Half-life, yr	Nuclide	Half-life, yr
^{238}U	4.47×10^{9}	^{232}Th	1.40×10^{10}
^{234}U	2.47×10^{5}	^{228}Ra	5.75
^{230}Th	7.52×10^{4}	^{228}Th	1.91
^{226}Ra	1.6×10^{3}		
^{210}Pb	22		

equivalent to saying that the activity (number of disintegrations per unit time) of each nuclide is the same, i.e.

$$\frac{\lambda_1 N_1}{\lambda_2 N_2} = \frac{\lambda_2 N_2}{\lambda_3 N_3} = \cdots = \frac{\lambda_{n-1} N_{n-1}}{\lambda_n N_n} = 1 \qquad (1)$$

The great strength of the disequilibria approach is that when radioactive equilibrium can be assumed the relative ratios of the nuclides of a decay series are determined from equation 1. For the present it is assumed that radioactive equilibrium exists in the mantle before the onset of magma formation, the limits of such an assumption being discussed later. In this hypothesis any disequilibrium that is observed between two members of a radioactive series is due to the magma formation process or to other processes that may have taken place after magma formation.

It is very important to note, however, that if the mantle volume that originates a magma could be considered as a closed system, radioactive disequilibria could hardly be observed in magmas at all. The mineral–melt partition coefficients for U and Th for relevant mantle minerals, in fact, are so low[37,38] that virtually all U and Th in the mantle source region would enter the melt. Fractional crystallization, which could eventually take place, would have no effect on the *relative ratios* of radioisotopes of U and Th in the magma for the very same reason. In these conditions in a zero age lava one should observe (isotopic ratios in brackets indicate activity ratios) $(^{230}Th/^{238}U) \simeq (^{226}Ra/^{238}U) \simeq 1$.

Measured $(^{230}Th/^{238}U)$ ratios range from 0.71 (Vesuvius[35]) to 1.61 (FAMOUS area[39]), but, much more important $(^{226}Ra/^{238}U)$ ratios in *primitive* rocks are generally higher than unity.[35,36,40,41,42] Radioactive equilibrium of the ^{238}U series in zero age lavas has been reported only for Hawaiian rocks.[43] For Vesuvius $(^{226}Ra/^{238}U)$ ratios range up to 10[35,36]—that is, ^{226}Ra is enriched up to ten times over U, which, in a closed-system framework, is supposed to be most effectively partitioned in the liquid. Oversby and Gast[36] suggested that Ra in Vesuvian lavas may have been extracted from crustal rocks. It was shown, however, that unrealistically large volumes of country rocks are required to account for the Ra excess in the lavas;[44] moreover, Ra was not extracted from crustal wallrocks by other magmas that did reside within the crust (Mt. St. Helens[42] and Vulcano, Vulcanello and Lipari[41]). High $(^{226}Ra/^{238}U)$ ratios are a common feature of primitive magmas, which is due to the magma-genetic processes themselves and is inexplicable in a closed-system framework.

If (1) the residence time of a magma within the earth plus its age of emplacement were very short in comparison with the half-life of ^{230}Th (75200 yr) and (2) the source region of U and Th in a magma was in secular equilibrium at the onset of melting, it can be assumed that $(^{230}Th/^{232}Th)_m = (^{238}U/^{232}Th)_s$, the subscripts m and s meaning 'in the magma' and 'in the source region', respectively.[36] The $^{232}Th/^{238}U$ ratio in the source region of a magma, as determined by Th isotopes (K_{Th}), is therefore

$$K_{Th} = (^{230}Th/^{232}Th)_m^{-1} \times 3.0567 \qquad (2)$$

The ^{230}Th dating method[45] is based on the implicit assumption that magma formation is a closed-system process: the $(^{230}Th/^{232}Th)$ ratios (isotopic composition of Th) of mineral phases $A, B, C, \ldots$, crystallizing from a magma m, should therefore be

$$(^{230}Th/^{232}Th)_A = (^{230}Th/^{232}Th)_B = \cdots = (^{230}Th/^{232}Th)_m \qquad (3)$$

These isotopic ratios will eventually evolve in time according to their $(^{238}U/^{232}Th)$ ratios.[45] Several papers have reported 'ages' obtained with this method[46,47,48] without the hypothesis of equation 3 being tested. Actual measurements of $(^{230}Th/^{232}Th)$ ratios in zero age volcanic rocks from the Stromboli, Etna, Vesuvius and Mt. St. Helens volcanoes show that the isotopic composition of Th in mineral separates is systematically *higher* than in host whole rocks.[35,42,49] These Th isotope composition data on zero age minerals and whole rocks are incompatible with a closed-system framework for magma generation and show that the ^{230}Th dating method is not valid, at least in the above-mentioned cases. ^{230}Th 'ages' were published for Etna and Stromboli,[47,48] where Th isotopic disequilibria were observed between coexisting minerals and whole rocks in zero-age samples.[49] Not surprisingly, in the one case where very precise K/Ar data are available (Stromboli, La Petrazza lava; four measurements from 45000 ± 10000 to 66000 ± 14000 yr[50]) the discordance with the ^{230}Th 'age' (156000 yr[47]) is large. Other researchers[51] tried to use the ^{230}Th dating method, but did not find any linear array in a $(^{230}Th/^{232}Th)$ versus $(^{238}U/^{232}Th)$ diagram, as hypothesized by Allègre.[45] In some cases[49] ^{230}Th 'ages' were obtained that were incompatible with the stratigraphic location of the studied rocks.

Mineral separates from Vesuvius lavas have Sr isotope ratios identical with those of their host lavas, and the Sr isotopic compositions of minerals from Vesuvian cumulate rocks are in the range defined by the lavas.[52] There is, however, a hyperbolic relationship between $(^{230}Th/^{232}Th)$ ratios and Th concentrations in the same materials (Fig. 1[35]). This suggests that Th was derived by mixing of two different components with different isotopic compositions of Th, and hence different K_{Th} ratios. The few available data on zero age minerals from Etna and Stromboli are compatible with a similar interpretation.[35] These data show that in these volcanoes a Th component is present that was derived from a source with a *low* Th/U ratio ($\leqslant 2.3$ for Vesuvius and Etna)—similar, in this respect, to the source region of oceanic basalts.[38,39] Th in the early crystallizing phases was essentially derived from such a low Th/U source.[35] The enrichment pattern of the Vesuvian lavas is $Ra \gg U \geqslant Th$, which strongly suggests that most U, Th and Ra in such lavas were fed by a fluid, which may have derived from a relatively high Th/U interstitial metasomatic mantle component.

K_{Th} ratios obtained from equation 2 for zero age rocks are, however, correct only if assumptions (1) and (2) (see earlier) are valid.

(1) The residence time of magmas within the earth is short in comparison to the half-life of ^{230}Th (75200 yr). This is probably a rather safe assumption. Capaldi *et al.*[40] and Bennett *et al.*,[42] based on the short-lived members disequilibria in the ^{232}Th series, evaluated semiquantitatively that magma generation took place some tens or hundreds of years before the eruption for zero-age rocks from the Stromboli, Etna and Mt. St. Helens volcanoes. Disequilibria data also suggest that chemically evolved magmas (up to rhyolites) erupted at Vulcano, Vulcanello and Lipari may have spent only a few thousands of years within the earth before eruption.[41]

(2) Radioactive equilibrium between ^{238}U and ^{230}Th exists in the source region(s) of U and Th at the onset of melting. Although Allègre and Condomines[53] suggested that this may be

a prevalent condition in the mantle, it is hard to devise specific tests for such an assumption. No specific evidence against it has, however, yet emerged from disequilibria studies. The point is that fractionation of U, Th and their daughters (and hence radioactive disequilibrium) *should* be expected, because it is produced by metasomatism, if metasomatism is a continuing process.[9] A reasonable explanation for this apparent contradiction is that mantle metasomatism is a *slow* process, i.e. that the time required for effective fractionation of U from Th is much longer than the half-life of ^{230}Th. If this is true, a slow change in Th/U would be produced in a mantle region that would always be essentially in radioactive equilibrium. Another possibility, which is discussed later, is that mantle metasomatism is not a steady-state process but has pulses of activity of a relatively limited duration.

It is conceptually very important to consider the open-system behaviour of the mantle *before* magma formation (mantle metasomatism) as a different phenomenon than the open-system behaviour of a mantle portion *during* magma formation. The duration of magma formation (here intended to mean the process by which Th, U and Ra reach their actual concentrations in a magma) is most probably very short—not only in comparison with the half-life of ^{230}Th but also in comparison with that of ^{226}Ra (1600 yr). In fact, disequilibria in the ^{232}Th chain could be interpreted[40] as being due to fluid transport fractionation within the magma column, which could be fed by a larger, buried magma body. Isotopic disequilibrium of Th between zero-age minerals and whole rocks, however, which had not been discovered in 1976, precludes this possibility. The leucite separated from the 1944 lava of Vesuvius (which has a higher (^{230}Th/^{232}Th) ratio than the host whole rock; Fig. 1) has a large ^{226}Ra excess[35] ((^{226}Ra/^{238}U) = 65). Because the high K_{Th} Th component and the Ra excess were not derived by crustal contamination, they must have been extracted from the mantle within a time interval that is short with respect to the half-life of ^{226}Ra.

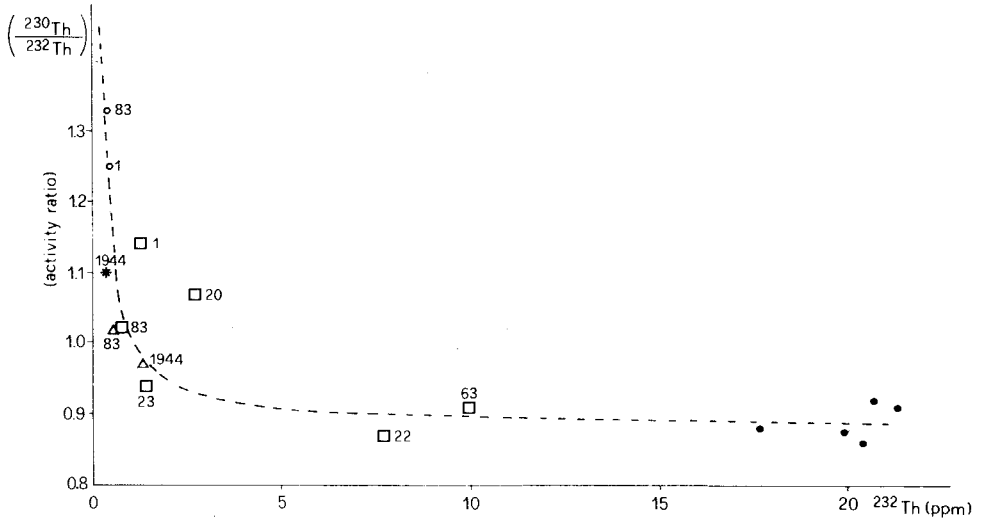

Fig. 1 (^{230}Th/^{232}Th) versus ^{232}Th plot for whole-rock and mineral separate zero-age samples from Vesuvius. From Capaldi and co-workers.[35] 1944 refers to mineral separates from the lava erupted in 1944; other numbers are laboratory numbers of cumulate ejecta. Most cumulates have large (^{226}Ra/^{238}U) ratios so their age is zero in comparison with half-life of ^{230}Th. Hyperbolic correlation strongly suggests that Th in Vesuvian lavas is derived by mixing of two components with different Th isotopic compositions (i.e. derived from two sources with different ^{232}Th/^{238}U ratios). Because data include whole-rock lavas and different minerals drawn hyperbola is not believed to be mixing curve of *magmas*

The enrichment of U, Th and Ra in a magma may be an increasing process that culminates at the moment of eruption.[35,40] The duration of magma formation, in the sense defined above, could therefore coincide with the residence time of a magma within the earth, as determined with short-lived members disequilibria in the ^{232}Th series. If the increase of U, Th and Ra in a magma really is such a fast process, the concept of mineral–melt partition coefficients would obviously be invalid for U, Th and Ra during magma formation because the minerals would represent systems that closed earlier than the liquid with respect to U, Th and Ra. One could perhaps devise an 'instantaneous partition coefficient' concept.

Indeed, the time scales of mantle metasomatism and magma formation do seem to be very different. They could be different aspects of essentially the same phenomenon, which perhaps is strongly enhanced at the onset of melting. As is seen next, however, there is some evidence that mantle metasomatism and magma formation may produce different effects on the Th/U fractionation.

U/Pb and U/Th fractionation in mantle processes

The first section of this paper is based on very strong evidence, and mantle metasomatism is a widely accepted concept. The conclusions of the second section may seem unorthodox, but, in the writer's opinion, they are based on compelling evidence. The present and the next sections deal with a very controversial matter: an interpretation is suggested, but no attempt is made to examine all the existing literature and possible alternative explanations.

Past events of U/Pb and U/Th fractionation can be traced by means of Pb isotopes.[54] If the mantle source of Pb in the erupted magmas had been a closed-system since the origin of the earth, the isotopic composition of Pb in magmas, in a ^{207}Pb/^{204}Pb versus ^{206}Pb/^{204}Pb plane, should plot on the 'geochron' (Fig. 2). This is not so, and most volcanic rocks plot to the right of the geochron (i.e. have negative or 'future' single-stage model ages[54]). Moreover, Pb isotopic data from many oceanic island and other volcanic areas (mid-oceanic ridge basalts, MORB; and also some continental areas) define linear arrays, both in a ^{207}Pb/^{204}Pb versus ^{206}Pb/^{204}Pb and in a ^{208}Pb/^{204}Pb versus ^{206}Pb/^{204}Pb plane (Fig. 2). These trends

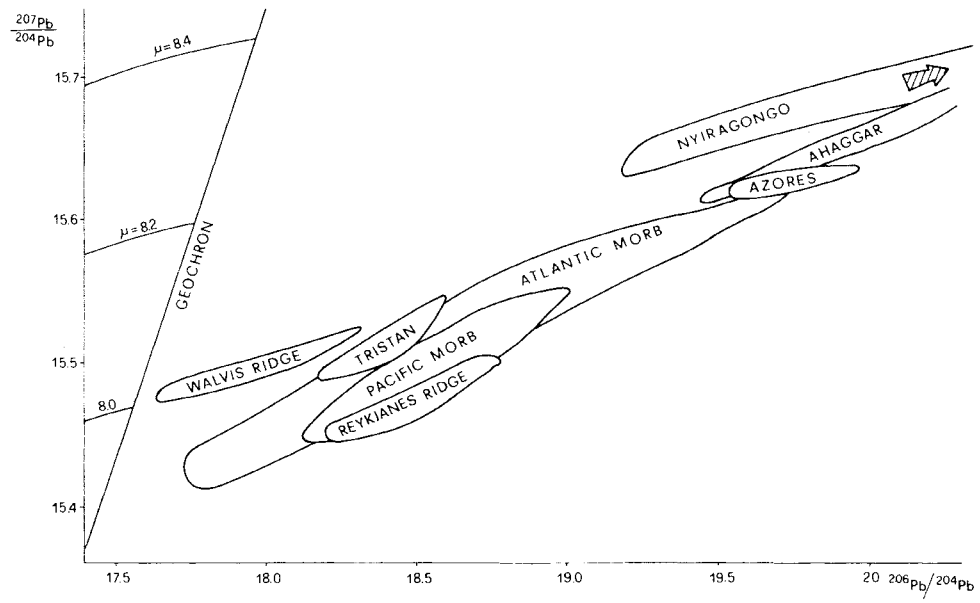

Fig. 2 $^{207}Pb/^{204}Pb$ versus $^{206}Pb/^{204}Pb$ plot for some oceanic and continental volcanics for which two-stage models can be computed. First- and second-stage model parameters reported in Table 2. All samples plot to right of geochron, i.e. have negative or future single-stage model ages. Linear arrays interpreted as secondary isochrons, following Chase[55]

can be interpreted in several ways (see Chase[55]). Chase[55] argued that the linear $^{207}Pb/^{204}Pb$ versus $^{206}Pb/^{204}Pb$ trends of some selected oceanic islands are most reasonably interpreted as secondary isochrons; he showed that two-stage histories can explain the Pb/Pb correlations.

The Pb sources of the oceanic islands studied[55] may have had a common first-stage history with the same $^{238}U/^{204}Pb$ (μ)-ratio of 7.91 ± 0.04. Secondary enrichment of U relative to Pb took place at different times (indicated by the secondary Pb/Pb isochrons), leading to a range of high μ values that can account for the observed data.[55] Here it is suggested that metasomatism has been responsible for the μ increase in the sources of many volcanic areas. Most researchers agree that the high second-stage μ values were more probably produced by U enrichment rather than Pb depletion.[18,20,38] Therefore, metasomatism should enrich a metasomatized mantle region more effectively in U than in Pb.

$^{232}Th/^{238}U$ (K) ratios can also be calculated for the first and second stages of Pb evolution. Table 2 reports μ and K values for the first stages (μ_1, K_1), isochron ages and K values for the second stages (K_2), together with the values obtained by Chase[55] for his reported oceanic islands. Data from Tristan were included (in spite of their poorly defined slope, Fig. 2) because relatively large slope variations do not have large effects on the computed μ_1, and because a comparison with the disequilibria data for Tristan[36] is interesting.

Table 2 Comparison of $^{238}U/^{204}Pb$ and $^{232}Th/^{238}U$ ratios for first-stage (μ_1, K_1) and $^{232}Th/^{238}U$ (K_2) ratios for second-stage lead model evolution in some volcanic areas

Volcanic area	Isochron age, billion years	μ_1	K_1	K_2	Reference
Azores	0.09	8.15	4.5	1.7	7
Nyiragongo	0.47	8.23	4.0	5.0	20
Walvis Ridge	0.57	8.00	4.4	3.2	25
Hawaii	0.94	7.92	4.1	2.4	55
Atlantic MORB*	1.23	7.91	3.8	3.4	7, 38
Ahaggar	1.26	7.98	7.5	3.3	64
Iceland	1.26	7.89	4.1	2.8	55
Ross	1.29	7.96	4.0	3.0	55
Trinidade	1.36	7.94	2.4	5.5	55
Reykjanes Ridge	1.46	7.97	4.3	3.5	62
Atlantic MORB*	1.66	7.89	3.5	3.9	7, 38, 60, 61
Pacific MORB	1.79	7.84	4.2	3.0	7, 30, 38
Canaries	1.79	7.86	4.1	3.2	55
Tristan	1.80	7.87	2.2	6.4	7, 63
Kerguelen	2.22	7.93	2.5	4.8	55
Reunion	2.47	7.84	4.3	3.5	55

*Two different sets of values are reported for Atlantic MORB in order to evaluate the effect of sampling on the computed parameters.

Many K_1 values cluster around 4.2, and K_2 values generally are lower. Tristan, however, like Trinidade and Kerguelen, yields a very low K_1 and a high K_2 value. It is difficult to evaluate how significant these results are—probably not very, because the calculation is based on the unrealistic assumption that secondary enrichment produced a range of μ_2 values but a single K_2 value. Moreover, although 'the primary μ is a very robust property of the system, and is not susceptible to masking by noise',[55] K is not. Table 2 shows the case of Atlantic MORB; if only selected Pb isotope composition data are used for the correlation, μ_1 values vary very little, but large variations result in the isochron age and K values. Nyiragongo, however, is an exception, and its high second-stage K value is very strongly constrained by the extremely radiogenic nature of some of the samples studied by Vollmer and Norry.[20] It seems that, in the case of Nyiragongo, $K_2 > K_1$.

A safer estimate of U/Th fractionation produced by metasomatism can probably be derived by a comparison of time-integrated K ratios obtained from Pb isotopes with K ratios obtained from Th isotopes (K_{Th}; equation 2). The mean K value of the Pb source of a magma, averaged over the entire history of the earth (K_{Pb}) can be obtained by simply dividing the growth equation of $^{208}Pb/^{204}Pb$ by that of $^{206}Pb/^{204}Pb$. Table 3 lists K_{Pb}, K_{Th} and K_m (measured $^{232}Th/^{238}U$ ratios) for some volcanic areas. K_{Pb} values cluster around 3.9, which is lower and not very far from many K_1 values in Table 2; the interesting feature is that the K_{Th} values are *always* lower than the corre-

Table 3 Comparison of average measured $^{232}Th/^{238}U$ ratios (K_m) with average $^{232}Th/^{238}U$ ratios as inferred from Th (K_{Th}) and Pb (K_{Pb}) isotopic data in historical rocks from some localities

Volcanic area	K_{Pb}	K_{Th}	K_m	Reference
Stromboli	3.94	3.34	3.59	41, 65
Vulcano, Vulcanello, Lipari	3.9–4.04	3.29	3.19	41, 65
Vesuvius	4.05	3.43	3.04	18, 35
Etna	3.85	3.17	3.00	40, 66
Tristan da Cunha	4.20	3.69	4.22	7, 36
Iceland 'A'	3.85	3.22	3.7	67, 68
Iceland 'B'	3.8–3.9	2.55	3.2	67, 68
Azores	3.8–3.9	2.60	3.79	7, 36
Hawaii	3.8–3.9	2.91	3.05	38, 59, 69
FAMOUS	3.8	2.46	3.05	39, 61
Mt. St. Helens	—	2.18	2.28	42

K_{Th} ratios calculated from equation 2; K_{Pb} ratios calculated by dividing growth equation of $^{208}Pb/^{204}Pb$ by that of $^{206}Pb/^{204}Pb$. Because Iceland magmas were interpreted in terms of mixing of two components[62, 67, 68] two values (*A* and *B*) listed are extreme values reported by Condomines *et al.*[68]

sponding K_{Pb} ratios. (A comparison of data in Table 2 with those in Table 3 shows that it is very unlikely that the K_1 value obtained for Tristan, as low as 2.2, is significant). Because the second-stage μ increase is generally interpreted as being due to U increase rather than Pb depletion, it should be concluded that the second-stage K decrease of many volcanic areas is caused by U over Th enrichment. Therefore, it is concluded that metasomatism produces a preferential enrichment of U over Pb and U over Th (with possible exceptions—e.g. Nyiragongo) in the metasomatized mantle region.

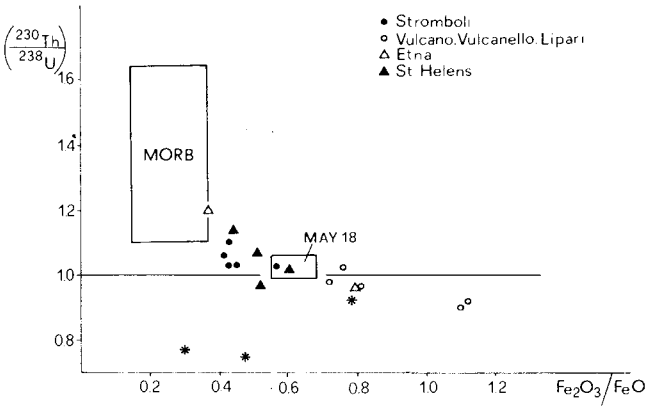

Fig. 3 Tentative plot of $(^{230}Th/^{238}U)$ versus Fe_2O_3/FeO for zero-age volcanic rocks from different tectonic environments. Quadrangle labelled 'May 18' refers to the products of 18 May, 1980, of Mt. St. Helens. Magmas with $(^{230}Th/^{238}U)$ ratios larger than unity preferentially enriched in Th rather than U, and vice-versa. MORB and oceanic islands basalts generally show Th/U enrichment (also at Tristan and Faial, not plotted; also unpublished data from writer's laboratory). Oxidizing conditions seem to favour U/Th enrichment. Vesuvius is apparent exception to trend; transport of U and Th seems to be controlled by factors other than oxygen fugacity

Present fractionation of U/Th in the mantle can be studied by comparing K_{Th} with K_m values in Table 3. K_m ratios are generally higher (Stromboli; oceanic islands and ridges), but can be lower (Vulcano, Vulcanello, Lipari; Vesuvius; Etna) than the corresponding K_{Th} ratios. Fig. 3 is a plot of $(^{230}Th/^{238}U)$ versus Fe_2O_3/FeO ratios for some very young volcanics. It should be remembered that $(^{230}Th/^{238}U) \equiv K_m/K_{Th}$, so if the mantle source of the measured U was in radioactive equilibrium before magma formation, $(^{230}Th/^{238}U)$ ratios larger than unity indicate enrichment of Th relative to U, and vice-versa. The plot in Fig. 3 is very tentative because the $(^{230}Th/^{238}U)$ and Fe_2O_3/FeO ratios should be measured on the same sample aliquot; in fact, both ratios may sometimes undergo large changes within a single flow (e.g. at Vesuvius). Instead, the plot in Fig. 3 is based on data reported in the literature. There does seem to be a tendency, however, to Th/U enrichment for low Fe_2O_3/FeO ratios, i.e. in conditions of low oxygen fugacity. In more oxidizing conditions U seems to be more efficiently extracted than Th. This probably suggests that U is not transported as the ionic species but that it forms ion complexes.

Both $\log(Fe_2O_3/FeO)$ and $\log(U^{+4}/U^{+5})$ are linearly correlated to $\log P_{O_2}$ in a magma (Fig. 7 in Calas[1]). Because the slopes of two such correlation lines are very similar, the following empirical relationship was derived from Calas' Fig. 7:[1]

$$\log(U^{+4}/U^{+5}) = \log(Fe_2O_3/FeO) - 0.85 \qquad (4)$$

The data in Fig. 3, therefore, can be replotted as a function of the oxidation percentage of U (Fig. 4). Vesuvius is a remarkable exception to the trends in Figs. 3 and 4: perhaps the transport of U and Th at Vesuvius is controlled prevalently by halogens, which are present in very large amounts in Vesuvian lavas.[56] Data from Faial and Tristan[36] (not plotted in Figs. 3 and 4) show $(^{230}Th/^{238}U)$ ratios higher than unity, and confirm that rocks from oceanic environments were prevalently enriched in Th rather than U.

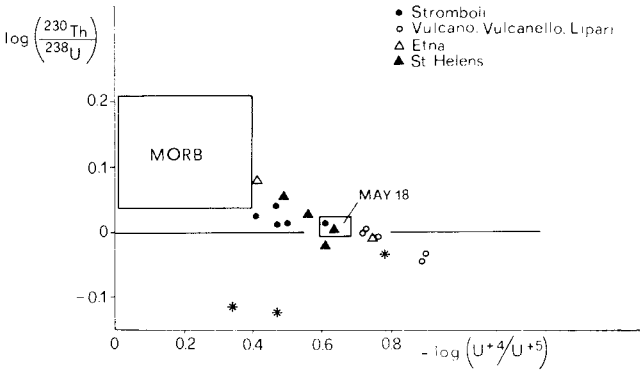

Fig. 4 Same data as in Fig. 3 plotted in $\log(^{230}Th/^{238}U)$ and $-\log(U^{+4}/U^{+5})$ coordinates. $\log(U^{+4}/U^{+5})$ obtained from empirical relationship based on experimental data of Calas[1] (see text)

It should be noted that the trends in Figs. 3 and 4 would be purely fortuitous if the source regions of the volcanics represented had not been in radioactive equilibrium at the moment of magma formation. Thus, these trends provide some further indirect evidence that the mantle generally is in radioactive equilibrium at the onset of melting.

Both enrichment (addition of metasomatic fluids) and depletion (extraction of magmas) therefore seem to generally produce *lower* K values in the mantle (the exceptions to this statement, significantly, seem to be confined to some continental alkaline volcanics and destructive plate margins, and may reflect a different nature of the fluids that enrich their sources). Variations of K ratios in the mantle, therefore, can indicate both enrichment and depletion and, as such, are not one to one geochemical tracers.

As was discussed previously, Th in lavas from Vesuvius, Stromboli, Etna and Mt. St. Helens contains a component (recorded in mineral phases) with a higher Th isotopic composition (lower K) than that of the host whole rocks. Because most Th in the whole rocks probably was fed to the magma from an interstitial, metasomatic mantle component, the lower K com-

ponent may have derived from a Th-poor, more refractory mantle component, which may have undergone a complex history of enrichment–depletion events.[16] These can more easily be studied by means of Sr and Nd rather than Pb and Th isotopes if the ages of these events are suitable.

'Lead paradox' and magma formation in an open system

The 'lead paradox' (so defined by Anderson[57]) is that the sources of some volcanics (e.g. MORB) are depleted in LIL elements relative to a chondritic earth, and Sr and Nd isotopes show that they have been depleted for a long time; yet they have very radiogenic Pb isotopes, which plot to the right of the geochron (Fig. 2). Anderson[57] showed how effective mixing is in resolving this contradiction: he suggested that magmas formed in a depleted source can mix with variable amounts of magmas formed in an enriched mantle region; this explains various apparent contradictions.

Nyiragongo,[20] however, is a recent case of Pb paradox that can hardly be explained by magma mixing. It has nearly primitive Sr and Nd isotope ratios (relative to a chondritic earth), but its Pb is so radiogenic (in one case $^{206}Pb/^{204}Pb = 62!$) that it is virtually impossible to conceive a wide mantle reservoir that can generate such a Pb. Vollmer and Norry[20] suggested that 'mantle metasomatism, by causing erratic and sometimes severe fractionations of U from Pb, could be responsible for the more complex evolution of the U–Pb system relative to the Rb–Sr and Sm–Nd systems observed in oceanic basalts'. Another difficulty of magma mixing is that it cannot generate the isotopic disequilibria of Th (but not of Sr) between minerals and host lavas. It is believed that open-system magma formation in a metasomatized mantle can well account for all the data.

The model that was proposed[35] for Vesuvius suggests that Th, U and Ra were fed to the magma in large amounts by a fluid, but Sr was not. Pb may be fed to the magma in the same way.[35] If this is so, and the fluids were derived from an interstitial, metasomatic mantle component, Sr, Nd, Pb and Th in a magma would be a mixture of two different sources—the metasomatic and the 'refractory', pre-metasomatic component. Church and Tatsumoto[30] proposed a similar explanation for the Pb/Pb arrays of MORB. But, in the present model, Sr and Nd would essentially represent the non-metasomatic component and Pb and Th the metasomatic component. Th and Pb in the *minerals* would represent the first melt, in which the 'refractory' component would be predominant; fluids would then add large amounts of Th, U, Ra and Pb from the metasomatic, interstitial component. The higher K_{Th} values of the latter would represent a more primitive component; the lower K_{Th} of the minerals would indicate a more complex enrichment–depletion history of the 'refractory' component, which could be traced by Sr and Nd isotopes. It is important to note that mixing of liquids derived by different percentages of partial melting (as in the interesting model of Ahern and Turcotte[58]), though very effective, cannot explain the disequilibria data; these require the intervention of some other fluid phase, because it is the only way to produce the recorded Ra/U fractionation.

The μ_1 values listed in Table 2 are all very similar and suggest that Pb from all the listed areas may have had a common first-stage history. The striking feature is that this interpretation fits volcanics from oceanic islands, oceanic ridges and continental areas. If Pb in all these volcanics represents, essentially, the metasomatic component, the common first-stage Pb history suggested by the μ_1 values in Table 2 should be that of the primary mantle reservoir, where Pb evolved *before* it was mobilized by metasomatism. The age significance that is attributed to the secondary Pb/Pb arrays[55] would then imply that metasomatism, rather than a steady-state process, would have pulses of activity. The range of μ_2 values required by the Pb secondary isochrons may be generated by erratic variations of metasomatism[20] and/or eventual depletion (melting) events.

Chase[55] found a shapeless scatter when he plotted the Hawaiian data in a $^{206}Pb/^{204}Pb$–1/Pb plane, and commented that two-component mixing is excluded for Hawaii. The writer thinks that *large-scale* mixing (e.g. magma mixing) is excluded, but small-scale mixing, which may have taken place *within* each magma batch, is not. In fact, the proposed model, strange as it may seem, has a good point in its favour—it is testable. It predicts (1) that Pb in mineral separates should be in isotopic disequilibrium with Pb in the host rock, as for Th but not Sr and Nd (this effect should be larger in continental alkaline volcanics) and (2) because Pb and Th are expected to derive from the same geochemical source, and to be transported by essentially the same mechanism, isotopes of Pb should correlate with isotopes of Th.

Summary and conclusions

(1) Metasomatism is an effective process in the mantle. It controls the distribution of U, Th and Pb in the mantle before the onset of magma formation.
(2) Radioactive disequilibria demonstrate that magma formation is an open-system very fast process in which Ra, U and Th are extracted in large amounts from a mantle source that is geochemically distinct from the mantle fraction from which the melt is formed (i.e. from the source of major and less mobile elements).
(3) Because the enrichment of U, Th and Ra in the magma is so fast, the concept of mineral–melt partition coefficient (which implies that magma formation is a closed-system process) is not valid for these elements during magma formation.
(4) Metasomatism seems to generally produce an *increase* in μ and a *decrease* in K of the metasomatized mantle region.
(5) Magma formation at oceanic ridges and islands seems to generally produce a *decrease* in K in its mantle source region. The fractionation of U/Th during magma formation seems to be often governed by oxygen fugacity conditions.
(6) The major source of U, Th, Ra *and* Pb in a magma probably is the metasomatic mantle component. Instead, the major source of Sr and Nd in a magma is the non-metasomatic, more 'refractory' mantle component. If this is so, the 'lead paradox' is easily explained.
(7) This proposed model is testable. It predicts isotopic disequilibrium of Pb between coexisting minerals and whole rocks, and a correlation of Pb with Th isotopes.

Postscript

Preliminary Pb isotopic data, obtained at the Open University, United Kingdom, on some minerals from Vesuvius, Etna and Stromboli suggest that both the conditions predicted by the writer's model are met. This supports the idea that Pb and Th in volcanic rocks may be a mixture of components derived from isotopically different sources. Much work has to be done, however, before this model can be used for quantitative purposes.

Acknowledgement

I am sincerely grateful to Ronald Vollmer, Enzo Locardi and Chris Hawkesworth for their critical reading of this manuscript. Giulio Ottonello showed me that the Th/U fractionation can be plotted as a function of the oxidation percentage of U, and provided very useful comments. His help is gratefully acknowledged.

References

1. Calas G. Etude expérimentale du comportement de l'uranium dans

les magmas: états d'oxydation et coordinance. *Geochim. cosmochim. Acta*, **43**, 1979, 1521–31.
2. Smith D. K. Uranium mineralogy. In *Uranium geochemistry, mineralogy, geology, exploration and resources* De Vivo B. *et al.* eds (London: IMM, 1984), 33–83.
3. Szalay S. and Sámsoni Z. Investigation of the leaching of uranium from crushed magmatic rocks. *Geochem. Int.*, **6**, 1969, 613–23.
4. Hamilton E. I. The abundance and distribution of uranium in some oceanic, continental ultramafic inclusions and host basalts. *Chem. Geol.*, **16**, 1975, 221–31.
5. Rich R. A. Holland H. D. and Petersen U. *Hydrothermal uranium deposits* (Amsterdam: Elsevier, 1977), 264 p.
6. Sun S.-S. and Nesbitt R. W. Chemical heterogeneity of the Archaean mantle, composition of the Earth and mantle evolution. *Earth Planet. Sci. Lett.*, **35**, 1977, 429–48.
7. Sun S.-S. Lead isotopic study of young volcanic rocks from mid-ocean ridges, ocean islands and island arcs. *Phil. Trans. R. Soc. Lond.*, **A297**, 1980, 409–45.
8. O'Nions R. K. and Pankhurst R. J. Early Archaean rocks and geochemical evolution of the earth's crust. *Earth Planet. Sci. Lett.*, **38**, 1978, 211–36.
9. Bailey D. K. Mantle metasomatism—continuing chemical change within the earth. *Nature, Lond.*, **296**, 1982, 525–30.
10. Lloyd F. E. and Bailey D. K. Light element metasomatism of the continental mantle: the evidence and the consequences. *Phys. Chem. Earth*, **9**, 1975, 389–416.
11. Boettcher A. L. *et al.* Metasomatism of the upper mantle and the genesis of kimberlites and alkali basalts. In *The mantle sample: inclusions in kimberlites and other volcanics* Boyd F. R. and Meyer H. O. A. eds (Washington, D.C.: American Geophysical Union, 1979), 173–82. (*Proc. 2nd Int. Kimberlite Conf.*, vol. 2)
12. Erlank A. J. *et al.* Mantle heterogeneity beneath southern Africa: evidence from the volcanic record. *Phil. Trans. R. Soc. Lond.*, **A297**, 1980, 295–307.
13. Erlank A. J. *et al.* Chemical and isotopic characterization of upper mantle metasomatism in peridotite nodules from the Bultfontein kimberlite. *Terra cognita*, **2**, 1982, 261–3.
14. Sutherland F. L. and Hollis J. D. Mantle–lower crust petrology from inclusions in basaltic rocks in Eastern Australia—an outline. *J. Volc. geotherm. Res.*, **14**, 1982, 1–29.
15. Menzies M. and Murthy V. R. Nd and Sr isotope geochemistry of hydrous mantle nodules and their host alkali basalts: implications for local heterogeneities in metasomatically veined mantle. *Earth Planet. Sci. Lett.*, **46**, 1980, 323–34.
16. Menzies M. Mantle ultramafic xenoliths in alkaline magmas; evidence for mantle heterogeneity modified by magmatic activity. In *Continental basalts and mantle xenoliths* Hawkesworth C. J. and Norry M. J. eds (London: Shiva Publications, 1983), 92–110.
17. Hawkesworth C. J. and Vollmer R. Crustal contamination versus enriched mantle: $^{143}Nd/^{144}Nd$ and $^{87}Sr/^{86}Sr$ evidence from the Italian volcanics. *Contr. Mineral. Petrol.*, **69**, 1979, 151–65.
18. Vollmer R. and Hawkesworth C. J. Lead isotopic composition of the potassic rocks from Roccamonfina (South Italy). *Earth Planet. Sci. Lett.*, **47**, 1980, 91–101.
19. Menzies M. and Murthy V. R. Enriched mantle: Nd and Sr isotopes in diopsides from kimberlite nodules. *Nature, Lond.*, **283**, 1980, 634–6.
20. Vollmer R. and Norry M. J. Unusual isotopic variations in Nyiragongo nephelinites. *Nature, Lond.*, **301**, 1983, 141–3.
21. Menzies M. and Murthy V. R. Mantle metasomatism as a precursor to the genesis of alkaline magmas—isotopic evidence. *Am. J. Sci.*, **280A**, 1980, 622–38.
22. Wass S. Y. and Rogers N. W. Mantle metasomatism—precursor to continental alkaline volcanism. *Geochim. cosmochim. Acta*, **44**, 1980, 1811–23.
23. Hawkesworth C. J. *et al.* $^{143}Nd/^{144}Nd$ and $^{87}Sr/^{86}Sr$ ratios from the Azores and their significance in LIL-element enriched mantle. *Nature, Lond.*, **280**, 1979, 28–31.
24. Schilling J.-G. Bergeron M. B. and Evans R. Halogens in the mantle beneath the North Atlantic. *Phil. Trans. R. Soc. Lond.*, **A297**, 1980, 147–78.
25. Richardson S. H. *et al.* Correlated Nd, Sr and Pb isotope variation in Walvis Ridge basalts and implications for the evolution of their mantle source. *Earth Planet. Sci. Lett.*, **59**, 1982, 327–42.
26. Haines E. L. and Zartman R. E. Uranium concentration and distribution in six peridotite inclusions of probable mantle origin. *Earth Planet. Sci. Lett.*, **20**, 1973, 45–53.
27. Zartman R. E. and Tera F. Lead concentration and isotopic composition in five peridotite inclusions of probable mantle origin. *Earth Planet. Sci. Lett.*, **20**, 1973, 54–66.
28. Wyllie P. J. The origin of kimberlite. *J. geophys. Res.*, **85**, 1980, 6902–10.
29. Spera F. J. Carbon dioxide in igneous petrogenesis: II. Fluid dynamics of mantle metasomatism. *Contr. Mineral. Petrol.*, **77**, 1981, 56–65.
30. Church S. E. and Tatsumoto M. Lead isotope relations in oceanic ridge basalts from the Juan de Fuca-Gorda ridge area, N.E. Pacific Ocean. *Contr. Mineral. Petrol.*, **53**, 1975, 253–79.
31. Gast P. W. Trace element fractionation and the origin of tholeiitic and alkaline magma types. *Geochim. cosmochim. Acta*, **32**, 1968, 1057–86.
32. Bailey D. K. and McDonald R. Fluorine and chlorine in peralkaline liquids and the need for magma generation in an open system. *Mineralog. Mag.*, **40**, 1975, 405–14.
33. Bailey D. K. Continental rifting and mantle degassing. In *Petrology and geochemistry of continental rifts* Neumann E.-R. and Ramberg I. B. eds (Dordrecht: Reidel, 1978), 1–13.
34. Somayajulu B. L. K. *et al.* Disequilibrium of the ^{238}U series in basalt. *Earth Planet. Sci. Lett.*, **1**, 1966, 387–91.
35. Capaldi G. Cortini M. and Pece R. Th isotopes at Vesuvius: evidence for open-system behaviour of magma-forming processes. *J. Volc. geotherm. Res.*, **14**, 1982, 247–60.
36. Oversby V. M. and Gast P. W. Lead isotope compositions and uranium decay series disequilibrium in recent volcanic rocks. *Earth Planet. Sci. Lett.*, **5**, 1968, 199–206.
37. Condomines M. Etude chronologique et géochimique du volcanism récent du Costa Rica à l'aide du déséquilibre radioactif ^{230}Th–^{238}U. Third cycle thesis, University of Paris, 1974, 69 p.
38. Tatsumoto M. Isotopic composition of lead in oceanic basalt and its implication to mantle evolution. *Earth Planet. Sci. Lett.*, **38**, 1978, 63–87.
39. Condomines M. Morand P. and Allègre C. J. ^{230}Th-^{238}U radioactive disequilibria in tholeiites from the FAMOUS zone (Mid-Atlantic Ridge, 36°50′N): Th and Sr isotopic geochemistry. *Earth Planet. Sci. Lett.*, **55**, 1981, 247–56.
40. Capaldi G. *et al.* Short-lived radioactive disequilibria in freshly erupted volcanic rocks and their implications for the preeruption history of a magma. *J. geophys. Res.*, **81**, 1976, 350–8.
41. Capaldi G. Cortini M. and Pece R. U and Th decay series disequilibria in historical rocks from the Eolian islands (Tyrrhenian sea). *Isotope Geosci.*, **1**, 1983, 39–55.
42. Bennett J. T. *et al.* The uranium and thorium decay series nuclides in Mt. St. Helens effusives. *Earth Planet. Sci. Lett.*, **60**, 1982, 61–9.
43. Krishnaswami S. Bennett T. J. and Turekian K. K. Uranium and thorium decay series nuclides in Hawaiian basalts. *EOS*, **63**, 1982, 1138. (Abstract)
44. Capaldi G. *et al.* U and Th distribution in sedimentary rocks from the Campanian Apennines. An evidence against an external source for the Ra excess of Vesuvius lavas. *Periodico Miner.*, **49**, 1980, 45–55.
45. Allègre C. J. ^{230}Th dating of volcanic rocks: a comment. *Earth Planet. Sci. Lett.*, **5**, 1968, 209–10.
46. Allègre C. J. and Condomines M. Fine chronology of volcanic processes using ^{238}U–^{230}Th systematics. *Earth Planet. Sci. Lett.*, **28**, 1976, 395–406.
47. Condomines M. and Allègre C. J. Age and magmatic evolution of Stromboli volcano from ^{230}Th–^{238}U disequilibrium data. *Nature, Lond.*, **288**, 1980, 354–7.
48. Condomines M. *et al.* Magmatic evolution of a volcano studied by ^{230}Th–^{238}U disequilibrium and trace elements systematics: the Etna case. *Geochim. cosmochim. Acta*, **46**, 1982, 1397–416.
49. Capaldi G. and Pece R. On the reliability of the ^{230}Th–^{238}U dating method applied to young volcanic rocks. *J. Volc. geotherm. Res.*, **11**, 1981, 367–72.
50. Gillot P. Y. and Villari L. K/Ar geochronological data on the Aeolian arc volcanism. A preliminary report. *Publ. Istit. int. Vulc.* no. 145, 1982.
51. Rose W. I. Jr and Bornhorst T. J. Uranium and thorium in selected Quaternary volcanic rocks of Guatemala and Sumatra: evidence for uranium redistribution. In *Uranium in volcanic and volcanoclastic rocks* Goodell P. C. and Waters A. C. eds. *AAPG Studies Geol.* no.

13, 1981, 13–21.
52. Cortini M. and Hermes O. D. Sr isotopic evidence for a multi-source origin of the potassic magmas in the Neapolitan area (S. Italy). *Contrib. Mineral. Petrol.*, **77**, 1981, 47–55.
53. Allègre C. J. and Condomines M. Basalt genesis and mantle structure studied through Th-isotopic geochemistry. *Nature, Lond.*, **299**, 1982, 21–4.
54. Faure G. *Principles of isotope geology* (New York: Wiley, 1977), 464 p.
55. Chase C. G. Oceanic island Pb: two-stage histories and mantle evolution. *Earth Planet. Sci. Lett.*, **52**, 1981, 277–84.
56. Baldridge W. S. Carmichael I. S. E. and Albee A. L. Crystallization paths of leucite-bearing lavas: examples from Italy. *Contrib. Miner. Petrol.*, **76**, 1981, 321–35.
57. Anderson D. L. Isotopic evolution of the mantle: the role of magma mixing. *Earth Planet. Sci. Lett.*, **57**, 1982, 1–12.
58. Ahern J. L. and Turcotte D. L. Magma migration beneath an ocean ridge. *Earth Planet. Sci. Lett.*, **45**, 1979, 115–22.
59. Condomines M. Bernat M. and Allègre C. J. Evidence for contamination of recent Hawaiian lavas from ^{230}Th–^{238}U data. *Earth Planet. Sci. Lett.*, **33**, 1976, 122–5.
60. Dupré B. and Allègre C. J. Pb–Sr–Nd isotopic correlation and the chemistry of the North Atlantic mantle. *Nature, Lond.*, **286**, 1980, 17–22.
61. Dupré B. *et al.* Limitations on the scale of mantle heterogeneities under oceanic ridges. *Nature, Lond.*, **294**, 1981, 552–4.
62. Sun S.-S. Tatsumoto M. and Schilling J.-G. Mantle plume mixing along the Reykjanes Ridge axis: lead isotopic evidence. *Science*, **190**, 1975, 143–7.
63. Cohen R. S. and O'Nions R. K. Identification of recycled continental material in the mantle from Sr, Nd and Pb isotope investigations. *Earth Planet. Sci. Lett.*, **61**, 1982, 73–84.
64. Allègre C. J. *et al.* The subcontinental versus suboceanic debate, I. Lead–neodymium–strontium isotopes in primary alkali basalts from a shield area: the Ahaggar volcanic suite. *Earth Planet. Sci. Lett.*, **52**, 1981, 85–92.
65. Cortini M. Aeolian island arc (South Tyrrhenian sea) magma heterogeneities in historical lavas: Sr and Pb isotopic evidence. *Bull. Volc.*, **44**, 1981, 711–22.
66. Carter S. R. and Civetta L. Genetic implications of the isotope and trace element variations in the Eastern Sicilian volcanics. *Earth Planet. Sci. Lett.*, **36**, 1977, 168–80.
67. Sun S.-S. and Jahn B. Lead and strontium isotopes in post-glacial basalts from Iceland. *Nature, Lond.*, **255**, 1975, 527–30.
68. Condomines M. *et al.* ^{230}Th–^{238}U disequilibria in historical lavas from Iceland. *Earth Planet. Sci. Lett.*, **55**, 1981, 393–406.

Transport and deposition of uranium in hydrothermal systems at temperatures up to 300°C: geological implications

Samuel B. Romberger
Department of Geology, Colorado School of Mines, Golden Colorado, U.S.A.

Many geologists accept that certain uranium deposits may have formed at elevated temperatures in the presence of aqueous fluids. Such deposits may range in nature from typical veins and fracture fillings to deposits in metamorphic terrains that exhibit a variety of structural controls. Fluid inclusion studies and mineral stability relationships from a variety of occurrences indicate that these deposits form at temperatures up to 300°C. The purpose of this paper is to outline the physicochemical conditions under which uranium is mobile and how it is transported, and also the conditions under which uranium is deposited, and to determine possible mechanisms of precipitation. Existing thermodynamic data were used to evaluate the relative stability of various uranium complexes in hydrothermal solutions up to 300°C. Subsequently, the conditions under which various aqueous uranium species and solids are stable were calculated in terms of oxidation potential (fugacity of oxygen, f_{O_2}) and pH. The stabilities of uranium species and minerals are compared against those of alteration and gangue minerals commonly associated with uranium mineralization. These natural assemblages are then used to determine the conditions of ore deposition, and possible mechanisms of deposition are proposed.

The phase diagrams used will be only as good as the data that are used to construct them. Even though there may be an error in the absolute position of stability boundaries, the diagrams are still quite useful in outlining relative mineral stabilities. Therefore, it is still possible to obtain approximate solution compositions from the mineral assemblages and also to speculate on the relative changes in solution parameters. Because of the lack of high-quality thermodynamic data for uranium species at high temperatures, a simple van't Hoff equation was used to calculate equilibria at high temperatures. The errors introduced by this approach increase with temperature.

General mineralizing environment

As a first approximation it can be assumed that uranium is transported in the U^{6+} oxidation state, and is insoluble in the U^{4+} state. Mineralizing solutions may be evolved meteoric water, formation waters and fluids released during metamorphism, as well as fluids liberated during magmatic processes. Uranium and associated metals may be derived locally in the rocks through which the mineralizing solutions migrate and need not come from a crystallizing magma.

The general mineralizing system is illustrated schematically in Fig. 1. It consists of the environment of mobilization, or source rock, environment of transport, and the environment of deposition. In the latter the uranium may be dispersed or concentrated, depending on the physical and chemical nature of the environment of deposition. The nature of each part of the system is dependent on the composition of the other parts. For example, the mechanisms of precipitation in the environment of deposition will depend on how the uranium is transported. This, in turn, may depend on the availability of suitable complexing agents in the source environment. Fig. 1 implies that the transport of uranium is favoured in systems with relatively high activities of electrons and protons, which is equivalent to assuming that uranium is soluble in acid oxidizing environments. Therefore, qualitatively, precipitation would be promoted by reduction and/or increase in pH of the transporting solutions.

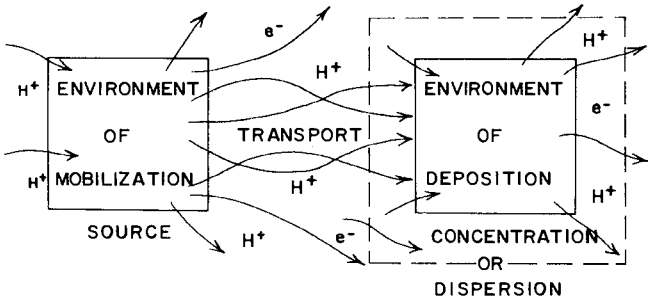

Fig 1 Schematic representation of environment of mineralization for uranium deposits

The source of uranium and associated elements has been a subject of significant controversy among uranium geologists. The long-held classical view that metals and other components in hydrothermal deposits were derived from differentiating silicate magmas cannot be applied to many deposits that are unassociated with igneous rocks. An alternative source for metals in these deposits may be the rocks through which the solutions pass (Fig. 2). For rocks to serve as adequate sources for uranium and other components the solutions must have access to these materials and the chemical components to be

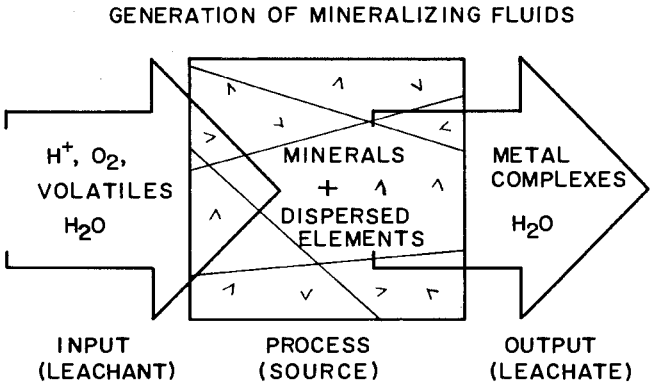

Fig. 2 Schematic representation of environment of mobilization for generation of mineralizing solutions

transported must be in a mobile, or soluble, form. The required permeability may be intrinsic to the formation, as in coarse conglomerates and sandstones; more commonly, the permeability is secondary, and is the result of fracturing or solution during the formation of karst features in carbonate sedimentary rocks.

Metals bonded within the crystal structure of rock-forming or accessory minerals will not be in a form easily dissolved by the mobilizing solutions. These minerals must experience some change during which the desired components can be released from the crystal lattices. Fig. 3 illustrates schematically that impurity elements can be removed to accessible sites by various processes of recrystallization, where the impurities are no longer accommodated by the new minerals. Such changes can occur during metamorphism and hydrothermal alteration. Metals dissolved in volcanic glass are also released during

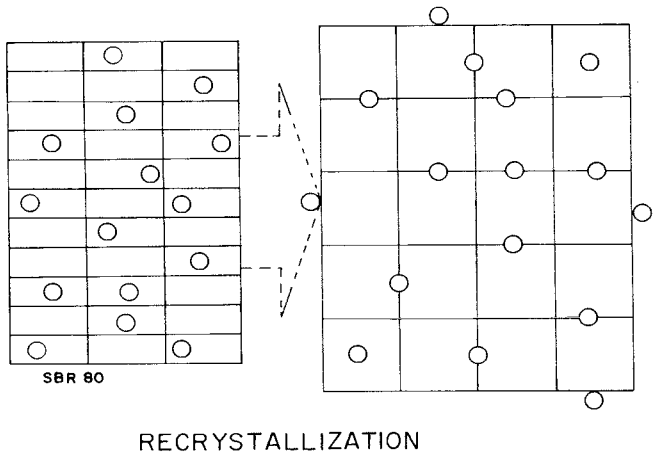

Fig. 3 Schematic representation for release of impurity components from rock-forming and accessory minerals through metamorphism or hydrothermal alteration, resulting in adsorbed metals on exchangeable sites in clays or secondary oxides

devitrification. Major redistribution of metals does not, however, occur during these processes. After the metallic components are released from crystal lattices they are quickly co-precipitated with various secondary oxides or are adsorbed on these oxides or secondary clay minerals. These loosely held metals can be dissolved by slightly acid oxidizing solutions. Where carbonate complexing of uranium is important, this metal may be mobilized by neutral to alkaline solutions as well. The source of the complexing agents may be the solutions that percolate through the source rocks or the source rocks themselves.

and U^{6+}. There are some 43 possible uranium complexes, the relative importance of each depending on temperature and the composition of the aqueous solution. In subsequent discussions the uranous complexes are neglected because of the low solubility of uranium as U^{4+}.

Table 1 List of uranyl and uranous complexes known to form with various anions

H_2O:	U^{4+}, UOH^{3+}, $U(OH)_2^{2+}$, $U(OH)_3^{+}$, $U(OH)_4^{\circ}$, $U(OH)_5^{-}$, UO_2^{2+}, UO_2OH^{+}, $UO_2(OH)_2^{\circ}$, $UO_2(OH)_3^{-}$, $U_2(OH)_5^{3+}$, $(UO_2)_2(OH)_2^{2+}$, $(UO_2)_3(OH)_5^{+}$, U^{3+}, UO_2^{+},
SULFATE:	USO_4^{2+}, $U(SO_4)_2^{\circ}$, $UO_2SO_4^{\circ}$, $UO_2(SO_4)_2^{2-}$,
CARBONATE:	$UO_2CO_3^{\circ}$, $UO_2(CO_3)_2^{2-}$, $UO_2(CO_3)_3^{4-}$,
PHOSPHATE:	$UHPO_4^{2+}$, $U(HPO_4)_2^{\circ}$, $U(HPO_4)_3^{2-}$, $U(HPO_4)_4^{4-}$, $UO_2HPO_4^{\circ}$, $UO_2(HPO_4)_2^{2-}$, $UO_2H_2PO_4^{+}$, $UO_2(H_2PO_4)_2^{\circ}$, $UO_2(H_2PO_4)_3^{+}$,
CHLORIDE:	UCl^{3+}, UO_2Cl^{+}.
FLUORIDE:	UF^{3+}, UF_2^{2+}, UF_3^{+}, UF_4°, UF_5^{-}, UF_6^{2-}, UO_2F^{+}, $UO_2F_2^{\circ}$, $UO_2F_3^{-}$, $UO_2F_4^{2-}$.

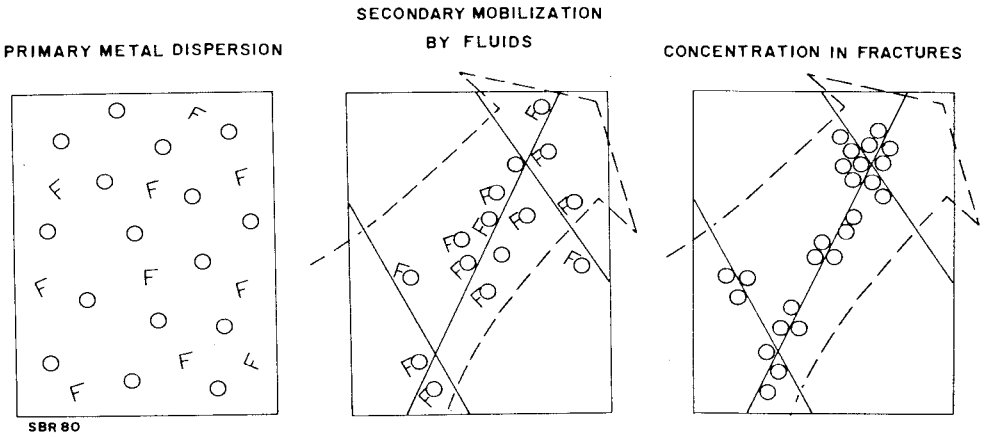

Fig. 4 Diagrammatic representation of process by which uranium can be mobilized from wallrock and concentrated in mineralized structures during hydrothermal activity

The process by which uranium dispersed in a source rock can be concentrated in favourable structures is illustrated in Fig. 4. The complexing agent that was responsible for transporting the uranium is assumed to be fluoride in this case, which is also dispersed in the source rock. Mobilization of the uranium requires fracture-induced permeability. Once the uranium is dissolved in the solutions that percolate through the fracture systems it can be precipitated as a result of the appropriate change in the physico-chemical conditions of the system.

Uranium transport

To determine the mechanisms of transport of uranium it is necessary to evaluate the various complexes that are formed by this metal. Table 1 lists the complexes known to form between various naturally occurring complexing agents and both U^{4+}

The relative stabilities of the various uranyl complexes are evaluated by use of distribution diagrams in which the distribution coefficient, α, is plotted versus pH at a constant temperature and concentration of complexing components. The distribution coefficient expresses the proportion of the total dissolved uranium that occurs as a given complex and is independent of the total uranium in solution. The activities of the complexing anions, such as F^-, HPO_4^{2-} and CO_3^{2-}, are a function of temperature and pH because their activities depend on the ionization of such weak acids as HF, H_3PO_4 and H_2CO_3, respectively. The concentration of the latter will depend on the partial pressure of carbon dioxide (P_{CO_2}) and this is specified in each diagram.

The distribution of uranyl complexes at 100°C in a solution that contains 10 ppm fluoride, 100 ppm sulphate, and 1 m NaCl

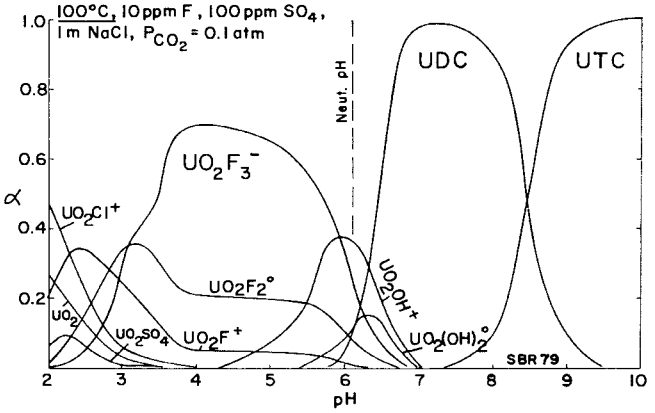

Fig. 5 Distribution diagram showing distribution of uranyl complexes at 100°C in solutions containing 10 ppm F, 100 ppm SO_4 and 1 m NaCl at P_{CO_2} of 0.1 atm

at a P_{CO_2} of 0.1 atm is shown in Fig. 5. Neutral pH at this temperature is 6.1. The alkaline region is dominated by the uranyl dicarbonate (UDC) and uranyl tricarbonate (UTC) complexes. A number of complexes occur at acid pH values, but fluoride complexes predominate even at this low concentration of fluoride. Chloride and sulphate complexes are generally weak, even at relatively high concentrations of these anions. In contrast, hydroxide complexes are quite stable and appear in the neutral region, even though the activity of hydroxyl ion is very small. The reactions responsible for uranium precipitation will depend on the mechanisms of transport: therefore, knowledge of the nature of these uranium

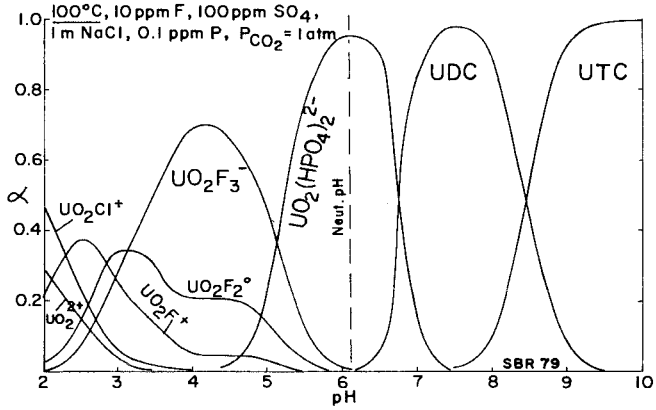

Fig. 6 Distribution diagram showing distribution of uranyl complexes at 100°C in solutions containing 10 ppm F, 100 ppm SO_4, 0.1 ppm P and 1 m NaCl at P_{CO_2} of 1 atm

complexes is essential. Fig. 6 shows the distribution of uranyl complexes in a solution similar to that for Fig. 5, except that 0.1 ppm phosphorus has been added and P_{CO_2} has been increased to 1 atm. The importance of phosphate complexes in the neutral region, even at such low concentrations of phosphorus, is well illustrated. Therefore, in certain hydrothermal uranium deposits that also contain phosphate minerals—for example, apatite—the activity of phosphate might have been sufficiently high for uranium to have been transported as phosphate complexes.

Fig. 7 illustrates the distribution of uranyl complexes at 200°C in a solution that contains 100 ppm fluoride, 100 ppm sulphate and 1 m NaCl at a P_{CO_2} of 1.0 atm. The general relationships at 200°C are similar to those at 100°C, except for the shift of the carbonate complexes to higher pH values. Neutral pH at 200°C is 5.6. Because of the buffering capacity of rocks most hydrothermal solutions have pH values within 2

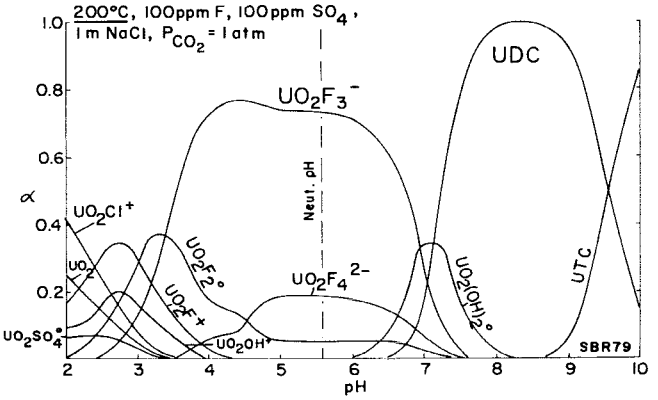

Fig. 7 Distribution diagram showing distribution of uranyl complexes at 200°C in solutions containing 100 ppm F, 100 ppm SO_4 and 1 m NaCl at P_{CO_2} of 1 atm

units on either side of neutrality. Therefore, fluoride complexes appear to be very important in solutions of this composition. Fig. 8 shows the distribution of uranyl complexes in a solution of similar composition to that for Fig. 7, except that 1 ppm phosphorus has been added. Under these conditions phosphate complexes predominate in slightly alkaline solutions.

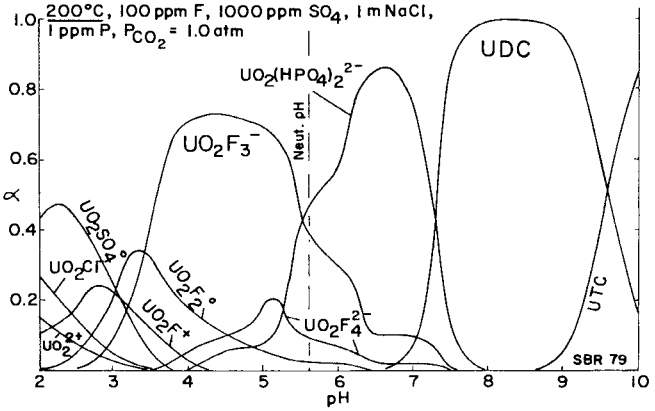

Fig. 8 Distribution diagram showing distribution of uranyl complexes at 200°C in solutions containing 100 ppm F, 1000 ppm SO_4, 1 ppm P and 1 m NaCl at P_{CO_2} of 1 atm

Fig. 9 shows the distribution of uranyl complexes at 300°C in solutions with 100 ppm fluoride, 1000 ppm sulphate and 1 m

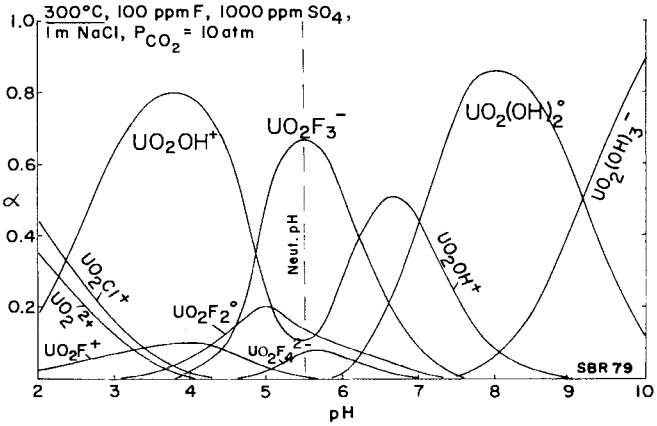

Fig. 9 Distribution diagram showing distribution of uranyl complexes at 300°C in solutions containing 100 ppm F, 1000 ppm SO_4 and 1 m NaCl at P_{CO_2} of 10 atm

NaCl at a P_{CO_2} of 10 atm. In a comparison of this diagram with those for lower temperatures it is apparent that carbonate complexes become unimportant, even in relatively alkaline solutions: this is the result of a decrease in the activity of CO_3^{2-} owing to the decrease in the second ionization constant for carbonic acid at elevated temperatures. Fluoride complexes are important only in neutral regions; neutral pH at 300°C is approximately 5.5. The decrease in importance of fluoride complexes is a result of the decrease in stability of the complexes themselves, and also the decrease in activity of fluoride ion because of the lowering of the ionization constant of HF as temperature increases. Hydroxide complexes predominate over a wide pH range even in the acid region: this is because the uranyl hydroxide complexes increase in stability as temperature increases, whereas the availability of other complexing anions decreases. Fig. 10 shows the distribution of uranyl complexes in solutions similar to those for Fig. 9, except that the fluoride concentration was decreased to 10 ppm and 1 ppm phosphorus has been added. Again, the importance of phosphate complexes in neutral solutions is apparent.

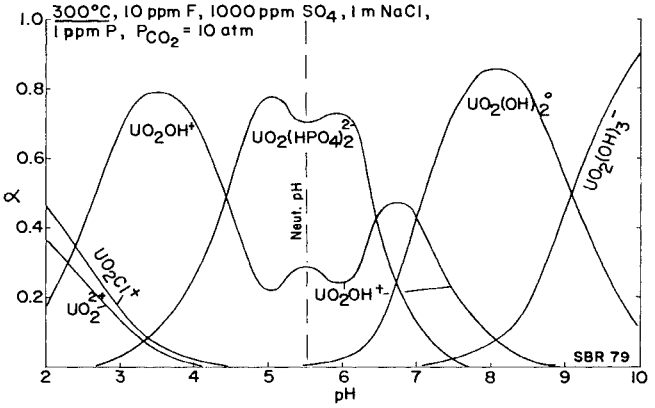

Fig. 10 Distribution diagram showing distribution of uranyl complexes at 300°C in solutions containing 10 ppm F, 1000 ppm SO_4, 1 ppm P and 1 m NaCl at P_{CO_2} of 10 atm

To summarize uranium complexing in hydrothermal solutions, the predominant species will depend on the concentration of complexing anions, which is, in turn, dependent on temperature and pH. The activity of fluoride in many uranium mineralizing systems appears to be significant, as is indicated by the abundance of fluorite and other fluoride-containing gangue minerals. In these systems uranyl fluoride complexes would predominate in acid to neutral solutions. At low temperatures carbonate complexes predominate in alkaline solutions, but, as temperature increases, carbonate complexes become less important. Phosphate complexes may be important in near-neutral solutions in which as little as 0.1 ppm phosphate is present. As temperature increases, hydroxide complexes become more important. At temperatures of 300°C and above hydroxide complexes may be the only soluble uranium species.

Mechanisms of deposition

Factors that may influence the solubility of uranium in a hydrothermal system are temperature, pressure, oxidation state, pH, activity of complexing anions and partial pressure of such volatile components as carbon dioxide. The solubility of uranium decreases with increase in temperature, so cooling cannot be a possible mechanism of deposition. The effect of pressure on uranium solubility is difficult to evaluate, but at the relatively low pressures of formation for many hydrothermal deposits the role of pressure is to affect the partial pressure of volatile components only. As pressure decreases, the partial pressure of CO_2 decreases, which will decrease the activity of carbonate ion available for uranium complexing. Also, pH may increase as pressure decreases because of the loss of volatile components. A very good mechanism by which the partial pressure of volatile components can be reduced is boiling. Other changes that can be responsible for the decrease in activity of complexing anions are dilution of the hydrothermal solutions and precipitation of gangue minerals that contain the appropriate anions. An example of the latter is the precipitation of fluorite, which results in the reduction of fluoride activity.

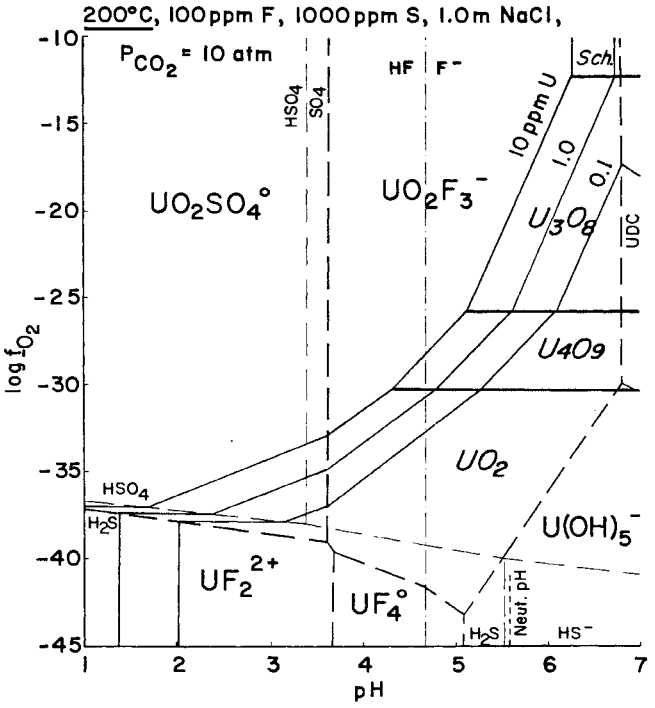

Fig. 11 Log f_{O_2}–pH diagram showing distribution of uranyl and uranous complexes and solubility of uranium oxides at 200°C in solutions containing 100 ppm F, 1000 ppm S and 1 m NaCl at P_{CO_2} of 10 atm (see text for explanation)

The effect of oxidation state and pH on the solubility of uranium can be evaluated by use of oxygen fugacity–pH diagrams at a constant temperature. Fig. 11 is a log f_{O_2}–pH diagram that shows the relative stability of uranium complexes at 200°C in solutions with 100 ppm fluoride, 1000 ppm sulphate and 1 m NaCl at a P_{CO_2} of 10 atm. The solubility of uranium oxide as these various complexes under these conditions has also been calculated. Solubility contours of 10, 1 and 0.1 ppm U are shown to demonstrate the trend of the solubility surface. The heavy dashed lines show the boundaries between the stability fields for the various uranium complexes. Uranyl complexes predominate at high f_{O_2} values, at which the sulphate complex is important in acid solutions; the fluoride complex is important in slightly acid to slightly alkaline pH values; and the carbonate complex (UDC) predominates at pH values above approximately 7. Various uranous complexes that involve fluoride and hydroxide are shown at low f_{O_2} values. The fine dashed lines show the boundaries between the fields of predominance for the aqueous sulphur species. The dot-dashed line separates the HF and F^- fields of predominance.

Even though uranium oxides of three distinct compositions are shown, natural phases usually consist of solid solutions with variable U:O ratios. It should be clear that this ratio will be a function of f_{O_2}, and will decrease as f_{O_2} decreases. The stability field of schoepite (Sch.) is shown in the upper right of Fig. 11. These phase relationships indicate that uranium is soluble over a wide range of f_{O_2} and pH values in the acid oxidizing region.

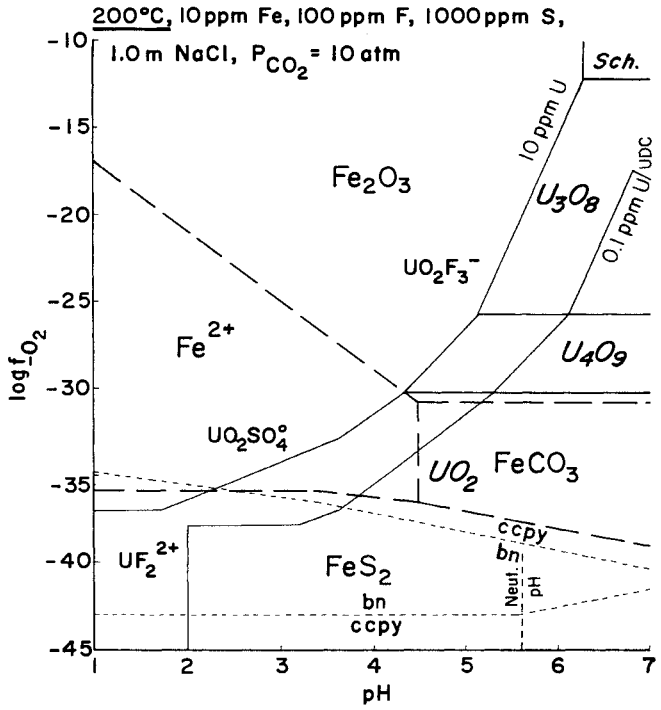

Fig. 12 Log f_{O_2}–pH diagram showing distribution of uranyl complexes, solubility of uranium oxides, distribution of iron phases and relative stability of chalcopyrite and bornite at 200°C in aqueous system containing 10 ppm Fe, 100 ppm F, 1000 ppm S and 1 m NaCl at P_{CO_2} of 10 atm (see text for explanation)

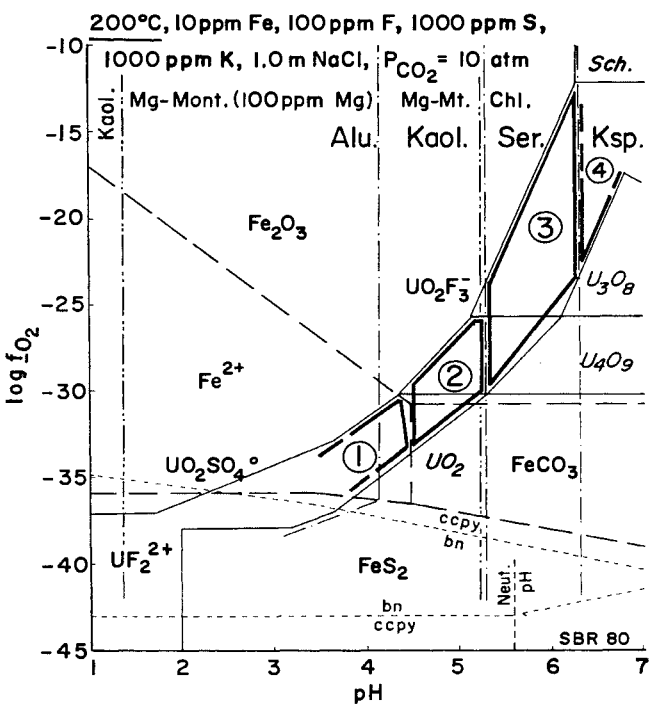

Fig. 13 Log f_{O_2}–pH diagram showing distribution of uranyl complexes, solubility of uranium oxides, distribution of iron phases, relative stability of chalcopyrite and bornite and relative stability of potassium and magnesium silicates at 200°C in aqueous system containing 10 ppm Fe, 100 ppm F, 1000 ppm S, 1000 ppm K, 100 ppm Mg and 1 m NaCl at P_{CO_2} of 10 atm (see text for explanation)

Precipitation of uranium oxide would occur if the composition of the transporting solution changed from upper left to lower right or during reduction and increasing pH. Because of the slopes of the various segments of the solubility contours the relative importance of reduction and increasing pH in promoting precipitation will depend on where the transporting solutions start out in the diagram and how the uranium is transported. At high pH values, where carbonate complexes predominate, reduction is the only geologically reasonable mechanism for deposition, as there are few processes that might cause alkaline solutions to become more acid.

Fig. 12 is a diagram similar to that shown in Fig. 11, except that the boundaries between aqueous species are neglected for simplicity and the stability fields for various iron solids and aqueous species are shown as heavy dashed lines, 10 ppm iron in solution being assumed. Iron would be transported under f_{O_2} and pH conditions within the boundaries of the Fe^{2+} field. At high f_{O_2} values hematite would be deposited; under reducing conditions pyrite would be stable; and at intermediate f_{O_2} values and slightly acid to alkaline pH values siderite would be the stable phase. These phase relationships indicate that if it can be assumed that between 0.1 and 10 ppm uranium are transported in solution, uranium oxides can be deposited with a wide range of iron minerals. The latter may be very useful in indicating the conditions of uranium deposition (see below).

The boundary that expresses the relative stability of bornite (bn) and chalcopyrite (ccpy) is shown as a fine dashed line. The field of bornite stability decreases in size with decrease in dissolved sulphur; in Fig. 12 total sulphur equals 1000 ppm. Chalcopyrite and pyrite are commonly associated with uranium mineralization, but the diagram suggests that the f_{O_2} and pH conditions for this assemblage to occur are limited. In these deposits the total dissolved sulphur content may be significantly less than 1000 ppm, and thus this assemblage puts an upper limit on sulphur activity.

Fig. 13 contains the same information as the earlier diagrams, except that the relative stability of potassium and magnesium silicates that commonly occur in uranium deposits as alteration minerals has been superimposed. These boundaries have been calculated for 200°C on the assumption of the presence of 1000 ppm potassium and 100 ppm magnesium in solution. The boundaries between the stability fields for the potassium silicates, kaolinite (kaol.), alunite (alu.), sericite (ser.) and adularia (ksp.) are shown as light dot-dashed lines. The boundaries between the fields for the magnesium silicates chlorite (chl.) and magnesian montmorillonite (Mg-Mont.) are shown as light double-dot–dashed lines. The position of all these boundaries will change slightly with change in cation activity. The composition of the chlorite is assumed to be a pure magnesium end member with no iron. Thus, its stability will be independent of oxygen fugacity.

The application of these diagrams to problems of ore genesis requires a carefully worked-out paragenesis to ensure that the minerals in a particular assemblage are cogenetic. By comparing the mineral assemblage in a uranium deposit, including ore, gangue and alteration minerals, with the stability relationships shown in these diagrams it is possible to determine the f_{O_2} and pH conditions of mineralization. This makes it possible to characterize the geochemical environment of deposition and thereby establish more reliable models for ore genesis.

Outlined in Fig. 13 are four possible areas of uranium mineralization based on the observed mineral assemblages. Area one would be a low f_{O_2}–low pH assemblage characterized by either alunite or kaolinite alteration accompanied by wallrock bleaching (removal of iron). At slightly lower f_{O_2} values, or higher dissolved iron concentrations, pyrite will be stable. Mineral assemblages in area two will be characterized by argillic alteration (kaolinite and/or montmorillonite) accompanied by hematite and/or iron carbonate. The size of the carbonate field will depend on P_{CO_2} and the activity of

iron. As P_{CO_2} increases, so does the size of the siderite field. The carbonate phase commonly associated with uranium mineralization is ankerite, where other cations substitute for iron. This would tend to decrease the size of the carbonate field.

Area three lies within the sericite and chlorite stability fields, so either one or both of these minerals will be associated with uranium oxide in deposits formed under these conditions of f_{O_2} and pH. The iron mineral associated with this assemblage would be hematite. Similarly, in area four adularia is the stable potassium silicate, so the assemblages associated with uranium in this area may be adularia–hematite or adularia–chlorite–hematite.

Natural chlorites may contain significant amounts of iron, and their stability will therefore depend on both pH and f_{O_2}. The lack of thermodynamic data on chlorites of variable composition prevents the calculation of a stability field for these minerals. Qualitative relationships suggest, however, that this field would superimpose over the siderite field and be slightly larger. This would further restrict the conditions of formation of deposits with iron-containing chlorite.

The slopes of the solubility contours in the neutral to slightly alkaline region of Fig. 13 suggest that changes in pH may be more important than reduction in the precipitation of uranium. Increase in pH may be produced by reactions between transporting solutions and carbonates or alkali silicates in the wallrocks, or by loss of acid volatile components during boiling. In this region uranium will be transported in the uranyl state, but the solid oxide will contain uranium in the U^{4+} state. Therefore, during this precipitation of uranium as a result of increased pH, uranium is being reduced. There must be a reservoir of available electrons to allow this reduction to occur. Sources of exchangeable electrons in natural systems may be ferrous iron or organic material in the wallrocks. This leads to the conclusion that ferric oxides associated with uranium mineralization may be a result of uranium deposition rather than the oxidation of ferrous iron being the cause of uranium precipitation.

The above results indicate that uranium can be transported as a variety of complexes, depending on the composition of the hydrothermal solutions. Deposition can occur as a result of increase in pH or reduction. These changes can occur as the solutions react with the wallrocks or as a result of boiling. The latter mechanism may be important in relatively shallow low-temperature open hydrothermal systems as the solutions percolate upward in an open fracture system. Reduction may be an important mechanism if the invaded rocks contain a suitable reductant such as sulphides or organic material.

A careful study of the paragenetic relationships between minerals and mineral assemblages can lead to valuable information on the environment of deposition and the mechanisms of uranium deposition. Of particular value are the alteration minerals as indicators of pH conditions and iron minerals as indicators of oxidation state of the mineralizing solutions. The results also indicate that no one set of physico-chemical conditions is unique to uranium deposition and that both uranium transport and deposition can occur over a wide range of pH and f_{O_2} conditions.

Geochemical behaviour of uranium in the supergene environment

Gaetano Dongarra
Istituto di Mineralogia, Petrografia e Geochimica, Palermo, Italy

Introduction

Chemical properties

Uranium (symbol U; atomic number 92) and 14 other elements (from actinium to lawrencium) form the actinide series. Uranium—from the Latin *Uranus*—was named in 1790 by Klaproth after Herschel had discovered the planet with the same name.

Although it was first recognized as an element in 1789 by Klaproth, uranium was chemically isolated as metallic uranium much later (1841) by thermal reduction of its anhydrous tetrachloride with potassium in a platinum crucible.

The electron configuration of the gaseous uranium atom is $5f^3 6d 7s^2$, and its atomic weight is 238.07. As might be expected, uranium shows valence states that range between 2+ and 6+. In minerals, however, only the valences 4+, 5+ and 6+ occur. Oxidation–reduction potential data for uranium are summarized in Table 1. Oxidation states 4+ and 6+ are the most important from a geochemical point of view.

Table 1 Oxidation potentials: $E°$ values computed from Gibbs free energy of reaction, ΔG_r°, which is related to voltage via relation $\Delta G_r^\circ = nFE°$; ΔG_r° computed from thermochemical data[10]

Reaction	$E°$, V
$U° = U^{3+} + 3e^-$	−1.661
$U° = U^{4+} + 4e^-$	−1.376
$U^{3+} = U^{4+} + e^-$	−0.520
$U^{4+} + 2H_2O = UO_2^+ + 4H^+ + e^-$	0.380
$U^{4+} + 2H_2O = UO_2^{2+} + 4H^+ + 2e^-$	0.273
$UO_2^+ = UO_2^{2+} + e^-$	0.165

The ionic radius of U^{4+} is very similar to that of tetravalent Th, and to those of many rare-earth ions (Table 2). This fact determines the occurrence of both Th and U in many rare earth bearing minerals. In the surficial environment, however, U^{4+} is readily oxidized to U^{6+}, which forms UO_2^{2+}, uranyl ion.

The chemical properties of uranyl significantly differ from those of thorium and rare-earth ions: this is significant geochemically as it accounts for the observed variability of Th/U ratios in surficial material, as well as for the lack of thorium and rare earths in secondary uranium minerals.

Table 2 Ionic radii for some elements. From Krauskopf[9]

Element	Oxidation state	Ionic radius, Å (sixfold coordination)
U	+4	0.97
U	+6	0.80
Ca	+2	0.99
Th	+4	1.02
La	+3	1.14
Ce	+3	1.07
Ce	+4	0.91
Ho	+3	0.91
Er	+3	0.89
Lu	+3	0.85
Hf	+4	0.78
Y	+3	0.92
Zr	+4	0.74

Natural isotopes

Uranium has three naturally occurring radioactive isotopes—^{238}U, ^{235}U and ^{234}U. Their relative abundances are 99.2739 ± 0.0007, 0.7204 ± 0.0007 and 0.0057 ± 0.0007%, respectively. ^{234}U is, in fact, a decay product of ^{238}U, so its natural abundance is a reflection of radioactive equilibrium with ^{238}U.

^{238}U and ^{235}U are parent isotopes for two separate decay series, which ultimately yield ^{206}Pb and ^{207}Pb, respectively.

In addition to the naturally occurring isotopes, several artificial short-lived uranium isotopes have been prepared, with mass numbers ranging from 227 to 240, but their short life precludes any natural occurrence.

Geochemical properties

The earth's surface, broadly speaking, includes atmosphere, hydrosphere and the upper section of its solid crust. It appears, then, to be the seat of physical flows, some visible and some subtle.

The flow of matter from continents to oceans and to the ocean floor is obviously visible: it is frequently termed 'exogenous' or 'minor cycle'. It describes the transfer of matter from the lithosphere to the hydrosphere and then back to the lithosphere. It is questionable whether a fragment of weathered rock, either crystalline or sedimentary in origin, moving in streams is part of the lithosphere.

In dealing with chemical processes, such as the transfer of matter from one molecular state to another and/or with separation of different substances from one another, the above description of the weathering process is, in general, inadequate.

Chemically, the molecular state of matter in sediments differs from that in crystalline rocks. Matter does not revert to its initial conditions by sedimentation. The geochemical cycle is not closed in the exogenous process: metamorphism, migmatization and anatexis must take place to bring matter back to its initial state. This forms the major, or endogenous, geologic cycle. Thus, one could say that the minor geologic cycle is not, in fact, a geochemical cycle, and that the union of the minor and the major geologic cycles corresponds with (we deliberately do not say *is*) the geochemical cycle.

Matter changes from one state (mineral lattice in crystalline rocks) to another (ions and molecules dissolved in liquid water) passing from lithosphere to hydrosphere: this process is termed alteration. By means of another process (that is, chemical sedimentation) some substances pass from the hydrosphere to yet another state in the lithosphere. In addition, some other substances build up in the hydrosphere.

The exogenous cycle of uranium is shown in Fig. 1. Igneous or, more generally, crystalline rocks are assumed to be the initial state of matter—the starting point of the exogenous cycle. The upper arrow, connecting the igneous rocks box with the sedimentary rocks box, represents flow of unaltered solids. Its starting point on the left corresponds with erosion; its termination on the right corresponds with mechanical sedimentation. Wherever this process is prevalent, i.e. sediments

are formed by sheer mechanical transport and sedimentation of nearly unaltered minerals, the final product is a *resistate* sediment. The lower arrow depicts chemical alteration—that is, the change of matter in igneous mineral lattices to the dissolved species in water. Transport across phase boundaries requires molecular diffusion. Diffusion, however, is not effective for regional scale transport in comparatively short geological times—for example, thousands or hundreds of kilometres in less than a million-year time span.

The surface waters box is a sub-field of the hydrosphere. Surface water flow to the oceans provides large-scale transport on the continental scale—say, 1000 km. No great change of state of matter is involved: it is just physical flow, similar to the movement of unaltered solid rock particles.

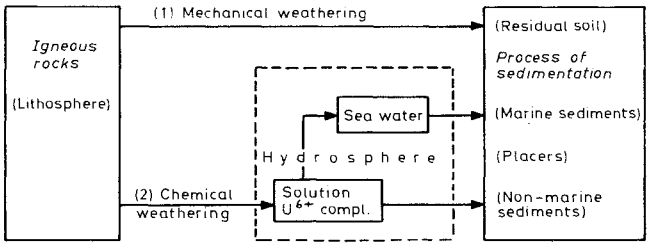

Fig. 1 Exogenous cycle of uranium (arrows depict flows, boxes reservoirs)

In Fig. 1 drainage and subsurface water flow is depicted by an arrow that connects the surface water box with the ocean water box. Subtle flow of dissolved substances takes place along with visible liquid water flow.

Chemical precipitation involves diffusion across phase boundaries, this time from liquid water to crystal lattice or from liquid water to adsorbing surfaces such as large molecules in colloidal systems. Biological systems are not explicitly depicted in Fig. 1 as they represent merely another form of the non-hydrosphere phase. They form bodies that may migrate into sediments.

Oceanic circulation forms a worldwide transportation system that makes substances available over the earth's surface within a geologically short time. Chemical precipitation is depicted by the arrow from the hydrosphere sea-water sub-box to marine sediments. The physical migration of suspended solids to sediments and to sedimentary rocks is left implicit.

One arrow is drawn to connect the surface water to the solid phase box: it represents chemical deposition, which also involves diffusion across phase boundaries. From the viewpoint of physical transport, however, it may correspond with either uranium going back to stream sediments or uranium remaining trapped in aquifer rocks.

This last step is significant with regard to the formation of supergene uranium ore deposits. The host rock can be whatever aquifer the uranium-carrying water is passing through. The meaning of this step with regard to physical transport remains to be determined. Uranium may well diffuse chemically into pore water of weathering granite only to precipitate along fissures in the same granite. This means that uranium may pass from the lithosphere into the hydrosphere and back into the lithosphere over a few hundred metres. Apart from its practical significance for uranium deposits, this example is useful in illustrating the distinctive chemical and physical transport processes.

Geochemical mobility

Let us assume the ratio of concentration of matter in ocean water, m, to concentration in sediments, y, to be m/y. The ratio m/y can be viewed approximately to correspond to solubility. It is only approximate since sediments are not just one solid phase. In reality molecules are bound in different solid phases in a sufficiently similar way that m/y approaches some sort of solubility, aptly referred to a defined class of solid. To avoid confusion the expression 'geochemical mobility' has been used with reference to the distribution between solid or immobile and liquid or mobile phases.

With reference to the marine environment let us also consider mM as the total amount of dissolved substance in the oceans, where M is the total mass of ocean water—the amount of each substance actually available for distribution over the earth. If Y is the total mass of sedimentary rocks, yY similarly represents the amount of the same substance stored in sedimentary formations.

The ratio mM/yY can also be termed 'geochemical mobility'. Inasmuch as M and Y are constant for all substances there is neither inconsistency nor ambiguity in the use of either definition.

By analogy, mobility in the surface drainage environment can also be defined as wW/xX or w/x, where x, X refer to altering igneous rocks, w and W to surface water. If W equals the *flow* of water through the drainage network for the hydrological cycle of water, xX/wW and yY/wW are equal to time spans. They represent, respectively, the time needed to remove the amount xX from the crystalline lithosphere and to introduce the amount yY into the sedimentary lithosphere. Inasmuch as xX and yY are close to each other, e.g. for insoluble or immobile substances, the time-span values are the same. The shorter the time, the greater is the mobility.

With x, y in the range of a few ppm U and X and Y some 150 kg/cm^2, $m = 0.001$ mg/kg, $M = 280$ kg/cm^2 and, in terms of flow, $W = 0.02$ kg/year cm^2 with $w = 0.0005$ mg/kg. The geochemical mobility of uranium can be expressed by assuming that about one-thousandth of its total mass in sediments, or of its total removed mass from crystalline lithosphere, is dissolved in ocean water and, hence, is available for transport and precipitation anywhere on earth.

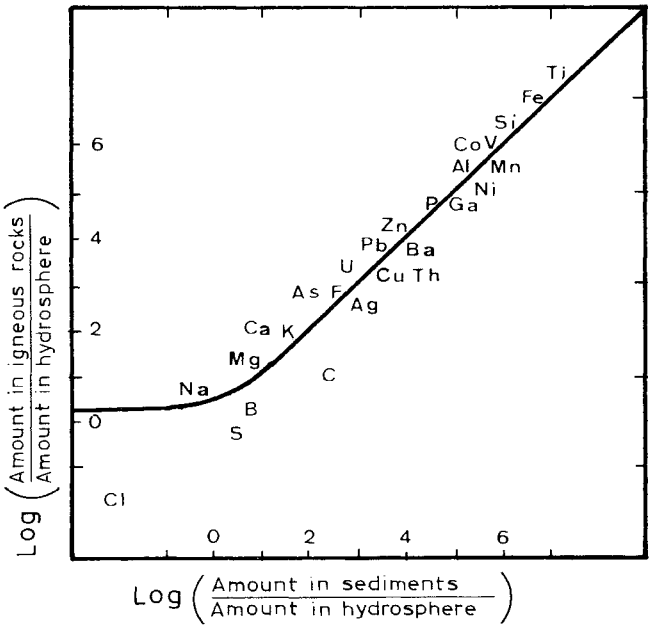

Fig. 2 Geochemical mobility of elements. From Dall'Aglio[8]

Comparison with other elements makes this assumption clear. The fraction of uranium removed from the crystalline lithosphere that is available for rapid redistribution over the ocean floor is hardly one order of magnitude greater than that

of zinc, two to four orders of magnitude in excess of that for such immobile elements as aluminium, manganese, iron and titanium and more than one order of magnitude less than that of calcium and potassium (Fig. 2).

The worldwide flow of uranium in the drainage network is $5 \times 10^{-4} \times 0.02$ mg/year cm^2, or 10^{-5} mg/year cm^2. If the amount of uranium in sediments or in the crystalline source rocks (150 kg/cm^2 × 2 mg/kg, i.e. 300 mg/cm^2) is divided by the value of the flow of uranium in the drainage network, the time obtained is 30 m.y. for the surface drainage system to transport it to the sedimentary environment or, put another way, to remove it from the crystalline lithosphere. On the other hand, the entire uranium in the oceans is replaced in only $0.3/10^{-5}$ or 30000 years, which compares with the turnover time of water itself, i.e. about 15000 years.

From the viewpoint of this study with regard to the behaviour of elements such as uranium, which form an extremely minute fraction of the bulk rock, the X and Y values of the total amount of sedimentary and crystalline rocks are externally fixed quantities.

Exogenous cycle of uranium

Source rock materials

Uranium geochemistry in the surface environment is closely related to its mode of occurrence in various igneous rock types. Table 3 shows the range of uranium content for different igneous rocks. The close relationship between uranium content and silicic rocks is immediately apparent. Such a relationship may be accepted as a valid generalization. Significant deviations from this relationship indicate that many factors affect uranium distribution in different igneous rocks. Alkaline rocks form the most striking exception as their uranium content is generally high, whereas their silica content is low.[5, 6, 14]

Table 3 Uranium in igneous rocks. From Adams and co-workers[2]

Rock	Uranium, ppm
Silicic intrusive	1–6
Silicic extrusive	2–7
Basic intrusive	0.3–2
Basic extrusive	0.2–4
Ultrabasic	0.001–0.03
Alkaline	0.1–30
Silicic pegmatite	1–4

Uranium occurs in igneous rocks—partly in the mineral lattices, where it substitutes for such elements as calcium or the rare earths, and partly as uranium minerals.

Accessory minerals are the major carriers of uranium in silicic intrusive rocks. Allanite, monazite and xenotime, for example, contain more uranium than zircon, apatite and sphene.

Uraninite, the most abundant uranium mineral, also occurs in rocks. Major constituents, such as quartz, feldspar, biotite, hornblende, pyroxene, all contain only a small fraction of total uranium at extremely low concentrations. In fact, uranium in major rock-forming minerals is generally in the ppb range. Rogers and Adams[13] ascribed its occurrence in major constituents to one or more of the following possible factors: (1) isomorphous substitution in the lattice; (2) concentration in lattice defects; (3) adsorption along crystal imperfections and grain borders; and/or (4) inclusion as microcrystals of uranium minerals. Agreement on the distribution of uranium in such different forms of occurrence has still to be established.

In basic intrusive rocks the most important uranium carrier is apatite, which may incorporate small quantities of uranium by isomorphic substitution of U^{4+} for Ca^{2+} ions. On the other hand, in extrusive rocks, whether acid or basic, rapid cooling of magma leaves a large part of the uranium scattered through the non- or cryptocrystalline matrix.

Chemical or mechanical weathering

The relative ratio between flows in processes 1 and 2 (Fig. 1) varies according to the distribution of uranium atoms in the different molecular sites in the source rock—indeed, such distribution determines the way in which uranium mobilization occurs. Uranium contained in insoluble accessories is leached to a very limited extent, so it is presumed to be transported to and concentrated in resistate sediments as clastic material. Adams and co-workers[2] estimated that 60–85% of the uranium in igneous rocks is present in mineral phases that are resistant to chemical alteration; approximately 15–40% is transported in the dissolved form by liquid water. The above fraction of uranium takes part in the processes of erosion and sedimentation (represented by the arrow in the upper part of Fig. 1 that connects the source rock box directly with the sediment box).

A large part of the uranium in igneous rocks is contained in heavy chemically resistant minerals the weathering of which is mainly mechanical. Thus, uranium in such form is transported by rivers and streams as clastic particles that are ultimately found in residual soils, in stream sediments and in common sedimentary rocks, either continental or marine. From the viewpoint of ore deposits the previously mentioned particles may accumulate in placer deposits.

U^{4+} oxide minerals are not common constituents of modern placers. Uranium undergoes oxidation to U^{6+} in an environment with abundant free oxygen and U-bearing placers have been considered to be very ancient (> 2400 m.y.) and they may have formed under low oxygen pressure in the earth's atmosphere.

Uranium in natural waters

A comprehensive review of uranium determinations in sea water was given by Rogers and Adams.[13] Ocean water contains uranium at a broadly uniform concentration (0.001–0.004 ppm). The average uranium concentration in stream water is less than 1 ppb U. Groundwater shows remarkable variability of concentration as a result of, for example, the presence of enriched mineralization, the time of contact of the water with the source rocks and the concentration of ligands that either form soluble uranium complexes or insoluble uranium compounds.

High concentrations of uranium may also occur in inland waters where evaporative processes prevail: a study of the uranium content in brines during solar salt production has shown that the evaporating water body becomes enriched in uranium while $CaSO_4$ and NaCl precipitate.[7]

A particular case of uranium enrichment is shown by $NaHCO_3$ waters: their high content of carbonate ions may be responsible for very effective leaching of uranium from weathering country rocks as a result of the formation of carbonate complexes.

Uranium speciation in natural waters

Uranium occurs in natural waters as U^{4+}, U^{5+} and U^{6+}. Species relationships in aqueous equilibria of the U–O_2–H_2O–CO_2 sub-system, as a function of Eh and pH, are shown in Fig. 3 for a temperature of 25°C and 1 atm pressure (the shaded area shows the stability field of uraninite (UO_2)). Dissolved uranium in water is mainly in the form of stable uranyl dicarbonate and tricarbonate complexes. Fig. 3 shows that the field of existence of soluble uranium complexes becomes wider as pH increases,

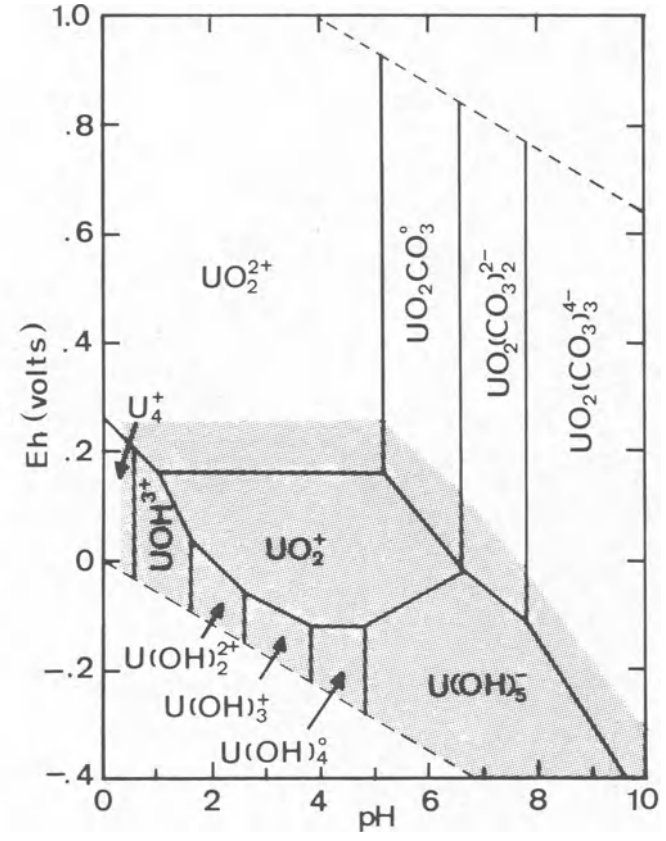

Fig 3 Eh–pH diagram of $U–O_2–H_2O–CO_2$ system at 25°C and 1 atm for $U = 10^{-6}$ M and $P_{CO_2} = 10^{-2}$ atm. Modified from Langmuir.[10] Upper and lower boundaries within diagram (dotted lines) are limits within which water itself is chemically stable. Above upper limit water is oxidized to give oxygen and below lower limit reduced to yield hydrogen. Stability field for crystalline uraninite shaded; predominant U species in solution indicated in various unshaded areas; unbroken lines represent equilibrium conditions

owing to the formation of uranyl carbonate complexes. This means that carbonate ions control uranium circulation. One should remember that dissolved CO_2 is always present one way or another in natural waters—even in rain water, where its partial pressure is $\geqslant 10^{-3.5}$ atm. CO_3^{2-} concentration is then dependent on the pH of the solution. Thus, taking account of the largest pH range that occurs in natural waters, many other ligands may bind uranium into complexes and so increase its solubility.

Langmuir[10] showed that, beside carbonate, uranyl complexes with hydroxyl, fluoride, sulphate or phosphate may predominate in oxidized surface and ground waters. More specifically, phosphate complexes are expected to predominate over other inorganic complexes of uranyl in waters in the pH range from 4 to 7.5 with $P_{CO_2} = 10^{-2.5}$ atm, $\Sigma m U^{6+} = 10^{-8}$ and $\Sigma m PO_4 = 10^{-6}$. These figures are consistent with dissolved components in typical natural waters.

Fig. 3 shows the stability field of U^{4+} species. Such U^{4+} compounds as UO_2 and $U(OH)_4$ are very insoluble, so the concentration of U^{4+} in water is extremely small. The field of stability of uraninite corresponds broadly with the fields in the Eh–pH graph where U^{4+} species are dominant. In Eh–pH fields where U^{6+} is greater the total amount of dissolved uranium can be much larger.

Chemical sedimentation of uranium

Marine sediments

In the supergene cycle uranium is removed from sea water by several processes, in which the ability of uranium to form stable complexes with various species may play an important role.

Marine limestones generally contain about 2 ppm of uranium. So far discussion of uranium behaviour in aqueous solution has stated that uranium stays in solution if carbonate ions are present.

According to Naumov and Mitronova,[12] the decomposition of uranyl carbonate complexes and the simultaneous reduction of uranium proceed the more readily with decreasing carbonate ion concentration. In fact, the potential of the $U^{6+}–U^{4+}$ couple in the presence of CO_3^{2-} ions is lower than that in carbonate-free waters—that is, more reducing conditions are required to remove uranium from carbonate-rich water in comparison with waters low in carbonate.

The uranium content in carbonate sediments is expected to be controlled more by biological factors than by pure chemical precipitation. Uranium may occur in the heavy mineral fraction of the carbonate sediments. Adams and Weaver[1] reported that only 20% of uranium in carbonate rocks is contained in the detrital, essentially shale, residue.

Uranium also accumulates in phosphatic sediments deposited from a marine environment. In this case uranium is believed either to be incorporated into the carbonate–fluorapatite lattice, where it substitutes for calcium,[4] or to be adsorbed on the surface of apatite crystals. Laboratory studies[11] have shown that phosphate rocks are among the most effective agents in the extraction of uranium from sea water. In this connexion marine black shales are especially significant because they contain comparatively high amounts of uranium. Marine black shales, the predominant clay mineral of which is illite, are believed to be deposited slowly under stagnant conditions and in the presence of abundant organic matter. In these conditions, with a very limited clastic contribution, deep-seated waters are readily depleted in oxygen and enriched in hydrogen sulphide, which is produced by the reduction of sulphate.

Generally speaking, a direct relationship between uranium concentration and increasing organic carbon content exists in marine black shales. Uranium content is also directly related to the colloidal size ranges of such sediments.

Many therefore believe that the enrichment of uranium in marine black shales is strictly related to the presence of organic matter in the sediments. This last, along with the H_2S, is deemed to be ultimately responsible for the reduction of uranyl ion to the insoluble form, uraninite. The Chattanooga Shale (U.S.A.) and the Alum Shale (Sweden), are the two best-known examples of uraniferous black shales.

Non-marine sediments

Minerogenetic studies and thermodynamic data suggest that uranium can be removed from weathering solutions by many processes, one of which is reduction—notably by organic matter among a number of reducing agents. Reduction commonly results in the formation of UO_2 or one of its hydrates.

Uranium may also undergo precipitation directly in its hexavalent state by a variety of anions—mainly phosphate and vanadate.

Among the geochemical factors possibly responsible for the reduction and precipitation of uranium from groundwater, Eh is most effective. Fe^{2+} and sulphides, in addition to organic matter, deserve mention. Insoluble uraninite may be precipitated according to the redox reaction

$$4UO_2^{2+} + HS^- + 4H_2O = 4UO_2 + SO_4^{2-} + 9H^+$$

or

$$4UO_2(CO_3)_3^{4-} + HS^- + 15H^+ = 4UO_2 + SO_4^{2-} + 12CO_2 + 8H_2O$$

or

$$4UO_2^{2+} + CH_4 + 2H_2O = 4UO_2 + CO_2 + 8H^+$$

In the last reaction CH_4 symbolizes organic matter in general.

Anaerobic bacteria prevalent in reducing environment are believed to play a significant role.

Humic constituents of alluvia and soils are very effective trapping material and remove uranium from natural waters. Their structure is only broadly known. They are insoluble at acid pH and soluble in alkaline medium. Their molecule consist of a polyaromatic skeleton that carries phenolic hydroxyl and carboxyl groups. Acidic hydrogen of the carboxyl group is exchanged with the uranyl ion: this process is so effective that very high enrichment factors may be obtained.

Many other natural materials, including several metal hydroxides (Fe, Al, Mn) as well as clays, are capable of adsorbing uranium. Sorption proceeds to a variable extent. It usually depends on the pH of the solution and the pH range for the greatest sorption of uranyl overlaps the pH range of minimal solubility of uranyl minerals.

With regard to mineral formation, removal is effective when adsorption is followed by reduction of U^{6+} to U^{4+}. If reduction does not take place, uranium is remobilized following changes of alkalinity and/or solution Eh.

Roll-type deposits

Some uranium deposits, formed in permeable sandstone units interbedded with less permeable strata, have a characteristic shape from which the name 'roll-type uranium deposits' arises.

The reducing capacity of the aquifer plays a key role in the formation of such deposits. Oxygenated waters that carry U^{6+}, as UO_2^{2+} and/or its carbonate complexes, attain reducing conditions during their downward migration. Uranium is then reduced to its tetravalent state, which entails its precipitation as uraninite or pitchblende. Reduction of U^{6+} is ascribed to the presence of organic material, pyrite, marcasite or H_2S. This last substance, for example, is produced from sulphate by sulphate-reducing bacteria in the presence of reducing matter. Hydrogen sulphide migrates easily and can be made available to groundwater. That seems to be the case for roll-type deposits in the Gulf Coast of Texas, where H_2S may come from underlying gas and oil deposits.[3]

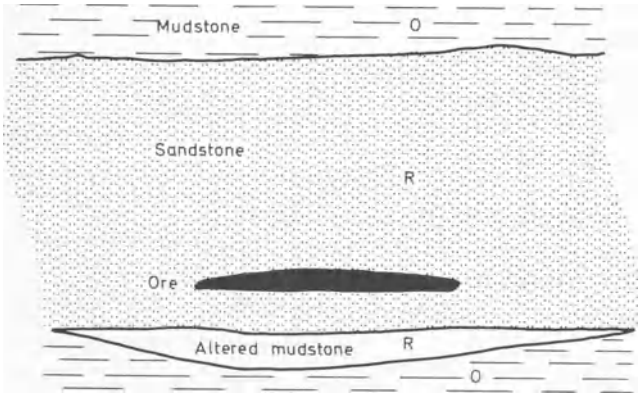

Fig. 4 Schematic diagram of 'roll-type' uranium deposit

Whether the reducing agents are indigenous to the sandstone (Wyoming) or rise along faults (Texas) is immaterial to the present discussion. It is noteworthy that deposition of large-size orebodies results from multiple cycles of reduction–oxidation, i.e. precipitation–dissolution, owing to inflows of oxygen-rich waters. Repeated mobilization–precipitation leads to uranium accumulation and, ultimately, the formation of roll-shaped deposits of uranium ore. The flow of mineralizing water is fairly similar in its effect to the movement of water in a chromatographic column.

Deposits of uranium ore that originate by the process described above take the shape shown in Fig. 4.

Carnotite and autunite ore deposits

The vanadate ion is a very effective precipitant for uranyl ions—as insoluble uranyl vanadate (carnotite, $K_2(UO_2)_2(VO_4)_2$ and tyuyamunite, $Ca(UO_2)_2(VO_4)_2$). Precipitation of carnotite, according to

$$2K^+ + 2UO_2^{2+} + 2H_2VO_4^- = K_2(UO_2)_2(VO_4)_2 + 4H^+$$

may take place under such favourable conditions as (*a*) solution pH in the range 4–8, (*b*) existence of an oxidizing environment, (*c*) UO_2^{2+} and $H_2VO_4^-$ ionic concentrations are sufficiently high to reach the solubility product of carnotite and (*d*) low content of carbonate ions.

Waters scarce in vanadium, but enriched in phosphate ions, may precipitate minerals of the autunite series in essentially the same conditions as those outlined above. In fact, autunite can precipitate instead of carnotite if ΣPO_4 exceeds ΣVO_4 by roughly a factor of 500.[10]

References

1. Adams J. A. S. and Weaver C. E. Thorium-to-uranium ratios as indicators of sedimentary processes—an example of concept of geochemical facies. *Bull. Am. Ass. Petr. Geol.*, **42**, 1958, 387–430.
2. Adams J. A. S. Osmond J. K. and Rogers J. J. W. The geochemistry of thorium and uranium. In *Phys. Chem. Earth*, **3**, 1959, 298–348.
3. Adler H. H. Concepts of uranium-ore formation in reducing environments in sandstones and other sediments. In *Formation of uranium ore deposits* (Vienna: I.A.E.A., 1974), 141–68.
4. Altschuler Z. S. Clarke R. S. Jr and Young E. S. Geochemistry of uranium in apatite and phosphorite. *Prof. Pap. U.S. geol. Surv.* 314-D, 1958, 90 p.
5. Bohse H. *et al.* On the behaviour of uranium during crystallization of magmas—with special emphasis on alkaline magmas. In *Formation of uranium ore deposits* (Vienna: I.A.E.A., 1974), 49–60.
6. Civetta L. and Gasparini P. A review of U and Th distributions in recent volcanics from southern Italy: magmatological and geophysical implications. In *The natural radiation environment II* Adams J. A. S. Lowder W. M. and Gesell T. S. eds (Houston, Texas: Rice University, Department of Geology, 1972), 483–516.
7. Dall'Aglio M. and Casentini E. The distribution of uranium between precipitates and brines in the solar salt plant of Margherita di Savoia. *Boll. Soc. geol. ital.*, **89**, 1970, 475–84.
8. Dall'Aglio M. Planning and interpretation criteria in hydrogeochemical prospecting for uranium. In *Uranium prospecting handbook* Bowie S. H. U. Davis M. and Ostle D. eds (London: IMM, 1972), 121–34.
9. Krauskopf K.B. *Introduction to geochemistry* (New York: McGraw Hill, 1967), 721 p.
10. Langmuir D. Uranium solution–mineral equilibria at low temperatures with applications to sedimentary ore deposits. *Geochim. cosmochim. Acta*, **42**, 1978, 547–69.
11. Moore G. W. Extraction of uranium from aqueous solution by coal and some other materials. *Econ. Geol.*, **49**, 1954, 652–8.
12. Naumov G. B. and Mitronova O. F. Migration of uranium in hydrothermal carbonate solutions (according to physicochemical data). In *Problems of geochemistry* Khitarov N. I. ed. (Jerusalem: Israel Program for Scientific Translations, 1969), 166–75.
13. Rogers J. J. W. and Adams J. A. S. Thorium and uranium. In *Handbook of geochemistry* Wedepohl K. E. ed. (Berlin, etc.: Springer, 1978), **II–V**, pt 90, 39 p. and pt 92, 50 p.
14. Saprykina T. V. Uranium. In *The geochemistry of the Lovozero alkaline massif, volume 2* (Canberra: Australian National University Press, 1968).

Uranium exploration techniques*

Chester E. Nichols
Nichols Associates, Reno, Nevada, U.S.A.

As would be expected from the scope and number of pages assigned to this paper, it is of necessity rather basic in nature. The main purpose is to present an introduction to how uranium is found, with the hope that an explorationist will find concepts that stimulate his thought.

Owing to its geochemical mobility (overall solubility), trace amounts of uranium occur in almost everything, living or otherwise. It occurs in most rock types, natural water, stream sediments, soils and plants (Table 1). It may be concentrated to tens or hundreds of times the geochemical average in the crust of the earth in a wide variety of rock types (Table 2). Orebodies generally consist of grades greater than 0.1% U_3O_8, and grades greater than 0.2% may be considered high, depending on the circumstances.

Genetic description of some uranium deposits

A good classification of the important Canadian uranium deposits was given by McMillan.[6] A much more complete classification was offered by Mickle.[7] Following this scheme, Mickle and Mathews edited a monograph[8] that described the recognition criteria of each category in some detail. The third paper in this series is a field guide,[9] but is also most useful as a lucid index to the monograph because of its abbreviated format, keyword index and cross-referenced pages.

One natural way to classify uranium deposits begins by categorizing the host rocks. The following is a brief description with genetic implications of a few interesting types of uranium mineralization.

Table 1 Typical concentrations of uranium in the natural environment

	U concentration	Remarks	Reference
Rocks	0.1–1.0 ppm	Basalts, tholeiitic and plateau, andesitic and alkali	1
	2 ppm	Av. in carbonate rocks of North America and Russian Platform	1
	2–4 ppm	Av. in Texas Gulf Coast (Tertiary) at the surface	2
	3.7 ppm	Av. for North America and Russian Platform	1
	2–15 ppm	Granites of U.S.A., U.S.S.R. and France	1
	3–20 ppm	Alkaline intrusives of U.S.S.R.	1
Waters	1–4 ppb	Sea water, worldwide	1
	0.5 ppb	Median of 155 stream water samples from Texas Gulf Coast*	2
	5.2 ppb	Median of 103 stream water samples from northwest Texas†	3
	0.7 ppb	Median of 75 stream water samples from Llano area, central Texas‡	4
	0.8 ppb	Median of 323 wells from Texas Gulf Coast*	2
	8.6 ppb	Median of 249 ground water samples from northwest Texas†	5
	0.6 ppb	Median of 49 wells from Llano area in central Texas‡	4
Stream sediments	1.1 ppm	Median of 463 samples from Texas Gulf Coast*	2
	1.7 ppm	Median of 161 samples from northwest Texas†	3
	1.2 ppm	Median of 95 samples in Llano uplift, central Texas‡	4
Plants	0.2–0.5 ppm	Median in ash of branches from 9 types of tree, Precambrian through Tertiary of Texas	(Table 4 of this paper)

* Pleistocene through Eocene.
† Tertiary, Permian, Triassic and Cretaceous.
‡ Cretaceous, Permian, Devonian, Mississippian, Cambrian and Precambrian.

Igneous rocks that concentrate uranium with other lithophile elements that form the earth's crust constitute the original source of uranium. Uranium is quite mobile in the presence of oxygen. Once in solution in surface water, it tends to continue downstream until an ocean is reached. Similarly, the oxygen in near-surface groundwater provides the environment for the leaching and transport of uranium down a hydrologic gradient in the subsurface. This uranium may be very efficiently precipitated when oxygen is lost, as by biologic demand. Most important types of uranium deposits form by some precipitating process that involves the reduction of uranium from an oxidized state, whether the host rock is sedimentary, metamorphic or igneous. Quartz-pebble conglomerate deposits are a major exception.

Sedimentary host rocks

Sandstones

In contrast to most of the rest of the world, the United States owes most of its reserves and production to deposits in sandstones. These rocks acted as conduits for uranium-bearing groundwater that passed through a redox change from oxidizing to reducing, resulting in the precipitation of uranium.

A key link to the understanding of sandstone districts is that they commonly form in rocks of deltaic origin. This environment is important in several respects. It provides permeable rocks encased in those which are less permeable to act as aquifers for uranium-bearing groundwater. The deltaic environment also implies a progressive reduction in the permeability of the channels basinward. This yields a district-wide trapping mechanism as opposed to a flushing through of groundwater.

Table 2 Principal rock types in which uranium mineralization occurs

Sedimentary	Metamorphic
Sandstone	Graphitic and pyritic schists
Calcrete	Quartz–chlorite schist
Lignite	Chlorite–sericite schist
Carbonate	Conglomerate
Phosphorite	Arkose
Black shale	Gneiss
Tuff	Psammite
Asphaltite	Carbonate
	Skarn
Igneous	Tuff
Granite	
Migmatite	
Pegmatite	

The sandstones of deltas are also typically oxidized in the upper reaches and reduced where they are deposited in standing water. Moreover, the reduced facies are frequently buffered with organic material and/or iron sulphides. A source of uranium may be found in fresh sediments deposited in the oxidizing environment. For example, volcanic glass in the form of ash is readily leached of several components, including uranium.

Uranium may also be derived from the upper reaches of a river basin, where any of the rock types listed in Table 2 may yield uranium by weathering. Groundwater that bears the dissolved components eventually enters the master stream, which transports its load to the deltaic environment. Part of the river water may flow through the deltaic sediments themselves before passing into the sea. In the upper portion of the delta this water can pass through a larger volume of oxidized sediments before being reduced. Farther downstream the river water that enters the sediments may be reduced in the first few centimetres of the river bed.

The distance that water travels in the ground before it enters a reducing environment relates in a general way to the shape of the orebody that is produced. Just as a lateral change in facies may be the same as a vertical or time change, so the implication that mineralization may occur while the sandstone is being deposited, or at some time thereafter, relates to the subdivision of orebodies into tabular and roll-front types.

Tabular deposits The Uravan district of southwestern Colorado is the most typical occurrence of tabular deposits, sometimes referred to as Colorado Plateau deposits. In general, the orebodies tend to lie in the lower portion of a reduced channel sandstone. They are roughly concordant to bedding, with horizontal dimensions much greater than the vertical. Except for the near-surface yellow ore found early in the history of the district, most of the ore is dark grey or black and lies within larger haloes of reduced rock. Indeed, the environment within the vicinity of the orebodies was so reducing that red siltstones adjacent to the channel sandstone were reduced to a distinctive medium green colour (Fig. 1).

The main mineralization in the Uravan district occurs in an arcuate belt that crosses the distributing channels of a delta (Fig. 2). Farther to the east the channels become finer-grained and,

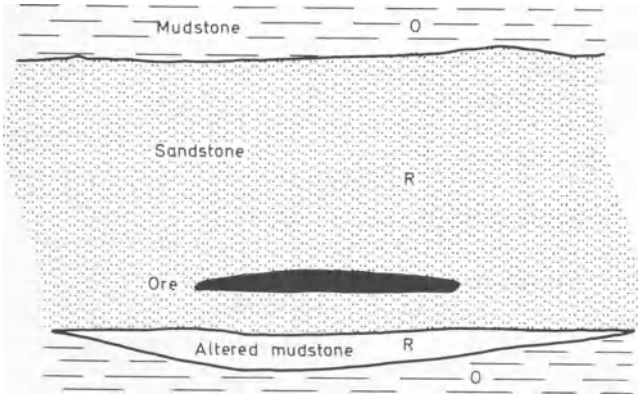

Fig. 1 Typical deposit, Uravan district

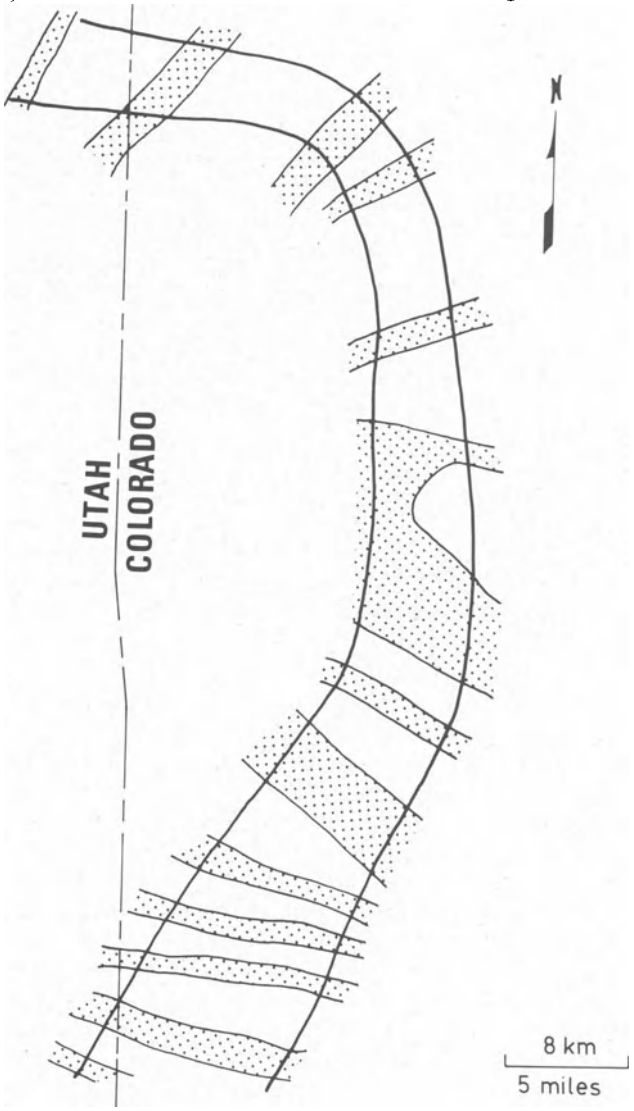

Fig. 2 Channel sandstones in Uravan mineral belt

with increased percentage of reduced ground, lose the redox boundaries that are found in the mineralized belt. The sandstone channel deposits that bear the orebodies are of the order of 1 km wide and 5–20 m thick. They crop out on canyon walls, but their actual lenticular cross-section is subtle owing to their superimposition and restricted length of exposure visible at any one place in the tortuous canyons.

The area is often thought of as a uranium district, but it actually produces several times as much vanadium by weight. Historically, the value of the vanadium that has been produced is approximately equivalent to that of uranium. Both metals are deposited by the same process. Probably the best theory for the origin of vanadium is that it was transported by a master river flowing from the west where the vanadiferous black Carlin shale was being eroded during the Jurassic time of deposition for the Morrison delta.

In core drilling three favourable features stand out as guides to ore: perhaps the most obvious is the percentage of carbon. In the ore carbon from leaf and wood fragments commonly exceeds 10% of the volume of the rock. The second feature is alteration in sandstone and adjacent siltstones. The thickness of alteration in the underlying or overlying siltstone, generally whichever is closer, is a contourable feature larger than the orebody. The siltstone reduction is often as thick as 1 or 2 m. Sandstone alteration is described in more detail in the section *Geologic techniques*. The third favourable feature is primary structure, such as cross bedding, which breaks the massive appearance of the sandstone.

Roll-front deposits The most typical roll-front deposits occur in Texas and Wyoming. In the Texas Gulf Coast province deposits occur in sandstone formations and group into districts by deltaic centres of deposition—called 'depocentres'.

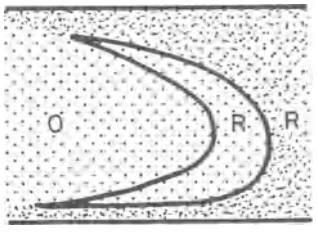

Fig. 3 *C* roll

In cross-section the orebodies of any particular sandstone tend to assume a characteristic *C* shape (Fig. 3). Groundwater moves faster near the centre of the aquifer, where it makes the orebody thicker and convex down the hydrologic gradient. The upper and lower limbs, or tails, of the orebody lag behind the nose of the roll.

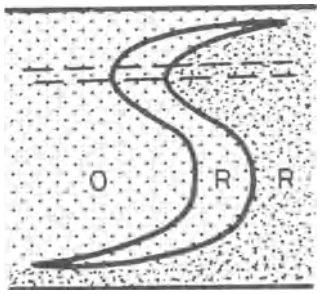

Fig. 4 *S* roll

Another configuration is the *S* roll, which is formed by reversing the bend of one side of a *C* roll around a permeability barrier (Fig. 4). In this case a mudstone split in the aquifer may interrupt the normal shape. The direction to another orebody may be indicated by the reversed tail of the *S*, which points downdip and toward the centre of the aquifer.

In plan view the nose of a roll will progress farthest downdip, where the best permeability lies. Thus, the axis of a front may be quite sinuous and many kilometres long. Where several sandstones are present the rolls may be stacked one above another, the roll in the uppermost (youngest) bed being generally the most offset in the direction of dip.

The serpentine nature of a roll front in plan view indicates that the groundwater that influences its movement does not have to cross the front at right angles. It only has to have some component of its movement crossing the front from the oxidized to the reduced side. In the case of a cylindrical host, which may be approximated by a channel sandstone deposit, the roll front may be tongue-shaped, mineralization being concentrated at the tip of the tongue. In cross-section, behind the end of the tongue where oxidized rock is surrounded by the tails of the orebody, the roll-front deposit may take the form of a mirror *C* (Fig. 5). Underground one might be tempted to believe that the ore is moving both left and right rather than perpendicular to the plane of the section. In this case the groundwater moved almost parallel to this part of the roll, and the best ore is likely to lie down the hydrologic gradient where the two *C* rolls meet. The most typical area for this shape of deposit is the Tertiary basins of Wyoming.

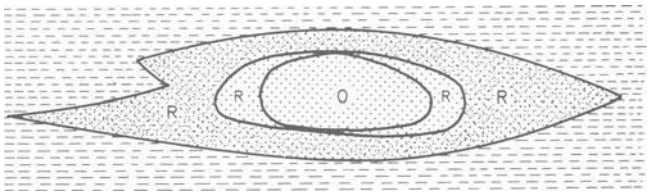

Fig. 5 Mirror roll

With time the redox front at the updip edge of the ore may move thousands of metres downdip, carrying the orebody with it and leaving behind alteration features in the oxidized ground. As erosion progresses, these features may be exposed at the surface or subsequently truncated in subcrop several kilometres from the location of the roll front that formed it.

A roll front is a subterranean surface between reduced and subsequently oxidized rock. It may be essentially unmineralized. Alternatively, it may concentrate metals other than uranium, such as iron, vanadium, molybdenum, silver[10] or heavy metals.[11] In addition, these metals may concentrate in any combination, but invariably in overlapping shells or zones in order of electromotive force (Fig. 6).

One popular concept holds that the metals are progressively leached from the host rock as the roll front passes through it. Uranium districts are found in areas where the background levels of uranium are elevated. Based on the nature of the alteration, leaching of the host rock on the oxidized side of a roll can be extremely intense. With the remarkable efficiency of the precipitating mechanism only a few parts per million of uranium have to be removed from the volume of oxidized rock associated with most roll-front deposits to account for the amount of uranium in the orebody.

One answer to the mystery of how the oxidation and reduction can be so intense at a roll front was given by Rackley,[12] who demonstrated that sulphur-oxidizing and sulphur-reducing bacteria can provide the driving force for a galvanic cell that controls the geochemical reactions. This seems to be the case where iron sulphide dominates the minerals that are precipitated in the mineralized ground.

Where sulphides are absent, or nearly so, organic material may be the food for other strains of micro-organisms. A third

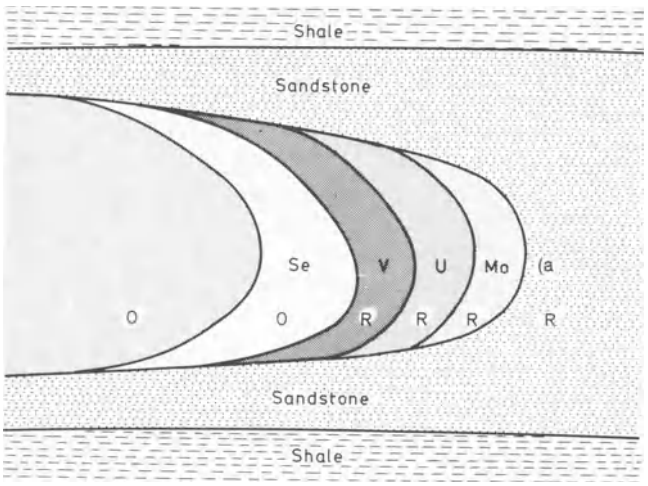

Fig. 6 Zonation of roll front

explanation for the precipitation of metals in the reduced ground involves chelation by organic acids of high molecular weight—for example, the humates found in significant amount in some orebodies of New Mexico.

Black shales

Most black shales are of marine origin, but reducing conditions in fresh water lakes and swamps are also potential sinks for uranium and associated metals. In each case the uranium and associated metals are introduced into the host rocks at the time of deposition.

The black shale of the Chattanooga Formation in Tennessee is an example of a large low-grade resource of uranium. The mineralized portion of this Devonian shale occupies several counties, but mineralized horizons tens of metres thick average only about 0.05% U_3O_8. For the most part, rocks of this type are not of economic importance, unless political considerations dictate otherwise.

Metamorphic host rocks

The world's largest and highest-grade uranium deposits occur in metamorphic rocks. An extensive review of the classification of uranium deposits was given by Ruzicka.[13] His classification of uranium vein deposits was subdivided into five types, based mainly on mineralogy.

Vein-like deposits were described as 'uranium deposits of uncertain genesis' by Mathews *et al*.[9] Except for a small number of these deposits in sedimentary rocks, the group is subdivided into unconformity-related deposits and deposits of metamorphic rocks. In a more genetic classification of the major (Proterozoic) vein-like deposits of the world, Dahlkamp and Adams[14] deciphered the relationship of diagenesis, metamorphism, metasomatism and weathering on uranium concentrations in various host rocks. The result is a logical genetic explanation for the spectrum of vein-like deposits observed today.

In a very generalized outline uranium concentrated in sedimentary rocks is reconcentrated by orogenic metamorphism in structures within the uraniferous strata. A deposit may be protected from surface weathering by a subsequent sedimentary cover, as at Beaverlodge in Canada. Magnesium and boron metasomatism may further concentrate uranium deposits near the unconformity, as at Ranger One in Australia. In the absence of sedimentary cover, intense subtropical weathering may produce a deep regolith with movement of uranium. Large deposits are not known to have been formed at this stage. After deep weathering the deposition of several thousand metres of continental sediments results in diagenetic reconcentration of uranium and nickel and the production of associated chlorite and kaolinite along the unconformity, as in the Athabasca Basin. In the last stage orebodies are degraded by faulting, fracturing and groundwater movement, redistributing uranium as sooty pitchblende and coffinite in the overlying sediments.

As was emphasized above, a wide variety of rocks are a potential source for uranium. One of the most significant of these are granitoids, which are associated with many of the major uranium districts around the world. The quantity of uranium that has been removed from these bodies is usually impressive. In the Granite Mountains of Wyoming, for example, all surface samples, and most drill core samples, appear to be 30–80% deficient in uranium relative to radiogenic lead.[15] Although none of the samples exhibited obvious signs of weathering below a depth of 60 m, uranium was removed to depths in excess of 400 m during geologically recent times. In addition to the obvious leaching of the uranium by surface waters, Rich and co-workers[16] concluded that red-bed sequences are the most likely source of oxidizing solutions for uranium vein deposits formed by ascending waters.

Except for the potential of decreasing the fugacity of oxygen by decreasing pressure and temperature, reducing agents are the key to the explanation of the accumulation of uranium. As massive pitchblende dominates vein-like deposits, a method of reducing uranium from the mobile hexavalent state to the tetravalent form is necessary. A number of reducing agents have been suggested, some of which were discussed earlier in the roll-front model—sulphides, graphite, carbon, biotite, amphiboles, chlorite, hydrogen sulphide and hydrocarbons. The association of these materials with vein-like deposits is obvious.

Rich and co-workers[16] showed that pitchblende formed before base-metal sulphides in 33 of 37 deposits where both were present. This indicates the possible need for another uranium-precipitating mechanism in addition to the oxidation of sulphides.

Clues to an interesting possibility may lie in recent studies of multi-element hot springs associated with centres of ocean-floor spreading. At an informal session of the Association of Exploration Geochemists annual meeting in June, 1982, S. D. Scott reported that samples from chimneys of 'smoking' springs collected from the Guaymas Basin were saturated with oil. Apparently, the rich organic material in the sea-floor sediments reaches unusually quick maturation as a result of the elevated temperatures that are associated with hydrothermal systems. Dr. Scott noted that spring waters with temperatures $<200°C$ contained several volume per cent of hydrocarbons. Some of the chimneys show deposits of wax and tar that may be analogous to the kerogen and bitumen that are found in exhalites today.

The association of oil with the hydrothermal environment of sea-floor spreading is consistent with the occurrence of major oil fields in aulocogens. The Gulf of Suez and the North Sea are examples of big oil-producing failed rifts. From the metals exploration standpoint the faster the sea-floor spreading, the greater is the heat flow and the bigger are the smoking springs and associated mineralization.

Although not brought out in any of the papers at that meeting of the Association of Exploration Geochemists, uranium vein deposits appear to be associated with the metamorphic equivalent of exhalites now dominated by assemblages of chlorite, sericite, quartz, banded iron formation and graphitic metapelite. This association may explain the origin of the heat drive for uranium vein deposits and a reducing mechanism related to the maturation of pelagic organic sediments. The relatively thin nature of these sediments is compatible with the limited depth extent of the deposits. It is significant that bituminous material seems to be associated with the pitchblende in most of the Athabasca veins. In addition, the initial stage of ore formation is

generally of about the same age as the host rock. This model could also explain how a recently discovered Canadian vein-like deposit is not close to an erosional unconformity.

Exploration techniques

Mineral exploration is properly an interdisciplinary field. In terms of the techniques used in the data-gathering phase, most activities may be classified as geologic, geophysical or geochemical. Each of the three is used on a scale of tens of kilometres to metres. Geochemistry is occasionally important down to the millimetre scale, as in dealing with the components of individual grains and crystal zones. Geology is the most scale-elastic, having exploration significance up to a continental scale, as in defining the boundary and understanding the genesis of metalliferous provinces.

Geologic techniques

Features for evaluation of the potential location of a uranium deposit may be considered in terms of source, transportation and precipitation. Understanding these stages is easier with the more lateral movement in sandstones than with metasediments, where upward movement may be overprinted with combinations of lateral and downward movement.

Alteration features in sandstones

The most widely recognized sources of uranium in sandstones are acid volcanics and rock rich in feldspar. During the 1950s and 1960s there was an argument among uranium geologists who favoured one or the other of these sources. Tuffaceous sediments are probably more important owing to the wide distribution of volcanic ash in Mesozoic and Caenozoic rocks and the ease with which the ash is leached. Except with experience, the ash is easily overlooked in a potential host rock unless it is a major part of the sediment.

Where uranium is derived from the components of a granitic rock it may weather directly from the intrusive and be carried in solution into adjacent sediments, or it may pass through an intermediate step by forming an arkosic granite wash near the edge of the basin. In either case at least one erosional cycle is required to free the uranium from a large source for subsequent concentration.

Thus, source rocks usually show features of oxidation and leaching. If the original rock is a light coloured sandstone, the change may be subtle and require examination at many locations for its detection. Most generally, there is both a shift toward a more oxidized iron colour and/or a lightening of the colour owing to the removal of metallic elements. Contrast of a few ppm uranium between the leached and unleached facies is quite adequate to derive the needed amount of metal when large volumes of rock are being weathered.

Identification of a uranium source rock is important because most alteration features indicative of a roll front do not establish the presence of uranium. Even in the strongest roll fronts uranium is probably not a necessary ingredient.

Grain size of the source rock may be quite fine. For example, a wide area of gently dipping tuff up to 100 m or more in thickness may be underlain by a favourable sandstone aquifer to which meteoric water percolates. A tuff, after being well altered, may become an unfavourable looking claystone. Near the surface a permeable sandstone may be completely silicated to an impermeable quartzite by release of silica from the tuff. On the other extreme of induration, as a rule of thumb, even the most impure and unlithified host must have some medium-grained sand to possess an adequate permeability for transportation.

The distance of uranium transportation from source rock to present mineralized location is ordinarily between 1 and 10 km. For the most part a roll front will have passed through the most rock updip from the mineralized trend. This emphasizes the value of recognizing some of the alteration features that are described below.

When a proper aquifer has hosted a roll front over a fetch measured in kilometres, the source rock may well be the same stratigraphic horizon as the present host of an ore trend. For this condition to obtain the host must have originally contained the few ppm uranium required for subsequent leaching.

In the process of dissolving and moving uranium in the groundwater a period of source rock and host rock erosion is implied. For this reason unconformities habitually overlie uranium orebodies. Presumably, the bigger and more intense the period of erosion the better, so long as the host rocks are not completely destroyed. On the other extreme, with ideal conditions of leaching, a good source rock and precipitation in a well-buffered host rock, the present cycle of continental erosion might suffice. Viable orebodies are found in rocks of Pliocene age in the Texas Gulf coast and, under the right conditions, it is reasonable to look for them in rocks of even younger age.

Most of the major sandstone deposits are Mesozoic and Caenozoic.[17] This is doubtless because rocks of this age contain the great piles of continental and marginal marine sandstones and the required periods of weathering and erosion. Most of the uranium introduced to Palaeozoic marine basins yielded little better than weakly mineralized black shales because of the lack of an efficient concentrating mechanism.

Various methods of precipitation have been proposed for uranium on the reducing side of a redox front. In the simplest model—and least likely to be mineralized—the front only represents the position of surface oxidation in an originally reduced but poorly buffered rock. In this case a low concentration of iron oxide may undergo a modest shift in its oxidation state under the influence of oxygenated groundwater. A typical colour change might be from light grey to light brown.

To concentrate uranium the host rock should be more reducing from the standpoint of reactive capacity per unit volume and negative redox potential. The former requirement may be fulfilled by sulphide minerals, organic material, such as plant remains and humates, or hydrocarbons. Humates have an unusual capacity to hold metal ions, including uranium, by ion exchange and chelation.[18] In general, however, it may be argued that the other materials are inadequate for the reduction of uranium, acting more importantly as a food source for anaerobic bacteria that create a very intense reducing environment.

Weathering and roll-front propagation both involve processes of oxidation. The latter involves not only a more intense oxidation but a precursive step of intense reduction when a geochemical cell is fully developed. Consequently, the alteration features that are associated with the movement of a roll front are more pronounced in degree and more varied in nature—indeed, when outcrop exposure of the host formation is good the various alteration colours can be mapped from the air or on coloured aerial photographs. In this way formations and basins may be surveyed at a rate far in excess of that which is possible by even the most generalized ground reconnaissance.

Reduced ore is generally some shade of grey. If the grade is very high, the colour intensity is black. Within a given area one can usually estimate the grade of ore by its darkness. When the values are completely removed by the intense biologic action in the oxidizing side of a geochemical cell a bleached or nearly white appearance may be attained.

High-grade ore may be stopped in its lateral movement by a permeable barrier or suddenly stranded by lowering of the groundwater-table. If it is also protected from the downward leaching of vadose water by an impermeable cap or suitably arid climate, the orebody can survive to be exposed by erosion at the surface. Even under these unusual conditions, however, it will normally be oxidized to a bright yellow before exposure.

Table 3 Redox colours

OXIDIZED		REDUCED	
Very light green	Light green	Medium green	Dark green
Very light greyish green	Light greyish green	Medium greyish green	Dark greyish green
Very light greenish grey	Light greenish grey	Medium greenish grey	Dark greenish grey
Very light grey	Light grey	Medium grey	Dark grey

Much more commonly, uranium is stripped from the host rock during passage of a roll front. The result in outcrop is barren oxidized sandstone. The colour is largely controlled by the oxidation state and amount of iron. Progressively, from the most oxidized colours to the most reduced, the series is roughly red, orange, yellow, green, grey, black. Ordinarily, the colour is not pure enough to fit directly into this sequence, having the further dimensions of greyness from light to dark and being mixed with other colours to yield some shade of brown, i.e. dark reddish brown, medium orange brown, light brownish yellow, etc.

Fortunately, iron is a sensitive indicator of oxidation state. It can be used even in subtle situations, such as a roll front smeared by lateral extension or a diffuse tabular deposit, to distinguish between the oxidized and reduced environments of uranium (Table 3). The redox line falls between light and medium in the greys and greens. When near mineralization, darkness increases with uranium content and sometimes greenness with increasing iron. These colour guidelines for the secondary enrichment of uranium and iron and degree of oxidation also can be used in metamorphic and igneous rocks.

Several other alteration features may be preserved in outcrop after passage of an intense redox cell. Some of these features are from the leading reduced side and some from the trailing oxidized side.

Calcite nodules and concretions generally form in advance of the precipitation of uranium[12] and may, therefore, be only slightly radioactive. The concretions can be 1 m or so across and erode to grotesque structures on pedestals. A significant form, generally overlooked, is called 'buck shot' calcite after the small rather closely packed spheres 1–2 cm in diameter. The spheres may form individually, but in the extreme case they represent various degrees of partial destruction from a complete calcite cementing in the host sandstone.

Colour bands are another feature that may be observed in outcrop. These are the ghosts of previous roll-front positions preserved as fluctuations in the amount and oxidation state of iron. Alternating colours form cycles that may be repeated many times in one outcrop. The cycle width may be from 0.1 cm to several tenths of a metre.

Colour bands are most easily recognized when they are not parallel to the bedding, as they commonly are near the tails of a roll. Any of the oxidized colours discussed above may be present—sometimes with striking brightness, but sometimes with barely discernible contrast. The stronger yellows and reds are probably the most favourable, especially when they are sufficiently extensive to indicate a large geochemical cell.

Just as roll fronts may be seen to drape around permeability barriers in a uranium mine, so the colour bands follow the same rules in detail on the surface. For example, a concretion may show a tear-shaped ring, the drawn-out apex pointing down the hydrologic gradient that moved the front.

Sometimes a second generation of colour bands cuts across an earlier set. This is generally expressed by weak colours arranged in cycles that have a medium to long length. This overprinting indicates a change of hydrologic flow directions and, probably, that altered rock can pass through another cycle of reduction and oxidation under the influence of a geochemical cell. The easiest explanation for this regeneration is that bacteria are the driving chemical force. The author speculates that sulphate-reducing bacteria could cause a reduction of oxidized ground charged with sulphate water if mineralization in a roll front temporarily plugged up the original direction of flow.

Another specialized case of colour banding is the thin concentric rings that may develop around a clay gall. These structures range from a few centimetres to a few tenths of a metre in size, and may involve up to 10 or 20 cycles.

'Kaolin nests' are distinctive light spots a few tenths of a centimetre in diameter that represent the filling of the intergranular space of a sandstone by kaolinite. The spots are usually spaced from 1 to 10 cm apart and scattered more or less evenly throughout the host. This common feature in oxidized rock is probably a specific indicator of a geochemical cell in both the roll-front situation and the less mobile tabular environment. Wanty and co-workers[19] found saturation anomalies with respect to kaolinite, illite, montmorillonite and two zeolites 1–2 km wide in the groundwater around two orebodies in south Texas.

A subtle but definitive alteration indicator is the destruction of mafic grains. This is particularly useful when drill cuttings, which do not preserve some of the other features of alteration, are all that is available for examination. A binocular microscope or hand lens may be used in the field to detect such alterations as biotite to chlorite or magnetite to hematite and limonite.

Other minerals are also altered. Perhaps the most obvious, when the host is arkosic, is the change in appearance of feldspar from its normal translucence to a lighter or 'dead' colour. Even quartz may be deeply corroded.

As one might expect, the direction of movement of a geochemical cell may not be down the present dip of the host bed. There are clues that indicate the direction of a drilling target from the centre of the most intense alteration in outcrop. If the exposure is large enough, and the third dimension visible, the axis of movement of the rolls may be seen directly from the colour banding. Smaller features near the centre of a large roll may also be useful—for example, the tear-drop banding mentioned above.

Where a knowledge of local tectonics and the exploration model suggest that the direction of the hydrologic gradient for the rolls is roughly the same as the primary slope on which the sediments were deposited, cross bedding and current ripple marks may be used. In the absence of any other reliable information, the direction of original sediment transport may be an indicator of the direction of roll-front movement.

Favourable features in metamorphic rocks

The best uranium deposits in metamorphic rocks occur near a major unconformity between a basal metamorphic sequence of early Proterozoic age and overlying sandstones. Uplifted granitic or gneissic core complexes provide an apparent source for the uranium. Orebodies are found at the intersection of altered and mineralized shear zones capable of channelling large volumes of uranium-bearing solutions past reducing graphitic and chloritic schists. Potential host rocks include a wide variety of metamorphic rock types, most notably schists dominated by quartz, chlorite, sericite, and graphite. Pathfinder elements for the uranium mineralization are most commonly nickel, cobalt, copper, zinc, lead, arsenic and bismuth.

The character of unconformity veins has been summarized thus:[7] 'They occur in faulted, fractured, and brecciated zones in sedimentary rocks and in retrogressively metamorphosed, chloritized metasedimentary rocks. Uranium veins contain pitchblende and varying amounts of sulfides and sulfarsenides and are commonly associated with pervasive hematitization'.

Vein-like deposits are related to both ascending and descending waters. The importance of each is a matter of current debate. Characteristics that may be used to distinguish ascending from descending solutions have been reviewed.[7] A few of these are lateral temperature zonation of an alteration sequence that may show decreasing or increasing temperature of formation away from the centre of a vein; fluid inclusions that may show high or low temperatures; asymmetric crystal growth that usually shows the direction of movement for the solution that formed them; and vertical extent of orebodies, as supergene mineralization seldom exceeds a depth of 200 m.

Geophysical techniques

The measurement of radioactivity is by far the most important geophysical method historically. In the last decade, with advances in instrumentation, there has been a change from total gamma counting to emphasis on gamma-ray spectrometry. Most recently, in terms of exploration dollars spent by industry, the induced pulse transient (INPUT) method has eclipsed radiometrics. This situation manifests a shift toward the search for blind unconformity vein deposits and the effectiveness of INPUT as perceived by exploration companies.

The use of methods for the detection of radon in soil and water is covered under *Geochemical techniques*. Other geophysical techniques applicable to the standard situations in which problems involve structure and lithology are beyond the scope of this paper.

Radiometric surveys

The original survey instruments were Geiger counters. In the United States during the 1950s thousands were sold to geologists and amateurs. For several years no one understood the finer points of uranium exploration, but this simple method of detecting uranium occurrences was responsible for the finding of many of the deposits during the first uranium boom. Starting with the latter part of the 1950s, geologists turned to scintillometers, and the best of these instruments were not surpassed in quality until the 1970s.

Hand-held methods Geiger counters are the simplest and least expensive instruments for measurement of radiation. Capable of distinguishing between beta- and gamma-rays, they can give useful information about the distribution of uranium as opposed to its daughter products. These instruments are still in use as a consequence of their advantage in measuring radiation from such small source areas as drill cores and their capability for probing piles of ore.

Scintillometers use a thallium-doped sodium iodide crystal that emits a small flash of light along the path of a captured gamma-ray. A photomultiplier tube converts this scintillation of light to an electrical pulse for each ray detected. These instruments are much more sensitive to the measurement of weak fluxes and distant sources than a Geiger counter. In use, they measure average gamma activity from larger areas. In models with large crystal volume they are the sensitive carborne and airborne measurers of gamma flux.

In determining the land to be recommended for acquisition it is a mistake to measure and contour average radioactivity of outcrops. In general, even in the largest outcrop areas, the most significant value is the highest found. Surface leaching commonly reduces radioactivity to near background levels. Small ghosts of previous mineralization may be found in concretions, clay galls, siltstone splits and other situations of reduced permeability. These vestiges are the best radiometric and geochemical indicators of where the mineralization was.

Only the highest radiometric value at each site is plotted. A recommended contour interval is one times background. If background is defined as the lowest common value found in the province, it is typically 0.005 milliröntgens per hour. A significant anomaly may be only about three times background.

It is recommended that flux fields be measured in milliröntgens per hour (mR/h). Many instruments read in counts per second (cps) or counts per minute (cpm), but these values vary widely from one type of instrument to another based on the size of the crystal and the geometry and efficiency of the instrument. Where several different instruments are used, either in a large survey or over a period of time, severe calibration problems can result in trying to compare the various measurements.

Gamma-ray spectrometers are usually scintillometers capable of distinguishing the energy level of individual rays. These instruments are available as small portable and large vehicle-mounted models. As a minimum they discriminate between gamma-rays that originate from the decay chains of potassium, uranium and thorium. This radioactivity accounts for virtually all natural gamma radiation that originates from the earth's surface.

Surface vehicle methods For traverses over areas measured in square kilometres the larger and more sensitive scintillometers and spectrometers may be mounted in or above a vehicle. The obvious advantage is an increase in the area that can be covered. Although one might use hand-held instruments to define the surface expression of a mineral deposit, surface-vehicle and airborne instruments are used to good advantage in locating districts that are larger areas and generally contain groups of deposits. An analogue or digital recorder needs to be linked to the detection instrument for accuracy and ease of recording and subsequent plotting. Advances in recent years have largely replaced surface-vehicle surveys by airborne methods.

Airborne methods During the 1950s the first airborne surveys used portable scintillometers in low-flying, light aircraft. Readings from the ratemeter were recorded on a map or air photograph for later field checking. This method is still useful for the quick and inexpensive evaluation of a moderate-size area where little radiometric information is available.

For larger areas the more sophisticated modern airborne systems are justified. Large crystal arrays greatly increase detection sensitivity. Multi-channel recorders are capable of logging details of the gamma spectrum in short time segments, the exact location of the aircraft and data to correct for extraterrestrial radiation and radiation from atmospheric dust. This wealth of

information is all stored for direct processing by a computer, which provides sophisticated statistical analyses and contour maps that show the distribution of potassium, uranium and thorium: individually, in sums, and in ratios. These maps may be used, for example, to distinguish areas of high granitic background from areas, perhaps weaker in total gamma activity, where a secondary uranium enrichment has occurred.

Input surveys

Radiometric surveys apply to all rock types, but as little as 1 m of cover can mask a very large anomaly. This section, which describes a type of airborne electromagnetic survey, applies particularly to the class of deposits broadly referred to as unconformity veins.

Bosschart and Pemberton[20] gave a good review of airborne electromagnetic methods, but our focus here is on the system that dominates in uranium exploration. The Induced Pulse Transient (INPUT) system developed by Barringer Research uses an airborne pulse input loop to induce a secondary field in natural ground conductors and then measures the decay of this field with a towed 'bird'. The survey normally incorporates magnetometer results. Methods for quantitative interpretation of aeromagnetic data were given by Morley and Bhattacharyya[21] and Spector.[22]

Paterson[23] summarized the response characteristics of AEM systems to natural conductive material. Conductors include sulphides, graphitic horizons, banded magnetite, serpentine bodies and water-filled faults. The importance of some of these conductors is discussed under *Exploration models.*

INPUT surveys yield depth penetration of up to a few hundred metres for large, good conductors. At the same time they give good definition of conductor shape, depth and conductivity, and good resolution to distinguish between adjacent conductors.

Two caveats should be noted: conductive overburden and human cultural items on the landscape can cause problems. A thick regolith or poorly consolidated Caenozoic cover can mask otherwise strong anomalies in the underlying rock. Interpretations can be made as long as some of the anomalous signal is detected.[24] Overburden can also harbour bogus anomalies that mimic those of an exploration model.[25] Man-made features such as power lines, pipelines and roads cause local interference. These features prohibit interpretation in industrialized or urbanized areas.

Examples of interpretation for horizontal and dipping tabular conductors were given by Lazenby.[26] Further refinements in qualitative and quantitiative interpretation were offered by Palacky and West[27] and Palacky.[28]

Geochemical techniques

Before a geochemical programme is started an appropriate sample type and sample spacing must be selected. The sample type is based mainly on the availability of the five types of samples for collection and the advantages and disadvantages of each. Water, rock or plants may be widely available in one survey area and virtually absent in another. Soil and stream sediments are usually even more widely available. Except, for example, for a desert covered by wind-blown sand, it is generally feasible to sample at least one type of surface material. In addition to the remarks on geochemical techniques that follow, Levinson[29] gave many more details on field and analytical methods.

Selection of sample type

Probably the reason that stream sediments are so popular in geochemical sampling is that they represent a natural integration of material from a large surface area. This implies the use of wide sample spacing and the ability to define metal provinces—the largest geochemical areas of enrichment. Of course, stream sediments may be used on much smaller scales, as in finding localized mineralization. But the advantage of this sample type is still in area integration to yield rapid identification of where more detailed work is required, perhaps with another sample type such as soil or rock.

For uranium deposits in igneous or metamorphic hosts rock samples are generally more reliable, being one step closer to the mineralizing process than stream sediments. Rock samples are also valuable when the host rock is sedimentary, but usually not as helpful as groundwater when it is available. In the absence of groundwater or rock, woody plants are often overlooked as a valid sampling medium. They are available with good sample spacing even in many arid lands, and their root systems may derive mineral components from well below the surface.

Where there is good coverage groundwater surveys generally give the best results. Otherwise, the strongest geochemical survey combines the advantages of more than one of the other sample types. At each collection site two or three types of samples may be taken—not necessarily the same combinations in adjacent sites. For example, in an area with poor water well coverage rocks would normally be the second best sample type. If restricted exposures yield large holes in coverage, at least two sample types should be taken at each site. Plants would probably be the next preferred type of sample, with soils last. Groundwater should be taken whenever it is available.

The simplest way to interpret a multi-sample type survey is to plot the results of surface samples in percentiles of each sample type. Most of the time, if one sample is anomalous at a site, another will be also. At any rate, good results are generally obtained by contouring at 5 or 10 percentile units based on the highest sample at each site. Groundwater samples need to be plotted and interpreted separately from the surface samples.

Determination of sample spacing

Reflecting a great flexibility of scales, geochemical means may be used to define provinces, districts and deposits. If a province is reasonably well defined by previous surveys or by geology, stream sediment sampling may not be necessary. Where the geology is known well enough, target areas may be defined and sampling may proceed at a spacing adequate to identify leaseable blocks.

If the area under consideration is too large to sample at this close a spacing, the survey gains efficiency by phasing with different sample spacings. The object might be to sample a large area and define districts that constitute 10 or 20% of that area.

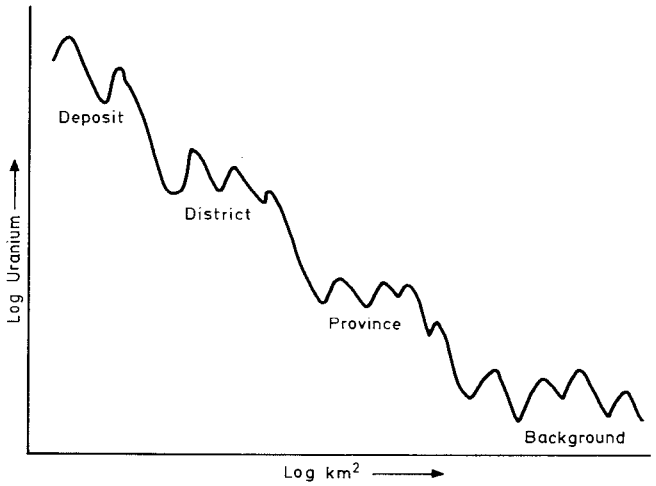

Fig. 7 Geochemical concentration versus proximity to uranium deposit

These targets may then be accorded priorities and sampled at a closer spacing to define leaseable blocks.

With geologic and radiometric information the final sample spacing should not have to be less than that which would give three adjacent anomalous samples in the smallest mineralized halo of interest. For many types of uranium deposit this spacing is about 1 or 2 km. Where doubt remains in target identification, additional samples may be taken at half the spacing. As a rule of thumb, spacing for finding districts or very large deposits might be about 5 km. Dyck[30] gave an example of contouring data from approximately such a spacing.

The concept of defining provinces, districts and deposits is illustrated in Fig. 7. Between each stage in the curve there is often a break or step from which a distinguishing or threshold value may be established. For any particular type of geochemical sample in a specified sub-continental area values may be assigned to the uranium axis.

Hydrogeochemistry

How to sample Perhaps the first rule in collecting water samples is to rinse the bottle and cap well with the water that is being collected. Normally, a 250-ml polyethylene bottle is adequate for multi-element programmes, but the size should be checked with the laboratory in advance. To exclude an air bubble when sealing, the cap should have an inverted conical polyethylene insert, sometimes referred to as a polyseal cap. New bottles should not need an acid wash to leach the inside surface of cations. Such a wash can actually increase adsorption of cations from the water sample.

Groundwater should be collected as near to the source as possible. Occasionally, it is necessary to sample at some distance from a well head. Generally, the water can be considered to be in equilibrium with the parts of a distribution system through which it passes—pump, pressure tank and pipes. It is preferable to run the water from a system as long as practical before sampling, especially if the system has been inactive.

The most controversial question in water sampling is whether to acidify the sample when it is collected. The author feels that it is generally not necessary. Sample acidification causes a loss of molybdenum, but makes no difference in uranium. When a stream water sample is murky or well water bears the slightest rust scale, acidification without prior fine filtering can falsely increase metal values one or more orders of magnitude.

At high latitudes uranium may be lost by the activity of natural bacteria, even in acidified water. In at least one case the problem was overcome by the addition of mercuric nitrate to samples at the time of collection (S.S. Shannon, Jr., 1976, personal communication).

Where practical, water samples are collected in the fastest-flowing part of a stream to optimize mixing and minimize local components. Other sampling instructions relate mainly to avoiding potential contamination, running various tests at the site and recording observations. Any condition that would reflect on the interpretation of the results should be recorded.

What to sample As was mentioned above, groundwater is a superior sampling medium. Usually, data from wells and springs can be plotted and interpreted together. In some areas where groundwater is not available but surface water is abundant, as in the northern latitudes, good results may be obtained from lakes in rapid aerial surveys.

In well-drained areas, and especially during periods of low flow, streams may derive a significant component of their discharge from groundwater. As is suggested by the uranium data in Table 1, there is a tendency for groundwater and stream water in a particular area to yield a similar distribution of results. Sampling during periods of high flow is not recommended.

Field measurements There are several measurements that can only be reliably made in the field. Probably the most common parameter for field determination in water samples is pH. In uranium exploration this measurement may give a direct indication of a geochemical cell. It is also necessary for equilibrium calculations.

A similar measurement for oxidation–reduction potential (Eh) is generally too difficult to accomplish. As a substitute dissolved oxygen can be determined reliably in about 2 min with a small commercially available kit.

A smaller and simpler kit measures carbonate and bicarbonate that relate to the solubility and mobility of uranium. Hydrogen sulphide, a reliable indicator for the environment of uranium precipitation, may be measured by yet another and even simpler kit.

As with other dissolved gases, radon is also usually measured in the field. In this case, however, it is the half-life of the unstable isotope more than the exsolution of the gas that requires field attention. The alpha-counting instrument that quantifies the specific radon daughter of uranium is field-portable but awkward. As a sample can be run in the evening or the next day with good results, and with the efficiency of a multiple-sample run, this measurement is usually not made at the collecting site. With normal groundwater movement the 3.8 day half-life of ^{222}Rn indicates that the ^{226}Ra from which it is derived cannot be far away. Ordinarily the uranium, from which it is alternately derived, is also nearby. In the fortuitous event of sampling water directly from an orebody the radon signal is three to five orders of magnitude above background, which is itself measured with an excellent sensitivity.

Laboratory measurements The determinations recommended in this, and the previous section on field measurements, are valuable in exploring both sandstone and vein deposits. Most should be used on any uranium survey. The more parameters that there are in the exploration model the less is the possibility of misinterpretation and the better the target definition. As a rule, a groundwater survey should not be attempted with less than determinations of pH, uranium, arsenic, sulphate and total dissolved solids. Helium, dissolved oxygen and bicarbonate are highly recommended. With a little experience hydrogen sulphide concentration can be estimated from the strength of its smell.

Uranium is the best indicator of uranium mineralization owing to its remarkable mobility in the oxidized environment. The primary value of arsenic is its large halo, which increases the likelihood of target detection and helps with verification of mineralization. Molybdenum is another good pathfinder for uranium. It has a much smaller halo, which may be located both along the strike of, and downdip from, the centre of mineralization. A laboratory needs good sensitivity to report values for this element.

A sulphate anomaly reveals the oxidized side of a geochemical cell or the oxidized top of a vein-type deposit. In the roll case the maximum value occurs near the front, with decreasing values up the hydrologic gradient. In the vein case the upper end of the anomaly is nearest the mineralization. Areas with evaporites may confuse the interpretation, but total dissolved solids help to resolve this problem as well as that of uranium anomalies related to water maturity rather than mineralization. In this case uranium is likely to increase more or less linearly with total dissolved solids down the hydrologic gradient. The same situation occurs with stream water maturity, uranium and total dissolved solids increasing continuously from the highest headwaters to the sea.

Helium is one of the decay products of both the uranium and thorium decay series. Except in the primary igneous environment, these two elements rarely are enriched in the same area owing to the relative insolubility of thorium. Thus, in sedimentary and metamorphic uranium districts a helium anomaly is

usually not derived from thorium mineralization. As eight atoms of helium are derived from the decay chain of each ^{238}U atom, and this noble gas represents the ultimate in mobility, the measurement of helium in groundwater can be a sensitive target identifier. Nearly all helium is of radiogenic origin, but the mass effect of the uranium and thorium of the earth's crust means that concentrating mechanisms such as deep faults and hydrocarbon reservoirs can cause interference.

Although some people regard the mass spectrometer, which measures helium, as a field-transportable instrument, laboratory analysis is recommended because of maintenance problems.

Both helium and radon are readily lost to the atmosphere from water, and both will pass through plastic containers. These gases need to be collected with minimum sample agitation and with no air bubble under the cap, as they are much more soluble in air than water. Radon may be collected in steel-capped glass jars, but samples for helium analysis are most safely collected in metal containers. Glass containers may be used if analysis is within a few weeks, but a correction should be made for loss of helium by diffusion through the container. The measurement of helium and radon in surface water is unlikely to yield success, with the exception of water from the bottom of lakes.

^{226}Ra, mother of the mobile ^{222}Rn, is an excellent indicator of uranium mineralization. Unfortunately, this isotope is difficult to measure and hence expensive to determine. Laboratory sensitivity is very good, however, and the element is recommended for target verification and delineation after potential targets have been identified.

An interesting example of a well water survey was given by Dyck[30] with emphasis on dissolved gases. He offered an interpretation for radon, helium, hydrogen sulphide, methane, oxygen, nitrogen, carbon dioxide, neon, argon and total dissolved gas. Other measurements are pH, Eh, conductivity, temperature, zinc, copper, lead and uranium. The result is a proposed new exploration target.

Petrogeochemistry

How and what to sample The standard sampling approach for orebodies requires that the chemical constituents of the sample closely represent a specific large body of rock. The philosophy for geochemical sampling of rock frequently violates this principle to the utmost by calling for the highest grade or most enriched sample to be collected. The principle of sample upgrading is justified because the most significant values that remain in the outcrop of a potential host sandstone are the best remains of the orebody that passed through it.

Thus, the material sampled is usually less permeable than the main sandstone body—siltstone or shale splits, contacts with siltstone or shale, claystone galls or concretions. The primary tool for identification of the exact spot to sample in an outcrop area is the scintillometer. One or more samples may be collected from an outcrop with dimensions as large as hundreds of metres.

Samples from an outcrop area are generally analysed separately unless they represent a lithology with low radiometric contrast with other parts of the outcrop. One may be satisfied with a single sample if it is several times the radiometric background. Otherwise, multi-grab samples help to define reproducible traces of mineralization in non-radioactive pathfinder elements.

Sample preparation and analysis As with sample collection, sample preparation gives an opportunity to increase the contrast between background and anomaly. Medium- and coarser-grained samples of sedimentary rocks, soils and stream sediments should be disaggregated rather than pulverized to avoid dilution by quartz. This helps to make results from fine-grained samples comparable with those from coarse-grained samples. The procedure may be applied to all of these three types of samples for simplicity and continuity of treatment. After disaggregation, the sample is sieved, preferably through bolting cloth to avoid contamination with a metal for which a subsequent analysis might be made.

Useful elements Uranium, arsenic and molybdenum are three of the most useful elements in rock sampling surveys. Uranium is most important in evaluating whether a small vestige of a pre-existing mineralized ground has been sampled and in determining whether a formation has adequate uranium to be considered a source rock. Arsenic and molybdenum, good pathfinder elements for uranium, may be considered favourable indicators. As long as there are adequate anomalous uranium occurrences in the target area to indicate the previous existence of a source, arsenic and molybdenum may be regarded as local proxies for uranium in rock, soil and stream sediment.

Other elements may also be useful, especially if they are known to be associated with uranium mineralization in the district or province under consideration. In an igneous body, for example, large fluctuations in the ratio of thorium to uranium generally indicate the removal of uranium, as thorium is relatively immobile. These large fluctuations may be an early hint of a secondary uranium mineralizing process. In a drill-hole the thorium/uranium ratio and subtle colour changes such as those described under *Alteration features in sandstones* can show the depth of surface oxidation and the zone of uranium precipitation. The redox level may actually be hundreds of metres deep in rock generally considered to be unaltered granite.

The Precambrian granites of the Granite Mountains in Wyoming are widely regarded as a source of uranium for the nearby major uranium districts hosted in rocks of Tertiary age. Stuckless and Nkomo[31] found that these granites, falling in the range of uranium concentrations generally thought to be normal, have lost at least 70% of their original uranium. Rosholt and co-workers[32] found an average uranium loss of approximately 75% without loss of thorium. Another calculation, based on radiogenic isotopic balances for granites from a 670-m core hole, demonstrated uranium loss of 80% since Cretaceous time.[33] The surprise was the depth to which the uranium loss occurred in granite that was not considered deeply weathered: 'Thorium anomalies in basement rocks may be better indicators of uranium provinces than uranium itself. If the thorium anomalies are accompanied by Th/U ratios greater than 5, uranium loss from the basement rock seems probable'. Conversely, if the ratio is less than 3, uranium was probably not lost.[34,35] The thorium content of most granites is in the range 10–30 ppm, whereas uranium in most granites averages 2–8 ppm.[1]

Data treatment Each element may be plotted on a separate overlay or combined with other elements on one overlay by colour or symbol coding. Where several related samples are taken at a single site or outcrop area, the highest value for each element may be used for contouring. One helpful method of interpreting multi-element results is to outline all adjacent sites that are anomalous for each type of determination.

Stream sediment geochemistry

How and what to sample Some of the more important guidelines for collecting stream sediments help to overcome the inherent erratic nature of results. The last deposited sediments, usually at the water's edge, have had the least opportunity for loss of the more mobile elements through weathering or gain through reduction. These so-called 'active sediments' are usually in the oxidized state. Where no water is present in the stream, the most recent sediment is collected.

When sediments *in situ* are kept wet, and particularly if comminuted organic material is included, they may discolour to the dark shades typical of a reduced environment. In this state the

sediments are capable of scavenging numerous metals from associated water. Active sediments should generally not be collected deeper than about 1 cm. Where there is a choice, an effort is made to collect the finest sediment. Except in some specific local circumstances, samples are sieved and the fine fraction is analysed to provide maximum anomalous contrast and to minimize the variable amount of quartz dilution between samples.

If the sediments of a stream appear to be homogeneous, a sample of six grabs over an interval of about ten times the width of the stream will normally suffice. When the sediments are inhomogeneous up to 20 grabs are recommended, depending on the degree of variability, the geologic environment and the elements analysed. In small streams the spacing between grabs should be at least 1 m, and preferably 3 m, to improve the representative nature of the sample.

Sample preparation It is recommended that stream sediments be dried overnight at 85°C, placed in a plastic envelope and disaggregated by impact with a rubber mallet. The fraction passing through a 100-mesh (150-μm) non-metallic sieve is blended and a 0.25-g aliquot is dissolved in 10 ml of 1:1 nitric–hydrofluoric acid. The sample is then evaporated to near dryness on a hot plate and diluted to 50 ml with 10% nitric acid. Further details of analysis were given by Nichols *et al.* [5]

Use of elements In a stream-sediment programme elements may be selected as indicators of both favourability and unfavourability. Negative indicators are helpful because the inherent mixing of geochemical environments and processes can result in bogus uranium anomalies.

One of the more helpful methods to resolve the origin of a uranium anomaly is to ratio the results of two different types of determinations. Several types of acid extractions may be arranged in order of increasing efficiency from stripping only surface-bonded uranium atoms to dissolving lattice-bonded uranium from refractory minerals. As is shown by delayed neutron activation analysis, even the most complete extraction methods, such as those which are typically used (Table 1), may leave 50–90% of the total uranium in the refractory minerals.[5] A ratio of determinations from two contrasting methods can be used to indicate the mineralogical origin of the uranium in the sample.[3]

A number of other elements may be added not only to indicate uranium anomalies related to unfavourable sources but to define associations of elements that distinguish such geologic sources as granite, mafic igneous rock, felsic igneous rock, metasediments and many more.[36,37] In addition, an overprinted process such as manganese scavanging can be identified.

Pedogeochemistry

Soil samples are useful in a detailed survey to find the small surface expression of a vein and may be taken where there is restricted availability of other sample types. Caution is needed in farming areas, where significant uranium can be added to soil and water if the ground is fertilized with phosphates.

How to sample Soils may have surprising lateral variations in radioactivity. Consistent with the principles of sample upgrading discussed under *Petrogeochemistry*, a scintillometer is recommended to survey each site for the purpose of finding the most radioactive spot to sample. In the absence of local radioactive contrast, a multi-grab sample is recommended. Uneconomic uranium potential is usually indicated where radioactive soil anomalies are related to heavy sands.

Useful elements For a soil survey the selection of elements, preparation of samples and interpretation of results are quite similar to those of rock and stream sediment surveys discussed above. Soils do, however, present some unique problems and opportunities. Uranium concentrations in soil are less than those in stream sediments, which, in turn, yield concentrations less than those of rock (Table 1). Thus, a significant contrast between uranium values in soil may be subtle, and there may be a potential problem with the detection level of some laboratories.

Emanometry On a more positive side, the natural porosity and ready availability of soil lead to the measurement of radiogenic gases emanating from soil and underlying permeable bedrock. Probing the soil for interstitial gas is more sensitive than sampling gas above the soil.

A good description of the theory and method for determining radon was given by Dyck,[38] who was a pioneer in the field. According to Morse,[39] 'In areas of shallow overburden, radon in soil gas can extend evaluation to depths beyond reach of the scintillometer . . . Day-to-day variations of radon content in soil gas are confusing, but seldom obscure trends and anomalies'.

Instruments are currently available that distinguish between ^{222}Rn from the ^{238}U decay series and ^{220}Rn from the thorium series.[40] They are field-worthy, sensitive, easy to use and popular. In addition, radon is trapped by snow, so measurements from the base of a snow cover are more reliable than those made in the soil without snow cover (R. H. Morse, 1980, verbal communication). There is a strong radon absorption (loss), however, for temperatures below −20°C.[41]

Although radon does enter snow from frozen soil, it does not emanate appreciably from solid rock.[42] A scintillometer should be used to complement any radon-measuring technique and especially in areas of outcrop. Czarnecki and co-workers[43] compared radon-measuring devices at 100 locations over a 1.5-km^2 area in the Red Desert of south-central Wyoming. A prototype microprocessor-controlled emanometer was found to be more reliable with a 13% coefficient of variation (standard deviation/mean) than an established emanometer with a coefficient of 31%.

In alpha-track detectors the carbonate etch method was found to be 20 times more sensitive than the nitrate track etch. The instruments that measured instantaneous radon did not correlate well with the possibly more reliable methods based on a 30-day sample time. All the radon-measuring techniques correlated poorly with the radiometric equivalent uranium in the soil, which led to the conclusion that the radon was coming from below the surface.

Possibly the most cost-effective method involves radon absorption on a small charge of activated charcoal that can be placed in an inexpensive polyethylene bag. The gamma-emitting radon decay products are measured by a scintillometer with an efficient collecting geometry, preferably approaching 4π.

Virtually all helium in the ground is generated by radioactive decay of unstable elements. Each ^{238}U atom, for example, gives off 8 He^4 atoms in the decay chain ending with ^{206}Pb. In recent years helium in soil has received wider attention for its potential in defining a geochemical halo for uranium deposits. Although the method is difficult to master, one firm claims to have a system worked out, but it has not published its secrets.[44]

Biogeochemistry

In their normal nutriment-gathering process plants sample most of the elements in the ground on which they grow. By sampling plants with deep root systems the effective penetration below surface materials may be several metres, especially in arid climates. Thus, plants are often the best readily available type of sample where allochthonous glacial material or aeolian sand covers the bedrock. Botanical sampling is uniquely applicable to extending the field season into winter if the ground is snow-covered. In addition, winter sampling has advantages in swampy areas where access is a problem during other seasons.

There is some concern about whether analytical results from trees of different genera can be compared with one another.

From some preliminary work with a few elements it appears that common deciduous trees of Minnesota and Wisconsin may be roughly comparable. The utility of uranium exploration with big sagebrush has been demonstrated in several western states.[45]

Nine types of trees that grow in Texas from the Gulf Coast, the Central Mineral District, and the northwest corner of the state have comparable uptakes of uranium based on the minimum, median and maximum value in the ash of limbs (Table 4). Both stream sediments and plants (Table 1) have a narrow range of uranium concentrations over a wide range of geologic terrains. Tree samples collected about 5 km apart in two Gulf Coast 1×2° quadrangles accurately defined the uranium province.[2]

Table 4 Uranium in trees, Texas, ppm

Tree type	Minimum	Median	Maximum	No. of samples	Reference
Cedar	0.18	0.48	5.54	50	4
Elm	<0.10	0.30	4.71	63	4
	0.12	0.26	1.51	33	5
Hackberry	<0.10	0.30	8.30	80	2
Huisache	<0.10	0.19	9.22	29	2
Live oak	0.10	0.37	4.92	23	2
	0.12	0.34	6.64	31	4
Mesquite	0.10	0.20	5.94	103	2
	<0.10	0.24	9.46	13	4
	0.10	0.23	0.60*	48	5
Salt cedar	0.10	0.22	1.40	20	5
Sycamore	0.13	0.47	3.99	44	4
Willow	0.20	0.47	1.64	16	2
	0.15	0.42	3.90	30	4

*Mesquite on soil derived from Permian rocks.

In the Llano area of central Texas tree types that grow in the same place were sampled for strict pair-wise testing for the significance of the difference in the mean concentration of metals from limb ash. The result was a hierarchy of mean concentrations for 11 elements in five types of trees.[4]

How and what to sample Plant samples are generally taken from the branches of the largest tree or shrub that is available for maximum depth of root penetration. To minimize seasonal variations in the metal composition of plant tissue twig material of at least a few years in age is recommended.

In the absence of a clue that one tree might contain higher values than another, sampling several trees makes for reproducible results. When more than one young branch is collected from a tree, as where only one or a few trees are available for sampling, the selection of branches should be spread evenly around the tree owing to the potential of asymmetry in uptake by the roots. Usually adequate material will be contained in 8–12 twigs 1–2 cm in diameter and about 20 cm long. The use of non-breathing plastic bags should be avoided as they promote decay of the wood.

Sample preparation and analysis During sample preparation at the laboratory all or most of *each* stick should be used, but 1 cm or so may be discarded from the ends to reduce the possibility of contamination. Table 4 shows that, as with stream sediment (Table 1), laboratory sensitivity should be good to tenths of a ppm.

If a volatile element—for example, arsenic—is to be determined, the sample should be ashed at a relatively low temperature to minimize sublimation. An alternate procedure with the use of hot acid digestion[46] is probably safer.

Combined sample types

Just as the use of more than one element strengthens the interpretation of a sample, so the collection of more than one type of sample broadens the base for interpretation of a survey. Results from well water and surface rock may be only indirectly related, yet both may be important to definition of the mineral potential. For example, groundwater samples might show evidence of a reducing environment and little or no uranium in solution, whereas analyses from the outcrop of the host formation could verify a good source of uranium in the rock.

Another reason for taking more than one sample type is substitution. The interpretation of data from rock, soil and plant ash can be expected to yield similar results. If rock cannot be sampled without gaping holes being left in the coverage, an additional sample medium may be needed. Indeed, trees might be sampled even with impressive rock outcrops nearby to cover another stratigraphic interval.

The problem of comparing the results from two different types of samples can be resolved by comparing the percentiles of the two populations. If the data-base is computerized, it is probably even easier to transform on the basis of the means and the standard deviations so that the population of each sample type has a mean of zero and a standard deviation of one. In this way, for example, the values of an element in rocks can be contoured directly with the same element in soils from other sites. The confidence level for this procedure may be established by taking more than one sample type at numerous sites where they are deemed to be equivalent.

What is anomalous?

The first problem that confronts a geologist in looking at his laboratory results is to designate the anomalous values for each element in each sample type. Values reported in the literature for similar situations provide a helpful beginning and Table 1 can be used as a starting point.

As would be expected, different lithologies yield different distributions of values. Usually, the rocks that are most likely to host a deposit are the highest in the various chemical parameters discussed here.

Unless the sample area is restricted to lithologies of middle and low background values, and mineralization has not occurred, the upper portion of the total distribution should indicate areas of real interest. Thus, the first rule of thumb for the 'old masters' was that the upper 10% of the sample distribu-

tion indicates the anomalous areas (J. M. Botbol, 1968, personal communication). This method makes false anomalies if no significant anomalies are present; the sampled area must have anomalies related to the formation of ore. Selection of a proper area is, of course, one of the fundamental responsibilities of the geologist.

A pilot survey around a known deposit or district is highly recommended to determine thresholds for elements of interest. Unfortunately, this type of study is not always feasible. The most common problems are lack of time or lack of a suitable test area.

After emphasizing 'that statistical methods should be used solely as a disciplinary guide', Hawkes and Webb[47] recommended estimation of the threshold of significance at two standard deviations above the median. The median is defined as the middle value after casting out the erratic high values. This is equivalent to selecting the threshold just below the upper $2^1/_2$% of the remaining values, and thus the method is generally not appropriate for detailed surveys in selected target areas.

A slightly more sophisticated method is applicable to any distribution whether normal, lognormal or otherwise. The Tchebycheff Inequality guarantees that at least 75% of the distribution will fall within two standard deviations of the mean and 89% within three standard deviations.[48] As with other arbitrary methods, it is well to examine a histogram of the data and consider the geology of the sampled area before accepting these guidelines.

A more refined method of plotting distributions on logarithmic probability paper gives a visual basis for separating mixed populations.[49] In the ideal case an optimum number can be selected that separates background values from those which represent mineralization. A straight line may indicate a single (background) distribution, but is also invariably obtained by mixing several distributions in surveys covering large areas. As an aid to determining the number of lines to fit a probability plot Lepeltier[50] gave a method for placing confidence limits on a line.

When the cumulative probability line has one or more inflection points the method of Sinclair[51] may be used to separate the populations and show their overlap. The advantage is obvious. If a two standard deviation rule is employed to define an anomaly in a population with 10 or 20% of its samples affected by a mineralizing process, most of the truly anomalous samples are interpreted as insignificant.

Most elements are properly plotted on lognormal, rather than normal, probability paper. Although many geochemical distributions are not truly lognormal, a few are more closely approximated by a normal distribution. A signal exception to the approximation of lognormality is the distribution of pH values that should be plotted on normal probability paper. These values, the negative logarithm of the hydrogen ion activity, are already log-transformed into a normal distribution.

Rose and co-workers [52] gave a good discussion of methods for selecting threshold values, including recognition of anomalous clusters on a map. Although much progress has been made in the science of defining anomalous levels, there is still an element of art in the process. Normally, a compromise should be struck from several methods.

Interpretation of results

In plotting results it may not be necessary to show or contour all values, but all sites do need to be plotted on the map. Values may be shown by symbols for anomalous, marginal and background categories. Thus, all adjacent sites on or above a specified threshold are outlined as an anomalous 'field', commonly partly surrounded by a marginal field.

In the simpler cases several pathfinders will collectively point to significant targets. In all cases, of course, the significance of the several elements must be interpreted in terms of the geology, and preferably with a model or ideal situation in mind. One should be flexible in constructing a model: it will usually be a creative composite of known situations and feasible alternatives. Adjacent anomalies need not fit the same model any more than adjacent mines need to reveal the same history of mineralization.

Large data arrays are encouraged by inductively coupled plasma atomic emission spectrometry because 20–30 elements can be obtained at a cost equivalent to that for a few elements by other means. Moreover, the average accuracy is better than for atomic absorption spectrophotometry, and output is computer-compatible without human interaction.

In a large survey a great deal of effort can be saved by computerizing the data base. This allows rapid machine plotting of all data, including maps, histograms and probability plots. Error checks can be run automatically on both field data and laboratory results. To specify samples for laboratory reruns or field resampling, samples that would not be obviously unusual by inspection of the multivariate data can be identified with a principal components test.[53] When thresholds are poorly established, each element can be contoured separately and significant levels inferred from interpretation around areas that are known to be mineralized.

Multiple regression may be used to remove confusing components from multi-element geochemical data, enhancing weak anomalies. Rose and co-workers[54] improved the resolution of significant anomalies in stream-sediment results by adjusting for (1) lithologies cropping out in the drainage basin and (2) scavenging by iron and manganese oxides.

Table 5 Ordered factor pattern matrix for results from well water

Factor 1		Factor 2		Factor 3		Factor 4		Factor 5	
SO_4	.87	Se	.08	Total alkalinity	.97	Se	.91	SO_4	.17
Conductivity	.85	Total alkalinity	.02	Bicarbonate	.93	Total alkalinity	.04	Conductivity	.15
U	.28	Bicarbonate	.01	U	.26	B	.04	pH	.05
B	.17	As	−.04	As	.11	As	.03	Se	.00
Se	.04	Ba	−.19	Ba	.09	Bicarbonate	.01	Total alkalinity	−.10
Mo	−.01	pH	−.19	V	.09	Conductivity	−.01	Bicarbonate	−.10
As	−.15	SO_4	−.19	Mo	.08	V	−.05	Ba	−.13
V	−.21	U	−.24	Se	.06	pH	−.06	B	−.15
Total alkalinity	−.23	Conductivity	−.38	Conductivity	−.19	SO_4	−.11	Mo	−.16
pH	−.27	V	−.41	B	−.19	Ba	−.12	U	−.25
Bicarbonate	−.29	B	−.82	pH	−.29	Mo	−.16	V	−.67
Ba	−.63	Mo	−.86	SO_4	−.29	U	−.19	As	−.89

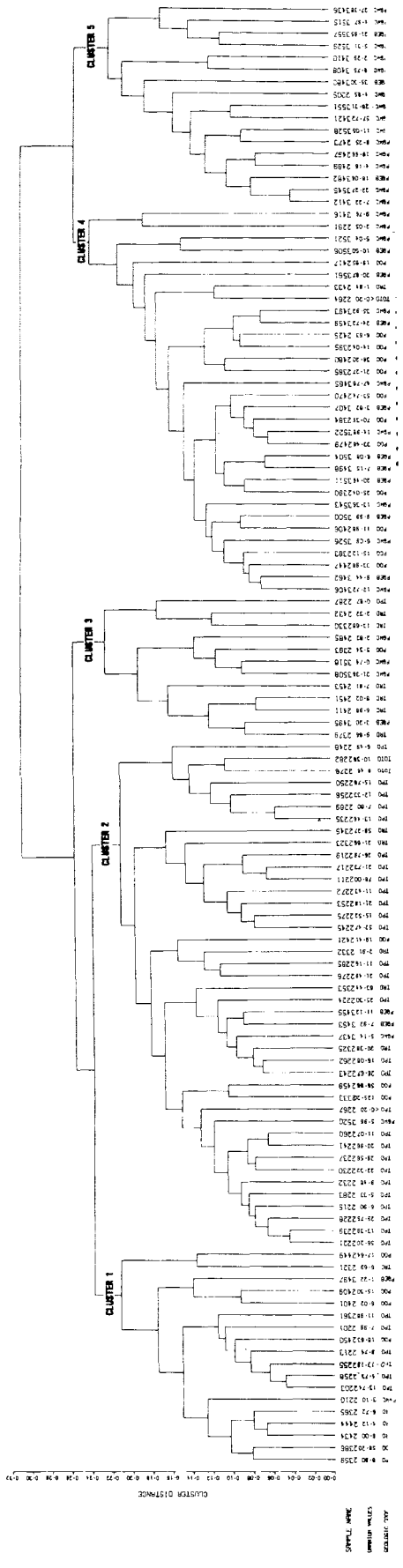

Fig. 8 Dendrogram for 121 samples of well water based on sum of weights for 10 significant elements from ordered factor pattern matrix

Universal kriging is a large and growing field within geostatistics. In spite of titles about applications to exploration,[55,56] the practice of 'regionalized variables' begins with the analysis of drilling results from an orebody—a subject beyond the scope of this paper.

Factor analysis is widely used in geology[57] to reveal the underlying components of data that can be expressed as a matrix. Typically, the matrix has along one axis a set of sample numbers and along the other several characteristics than can be quantified. In exploration geochemistry a matrix might consist of 10 or 15 measurements for hundreds or even thousands of samples.

The problem is to define mathematical factors composed of different weights of the elements in each sample that can be used to regenerate the original matrix. A perfect fit occurs when the number of factors equals the number of elements, but in this case nothing is accomplished in simplifying the matrix.

Ten of 15 factors, however, might explain 99% of the original data, and six factors 95%. In this case five factors contribute essentially no information to the geochemical processes that operate on the data and can be dropped from subsequent consideration. Four additional factors are probably also not significant.

Invariably, the few factors that explain most of the data can be related to geochemical processes. In Table 5 five factors explain 82% of a total matrix of 121 groundwater samples and 12 determinations. Elements of low significance in each factor occur between the horizontal bars. The remaining parameters suggest the geochemical process represented by each factor: (1) the maturity of the water, (2) the tendency for elements to become mobilized, (3) the tendency for the water to become alkaline, (4) the tendency for selenium to go into solution if available and (5) the large-scale occurrence of pathfinder elements for uranium.

Uranium, which is influenced by all these processes, is not important in all of them (Table 5). If the samples are clustered by weights from a simplification of the factor loadings shown, the arrangement looks something like Fig. 8.

When these clusters are plotted on a map the groupings suggest areas where uranium in saline water is unrelated to mineralization and where redox fronts should lie based on belts of mobile elements (oxidized zones) and other adjacent groups of favourability indicators.[5] The interpretation is further strengthened by dramatic decreases in dissolved uranium down the hydrologic gradient and other details of geochemical contrast between wells. The original contour plot of uranium values gave little hint of the geochemical processes that operated on the groundwater.

Good introductions to factor analysis were given by Koch and Link,[58] Klovan[59] and Jöreskog and co-workers.[57] Nichol and co-workers were pioneer practitioners in the use of factor analysis for the interpretation of geochemical data and wrote a milestone paper on its application to stream sediments.[36]

Two limitations of factor analysis were put forward by Nichol:[60] the number of factors cannot be more than the number of variables measured and processes significant to the interpretation of the survey must be reflected in the distribution of the variables selected. Ordinarily, at least six parameters should be measured—except for the smallest surveys with the simplest exploration models.

A purer form of factor analysis, called correspondence analysis, provides an unbiased interpretation of the structure of a multidimensional cloud of data points. It eliminates cumbersome steps that influence the results according to the subjective ability of the geochemist. Among these steps are assigning factor loadings, selecting the significance cutoff of factors to be used, selecting the cluster level for plotting sample groups and, after a preliminary interpretation of the results, going back through the judgement process in an attempt to improve these results.

Correspondence analysis is more direct in its approach, without imposing assumptions on the process of data manipulation. It deals strictly with the Euclidean distances between groups of n-dimensional points without the restrictions of hierarchical classification of the samples.[61]

As elucidated by David and co-workers,[62] the breakthrough is combining R-mode (variable) and Q-mode (sample) analysis in one operation that is much simpler than Q-mode analysis alone. The resulting factors, which simplify the description of the cloud of multidimensional data points, represent the combinations of variables that are related to the geochemical processes that cause the measured distributions of the data points.

Thus, a map with contours on the influence of a factor in each sample shows the relative geographic importance of each geochemical process. To further understand the relationship between the factors they may be plotted as multidimensional representations in a plane of the principal axis of any two factors, usually two that are dominant.

Exploration models

Every explorationist appreciates the necessity of a good working model that explains in some detail the genesis and recognition criteria of the type of mineralization for which he searches. Subtle features that distinguish sub-economic mineralization from real orebodies are quite important, as it becomes increasingly expensive to test the application of a model to ever blinder targets and as competitive activity reduces the time available to find, recommend and acquire properties.

Geochemical model for roll-front deposits

For decades the uranium literature has tended to emphasize the difference between types of sandstone deposits. Articles that described deposits, or abstracted salient features from several deposits into an exploration model, rightly emphasized stratigraphy, structure, source of uranium and host rock alteration. These subjects were reviewed earlier. A generalized geochemical model is to be presented for groundwater associated with a roll front, but let us first consider reducing and oxidizing agents and the zonation of metals in the reduced ground.

Reducing agents

The concepts that organic remains are associated with reduced ground and that these remains are also associated with uranium deposits are very old. Even before these two concepts were combined with the realization that large uranium deposits should be found below the level of surface oxidation, shallow oxidized deposits were known to be associated with logs and other vegetative remains.

Another old concept is that sulphide minerals indicate reduced conditions. In the usual case sulphide minerals, especially those of iron, occur closely associated with the mineralization of uranium and associated elements.

Organic material Schmidt-Collerus is a leader in the study of organic materials in uranium deposits. His latest comprehensive tome[63] provided details of the evolution of organic compounds, their migration, complexing and chelation of uranium, their degradation by anaerobic bacteria and the mechanism for the ultimate development of uraninite or coffinite. An excellent review of the origin of organic material and its importance in ore formation in the Grants region was given by Adams and Saucier.[64] The ores of this region are the outstanding example of the efficiency by which uranium is accumulated by and incorporated into organic material of humic affinity. This material is also involved in such alteration phenomena as corrosion of quartz, replacement of feldspars and alteration of clays.

Adams and Saucier[64] summarized the importance of

organics in the Grants region: 'The uranium mineralization is everywhere co-extensive with the humic organic matter in the standstones. The uranium is much more often associated with the unstructured humate than with the carbonized plant debris. . . . .Humic matter is approximately equal to the uranium content in weight percent. . . . Because the organic material is so much lighter, it is greatly in excess over uranium in volume, and therefore, it is primarily responsible for the dark gray to black colors of the ores. Because of the high geochemical enrichment factor for uranium, it takes only a small amount of humic material to accumulate uranium to ore grade'. They went on to stress the role of humic substances in the transportation, concentration and preservation of uranium.

Organic carbon has long been regarded as a precipitating agent for uranium, but all carbonized wood and trash does not accumulate and retain uranium, even when the element is suitably available.[64] Barren carbonaceous material associated with uranium mineralization has been found to be leached of the active ingredients, fulvic and humic acids.

A well-developed model for the origin of deposits in the Morrison Formation (Jurassic) near the Henry Mountains of Utah emphasized the significance of organic acids: 'Humic and fulvic acids generated in the offshore muddy sediments of humus-bearing lakes were expelled by compaction or seepage into nearby sandstone beds where the organic acids were fixed as tabular humate deposits. Subsequently, uranium-bearing ground water passed through the sandstone where the humate fixed and concentrated the uranium, forming tabular sandstone uranium deposits'.[65] Perhaps the close association of organic carbon with ore in the Gas Hills district of Wyoming[66,67] also involves unstructured humates.

Hydrogen sulphide The sandstone uranium deposits of Texas are noted for the negligible quantities of organic material.[68] The principal reducing agent—hydrogen sulphide—evolved from intense reduction by anaerobic bacteria. Examples are hydrogen sulphide associated with upward leakage of hydrocarbons, as at the Felder deposit,[69] or derived from the cap of a salt dome, as at the Palangana deposit, also in the Gulf Coast of Texas.

Thus, the reducing mechanism of these deposits is driven biochemically, analogous to the geochemical cells described in Wyoming.[12] In a salt dome the sulphur comes from anhydrite, which hydrates to gypsum. After the gypsum dissolves in the groundwater the sulphate is reduced by bacteria, and available iron combines with hydrogen sulphide to form pyrite.

In addition to reactions dominated by ions in solution, hydrogen sulphide can cause iron–titanium oxides to be replaced by pyrite—a useful guide to mineralization.[70,71] Pyrite and marcasite are more the indicators of a favourable reducing environment than the reducing agents for uranium and its associated metals, including iron.

Oxidizing agents

Just as bacteria are of immense significance in creating the intense environment of reduction for uranium, they are probably critical in explaining the remarkable mobilization and bleaching that is sometimes found on the oxidized side of a geochemical cell.[12] Given the limited rate of inorganic oxidation of sulphides by meteoric water, Hoag and Webber[72] showed that oxidizing bacteria create a low pH and dominate the production of sulphate in groundwater associated with gossans. In the case of roll fronts the environment is intense enough to dissolve feldspars, corrode quartz grains and leave kaolinite.

Zonation

It is axiomatic that what precipitates in a roll front is largely dependent on what is available to the system. The redox boundary of a roll front is taken as the line, sometimes very sharp, between the oxidized (and commonly bleached) facies and the dark reduced zone of pyrite and associated metallic minerals. The formation of marcasite is favoured over pyrite when the pH is less than about 6 and when elemental sulphur is present.[73]

'Conditions that favor marcasite as the dominant ore-stage iron disulfide are most likely to arise in non-carbonaceous rocks. In rocks with considerable organic matter "the presence of polysulfide ions and pH buffering by anerobic bacterial metabolic processes apparently lead to the formation of ore-stage pyrite." In the preceding descriptions of the Wyoming roll-type deposits, we have noted that most of the ore-stage iron sulfide minerals are pyrite—a clear implication that biochemical activity was responsible for reduction of the deposits. Austin (1970) [see reference 75] reached a similar conclusion based on his sulfur isotope studies of the Wyoming deposits, noting the well-defined oxidation-reduction interface for iron, the lack of identification of intermediate sulfur species resulting from non-biochemical processes, and the ubiquitous nature of sulfate-reducing bacteria.'[74]

Fig. 6 is a diagrammatic sketch of the five most common metals that occur in a roll front. The metal zones usually overlap so the redox boundary between selenium and vanadium may be the only visible line. In addition, one or more of the zones is likely to be absent in any given area: for example, if vanadium is absent, uranium is found at the redox boundary with selenium.

Native selenium gives a distinctive reddish bloom,[11] whereas the overlapping grey vanadium and uranium zones are generally more distinguishable by radioactivity. Shades of brownish colour may be due to the oxidation of vanadium. In general, the darker the grey, the higher the grade of ore, though humic matter may confuse the issue. In total, the concentration of metals is greater near the redox front and decreases away from it. This includes selenium, with a concentration gradient reversed with respect to the direction of groundwater flow. Selenium concentration decreases up the hydrologic gradient.

The zone of molybdenum, which usually occurs as the sulphide, jordisite, may be separated from the uranium zone.[12] The zone most remote from the front is calcium, which precipitates as calcite in response to increasing pH. Massive pods of calcite can be enclosed by encroaching zones and may persist until they are exposed at the surface by erosion.

At both the Rifle and the Garfield mines in Colorado a thin zone of non-radiogenic galena and clausthalite, a lead selenide, lies at the redox front next to the vanadium ore.[11] This band, generally less than 1 cm in thickness, assays about 3% lead, with much lower concentrations in the ore zone. In the oxidized ground adjacent to the high lead band there is a zone of green chromium-bearing mica roughly 0.5 m thick where chromium concentration may reach a few tenths of a percent.

Although small amounts of copper do occur in uranium ore in the Uravan district, the dominant elements that are associated with uranium mineralization 'are ones that either must or can be readily transported in neutral to somewhat alkaline solutions; elements that require acid solutions for mobility, such as copper, are lacking in the ore'.[67] Harshman and Adams[74] gave an excellent summary of the geochemistry of roll fronts, including an Eh–pH diagram to explain the zonation of a roll front in terms of dissolved and solid species.

Generalized model

A generalized discussion follows of the groundwater geochemistry associated with such roll-front deposits as those which are found in Texas or Wyoming. The model is useful for exploration where wells produce water from mineralized sandstone and, in the absence of existing wells, where water is tested from holes drilled in an exploration programme. It is not very useful where the mineralized sandstone is above the water-

table, as is common in the Colorado Plateau.

This generalized model has wide application because of the similarities in groundwater geochemistry that occur in a variety of sandstone uranium deposits. Chemistry provides a powerful common denominator in spite of differing source rocks, trap structures, sandstone host facies, redox agents, scale and shape of mineralization, ages of host rocks and time of mineralization with respect to the diagenetic cycle. The model has been tested by many thousands of water samples and has been applied successfully over a period of 13 years to areas as diverse as the Texas Gulf Coast, the west flank of the San Juan Basin, New Mexico, and northwestern Nebraska.

The application of the model is greatly strengthened when several parameters fit. One need not expect all the parameters to fit any particular situation, but certain combinations are unequivocal indicators of mineralization. A target must be drilled, of course, to define its economic significance.

On the oxidized side of a mineralized roll front there is a zone of mobilization most typically marked by high concentrations of uranium, sulphate, alkalinity and total dissolved solids (Fig. 9). A decrease in these parameters on the reduced side of the front implies precipitation between wells.

No horizontal scale appears in Fig. 9 because the spacing between the axis of maximum uranium concentration in the groundwater and the axis of minimum uranium concentration as interpreted from the samples is largely a function of the sample spacing. As the sample spacing is reduced, the apparent axes move closer together and the maximum and minimum uranium values become more extreme. The distance between the two interpreted axes may be as much as 5 km or less than 100 m as the sample spacing varies over the same range.

Helium dissolved in groundwater is useful in defining a uranium target. Values greater than 200 ppb above background are probably anomalous, and may reach 10–100 times that level. The maximum helium will be measured in the first well down the hydrologic gradient from its source (Fig. 9). The rate of decline in the concentration is determined mainly by the groundwater velocity and the rate of helium leakage from the aquifer.

A consideration of other elements associated with roll-front deposits improves the accuracy and confidence in locating favourable trends (Fig. 9). Sulphate concentration and conductivity increase toward the redox front and then decrease abruptly owing to precipitation of iron sulphide, followed by calcium carbonate. High values of bicarbonate and selenium also contribute to identification of the zone of uranium mobilization on the oxidized side of the front. Molybdenum concentrations are normally associated with sandstone deposits, but haloes in the groundwater may be to the side of or farther down-dip than the centre of the geochemical cell. Arsenic is most valuable for its regional halo around areas of mineralization.

As with the uranium and helium curves shown in Fig. 9, there is no scale for the Eh and pH values because the actual numbers depend on the district and the sample spacing. As a rule the Eh lies within a few hundred millivolts of zero. The pH will usually range between 5 and 9 with the mode of the distribution greater than 7 in arid climates and less than 7 in temperate zones.

Owing to slightly greater asymmetry in the curve, Eh, if properly measured, is more valuable than pH as an indicator of the direction to a redox front. The Eh and pH curves show sharp

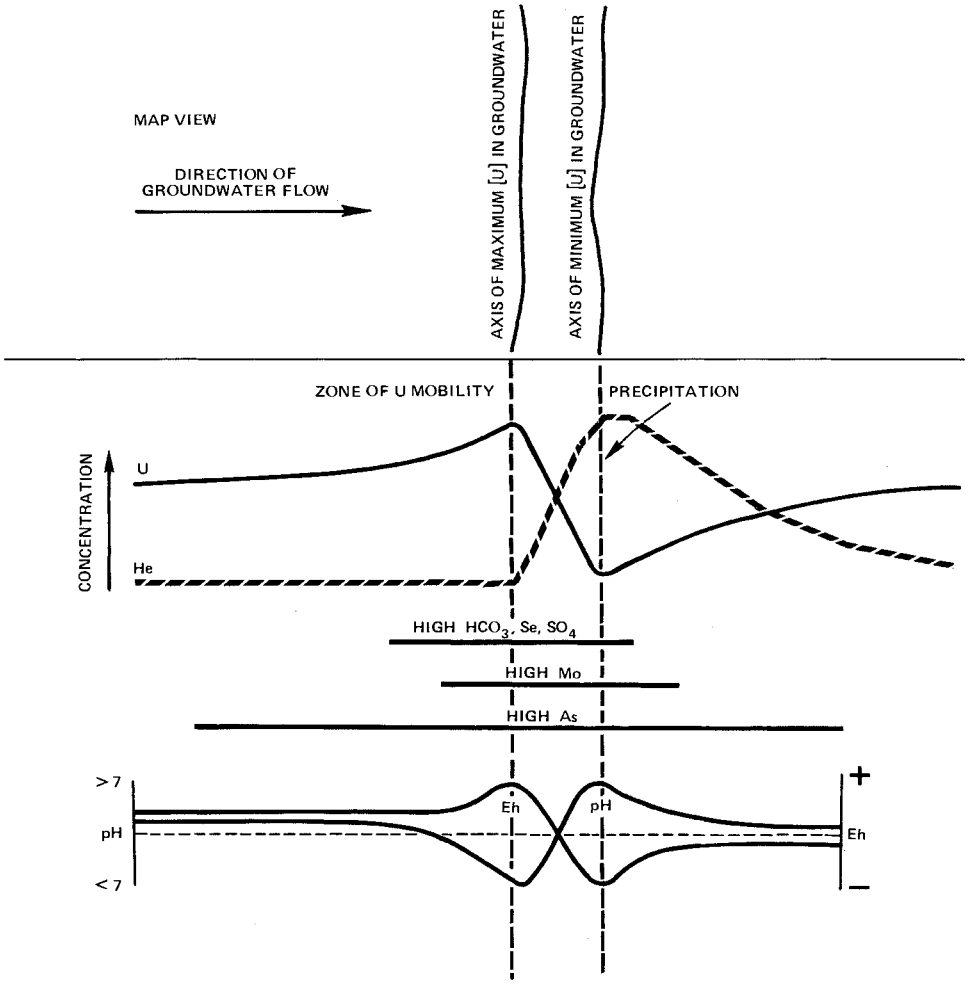

Fig. 9 Geochemical model for groundwater associated with U mineralization

reversals in the vicinity of a redox front (Fig. 9). At a sample spacing of 5 km evidence of one side of the redox front is likely to be missed, so the *S*-shape becomes a simple peak or trough. For example, proximity to a front may be indicated by a drop in pH without any unusually high values. The key is to look for sharp changes in adjacent wells that produce from the same aquifer.

Based on results from Texas and Wyoming, 'radiogenic radium and radon are excellent short-range indicators of uranium mineralization'.[76] Radon greater than 1000 pCi/l may indicate zones of economic significance.[19]

At a sample spacing of 5 km very few wells will be near a redox front. Nevertheless, with a proper model and knowledge of the hydrologic gradient the position of a front is quite interpretable.[5]

The axis of maximum uranium concentration, plotted in Fig. 9 for samples collected on a scale of kilometres, is generally not the correct trend to lease. Attention should be focused on the area between the maximum and minimum uranium concentration and the edge of the area where wells bear even a trace of hydrogen sulphide.

A target area is most closely defined by sharp changes in pH and Eh (or dissolved oxygen) and by dissolved radon and radium. The latter two elements may be used to calculate the minimum product of grade times thickness that could produce the anomaly. The most conservative assumption is that the well penetrates the centre of the mineralization. The farther the water travels to the well, the larger is the uranium source for a measured concentration of radon.

The most recent development in sophisticated geochemical indicators of mineralization is Langmuir's saturation index (*SI*). The method yields a measure of the stability of uranium-bearing and associated minerals based on pH, Eh and major and trace elements in the groundwater. 'Positive SI values for uraninite or coffinite are . . . strong indicators of the nearby presence of ore, as are positive SI values for the reduced phases of As, Mo, and Se. Regional trends in uraninite or coffinite SI values may exist, and should help locate possible ore zones even if no samples are close enough to the ore to show positive SI values for these phases.'[19]

Geochemical modelling will probably be the most useful technique in delineating the next generation of exploration targets. Its utility for near-surface mineralization related to the current hydrologic cycle is established. In addition, deeper targets, located well below the water-table and possibly well within reduced ground, may be found by testing water from exploration drill-holes.

Radiogenic helium, radon and radium, each with a different mechanism of migration, should be effective even in completely reduced systems. Examples of these occurrences are tabular Colorado Plateau type deposits related to reducing conditions in a palaeo-river bed and rereduced host rocks where roll fronts are no longer in proximity to surface oxidation.

Geologic model for vein-like deposits

The term 'vein-like' is used to distinguish the unconformity-related deposits of Lower and Middle Proterozoic age from the classical vein deposits of, for example, Beaverlodge in Saskatchewan, Schwartzwalder in Colorado and the Massif Central in France. At a mining and milling cost of $50/lb 5% of reasonably assured Western world resources are of the classical vein type and 16% of the unconformity type.[77] Subsequent to the 1968 discovery of the Rabbit Lake deposit in Saskatchewan and the 1970 discovery of the East Alligator Rivers district in the Northern Territory of Australia the vein-like deposits were found to have an average grade and tonnage of contained uranium that greatly surpassed that of sandstone deposits.

Because of the scope of this paper, only generalized statements of an introductory nature can be made about vein-like deposits. As might be expected from such a recently discovered deposit type and its economic importance, exploration models are evolving rapidly. Much more information will be developed as the deposits are mined. Given the current incomplete knowledge, a masterly synthesis of the vein-like Proterozoic deposits of the world was provided by Dahlkamp and Adams.[14] Their genetic classification, though presented provisionally, is a quantum jump in the understanding of these deposits.

Generalized model

Although this section refers to unconformity-related vein-like deposits, in the most general sense there are some striking similarities to the classical vein deposits. Both bear pitchblende in zones of structural ground preparation and exhibit retrogressively metamorphosed and chloritized metasediments, sulphides and sulpharsenides, and pervasive hematization. In a broad sense the paragenesis of these deposits involves hematization, chloritization, pitchblende mineralization and the deposition of sulphides, carbonates and quartz. Origins for hematite and chlorite were suggested by McMillan[6] in his summary of metamorphic and weathering reactions. Pitchblende is habitually associated with graphitic or chloritic schists or with carbonates.

It may come as a surprise that, when groundwater can be sampled, there is a remarkable similarity between the geochemical model described for sandstone deposits and the geochemistry of vein-like deposits. When the mineralization lies near the groundwater-table, water sampled on a scale of kilometres gives similar results for these two diverse cases in uranium, molybdenum, arsenic, radon, helium, sulphate, total dissolved solids, pH and alkalinity.

Referring more strictly to vein-like deposits, Dahlkamp and Adams[14] noted features in common for all the deposits in Saskatchewan and the Northern Territory of Australia: 'They occur in metasediments which were (a) originally deposited upon Archean granitic basement in upper Lower Proterozoic time, (b) metamorphosed between about 1700 to 1900 m.y. ago, and (c) then covered by Middle Proterozoic continental sandstones, in part after a period of strong weathering'.

Favourable features common to vein-like districts associated with the Lower to Middle Proterozoic unconformity were given by Dahlkamp and Adams.[14] Where Lower to Middle Proterozoic uraniferous sediments are present several recognition criteria are regarded as favourable indicators for the occurrence of vein-like deposits: (1) a preexisting source of uranium, such as Archaean granitoids; (2) favourable host rocks, especially carbon-rich metasediments composed of mixed pelites, psammites and carbonate rocks; (3) alteration, like albitization, magnesium, boron and lithium metasomatism, and magnesium and iron chloritization; (4) an unconformity, preferably overlain by sandstone; (5) a well-developed regolith; and (6) proximity to an Archaean dome.

Most vein-like deposits are in or near a series of graphitic mica schists, biotite–garnet schists, and dolomitic marbles, which are the metamorphic equivalents of marine sediments marginal to Archaean granite–gneiss complexes.[77] The host rocks are then syngenetically and diagenetically enriched in uranium and other elements provided by the chemically diverse sediments. Sub-economic sedimentary preconcentrations are subsequently metamorphically upgraded in the amphibolite facies near migmatized sedimentary rocks and reactivated Archaean granitoid domes. The smaller deposits, such as Rum Jungle, tend to occur in the greenschist facies. Subsequent supergene enrichment during chemical weathering on the unconformity appears to be important in the Key Lake deposit

but not generally in other deposits. Most of the highest-grade orebodies were formed by remobilization under a thick sandstone cover.

Additional recognition criteria[78] include proximity of high-grade metamorphism and a covering sandstone. Nash granted that 'supergene enrichment can upgrade the ores', but concluded 'that these deposits can form without processes operating at the paleosurface' and played down the importance of the age of the rocks in favour of a wider application of geochemical processes.

One of the more controversial problems in explaining the genesis of the vein-like deposits is the amount of mineralization in the overlying sandstone. The most unusual model to explain this distribution is based on the conductivity of the steeply dipping graphitic zones that extend from the oxidized sandstone above the unconformity into intensely reduced metasediments. Tilsley[79] hypothesized that the resulting galvanic cell causes ionic movement and precipitation of metals near the upper pole. After the orebody is formed and covered by a thick accumulation of basin sediments, radiogenic heat drives a geothermal cell that redistributes uranium into the base of the sandstone.

Hoeve and Sibbald[80,81] reviewed the arguments of the near-surface supergene school and the magmatic and metamorphic hydrothermal school and concluded that a diagenetic-hydrothermal model provides a better fit to the observations: 'The model envisions that at elevated temperatures and under a thick sedimentary cover, oxidizing diagenetic solutions of the Athabasca Formation penetrated the metamorphic basement along breccia and fault zones and reacted with graphitic rocks to yield reducing solutions containing carbon dioxide and methane'. Uranium was precipitated next to the graphitic metapelite, where oxidizing groundwater became reduced, and above, where methane-bearing solutions mixed with oxidized diagenetic solutions that carried ore constituents. The remarkable lateral deflection of the upper orebodies at Key Lake and Collins Bay appears to reflect the direction of movement of groundwater in the basal Athabasca Formation at the time of ore deposition.

Summary

This paper provides a general review of exploration methods for major types of uranium deposits. The author has been active in exploration for deposits hosted by rocks of Precambrian, Palaeozoic, Mesozoic and Caenozoic age. Much of this work involved deposits in sandstones, but the geochemical principles also apply to many of the Precambrian deposits.

Acknowledgement

A. A. Levinson, A. W. Rose and S. S. Adams must be thanked for their very helpful comments.

References

1. Rogers J. J. W. and Adams J. A. S. Thorium and uranium. In *Handbook of geochemistry* Wedepohl K. E. ed. (Berlin, etc.: Springer, 1978, **II–V**, pt 90, 39 p. and pt 92, 50 p.
2. Nichols C. E. *et al.* Uranium geochemical survey in the Crystal City and Beeville quadrangles, Texas. *Open File Rep. U.S. Dep. Energy* GJBX-19(77), 1977, 326 p.
3. Nichols C. E. *et al.* Wide-spaced uranium geochemical survey in the Plainview, Lubbock, and Big Spring quadrangles, Texas. *Open File Rep. U.S. Dep. Energy* GJBX-73(78), Dec. 1977, 229 p.
4. Nichols C. E. *et al.* Hydrogeochemical and stream sediment pilot survey of Llano area, Texas. *Open File Rep. U.S. Dep. Energy* GJBX-36(76), 1976, 152 p.
5. Nichols C. E. *et al.* Northwest Texas pilot geochemical survey. *Open File Rep. U.S. Dep. Energy* GJBX-60(76), 1976, 227 p.
6. McMillan R. H. Genetic aspects and classification of important Canadian uranium deposits. In *Short course in uranium deposits: their mineralogy and origin* Kimberley M. M. ed. (Toronto: The University Press for Mineralogical Association of Canada, 1978), 187–204.
7. Mickle D. G. ed. A preliminary classification of uranium deposits. *Open File Rep. U.S. Dep. Energy* GJBX-63(78), May 1978, 77 p.
8. Mickle D. G. and Mathews G. W. eds. Geological characteristics of environments favorable for uranium deposits. *Open File Rep. U.S. Dep. Energy* GJBX-67 (78), Nov. 1978, 250 p.
9. Mathews G. W. *et al.* Preliminary recognition criteria for uranium occurrences: a field guide. *Open File Rep. U.S. Dep. Energy* GJBX-32(79), Feb. 1979, 47 p.
10. Shockey P. N. Renfro A. R. and Peterson R. J. Copper–silver solution fronts at Paoli, Oklahoma. *Econ. Geol.*, **69**, 1974, 266–8.
11. Fischer R. P. Vanadium–uranium deposits in the Rifle Creek area, Garfield county, Colorado. *Bull. U.S. geol. Surv.* 1101, 1960, 52 p.
12. Rackley R. I. Environment of Wyoming Tertiary uranium deposits. *Mountain Geol.*, **9**, no. 2–3 1972, 143–57.
13. Ruzicka V. Geological comparison between East European and Canadian uranium deposits. *Pap. geol. Surv. Can.* 70-48, 1971, 196 p.
14. Dahlkamp F. J. and Adams S. S. Geology and recognition criteria for veinlike uranium deposits of the Lower to Middle Proterozoic unconformity and strata-related types. *Open File Rep. U.S. Dep. Energy* GJBX-5(81), Jan. 1981, 253 p.
15. Stuckless J. S. *et al.* Geochemical and petrological studies of an uraniferous granite from the Granite Mountains, Wyoming. *J. Res. U.S. geol. Surv.*, **5**, 1977, 61–81.
16. Rich R. A. Holland H. D. and Petersen U. *Hydrothermal uranium deposits* (Amsterdam, etc.: Elsevier, 1977), 264 p.
17. Dahlkamp F. J. Typology and geographic/geotectonic distribution of uranium deposits. In *Energy resources* Burollet P. F. and Ziegler V. eds (Paris: Edition Technip, 1980), 499–536. (*26th Int. geol. Congr., Colloque* C2)
18. Jennings J. K. and Leventhal J. S. A new structural model for humic material which shows sites for attachment of oxidized uranium species. In *Short papers of the U.S. Geological Survey uranium–thorium symposium, 1977* Campbell J. A. ed. *Circ. U.S. geol. Surv.* 753, 1977, 10–11.
19. Wanty R. B. Langmuir D. and Chatham J. R. Ground water prospecting for sandstone-type uranium deposits; the merits of mineral–solution equilibria versus single element tracer methods, volume II. *Rep. U.S. Dep. Energy* GJO 79-360-E, 1981, 91 p.
20. Bosschart R. A. and Pemberton R. H. Applications and limitations of airborne electromagnetic systems in mineral exploration. *Min. Canada*, **42**, May 1969, 19–28.
21. Morley L. W. and Bhattacharyya B. K. Quantitative treatment of aeromagnetic data in mineral areas. *Can. Min. metall. Bull.*, **59**, 1966, 733–42.
22. Spector A. Aeromagnetic map interpretation with the aid of the digital computer. *Can. Min. metall. Bull.*, **64**, July 1971, 27–33.
23. Paterson N. R. Airborne electromagnetic methods as applied to the search for sulphide deposits. *Can. Min. metall. Bull.*, **64**, Jan. 1971, 29–38.
24. Palacky G. J. Interpretation of INPUT AEM measurements in areas of conductive overburden. *Geophysics*, **40**, 1975, 490–502.
25. Scott W. J. and Fraser D. C. Drilling of EM anomalies caused by overburden. *Can. Min. metall. Bull.*, **66**, July 1973, 72–7.
26. Lazenby P. G. New developments in the INPUT airborne EM system. *Can. Min. metall. Bull.*, **66**, April 1973, 96–104.
27. Palacky G. J. and West G. F. Quantitative interpretation of INPUT AEM measurements. *Geophysics*, **38**, 1973, 1145–58.
28. Palacky G. J. Use of decay patterns for the classification of anomalies in time-domain AEM measurements. *Geophysics*, **41**, 1976, 1031–41.
29. Levinson A. A. *Introduction to exploration geochemistry* (Calgary, Alberta: Applied Publishing Ltd., 1974), 612 p.
30. Dyck W. Uranium, radon, helium and other trace elements and gases in well waters of parts of the St. Lawrence lowlands (Ottawa region), Canada. *J. geochem. Explor.*, **13**, 1980, 27–39.
31. Stuckless J. S. and Nkomo I. T. Uranium–lead isotope systematics in uraniferous alkali-rich granites from the Granite Mountains, Wyoming; implications for uranium source rocks. *Econ. Geol.*, **73**, 1978, 427–41.
32. Rosholt J. N. Zartman R. E. and Nkomo I. T. Lead isotope systematics and uranium depletion in the Granite Mountains, Wyoming. *Bull. geol. Soc. Am.*, **84**, 1973, 989–1002.
33. Price T. J. Callihan M. C. and Young R. G. Pedro Mountain drill-

ing project, Carbon county, Wyoming. *Open File Rep. U.S. Dep. Energy* GJBX-56(76), 1976, 19 p.
34. Stuckless J. S. Uranium and thorium concentrations in Precambrian granites as indicators of a uranium province in central Wyoming. *Contrib. Geology, Univ. Wyo.*, **17**, no. 2 1979, 173–8.
35. Rosholt J. N. and Bartel A. J. Uranium, thorium and lead systematics in Granite Mountains, Wyoming. *Earth Planet. Sci. Lett.*, **7**, 1969, 141–7.
36. Nichol I. Garrett R. G. and Webb J. S. The role of some statistical and mathematical methods in the interpretation of regional geochemical data. *Econ. Geol.*, **64**, 1969, 204–20.
37. Chaffee M. A. Botbol J. M. and Hamilton J. C. The distribution of selected elements in stream sediments, central Maine. *Open File Rep. U.S. geol. Surv.*, 1972, 8 p.
38. Dyck W. Field and laboratory methods used in the Geological Survey of Canada in geochemical surveys, no. 10: radon determination apparatus for geochemical prospecting for uranium. *Pap. geol. Surv. Can.* 68-21, 1969, 30 p.
39. Morse R. H. Getting the most out of radon geochemistry: abstract. *Bull. Am. Ass. Petrol. Geol.*, **64**, May 1980, 754.
40. Morse R. H. Radon counters in uranium exploration. In *Exploration for uranium ore deposits: proceedings of a symposium, Vienna, 1976* (Vienna: IAEA, 1976), 229–39.
41. Barretto P. M. C. Radon-222 emanation characteristics of rocks and minerals. In *Radon in uranium mining: proceedings of a panel, Washington, D.C., December 1973* (Vienna: IAEA, 1975), 129–50.
42. Morse R. H. Wealth of field experience becomes available to help fine-tune portable radon detectors. *North. Miner*, **64**, March 8 1979, C12–13.
43. Czarnecki R. F. Pacer J. C. and Freeman R. W. Advances in radon exploration techniques for uranium: abstract. *Bull. Am. Ass. Petrol. Geol.*, **64**, May 1980, 695.
44. Pogorski L. A. and Quirt G. S. Helium surveying for deeply buried uranium deposits: abstract. *Bull. Am. Ass. Petrol. Geol.*, **64**, May 1980, 766–7.
45. Erdman J. A. and Harrach G. H. Uranium in big sagebrush from western U.S. and evidence of possible mineralization in the Owyhee Mountains of Idaho. *J. geochem. Explor.*, **14**, 1981, 83–94.
46. Vijan P. N. *et al.* A semi-automated method for the determination of arsenic in soil and vegetation by gas-phase sampling and atomic absorption spectrometry. *Analyt. chim. Acta*, **82**, 1976, 329–36.
47. Hawkes H. E. and Webb J. S. *Geochemistry in mineral exploration* (New York: Harper and Row, 1962), 415 p.
48. Bowker A. H. and Liberman G. J. *Engineering statistics* (Englewood Cliffs, N.J.: Prentice-Hall, 1959), 585 p.
49. Tennant C. B. and White M. L. Study of the distribution of some geochemical data. *Econ. Geol.*, **54**, 1959, 1281–90.
50. Lepeltier C. A simplified statistical treatment of geochemical data by graphical representation. *Econ. Geol.*, **64**, 1969, 538–50.
51. Sinclair A. J. Selection of threshold values in geochemical data using probability graphs. *J. geochem. Explor.*, **3**, 1974, 129–49.
52. Rose A. W. Hawkes H. E. and Webb J. S. *Geochemistry in mineral exploration, 2nd edn* (London, etc.: Academic Press, 1979), 657 p.
53. Kane V. E. Baer T. and Begovich C. L. Principal component testing for outliers. *Open File Rep. U.S. Dep. Energy* GJBX-71(77), 1977, 77 p.
54. Rose A. W. Dahlberg E. C. and Keith M. L. A multiple regression technique for adjusting background values in stream sediment geochemistry. *Econ. Geol.*, **65**, 1970, 156–65.
55. David M. Geostatistics—bloodhound of uranium exploration. *Can. Min. J.*, **100**, May 1979, 111–3.
56. Journel A. G. Geological reconnaissance to exploitation—a decade of applied geostatistics. *Can. Min. metall. Bull.*, **68**, June 1975, 75–84.
57. Jöreskog K. G. Klovan J. E. and Reyment R. A. *Geological factor analysis* (New York, etc.: Elsevier, 1976), 178 p.
58. Koch G. S. Jr. and Link R. F. *Statistical analysis of geological data, vol. II* (New York, etc.: Wiley, 1971), 438 p.
59. Klovan J. E. R- and Q-mode factor analysis. In *Concepts in geostatistics* McCammon R. B. ed. (New York, etc.: Springer, 1975), 21–69.
60. Nichol I. The role of computerized data systems in geochemical exploration. *Can. Min. metall. Bull.*, **66**, Jan. 1973, 59–68.
61. Froidevaux R. Jaquet J. M. and Thomas R. L. AGCL, a Fortran IV program for agglomerative, nonhierarchical Q-mode classification of large data sets. *Computers Geosci.*, **3**, no. 1-C 1977, 31–48.
62. David M. Dagbert M. and Beauchemin Y. Statistical analysis in geology: correspondence analysis method. *Colo. Sch. Mines Q.*, **72**, no. 1 1977, 60 p.
63. Schmidt-Collerus J. J. Investigation of the relationship between organic matter and uranium deposits. *Open File Rep. U.S. Dep. Energy* GJBX-130(79), 1979, 281 p.
64. Adams S. S. and Saucier A. E. Geology and recognition criteria for uraniferous humate deposits, Grants uranium region, New Mexico. *Open File Rep. U.S. Dep. Energy* GJBX-2(81), 1980, 226 p.
65. Peterson F. and Turner-Peterson C. E. Lacustrine-humate model: sedimentologic and geochemical model for tabular sandstone uranium deposits in the Morrison Formation, Utah, and application to uranium exploration. *Open File Rep. U.S. geol. Surv.* 80-319, 1980, 46 p.
66. King J. W. and Austin S. R. Some characteristics of roll-type uranium deposits at Gas Hills, Wyoming. *Min. Engng, N.Y.*, **18**, May 1966, 73–80.
67. Harshman E. N. Distribution of elements in some roll-type uranium deposits. In *Formation of uranium ore deposits* (Vienna: IAEA, 1974), 169–83.
68. Adams S. S. and Smith R. B. Geology and recognition criteria for sandstone uranium deposits in mixed fluvial–shallow marine sedimentary sequences, South Texas. *Open File Rep. U.S. Dep. Energy* GJBX-4(81), 1981, 143 p.
69. Klohn M. L. and Pickens W. R. Geology of the Felder uranium deposit, Live Oak county, Texas. *AIME Preprint* 70-1-38, 1970, 19 p.
70. Reynolds R. L. and Goldhaber M. B. Origin of a South Texas roll-type uranium deposit: I. Alteration of iron–titanium oxide minerals. *Econ. Geol.*, **73**, 1978, 1677–89.
71. Goldhaber M. B. Reynolds R. L. and Rye R. O. Origin of a South Texas roll-type uranium deposit: II. Sulfide petrology and sulfur isotope studies. *Econ. Geol.*, **73**, 1978, 1690–705.
72. Hoag R. B. Jr. and Webber G. R. Significance for mineral exploration of sulphate concentrations in groundwaters. *CIM Bull.*, **69**, Dec. 1976, 86–91.
73. Goldhaber M. B. and Reynolds R. L. Origin of marcasite and its significance for understanding the genesis of roll-front uranium deposits. *Open File Rep. U.S. geol. Surv.* 79-1696, 1979, 38 p.
74. Harshman E. N. and Adams S. S. Geology and recognition criteria for roll-type uranium deposits in continental sandstones. *Open File Rep. U.S. Dep. Energy* GJBX-1(81), 1981, 185 p.
75. Austin S. R. Some patterns of sulfur isotope distribution in uranium deposits. *Earth Sci. Bull.*, **3**, no. 2 1970, 5–22.
76. Chatham J. R. Wanty R. B. and Langmuir D. Groundwater prospecting for sandstone-type uranium deposits: the merits of mineral–solution equilibria versus single element tracer methods. *Rep. U.S. Dep. Energy* GJ079-360-E, 1981, 197 p.
77. Nash J. T. Granger H. C. and Adams S. S. Geology and concepts of genesis of important types of uranium deposits. *Econ. Geol. 75th anniversary vol.*, 1981, 63–116.
78. Nash J. T. Empirical recognition criteria for unconformity-type uranium deposits applied to some Proterozoic terranes in the United States. *Open File Rep. U.S. geol. Surv.* 81-793, 1981, 18 p.
79. Tilsley J. E. Continental weathering and development of palaeosurface-related uranium deposits: some genetic considerations. In *Uranium in the Pine Creek Geosyncline: proceedings of the international uranium symposium, Sydney, 1979* Ferguson J. and Goleby A. B. eds (Vienna: IAEA, 1980), 721–32.
80. Hoeve J. and Sibbald T. I. I. Uranium concentration related to the sub-Athabasca unconformity, northern Saskatchewan, Canada. Reference 6, 475–84.
81. Hoeve J. and Sibbald T. I. I. Uranium metallogenesis and its significance to exploration in the Athabasca Basin. In *Uranium exploration techniques* Parslow G. R. ed. *Spec. Publ. Sask. geol. Soc.* no. 4, 1978, 161–88.

Uranium mineralogy

Deane K. Smith Jr.

Department of Geosciences, Pennsylvania State University, University Park, Pennsylvania, U.S.A.

Fleischer[60,61] has shown that more than 160 species can be identified that contain uranium as an essential element. In many additional species uranium is known to play a significant substitutional role. For an element as rare as uranium (2.5 ppm in the earth's crust) this large proportion of the known species—more than 5%—seems highly surprising. There are several reasons for this situation, probably the most important of which is the complex chemistry of the element, including its multiple valence states. Also, because of the energy potential, uranium has received special attention both in the exploration aspects as well as in the laboratory. With modern instrumentation even very small quantities of a phase can be adequately characterized to establish a new species. A third factor is the beautiful array of colours that is exhibited by most uranium minerals. These colours increase the interest in collecting and characterizing specimens, and subtle shade differences are often the keys to the first spotting of a new species.

Uranium is classified as a lithophile element, and its abundance in granitic rocks is about double its average crustal abundance. In fact, the weathering of granites is probably the major primary source for the uranium that presently occurs in sedimentary host rocks. Although reported to have all valence states from 2+ to 6+, only the 4+ and 6+ states are important in minerals. There is some evidence for a 5+ state both as a solution species and in some of the uranium oxides, but its role in mineral structures is not confirmed.

Uranium minerals are usually divided into two main groups—the so-called 'primary' and 'secondary' minerals. This classification was based on the initial belief that all uranium was first deposited as uraninite, which was the only really economic ore mineral, oxidation then resulting in the formation of other minerals. It is now recognized that several uranyl minerals have formed directly from source solutions without primary uraninite and produced concentrations sufficient for economic exploitation. Also, several new uranous minerals were recognized that proved to be ore minerals in some major deposits. Some minerals that are original ore minerals in one deposit are alteration products in others. Mineralogically, it is probably better to divide the uranium minerals on the basis of the valence state of the uranium. Thus, there is a 'reduced' family with U^{4+} as the dominant valence state and an 'oxidized' family in which all or most of the uranium exists as U^{6+}. Most U^{6+} minerals involve the uranyl ion UO_2^{2+}. Because of the complexity of the oxidized family the minerals are further divided chemically by use of the associated anionic group or groups. The terms 'primary' and 'secondary' should be used to describe the initially deposited and the alteration minerals, respectively.

Most uranium minerals occur in all of the several types of ore deposits. A given deposit usually has no more than two reduced minerals. The oxidized minerals that occur in the deposit depend on the Eh–pH conditions and the availability of reactive anions. In the absence of reactive anions, hydrated oxides and uranates form. The uranyl ion is, however, fairly soluble and groundwater can effectively disperse it a considerable distance from the reduced source. The uranyl minerals that are then deposited are complex compounds that employ available oxyanions. The rate of formation of these secondary minerals can be very rapid, as is evidenced by mineral formation on the walls of mine drifts in a matter of months after the drifts have been opened. In all deposits there is usually a zonation of mineralogy in which a reduced mineral is surrounded by hydrated oxides within the first few centimetres of the oxidation zone, followed by complex uranates and, finally, uranyl oxysalts. The specific oxysalt depends on the solubility and availability of the given anion, silicates and phosphates being the most common and carbonates and sulphates relatively rare.

The principal deposits of uranium are in pegmatites or in sedimentary host rocks. The pegmatites represent direct concentrations from igneous processes. The reduced minerals are usually uraninite with or without associated rare earths and other actinide elements. Niobate, tantalate and titanate minerals are also common as primary minerals. Oxidized minerals are usually hydrated oxides, silicates and phosphates, but minerals of all groups may occur. Deposits in sedimentary rocks represent concentrations of previously dispersed uranium, perhaps all igneous in origin. Uraninite is the dominant reduced mineral, but such newly recognized minerals as coffinite and brannerite are also important. The secondary minerals, as in the pegmatites, are usually hydrated oxides, silicates and phosphates. Some deposits may show only a few other species, but many show 20 or more uranium minerals.

The most complete description of uranium minerals was by Frondel.[63] His monograph followed the format of Dana's *System of mineralogy* in reviewing the synonymy, composition, crystallography, physical and optical properties, synthesis, identification and occurrences in detail for each species. Around 70 valid uranium species and many since discredited or ill-defined other phases were included. Several other general discussions of uranium minerals exist. Those by Soboleva and Pudovkina,[163,164] Gerasimovsky,[73] Getseva and Saveleva[74] and Heinrich[79] are the most comprehensive, but they are contemporaneous and nowhere as complete as the work by Frondel.[63] Recent summaries[113,167] discussed the uranium mineralogy of Canada and listed most of the known minerals, including some archaic terminology. The most current listing of minerals is that by Fleischer,[60] which reflected the nomenclature accepted by the Commission on New Minerals and Mineral Names of the International Mineralogical Association. This nomenclature will be followed in the descriptions that follow.

The presentation of uranium mineralogy here concentrates on the chemical and structural classification of the uranium minerals, including the recognition of many closely related species. Individual minerals will only be discussed in detail for species that were not described by Frondel.[63] There is insufficient space in this presentation to list all the data as offered by Frondel, but references to such descriptive data are given for all new minerals.

The order of presentation of the uranium minerals will follow chemical groups. The U^{4+} minerals are discussed first, followed by the niobates, tantalates and titanates. These two groups include the 'primary' reduced minerals. The uranyl minerals are considered in the order hydrated oxides, silicates, phosphates and arsenates, vanadates, molybdates, sulphates, carbonates, and selenates and tellurates. Each section includes an evaluation of the known crystal chemistry and its effect on chemical variability and occurrence of mineral species.

U^{4+} minerals

The lowest valence state for uranium in nature is 4+, and in this state it forms severals minerals. In this valence state uranium is also substitutional in many other minerals—particularly the

Table 1 U^{4+} minerals

Mineral	Formula	Structure type	System	Lattice constants, Å (symmetry)
Brannerite (F)	$(U,Ca,Ce)(Ti,Fe)_2O_6$	$ThTi_2O_6$	Mono.	$a=9.79$ $b=3.72$ $c=6.87$ $\beta=118°25'$ $(C2/m)$
Coffinite (F)	$U(SiO_4)_{1-x}(OH)_{4x}$	Zircon	Tetra.	$a=6.979$ $c=6.253$ $(I4_1/amd)$
Ishikawaite	$(U,Fe,Y,Ca)(Nb,Ta)O_4$	Columbite		
Lermontovite	$(U,Ca,Ce)PO_4(OH)\cdot H_2O$			
Mourite	$UMo_5O_{12}(OH)_{10}$		Mono.	
Ningyoite	$(U,Ca,Ce)_2(PO_4)_2\cdot 1\text{–}2H_2O$	Rhabdophane	Orth.	$a=6.78$ $b=12.10$ $c=6.38$ $(P222)$
Petscheckite	$UFe(Nb,Ta)_2O_8$	UTa_2O_8	Hex.	$a=6.42$ $c=4.02$ $(P\bar{3}1m)$
Sedovite	$U(MoO_4)_2$		Orth.	$a=3.36$ $b=11.08$ $c=6.42$
Uraninite (F)	$UO_{2+x}(0.0<X<0.25)$	Fluorite	Cubic	$a=5.470-5.443$ $(Fm3m)$
Uranmicrolite	$(U,Ca,Ce)_2(Nb,Ta)_2O_6(OH,F)$	Pyrochlore	Cubic	$a=10.40$ $(Fd3m)$
Uranpyrochlore	$(U,Ca,Ce)_2(Ta,Nb)_2O_6(OH,F)$	Pyrochlore	Cubic	$a=10.44$ $(Fd3m)$

(F) indicates described in Frondel.[63]

rare-earth tantalates and niobates. For a long time uraninite was the only known U^{4+} mineral, but the list now contains 11 species (Table 1). Assignment of a species to this list is complicated by the chemistry of uranium—in particular, its tendency to partially oxidize. There are several known species that contain uranium in which the average valence state is definitely higher than 4+ but less than 6+ (Table 2). In addition, uranium is commonly found in the rare-earth tantalates and niobates, but the valence states of the uranium are not well established. Although many of these minerals probably formed with the uranium initially in the 4+ state, chemical analyses indicate that both 4+ and 6+ are present. These minerals are listed separately in Table 3.

Uraninite

Uraninite is still the best known and most common reduced mineral. It is found in all types of uranium deposits, except where the zone of oxidation has eliminated the reduced mineralization. Finding uraninite in an orebody is usually considered as evidence for finding the primary deposit.

Table 2 U^{4+}–U^{6+} minerals

Mineral	Formula	Structure type	System	Lattice constants, Å (symmetry)
Ianthinite (F)	$U(UO_2)_5(OH)_{14}\cdot 3H_2O$		Orth.	$a=11.52$ $b=7.15$ $c=30.3$
Liandratite	$U(Nb,Ta)_2O_8$	UTa_2O_8	Hex.	$a=6.36$ $c=4.01$ $(P\bar{3}1m)$
Moluranite	$H_4U(UO_2)_3(MoO_4)_7\cdot 18H_2O$		Amorphous	
Orthobrannerite	$UUTi_4O_{12}(OH)_2$		Orth.	$a=7.415$ $b=11.77$ $c=6.830$ $(P2_122[?])$
Unnamed	α-U_3O_7	CaF_2(fluorite)	Tetr.	$a=5.472$ $c=5.397$ $(F4mmm[?])$
Wyartite	$Ca_3U(UO_2)_6(CO_3)_2(OH)_{18}\cdot 3\text{–}5H_2O$		Orth.	$a=11.25$ $b=7.10$ $c=16.83$ $(Pnma)$ and $a=11.25$ $b=7.10$ $c=20.80$ $(P2_12_12_1[?])$

Uraninite as a mineral received considerable attention in the 1940s and 1950s, and much of this mineralogy has been reviewed by Frondel.[63] More recent studies have concentrated on its properties in the nuclear ceramics field. Much of the emphasis has been on its role in the U–O system, which contains many compounds between U and UO_3. Uraninite is especially interesting because it is the only U–O compound that occurs

Table 3 Uranium niobates, tantalates and titanates (U substitutional but not dominant ion)

Mineral	Formula	Structure type	System	Lattice constant, Å (symmetry)
Ashanite	$(Nb,Ta,U,Fe,Mn)_4O_8$	Ixiolite	Orth.	$a=5.869$ $b=4.873$ $c=5.216$ $(Pbcn)$
Betafite (F)	$(Ca,Na,U)(Ti,Nb,Ta)_2O_6(OH)$	Pyrochlore	Cubic	$a=10.29$ $(Fd3m)$
Davidite (F)	$(Fe,La,U,Ca)_6(Ti,Fe)_{15}(O,OH)_{36}$	Crichtonite	Hex.	$a=10.37$ $c=20.87$
Euxenite	$(Y,Ca,Ce,U,Th)(Nb,Ta,Ti)_2O_6$	Columbite	Orth.	$a=5.520$ $b=14.57$ $c=5.166$ $(Pbcn)$
Kobeite	$(Y,U)(Ti,Nb)_2(O,OH)_6$	Columbite		
Pisekite (F)	$(As,Ca,U)(Nb,Ta,Ti)O_4$			
Plumbobetafite	$(Pb,U,Ca)(Nb,Ti)_2O_6(OH,F)$	Pyrochlore		
Plumbomicrolite	$(Pb,Ca,U)Ta_2O_6(OH)$	Pyrochlore		
Plumbopyrochlore	$(Pb,Y,U,Ca)_{2-x}Nb_2O_6(OH)$	Pyrochlore	Cubic	$a=10.534$ $(Fd3m)$
Polycrase	$(Y,Ca,Ce,U,Th)(Ti,Nb,Ta)_2O_6$	Columbite		
Samarskite	$(Y,Ce,U,Ca,Pb)(Nb,Ta,Ti,Sn)_2O_6$	Columbite		
Tanteuxenite	$(U,Fe,V)(Ti,Sn)_2O_6$	Columbite		
Thorutite	$(Th,U,Ca)Ti_2(O,OH)_6$	Brannerite		
Yttrobetafite	$(Y,U,Ce)_2(Ti,Nb,Ta)_2O_6(OH)$	Pyrochlore		
Yttrocolumbite	$(Y,U,Fe)(Nb,Ta)O_4$	Stannocolumbite?		
Yttrocrasite	$(Y,Th,Ca,U)(Ti,Fe)_2(O,OH)$	Columbite		
Yttromicrolite (hjelmite)	$(Y,Ca,U)_2(Ta,Nb)_2O_6(OH)$	Pyrochlore		
Yttropyrochlore	$(Y,Na,Ca,U)_{1-2}(Nb,Ta,Ti)_2O_6(OH)$	Pyrochlore	Cubic	$a=10.3$ $(Fd3m)$

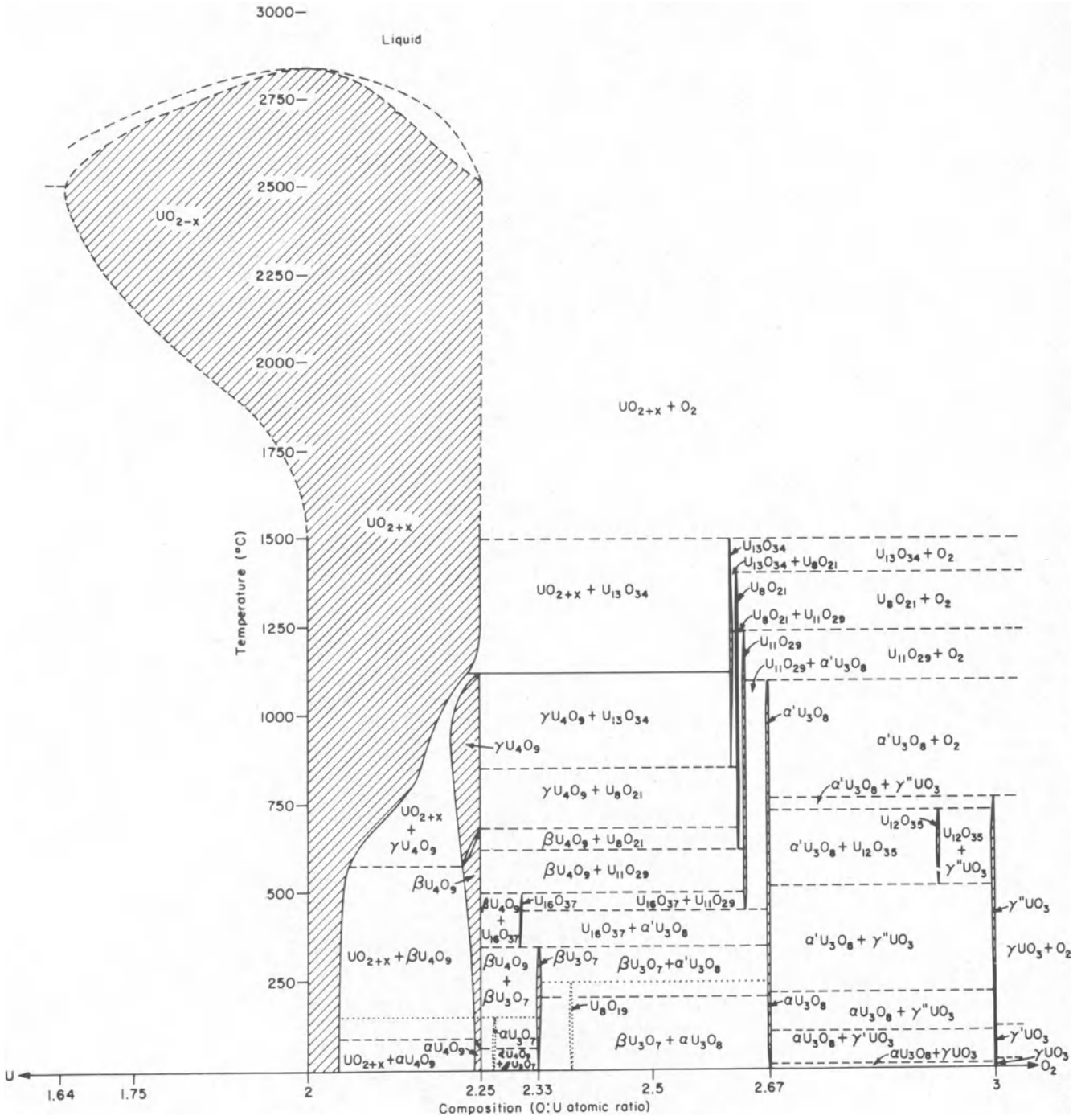

Fig. 1 Phase relations in uranium–oxygen system

in nature in any degree of abundance.

The effects of the oxidation of uranium complicate the nature of uraninite behaviour. Its composition is nominally UO_2, but it always shows a higher degree of oxidation. In fact, stoichiometric $UO_{2.00}$ may not exist in nature. There are reports of hypostoichiometric uraninite, but these reports may be doubted. The composition of uraninite appears to be restricted to the range $UO_{2.00}$ to $UO_{2.25}$—and more probably to $UO_{2.07}$ to $UO_{2.25}$.

Fig. 1 is a composite T–X phase diagram for the U–O system. The geologically significant portion of this system is probably below 1000°C and from $UO_{2.0}$ to $UO_{3.0}$. Uraninite in this region shows a solid solution the composition range of which is a function of temperature, but with an upper limit at low temperatures of around $UO_{2.07}$. This composition probably represents the limit of natural uraninite. If a sample of stoichiometric $UO_{2.00}$ is prepared in a reducing atmosphere, the resulting compound is brick red. When this material is exposed to air it quickly darkens to a brown colour and the composition oxidizes to $UO_{2.04}$. Further oxidation to $UO_{2.07}$ results in a black sample after long times in air. If the sample is heated at 100°C, it quickly oxidizes to $UO_{2.25}$ and is black in colour.

Uraninite, UO_2, is isostructural with fluorite, CaF_2, and consists of U in eightfold cubic coordination (Fig. 2). Cerianite, CeO_2, and thorianite, ThO_2, have the same structure and form complete solid solutions with uraninite, which accounts for the high rare-earth and thorium content of many pegmatitic uraninites. Grønvold[76] has shown that UO_2 oxidation occurs by an oxygen interstitial mechanism and that the proper formulation for uraninite should be UO_{2+x}. The usual way to determine the stoichiometry is to measure the unit cell constant. For $UO_{2.00}$ $a = 5.470$ Å. The cell size varies linearly with composition, $a_O = 5.470 - 0.1080X$, where X is the deviation from stoichiometry of the oxygen. Willis[190] has discussed the details of the structural aspects of this oxidation. The limiting value for X is 0.25: above this composition the cubic structure gives

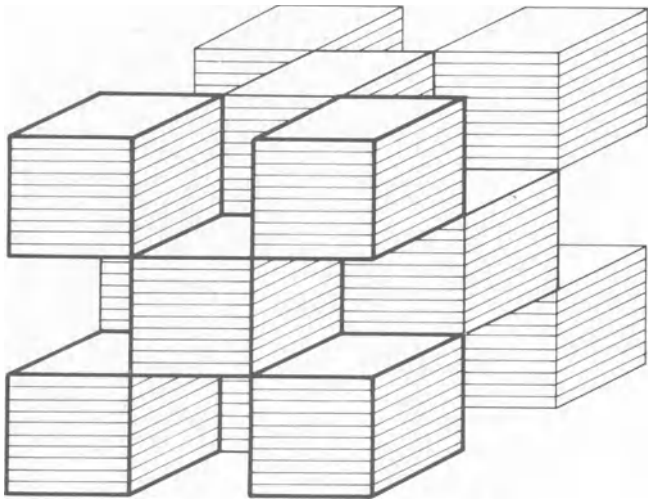

Fig. 2 Structure of uraninite, UO_2 (figure shows cubic UO_8 coordination polyhedra which are edge-shared in face-centred-cubic arrangement)

way to a related tetragonal form. Frondel[63] listed many uraninite cell determinations that could be translated into compositions in the range $UO_{1.21}$ to $UO_{2.94}$, but the data are obviously complicated by either interfering ionic substitutions or poor uncorrected X-ray data. Experimental evidence on pure uranium oxides with carefully measured data shows that compositions only between $UO_{2.0}$ and $UO_{2.25}$ are possible.

Natural uraninites with compositions above $UO_{2.07}$ usually show broad diffraction lines, which are probably indicative of a range of compositions. Shaner[151] has shown by metallography that samples fired at high temperatures in controlled atmospheres do not quench but separate into two phases, one oxygen-rich and the other oxygen-poor. The details of the two-phase field UO_{2+x}–U_4O_9 in Fig. 1 were determined in this manner. Natural samples probably behave in a similar manner in that the oxidation to $UO_{2.25}$ probably occurs stepwise, affecting only part of a sample at a time.

The composition $UO_{2.25}$ usually shows a fairly sharp diffraction pattern. The compound may show an ordered state if it has been carefully annealed. Three forms of U_4O_9 have been reported by Masaki,[102] Masaki and Doi[103] and Naito,[116] all of which are cubic and based on a superstructure of the uraninite cell. None of these ordered compounds has been reported in natural samples. Although $UO_{2.25}$ has been reported, the required annealing has evidently not occurred. Careful studies on natural samples may reveal the weak characteristic ordering lines. The phase should exist in natural systems.

Uraninite samples, even in a finely powdered state, seem to be stable in air for long periods of time at ambient conditions once they have oxidized to $UO_{2.25}$. If samples are heated to 150°C in air, they oxidize further to $UO_{2.33}$ and assume a tetragonal structure. Several phases around this composition are known, and that which forms is dependent on the thermal history of the sample. The most commonly encountered form is designated α-U_3O_7, and it has been reported by Voultsidis and Clasen[179] to occur at Key Lake, Saskatchewan, Canada. By analogy with the phase information it may imply oxidation at a slightly elevated temperature. All the U_3O_7 phases may be metastable, as they are only formed in oxidation experiments. They cannot be formed by reduction of higher oxides.

Further oxidation at higher temperatures readily forms a series of oxides in the range $UO_{2.61}$ to $UO_{2.67}$ and ultimately to UO_3. All of these compounds have crystal structures that differ significantly from the fluorite structure type found in phases with compositions up to $UO_{2.37}$. The phase relations imply that γ-UO_3 should be the stable phase at the earth's surface. To date, none of these compounds has been reported in nature. Evidently, in the oxidation of uraninite these higher oxides have a strong affinity for water and form hydrated compounds instead of simple oxides. Natural specimens usually show a massive uraninite core surrounded by a yellow to orange microcrystalline zone that is usually termed 'gummite'—a complex mixture of uranium oxide hydrates. It may contain such minerals as ianthinite that are not fully oxidized, but this zone usually consists of U^{6+} minerals. If oxidation were to occur in the absence of water, one of the U_3O_8 forms would probably form—α-U_3O_8 being the most likely. Further oxidation usually produces either α-UO_3 or γ-UO_3. The α-form is structurally related to the U_3O_8 forms.

Uraninite occurs in many varieties from crystals to dense massive microcrystalline samples to finely divided powdery coatings. The term pitchblende has been used for the dense botryoidal variety that is commonly found in vein deposits, but there is no justification for the continuation of this usage. All studies show that there is no real distinction and the practice should be discontinued. Uraninite is easily identified by its X-ray diffraction pattern, and all UO_{2+x} show the same pattern, except for the changes in spacing due to composition.

Coffinite

Coffinite was first described as a new mineral by Stieff and co-workers[168] from several localities in the sandstones of the Colorado Plateau deposits often intimately associated with asphaltic material. It was also found in vein-type deposits in Spain by Arribas[8] and has since been found in almost all types of deposits. The composition has been reported as $U(SiO_4)_{1-x}(OH)_{4x}$, but samples were never sufficiently purified to validate this composition. Organic matter was always present and organometallic complexes of uranium may have accounted for the excess uranium rather than requiring excess (OH) to account for the U : Si ratio deviating from unity. $USiO_4$ has been prepared by Fuchs and Gebert[66] with no evidence of OH substitution.

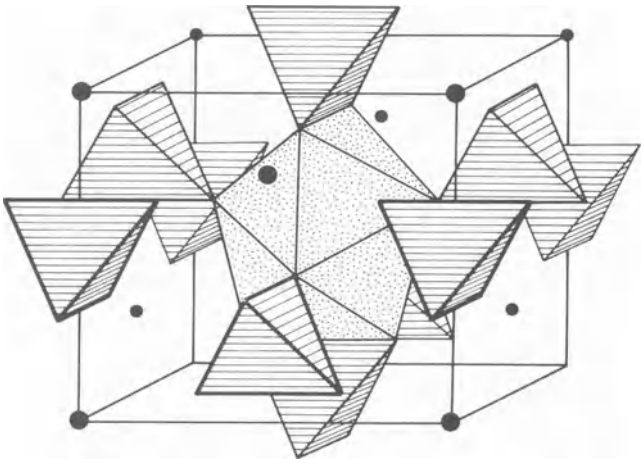

Fig. 3 Structure of coffinite, $USiO_4$ (uranium is in 8-fold coordination shown stippled; SiO_4 tetrahedra are ruled)

Coffinite is isostructural with zircon, thorite and hafnon and may show significant solid solution with each of these minerals. Its structure is shown in Fig. 3. No specific structural study has been done on coffinite. Crystals are always extremely small. The structure of the $(OH)_4$ group may be implied by analogy with hydrogarnets.[40, 62] Its role in the stability of coffinite is totally unknown.

Bayushkin and Il'menev[9] described some microscopic crystals from the U.S.S.R. More commonly, it is disseminated as a very fine black powder. Its association with organic matter masks its true properties, as it is usually only observable under the microscope. Like uraninite, stoichiometric $USiO_4$ is prob-

ably not black. Natural material owes its colour to the organic matter that is invariably present and, probably, to some degree of oxidation as well. Identification of coffinite is very easy by use of its powder diffraction pattern.

Brannerite

Brannerite is the third most important reduced uranium mineral in that it occurs in many different types of deposits and is the chief uranium producer in the conglomerates of Blind River–Elliot Lake, Ontario, Canada. Although it has been found in pegmatites, hydrothermal and sedimentary deposits, it is always associated with uraninite and probably forms through reactions with uraninite and titanium phases that are also present.

Brannerite is nominally UTi_2O_6, but the U may be partially oxidized and partially replaced by Ca and rare earths. Fe may replace some of the Ti and partial hydration may occur. The formula of brannerite may be $(U,Ca,RE)(Ti,Fe)_2O_{6-8}(OH)_X$. The variable oxygen content reflects the oxidation of the U that may not be compensated by the Ca and rare-earth substitutions. A new phase, orthobrannerite, with a proposed formula of $U^{4+}U^{6+}(Ti,Fe)_4O_{12}(OH)_2$ has been reported by the Peking Institute of Uranium Geology.[121] The orthorhombic nature of this new phase is partly implied on the basis of crystal morphology. All brannerites are metamict and must be heated to develop crystallinity. Care must be taken during heating not to change the oxidation states. True brannerite appears to crystallize as a monoclinic phase that is isostructural with $ThTi_2O_6$.[145] The X-ray data of orthobrannerite can be indexed on an orthorhombic lattice, which, coupled with the orthorhombic morphology, implies that this phase formed as orthobrannerite and was not the product of oxidation during the heating to crystallize the specimen.

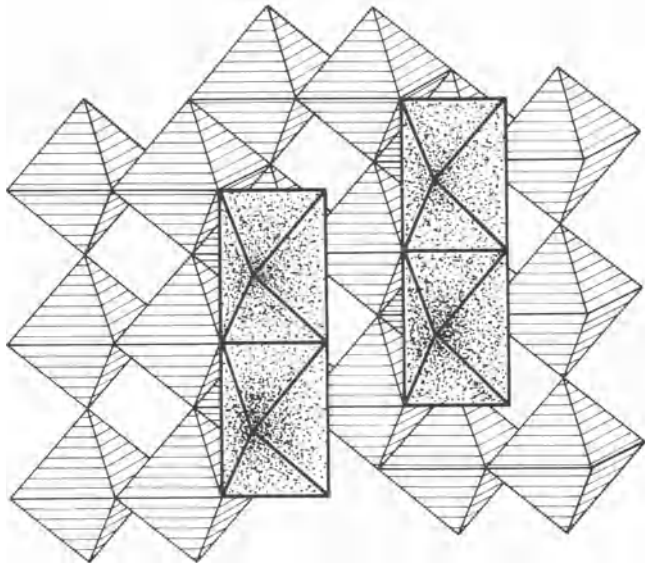

Fig. 4 Structure of brannerite, UTi_2O_6 (TiO_6 octahedra (ruled) share corners and edges to form a layer bridged by UO_6 octahedra (stippled))

Brannerite, when fully reduced, is brown in colour but, like uraninite, it darkens with oxidation to a pitchy black colour. Its crystal structure is related to the perovskites, pyrochlores and columbites in that it is based on a framework of linked octahedra of $(Ti,Ta,Nb)O_6$ units with interstitial U, Ca, Th and rare earths. These ions substitute rather freely for one another. The brannerite structure is shown in Fig. 4. The structural unit is a sheet of corner and edge-shared TiO_6 octahedra with UO_6 octahedra cross-linking these sheets. The sheet structure is closely related to the anatase form of TiO_2. The monoclinic structure results from the nature of the sheet, which steps one-half an octahedral width in the a-axis direction for every pair of octahedra in the c-axis direction. Orthobrannerite probably has a related sheet structure in which the step alternates $\pm a$ rather than only $+a$. The cell of orthobrannerite has $a = a_b$, $b \simeq 2b_b$, $c \simeq 2c_b$. It is not a polymorph. Orthobrannerite probably conforms to Kirvokoneva's[90] phase X, quoted as $U^{6+}Ti_2O_7$.

Mineral varieties of the brannerite series include lodochnikite, absite and thorutite. Absite is a thorian-rich brannerite and does not warrant species status. Lodochnikite is a uranium-rich brannerite, possibly significantly oxidized. Heating produces a brannerite-like X-ray pattern, but with differing intensities. It probably does not warrant species status either. Thorutite is the thorium end member.

The brannerite group can be identified by the X-ray powder patterns that are obtained on heating. The heating to crystallize the metamict structure is usually done in air, and some surface oxidation necessarily occurs. Usually, traces of U_3O_8 and TiO_2 can be detected. If the grains are coarse and the heating time is kept to a minimum, the interior of the grains may retain the original composition.

Ningyoite

The mineral ningyoite was first reported by Muto *et al.*[115] from Ningyo-toge mine, Tottori Prefecture, Japan, where it occurs as the principal uranium mineral in a Tertiary conglomerate. It is associated with sulphides, apatite, chlorite and gypsum, which appear to have been deposited by laterally moving solutions. Ningyoite occurs only as thin microcrystalline coatings on the surface or in cracks of the pebbles, and a pure sample was not obtainable for analysis. The mineral is structurally and chemically related to rhabdophane and probably has a formula $U_{1-X}Ca_{1-X}RE_{2X}(PO_4)\cdot 1-2H_2O$. Synthesis of a closely related compound $UCa(PO_4)_2\cdot 0.5H_2O$ suggests that the two materials are isostructural with a coupled substitution of $2RE^{3+} \rightleftharpoons Ca^{2+} + U^{4+}$ up to several per cent. The structural relation to rhabdophane is apparent in the diffraction patterns, but the probable ordering of Ca and U on the RE sites lowers the symmetry to orthorhombic.

Ningyoite is not known from other localities, although its microcrystalline nature may have precluded its recognition. It is brownish green to brownish in thin section, which suggests partial oxidation as the synthetic analogue is green. Crystals may be acicular or elongated. The principal way to identify it is by its X-ray pattern.

Lermontovite

Another uranium phosphate mineral, lermontovite, has been described by Soboleva and Pudovkina.[163,164] This mineral occurs as botryoidal aggregates of radial fibrous needles. The formula is apparently $U_3(PO_4)_4\cdot 6H_2O$ with some substitution of Ca and RE for the U. The material is poorly characterized. It is associated with molybdenum sulphate, marcasite, hydrous silicates and 'thallium ochre'. This phase requires more careful characterization.

U^{4+} molybdates

Uranium is often associated with molybdenum in its deposits, and several uranium–molybdenum minerals are known. Two of these minerals contain U^{4+}—mourite and sedovite—which were reported by Kopchenova *et al.*[93] and Skvortsova *et al.*[159] to occur in the supergene zone over a uraninite–molybdenite deposit. Sedovite is $U^{4+}(Mo^{6+}O_4)_2$ and forms the core of sedovite–mourite clusters. Its colour is brown to reddish brown, which indicates that the uranium is in one valence state. Mourite is given as $U^{4+}Mo^{6+}_5O_{12}(OH)_{10}$ and shows a deep violet colour. The valence states of U and Mo were not determined and the deep colour indicates some electron exchange suggestive of partial oxidation of the U or reduction of the Mo. Both

minerals were reported from only one deposit.

Moluranite is another uranium molybdate with at least some reduced uranium.[54] It is also very dark in colour, showing brown only in very thin fragments. It shows no X-ray pattern and appears to be amorphous or possibly metamict. It occurs in fine fissures in granulated albitite associated with molybdenite and other sulphides, brannerite and other U–Mo compounds. It is only known from one locality.

U^{4+} pyrochlores

Many minerals of the pyrochlore group, which includes the betafites and the microlites, often contain significant quantities of uranium along with rare-earth elements. These minerals are usually associated with rare-earth pegmatite deposits or as accessory minerals in granitic rocks. Detrital grains are also known in placer deposits. The pyrochlores have a general formula $A_2B_2O_6(O,OH,F)$, where U^{4+} (or U^{6+}) occurs in the A site and B = Ta,Nb,Ti,Sn. The nomenclature of the pyrochlore series was discussed by Hogarth.[81] The master name refers to the dominant element in the B site. Betafite refers to Ti, microlite to Ta and pyrochlore to Nb. Uranmicrolite (formerly called djalmaite) and uranpyrochlore (formerly called ellsworthite or hachettolite) are two species in which U dominates the A sites. Several other pyrochlore family minerals with significant reported U are listed in Table 3.

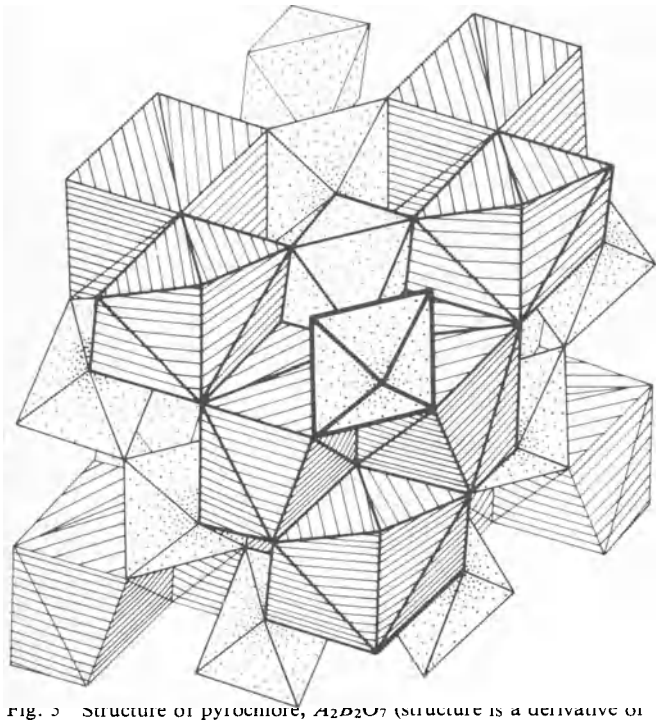

Fig. 5 Structure of pyrochlore, $A_2B_2O_7$ (structure is a derivative of fluorite (Fig. 1) in which one O in eight is missing and concomitant atomic shifts result in A site (ruled) remaining 8-coordinated in a distorted cubic array and B site (stippled) becoming octahedrally coordinated; uranium usually occurs in A sites)

The pyrochlore structure is three-dimensional framework of corner-shared $(Ti,Ta,Nb)O_6$ octahedra. The A site lies within this framework and is 8-coordinated. The octahedra can articulate to allow for a fair range in sizes of the A cation, which accounts for the variable compositions of most of these compounds. Part of the structure is depicted in Fig. 5. The A coordination is a distorted cube, the size and degree of distortion depending on the amount of tipping of the B octahedra. Many pyrochlores show deviations from the $A_2B_2O_6(O,OH,F)$ stoichiometry, some of which are probably defect structures that result from charge balance effects and coupled substitutions. The U in the minerals was probably originally present as U^{4+}, but U^{6+} is often reported in analyses, probably as a result of oxidation either naturally or after sampling. Chevalier and Gasperin[35] showed evidence for ordering of atoms on the A sites in some uraniferous pyrochlores.

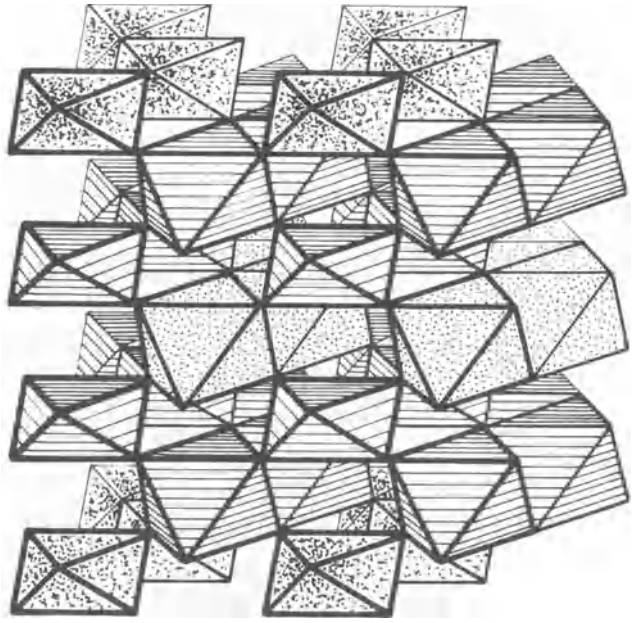

Fig. 6 Structure of columbite, AB_2O_6 (structure is hexagonally close packed with all A and B atoms in octahedral coordination; A octahedra stippled and B octahedra ruled)

U^{4+} columbites—AB_2O_6

Members of the columbite–tantalite family of minerals also often contain significant U along with rare earths, Fe, Ca and Th. The B site is either Nb or Ta. Like the pyrochlores, these minerals are associated with rare-earth pegmatites and are also known from placer deposits. Most of the compounds probably formed initially with U^{4+}—most probably as a coupled substitution $Ca^{2+} + U^{4+}$ for a trivalent ion. Oxidation occurs easily, however, and most specimens contain significant amounts of U^{6+}. Those minerals which contain radioactive elements are usually metamict and require heating to develop crystallinity.

The structure of the columbites is based on hexagonal close-packed oxygens in which the cations occupy one-half the available octahedral sites. The B cations form double layers of edge-shared octahedra that alternate with single A layers. The structure is illustrated in Fig. 6. Various other stacking sequences are possible, and some of the phases of Table 3 may have different arrangements of A and B atoms in the octahedra. Euxenite and samarskite appear to be analogous to columbite. X-ray data are generally lacking on other phases assigned to this group. The assignment of kobeite to this group is based on the first detected pattern on heating, which suggests a 14.3-Å cell constant.[86] Higher temperatures produce a changed structure more indicative of a uraninite-type structure. Ashanite has been assigned to this group, although it may be more closely associated with the ixiolite sub-group.

Petscheckite and liandratite

Two new minerals—petscheckite and its closely related alteration product liandratite—have been reported from a pegmatite in Madagascar.[114] Like other niobates and tantalates they are metamict, even though they occur as well-defined crystals, and heating is required to produce crystallinity. The resulting structure is most closely related to UTa_2O_8,[72] which is a derivative structure of U_3O_8, so they are not related to minerals discussed

above. Because U_3O_8 has not been reported in nature, these minerals must be considered as a new group.

Liandratite appears to be an oxidation product of petscheckite as it is always intimately associated on the surface of petscheckite crystals. It occurs as a glassy translucent coating 1–2 mm thick. It probably represents the fully oxidized U^{6+} form. Petscheckite as found shows partly oxidized and partly hydrated varieties. The oxy-petscheckite probably forms first from the original $UFe(Nb,Ta)_2O_8$ as the Fe^{2+} oxidizes and is removed from the structure. Hydration leads to a hydroxy-petscheckite form, which is distinguished from the oxy-petscheckite by colour reflectivity and texture in polished section. All these phases are essentially opaque and very dark in colour, which indicates that mixed valence states are present.

Minerals with minor U—probably U^{4+}

Many minerals incorporate minor amounts of uranium, but the uranium is not an essential component. Most of these minerals are igneous or pegmatitic in origin and may represent the source minerals from which weathering allowed the release of uranium into the groundwater system. No effort will be made to describe them. For the sake of completeness of the description of uranium-bearing minerals they have been listed in Table 4.

Table 4 Minerals with traces of uranium

Mineral	Formula	Structure type
Aeschynite	$(Ce,Ca...)(Ti,Nb)_2(O,OH)_6$	Aeschynite
Allanite	$(Ce,Ca,Y,U)(Al,Fe)_3(SiO_4)_3(OH)$	Epidote
Belovite	$(Sr,Ce,Na,Ca)_5(PO_4)_3(OH)$	Apatite
Britholite	$(Ce,Ca)_5([Si,P]O_4)_3(OH,F)$	Apatite
Cerianite	$(Ce,U)O_2$	Fluorite
Cheralite	$(Ca,Ce,Th)(P,Si)O_4$	Monazite
Ekanite	$(Th,U)(Ca,Fe,Pb)_2Si_8O_{20}$	Ekanite
Ewaldite	$Ba(Ca,RE)(CO_3)_2$	Ewaldite
Fergusonite	$YNbO_4$	Fergusonite
Formanite	$YTaO_4$	Fergusonite
Iimoriite	$(Y,Ca,Zr)_{15}(Mg,Fe,Al)(Si,Al,P)_9O_{34}(OH)_{16}$	Apatite
Iraqite	$(La,Ce,Th,U)_2(K,Y)_2(Ca,La,Ce,Na)_4(Si,Al)_{16}O_{40}$	Ekanite
Melanocerite	$(Ce,Ca)_5(Si,B)_3O_{12}(OH,F)\cdot nH_2O$	Apatite
Monazite	$(Ce,Th,Ca,U)PO_4$	Monazite
Niobo-aeschynite	$(Ce,Ca,Th)(Nb,Ti)_2(O,OH)_6$	Aeschynite
Rhabdophane	$(Y,..)PO_4\cdot H_2O$	Rhabdophane
Thorianite	$(Th,U)O_2$	Fluorite
Thorite	$(Th,U)SiO_4$	Zircon
Umbozerite	$(Na,K)_3(Sr,Ba)_4(Th,U,Fe)_3O_{24}$	Umbozerite

U^{6+} minerals

Uranium in its highest valence state forms a large number of colourful minerals that may deposit in the oxidized zone associated with the primary deposit or the uranium may go into solution and be transported a considerable distance from its source area before reprecipitation. Minerals that form at the source may mimic the original phases by direct replacement, but more often they form a nondescript mass that destroys any original structure. These minerals are usually hydrated uranyl oxides, silicates or phosphates. Further from the source the minerals usually form as one or more of the many hydrated uranyl oxysalts.

The uranyl minerals are considered in groups, depending on their associated anion. This approach is useful because each of these groups has many characteristics in common, including those of occurrence and crystal chemistry. Within each group sub-classification by $UO_2 : XO_n$ ratios leads to interesting comparisons and some very specific mineral families.

Uranyl oxide hydrates

Those minerals which form as the direct alteration of uraninite, usually as a boxwork of criss-crossing veinlets or as an alteration rind, are collectively called 'gummite'. The name derives from the gum-like or waxy appearance of these microcrystalline, intimately intergrown minerals. These minerals are usually hydrated uranyl oxides, alkali or alkaline-earth uranyl oxides along with uranyl silicates and phosphates. The fine-grained poorly crystalline nature of this material usually makes positive identification difficult or impossible, and many ill-defined minerals have been described. Many of these old minerals are unavailable for study, so it is not possible to clarify some of the earlier designations. Much of the mineral characterization has had to rely on analogies with synthetic phase studies, especially in the UO_3–H_2O system. The most complete review of this system by Hoekstra and Siegel[80] is a good guide to what may or may not exist in natural specimens.

The higher oxides of uranium (U_3O_8 and UO_3) do not appear to be stable in the presence of water. Neither U_3O_8 nor UO_3 has ever been found to occur naturally, though there is no real reason other than the ubiquitous presence of water in the oxidation zone to prevent such formation. In their place one usually finds hydrated oxides. The naturally occurring uranyl oxide hydrates are listed in Table 5. The list of verified synthetic phases is presented in Table 6.[80] The two lists show very little correspondence.

The ianthinite phase is a rare mineral in which the uranium is not fully oxidized. It occurs as a violet alteration product of uraninite in several localities and may form small crystals. Its colour distinguishes it from all other hydrated oxides and is undoubtedly due to electron exchange absorption caused by the mixed valence state of uranium. A synthetic $UO_{2.84}\cdot 1.5H_2O$ phase has been prepared by Bignand,[13] which is undoubtedly analogous based on its diffraction pattern. There was reluctance on the part of Frondel[63] to accept this analogy, but the evidence is clear, and ianthinite can be considered as a distinct mineral. On the other hand, the mineral epi-ianthinite was described initially by Schoep and Stradiot[148] as 'a yellow hydrated oxide which is not fully oxidized'. This description is a contradiction, and in view of the lack of chemical verification the material described must be considered a fully oxidized hydrate and probably one of the phases in the list in Table 6.

The only UO_3 hydrates verified from nature are three slightly different forms of $UO_3\cdot 2H_2O$ as described by Christ and Clark.[37] These minerals—schoepite, metaschoepite and paraschoepite (designated, respectively, in earlier literature as schoepite I, II and III)—seem to have slightly different unit

Table 5 Uranyl oxide hydrates (gummite minerals)

Mineral	Formula	System	Lattice constants, Å (symmetry)
Ianthinite (F)	$UO_2 \cdot 5UO_3 \cdot 10H_2O$	Orth.	$a=11.52$ $b=30.3$ $c=7.15$
Metaschoepite (schoepite II) (F)	$UO_3 \cdot 2H_2O$	Orth.	$a=14.73$ $b=16.72$ $c=13.99$ (*Pbna*)
Paraschoepite (schoepite III) (F)	$UO_3 \cdot 2H_2O$	Orth.	$a=15.22$ $b=16.83$ $c=14.12$ (*Pbca*)
Schoepite (schoepite I) (F)	$UO_3 \cdot 2H_2O$	Orth.	$a=14.74$ $b=16.66$ $c=14.36$ (*Pbca*)
Studtite* (F)	$UO_4 \cdot 4H_2O$	Mono.	$a=11.85$ $b=6.80$ $c=4.25$ $\beta=93°51'$ (*C2/m*)
Metastudtite	$UO_4 \cdot 2H_2O$	Orth.	$a=6.51$ $b=8.78$ $c=4.21$ (*Immm*)

* Misidentified in Frondel[63] as a carbonate.

Table 6 Crystal data on synthetic UO_3–H_2O compounds

Compound	System	Lattice constants, Å (symmetry)
$(UO_3)_3 \cdot H_2O = U_3O_8(OH)_2$	Tricl.	$a=6.802$ $b=7.417$ $c=5.556$ $\alpha=108.5$ $\beta=125.5°$ $\gamma=88.2$ ($P\bar{1}$)
$UO_3 \cdot 0.8H_2O$	Orth.	$a=4.27$–4.30 $b=10.19$–10.24 $c=6.86$–6.96
$UO_3 \cdot H_2O$ = α-$UO_2(OH)_2$	Orth.	$a=4.242$ $b=10.302$ $c=6.868$ (*Cmca* or *C2cb*)
$UO_3 \cdot H_2O$ = β-$UO_2(OH)_2$	Orth.	$a=5.6438$ $b=6.2867$ $c=9.9372$ (*Pbca*)
$UO_3 \cdot H_2O$ = γ-$UO_2(OH)_2$	Mono.	$a=6.419$ $b=5.518$ $c=5.561$ $\beta=112.77°$ ($P2_1/c$)
$UO_3 \cdot 2H_2O$	Orth.	$a=13.977$ $b=16.696$ $c=14.672$ (*Pbna*)

cells that are distinct from one another. These slightly different crystal structures are probably due to small structural rearrangements caused by differences in the state of hydration. Schoepite is most likely the original mineral with the highest hydration state. It is darker and more brown that the other two, which are bright yellow. The minerals do not appear to be true polymorphs. Analogous synthetic products have been reported only for schoepite.

The crystal structures of the schoepites and ianthinite are derivatives of the structure of U_3O_8.[57,98] Uranyl ions, which form five axial ligands to oxygen or hydroxyl ions, result in layered arrangements. Water molecules and oxonium ions cross-link these layers to form the structure. Subtle adjustments may occur in the layers, which result in slightly different structures, as evidenced in the many forms of U_3O_8. These changes may be analogous to the changes that occur in the schoepites. Further study is necessary to understand the true nature of the schoepites.

Studtite is an extremely unusual mineral in that it is a uranyl peroxide indicative of very strong oxidizing conditions during its formation. It was identified by Walenta[183] by analogy with synthetic $UO_4 \cdot 4H_2O$. It is known from only one locality and may prove to be extremely rare. Metastudtite, $UO_4 \cdot 2H_2O$, has recently been described by Deliens and Piret.[50a]

Alkali and alkaline-earth uranyl oxide hydrates

Table 7 lists 19 known minerals that may be classified as alkali or alkaline-earth uranyl oxide hydrates. They have often been referred to as uranates as well as uranyl oxides, but as details of their crystal structures become known it is apparent that they are closely related to the uranyl oxides described above. In fact, Sobry[165] and Noe-Spirlet and Sobry[119] have shown that substitutional series exist between schoepite and all the minerals on the list. It was proposed that the minerals can be explained by the general formula

$$mXO \cdot 2UO_3 \cdot (4-2m)H_2O$$

Table 7 Alkali and alkaline-earth uranyl oxide hydrates

Mineral	Formula	System	Lattice constants, Å (symmetry)
Agrinierite	$(K_2Ca,Sr)U_3O_{10}$	Orth.	$a=14.3$ $b=24.07$ $c=14.04$ (*Cmmm*)
Bauranoite	$BaU_2O_7 \cdot 4$–$5H_2O$		
Becquereite (F)	$Ca(UO_2)_6O_4(OH)_6 \cdot H_2O$	Orth.	$a=13.82$ $b=14.94$ $c=12.39$ (*Pnma*)
Billietite (F)	$Ba(UO_2)_6O_4(OH)_6 \cdot 8H_2O$	Orth.	$a=14.22$ $b=15.02$ $c=12.03$ (*Pnmn*)
Calciouranoite	$(Ca,Ba,Pb)U_2O_7 \cdot 5H_2O$	Metamict	
Clarkeite (F)	$(Na,Ca,Pb)_2U_2(O,OH)_7$		
Compreignacite	$K_2(UO_2)_6O_4(OH)_6 \cdot 8H_2O$	Orth.	$a=12.14$ $b=14.88$ $c=7.16$ (*Pnmn*)
Curite (F)	$Pb_2U_5O_{17} \cdot 4H_2O$	Orth.	$a=12.50$ $b=13.01$ $c=8.40$ (*Pna2*)
Fourmarierite (F)	$PbU_4O_{13} \cdot 6H_2O$	Orth.	$a=14.39$ $b=16.47$ $c=14.00$ (*Pbnm*)
Masuyite* (F)	$Pb_3U_8O_{27} \cdot 10H_2O$	Orth.	$a=41.93$ $b=42.61$ $c=24.22$ (*Pbmn*)
Metacalciouranoite	$(Ca,Na,Ba)U_2O_7 \cdot 2H_2O$	Metamict	
Metavandendriesscheite	$PbU_7O_{22} \cdot nH_2O (n<12)$		
Rameauite	$K_2CaU_6O_{20} \cdot 9H_2O$	Mono.	$a=14.22$ $b=14.26$ $c=13.97$ $\beta=121°1'$ (*C2/c*)
Richetite (F)	Pb–U oxide		
Roubaultite	$Cu_2(UO_2)_3(OH)_{10} \cdot 5H_2O$	Tricl.	$a=7.73$ $b=10.87$ $c=6.87$ $\alpha=86°29'$ $\beta=93°10'$ $\gamma=134°12'$ ($P\bar{1}$)
Uranosphaerite (F)	$Bi_2U_2O_9 \cdot 3H_2O$		
Vandenbrandeite (F)	$Cu(UO_2)(OH)_4$	Tricl.	$a=7.86$ $b=5.44$ $c=6.10$ $\alpha=91°52'$ $\beta=102°$ $\gamma=89°37'$ ($P\bar{1}$)
Vandendriesscheite (F)	$PbU_7O_{22} \cdot 22H_2O$	Orth.	$a=40.85$ $b=43.33$ $c=14.07$ (*Pmma*)
Wolsendorfite† (F)	$(Pb,Ca)U_2O_7 \cdot 2H_2O$	Orth.	$a=11.92$ $b=13.96$ $c=6.90$

*Listed in Frondel[63] as $UO_2 \cdot 4H_2O$.
†Listed in Frondel[63] under fourmarierite.

or

$$mX\text{OH}\cdot 2UO_3\cdot(4-2m)H_2O$$

The replacement mechanism is evidently either the simple substitution $(H_3O)^+ \leftrightarrow X^+$ or the coupled substitution $(H_3O)^+ \leftrightarrow X^{2+}$ and $(OH)^- \leftrightarrow O^{2-}$. These mechanisms suggest that the formula can be rewritten

$$X_m^{2+}(H_3O)_{2-m}^{+}\ [(UO_2)_2O_{2+m}(OH)_{2-m}]$$

or

$$X_m^{+}(H_3O)_{2-m}^{+}\ [(UO_2)_2O_2(OH)_2]$$

for $m=0$ both formulas give

$$(H_3O)_2\ [(UO_2)_2O_2(OH)_2]$$

which is a possible structural formula for schoepite.

Christ and Clark[37] proposed a crystal structure for these compounds that is a derivative of that proposed for UO_2F_2 by Zacharisen.[192] This structure consists of layers of 2–6* coordinated uranium in which the hexagonal dipyramidal polyhedra share edges. These layers are basically hexagonal in symmetry with the uranyl ion axis normal to the sheet direction. Oxygen atoms in the sheet are displaced small distances above and below the plane of the uranium atoms to accommodate closer packing. The formula of this layer is $[(UO_2)(O,OH)_2]$. Interlayer ions include monovalent or divalent cations and water molecules. The sheet is shown in Fig. 7(*a*). This structure has been reported for α-$UO_2(OH)_2$ by Taylor.[171]

Evans[57] proposed that the sheets are composed of 2–5 coordinated uranium atoms, the pentagonal dipyramidal polyhedra sharing edges and corners. This configuration is shown in Fig. 7(*b*). The uranium atom positions in the two configurations are very nearly the same. This pentagonal array has been reported for the structure of U_3O_8 by Loopstra,[98] and 2–5 coordination of uranium occurs in many other uranyl compounds (see later). The pentagonal array may be derived from the hexagonal array by replacing two OH atoms that are shared by two U atoms in the hexagonal array with a single O atom. It is interesting that this pentagonal array may have three-fold symmetry. The formula of a layer of this array becomes $[(UO_2)_6(O,OH)_{10}]$.

The proposal of Sobry[165] that water can continuously substitute for the cations maintaining charge balance by existing as oxonium ions is compatible with the structures proposed by Christ and Clark[37] but not with the structures proposed by Evans[57] or the structure of curite proposed by Mereiter.[106] It is difficult to distinguish the two structures with X-ray diffraction data because of the low quality of the data and the difficulty of obtaining accurate information on O in the presence of U. Good single crystal X-ray data or powder neutron data will be needed to resolve this problem. Infrared data could show the presence of oxonium, eliminating Evans' model.

In view of the fact that α-$UO_2(OH)_2$ exists with a hexagonal array and both β- and γ-$UO_2(OH)_2$[138, 157] show a square 2–4 coordination array (Fig. 7(*c*)), the existence of a pentagonal array must be questioned. The structure of $U_3O_8(OH)_2$, reported by Siegel and co-workers[158] and Taylor and Wilson,[172] shows uranium in both the 2–4 and 2–5 coordinations. Accepting Sobry's arguments, the nature of the layers must be considered to be essentially hexagonal. The structures of the various species then depend on the orderly nature of the substitutions and local distortions due to OH for O substitutions in the layers and stacking to achieve the most effective coordination and charge compensation with the interlayer cations. All the struc-

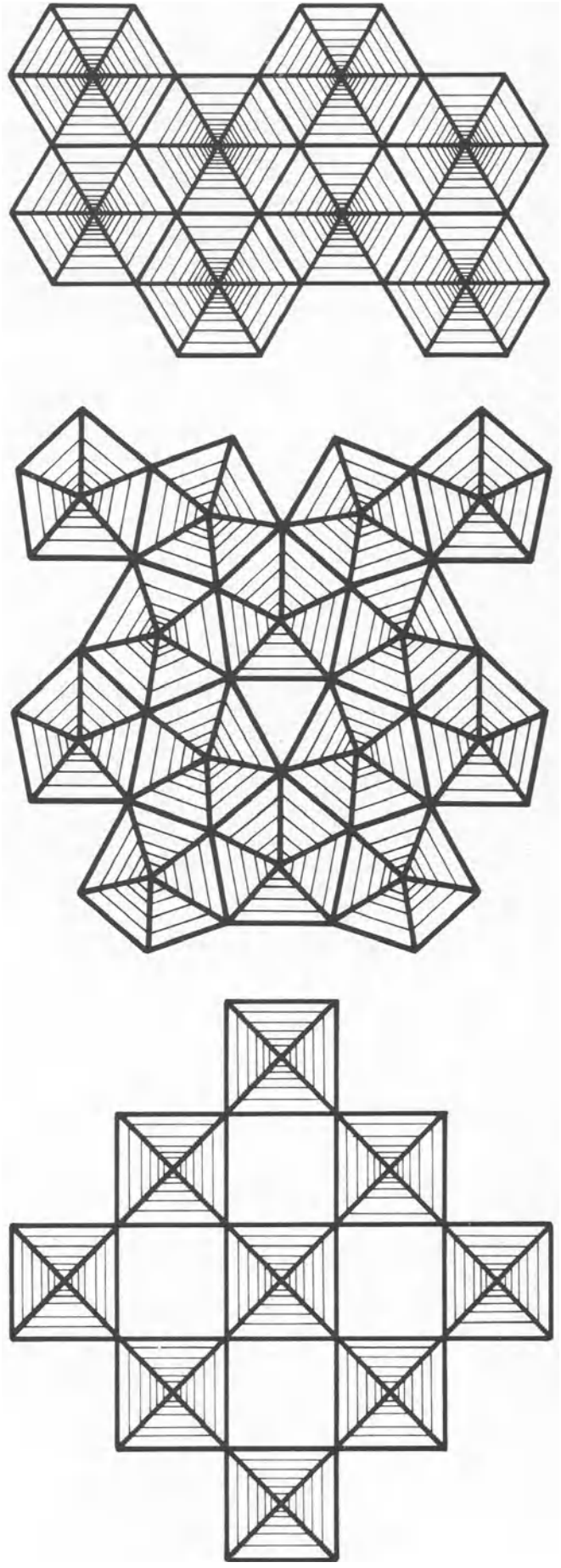

Fig. 7 Possible structures of U(O,OH) layers in hydrated uranyl oxides: (*a*) (*top*), arrangement with 2–6 coordination as found in α-$UO_2(OH)_2$; (*b*) (*centre*), arrangement with 2–5 coordination as reported for U_3O_8; (*c*) (*bottom*), arrangement with 2–4 coordination as reported for β- and γ-$UO_2(OH)_2$

*The coordination of uranium in U^{6+} compounds is invariably dipyramidal. The linear uranyl ion, $(UO_2)^{2+}$, surrounded by 4, 5 or 6 other oxygens with U–O distances longer than in the uranyl unit. These coordinations will be designated 2–4, 2–5 and 2–6, respectively.

tures are based on an orthohexagonal pseudo-cell $a' = 7$Å, $b' = 4$Å, $c' = 7.1$Å. Large cells, such as those reported for vandendriesscheite and masuyite, imply complex ordering patterns for the interlayer cation and substituting oxonium rather than disorder and justify the species distinctions that have been recognized. This interpretation of structural variations with substitution also helps explain paragenesis in some alteration zones around uraninite, as described by Deliens[46] for the famous Shinkolobwe deposits in Katanga, Zaire. Vandenbrandeite[140] shows a layer structure with uranium in 2–5 coordination. UO_7 dipyramids share one edge to form U_2O_{12} dimers that edge share with planar Cu_2O_6 dimers to form the layers in a structure that is different from any other known uranium compound.

The Pb-containing minerals form a series, which is listed in Table 8. The mineral masuyite has been variously described as a uranyl oxide hydrate[63] and a Pb-containing phase.[37] Deliens[45] has verified the existence of the Pb in all examined samples and suggested that it corresponds to the synthetic product of Protas[133,134] with the formula $Pb_3U_8O_{27}\cdot 10H_2O$. The formula of fourmarierite also has been variously reported with 4–$8H_2O$ per formula unit, but to fit the Sobry scheme $6H_2O$ is appropriate. Metavandendriesscheite obviously represents the dehydrated state for the Pb:U = 1:7 phase, and the existence of vandendriesscheite indicates that additional water may be accommodated in the interlayer volume. The layers separate and possibly shift to allow for this accommodation as in the autunite–meta-autunite minerals. A similar relationship exists in the Ca and Ba phases, metacalciouranoite representing the fully dehydrated phase and calciouranoite and bauranoite higher hydrates. As more becomes known about the other minerals, they may be expected to fit into similar series.

tion is the best way to distinguish these phases.

Many of the uranyl oxides were described by Frondel,[63] but several new minerals have been identified since then, and new data are available on some of the older minerals. Agrinierite and rameauite were described by Cesbron *et al.*[27] from the Margnac deposit, France, where they form in the oxidation zone. Agrinierite occurs as small orange crystals with uranophane in cavities in gummite. Rameauite occurs as 1-mm orange crystals with uranophane on uraninite. Bauranoite and metacalciouranoite were characterized by Rogova *et al.*[136] from a U–Mo deposit where they are found replacing uraninite and being replaced by uranophane. Bauranoite is reddish brown; metacalciouranoite is orange. Calciouranoite was described later by Rogova *et al.*[137] from the same deposit. It appears to be a higher hydrate of metacalciouranoite and occurs as poorly crystalline coatings that must be heated to yield a diffraction pattern. Compreignacite was identified by Protas[135] from the Margnac deposit, where it occurs closely associated with uraninite. Brindley and Bastovanov[19] have presented new data on synthetic compreignacite and its sodium analogue. A structure of a related phase $K_2U_7O_{22}$ was reported by Kovba,[94] but it does not appear to have a natural counterpart. Roubaultite was described by Cesbron and co-workers[30] from Shinkolobwe, Katanga, where it occurs as rosettes of platy green crystals on uraninite associated with other uranyl oxides and silicates. Wolsendorfite was described in Frondel[63] as fourmarierite, but simultaneously recognized as a distinct specie by Protas.[132] Deliens[45] showed that the two descriptions were identical and also showed that masuyite was a Pb mineral rather than a straight hydrated uranyl oxide. Sobry[166] prepared synthetic wolsendorfite, becquerelite and billietite and presented much new data on the phases. Protas[133,134] described a Ca–Sr

Table 8 Structural formulae of Pb, Ca and Ba uranyl oxide hydrates

Mineral	Formula	X:U	Sobry formula	*m*
Wolsendorfite	$PbU_2O_7\cdot 2H_2O$	1:2	$Pb(H_3O)[(UO_2)_2O_3(OH)]$	1.0
Curite	$Pb_2U_5O_{17}\cdot 4H_2O$	2:5	$Pb_4(H_3O)_6[(UO_2)_{10}O_{14}(OH)_6]$	0.8
Masuyite	$Pb_3U_8O_{27}\cdot 10H_2O$	3:8	$Pb_3(H_3O)_5[(UO_2)_8O_5(OH)_5]$	0.75
Fourmarierite	$PbU_4O_{13}\cdot 6H_2O$	1:4	$Pb(H_3O)_3[(UO_2)_4O_5(OH)_3]$	0.5
Metavandendriesscheite	$PbU_7O_{22}\cdot 12H_2O$	1:7	$Pb(H_3O)_6[(UO_2)_7O_8(OH)_6]$	0.28
Vandendriesscheite	$PbU_7O_{22}\cdot 22H_2O$	1:7	$Pb(H_3O)_6[(UO_2)_7O_8(OH)_6]\cdot 10H_2O$	0.28
Calciouranoite	$CaU_2O_7\cdot 5H_2O$	1:2	$X(H_3O)[(UO_2)_2O_3(OH)]\cdot 3H_2O$	1.0
Bauranoite	$BaU_2O_7\cdot 5H_2O$	1:2		
Metacalciouranoite	$CaU_2O_7\cdot 2H_2O$	1:2	$X(H_3O)[(UO_2)_2O_3(OH)]$	1.0
Becquerelite	$CaU_6O_{19}\cdot 10H_2O$	1:6	$X(H_3O)_5[(UO_2)_6O_7(OH)_5]$	0.33
Billietite	$BaU_6O_{19}\cdot 10H_2O$	1:6		

The crystal structure of curite casts considerable doubt on the Sobry scheme. The studies by Mereiter[106] and Taylor[171a] showed that the layers are corrugated sheets of uranium in both 2–4 and 2–5 coordination. The structural formula is $[Pb_{6.56}(H_2O,OH)_4][(UO_2)_8O_8(OH)_6]_2$, where the first bracketed term is the inter-sheet contents and the second is the sheet formula. This formula does not agree with the Sobry formula for curite given in Table 8. Evidently, the situation is more complicated than has heretofore been recognized and much more work is necessary to clarify the true structure relationships.

This group of uranyl minerals occurs almost exclusively in alteration haloes on uraninite in association with the uranyl oxide hydrates. The Pb minerals are common because of the available radiogenic Pb especially in geologically older deposits. The phases are usually very fine-grained and intimately intergrown with other minerals or with one another. Only rarely do they form as recognizable small crystals. Colour can be a guide to specific mineral identifications, but X-ray diffrac-

uranyl oxide from Margnac that was never named.

A provocative web of mineral associations has been proposed by Deliens[46] (Fig. 8). It is interesting to note that the Pb–uranyl oxide hydrates diverge considerably in their associations. Work should be performed to verify this divergence in other deposits where many secondary minerals exist. Curite, in particular, is suggested as a major precursor of many phosphates and silicates. Synthetic studies by Vochten and Deliens[177] and Vochten *et al.*[178] have shown that curite can be transformed easily into meta-autunite and metatorbernite.

Uranyl silicates

The uranyl silicate minerals occur in all types of deposits. They may be found close to the uraninite or other primary minerals as one of the first-formed oxidation products, or they may be found in isolated occurrences as trace coatings far from any obvious source. By far the most common silicate is uranophane, which may actually be the most common of all the

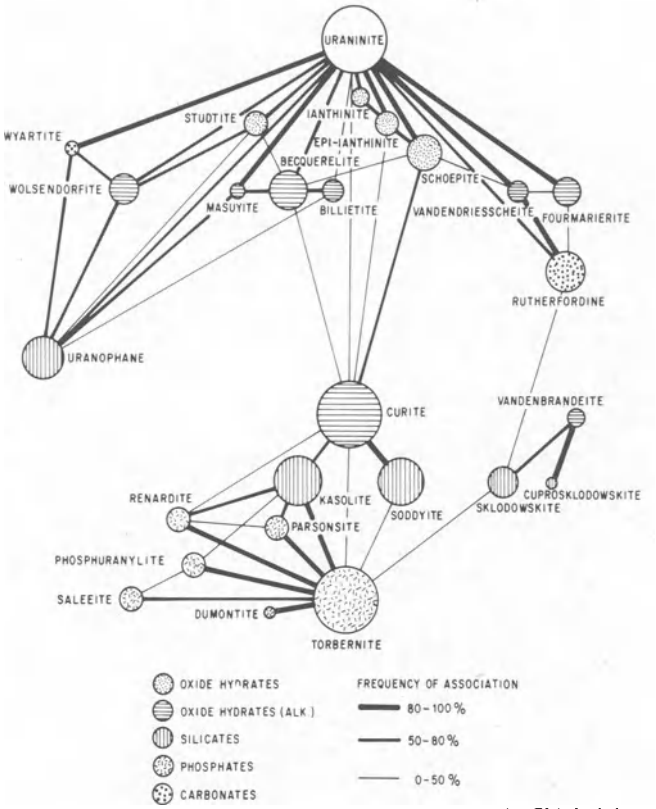

Fig. 8 Paragenesis of oxidized uranium minerals in Shinkolobwe deposit, Zaire. After Deliens[46]

uranyl minerals.

New uranyl silicates described since 1958[63] include boltwoodite, sodium boltwoodite, haiweeite, weeksite and several unnamed minerals. Each of the named minerals has since been found in multiple localities. Boltwoodite[64] was discovered in sandstone deposits of the Colorado Plateau, U.S.A. Honea[83] described the mineral more thoroughly. Sodium boltwoodite was characterized by Chernikov and co-workers[34] from the arid regions of the U.S.S.R., where it forms thin powdery crusts. Weeksite, the first of the 1:3 uranyl silicates to be recognized (around 1950), was described by Outerbridge *et al.*[120] It resembles uranophane and occurs in rhyolites and sandstones. The sodium analogue of weeksite can be synthesized hydrothermally at around 150–300°C. Haiweeite is a chemical analogue of weeksite, which contains Ca rather than K. It was described by McBurney and Murdoch[104] from the Haiwee reservoir in California, U.S.A., where it occurs as yellow spherulitic aggregates on fracture surfaces in granite. Chernikov and co-workers[33] described a mineral called ursilite, which is evidently equivalent to haiweeite. It also occurs in cracks in granitic rocks. One of the specimens that they described is Mg-rich and probably represents a magnesium haiweeite as a valid mineral species. A mineral described as gastunite[82] has been shown to be equivalent to haiweeite by Ertl and Ertl.[55] Ranquilite[1] is also probably equivalent to haiweeite. Several unnamed uranyl silicate minerals have been described by Threadgold[173] from Northern Territory, Australia, Walenta[183] from Menzenschwand, Germany, Emerson and Wright[53] from Montana, U.S.A., and Stohl and Smith[169] from New

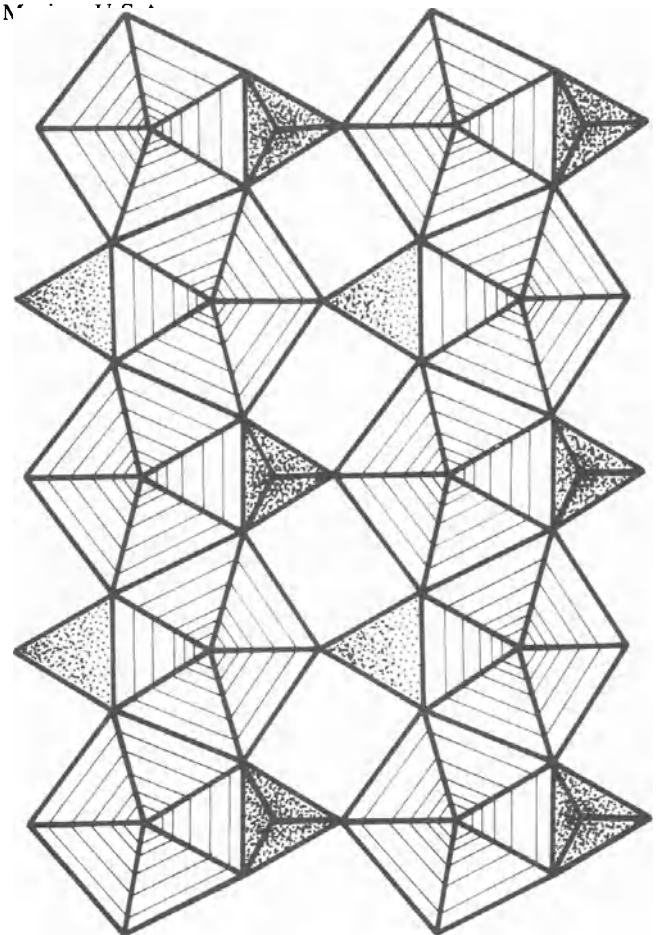

Fig. 9 Uranyl silicate chain and sheet structure as found in 1:1 uranyl silicates (uranium 2–5 polyhedra ruled and SiO_4 tetrahedra stippled)

Chemically, the uranyl silicates form three groups depending on the uranium/silicon ratio. The most populated group, the 1:1 group, is one of the best studied. Stohl and Smith[169] and Sidorenko and co-workers[156] reviewed the crystal chemistry of these minerals. They showed that all 1:1 minerals have essentially the same basic structural unit $[(UO_2)SiO_4]_n^{2n+}$, an infinite chain of edge-shared uranyl pentagonal dipyramids and silicate

Table 9 Uranyl silicates

$(UO_2):(TO_4)$	Mineral	Formula	System	Lattice constants, Å (symmetry)
2:1	Soddyite (F)	$(UO_2)_2SiO_4 \cdot 2H_2O$	Orth.	$a=8.32$ $b=11.21$ $c=18.71$ ($Fddd$)
1:1	Betauranophane (F)	$(H_3O)_2Ca(UO_2)_2(SiO_4)_2 \cdot 3H_2O$	Mono.	$a=6.64$ $b=15.55$ $c=14.01$ $\beta=91°$ ($P2_1/a$)
	Boltwoodite	$K_2(UO_2)_2(SiO_3OH)_2 \cdot 5H_2O$	Mono.	$a=13.71$ $b=7.14$ $c=12.35$ $\beta=102.2$ ($P2_1$)
	Cuprosklodowskite (F)	$(H_3O)_2Cu(UO_2)_2(SiO_4)_2 \cdot 4H_2O$	Tricl.	$a=9.21$ $b=6.63$ $c=7.06$ $\alpha=90°$ $\beta=110°$ $\gamma=108°30'$ ($P\bar{1}$)
	Kasolite (F)	$Pb_2(UO_2)_2(SiO_4)_2 \cdot 2H_2O$	Mono.	$a=13.31$ $b=7.02$ $c=6.72$ $\beta=104.7$ ($P2_1/c$)
	Sklodowskite (F)	$(H_3O)_2Mg(UO_2)_2(SiO_4)_2 \cdot 4H_2O$	Mono.	$a=17.28$ $b=7.03$ $c=6.56$ $\beta=105.88$ ($C2/m$)
	Sodium boltwoodite	$(H_3O)_2(Na,K)_2(UO_2)_2(SiO_4)_2 \cdot 2H_2O$	Orth.	$a=27.40$ $b=7.02$ $c=6.65$
	Uranophane (F)	$(H_3O)_2Ca(UO_2)_2(SiO_4)_2 \cdot 3H_2O$	Mono.	$a=15.87$ $b=7.05$ $c=6.66$ $\beta=97°15'$ ($P2_1$)
1:3	Haiweeite	$Ca(UO_2)_2Si_6O_{15} \cdot 5H_2O$	Mono.	$a=15.4$ $b=7.05$ $c=7.10$ $\beta=107°52'$ ($P2/c$)
	Weeksite	$K_2(UO_2)_2Si_6O_{15} \cdot 4H_2O$	Orth.	$a=14.26$ $b=35.88$ $c=14.20$ ($Fmmm$)
	Haiweeite-(Mg)	$Mg(UO_2)_2Si_6O_{15} \cdot 9H_2O$		

tetrahedra. These chains, shown in Fig. 9, cross-link through corner sharing to form infinite sheets. All the minerals of this group have these sheets, with slight differences, depending on how the free apex of the SiO_4 groups is arranged. The interlayer region contains the cations, oxonium and water molecules. Oxonium ions are an essential part of all structures except kasolite and possibly boltwoodite. Their role may be similar to that of oxonium in the uranyl oxide hydrates. The water of hydration seems to be of two types—that which forms part of the coordination sphere around the cation and additional water that appears to lie in open channels and behaves like that in a zeolite. This zeolitic water accounts for the variability in chemical analyses that have been reported.

When crystalline, all the 1:1 minerals show a bladed to acicular crystal habit. Often, the crystals form radiating sprays sometimes up to 5 cm in diameter. Individual crystals are rare; usually needles are many crystals in near-parallel orientation. Except for cuprosklodowskite, which is green, and kasolite, which is yellow-orange, the minerals are yellow to pale yellow. Uranophane and beta-uranophane show a weak yellow-green fluorescence in shortwave ultraviolet. Colour and crystal habit are the best field guides for identification, but X-ray diffraction is the best method for positive characterization.

The 1:3 uranyl silicates comprise haiweeite and weeksite. These minerals have the same occurrences as the 1:1 minerals, but they are not as common. These minerals also show acicular to prismatic habits and yellow to white colours. The mineral ranquilite, which was described by de Abeledo and co-workers[1] is evidently identical with haiweeite. Ursilite may be a valid magnesium haiweeite, but more work is needed to validate its existence. A sodium analogue of weeksite occurs in hydrothermal experiments at 300°C with synthetic nuclear reactor waste.[105]

Six of the members of the 1:1 minerals have had structure determined by Smith and co-workers[161] and has been refined by Stohl and Smith.[169] The structure of beta-uranophane was determined by Smith and Stohl.[162] A structure analysis of boltwoodite was reported by Stohl and Smith.[169] The structure of kasolite was originally carried out by Huynen and co-workers[87] and was refined by Mokeeva[111] and by Rosenzweig and Ryan.[141] The sklodowskite structure was analysed by Mokeeva[109] and refined by Huynen and Van Meerssche,[88] Mokeeva[110] and Ryan and Rosenzweig.[147] The cuprosklodowskite structure was originally determined by Piret-Meunier and Van Meerssche[130] and was refined by Rosenzweig and Ryan.[139] An anhydrous $Na_2(UO)_2SiO_4$ was reported by Shashkin and co-workers,[153] which shows an unrelated structure with uranium in 2–4 coordination.

Crystal structure analyses of weeksite and the synthetic sodium analogue by Stohl and Smith[169] and Anderson[4] have shown that the basic structural unit is the $[(UO_2)SiO_4]$ infinite chain as found in the 1:1 compounds. The chains lie parallel (as shown in Fig. 10), but do not cross link. Instead, the additional SiO_4 tetrahedra form bridges between the chains. These bridges have not been resolved in the crystal structure studies. The interlayer cations and water molecules have the same roles as in the 1:1 compounds. Further structural studies are needed.

The 2:1 mineral soddyite also occurs in ways similar to the other uranyl silicates. No structure study has been accomplished on soddyite, but it is evidently isostructural with $(UO_2)_2GeO_4{\cdot}2H_2O$, $a = 8.179$ Å, $b = 11.515$ Å, $c = 19.297$ Å.[97] In this compound the same type of uranyl silicate chains exist, but they cross link by having each Si tetrahedrum part of two chains, as shown in Fig. 11. The resulting structure is a framework of chains crossing at 90°. Water molecules occupy sites within the framework.

Several compositions have been reported for soddyite and there may be several related minerals rather than only one. Gorman[75] described the physical properties of soddyite, indicating that crystals are usually zoned, but the different parts show the same X-ray powder pattern. Stohl and Smith[169] described another specimen that shows the same X-ray powder

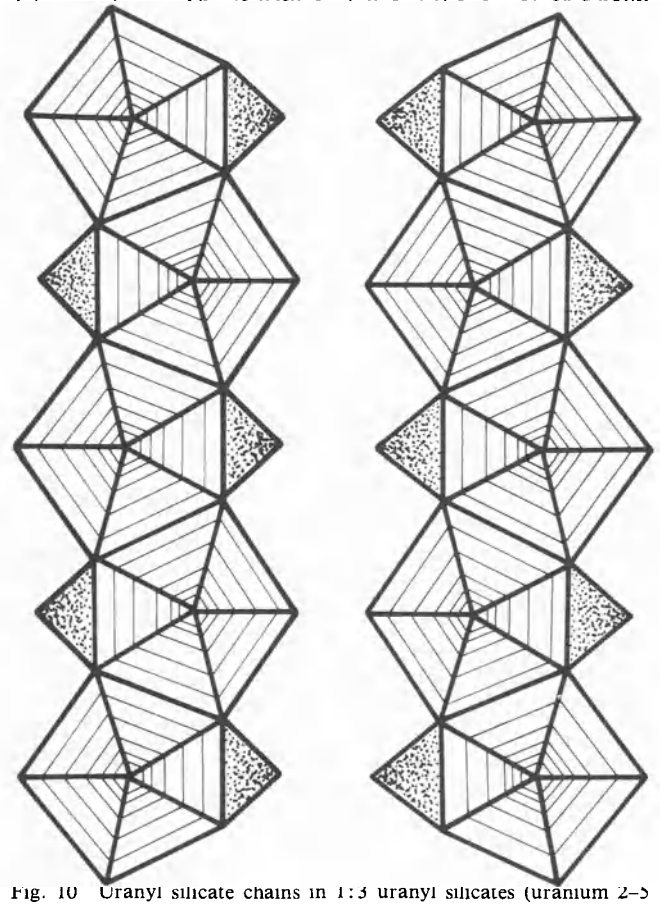

Fig. 10 Uranyl silicate chains in 1:3 uranyl silicates (uranium 2–5 polyhedra ruled and SiO_4 tetrahedra stippled)

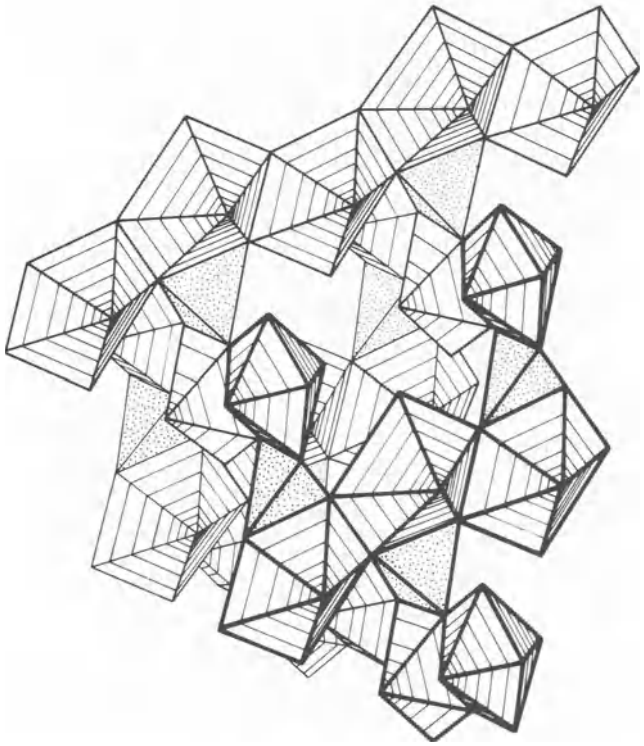

Fig. 11 Structure of soddyite, $(UO_2)_2SiO_4{\cdot}2H_2O$ (uranium 2–5 polyhedra ruled and SiO_4 tetrahedra stippled; chains, as found in other uranyl silicates, lie 90° to one another and share SiO_4 tetrahedra)

pattern but on which single crystal studies show a triclinic unit cell rather than the orthorhombic cell that is usually reported. It is quite evident that this group of minerals requires much work to clear up these problems.

Uranyl phosphates and arsenates

The uranyl phosphates and arsenates comprise the largest group of uranium minerals and, except for uranophane, the most abundant mineral group. Table 10 lists the known minerals in this group. The autunite and meta-autunite families are expanded and listed as individual species in Tables 11 and 12. This group shows several divisions based on the $UO_2:TO_4$ ratio, and the individual divisions show considerable structural similarity.* The phosphates and arsenates are grouped together because of the many analogies that exist.

Table 10 Uranyl phosphates and arsenates

$UO_2:TO_4$	Mineral	Formula	System	Lattice constants, Å (symmetry)
4:2	Arsenuranylite	$Ca(UO_2)_4(AsO_4)_2(OH)_4\cdot 6H_2O$ possibly $Ca_2(UO_2)_3(AsO_4)_2(OH)_4\cdot 6H_2O$	Orth.	$a=15.40$ $b=17.40$ $c=13.77$
	Bergenite	$Ba(UO_2)_4(PO_4)_2(OH)_4\cdot 8H_2O$ possibly $Ba_2(UO_2)_3(PO_4)_2(OH)_4\cdot 8H_2O$	Orth.	$a=16.05$ $b=17.76$ $c=13.86$ (*Bmmb*)
	Kivuite	$(Th,Ca,Pb)(H_3O)_2(UO_2)_4(PO_4)_2(OH)_8\cdot 5H_2O$ possibly $(Th,Ca,Pb)(H_3O)_2(UO_2)_3(PO_4)_2(OH)_6\cdot 5H_2O$	Orth.	$a=15.88$ $b=17.24$ $c=13.76$ (*Bmmb*)
	Renardite (F)	$Pb(UO_2)_4(PO_4)_2(OH)_4\cdot 7H_2O$ possibly $Pb_2(UO_2)_3(PO_4)_2(OH)_4\cdot 7H_2O$	Orth.	$a=15.9$ $b=17.6$ $c=13.8$
3:2	Dumontite (F)	$Pb_2(UO_2)_3(PO_4)_2(OH)_4\cdot 3H_2O$	Mono.	$a=8.16$ $b=16.73$ $c=7.02$ $\beta=110°$
	Huegelite	$Pb_2(UO_2)_3(AsO_4)_2(OH)_4\cdot 3H_2O$	Similar to dumontite	
	Phosphuranulite (F)	$(H_3O)_2Ca(UO_2)_3(PO_4)_2(OH)_4\cdot 4H_2O$	Orth.	$a=15.85$ $b=17.42$ $c=13.76$ (*Bmmb*)
	Phurcalite	$Ca_2(UO_2)_3(PO_4)_2(OH)_4\cdot 4H_2O$	Orth.	$a=17.366$ $b=15.957$ $c=13.548$ (*Pbca*)
	Phuralumite	$Al_2(UO_2)_3(PO_4)_2(OH)_6\cdot 10H_2O$	Mono.	$a=13.87$ $b=20.79$ $c=9.38$ $\beta=112°$ ($P2_1/a$)
	Upalite	$Al(UO_2)_3(PO_4)_2(OH)_3$	Orth.	$a=34.68$ $b=16.81$ $c=13.72$ (*Bbcm*)
	Vanmeersscheite	$U(UO_2)_3(PO_4)_2(OH)_6\cdot 4H_2O$	Orth.	$a=17.04$ $b=16.76$ $c=7.023$ ($P2_1mn$)
	Metavanmeersscheite	$U(UO_2)_3(PO_4)_2(OH)_4\cdot 2H_2O$	Orth.	$a=34.18$ $b=33.88$ $c=14.074$ ($Fαd2$)
1:1	Autunite family (F)	$R_{1-2}(UO_2)_2(TO_4)_2\cdot 8\text{–}12H_2O$	See Table 11	
	Dewindtite (F)	$Pb(UO_2)_2(PO_4)_2\cdot 3H_2O$	= renardite?	
	Meta-autunite I family (F)	$R_{1-2}(UO_2)_2(TO_4)_2\cdot 6\text{–}8H_2O$	See Table 12	
2:3	Coconinoite	$Fe_2Al_2(UO_2)_2(PO_4)_2(SO_4)(OH)_2\cdot 20H_2O$	Mono.	
2:4	Furongite	$Al_2(UO_2)(PO_4)_2(OH)_2\cdot 8H_2O$	Tricl.	$a=17.87$ $b=14.18$ $c=12.18$ $\alpha=67.8°$ $\beta=77.5$ $\gamma=79.9$
	Hallimondite	$Pb(UO_2)(AsO_4)_2\cdot nH_2O$	Tricl.	$a=7.123$ $b=10.469$ $c=6.844$ $\alpha=100°34'$ $\beta=94°48'$ $\gamma=91°16'$
	Parsonite (F)	$Pb(UO_2)(PO_4)_2\cdot nH_2O$	Tricl.	$a=6.862$ $b=10.425$ $c=6.684$ $\alpha=101°26'$ $\beta=98°15'$ $\gamma=86°17'$
	Pseudo-autunite	$(H_3O)_4Ca_2(UO_2)_2(PO_4)_4\cdot 5H_2O$	Orth.	$a=6.95$ $b=6.95$ $c=12.88$
	Walpurgite (F)	$(BiO)_4(UO_2)_2(AsO_4)_4\cdot 6H_2O$	Tricl.	$a=7.135$ $b=10.426$ $c=5.494$ $\alpha=101.47°$ $\beta=110.82°$ $\gamma=88.20°$
	Walpurgite–(P)	$(BiO)_4(UO_2)_2(PO_4)_4\cdot 6H_2O$	Tricl.	

Many of the phosphate–arsenate minerals have been described since Frondel.[63] Arsenuranylite was described by Belova[12] from the oxidized zone of a sulphide deposit, where it occurs as orange lichen-like growths with other uranium minerals. It was considered as the arsenate analogue of phosphuranylite and probably should have a different formula. Bergenite, described by Bültemann and Moh,[21] and kivuite, described by Van Wambeke,[176] also were considered analogues of phosphuranylite–renardite and need more data on the true formula. Bergenite is found in dumps at a mine at Streuberg in Saxony, where it forms yellow crusts with other uranium minerals. Kivuite is from the Kobokobo pegmatite, Kivu, Zaire, where it occurs as yellow earthy masses. Walenta and Wimmenauer[187] showed that huegelite, originally described as a vanadate, was actually a Pb uranyl arsenate very similar to dumontite. It occurs as orange-yellow crystals in cavities in a hornstone breccia near Lahr, Baden. It is considered to be the arsenate analogue of dumontite. Phurcalite, phuralumite and upalite were described by Deliens and Piret.[47,49] Phurcalite is from the Bergen, Vogtland, Saxony area, where it occurs as yellow platelets with specular hematite. Phuralumite and upalite are from Kobokobo, Kivu, Zaire, where both occur in a beryl–columbite pegmatite. Vanmeersscheite and metavanmeersscheite, also from Kobokobo, have been described by Piret and Deliens.[127a]

Coconinoite, a phosphate–sulphate, was described by Young and co-workers[191] from several deposits in the Colorado Plateau, Arizona and Utah, U.S.A. It occurs as light yellow, soft encrustations in sandstones. It seems to represent a unique mineral group.

Furongite was described by the Hunan 230 Laboratory[84] as a yellow, minutely crystalline deposit on carbonaceous shale in the oxidized zone of an illuvial-type uranium deposit. Walenta and Wimmenauer[187] described hallimondite from Lahr, Baden. It is very similar to parsonsite. Pseudo-autunite was characterized by Sergeev[150] from fenitized rocks of the exocontact zone of a massif of ultrabasic–alkaline rocks of northern Karelia, U.S.S.R. Walpurgite-(P), an unnamed phosphate analogue of walpurgite, was described in Soboleva and Pudovkina.[163]

*In a general crystal-chemical formula T stands for any of several tetrahedrally coordinated cations and X for any three-coordinated cations.

Table 11 The autunite family

Mineral	Formula	System	Lattice constants, Å (symmetry)
Arsenuranospathite	$HAl(UO_2)_4(AsO_4)_4 \cdot 40H_2O$	Tetr.	$a = 7.00$ $c = 20.64$ ($I4/mmm$)
Autunite (F)	$Ca(UO_2)_2(PO_4)_2 \cdot 8\text{–}12H_2O$	Tetr.	$a = 7.00$ $c = 20.67$ ($I4/mmm$)
Fritzcheite* (F)	$Mn(UO_2)_2(VO_4)_2 \cdot 10H_2O$		
Heinrichite	$Ba(UO_2)_2(AsO_4)_2 \cdot 10\text{–}12H_2O$	Tetr.	$a = 7.13$ $c = 20.56$
Kahlerite (F)	$Fe(UO_2)_2(AsO_4)_2 \cdot 10\text{–}12H_2O$	Tetr.	$a = 14.30$ $c = 21.97$ ($P4_2/n$)
			$a = 7.16$ $c = 20.19$
Novacekite (F)	$Mg(UO_2)_2(AsO_4)_2 \cdot 12H_2O$	Tetr.	$a = 14.30$ $c = 22.00$ ($P4_2/n$)
Sabugalite (F)	$HAl(UO_2)_4(PO_4)_4 \cdot 16H_2O$	Tetr.	$a = 6.96$ $c = 19.3$
Saleeite (F)	$Mg(UO_2)_2(PO_4)_2 \cdot 10H_2O$	Tetr.	$a = 6.98$ $c = 19.71$ ($P4/nmm$)
Threadgoldite	$Al(UO_2)_2(PO_4)_2(OH) \cdot 8H_2O$	Mono.	$a = 20.25$ $b = 9.85$ $c = 19.75$ $\beta = 111.4°$ ($C2/c$)
Torbernite (F)	$Cu(UO_2)_2(PO_4)_2 \cdot 8\text{–}12H_2O$	Tetr.	$a = 7.06$ $c = 20.54$ ($I4/mmm$)
Uranocircite (F)	$Ba(UO_2)_2(PO_4)_2 \cdot 12H_2O$	Tetr.	$a = 7.01$ $c = 20.46$
Uranospathite (F)	$HAl(UO_2)_4(PO_4)_4 \cdot 40H_2O$	Tetr.	$a = 7.00$ $c = 30.02$ ($P4_2/n$[?])
Uranospinite (F)	$Ca(UO_2)_2(AsO_4)_2 \cdot 10H_2O$	Tetr.	$a = 7.16$ $c = 20.4$ ($I4/mmm$)
Xiangjiangite	$(Fe,Al)(UO_2)_4(PO_4)_2(SO_4)_2(OH) \cdot 22H_2O$	Orth.	$a = 7.17$ $b = 7.17$ $c = 22.22$
Zeunerite (F)	$Cu(UO_2)_2(PO_4)_2 \cdot 40H_2O$	Tetr.	$a = 7.18$ $c = 20.79$ ($P4/nnc$)

* More likely a member of the carnotite group.

Table 12 The meta-autunite family

Mineral	Formula	System	Lattice constants, Å (symmetry)
Abernathyite (F)	$K_2(UO_2)_2(AsO_4)_2 \cdot 8H_2O$	Tetr.	$a = 7.176$ $c = 18.126$ ($P4/ncc$)
Bassettite (F)	$Fe(UO_2)_2(PO_4)_2 \cdot 8H_2O$	Mono.	$a = 6.98$ $b = 17.07$ $c = 7.01$ $\beta = 90°32'$
Meta-ankoleite	$K_2(UO_2)_2(PO_4)_2 \cdot 6H_2O$	Tetr.	$a = 6.993$ $c = 8.891$ ($P4/nmm$)
Meta-autunite (F)	$Ca(UO_2)_2(PO_4)_2 \cdot 6H_2O$	Tetr.	$a = 6.972$ $c = 8.47$ ($P4/nmm$) $a = 19.65$ $c = 8.47$
Meta-autunite II (F)	$Ca(UO_2)_2(PO_4)_2 \cdot 4\text{–}6H_2O$	Orth.	$a = 6.551$ $b = 7.053$ $c = 8.164$ ($Pmmm$)
Metaheinrichite	$Ba(UO_2)_2(AsO_4)_2 \cdot 8H_2O$	Tetr.	$a = 7.07$ $c = 17.74$ ($P4_2/m$)
Metakahlerite	$Fe(UO_2)_2(AsO_4)_2 \cdot 8H_2O$	Tetr.	$a = 7.18$ $c = 8.58$
Metakirchheimerite	$Co(UO_2)_2(AsO_4)_2 \cdot 8H_2O$	Tetr.	$a = 7.16$ $c = 8.60$
Metalodevite	$Zn(UO_2)(AsO_4)_2 \cdot 10H_2O$	Tetr.	$a = 7.16$ $c = 17.20$ ($P4_2/m$)
Metanovacekite (F)	$Mg(UO_2)_2(AsO_4)_2 \cdot 4\text{–}8H_2O$	Tetr.	$a = 7.16$ $c = 8.58$ ($P4/n$)
Metatorbernite (F)	$Cu(UO_2)_2(PO_4)_2 \cdot 8H_2O$	Tetr.	$a = 6.969$ $c = 17.306$ ($P4/n$)
Meta-uranocircite (F)	$Ba(UO_2)_2(PO_4)_2 \cdot 8H_2O$	Tetr.	$a = 6.94$ $c = 17.65$ ($P4_2/m$) $a = 7.19$ $c = 8.81$ ($P4/nmm$)
Meta-uranocircite II (F)	$Ba(UO_2)_2(PO_4)_2 \cdot 6H_2O$	Mono.	$a = 9.855$ $b = 9.756$ $c = 16.84$ $\gamma = 90°36'$ ($P2_1$)
Meta-uranospinite (F)	$Ca(UO_2)_2(AsO_4)_2 \cdot 8H_2O$	Tetr.	$a = 7.14$ $c = 17.00$ ($P4/nmm$)
Metazeunerite (F)	$Cu(UO_2)_2(AsO_4)_2 \cdot 8H_2O$	Tetr.	$a = 7.10$ $c = 17.42$ ($P4_2/n$)
Przhevalskite	$Pb(UO_2)_2(PO_4)_2 \cdot 2H_2O$	Orth.	
Ranunculite	$(H_3O)Al(UO_2)(PO_4)(OH)_3 \cdot 3H_2O$	Mono.	$a = 11.1$ $b = 17.7$ $c = 18.0$ $\beta = 90°$
Sodium meta-autunite	$(Na_2,Ca)(UO_2)_2(PO_4)_2 \cdot 8H_2O$	Tetr.	$a = 6.97$ $c = 8.96$ ($P4/nmm$)
Sodium uranospinite	$(Na_2,Ca)(UO_2)_2(AsO4)_2 \cdot 5H_2O$	Tetr.	$a = 7.12$ $c = 8.70$ ($P4/nmm$)
Trögerite (F)	$UO_2(UO_2)_2(AsO_4)_2 \cdot 8H_2O$	Tetr.	$a = 7.16$ $c = 8.80$ ($P4/nmm$)
Trögerite-(P)	$UO_2(UO_2)_2(PO_4)_2 \cdot 8H_2O$	Tetr.	$a = 7.02$ $c = 8.49$ ($P4/nmm$)
Uramphite	$(NH_4)_2(UO_2)_2(PO_4)_2 \cdot 4\text{–}6H_2O$	Tetr.	$a = 7.01$ $c = 9.05$

Several new autunite-like and meta-autunite-like minerals include arsenuranospathite,[186] heinrichite and metaheinrichite,[11,77] threadgoldite,[50] xiangjiangite,[85] meta-ankoleite,[70] metakirchheimerite,[180] metalodevite,[2] metakahlerite and meta-uranospinite,[181] przhevalskite,[163,164] ranunculite,[48] sodium meta-autunite,[32] sodium uranospinite,[92] trögerite-(P)[155] and uramphite.[117] These new minerals occur in all types of secondary uranium deposits, including igneous and sedimentary terrains and pegmatites.

The common nature of the uranyl phosphates and arsenates is evidently related to the ease of forming UO_2–PO_4 or UO_2–AsO_4 complexes in solution.[95] Phosphorus and, apparently, arsenic are available in sufficient abundance around uranium deposits to allow these complexes to be significant factors in the transport of uranium in groundwater. These complexes can encounter the various cations represented in the mineral list and precipitate directly as the mineral species or a pre-existing mineral may exchange its cations with another in solution. Evidently, more than one complex may exist in solution, as suggested by the several types of crystal structures encountered.

Chemically, the uranyl phosphates fall into five distinct groups, depending on the UO_2:TO_4 ratio, though the classification of some of the species is in doubt. Phosphuranulite, for example, has been reported with U:P both 4:2 and 3:2. The similarity of the unit cells in the 4:2 and 3:2 groups suggests that this problem may be more prevalent. Crystal structures for dumontite,[129] phosphuranylite,[154] phurcalite[123] and phuralumite[128] verify the 3:2 ratio and show a chain unit, $[(UO_2)_3(PO_4)_2(OH)_2]$, which is the basic unit of this group. This structure is shown in Fig. 12. Pentagonal and hexagonal dipyramids of uranium polyhedra share edges with other dipyramids and with PO_4 tetrahedra. Corner sharing results in a sheet-like unit. Cations and water molecules occupy interlayer sites. No structural study has been made on any of the 4:2 compounds, but their powder patterns and cell dimensions are very similar to phurcalite and the other 3:2 compounds, which suggests that they may actually be 3:2 compounds.

By far the largest and best studied group of phosphates and arsenates is the 1:1 compounds. Except for dewindtite, which is a doubtful phase, possibly equivalent to renardite, this group

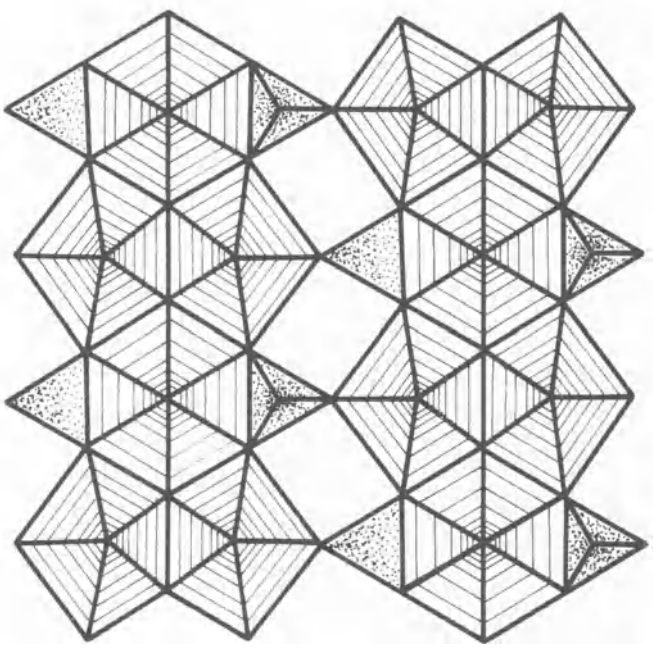

Fig. 12 Uranyl phosphate chain and sheet structure as found in 3:2 uranyl phosphates (uranium 2–5 and 2–6 polyhedra ruled and PO_4 tetrahedra stippled)

may be divided into two families—the autunites and the meta-autunites. Both these families have the same basic structural unit, an infinite sheet, and differ primarily in the degree of hydration and the way in which the sheets are stacked. If the mineral is near maximum hydration, the layer spacing is around 10 Å (or 20 Å for doubled cells). These minerals comprise the autunites. The sheet unit is usually $[(UO_2)_2(TO_4)_2]$, and the corresponding level of hydration is usually $10–12H_2O$. When the hydration level is $6–8H_2O$, the layers collapse somewhat, and the layers spacing is around 9 Å (or 18 Å). These minerals comprise the meta-autunites. So many pairs of minerals have the same composition, but differ in water content, that it is now customary to use the same name and add the 'meta' prefix to the lower hydrate. Even when an equivalent higher hydrate is not known to occur naturally, it is now the practice to use the 'meta' prefix if the layer spacing is 9 Å. Thus, meta-ankoleite and metalodevite are used, even though ankoleite or lodevite have not been described.

The meta-autunite family is the largest family, probably because many of the minerals are found in sandstone deposits in arid or semi-arid climates. Actually, practically all museum specimens of the autunite minerals prove to be meta-autunites when rechecked. This situation suggests that many specimens were initially misidentified or it may be that they have dehydrated in the museum atmosphere during storage. Once an autunite has dehydrated, which appears to happen readily, rehydration does not occur. The occurrence of an autunite thus implies formation in a cool humid climate and minerals from such localities should be carefully collected and maintained in a humid state for study.

Crystal structure studies have only been made on members of the meta-autunite family. Abernathyite and metatorbernite have been studied by Ross and Evans,[143] and Ross and co-workers,[144] meta-uranocircite by Zolensky[193] and Khosrawan-Sazedj,[89a] threadgoldite by Piret and co-workers,[124] and hydrogen–meta-autunite by Morosin.[112] These studies verify the general meta-autunite structure proposed by Beintema,[10] but show that there are subtle structural differences among the species. The basic unit is an infinite sheet of 2–4 UO_6 polyhedra and $(P,As)O_4$ tetrahedra, which share corners. Ideally, this sheet has tetragonal symmetry. It is shown in Fig. 13, which also shows how the sheets are proposed to

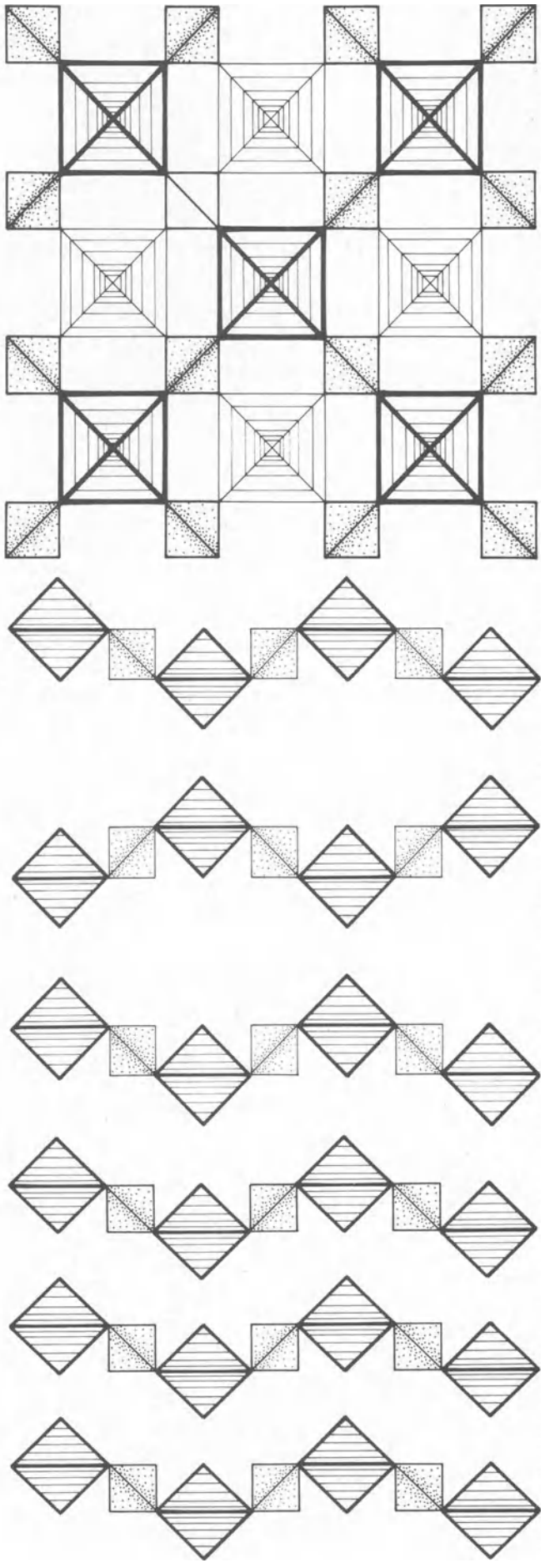

Fig. 13 Ideal uranyl phosphate sheet structure as found in autunite and meta-autunite families. (*a*) (*top*), structure of $[(UO_2)(TO_4)]$ sheet; (*b*) (*centre*), stacking of sheets in autunite family; (*c*) (*bottom*), stacking of sheets in meta-autunite family. After Beintema[10]

stack in autunite and meta-autunite. In all the examined structures the tetrahedra articulate from the ideal orientation due to hydrogen bonding. The actual structure of the sheet in abernathyite is shown in Fig. 14(*a*). The rotation of the tetrahedra results in a more efficient packing of atoms. The sheets are corrugated in that uranyl groups are alternately displaced plus or minus from the average plane of the sheet, depending on which corner of the PO_4 tetrahedra they link to. As proposed by Beintema,[10] the corrugations of the sheet arrange themselves in parallel in the meta-autunite structures but antiparallel in the autunite compounds. Clusters of water molecules occur in the pockets between the sheets along with the alkali-earth or alkali cation. Two arrangements have been found for these interlayer ions. In metatorbernite (Fig. 14(*b*)) distinct Cu ions lie at the centre of a square of four water molecules and between the uranyl ions of the sheet. In abernathyite, meta-uranocircite and hydrogen–meta-autunite the cation site is not occupied and the K^+, Ba^{+2} or $(H_3O)^+$ appears to replace one of the water molecules of the square array in a disordered fashion. The very low true symmetry of the low-temperature form of meta-uranocircite suggests that the Ba may order, but this effect has not yet been confirmed.

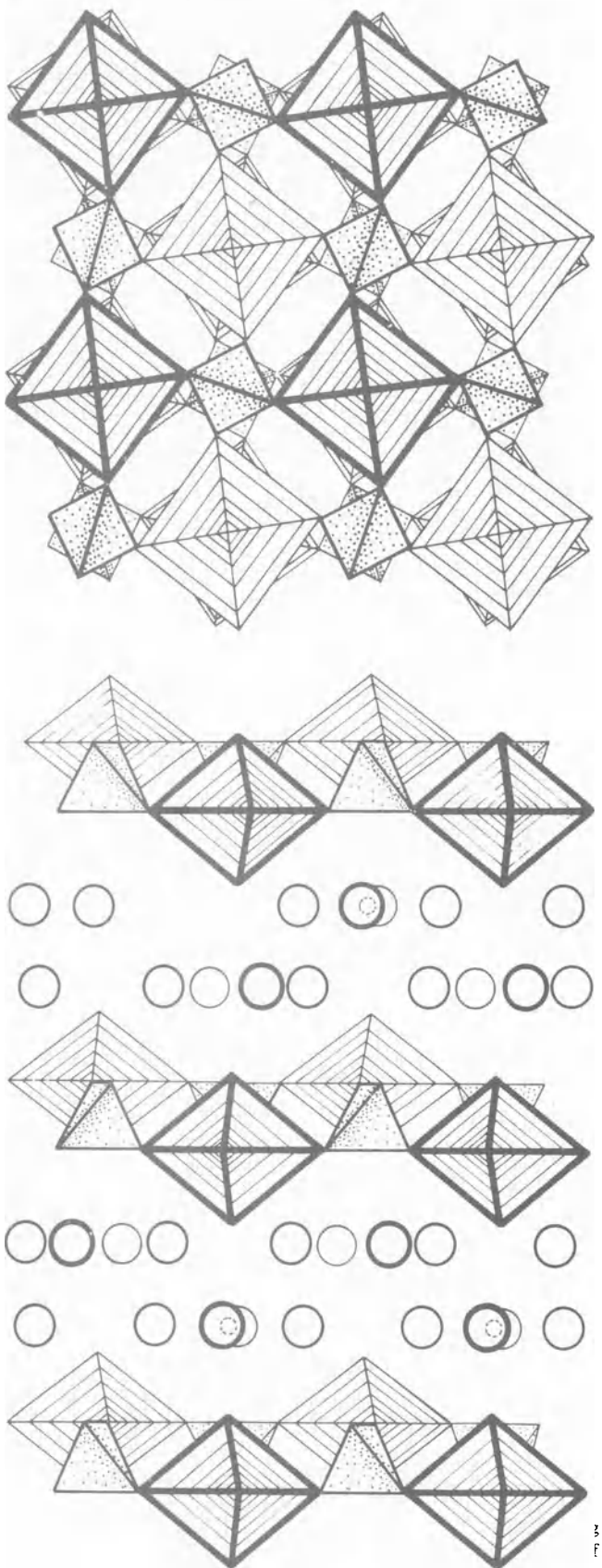

two superimposed $[(UO_2)(AsO_4)]$ sheets showing alternating articulation of polyhedra in adjacent sheets; (*b*) (*bottom*), stacking of sheets in metatorbernite showing interlayer water and cations. Cu atom is the small circle. In abernathyite Cu site is not occupied and K is disordered on H_2O sites. After Ross and Evans[143] and Ross and co-workers[144]

Specimens of trögerite and meta-uranocircite are known to transform from tetragonal to lower symmetry at temperatures near room temperature. For trögerite the transformation is around 25°C;[44] for meta-uranocircite it is at 108°C.[193] A slight distortion in the structure results and the crystals show an extensive cross-grid twinning. Similar transformations occur in other minerals also—for example, Ca and Pb meta-autunites, and may explain the reported meta-autunite II, which is orthorhombic.

The structure of threadgoldite determined by Piret and co-workers[124] shows a complicated derivative of the autunite structure. The structure consists of $[UO_2PO_4]_n^{n-}$ layers that are only slightly distorted from the square array. The stacking of the layers shifts parallel to *c* (the *a*-axis corresponds to the *c*-axis in the tetragonal forms) to accommodate an interlayer Al_2O_{10} double octahedral cluster and to yield a monoclinic structure.

The 2:4 compounds appear to have unrelated crystal structures. Walpurgite shows a chain unit of 2–4UO_6 edge-shared polyhedra with attached AsO_4 tetrahedra.[106b] Pseudo-autunite may be related to the autunite family with extra PO_4 tetrahedra. The other compounds probably have a sheet-like structure also. Coconinoite is a mixed phosphate–sulphate and is therefore quite unique. Until the X-ray powder pattern is indexed and a unit cell is determined, no comments on its character can be made.

The mineral fritzcheite is an enigma. It has been reported to be a member of the autunite group, but this classification is based primarily on morphology. No X-ray data exist and optical data reported by Fairchild[59] indicate a biaxial character. As a vanadate it is more probable that fritzcheite should be grouped with the other vanadates. There is a report of a synthetic Mn phase that supposedly shows a structure related to the autunites,[63] but Cesbron[24] reported a $Mn(UO_2)_2V_2O_8{\cdot}4H_2O$ that is related to other vanadates based on its unit cell. This question cannot be resolved unless the original type material could be examined, but on the basis of the information available it is best to consider fritzcheite along with the other vanadates.

Uranyl vanadates

The uranyl vanadates form mineral groups distinct from the phosphates and arsenates because of the markedly different chemistry of the vanadium ion. Like uranium, vanadium shows several valence states in nature, and its detailed mineralogy is very complex. The crystal chemistry of vanadium was reviewed by Evans.[56] In its lower valence states it forms distinct vanadium minerals, but in its higher valence state 5+ it com-

bines with U^{6+} to form several minerals. These minerals are listed in Table 13.

Table 13 Uranyl vanadates

Mineral	Formula	System	Lattice constants, Å (symmetry)
Carnotite group			
Carnotite (F)	$K_2(UO_2)_2V_2O_8 \cdot 3H_2O$	Mono	$a=10.471$ $b=8.41$ $c=6.59$ $\beta=103°50'$ ($P2_1/a$)
Curienite	$Pb(UO_2)_2V_2O_8 \cdot 5H_2O$	Orth.	$a=10.40$ $b=8.45$ $c=16.34$ (*Pcan*)
Francevillite	$Ba(UO_2)_2V_2O_8 \cdot 5H_2O$	Orth.	$1=10.41$ $b=8.51$ $c=16.76$ (*Pcan*)
Fritzcheite (F)	$Mn(UO_2)_2V_2O_8 \cdot 10H_2O$	Orth.	$a=10.59$ $b=8.25$ $c=15.54$* (*Pnam*)
Margaritasite	$Cs(UO_2)_2V_2O_8 \cdot 1.5H_2O$	Mono.	$a=10.51$ $b=8.45$ $c=7.32$ $\beta=106°5'$ ($P2_1/a$)
Metatyuyamunite (F)	$Ca(UO_2)_2V_2O_8 \cdot 3\text{-}5H_2O$	Orth.	$a=10.54$ $b=8.49$ $c=17.34$ (*Pnam*)
Metavanuralite	$Al(UO_2)_2V_2O_8(OH) \cdot 8H_2O$	Tricl.	$a=10.46$ $b=8.44$ $c=10.43$ $\alpha=75°53'$ $\beta=102°50'$ $\gamma=90°$ ($P\bar{1}$)
Sengierite (F)	$Cu_2(UO_2)_2V_2O_8(OH)_2 \cdot 6H_2O$	Mono.	$a=10.62$ $b=8.10$ $c=10.11$ $\beta=103°36'$ ($P2_1/a$)
Strelkinite	$Na_2(UO_2)_2V_2O_8 \cdot 6H_2O$	Orth.	$a=10.64$ $b=8.36$ $c=32.72$ (*Pnmm*)
Tyuyamunite (F)	$Ca(UO_2)_2V_2O_8 \cdot 8H_2O$	Orth.	$a=10.36$ $b=8.36$ $c=20.40$ (*Pnan*)
Vanuralite	$Al(UO_2)_2V_2O_8(OH) \cdot 11H_2O$	Mono.	$a=10.55$ $b=8.44$ $c=24.52$ $\beta=103°$ (*A2/a*)
Vanuranylite	$(H_3O)_2(UO_2)_2V_2O_8 \cdot 4H_2O$	Mono.	$a=10.49$ $b=8.37$ $c=20.30$ $\beta=90°$?
Unclassified			
Ferghanite (F)	$(UO_2)_3V_2O_8 \cdot 6H_2O$		
Rauvite (F)	$Ca(UO_2)_2V_{10}O_{28} \cdot 16H_2O$		
Unnamed	$Ca\text{-}U\text{-}V\text{-}O\text{-}H_2O$		
Unnamed	$Pb\text{-}U\text{-}V\text{-}O\text{-}H_2O$		
Uvanite (F)	$(UO_2)_2V_6O_{17} \cdot 15H_2O$		

* Data from synthetic $Mn(UO_2)_2V_2O_8 \cdot 4H_2O$.[24] (F)[63]

The uranyl vanadate minerals are most commonly found in the sandstone uranium deposits. In the Colorado Plateau area of the United States they are, in fact, very abundant. Langmuir[95] has shown that uranyl vanadates are the least soluble of all the uranium minerals, which indicates that if any vanadium is present, it will effectively precipitate the uranium. Concentrations of carnotite and tyuyamunite are large enough in some areas to be actually the major ore mineral in some deposits. Carnotite is the dominant mineral in some calcrete deposits in Australia.[101] Usually, the minerals occur as fine coatings on sand grains and in the pore spaces. Rarely are they sufficiently coarse-grained to reveal distinct crystals. Carnotite and tyuyamunite are usually recognized by their greenish-yellow colour, which is rather distinctive but not unique among the yellow uranium minerals. The better crystalline forms are bright yellow. Most of the other vanadates are also yellow, except for sengierite, which is green owing to the Cu, and rauvite and uvanite, which are brown or blackish violet. Rauvite and uvanite often show a waxy appearance and coat slickensided surfaces. Individual crystals of these two minerals have never been obtained.

About half these minerals have been described since Frondel's[63] monograph. Curienite was identified as a new mineral by Cesbron and Morin[28] from the mineralized sandstones of Mounana mine, Gabon, where it occurs with francevillite. Francevillite was recognized by Branche *et al.*[15] from the region of Franceville, Gabon, where it occurs as impregnations, cryptocrystalline veinlets and in moderate-size crystals. It has since been found in several localities, including other sandstone deposits and alteration zones in pegmatites. Strelkinite was described by Alekseeva *et al.*[3] from Palaeozoic carbonaceous–siliceous shales and has since been found in other related rocks. Vanuralite was first characterized by Branche *et al.*[16] from Mounana, Gabon. Cesbron[23] recognized two hydration states and fully characterized vanuralite as well as metavanuralite. Vanuranylite is the oxonium member of this group and is found in sandstone deposits in the U.S.S.R. It was described by Buryanova and co-workers.[22] Margaritasite, the newest mineral to be described, was found in Mexico by Wenrich-Verbeek *et al.*[189]

In the crystal chemistry review of the vanadium minerals it was shown[56] that vanadium occurs as different complex units in the structures. The V^{5+} may form discrete VO_4 groups as in vanadinite, but only fritzcheite has been proposed to have this anion. More commonly, vanadates polymerize into complex anions. Of the known polyanions only $(V_2O_8)^{6-}$ and $(V_{10}O_{28})^{6-}$ have been verified in uranium vanadates. The structural unit in

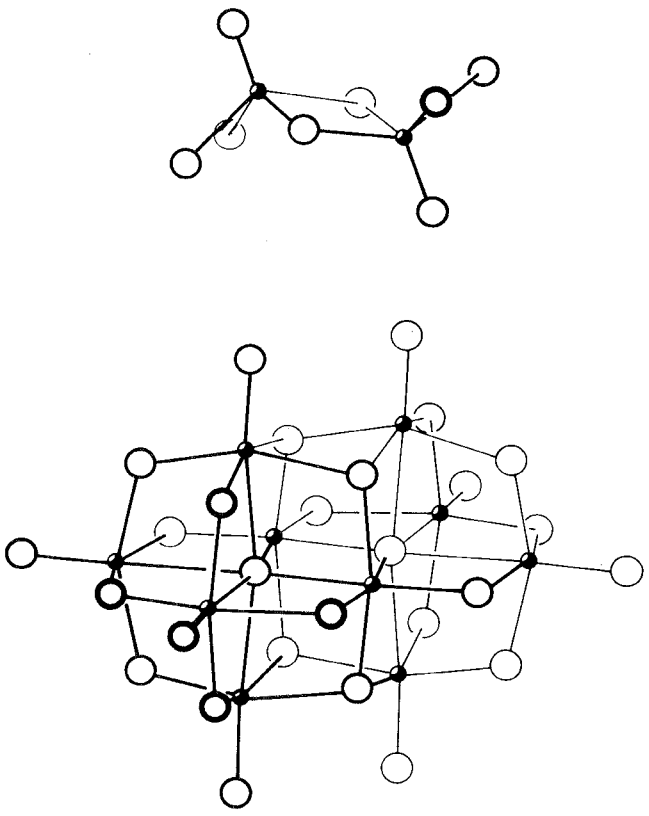

Fig. 15 Complex vanadate ions found in uranyl vanadate minerals. (*a*) (*top*), $(V_2O_8)^{6-}$ unit of carnotite family. After Cesbron and Borène.[25] (*b*) (*bottom*), $(V_{10}O_{28})^{6-}$ ion as found in rauvite. After Swallow and co-workers[170]

uvanite is not known, but it may be $(V_6O_{17})^{4-}$.

The vanadates in Table 13 have been grouped into a carnotite family and other minerals. The carnotite family is characterized by the crystal unit cells with essentially the same *a* and *b* dimensions, the structures having V_2O_8 polyanions. The V_2O_8 ion results from the edge sharing of two VO_5 groups. Each VO_5 group is a square pyramid with the V centrally located. Two pyramids share base oxygens, so the bases are essentially coplanar and the apices point in opposite directions (Fig. 15(*a*)). All the minerals of this family are comprised of a sheet of uranyl pentagonal dipyramids and these V_2O_8 polyhedra. This sheet and its stacking, from francevillite, is shown in Fig. 16. The sheet lies parallel to the (001) plane in all the carnotite minerals. The structures of the minerals differ in the ways in which these sheets stack and in the arrangement of the interlayer ions.

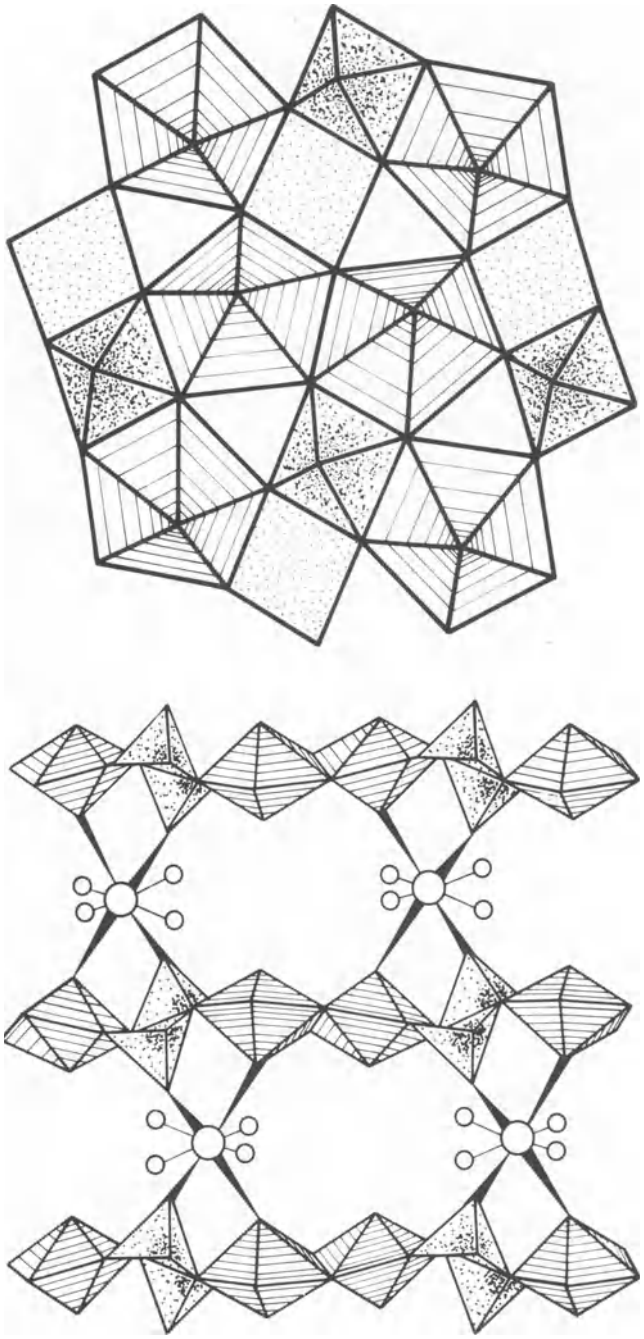

Fig. 16 Structure of francevillite, $Ba(UO_2)_2V_2O_8{\cdot}5H_2O$. (*a*) (*top*), structure of $[(UO_2)_2V_2O_8]$ unit; (*b*) (*bottom*), stacking of sheets showing interstitial cations and water molecules (uranium 2–5 polyhedra ruled and V_2O_8 groups stippled. After Shashkin[152])

Crystal structures have been determined or proposed for almost every member of the carnotite family and some additional synthetic analogues as well. A synthetic anhydrous carnotite and anhydrous margaritasite were described by Appleman and Evans.[7] Curienite was solved by Borène and Cesbron,[14] francevillite by Shashkin,[152] sengierite by Piret and co-workers[125] and a synthetic Ni analogue by Borène and Cesbron.[14] Structures for vanuralite and metavanuralite have been proposed by Borène and Cesbron.[14] The structures do differ in that adjacent sheets may be parallel or antiparallel and they may be directly over the underlying sheet or shifted significantly. Fig. 16(*b*) shows the stacking of the sheets in francevillite. Fig. 17 shows five different ways in which the sheets can stack. Each stacking results in a different unit cell and crystal symmetry. There are probably other ways in which the stacking may develop, as suggested by the various values reported for the *c*-axis and symmetry differences.

The meta designation in this family implies a loss in water, as in the autunites. This loss of water results in shifts in the stacking of sheets, a change in the sheet spacing and possibly changes in the number of sheets in a unit repeat along the *c*-axis. As in the autunites once the dehydration occurs, it is very difficult to rehydrate the phase.

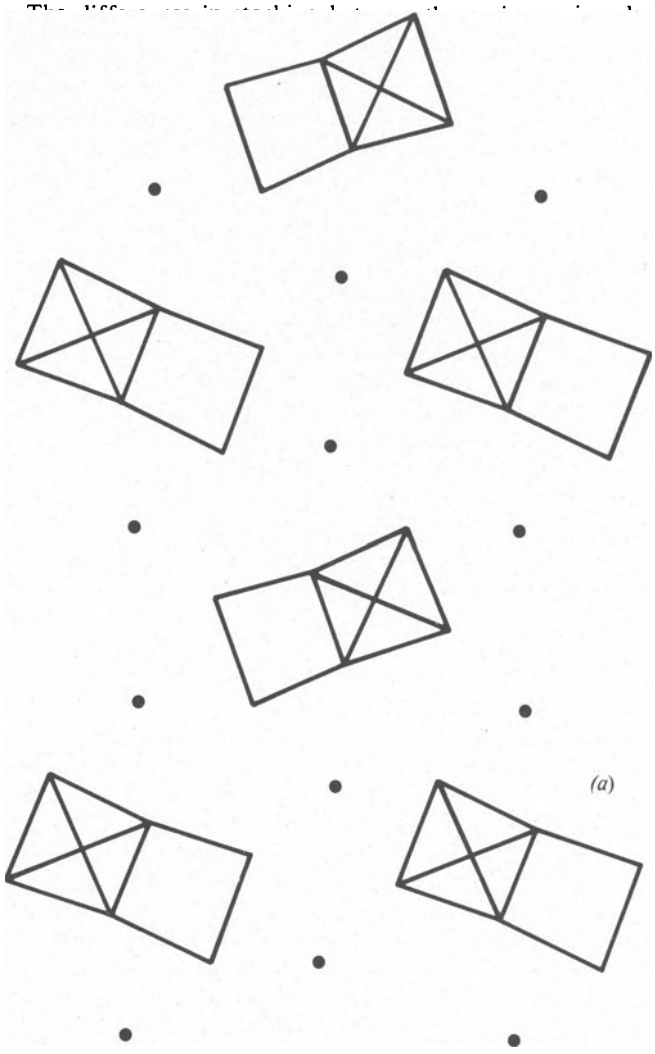

Fig. 17 Stacking of adjacent $[(UO_2)_2V_2O_8]$ sheets in minerals of carnotite family. (*a*) (*above*), $Ni(UO_2)_2V_2O_8{\cdot}4H_2O$, *Pnam*; (*b*) (*top left*), Carnotite, $K_2(UO_2)_2V_2O_8{\cdot}3H_2O$, $P2_1/a$; (*c*) (*bottom left*), curienite, $Pb(UO_2)_2V_2O_8{\cdot}5H_2O$, *Pcan*; (*d*) (*top right*), metavanuralite, $Al(UO_2)_2V_2O_8(OH){\cdot}8H_2O$, $P\bar{1}$; (*e*) (*bottom right*), vanuralite, $Al(UO_2)_2V_2O_8(OH){\cdot}11H_2O$, *A2/a*. After Borène and Cesbron[14] (V_2O_8 groups shown along with positions of uranium) (*See also facing page*)

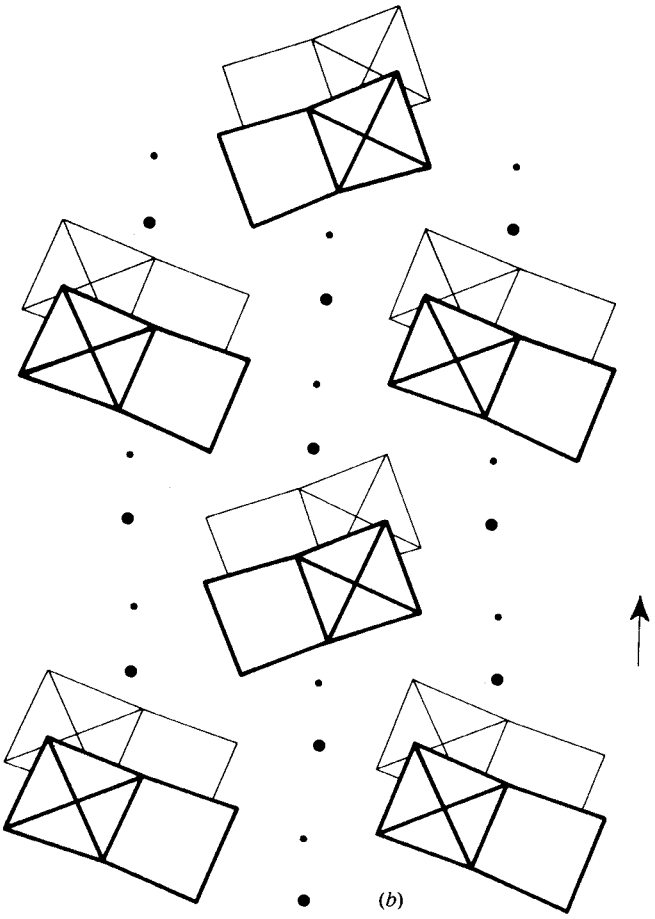

(b)

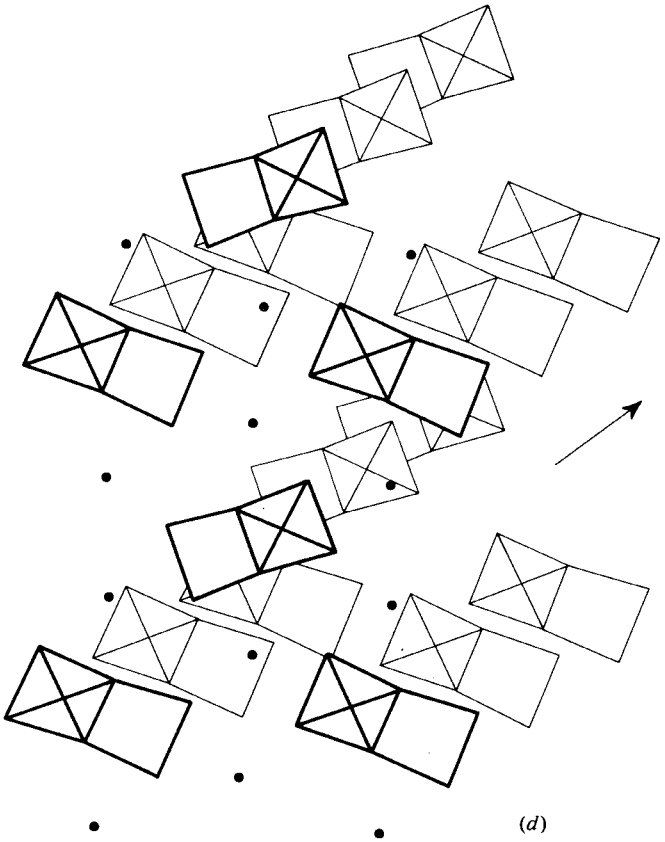

(d)

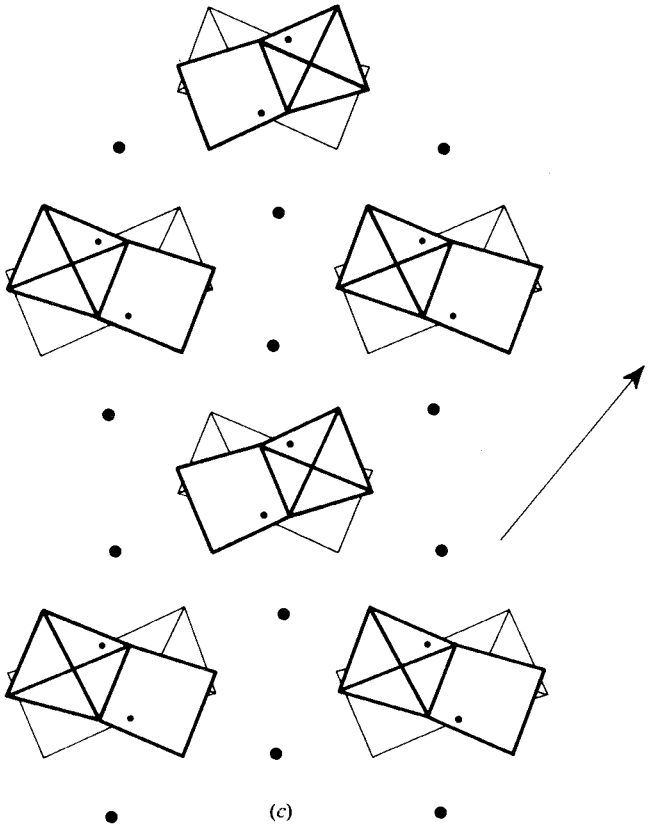

(c)

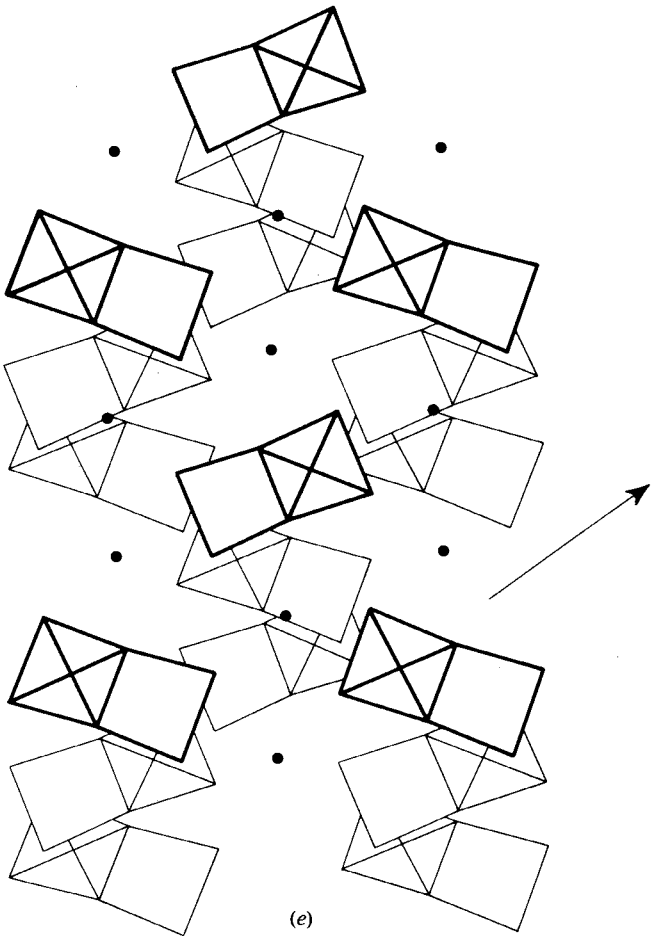

(e)

have another consequence. It is evident that some substitution of the interlayer cation may take place, but complete exchange of many of the cations will be impossible because of the structural differences. Ba can probably replace Pb but not Ca or Al. This situation is quite different from that in the autunites, where essentially complete exchange of all ion pairs is possible.

The only other polyanion to be verified among the uranyl vanadates is the decavanadate $(V_{10}O_{28})^{6-}$. The structure of this ion was found by Evans[58] for $K_2Zn_2V_{10}O_{28}\cdot H_2O$ and Swallow and co-workers[170] in pascoeite, $Ca_3V_{10}O_{28}\cdot 17H_2O$. Its structure is shown in Fig. 15(*b*). This ion probably occurs in rauvite. It has been verified in hureaulite, $Na_4MgV_{10}O_{28}\cdot 24H_2O$. The mineral uvanite appears to have a group $(V_6O_{17})^{4-}$, but this unit has not been found in any other vanadium compound.

Two unnamed and poorly characterized uranyl vanadates have been reported by Threadgold[173] from El Sherana mine, Northern Territory, Australia.

Uranyl molybdates

The uranyl molybdate minerals are relatively poorly characterized. The first uranyl molybdate mineral was recognized by Brophy and Kerr,[20] but since then a number of minerals that belong to this group have been described from many different deposits (Table 14). An affinity of uranium and molybdenum, especially in roll-front type deposits, has been known for some time. Initially, only minerals with U^{6+} were recognized, but the occurrence of such minerals as sedovite[159] shows that U^{4+} compounds also exist.

Table 14 Uranyl molybdates

Mineral	Formula	System	Lattice constants, Å (symmetry)
Calcurmolite	$Ca(UO_2)_3(MoO_4)_3(OH)_2\cdot 11H_2O$		
Cousinite	$Mg(UO_2)_2(MoO_4)_2(OH)_2\cdot 5H_2O$		
Iriginite	$(UO_2)Mo_2O_7\cdot 3H_2O$	Orth.	$a=12.77\ b=6.715\ c=11.53$ ($Pca2_1$)
Moluranite	$H_4U(UO_2)_3(MoO_4)_7$		
Mourite	$UMo_5O_{12}(OH)_{10}$	Mono.	$a=24.426\ b=7.185\ c=9.895\ \beta=102°10'$
Sedovite	$U(MoO_4)_2$		
Umohoite (F)	$(UO_2)(MoO_2)(OH)_4\cdot 2H_2O$	Mono.	$a=6.32\ b=7.50\ c=57.8\ \beta=94°$ ($P2_1/c$)

Umohoite was first described from a hydrothermal deposit at Marysvale, Utah, U.S.A., and has since been found in sandstone deposits by Coleman and Appleman[41] and at Katanga, Zaire.[126] It usually occurs at the edge of the unoxidized zone as intergrowths with other minerals, including uranium oxides. It is definitely a $U^{6+}Mo^{6+}$ compound and evidently represents one of the first oxidized uranium compounds to form. It is a difficult mineral to recognize when associated with U^{4+} minerals because of its blue-black colour, and it is probably more common than might be suspected.

Other minerals of this group include calcurmolite, described by Rupnitskaya[146] from a hydrothermal vein, and cousinite, recognized by Vaes[174] from Katanga, Zaire. Iriginite and moluranite were described by Epstein[54] from a granulated albitite in the U.S.S.R. Mourite[93] and sedovite[159] contain U^{4+} and were discussed under uranous minerals.

The only mineral in this group that has been studied extensively is umohoite. Several X-ray studies have been made.[5,41,89,126,160] The proposed cells do not agree. Although $a\simeq 6.38$ Å and $b\simeq 7.50$ Å are similar in all reports, the *c*-axes differ and the cells are described as both monoclinic and orthorhombic. Makarov and Anikina[100] reported a structure for umohoite, which may help to explain the differences that have been observed. The basic structure (Fig. 18) consists of double layers of composition $[(UO_2)(MoO_2)(OH)_4]_n$. These layers are composed of hexagonal dipyramids of both U and Mo, which edge share to form the continuous sheets. Two sheets cross-link through hydrogen bonds between the OH ions and the O of the uranyl and molybdenyl ions. These double layers are electrically neutral and may stack in different ways, depending on the amount and nature of interlayer molecules. The hydrogen bonding probably distorts the sheets from ideal configurations as well. These potential differences suggest that more than one form of umohoite exists.

The layer structure of umohoite may be the basis for a family of minerals with U : Mo = 1 : 1. Both calcurmolite and cousinite fit this condition. By replacing OH^- ions in the sheets with O^{-2} ions, a charge can be created on the double layer that must be compensated by interlayer cations. Available X-ray data are not sufficient for this theory to be tested.

The mineral iriginite has been studied by Serezhkin *et al.*[149] The structure is quite different from that of umohoite. The uranium is in 2–5 coordination and the molybdenum is 6-coordinated. The $MoO_5(H_2O)$ octahedra share edges in pairs and with the UO_7 dipyramids. A chain structure results that corner links to form the sheet as shown in Fig. 19. The sheets are held together through hydrogen bonds.

Uranyl sulphates

Minerals of the uranyl sulphate group are fairly widespread in occurrence, but usually are not found in any abundance. This distribution is undoubtedly due to the moderate to high solubility of these compounds and the rather limited conditions under which they may form. Their formation requires the absence of other oxyanions, such as VO_4, PO_4 and AsO_4. They are usually found very close to actively oxidizing uraninite and sulphide minerals. Most commonly, they form in cracks and veinlets and as efflorescences on mine walls soon after an adit is opened. One of the most spectacular occurrences is at Happy Jack mine in Utah, U.S.A., where adit walls show thick coatings of uranopilite, zippeite and johannite along with schoepite. The strong fluorescence of these minerals results in remarkable displays under shortwave ultraviolet.

The uranyl sulphates listed in Table 15 are surprisingly poorly characterized. Only johannite and sodium zippeite have even yielded crystal unit cells. For a long time the zippeite family was the least understood, but Frondel *et al.*[65] has shown that a series of zippeite-related minerals have different alkali, alkaline-earth or divalent transition cations in combination with uranyl and sulphate. All of the powder patterns are very similar, but are based on superstructures of an $a=8.82$ Å, $b=17.12$ Å, $c=7.32$ Å pseudo-cell. No crystal structure has been proposed for these compounds but, by analogy with other uranyl tetrahedral anion compounds, it is either a sheet structure or a chain structure. Several sulphate structures have been studied, none of which has natural counterparts. The compound $Cs_2(UO_2)_2(SO_4)_3$ solved by Ross and Evans[142] has a sheet structure with uranium in 2–5 coordination. The configuration of this sheet is shown in Fig. 20. It might be related to the structure of coconinoite. Structures have also been reported for $UO_2SO_4\cdot 2.5H_2O$ by Van der Putten and Loopstra[175] and $UO_2SO_4\cdot 3.5H_2O$ by Brandenburg and

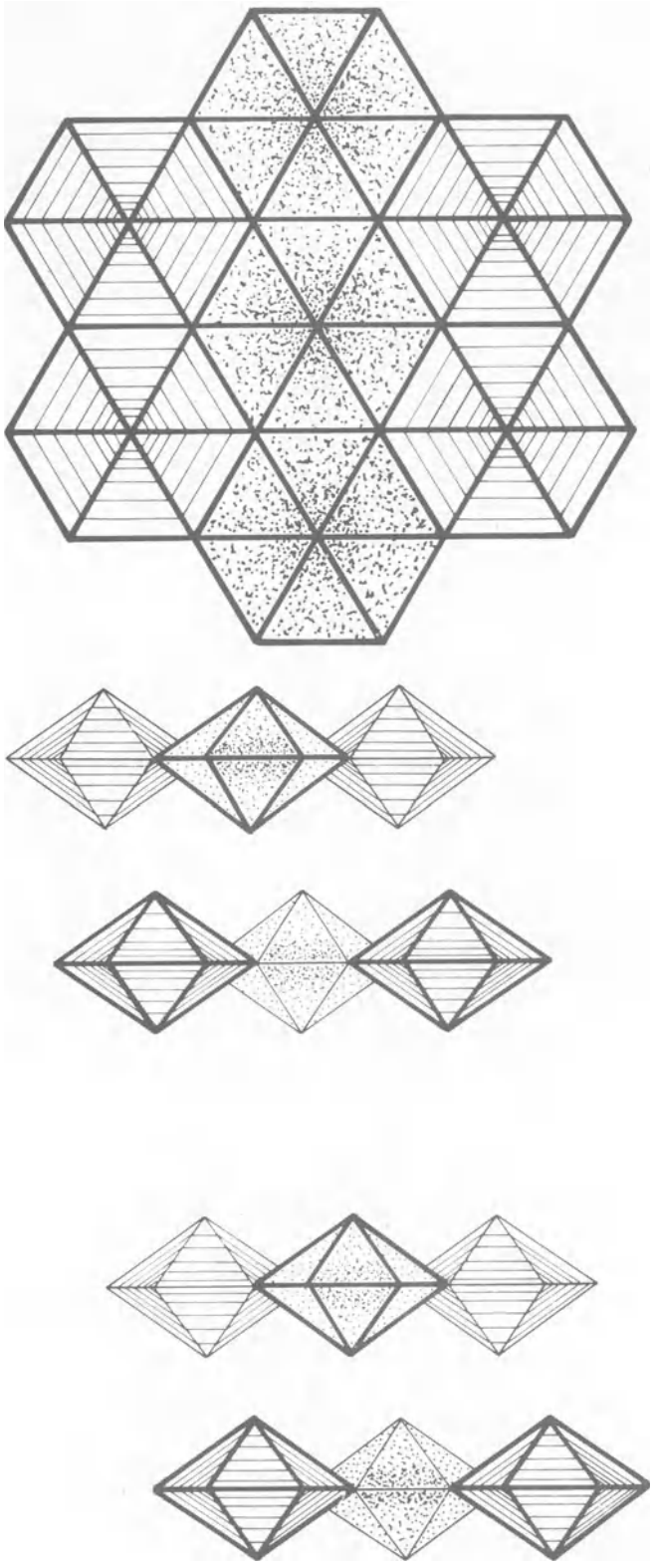

Fig. 18 Structure of umohoite, $UO_2MoO_4 \cdot 4H_2O$ (uranium 2–6 polyhedra ruled and molybdenum 2–6 polyhedra stippled). (*a*) (*top*), projection of one $[UO_2MoO_2(OH)_4]$ sheet; (*b*) (*bottom*), stacking of sheets. Modified from Makarov and Anikina[100]

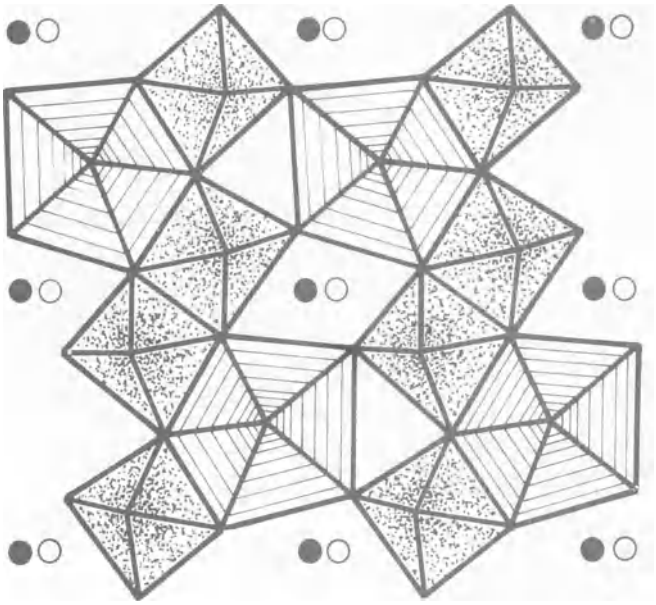

Fig. 19 Structure of iriginite, $UO_2Mo_2O_7 \cdot 3H_2O$ (uranium 2–5 polyhedra ruled and MoO_6 octahedra stippled; interlayer water molecules shown as circles)

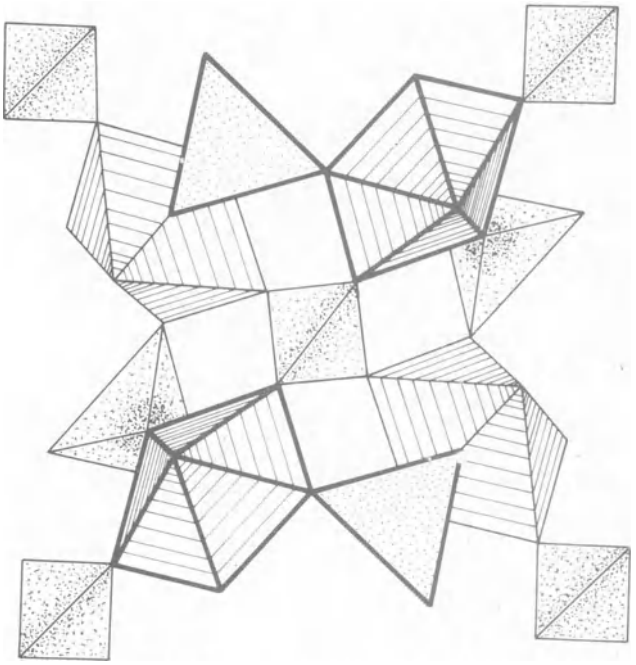

Fig. 20 Structure of sheet found in $Cs_2(UO_2)_2(SO_4)_3$ (uranium 2–5 polyhedra ruled and SO_4 tetrahedra stippled)

Loopstra.[17] These compounds have chain structures, shown in Fig. 21, which may be analogous to johannite. Niinisto and co-workers[118] described the structures of other complex uranyl sulphates.

The minerals uranopilite and meta-uranopilite were adequately discussed by Frondel.[63] New data on johannite are available.[106a] A synthetic $(UO_2)_6SO_4(OH)_{10} \cdot 13H_2O$ has been prepared by Cordfunke,[43] but it does not seem to correspond to uranopilite. The sulphate-containing minerals coconinoite and schroeckingerite are discussed elsewhere in this paper.

Walenta[185] has described an unnamed mineral of Na, Mg, U, with borate and sulphate. A Ca, Mg uranyl sulphate has also been described by Kiss.[91] Neither of these minerals has yielded sufficient information to characterize them adequately. A large number of synthetic uranyl sulphates have been described in the *Powder diffraction file*,[131] some of which may well occur naturally.

Uranyl carbonates

The uranyl carbonate minerals are found as coatings on a variety of other uranium minerals and usually occur in deposits located in arid climates or on the walls of mine adits, where they form as efflorescences. The minerals are all very soluble in water, and evidence in many localities indicates very recent deposition from water migrating away from primary deposits. Most uranium carbonates show low radioactivity, which

Table 15 Uranyl sulphates

$UO_2:TO_4$	Mineral	Formula	System	Lattice constants, Å (symmetry)
6:1	Meta-uranopilite (F)	$(UO_2)_6(SO_4)(OH)_{10}\cdot 5H_2O$		
	Uranopilite (F)	$(UO_2)_6(SO_4)(OH)_{10}\cdot 12H_2O$	Mono.	
2:1	Cobalt zippeite	$Co_2(UO_2)_6(SO_4)_3(OH)_{10}\cdot 16H_2O$	Orth.	
	Magnesium zippeite	$Mg_2(UO_2)_6(SO_4)_3(OH)_{10}\cdot 16H_2O$	Orth.	
	Nickel zippeite	$Ni_2(UO_2)_6(SO_4)_3(OH)_{10}\cdot 16H_2O$	Orth.	
	Sodium zippeite	$Na_4(UO_2)_6(SO_4)_3(OH)_{10}\cdot 16H_2O$	Orth.	$a=8.80$ $b=68.48$ $c=14.55$*
	Zinc zippeite	$Zn_2(UO_2)_4(SO_4)_3(OH)_{10}\cdot 16H_2O$	Orth.	
	Zippeite (F)	$K_4(UO_2)_6(SO_4)_3(OH)_{10}\cdot 16H_2O$	Orth.	
1:1	Johannite (F)	$Cu(UO_2)_2(SO_4)_2(OH)_2\cdot 8H_2O$	Tricl.	$a=8.903$ $b=9.499$ $c=6.812$ $\alpha=109.87°$ $\beta=112.01°$ $\gamma=100.40°$ $(P\bar{1})$
2:3	Coconinoite	$Fe_2Al_2(UO_2)_2(PO_4)_2SO_4(OH)_2\cdot 20H_2O$	Mono.	
1:2	Schroeckingerite (F)	$NaCa_3(UO_2)_2(CO_3)_3SO_4F\cdot 10H_2O$	Tricl.	$a=9.60$ $b=9.62$ $c=14.46$ $\alpha=91°42'$ $\beta=91°48'$ $\gamma=120°05'$ $(P\bar{1})$

*

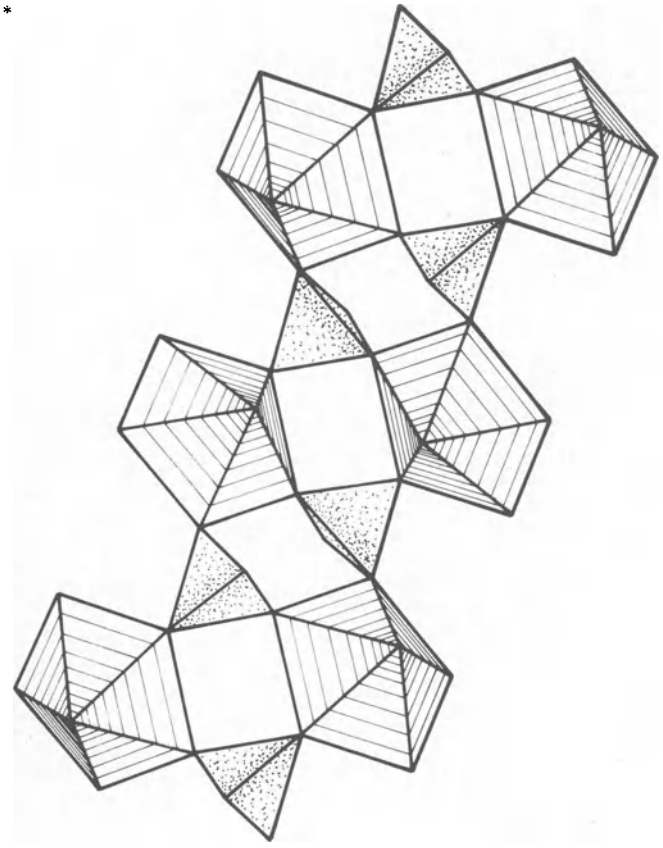

Fig. 21 Structure of UO_2SO_4 chains in 1:1 uranyl sulphates as found in $UO_2SO_4\cdot 3\frac{1}{2}H_2O$ (uranium 2–5 polyhedra ruled and SO_4 tetrahedra stippled. After Brandenburg and Loopstra[17])

suggests that recent solution separated out daughter products before reprecipitation. Rainfall in desert areas often dissolves carbonate minerals at the surface (including mine dumps) and redeposits them below the surface.

The uranyl carbonates as a group are relatively easy to recognize visually because of their strong fluorescence and greenish-yellow colours. They may occur as thin coatings, as crystals in pore spaces or veinlets in cracks. Many members of this group were described in Frondel.[63] Schroeckingerite is the most common mineral of this group and has been mined in a few small surface deposits as the principal ore mineral. Andersonite, liebigite, rutherfordine and bayleyite have also been reported at numerous localities. The other minerals of the list in Table 16 are relatively rare.

Using the classification scheme based on $UO_2:CO_3$ ratios, the minerals fall into several groups. The 1:3 group is the most populated, probably because of the ease of formation of the structural unit $[UO_2(CO_3)_3]^{4-}$. This unit has been found in the structures of andersonite and liebigite[106c] and has been verified as a stable solution complex by Langmuir.[95] The structure of this complex is shown in Fig. 22. Three CO_3 groups edge share with a uranyl ion to form a 2–6 coordination around the uranium. In the structure of andersonite[39] and liebigite[6] these units are cross linked through alkali and alkaline-earth cations to form a three-dimensional structure. The cell constants do not indicate any similarities within the various groups except for zellerite–metazellerite. The only other group from which

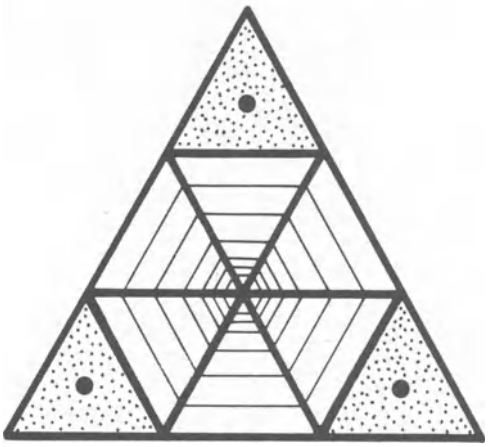

Fig. 22 $[UO_2(CO_3)_3]^{4-}$ unit as found in liebigite and andersonite (three CO_3 groups (stippled) edge share with uranium 2–6 polyhedron)

structural information has been produced is the 1:1 group. Rutherfordine has been solved by Christ and co-workers[36] and exhibits a layer structure. The carbonate groups lie in planes arranged in a close-packed hexagonal array. Four CO_3 groups surround a UO_2^{2+} ion, so two edge share and two corner share to give the uranium a 2–6 coordination. This sheet is electrically neutral and there is some disorder in the way in which sheets stack. The sheet structure is shown in Fig. 23. Evidently, variable amounts of water can enter the interlayer region, yielding sharpite and joliotite. Based on the unit cell data, the structures of the hydrated forms differ considerably from the anhydrous rutherfordine.

Several uranyl carbonate minerals have been described since Frondel.[63] Wyartite was described by Guillemin and Protas,[78] who recognized that specimens labelled ianthinite from Katanga, Zaire, were actually a carbonate that formed as a second-stage alteration product of uraninite. Like ianthinite, it

Table 16 Uranyl carbonates

$UO_2:CO_3$	Mineral	Formula	System	Lattice constants, Å (symmetry)
3:1	Wyartite	$Ca_3U(UO_2)_6(CO_3)_2(OH)_{18}\cdot 3\text{–}5H_2O$	Orth.	$a=11.25$ $b=7.10$ $c=16.83$ (*Pnma*)
				$a=11.25$ $b=7.10$ $c=20.80$ ($P2_12_12_1$)
1:1	Joliotite	$(UO_2)(CO_3)\cdot 1.5\text{–}2H_2O$	Orth.	$a=8.16$ $b=10.35$ $c=6.32$ (*Pmmm*)
	Rutherfordine (F)	$(UO_2)(CO_3)$	Orth.	$a=4.845$ $b=9.205$ $c=4.296$ (*Pmmn*)
	Sharpite (F)	$(UO_2)(CO_3)\cdot H_2O$	Orth.	
1:2	Metazellerite	$Ca(UO_2)(CO_3)_2\cdot 3H_2O$	Orth.	$a=9.718$ $b=18.226$ $c=4.965$ (*Pbnm*)
	Zellerite	$Ca(UO_2)(CO_3)_2\cdot 5H_2O$	Orth.	$a=11.220$ $b=19.252$ $c=4.933$ (*Pmnm*)
1:3	Andersonite (F)	$Na_2Ca(UO_2)(CO_3)_3\cdot 6H_2O$	Hex.	$a=18.009$ $c=23.838$ ($R\bar{3}$)
	Bayleyite (F)	$Mg_2(UO_2)(CO_3)_3\cdot 18H_2O$	Mono.	$a=26.65$ $b=15.31$ $c=6.53$ $\beta=93°4'$ ($P2/a$)
	Grimselite	$K_3Na(UO_2)(CO_3)_3\cdot H_2O$	Hex.	$a=9.30$ $c=8.26$ ($P\bar{6}2c$)
	Liebigite (F)	$Ca_2(UO_2)(CO_3)_3\cdot 11H_2O$	Orth.	$a=16.699$ $b=17.577$ $c=13.697$ (*Bba2*)
	Rabbittite (F)	$Ca_3Mg_3(UO_2)_2(CO_3)_6(OH)_4\cdot 18H_2O$	Mono.	$a=32.6$ $b=23.8$ $c=9.45$ $\beta\approx 90°$
	Schroeckingerite (F)	$NaCa_3(UO_2)(CO_3)_3SO_4F\cdot 10H_2O$	Tricl.	$a=9.60$ $b=9.62$ $c=14.46$
				$\alpha=91°42'$ $\beta=91°48'$ $\gamma=120°05'$
	Swartzite	$CaMg(UO_2)(CO_3)_3\cdot 12H_2O$	Mono.	$a=11.21$ $b=14.72$ $c=6.47$ $\beta=99°26'$ ($P2_1/m$)
	Widenmannite	$Pb_2(UO_2)(CO_3)_3$	Orth.	$a=8.99$ $b=9.36$ $c=4.95$ (*Pnmm*)
1:4	Voglite (F)	$Ca_2Cu(UO_2)(CO_3)_4\cdot 6H_2O$	Mono.	$a=25.94$ $b=24.50$ $c=10.70$ $\beta=104.0°$ ($P2_1/*$)
1:6	Mckelveyite	$Ca_3Na(Ca,U)Y(CO_3)_6\cdot 3H_2O$	Hex.	$a=9.174$ $c=19.154$ ($P\bar{3}$)

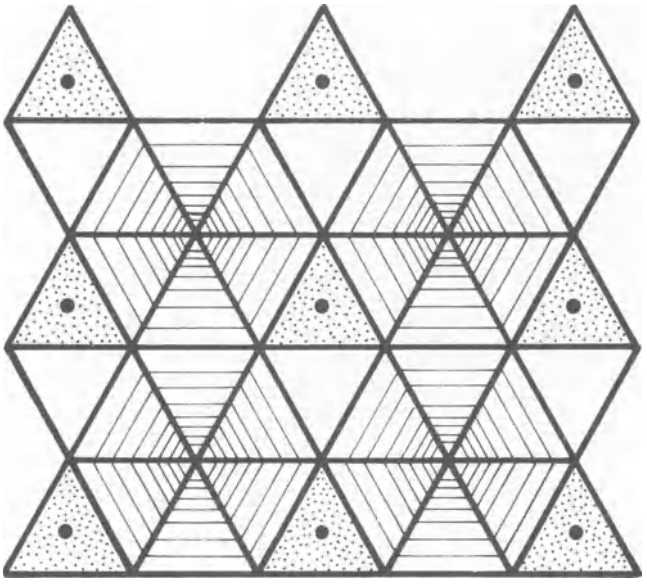

Fig. 23 Structure of rutherfordine, UO_2CO_3 (uranium 2–6 polyhedra ruled and CO_3 triangles stippled. After Christ *et al.*[36])

is not fully oxidized. Wyartite is a dark violet black colour indicative of the presence of mixed valence state of uranium. It may occur in several states of hydration with consequent changes in X-ray pattern similar to the behaviour of schoepite. Two forms of wyartite have been verified by Clark,[38] which show different *c*-axis lengths.

Joliotite and widenmannite were described by Walenta and Wimmenauer[187] and Walenta[184] from the Michaelgang in Germany, where they occur as small radiating clusters. The later study fixed the composition of widenmannite and determined that it was one of the 1:3 minerals. Metazellerite and zellerite were described by Coleman and co-workers[42] from Wyoming, U.S.A., where they occur as pincushion clumps of needle-like crystals on uranium ore intimately associated with gypsum and iron oxides. These minerals, which evidently have a layer structure, show different states of hydration analogous to the autunites. Grimselite was also described by Walenta.[182] It occurs with schroeckingerite and two unknown non-uranium carbonates. The crystals are yellow and granular, so the mineral probably has a structure similar to andersonite and liebigite. The occurrence is in mineralized aplitic granite. New data on voglite have been presented by Piret and Deliens[127] on specimens from Jachymov, Czechoslovakia, and Utah, U.S.A.

Mckelveyite has been described by Milton *et al.*[108] from the fresh water lake beds of the Green River formation in Wyoming, U.S.A. The occurrences are in a uranium district, but are not associated with other uranium minerals. It is a unique carbonate as it contains significant quantities of rare-earth elements and may be related to rhapdophane. It does occur with another rare-earth mineral burbankite. Donnay and Donnay[51] showed that mckelveyite was intergrown with ewaldite, another carbonate with a trace of uranium included. Donnay and Preston[52] reported a structure for ewaldite.

Uranyl selenates and tellurates

A totally new group of minerals, all of which have been described since Frondel,[63] comprises the uranyl selenates and tellurates. Although other selenate and tellurate minerals have been reported as occurring in many types of uranium deposits, the uranyl compounds have only been recognized at two rather different localities. A Au–Te deposit near Moctezuma, Mexico, has yielded moctezumite, cliffordite and schmitterite[67,68,69] and the Musonoi Cu–Co deposit at Katanga, Zaire, has produced the other minerals. Schmitterite has also been found at the Shinkolobwe uranium deposit in Katanga. All the minerals are secondary.

The listing of the minerals in Table 17 by the $UO_2:XO_3$ ratio does not show any similarities. Each category has one selenate, and three categories have one tellurate. The tellurates are all anhydrous, whereas the selenates are all hydrous. Crystal structures are known for two of the tellurates, cliffordite[71] and schmitterite,[99,107] and a related $Pb_2(UO_2)(TeO_3)_3$.[18] Although the structure for none of the selenate minerals has been solved, the structure of UO_2SeO_3 has been determined by Loopstra and Brandenburg[99] and shows some interesting contrasts to UO_2TeO_3 that may be of significance in the mineral kingdom. The compound UO_2SeO_3 is unstable in air and with respect to water, whereas UO_2TeO_3 is quite stable. The crystal structures shown in Fig. 24 have almost the same topologies; however, in UO_2TeO_3 the uranium shows a 2–5 coordination and the Te is 4 coordinated, whereas in UO_2SeO_3 the U shows a 2–6 coordination and the Se is 3 coordinated. These structures are shown in Fig. 24. In schmitterite, where the $UO_2:XO_3$ ratio is 1:1, it is the uranium coordination polyhedra that share edges to form chains, which are the main structural unit. In cliffordite the U is 2–6 coordinated and the Te is 4 coordinated. The cliffordite structure is shown in Fig. 25. It is the TeO_4 tetrahedra that corner share to form a framework that creates the main structural unit, which encloses the uranyl ion. Evidently,

Table 17 Uranyl selenates and tellurates

$UO_2:XO_3$	Mineral	Formula	System	Lattice constants, Å (symmetry)	Colour
3:2	Guilleminite	$Ba(UO_2)_3(SeO_3)_2(OH)_4 \cdot 3H_2O$	Orth.	$a=7.25$ $b=16.84$ $c=7.08$	Yellow
1:1	Marthozite	$Cu(UO_2)_3(SeO_3)_3(OH)_2 \cdot 7H_2O$	Orth.	$a=16.40$ $b=17.20$ $c=6.98$	Yellow-green
	Schmitterite	UO_2TeO_3	Orth.	$a=7.860$ $b=10.089$ $c=5.363$ (*Pbcm*)	Straw yellow
1:2	Derricksite	$Cu_4(UO_2)(SeO_3)_2(OH)_6 \cdot H_2O$	Orth.	$a=5.57$ $b=19.07$ $c=5.96$	Green
	Moctezumite	$Pb(UO_2)(TeO_3)_2$	Mono.	$a=7.189$ $b=7.070$ $c=13.836$ $\beta=93°37'$	Orange
1:3	Cliffordite	$UO_2Te_3O_7$	Cub.	$a=11.371$ (*Pa*3)	Yellow
	Demesmaekerite	$Pb_2Cu_5(UO_2)_2(SeO_3)_6(OH)_6 \cdot 2H_2O$	Tricl.	$a=11.94$ $b=10.02$ $c=5.62$ $\alpha=90$ $\beta=100$ $\gamma=91°55'$	Green

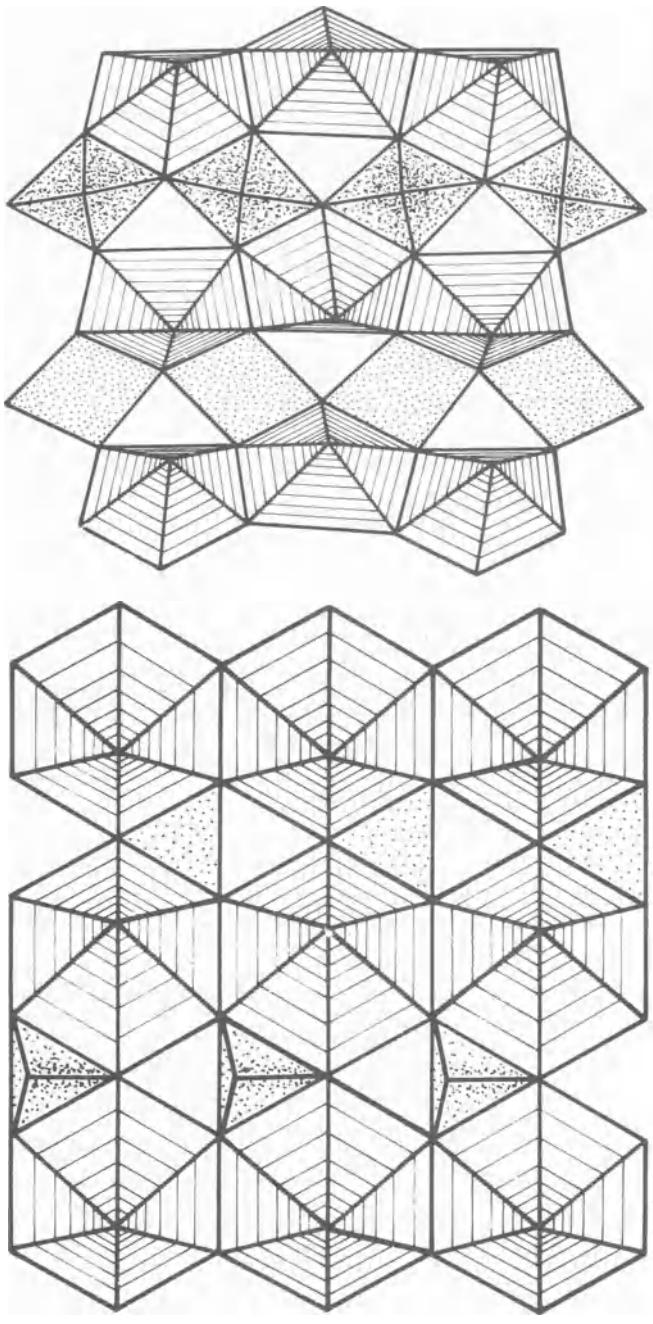

Fig. 24 Structure of schmitterite, UO_2TeO_3, and UO_2SeO_3. (*a*) (*top*), schmitterite (uranium 2–5 polyhedra ruled and TeO_5 pyramids stippled. After Meunier and Galy[107]). (*b*) (*bottom*), UO_2SeO_3 (uranium 2–6 polyhedra ruled and SeO_3 pyramids stippled. After Loopstra and Brandenburg[99])

the selenate and tellurate structures are all sufficiently different that isostructural pairs do not form.

The selenate minerals are all found in the same deposit in an altered dolomite at Musonoi, Katanga. Pierrot and co-workers[122] described guilleminite from some coatings in the oxidized zone and in some geodes. Marthozite was characterized by Cesbron and co-workers[29] as millimetre-size green crystals in the oxidized zone that appear to have formed prior to the closely associated guilleminite and demesmaekerite.[26] Derricksite,[31] the latest of this group to be recognized, occurs as microcrystalline crusts on selenian digenite associated with the demesmaekerite. All of these phases are well represented by powder diffraction data, which is the best way to achieve positive identification among these minerals.

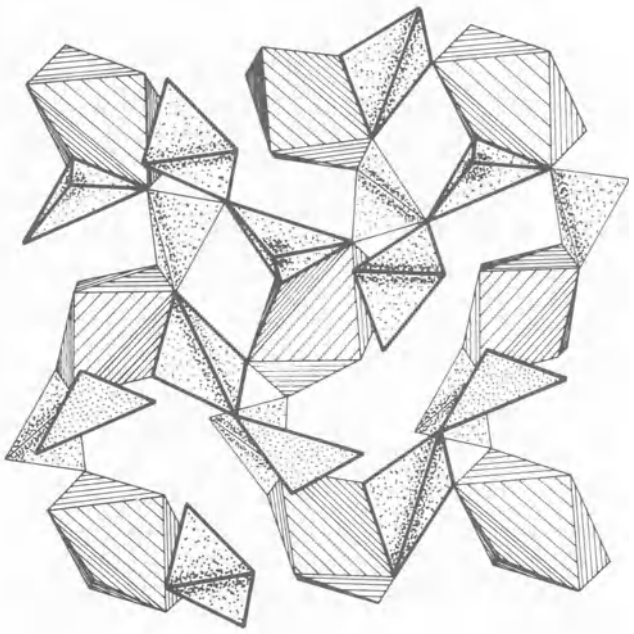

Fig. 25 Structure of cliffordite, $UO_2Te_3O_7$ (heavy outlined TeO_4 units have Te close to $Z=0.75$; lightly outlined UO_8 and TeO_4 units have U at $Z=0.5$ and Te close to $Z=0.5$; uranium 2–6 polyhedra ruled and TeO_4 tetrahedra stippled. After Galy and Meunier[71])

Identification of uranium minerals

Uranium minerals pose some interesting problems in their identification. All the U^{4+} minerals are very dark or black in colour and, except for uraninite and some pegmatitic niobate–tantalates, they occur as coatings or very minute crystals intimately associated with other minerals. Even uraninite in massive form rarely shows distinguishing visual properties other than its high radioactivity and density. In polished section all these minerals are low reflecting and usually without structure. The techniques of X-ray powder diffraction are the most useful means of positive identification, but many of the minerals are metamict and produce no pattern unless the specimen is heated to improve the crystallinity. This heating must be done carefully to prevent oxidation or other reactions that would yield new compounds and alter the original atomic arrangement. Heating is best done quickly with the use of fairly

large pieces. The samples may be fired in an open crucible either in air or an oxygen-free atmosphere. Temperatures usually must reach >600°C to produce crystallinity and may require 1000°C to achieve sufficient crystallinity to yield decent X-ray powder patterns. This rather drastic heat-treatment always leaves open the question of how much the original structure was altered and whether two or more minerals yield the same structure after firing. Chemical analyses, primarily by the electron microprobe, may be required to distinguish some varieties, especially among the pyrochlore-type minerals.

The oxidized minerals pose quite different problems in their identification. All the minerals are brightly coloured and most of them are some shade of yellow, orange or brown. Although the colour can often be used to distinguish a uranium mineral from associated non-uranium minerals, the colour shades overlap so much among the U mineral groups that it is useless to distinguish individual species. There are also several non-uranium minerals the colours of which are too close for positive distinction. Crystal morphology, when crystals are present, may be used to recognize some of the mineral families as defined in this section, but many groups are fibrous owing to the dominance of the chain structural unit and several are platy owing to the sheet structures. The only groups that usually can be recognized with some certainty based on crystal morphology are the autunite–meta-autunite minerals, which show square-tabular habits. Microchemical tests can distinguish anions and most of the cations, but they are rarely used today. As with the U^{4+} minerals, X-ray powder diffraction is the most useful and surest method to distinguish individual species. Electron-microprobe analyses may be necessary to distinguish individual chemical varieties and infrared spectra are especially useful to characterize the role of water and interlayer cations present in almost all minerals. Optical refractive indices can prove useful to distinguish many of the species, especially within specific mineral groups. Examples include the autunites and meta-autunites, where the indices for the arsenate species are higher than those for their phosphate counterparts.

Identification by all techniques is usually complicated by the fine-grained nature of most minerals and by the likelihood that two or more species are intergrown intimately. Fortunately, all the techniques, XRPD, EM, IR and optics, can utilize small amounts of material. Careful preparation can require separation of material under a microscope. It is usually imperative to utilize single-phase samples to facilitate the interpretation of the experimental data. Many questionable identifications can be traced to poor sample preparation.

Appendices 1 and 2 have been prepared to assist in the mineral identification of uranium-bearing species. Appendix 1 contains the five strongest powder X-ray diffraction lines arranged in three-entry Hanawalt format. The data are mostly from the *Powder diffraction file*[131] and used with permission of JCPDS—International Centre for Diffraction Data. Data for newly described minerals were obtained from original references already mentioned. This list may be used as a mini-search manual for identification of mineral specimens known to contain uranium. Appendix 2 lists the optical indices of refraction for the transparent uranium-bearing minerals.

Conclusions

It is quite evident that the interest in uranium will continue, and new species of minerals will be described. As old specimens are reviewed with modern analytical methods, old confusions will be clarified and new minerals recognized. As new mineral deposits are found, the discovery of new mineral species and perhaps better specimens of older species can be expected.

The crystal-chemical classification used in this chapter will help in the recognition of similarities among the many minerals that have been described, and new minerals may fill in some of the gaps or fulfil predictions that fall out of the classification scheme. Crystal structure analysis is one of the most powerful tools in the understanding of the nature and properties of the various minerals. Structure studies are hindered by the difficulties of obtaining suitable crystals and experimental difficulties encountered from the use of small crystals with high absorption in which the uranium dominates the diffraction intensities. Nevertheless, the information obtained has been worth the effort. From the structural information it is possible to predict new minerals that should be encountered. Rules governing structure types and solid solution or chemical substitutions are evident, but further structural studies are necessary to delineate the small differences that occur in individual species in the larger groups, such as the autunites and meta-autunites.

It is evident that new analytical methods, especially the techniques of spectroscopy, have much to offer in the further characterization. The work of Sobry[165] has shown the need to distinguish oxonium ions as an integral part of the compound. There is still much to be learned. Obviously, uranium minerals will hold our fascination for many years and new data will continue to appear.*

Acknowledgement

The author would like to thank the several students and colleagues who have contributed to this study of uranium minerals. Frances V. Stohl, Christine A. Anderson and Barry E. Scheetz have contributed greatly to the study of the uranyl silicates. Michael E. Zolensky is still engaged in the studies of the uranyl phosphates. He has also helped review this manuscript. Steve A. Markgraf assisted with the literature search and compiling of data used in the tables.

References

1. de Abeledo M. J. de Benyacar M. R. and Galloni E. E. Ranquilite, a calcium uranyl silicate. *Am. Miner.*, **45**, 1960, 1078–86.
2. Agrinier H. *et al.* Une nouvelle espèce minérale: la meta-lodèvite (arséniate hydraté d'uranium et de zinc). *Bull. Soc. fr. Minér. Cristallogr.*, **95**, 1972, 360–4.
3. Alekseeva M. A. *et al.* Strelkinite, a new uranyl vanadate. *Zap. vses. miner. Obshch.*, **103**, 1974, 576–80. (Russian text)
4. Anderson C. A. F. The crystal structure of weeksite. M.S. thesis, Pennsylvania State University, 1980.
5. Anikina L. I. and Makarov Ye. S. Unit cell of umohoite, $UO_2MoO_4 \cdot 4H_2O$. *Dokl. Akad. Nauk SSSR*, **137**, 1961, 942–3; *Dokl. Acad. Sci. USSR, Earth Sci. Sect.*, **137**, 1961, 449–50.
6. Appleman D. E. Crystal structure of liebigite. *Bull. geol. Soc. Am.*, **67**, 1956, 1666.
7. Appleman D. E. and Evans H. T. Jr. The crystal structures of synthetic anhydrous carnotite, $K_2(UO_2)_2V_2O_8$, and its cesium analogue, $Cs_2(UO_2)_2V_2O_8$. *Am. Miner.*, **50**, 1965, 825–42.
8. Arribas A. Nuevos datos sobre la coffinita. *Estudios geol. Inst. Invest. geol. Lucas Mallada*, **22**, 1967, 45–56.
9. Bayushkin I. M. and Il'menev Ye. S. Coffinite crystals from molybdenum–uranium deposits. *Izv. vyssh. ucheb. Zaved. Geol. Razved.*, **12**, no. 11 1969, 39–42. (Russian text)
10. Beintema J. On the composition and the crystallography of autunite and the meta-autunites. *Recl Trav. chim. Pays-Bas Belg.*, **57**, 1938, 155–75.
11. Belova L. N. Arsenuranocircite, $Ba(UO_2)_2(AsO_4)_2 \cdot 8H_2O$. In *Proceedings of the second United Nations international conference on the peaceful uses of atomic energy, Geneva, 1958, volume 2* (Geneva: U.N., 1958), 294.

Postscript The 1984 additions and corrections to the *Glossary of mineral species* list the following new uranium minerals not discussed in this text: oursinite, $(CO,Mg)(UO_2)_2Si_2O_7 \cdot 6H_2O$, sayrite, $Pb_2(UO_2)_5O_6(OH)_2 \cdot 4H_2O$, triangulite, $Al_3(UO_2)_4(PO_4)_4(OH)_5 \cdot 5H_2O$, and uranosilite, $U^{+6}Si_7O_{17}$ (Mineralogical Record, 1984); swamboite, $V_{0.3}H_2(UO_2)_2(SiO_4)_2 \cdot 10H_2O$; bijvoetite, $(RE)_2(UO_2)_4(CO_3)_4(OH)_6$, and lepersonnite, $Ca(RE)_2U_{24}(CO_3)_8Si_{4.2}O_{76} \cdot 60H_2O$.[194, 195]

12. Belova L. N. Arsenuranylite, the arsenic analogue of phosphuranylite. *Zap. vses. miner. Obshch.*, **87**, 1958, 589–602. (Russian text)
13. Bignand C. Sur les propriétés et les synthèses de quelques minéraux uranifères. *Bull. Soc. fr. Minér. Cristallogr.*, **78**, 1955, 1–26.
14. Borène J. and Cesbron F. Structure cristalline de la curiénite $Pb(UO_2)_2(VO_4)_2 \cdot 5H_2O$. *Bull. Soc. fr. Minér. Cristallogr.*, **94**, 1971, 8–14.
15. Branche G. *et al.* La francevillite, nouveau minérale uranifère. *C.R. Acad. Sci., Paris*, **245**, 1957, 89–91.
16. Branche G. *et al.* La vanuralite, nouveau minérale uranifère. *C.R. Acad. Sci., Paris*, **256**, 1963, 5374–6.
17. Brandenburg N. P. and Loopstra B. O. Uranyl sulfate hydrate, $UO_2SO_4 \cdot 3\frac{1}{2}H_2O$. *Cryst. Struct. Commun.*, **2**, 1974, 243–6.
18. Brandstätter F. Synthesis and crystal structure determination of lead uranyl tellurate: $Pb_2(UO_2)(TeO_3)_3$. *Z. Kristallogr.*, **155**, 1981, 193–200.
19. Brindley G. W. and Bastovanov M. Interaction of uranyl ions with synthetic zeolites of type A and formation of compreignacite-like and becquerelite-like products. *Clays Clay Minerals*, **30**, 1982, 135–42.
20. Brophy G. P. and Kerr P. F. Hydrous uranium molybdate in Marysvale ore. *U.S. Atomic Energy Commn Rep.* RME-3046, 1953, 45–51.
21. Bültemann H. W. and Moh G. H. Bergenit, ein neues Mineral der Phosphuranylite-Gruppe. *Neues Jb. Miner. Mh.*, 1959, 232–3.
22. Buryanova E. Z. Stokova G. S. and Shitov V. A. Vanuranylite, a new mineral. *Zap. vses. miner. Obshch.*, **94**, 1965, 437–43. (Russian text)
23. Cesbron F. Nouvelles données sur la vanuralite. Existence de la méta-vanuralite. *Bull. Soc. fr. Minér. Cristallogr.*, **93**, 1970, 242–8.
24. Cesbron F. Etude cristallographique et comportement thermique des uranyl-vanadates de Ba, Pb, Sr, Mn, Co et Ni. *Bull. Soc. fr. Minér. Cristallogr.*, **93**, 1970, 320–7.
25. Cesbron F. and Borène J. Structure cristalline de l'uranyl-vanadate de nickel tétrahydraté $Ni(UO_2)_2(VO_4)_2 \cdot 4H_2O$. *Bull. Soc. fr. Minér. Cristallogr.*, **93**, 1970, 426–32.
26. Cesbron F. Bachet B. and Oosterbosch R. La demesmaekerite, sélénite hydraté d'uranium, cuivre et plomb. *Bull. Soc. fr. Minér. Cristallogr.*, **88**, 1965, 422–5.
27. Cesbron F. *et al.* Rameauite and agrinierite, two new hydrated complex uranyl oxides from Margnac, France. *Mineralog. Mag.*, **38**, 1972, 781–9.
28. Cesbron F. and Morin N. Une nouvelle espèce minérale: la curiénite. Etude de la série francevillite–curiénite. *Bull. Soc. fr. Minér. Cristallogr.*, **91**, 1968, 453–9.
29. Cesbron F. Oosterbosch R. and Pierrot R. Une nouvelle espèce minérale: la marthozite, uranyl sélénite de cuivre hydraté. *Bull. Soc. fr. Minér. Cristallogr.*, **92**, 1969, 278–83.
30. Cesbron F. Pierrot R. and Verbeek T. La roubaultite, $Cu_2(UO_2)_3(OH)_{10} \cdot 5H_2O$, une nouvelle espèce minérale. *Bull. Soc. fr. Minér. Cristallogr.*, **93**, 1970, 550–4.
31. Cesbron F. Pierrot R. and Verbeek T. La derriksite, $Cu_4(UO_2)(SeO_3)_2(OH)_6 \cdot H_2O$, une nouvelle espèce minérale. *Bull. Soc. fr. Minér. Cristallogr.*, **94**, 1971, 534–7.
32. Chernikov A. A. Krutetskaya O. V. and Organova N. I. Sodium-autunite. *Atomn. Energ.*, **3**, 1957, 135–40. (Russian text)
33. Chernikov A. A. Krutetskaya O. V. and Sidelnikova V. D. Ursilite—a new silicate of uranium. In *Voprosy Geol. Urana (Atomn. Energ. Prilozh.* no. 6), 1957, 73–7. (Russian text); English transl., Consultants Bureau, 1958, 61–5.
34. Chernikov A. A. Shaskin D. P. and Gavrilova I. N. Sodium boltwoodite. *Dokl. Akad. Nauk SSSR*, **221**, 1975, 195–7.
35. Chevalier R. and Gasperin M. Mise en évidence d'une transformation ordre–disordre dans un cristal de type pyrochlore. *Acta Crystallogr.*, **28B**, 1972, 985–6.
36. Christ C. L. Clark J. R. and Evans H. T. Jr. Crystal structure of rutherfordine, UO_2CO_3. *Science*, **121**, 1955, 472–3.
37. Christ C. L. and Clark J. R. Crystal chemical studies of some uranyl oxide hydrates. *Am. Miner.*, **45**, 1960, 1026–61.
38. Clark J. R. X-ray study of alteration in the uranium mineral wyartite. *Am. Miner.*, **45**, 1960, 200–8.
39. Coda A. Ricerche sulla struttura cristallina dell'andersonite. *Rendiconte Classe Sci. fis. mat. natur., Accademia nazionale dei Lincei*, **34**, 1963, 299–304.
40. Cohen-Addad C. *et al.* Détermination de la position des atomes d'hydrogen dans l'hydrogarnet $Al_2O_3 \cdot 3CaO \cdot 6H_2O$ par résonance nucleaire et diffraction neutronique. *J. Phys.*, **25**, 1964, 478–83.
41. Coleman R. G. and Appleman D. E. Umohoite from the Lucky Mc mine, Wyoming. *Am. Miner.*, **42**, 1957, 657–60.
42. Coleman R. G. Ross D. R. and Meyrowitz R. Zellerite and metazellerite, new uranyl carbonates. *Am. Miner.*, **51**, 1966, 1567–78.
43. Cordfunke E. H. P. $UO_2SO_4 \cdot 5UO_3 \cdot 18H_2O$. *Powder diffraction file* 28-1419, 1974. (Joint Committee on Powder Diffraction Standards, Swarthmore, Pa., U.S.A.)
44. de Benyacar M. A. R. and de Abeledo M. E. J. Phase transition in synthetic troegerite at room temperature. *Am. Miner.*, **59**, 1974, 763–7.
45. Deliens M. Review of the hydrated oxides of U and Pb, with new X-ray powder data. *Mineralog. Mag.*, **41**, 1977, 51–7.
46. Deliens M. Associations de minéraux secondaires d'uranium à Shinkolobwe (région du Shaba, Zaire). *Bull. Soc. fr. Minér. Cristallogr.*, **100**, 1977, 32–8.
47. Deliens M. and Piret P. La phurcalite, $Ca_2(UO_2)_3(PO_4)_2(OH)_4 \cdot 4H_2O$, nouveau minéral. *Bull. Soc. fr. Minér. Cristallogr.*, **101**, 1978, 356–8.
48. Deliens M. and Piret P. Ranunculite, $AlH(UO_2)(PO_4)(OH_3) \cdot 4H_2O$, a new mineral. *Mineralog. Mag.*, **43**, 1979, 321–3.
49. Deliens M. and Piret P. Les phosphates d'uranyl et d'aluminium de Kobokobo. II. La phuralunite $Al_2(UO_2)_3(PO_4)_2(OH)_6 \cdot 10H_2O$ et l'upalite $Al(UO_2)_3(PO_4)_2(OH)_3$, nouveaux minéraux. *Bull. Soc. fr. Minér. Cristallogr.*, **102**, 1979, 333–7.
50. Deliens M. and Piret P. Les phosphates d'uranyl et d'aluminium de Kobokobo. IV. La threadgoldite, $Al(UO_2)_2(PO_4)_2(OH) \cdot 8H_2O$, nouveau minéral. *Bull. Soc. fr. Minér. Cristallogr.*, **102**, 1979, 338–41.
50a. Deliens M. and Piret P. Metastudtite $UO_4 \cdot 2H_2O$, a new mineral from Shinkolobwe, Shaba, Zaire. *Am. Miner.*, **68**, 1983, 456–8.
51. Donnay G. and Donnay J. D. H. Ewaldite, a new barium calcium carbonate: I. Occurrence of ewaldite in syntactic intergrowths with mackelveyite. *Tschermaks miner. petrogr. Mitt.*, **15**, 1971, 185–200.
52. Donnay G. and Preston H. Ewaldite, a new barium calcium carbonate: II. Its crystal structure. *Tschermaks miner. petrogr. Mitt.*, **15**, 1971, 201–12.
53. Emerson D. O. and Wright H. D. Secondary uranium minerals at the W. Wilson mine in the Boulder batholith, Montana. *Am. Miner.*, **42**, 1957, 222–39.
54. Epstein G. Yu. On molybdates of uranium—moluranite and iriginite. *Zap. vses. miner. Obshch.*, **88**, 1959, 564–70. (Russian text)
55. Ertl R. F. and Ertl S. Mineraliensammeln und Goldwaschen bei Heiligenbluth in Kärnten; Alphabetische Übersicht über die Mineralvorkommen in der Umgebung von Heiligenbluth. *Aufschluss*, **25**, 1974, 237–46; 246–95.
56. Evans H. T. Jr. The crystal chemistry and mineralogy of vanadium. *Prof. Pap. U.S. geol. Surv.* 320, 1959, 91–102.
57. Evans H. T. Jr. Uranyl ion coordination. *Science*, **141**, 1963, 154–7.
58. Evans H. T. Jr. The molecular structure of the isopoly complex ion, decavanadate ($V_{10}O_{28}^{6-}$). *Inorg. Chem.*, **5**, 1966, 967–77.
59. Fairchild J. G. Base exchange in artifical autonites. *Am. Miner.*, **14**, 1929, 265–75.
60. Fleischer M. *Glossary of mineral species 1980* (Tucson, Arizona: Mineralogical Record, 1980), 192 p.
61. Fleischer M. Additions and corrections to the glossary of mineral species 1980. *Mineralog. Rec.*, **12**, 1981, 61–3.
62. Foreman D. W. Jr. Neutron and X-ray diffraction of $Ca_3Al_2(O_4D_4)_3$, a garnetoid. *J. chem. Phys.*, **48**, 1968, 3037–41.
63. Frondel C. Systematic mineralogy of uranium and thorium. *Bull. U.S. geol Surv.* 1064, 1958, 400 p.
64. Frondel C. and Ito J. Boltwoodite, a new uranium silicate mineral. *Science*, **124**, 1956, 931.
65. Frondel C. *et al.* Mineralogy of the zippeite group. *Can. Mineralogist*, **14**, 1976, 429–36.
66. Fuchs L. H. and Gebert E. X-ray studies of synthetic coffinite, thorite and uranothorites. *Am. Miner.*, **43**, 1958, 243–8.
67. Gaines R. V. Moctezumite, a new lead uranyl tellurate. *Am. Miner.*, **50**, 1965, 1158–63.
68. Gaines R. V. Cliffordite—a new tellurite mineral from Moctezuma, Sonora, Mexico. *Am. Miner.*, **54**, 1969, 697–701.
69. Gaines R. V. Schmitterite—a new uranyl tellurite from Moctezuma, Sonora. *Am. Miner.*, **56**, 1971, 411–5.
70. Gallagher M. J. and Atkin D. Meta-ankoleite, hydrated potassium

uranyl phosphate. *Bull. geol. Surv. Gt Br.* 25, 1966, 49–54.
71. Galy J. and Meunier G. A propos de la cliffordite UTe_3O_8. Le système UO_3–TeO_2 à 700°C. Structure cristalline de UTe_3O_9. *Acta crystallogr.*, **B27**, 1971, 608–16.
72. Gasperin M. Contribution à l'étude de quelques oxydes doubles que forme le tantale avec l'étain, l'uranium et le calcium. *Bull. Soc. fr. Minér. Cristallogr.*, **83**, 1960, 1–21.
73. Gerasimovsky V. I. Minerals of uranium. *Atomn. Energ.*, **4**, 1956, 573–85. (Russian text)
74. Getseva R. V. and Saveleva K. T. *Handbook for the determination of uranium minerals* (Moscow: Gosgeoltekhizdat, 1956), 260 p.
75. Gorman D. H. Studies of radioactive compounds: V—soddyite. *Am. Miner.*, **37**, 1952, 386–93.
76. Grønvold F. High temperature X-ray of uranium oxides in the UO_2–U_3O_8 region. *J. inorg. nucl. Chem.*, **1**, 1955, 357–70.
77. Gross E. B. *et al.* Heinrichite and metaheinrichite, hydrated barium uranyl arsenate minerals. *Am. Miner.*, **43**, 1958, 1134–43.
78. Guillemin C. and Protas J. Ianthinite et wyartite. *Bull Soc. fr. Minér. Cristallogr.*, **82**, 1959, 80–6.
79. Heinrich E. W. *Mineralogy and geology of radioactive raw materials* (New York: McGraw-Hill, 1958), 614 p.
80. Hoekstra H. R. and Siegel S. The uranium trioxide–water system. *J. inorg. nucl. Chem.*, **35**, 1973, 761–79.
81. Hogarth D. D. Classification and nomenclature of the pyrochlore group. *Am. Miner.*, **62**, 1977, 403–10.
82. Honea R. M. New data on gastunite, an alkali uranyl silicate. *Am. Miner.*, **44**, 1959, 1047–56.
83. Honea R. M. New data on boltwoodite, an alkali uranyl silicate. *Am. Miner.*, **46**, 1961, 12–25.
84. Hunan 230 Laboratory, Hunan 305 Geological Team and X-ray Laboratory, Wuhan Geological Institute. Furongite—a new uranium mineral found in China. *Acta Geol. Sin.*, **2**, 1976, 203–4. (Chinese text)
85. Hunan 230 Institute and X-ray Laboratory, Wuhan Geologic College. Xiangjiangite—a new mineral discovered in China. *Scientia Geol. Sin.* no. 2, 1978, 183–8. (Chinese text; English abstract)
86. Hutton C. O. Kobeite from Paringa River, South Westland, New Zealand. *Am. Miner.*, **42**, 1957, 342–53.
87. Huynen A. M. Piret-Meunier J. and Van Meerssche M. Structure de la kasolite. *Bull. Acad. r. Belg. Cl. Sci.*, **49**, 1963, 192–201.
88. Huynen A. M. and Van Meerssche M. Confirmation de la structure de la sklodowskite. *Bull. Acad. r. Belg. Cl. Sci.*, **48**, 1962, 742–50.
89. Kamhi S. R. An X-ray study of umohoite. *Am. Miner.*, **44**, 1959, 920–5.
89a. Khosrawan-Sazedj F. The crystal structure of meta-uranocircite: II. $Ba(UO_2)_2(PO_4)_2{\cdot}6H_2O$. *Tschermaks miner. petrogr. Mitt.*, **29**, 1982, 193–204.
90. Kirvokoneva G. K. Phase transitions of brannerite upon heating. *Dokl. Akad. Nauk SSSR*, **194**, 1970, 1168–71; *Dokl. Acad. Sci. USSR, Earth Sci. Sect.*, **194**, 1970, 137–40.
91. Kiss J. Constitution minéralogique propriétés, et problèmes de génèse du gisement uranifère de la Montagne Mecsek. *Annls Univ. Scient. Budapest Rolando Eötvòs, Sect. Geol.*, **9**, 1965, 139–61.
92. Kopchenova E. V. and Skvortsova K. V. Sodium uranospinite. *Dokl. Akad. Nauk SSSR*, **114**, 1957, 634–6. (Russian text)
93. Kopchenova E. V. *et al.* Mourite, a new supergene uranium molybdenum mineral. *Zap. vses. miner. Obshch.*, **91**, 1962, 67–71. (Russian text)
94. Kovba L. M. Crystal structure of potassium uranium oxide $K_2U_7O_{22}$. *Zh. strukt. Khim.*, **13**, 1972, 256–9.
95. Langmuir D. Uranium solution-mineral equilibria at low temperatures with application to sedimentary ore deposits. *Geochim. cosmochim. Acta*, **42**, 1978, 547–69.
96. Larsen E. S. Jr. and Berman H. The microscopic determination of nonopaque minerals, 2nd edition. *Bull. U.S. geol Surv.* 848, 1934, 266 p.
97. Legros J. P. and Jeannin Y. Coordination de l'uranium par l'ion germanate, II. Structure du germanate d'uranyle dihydraté $(UO_2)_2GeO_4(H_2O)_2$. *Acta crystallogr.*, **B31**, 1975, 1140–3.
98. Loopstra B. O. Neutron diffraction investigation of U_3O_8. *Acta crystallogr.*, **17**, 1964, 651–3.
99. Loopstra B. O. and Brandenburg N. P. Uranyl selenite and uranyl tellurite. *Acta crystallogr.*, **B34**, 1978, 1335–7.
100. Makarov Ye. S. and Anikina L. I. Crystal sturcture of umohoite $(UMoO_6(H_2O)_2){\cdot}2H_2O$. *Geokhimiya*, **1**, 1963, 15–22.
101. Mann A. W. Chemical ore genesis models for the precipitation of carnotite in calcrete. *Rep. C.S.I.R.O. Div. Miner.* FP7, 1974, 18 p.
102. Masaki N. Structure of U_4O_9 below and above the transition temperature. *Acta crystallogr.*, **A28**, 1972, S54.
103. Masaki N. and Doi K. Analyses of the superstructure of U_4O_9 by neutron diffraction. *Acta crystallogr.*, **B28**, 1972, 785–91.
104. McBurney T. C. and Murdoch J. Haiweeite, a new uranium mineral from California. *Am. Miner.*, **44**, 1959, 839–43.
105. McCarthy G. J. *et al.* Interactions between nuclear waste and surrounding rock. *Nature, Lond.*, **273**, 1978, 216–7.
106. Mereiter K. The crystal structure of curite $[Pb_{6.56}(H_2O, OH)_4][(UO_2)_8O_8(OH)_6]_2$. *Tschermaks miner. petrogr. Mitt.*, **26**, 1979, 279–92.
106a. Mereiter K. The crystal structure of johannite $Cu(UO_2)_2(OH)_2(SO_4)_2{\cdot}8H_2O$. *Tschermaks miner. petrogr. Mitt.*, **30**, 1982, 47–57.
106b. Mereiter K. The crystal structure of walpurgite $(UO_2)Bi_4O_4(AsO_4)_2{\cdot}2H_2O$. *Tschermaks miner. petrogr. Mitt.*, **30**, 1982, 129–39.
106c. Mereiter K. The crystal structure of liebigite $Ca_2(UO_2)(CO_3)_3{\cdot}11H_2O$. *Tschermaks miner. petrogr. Mitt.*, **30**, 1982, 277–88.
107. Meunier G. and Galy J. Structure crystalline de la schmitterite synthétique $UTeO_5$. *Acta crystallogr.*, **B29**, 1973, 1251–5.
108. Milton C. *et al.* Mckelveyite, a new hydrous sodium barium rare-earth uranium carbonate mineral from the Green River Formation Wyoming. *Am. Miner.*, **50**, 1965, 593–612.
109. Mokeeva V. I. The crystal structure of sklodowskite. *Soviet Phys. Dokl.*, **4**, 1958, 27–9.
110. Mokeeva V. I. The structure of sklodowskite. *Kristallografiya*, **9**, 1964, 277–8.
111. Mokeeva V. I. The crystal structure of kasolite. *Soviet Phys. Crystallogr.*, **9**, 1965, 621–2.
112. Morosin B. Hydrogen uranyl phosphate tetrahydrate, a hydrogen ion solid electrolyte. *Acta crystallogr.*, **B34**, 1978, 3732–4.
113. Morton R. D. The identification of uraniferous minerals. In *Short course in uranium deposits: their mineralogy and origin* Kimberley M. M. ed. (Toronto: The University Press for Mineralogical Association of Canada, 1978), 141–83.
114. Mücke A. and Strunz H. Petscheckite and liandratite, two new pegmatite minerals from Madagascar. *Am. Miner.*, **63**, 1978, 941–6.
115. Muto T. *et al.* Ningyoite, a new uranous phosphate mineral from Japan. *Am. Miner.*, **44**, 1959, 633–50.
116. Naito K. Phase transitions of U_4O_9. *J. nucl. Mater.*, **15**, 1974, 126–35.
117. Nekrasova Z. A. A hydrous uranyl ammonium phosphate (uramphite), $NH_4(UO_2)(PO_4){\cdot}3H_2O$. In *Voporsy Geol. Urana (Atomn. Energ. Prilozh.* no. 6), 1957, 67–72. (Russian text); English transl., Consultants Bureau, 1958, 56–60.
118. Niinisto L. Toivonen J. and Valkanen J. Structures of complex uranyl VI sulfates. In *Fourth European crystallographic meeting, Oxford, 1977* Prout C. K. convenor (Oxford, 1977), 572.
119. Noe-Spirlet M. R. and Sobry R. Les uranates hydratés ne forment pas une série continue. *Bull. Soc. r. Sci. Liège*, **43**, 1974, 164–71.
120. Outerbridge W. F. *et al.* Weeksite, a new uranium silicate from the Thomas Range, Juab county, Utah. *Am. Miner.*, **45**, 1960, 39–52.
121. Peking Institute of Uranium Geology and X-ray Laboratory, Wuhan Geological College. Orthobrannerite—a new mineral of the brannerite group. *Acta Geol. Sin.*, 1978, 241–51. (Chinese text; English abstract)
122. Pierrot R. Toussaint J. and Verbeek T. La guilleminite, une nouvelle espèce minérale. *Bull. Soc. fr. Minér. Cristallogr.*, **88**, 1965, 132–5.
123. Piret P. and Declercq J. P. Phurcalite. *Acra crystallogr.*, **B34**, 1978, 1677–9.
124. Piret P. Declercq J. P. and Wauters-Stoop D. Structure of threadgoldite. *Acta crystallogr.*, **B35**, 1979, 3017–20.
125. Piret P. Declercq J. P. and Wauters-Stoop D. Structure cristalline de la sengiérite. *Bull. Soc. fr. Minér. Cristallogr.*, **103**, 1980, 176–8.
126. Piret P. and Deliens M. Nouvelles données sur une umohoite magnésienne de Shinkolobwe (region du Shaba, Republique du Zaire). *Annls Soc. géol. Belg.*, **99**, 1976, 205–9.
127. Piret P. and Deliens M. New crystal data for Ca, Cu, UO_2 hydrated carbonate: voglite. *J. appl. Crystallogr.*, **12**, 1979, 616.
127a. Piret P. and Deliens M. Vanmeersscheite, $U(UO_2)_3(PO_4)_2(OH)_6{\cdot}4H_2O$ and meta-vanmeersscheite $U(UO_2)_3(PO_4)_2(OH)_6{\cdot}2H_2O$, new minerals. *Bull. Minéralogie*, **105**, 1982, 125–8.
128. Piret P. Piret-Meunier J. and Declercq J. P. Structure of

phuralumite. *Acta crystallogr.*, **B35**, 1979, 1880–2.
129. Piret-Meunier J. Léonard A. and Van Meerssche M. Structure de la dumontite, $Pb_2(UO_2)_3(PO_4)_2(OH)_4 \cdot 3H_2O$. *Bull. Acad. r. Belg. Cl. Sci.*, **48**, 1962, 751–60.
130. Piret-Meunier J. and Van Meerssche M. Structure de la jachimovite, $Cu_2H_2(UO_2SiO_4)_2 \cdot 5H_2O$. *Bull. Acad. r. Belg. Cl. Sci.*, **49**, 1963, 181–91.
131. *Powder diffraction file 1980* (Swarthmore, Pa.: Joint Committee on Powder Diffraction Standards, International Centre for Diffraction Data, 1980).
132. Protas J. La wölsendorfite, nouvelle espèce uranifère. *C.r. Acad. Sci. Paris*, **244**, 1957, 2942–4.
133. Protas J. Contribution a l'étude des oxydes d'uranyle hydratés. Thèse, Faculté des Sciences, Université de Paris, 1959.
134. Protas J. Contribution à l'étude des oxydes d'uranyle hydratés. *Bull. Soc. fr. Minér. Cristallogr.*, **82**, 1959, 239–72.
135. Protas J. Une nouvelle espèce minérale: la compreignacite, $K_2O \cdot 6UO_3 \cdot 11H_2O$. *Bull. Soc. fr. Minér. Cristallogr.*, **87**, 1964, 365–71.
136. Rogova V. P. *et al.* Bauranoite and metacalciouranoite, new minerals of the group of hydrous uranium oxides. *Zap. vses. miner Obshch.*, **102**, 1973, 75–81.
137. Rogova V. P. *et al.* Calciouranoite, a new hydroxide of uranium. *Zap. vses. miner. Obshch.*, **103**, 1974, 108–9.
138. Roof R. B. Jr. Cromer D. T. and Larsen A. C. The crystal structure of uranyl dihydroxide, $UO_2(OH)_2$. *Acta crystallogr.*, **17**, 1964, 701–5.
139. Rosenzweig A. and Ryan R. R. Refinement of the crystal structure of cuprosklodowskite, $Cu[(UO_2)_2(SiO_3OH)_2] \cdot 6H_2O$. *Am. Miner.*, **60**, 1975, 448–53.
140. Rosenzweig A. and Ryan R. R. Vandenbrandeite, $CuUO_2(OH)_4$. *Cryst. Struct. Commun.*, **6**, 1977, 53–6.
141. Rosenzweig A. and Ryan R. R. Kasolite, $Pb(UO_2)(SiO_4) \cdot H_2O$. *Cryst. Struct. Commun.*, **6**, 1977, 617–21.
142. Ross M. and Evans H. T. Jr. Crystal structure of cesium biuranyl trisulfate, $Cs_2(UO_2)_2(SO_4)_3$. *J. inorg. nucl. Chem.*, **15**, 1960, 338–51.
143. Ross M. and Evans H. T. Jr. Studies of the torbernite minerals (I): the crystal structure of abernathyite and the structurally related compounds, $NH_4(UO_2AsO_4) \cdot 3H_2O$ and $K(H_3O)(UO_2AsO_4)_2 \cdot 6H_2O$. *Am. Miner.*, **49**, 1964, 1578–602.
144. Ross M. Evans H. T. Jr. and Appleman D. E. Studies of the torbernite minerals (II): the crystal structure of meta-torbernite. *Am. Miner.*, **49**, 1964, 1603–21.
145. Ruh R. and Wadsley A. D. The crystal structure of $ThTi_2O_6$ (brannerite). *Acta crystallogr.*, **21**, 1966, 974–8.
146. Rupnitskaya L. S. Calcium uranium molybdate, $Ca(UO_2)_3(MoO_4)_3(OH)_2 \cdot 8H_2O$. Reference 11, 286.
147. Ryan R. R. and Rosenzweig A. Sklodowskite, $MgO \cdot 2UO_2 \cdot 2SiO_2 \cdot 7H_2O$. *Cryst. Struct. Commun.*, **6**, 1977, 611–5.
148. Schoep A. and Stradiot S. Paraschoepite and epiianthinite, two new uranium minerals from Shinkolobwe (Belgian Congo). *Am. Miner.*, **32**, 1947, 344–50.
149. Serezhkin V. N. *et al.* The structure of synthetic iriginite. *Dokl. Akad. Nauk SSSR*, **210**, 1973, 873–6.
150. Sergeev A. S. Pseudo-autunite, a new hydrous calcium uranyl phosphate. *Miner. Geokhim. Leningrad Univ. Sbornik Statei* no 1, 1964, 31–9.
151. Shaner B. E. Metallographic determination of the UO_2–U_4O_9 phase diagram. *J. nucl. Mater.*, **2**, 1960, 110–20.
152. Shashkin D. P. Crystal structure of francevillite, $Ba[(UO_2)_2(VO_4)_2] \cdot 5H_2O$. *Dokl. Akad. Nauk SSSR*, **220**, 1974, 1410–3.
153. Shashkin D. P. Lur'e E. A. and Belov N. V. Crystal structure of sodium uranyl silicate, $Na_2(UO_2)SiO_4$. *Kristallografiya*, **19**, 1974, 958–63.
154. Shashkin D. P. and Sidorenko G. A. Crystal structure of phosphuranylite, $Ca[(UO_2)_3(PO_4)_2] \cdot 6H_2O$. *Dokl. Akad. Nauk SSSR*, **220**, 1974, 1161–4.
155. Shchipanova O. V. *et al.* New data on the structure and identification of trögerite and hydrogen uranospinite. *Dokl. Akad. Nauk SSSR*, **197**, 1971, 178–81; *Dokl. Acad. Sci. USSR Earth Sci. Sect.*, **197**, 1971, 109–11.
156. Sidorenko G. A. Moroz I. Kh. and Zhiltsova I. G. Crystal chemistry of uranium silicates. *Zap. vses. miner. Obshch.*, **104**, 1975, 559–67.
157. Siegel S. Hoekstra H. R. and Gebert E. The structure of γ-uranyl dihydroxide, $UO_2(OH)_2$. *Acta crystallogr.*, **B28**, 1972, 3469–73.
158. Siegel S. Viste A. and Hoekstra H. R. The structure of hydrogen triuranate. *Acta crystallogr.*, **B28**, 1972, 117–21.
159. Skvortsova K. V. and Sidorenko G. A. Sedovite, a new supergene mineral of uranium and molybdenum. *Zap. vses. miner. Obshch.*, **94**, 1965, 548–54. (Russian text)
160. Skvortsova K. V. *et al.* Conditions of the formation of umohoite in the uranium–molybdenum deposits of the USSR. *Geologiya rudn. mestorozh.*, **3**, no. 5, Sept.–Oct. 1961, 53–63. (Russian text)
161. Smith D. K. Jr. Gruner J. W. and Lipscomb W. N. The crystal structure of uranophane $[Ca(H_3O)_2](UO_2)_2(SiO_4)_2 \cdot 3H_2O$. *Am. Miner.*, **42**, 1957, 594–618.
162. Smith D. K. Jr. and Stohl F. V. Crystal structure of beta-uranophane. *Mem. geol. Soc. Am.*, **135**, 1972, 281–8.
163. Soboleva M. V. and Pudovkina I. A. *Mineraly urana: Spravochnik (Uranium minerals: a reference book)* (Moscow: Gosgeoltekhizdat, 1957), 408 p. (Russian text); *Mineralog. Abstr.*, **14**, 1959–60, 13–14.
164. Soboleva M. V. and Pudovkina I. A. *Uranium minerals: a reference book.* U.S. Atomic Energy Commision Translation Series 4487, 1961, 433 p.
165. Sobry R. Water and interlayer oxonium in hydrated uranates. *Am. Miner.*, **56**, 1971, 1065–76.
166. Sobry R. Indexation de radiogrammes de poudères d'uranates hydratés. *Bull. Soc. r. Sci. Liège*, **41**, 1972, 542–52.
167. Steacy H. R. and Kaiman S. Uranium minerals in Canada: their description, identification and field guides. Reference 113, 107–40.
168. Stieff L. R. Stern T. W. and Sherwood A. M. Coffinite, a uranous silicate with hydroxyl substitution: a new mineral. *Am. Miner.*, **41**, 1956, 675–88.
169. Stohl F. V. and Smith D. K. Jr. The crystal chemistry of the uranyl silicates. *Am. Miner.*, **66**, 1981, 610–25.
170. Swallow A. G. Ahmed F. R. and Barnes W. H. The crystal structure of pascoeite, $Ca_3V_{10}O_{28} \cdot 17H_2O$. *Acta crystallogr.*, **21**, 1966, 397–405.
171. Taylor J. C. The structure of the α form of uranyl hydroxide. *Acta crystallogr.*, **B27**, 1971, 1088–91.
171a. Taylor J. C. Stuart W. K. and Momme I. A. The crystal structure of curite. *J. inorg. nucl. Chem.*, **43**, 1981, 2419–23.
172. Taylor J. C. and Wilson P. W. The deuterium location in deuterium triuranate $D_2U_3O_{10}$ by neutron diffraction. *Acta crystallogr.*, **B30**, 1974, 151–4.
173. Threadgold I. M. The mineral composition of some uranium ores from the South Alligator River area, Northern Territory. *Mineralog. Invest. CSIRO Tech. Pap.* no. 2, 1960.
174. Vaes J. F. Cousiniet, een nieuw uraanmineraal. *Geologie Mijnb.*, **20**, 1958, 449.
175. Van der Putten N. and Loopstra B. O. Uranyl sulfate hydrate. *Cryst. Struct. Commun.*, **3**, 1974, 377–80.
176. Van Wambeke L. Contribution à l'étude de la minéralisation radioactive de la pegmatite de Kobokobo et déscription d'une nouvelle espèce minérale radioactive de la série phosphuranylite–renardite: la kivuite. *Bull. Soc. belge Géol. Paléont. Hydrol.*, **67**, 1958, 383–403.
177. Vochten R. and Deliens M. Transformation of curite into meta-autunite: paragenesis and electrokinetic properties. *Phys. Chem. Minerals*, **6**, 1980, 129–43.
178. Vochten R. *et al.* Formation of meta-torbernite starting from curite: crystallographic data and electrokinetic properties. *Phys. Chem. Minerals*, **4**, 1979, 281–90.
179. Voultsidis V. and Clasen D. Probleme und Grenzbereiche der Uranmineralogie. *Erzmetall*, **31**, 1978, 8–13.
180. Walenta K. Die sekundären Uranmineralien des Schwarzwaldes. Preliminary report. Technische Hochschule Stuttgart, 1958; Abstract in *Bull. Soc. fr. Minér. Cristallogr.*, **81**, 1958, 67–8.
181. Walenta K. Die sekundären Uranmineralien des Schwarzwaldes. *Jh. geol. Landesamt Baden-Württ.*, **3**, 1958, 17–51.
182. Walenta K. Grimselit ein neues Kalium–Natrium–Uranyl-Karbonat aus dem Grinselgebiet (Oberhasli, Kanton Bern, Schweiz). *Schweiz. mineral. petrogr. Mitt.*, **52**, 1972, 93–108.
183. Walenta K. On studtite and its composition. *Am. Miner.*, **59**, 1974, 166–71.
184. Walenta K. Widenmannit und Joliotit, zwei neue Uranyl-karbonatmineralien aus dem Schwarzwald. *Schweiz. mineral. petrogr. Mitt.*, **56**, 1976, 167–85.
185. Walenta K. Uranium minerals from the Schildmauer gypsum

deposit near Admont, Styria. *MittBl. Landesmuseums Joanneum Abt. Miner.*, **44**, 1976, 35–41. (German text)
186. Walenta K. Uranospathite and arsenuranospathite. *Mineralog. Mag.*, **42**, 1978, 117–28.
187. Walenta K. and Wimmenauer W. Der Mineralbestand des Michaelganges im Weiler bei Lahr (Schwarzwald). *Jh. geol. Landesamt Baden-Württ.*, **4**, 1961, 7–37.
188. Weeks A. D. and Thompson M. E. Identification and occurrence of uranium and vanadium minerals from the Colorado Plateaus. *Bull. U.S. geol. Surv.* 1009B, 1954, 13–62.
189. Wenrich-Verbeek K. J. *et al.* Margaritasite: a new mineral of hydrothermal origin from the Peña Blanca uranium district, Mexico. *Am. Miner.*, **67**, 1982, 1273–89.
190. Willis B. T. M. The defect structure of hyper-stoichiometric uranium dioxide. *Acta crystallogr.*, **A34**, 1978, 88–90.
191. Young E. J. Weeks A. D. and Meyrowitz R. Coconinoite, a new uranium mineral from Utah and Arizona. *Am. Miner.*, **51**, 1966, 651–63.
192. Zacharisen W. H. Crystal chemical studies of the 5f-series of elements: III. A study of the disorder in the crystal structure of anhydrous uranyl fluoride. *Acta crystallogr.*, **1**, 1948, 277–81.
193. Zolensky M. E. The crystal structure and twinning of barium uranyl phosphate hexahydrate (meta-uranocircite), and comparison to the other members of meta-autunite group. Ph.D. thesis, Pennsylvania State University, 1983.
194. Deliens M. and Piret P. La swamboite, nouveau silicate d'uranium hydraté du Shaba, Zaire. *Can. Mineralogist*, **19**, 1981, 553–7.
195. Deliens M. and Piret P. Bijvoetite et lepersonnite, carbonates hydratés d'uranyle et des terres rares de Shinkolobwe, Zaire. *Can. Mineralogist*, **20**, 1982, 231–8.

Appendix 1

X-ray data for uranium minerals

The accompanying table is compiled from data of several sources but primarily the *Powder diffraction file* published by the Joint Committee on Powder Diffraction Standards-International Centre for Diffraction Data and is used with their permission.* Other data are taken from primary references on the specific minerals and will appear in the PDF in the near future. These data are indicated when no PDF number is listed.

The table is a modified Hanawalt search manual. Each X-ray pattern is represented by its five strongest lines. The strong lines are permuted following Hanawalt rules to create three entries and expanded to include entries under the fourth and fifth lines. If d_1, d_2, d_3, d_4 and d_5 are the d-spacings listed in order of decreasing intensity, the five entries are as follows:

$$\begin{array}{ccccc} d_1 & d_2 & d_3 & d_4 & d_5 \\ d_2 & d_3 & d_1 & d_4 & d_5 \\ d_3 & d_1 & d_2 & d_4 & d_5 \\ d_4 & d_1 & d_2 & d_3 & d_5 \\ d_5 & d_1 & d_2 & d_3 & d_4 \end{array}$$

These entries are then grouped into 45 Hanawalt groups as indicated by the heading divider and ordered within each group according to the second line in the list.

This appendix is intended to be a mini-search manual for the uranium minerals. Once the possible pattern matches are located using this abbreviated table, it will be necessary for the user to refer to the original data or the PDF for final confirmation of any identification.

Several uranium minerals have no recorded X-ray pattern. These minerals are listed separately. If any user has patterns for any one of these minerals, they should adequately characterize the specimen and submit the pattern to JCPDS–ICDD for inclusion in the PDF.

Although the list of 231 X-ray patterns has been essentially restricted to accepted uranium mineral species, several poorly described unnamed minerals have been included along with the best characterized uranyl oxide hydrates. These latter synthetic phases have been listed because of the possible existence in the 'gummite' alteration rinds often associated with uraninite.

D	I	D	I	D	I	D	I	D	I	MINERAL NAME	PDF NO.
99.990 - 10.000											
12.600	(100)	8.700	(100)	9.650	(80)	7.100	(60)	4.320	(50)	VOGLITE	33- 274
10.200	(100)	8.620	(80)	4.310	(50)	3.639	(40)	2.868	(35)	FURONGITE	29- 98
16.800	(70)	8.420	(100)	5.600	(100)	3.350	(78)	2.791	(45)	UMOHOITE,17A	12- 778
11.300	(50)	8.240	(100)	7.790	(80)	4.370	(80)	4.710	(70)	RABBITTITE	7- 365
10.300	(100)	7.960	(90)	3.080	(80)	2.870	(80)	5.880	(60)	KIVUITE	13- 419
13.000	(100)	7.930	(100)	5.670	(100)	3.680	(100)	5.230	(80)	ANDERSONITE	20-1092
14.620	(100)	7.620	(100)	3.490	(90)	5.030	(80)	3.590	(60)	ARSENURANOSPATHITE	31- 586
15.200	(100)	7.600	(100)	4.930	(100)	3.500	(80)	0.000	(0)	URANOSPATHITE	31- 587
14.300	(30)	7.260	(100)	4.800	(80)	8.480	(70)	2.876	(70)	SCHROECKINGERITE	8- 397
14.100	(25)	7.100	(100)	3.220	(50)	3.180	(25)	4.740	(20)	UMOHOITE,14A	11- 375
12.000	(100)	5.980	(90)	3.980	(80)	3.230	(80)	3.180	(80)	VANURALITE	23- 769
11.100	(100)	5.560	(40)	3.300	(20)	5.640	(18)	4.590	(14)	COCONINOITE	25- 16
11.100	(80)	5.550	(50)	3.530	(100)	3.590	(50)	1.603	(40)	KAHLERITE	17- 145
10.400	(100)	5.190	(50)	3.580	(45)	4.960	(25)	4.480	(20)	AUTUNITE	12- 418
10.300	(100)	5.190	(30)	3.470	(10)	3.280	(10)	7.600	(5)	WYARTITE-(20A)	12- 635
10.100	(60)	5.100	(100)	2.040	(100)	1.462	(60)	2.160	(50)	URANOCIRCITE	18- 199
10.200	(100)	5.020	(90)	3.200	(50)	2.040	(40)	6.620	(30)	TYUYAMUNITE	6- 17
10.300	(100)	4.940	(90)	3.580	(90)	3.510	(80)	6.610	(40)	TORBERNITE	8- 360
11.000	(40)	4.490	(100)	3.930	(50)	2.990	(60)	2.450	(60)	SHARPITE	12- 164
12.200	(30)	4.130	(100)	3.200	(50)	3.150	(40)	6.180	(30)	UMOHOITE,12A	12- 693
13.100	(90)	3.830	(60)	7.660	(100)	2.690	(50)	2.210	(50)	BAYLEYITE	4- 130
11.100	(100)	3.740	(80)	3.290	(80)	2.938	(70)	4.620	(60)	XIANGJIANGITE	29-1401
10.000	(80)	3.620	(100)	3.410	(90)	5.210	(80)	4.970	(80)	URANOSPINITE	29- 390
10.700	(100)	3.590	(90)	5.040	(80)	3.390	(70)	1.930	(60)	ZEUNERITE	4- 90
13.200	(100)	3.580	(90)	5.060	(80)	3.350	(50)	6.800	(40)	NOVACEKITE	8- 286
10.000	(100)	3.570	(100)	5.020	(80)	1.588	(50)	3.350	(40)	NOVACEKITE	17- 148
10.900	(100)	3.540	(100)	3.220	(70)	5.490	(60)	5.030	(40)	NOVACEKITE	17- 147
10.000	(100)	3.530	(100)	3.350	(80)	5.090	(70)	1.600	(70)	HEINRICHITE	29- 210
11.000	(90)	3.370	(90)	3.190	(100)	3.060	(90)	5.530	(80)	SEDOVITE	18-1425
10.400	(100)	3.080	(80)	5.170	(70)	3.400	(50)	3.470	(40)	PHURALUMITE	33- 38
10.700	(100)	2.950	(50)	3.490	(40)	2.620	(30)	3.870	(20)	RAUVITE	8- 288

* *Powder diffraction file* (Swarthmore, Pa.: Joint Committee on Powder Diffraction Standards, International Centre for Diffraction Data).

9.990 - 8.000

9.650(80)	12.600(100)	8.700(100)	7.100(60)	4.320(50)	VOGLITE	33- 274
8.700(100)	9.650(80)	12.600(100)	7.100(60)	4.320(50)	VOGLITE	33- 274
8.070(30)	9.160(100)	4.590(70)	4.430(60)	3.200(40)	HAIWEEITE	22- 160
9.250(70)	8.530(100)	3.660(90)	1.600(90)	1.530(80)	TROEGERITE-(P)	26- 887
8.300(50)	7.800(100)	3.210(80)	3.890(60)	1.990(50)	CALCURMOLITE	16- 145
8.240(100)	7.790(80)	4.370(80)	4.710(70)	11.300(50)	RABBITTITE	7- 365
8.410(80)	7.720(100)	3.850(100)	3.130(80)	3.420(70)	ARSENURANYLITE	14- 268
8.180(40)	7.680(100)	3.950(80)	4.080(60)	3.200(50)	STRELKINITE	27- 822
8.390(100)	7.290(100)	3.550(80)	6.680(60)	3.040(60)	GUILLEMINITE	18- 582
8.490(70)	7.260(100)	4.800(80)	2.876(70)	14.300(30)	SCHROECKINGERITE	8- 397
8.980(80)	7.110(100)	5.570(90)	3.550(70)	3.300(70)	WEEKSITE	12- 462
9.620(35)	7.080(100)	3.540(50)	3.440(35)	3.100(25)	ZINC-ZIPPEITE	29-1395
8.420(100)	5.600(100)	3.350(78)	16.800(70)	2.791(45)	UMOHOITE,17A	12- 778
8.760(100)	5.500(100)	7.310(90)	4.820(80)	2.910(80)	SWARTZITE	4- 111
8.680(90)	5.400(90)	6.810(100)	4.550(60)	3.100(60)	LIEBIGITE	11- 296
9.790(90)	5.000(80)	3.500(100)	4.480(60)	3.310(60)	SALEEITE	29- 874
9.820(100)	4.910(80)	3.740(60)	3.197(60)	3.179(60)	SENGIERITE	8- 398
8.590(60)	4.890(100)	3.460(100)	2.200(60)	4.250(30)	BASSETTITE	7- 288
9.690(100)	4.860(90)	3.470(80)	2.188(60)	4.390(40)	SABUGALITE	5- 107
9.660(100)	4.850(50)	5.590(35)	3.650(35)	4.410(25)	ZELLERITE	19- 257
8.160(100)	4.820(90)	6.060(70)	3.530(70)	3.290(40)	CUPROSKLODOWSKITE	19- 413
9.300(100)	4.620(45)	4.470(40)	3.340(30)	3.037(30)	HAIWEEITE	13- 118
9.160(100)	4.590(70)	4.430(60)	3.200(40)	8.070(30)	HAIWEEITE	22- 160
9.260(100)	4.530(80)	4.410(50)	3.180(40)	7.090(30)	HAIWEEITE	12- 721
8.620(80)	4.310(50)	10.200(100)	3.639(40)	2.868(35)	FURONGITE	29- 98
8.550(90)	4.290(60)	3.590(100)	5.110(50)	2.150(50)	METAKAHLERITE	12- 576
9.180(80)	4.280(80)	7.120(100)	3.650(50)	5.510(40)	URANOPILITE	8- 443
8.340(80)	4.230(40)	3.600(100)	4.270(35)	5.350(30)	META-URANOCIRCITE II	25-1468
8.460(100)	4.220(20)	3.470(20)	3.560(10)	3.030(10)	WYARTITE-(17A)	12- 636
8.420(100)	4.190(80)	3.270(70)	3.520(60)	3.000(60)	SKLODOWSKITE	29- 875
8.400(100)	4.180(80)	3.430(80)	3.170(70)	4.240(60)	UPALITE	33- 37
9.920(100)	4.170(90)	3.160(90)	4.090(80)	3.240(80)	METAVANURALITE	23- 770
8.180(100)	4.090(90)	2.970(80)	4.820(70)	6.100(60)	CUPROSKLODOWSKITE	8- 290
8.170(100)	4.000(55)	4.140(30)	3.510(14)	2.718(14)	META-AUTUNITE	14- 75
9.100(100)	3.830(85)	3.340(80)	3.590(75)	5.640(70)	ABERNATHYITE	16- 386
9.020(100)	3.800(100)	3.260(90)	2.760(80)	2.160(80)	URAMPHITE	29- 121
9.100(100)	3.790(50)	4.700(35)	4.800(35)	4.550(18)	METAZELLERITE	19- 258
8.590(100)	3.790(90)	3.300(80)	5.500(70)	4.350(70)	TROEGERITE	8- 326
9.090(100)	3.780(100)	3.270(90)	3.510(80)	5.530(70)	META-ANKOLITE	29-1061
8.900(100)	3.750(80)	5.540(60)	4.420(60)	3.550(60)	METAHEINRICHITE	24- 128
8.930(100)	3.730(80)	5.480(70)	3.230(60)	1.658(50)	META-URANOCIRCITE	17- 758
8.920(100)	3.730(65)	3.250(55)	4.930(50)	3.490(50)	META-ANKOLITE	19-1008
8.860(100)	3.730(100)	5.570(80)	3.300(80)	3.570(70)	METAZEUNERITE	17- 146
8.710(100)	3.680(100)	3.480(80)	3.230(90)	5.440(75)	METATORBERNITE	16- 404
8.530(100)	3.660(90)	1.600(90)	1.530(80)	9.250(70)	TROEGERITE-(P)	26- 887
8.420(100)	3.630(90)	3.270(80)	5.440(70)	3.550(70)	SODIUM URANOSPINITE	8- 446
9.490(50)	3.610(100)	9.080(90)	1.620(60)	1.530(60)	PRZHEVALSKITE	29- 787
8.550(100)	3.610(90)	5.390(70)	3.210(70)	4.250(60)	META-URANOCIRCITE II	17- 789
8.470(100)	3.610(85)	2.110(70)	4.230(65)	5.370(45)	META-AUTUNITE	12- 423
8.860(100)	3.590(100)	1.610(70)	2.540(60)	2.280(60)	METAKAHLERITE	17- 151
8.850(100)	3.590(90)	3.340(80)	5.100(70)	5.570(60)	META-URANOSPINITE	8- 319
8.780(100)	3.570(100)	5.080(60)	4.300(60)	3.010(60)	METAKIRCHHEIMERITE	12- 586
8.650(100)	3.570(100)	3.310(90)	5.530(80)	3.000(50)	META-URANOSPINITE	18- 309
8.520(100)	3.570(90)	2.140(60)	4.290(50)	2.530(50)	METANOVACEKITE	17- 152
9.430(100)	3.474(80)	3.366(60)	2.197(60)	5.350(50)	THREADGOLDITE	33- 39
9.630(35)	3.450(100)	7.100(95)	3.100(65)	3.560(40)	NICKEL-ZIPPEITE	29- 944
8.090(100)	3.420(90)	3.180(80)	4.100(50)	1.882(40)	JOLIOTITE	29-1378
9.000(100)	3.133(80)	4.700(50)	2.978(40)	1.850(40)	RANUNCULITE	33- 972
9.900(40)	3.110(100)	3.250(50)	3.050(50)	2.720(40)	WALPURGITE	8- 324
8.050(100)	3.100(80)	3.090(80)	2.878(70)	3.390(50)	PHURCALITE	29- 391
8.230(100)	3.090(100)	3.220(90)	2.900(90)	3.500(80)	MARTHOZITE	25- 320
8.090(80)	3.080(80)	5.760(100)	3.650(70)	2.860(70)	GRIMSELITE	25- 679
8.190(100)	3.010(100)	4.100(30)	5.130(60)	4.220(60)	CURIENITE	22- 402
8.400(100)	3.000(100)	5.200(60)	4.260(60)	2.126(60)	FRANCEVILLITE	21- 381
8.160(100)	2.990(100)	4.070(90)	4.230(70)	5.110(60)	UNNAMED-(PB)	15- 496
8.660(70)	2.980(60)	3.590(100)	5.090(40)	3.500(30)	METALOOEVITE	25-1239
9.080(90)	1.620(60)	3.610(100)	1.530(60)	9.490(50)	PRZHEVALSKITE	29- 787

7.990 - 7.000

7.660(100)	13.100(90)	3.830(60)	2.690(50)	2.210(50)	BAYLEYITE	4- 130
7.100(60)	12.600(100)	8.700(100)	9.650(80)	4.320(50)	VOGLITE	33- 274
7.600(5)	10.300(100)	5.190(30)	3.470(10)	3.280(10)	WYARTITE-(20A)	12- 635
7.090(30)	9.260(100)	4.530(80)	4.410(50)	3.180(40)	HAIWEEITE	12- 721
7.120(100)	9.180(80)	4.280(80)	3.650(50)	5.510(40)	URANOPILITE	8- 443
7.310(90)	8.760(100)	5.500(100)	4.820(80)	2.910(80)	SWARTZITE	4- 111
7.910(100)	7.320(90)	3.280(60)	3.560(40)	5.810(30)	UO3.H2O UNNAMED	15- 569
7.740(90)	6.880(80)	5.550(100)	3.450(80)	3.230(80)	ROUBAULTITE	25- 318
7.730(100)	6.160(90)	3.410(80)	3.870(70)	3.130(70)	JOHANNITE	17- 530
7.930(100)	5.670(100)	13.000(100)	3.680(100)	5.230(80)	ANDERSONITE	20-1092
7.110(100)	5.570(90)	8.980(80)	3.550(70)	3.300(70)	WEEKSITE	12- 462
7.360(80)	5.280(100)	3.310(100)	2.640(100)	3.380(80)	IRAQITE	29- 995
7.280(100)	5.080(70)	3.440(25)	3.660(15)	3.510(12)	SCHOEPITE	13- 407
7.600(100)	4.930(100)	15.200(100)	3.500(80)	0.000(0)	URANOSPATHITE	31- 587
7.260(100)	4.800(80)	8.480(70)	2.876(70)	14.300(30)	SCHROECKINGERITE	8- 397
7.790(80)	4.370(80)	8.240(100)	4.710(70)	11.300(50)	RABBITTITE	7- 365
7.970(100)	3.990(90)	5.830(80)	3.130(80)	3.090(80)	RENAROITE	8- 328
7.930(80)	3.990(60)	1.997(60)	2.140(50)	3.580(40)	URANOPHANE-(BA)	-
7.680(100)	3.950(80)	4.080(60)	3.200(50)	8.180(40)	STRELKINITE	27- 822
7.880(100)	3.940(90)	2.990(80)	2.910(80)	1.969(70)	URANOPHANE	8- 442
7.830(100)	3.900(90)	3.510(60)	3.190(50)	2.590(50)	BETAURANOPHANE	8- 301

7.780(100)	3.880(100)	3.080(100)	2.976(80)	3.440(60)	BERGENITE	20- 154
7.720(100)	3.850(100)	8.410(80)	3.130(80)	3.420(70)	ARSENURANYLITE	14- 268
7.630(100)	3.810(80)	3.240(80)	3.590(60)	3.350(60)	IANTHINITE	12- 272
7.810(100)	3.760(70)	3.890(60)	3.290(40)	2.150(40)	UNNAMED-(GA)	15- 609
7.350(100)	3.660(50)	3.240(10)	2.446(10)	3.210(4)	SCHOEPITE	13- 241
7.340(100)	3.660(55)	3.490(45)	3.150(35)	2.858(15)	SODIUM-ZIPPEITE	29-1285
7.250(100)	3.610(100)	3.170(75)	1.985(40)	3.530(25)	VANDENDRIESSCHEITE	13- 117
7.370(100)	3.590(100)	3.240(80)	3.520(60)	3.170(50)	SCHOEPITE	29-1376
7.210(100)	3.590(45)	3.120(30)	3.470(20)	1.963(12)	COBALT-ZIPPEITE	29- 520
7.210(100)	3.590(45)	3.120(30)	1.963(12)	2.491(11)	NICKEL-ZIPPEITE	29-1434
7.200(100)	3.580(50)	3.180(50)	3.550(18)	3.140(12)	FOURMARIERITE	13- 116
7.140(90)	3.560(100)	3.480(100)	3.130(90)	2.620(80)	RICHETITE	25- 467
7.480(100)	3.550(80)	3.200(80)	3.140(60)	3.730(40)	BECQUERELITE	12- 176
7.290(100)	3.550(80)	8.390(100)	6.680(60)	3.040(60)	GUILLEMINITE	18- 582
7.080(100)	3.540(50)	9.620(35)	3.440(35)	3.100(25)	ZINC-ZIPPEITE	29-1395
7.400(100)	3.530(80)	3.190(80)	3.700(60)	3.580(60)	COMPREIGNACITE	17- 167
7.080(100)	3.520(70)	3.120(50)	3.560(35)	3.480(20)	MASUYITE	13- 408
7.530(80)	3.500(70)	3.180(100)	3.760(50)	2.039(50)	BILLIETITE	29- 208
7.120(100)	3.500(100)	3.140(100)	3.120(100)	3.570(90)	RAMEAUITE	25- 631
7.060(100)	3.500(90)	3.120(80)	2.870(40)	2.650(40)	ZIPPEITE	29-1062
7.620(100)	3.490(90)	14.620(100)	5.030(80)	3.590(60)	ARSENURANOSPATHITE	31- 586
7.200(80)	3.480(80)	3.560(100)	3.110(60)	2.740(30)	MAGNESIUM-ZIPPEITE	29- 876
7.020(100)	3.480(90)	3.130(90)	1.960(60)	1.750(50)	ZIPPEITE	8- 138
7.320(90)	3.280(60)	7.910(100)	3.560(40)	5.810(30)	UO3.H2O UNNAMED	15- 569
7.770(100)	3.250(100)	3.000(100)	4.130(90)	6.520(80)	FRITZCHEITE	23-1249
7.370(100)	3.220(100)	3.700(80)	3.610(80)	3.160(80)	UO2(OH)2	28-1415
7.350(100)	3.220(50)	3.590(40)	3.160(30)	3.670(25)	UO3.2H2O (BETA)	18-1436
7.100(100)	3.220(50)	14.100(25)	3.180(25)	4.740(20)	UMOHOITE,14A	11- 375
7.800(100)	3.210(80)	3.890(60)	8.300(50)	1.990(50)	CALCURMOLITE	16- 145
7.490(100)	3.210(80)	3.550(40)	3.740(35)	3.160(30)	BECQUERELITE	29- 389
7.440(100)	3.200(35)	3.730(30)	3.540(20)	2.566(10)	BECQUERELITE	13- 405
7.960(80)	3.160(100)	3.090(100)	2.880(100)	5.860(80)	PHOSPHURANULITE	19- 898
7.080(100)	3.130(100)	3.490(90)	3.153(90)	3.520(80)	AGRINIERITE	25- 630
7.100(95)	3.100(65)	3.450(100)	3.560(40)	9.630(35)	NICKEL-ZIPPEITE	29- 944
7.960(90)	3.080(80)	10.300(100)	2.870(80)	5.880(60)	KIVUITE	13- 419

6.990 - 6.000

6.610(40)	10.300(100)	4.940(90)	3.580(90)	3.510(80)	TORBERNITE	8- 360
6.800(40)	10.200(100)	3.580(90)	5.060(80)	3.350(50)	NOVACEKITE	8- 286
6.620(30)	10.200(100)	5.020(90)	3.200(50)	2.040(40)	TYUYAMUNITE	6- 17
6.810(100)	8.680(90)	5.400(90)	4.550(60)	3.100(60)	LIEBIGITE	11- 296
6.680(60)	8.390(100)	7.290(100)	3.550(80)	3.040(60)	GUILLEMINITE	18- 582
6.100(60)	8.180(100)	4.090(90)	2.970(80)	4.820(70)	CUPROSKLODOWSKITE	8- 290
6.060(70)	8.160(100)	4.820(90)	3.530(70)	3.290(40)	CUPROSKLODOWSKITE	19- 413
6.520(80)	7.770(100)	3.250(100)	3.000(100)	4.130(90)	FRITZCHEITE	23-1249
6.880(80)	5.550(100)	7.740(90)	3.450(80)	3.230(80)	ROUBAULTITE	25- 318
6.140(55)	4.270(100)	3.000(85)	2.950(85)	3.480(70)	DUMONTITE	12- 158
6.510(100)	4.220(80)	3.260(60)	3.050(60)	5.190(40)	METATYUYAMUNITE	6- 287
6.970(100)	4.210(90)	5.440(60)	2.880(60)	5.870(50)	URANOPILITE	8- 131
6.180(30)	4.130(100)	3.200(50)	3.150(40)	12.200(30)	UMOHOITE,12A	12- 693
6.965(100)	3.600(70)	3.344(70)	3.489(70)	3.231(50)	MARGARITASITE	-
6.360(100)	3.530(80)	3.210(80)	4.220(60)	3.140(60)	CARNOTITE	11- 338
6.040(35)	3.440(100)	3.350(100)	4.740(95)	3.020(35)	BRANNERITE	12- 477
6.160(90)	3.410(80)	7.730(100)	3.870(70)	3.130(70)	JOHANNITE	17- 530
6.010(100)	3.400(90)	3.540(70)	2.910(70)	1.908(60)	BOLTWOODITE	29-1026
6.140(80)	3.320(100)	4.480(90)	2.690(70)	2.470(60)	SODDYITE	12- 180
6.200(100)	3.250(100)	1.920(90)	2.950(80)	2.190(80)	PSEUDO-AUTUNITE	18-1084
6.400(19)	3.230(100)	5.290(30)	3.130(25)	2.974(19)	IRIGINITE	29-1372
6.330(100)	3.210(100)	2.620(55)	4.280(50)	5.250(45)	IRIGINITE	18-1426
6.230(100)	3.140(80)	3.960(70)	3.060(50)	3.520(40)	CURITE	14- 267
6.560(100)	3.120(70)	3.530(50)	4.250(30)	3.250(30)	CARNOTITE	8- 317
6.910(35)	3.090(100)	3.460(75)	1.730(40)	1.913(80)	WOLSENDORFITE	29- 786
6.390(80)	3.090(100)	3.470(80)	3.130(60)	3.510(40)	WOLSENDORFITE	12- 159
6.070(60)	3.020(100)	4.400(80)	2.830(80)	2.150(80)	RHABDOPHANE	12- 277
6.400(35)	2.940(100)	4.470(85)	2.650(40)	3.320(30)	MCKELVEYITE	18- 901
6.710(100)	2.920(100)	4.700(80)	3.490(80)	3.370(80)	SODIUM BOLTWOODITE	29-1044

5.990 - 5.500

5.670(100)	13.000(100)	7.930(100)	3.680(100)	5.230(80)	ANDERSONITE	20-1092
5.640(18)	11.100(100)	5.560(40)	3.300(20)	4.590(14)	COCONINOITE	25- 16
5.880(60)	10.300(100)	7.960(90)	3.080(80)	2.870(80)	KIVUITE	13- 419
5.590(35)	9.660(100)	4.850(50)	3.650(35)	4.410(25)	ZELLERITE	19- 257
5.640(70)	9.100(100)	3.830(85)	3.340(80)	3.590(75)	ABERNATHYITE	16- 386
5.530(70)	9.090(100)	3.780(100)	3.270(90)	3.510(80)	META-ANKOLITE	29-1061
5.570(90)	8.980(80)	7.110(100)	3.550(70)	3.300(70)	WEEKSITE	12- 462
5.540(60)	8.900(100)	3.750(80)	4.420(60)	3.550(60)	METAHEINRICHITE	24- 128
5.570(80)	8.860(100)	3.730(100)	3.300(80)	3.570(70)	METAZEUNERITE	17- 146
5.570(60)	8.850(100)	3.590(90)	3.340(80)	5.100(70)	META-URANOSPINITE	8- 319
5.530(80)	8.650(100)	3.570(100)	3.310(90)	3.000(50)	META-URANOSPINITE	18- 309
5.530(70)	8.590(100)	3.790(90)	3.300(80)	4.350(70)	TROEGERITE	8- 326
5.760(100)	8.090(80)	3.080(80)	3.650(70)	2.860(70)	GRIMSELITE	25- 679
5.830(80)	7.970(100)	3.990(90)	3.130(80)	3.090(80)	RENARDITE	8- 328
5.810(30)	7.910(100)	7.320(90)	3.280(60)	3.560(40)	UO3.H2O UNNAMED	15- 569
5.550(100)	7.740(90)	6.880(80)	3.450(90)	3.230(80)	ROUBAULTITE	25- 318
5.500(100)	7.310(90)	8.760(100)	4.820(80)	2.910(80)	SWARTZITE	4- 111
5.510(40)	7.120(100)	9.180(80)	4.280(80)	3.650(50)	URANOPILITE	8- 443
5.870(50)	6.970(100)	4.210(90)	5.440(60)	2.880(60)	URANOPILITE	8- 131
5.980(90)	3.980(80)	12.000(100)	3.230(80)	3.180(80)	VANURALITE	23- 769
5.550(50)	3.530(100)	11.100(80)	3.590(50)	1.603(40)	KAHLERITE	17- 145
5.880(100)	3.390(30)	3.400(20)	3.490(18)	4.230(12)	STUDTITE	16- 206
5.600(100)	3.350(78)	8.420(100)	16.800(70)	2.791(45)	UMOHOITE,17A	12- 778

5.560(40)	3.300(20)	11.100(100)	5.640(18)	4.590(14)	COCONINOITE	25- 16
5.530(80)	3.190(100)	11.000(90)	3.370(90)	3.060(90)	SEDOVITE	18-1425
5.770(80)	3.170(100)	3.340(90)	1.970(80)	1.860(60)	CLARKEITE	8- 315
5.860(80)	3.160(100)	3.090(100)	2.880(100)	7.960(80)	PHOSPHURANULITE	19- 898
5.500(20)	3.020(100)	2.950(100)	3.090(25)	2.970(20)	AESCHYNITE,HEATED	18- 765
5.540(20)	2.980(100)	3.050(70)	3.130(40)	3.450(20)	NIOBO-AESCHYNITE	29- 311
5.890(60)	2.970(100)	5.420(80)	3.340(60)	5.140(45)	DEMESAEKERITE	18- 692
5.900(60)	2.940(100)	1.710(90)	2.240(80)	1.484(70)	UVANITE	8- 322
5.790(60)	2.940(100)	4.600(70)	1.701(50)	2.210(40)	UVANITE	8- 323
5.970(100)	2.890(40)	3.302(25)	3.226(25)	3.181(25)	MOURITE	24-1359

5.490 - 5.000

5.030(80)	14.620(100)	7.620(100)	3.490(90)	3.590(60)	ARSENURANOSPATHITE	31- 586
5.230(80)	13.000(100)	7.930(100)	5.670(100)	3.680(100)	ANDERSONITE	20-1092
5.490(60)	10.900(100)	3.540(100)	3.220(70)	5.030(40)	NOVACEKITE	17- 147
5.030(40)	10.900(100)	3.540(100)	3.220(70)	5.490(60)	NOVACEKITE	17- 147
5.040(80)	10.700(100)	3.590(90)	3.390(70)	1.930(60)	ZEUNERITE	4- 90
5.170(70)	10.400(100)	3.680(80)	3.400(50)	3.470(40)	PHURALUMITE	33- 38
5.050(80)	10.200(100)	3.580(90)	3.350(50)	6.800(40)	NOVACEKITE	8- 286
5.040(70)	10.000(100)	3.530(100)	3.350(80)	1.600(70)	HEINRICHITE	29- 210
5.020(80)	10.000(100)	3.570(100)	1.588(50)	3.350(40)	NOVACEKITE	17- 148
5.350(50)	9.430(100)	3.474(80)	3.366(60)	2.197(60)	THREADGOLDITE	33- 39
5.480(70)	8.930(100)	3.730(80)	3.230(60)	1.658(50)	META-URANOCIRCITE	17- 758
5.100(70)	8.850(100)	3.590(90)	3.340(80)	5.570(60)	META-URANOSPINITE	8- 319
5.030(60)	8.780(100)	3.570(100)	4.300(60)	3.010(60)	METAKIRCHHEIMERITE	12- 586
5.440(75)	8.710(100)	3.680(100)	3.480(30)	3.230(80)	METATORBERNITE	16- 404
5.390(70)	8.550(100)	3.610(90)	3.210(70)	4.250(60)	META-URANOCIRCITE II	17- 789
5.370(45)	8.470(100)	3.610(85)	2.110(70)	4.230(65)	META-AUTUNITE	12- 423
5.440(70)	8.420(100)	3.630(90)	3.270(80)	3.550(70)	SODIUM URANOSPINITE	8- 446
5.200(50)	8.400(100)	3.000(100)	4.260(60)	2.126(60)	FRANCEVILLITE	21- 381
5.130(60)	8.190(100)	3.010(100)	4.100(80)	4.220(60)	CURIENITE	22- 402
5.110(60)	8.160(100)	2.990(100)	4.070(90)	4.230(70)	UNNAMED-(PB)	15- 496
5.440(60)	6.970(100)	4.210(90)	2.880(60)	5.870(50)	URANOPILITE	8- 131
5.400(90)	6.810(100)	8.680(90)	4.550(60)	3.100(60)	LIEBIGITE	11- 296
5.190(40)	6.510(100)	4.220(80)	3.260(60)	3.050(60)	METATYUYAMUNITE	6- 287
5.250(45)	6.350(100)	3.210(100)	2.620(55)	4.280(50)	IRIGINITE	18-1426
5.420(80)	5.890(60)	2.970(100)	3.340(60)	5.140(45)	DEMESAEKERITE	18- 692
5.060(40)	4.290(100)	2.920(80)	2.090(30)	1.850(80)	VANDENBRANDEITE	4- 340
5.210(80)	3.620(100)	3.410(90)	10.000(80)	4.970(80)	URANOSPINITE	29- 390
5.350(30)	3.600(100)	8.340(80)	4.230(40)	4.270(35)	META-URANOCIRCITE II	25-1468
5.110(50)	3.590(100)	8.550(90)	4.290(60)	2.150(50)	METAKAHLERITE	12- 576
5.090(40)	3.590(100)	8.660(70)	2.980(60)	3.500(30)	METALODEVITE	25-1239
5.190(50)	3.580(45)	10.400(100)	4.960(25)	4.480(20)	AUTUNITE	12- 418
5.000(80)	3.500(100)	9.790(90)	4.480(60)	3.310(60)	SALEEITE	29- 874
5.190(30)	3.470(10)	10.300(100)	3.280(10)	7.600(5)	WYARTITE-(20A)	12- 635
5.080(70)	3.440(25)	7.280(100)	3.660(15)	3.510(12)	SCHOEPITE	13- 407
5.151(85)	3.434(32)	3.406(100)	2.488(27)	2.857(26)	UO2(OH)2 (ALPHA)	25-1116
5.110(100)	3.430(100)	3.450(80)	2.857(60)	2.487(60)	UO3.0.8H2O	10- 309
5.300(45)	3.380(100)	3.320(55)	2.640(40)	2.000(25)	EKANITE	25- 677
5.280(100)	3.310(100)	2.640(100)	7.360(80)	3.380(80)	IRAQITE	29- 995
5.000(100)	3.230(100)	2.110(80)	1.970(80)	2.050(50)	VANURANYLITE	19-1417
5.020(90)	3.200(50)	10.200(100)	2.040(40)	6.620(30)	TYUYAMUNITE	6- 17
5.250(60)	3.160(100)	1.830(80)	3.870(70)	3.470(60)	URANOSPHAERITE	8- 321
5.290(30)	3.130(25)	3.230(100)	6.400(19)	2.974(19)	IRIGINITE	29-1372
5.350(90)	3.100(90)	3.690(100)	4.730(80)	3.170(80)	SCHMITTERITE	25-1001
5.480(25)	2.980(100)	3.020(80)	3.110(35)	2.698(30)	AESCHYNITE	15- 864
5.260(90)	2.970(80)	4.440(100)	2.590(70)	2.030(60)	VANDENBRANDEITE	8- 325
5.140(45)	2.970(100)	5.420(80)	5.890(60)	3.340(60)	DEMESAEKERITE	18- 692
5.100(100)	2.040(100)	10.100(60)	1.462(60)	2.160(50)	URANOCIRCITE	18- 199

4.990 - 4.600

4.930(100)	15.200(100)	7.600(100)	3.500(80)	0.000(0)	URANOSPATHITE	31- 587
4.620(60)	11.100(100)	3.740(80)	3.290(80)	2.938(70)	XIANGJIANGITE	29-1401
4.960(25)	10.400(100)	5.190(50)	3.580(45)	4.480(20)	AUTUNITE	12- 418
4.800(35)	9.100(100)	3.790(50)	4.700(35)	4.550(18)	METAZELLERITE	19- 258
4.700(35)	9.100(100)	3.790(50)	4.800(35)	4.550(18)	METAZELLERITE	19- 258
4.700(50)	9.000(100)	3.133(80)	2.978(40)	1.850(40)	RANUNCULITE	33- 972
4.930(50)	8.920(100)	3.730(65)	3.250(55)	3.490(50)	META-ANKOLITE	19-1008
4.820(80)	8.760(100)	5.500(100)	7.310(90)	2.910(80)	SWARTZITE	4- 111
4.800(80)	8.480(70)	7.260(100)	2.876(70)	14.300(30)	SCHROECKINGERITE	8- 397
4.710(70)	8.240(100)	7.790(80)	4.370(80)	11.300(50)	RABBITTITE	7- 365
4.820(70)	8.180(100)	4.090(90)	2.970(80)	6.100(60)	CUPROSKLODOWSKITE	8- 290
4.740(20)	7.100(100)	3.220(50)	14.100(25)	3.180(25)	UMOHOITE,14A	11- 375
4.700(80)	6.710(100)	2.920(100)	3.490(80)	3.370(80)	SODIUM BOLTWOODITE	29-1044
4.820(90)	6.060(70)	8.160(100)	3.530(70)	3.290(40)	CUPROSKLODOWSKITE	19- 413
4.600(70)	5.790(60)	2.940(100)	1.701(50)	2.210(40)	UVANITE	8- 323
4.850(50)	5.590(35)	9.660(100)	3.650(35)	4.410(25)	ZELLERITE	19- 257
4.620(45)	4.470(40)	9.300(100)	3.340(30)	3.037(30)	HAIWEEITE	13- 118
4.610(100)	4.300(70)	3.230(40)	3.920(30)	2.640(25)	RUTHERFORDINE	11- 263
4.910(80)	3.740(60)	9.820(100)	3.197(60)	3.179(60)	SENGIERITE	8- 398
4.730(80)	3.680(100)	5.350(90)	3.100(90)	3.170(80)	SCHMITTERITE	25-1001
4.970(80)	3.620(100)	3.410(90)	10.000(80)	5.210(80)	URANOSPINITE	29- 390
4.940(90)	3.580(90)	10.300(100)	3.510(80)	6.610(40)	TORBERNITE	8- 360
4.860(90)	3.470(80)	9.690(100)	2.188(60)	4.390(40)	SABUGALITE	5- 107
4.890(100)	3.460(100)	8.590(60)	2.200(60)	4.250(30)	BASSETTITE	7- 288
4.740(95)	3.440(100)	3.350(100)	6.040(35)	3.020(35)	BRANNERITE	12- 477
4.780(100)	3.380(80)	3.120(70)	2.620(70)	2.030(70)	DERRICKSITE	25- 319
4.990(100)	3.070(100)	2.300(90)	2.070(90)	4.590(80)	HAIWEEITE-(MG)	17- 463
4.620(50)	2.960(100)	3.500(80)	2.670(80)	1.630(60)	ALLANITE,HEATED	9- 474

4.650(40)	2.900(100)	1.880(60)	3.500(40)	2.160(40)	COFFINITE-(Y)	17- 460
4.720(85)	2.680(75)	3.550(100)	1.834(65)	2.842(45)	THORITE	11- 419
4.640(95)	2.640(95)	3.480(100)	1.803(70)	2.789(45)	COFFINITE	11- 420
4.969(48)	2.601(23)	3.868(100)	1.927(14)	3.143(12)	UO2(OH)2 (BETA)	24-1160

4.590 - 4.300

4.320(50)	12.600(100)	8.700(100)	9.650(80)	7.100(60)	VOGLITE	33- 274
4.590(14)	11.100(100)	5.560(40)	3.300(20)	5.640(18)	COCONINOITE	25- 16
4.480(20)	10.400(100)	5.190(50)	3.580(45)	4.960(25)	AUTUNITE	12- 418
4.310(50)	10.200(100)	8.620(80)	3.639(40)	2.868(35)	FURONGITE	29- 98
4.390(40)	9.690(100)	4.860(90)	3.470(80)	2.188(60)	SABUGALITE	5- 107
4.410(25)	9.660(100)	4.850(50)	5.590(35)	3.650(35)	ZELLERITE	19- 257
4.470(40)	9.300(100)	4.620(45)	3.340(30)	3.037(30)	HAIWEEITE	13- 118
4.410(50)	9.260(100)	4.530(80)	3.180(40)	7.090(30)	HAIWEEITE	12- 721
4.430(60)	9.160(100)	4.590(70)	3.200(40)	8.070(30)	HAIWEEITE	22- 160
4.550(18)	9.100(100)	3.790(50)	4.700(35)	4.800(35)	METAZELLERITE	19- 258
4.420(60)	8.900(100)	3.750(80)	5.540(60)	3.550(60)	METAHEINRICHITE	24- 128
4.300(60)	8.780(100)	3.570(100)	5.080(60)	3.010(60)	METAKIRCHHEIMERITE	12- 586
4.350(70)	8.590(100)	3.790(90)	3.300(80)	5.500(70)	TROEGERITE	8- 326
4.370(80)	8.240(100)	7.790(80)	4.710(70)	11.300(50)	RABBITTITE	7- 365
4.550(60)	6.810(100)	8.680(90)	5.400(90)	3.100(60)	LIEBIGITE	11- 296
4.480(90)	6.140(80)	3.320(100)	2.690(70)	2.470(60)	SODDYITE	12- 180
4.440(100)	5.260(90)	2.970(80)	2.590(70)	2.030(60)	VANDENBRANDEITE	8- 325
4.590(80)	4.990(100)	3.070(100)	2.300(90)	2.070(90)	HAIWEEITE-(MG)	17- 463
4.590(70)	4.430(60)	9.160(100)	3.200(40)	8.070(30)	HAIWEEITE	22- 160
4.530(80)	4.410(50)	9.260(100)	3.180(40)	7.090(30)	HAIWEEITE	12- 721
4.500(20)	4.160(100)	3.740(60)	3.130(60)	3.500(20)	KOBEITE	11- 259
4.490(100)	3.930(60)	2.990(60)	2.450(60)	11.000(40)	SHARPITE	12- 164
4.480(60)	3.500(100)	9.790(90)	5.000(80)	3.310(60)	SALEEITE	29- 874
4.550(25)	3.450(100)	2.560(50)	1.770(50)	2.150(25)	XENOTIME	11- 254
4.540(25)	3.440(100)	2.560(60)	1.760(45)	2.145(25)	XENOTIME	9- 377
4.410(50)	3.400(100)	2.840(90)	1.740(60)	1.696(50)	HALLIMONDITE	16- 706
4.570(90)	3.380(100)	3.030(100)	1.832(90)	1.160(90)	HAIWEEITE	17- 462
4.300(70)	3.230(40)	4.610(100)	3.920(30)	2.640(25)	RUTHERFORDINE	11- 263
4.390(80)	3.070(100)	3.670(90)	3.153(80)	2.858(80)	RENARDITE	11- 215
4.330(60)	3.020(100)	2.810(80)	2.130(80)	3.380(60)	NINGYOITE	12- 273
4.400(90)	2.830(80)	3.020(100)	2.150(80)	6.070(60)	RHABDOPHANE	12- 277
4.470(85)	2.650(40)	2.940(100)	6.400(35)	3.320(30)	MCKELVEYITE	18- 901

4.290 - 4.100

4.250(60)	8.550(100)	3.610(90)	5.390(70)	3.210(70)	META-URANOCIRCITE II	17- 789
4.290(50)	8.520(100)	3.570(90)	2.140(60)	2.530(50)	METANOVACEKITE	17- 152
4.230(65)	8.470(100)	3.610(85)	2.110(70)	5.370(45)	META-AUTUNITE	12- 423
4.260(60)	8.400(100)	3.000(100)	5.200(60)	2.126(60)	FRANCEVILLITE	21- 381
4.240(60)	8.400(100)	4.180(80)	3.430(80)	3.170(70)	UPALITE	33- 37
4.220(60)	8.190(100)	3.010(100)	4.100(80)	5.130(60)	CURIENITE	22- 402
4.100(80)	8.190(100)	3.010(100)	5.130(60)	4.220(60)	CURIENITE	22- 402
4.140(30)	8.170(100)	4.000(55)	3.510(14)	2.718(14)	META-AUTUNITE	14- 75
4.230(70)	8.160(100)	2.990(100)	4.070(90)	5.110(60)	UNNAMED-(PB)	15- 496
4.100(50)	8.090(100)	3.420(90)	3.180(80)	1.882(40)	JOLIOTITE	29-1378
4.130(90)	7.770(100)	3.250(100)	3.000(100)	6.520(80)	FRITZCHEITE	23-1249
4.280(80)	7.120(100)	9.180(80)	3.650(50)	5.510(40)	URANOPILITE	8- 443
4.250(30)	6.560(100)	3.120(70)	3.530(50)	3.250(30)	CARNOTITE	8- 317
4.220(60)	6.360(100)	3.530(80)	3.210(80)	3.140(60)	CARNOTITE	11- 338
4.290(50)	6.350(100)	3.210(100)	2.620(55)	5.250(45)	IRIGINITE	18-1426
4.230(12)	5.880(100)	3.390(30)	3.400(20)	3.490(18)	STUDTITE	16- 206
4.210(90)	5.440(60)	6.970(100)	2.880(60)	5.870(50)	URANOPILITE	8- 131
4.250(30)	4.890(100)	3.460(100)	8.590(60)	2.200(60)	BASSETTITE	7- 288
4.160(100)	3.740(60)	3.130(60)	4.500(20)	3.500(20)	KOBEITE	11- 259
4.270(35)	3.600(100)	8.340(80)	4.230(40)	5.350(30)	META-URANOCIRCITE II	25-1468
4.230(40)	3.600(100)	8.340(80)	4.270(35)	5.350(30)	META-URANOCIRCITE II	25-1468
4.290(60)	3.590(100)	8.550(90)	5.110(50)	2.150(50)	METAKAHLERITE	12- 576
4.220(20)	3.470(20)	8.460(100)	3.560(10)	3.000(10)	WYARTITE-(17A)	12- 636
4.180(80)	3.430(80)	8.400(100)	3.170(70)	4.240(60)	UPALITE	33- 37
4.230(65)	3.280(100)	3.250(100)	3.410(65)	3.160(45)	PARSONSITE	12- 259
4.190(80)	3.270(70)	8.420(100)	3.520(60)	3.000(60)	SKLODOWSKITE	29- 875
4.220(80)	3.260(60)	6.510(100)	3.050(60)	5.190(40)	METATYUYAMUNITE	6- 287
4.130(100)	3.200(50)	3.150(40)	12.200(30)	6.180(30)	UMOHOITE,12A	12- 693
4.170(90)	3.160(90)	9.920(100)	4.090(80)	3.240(80)	METAVANURALITE	23- 770
4.170(25)	3.090(100)	2.870(70)	3.300(50)	3.510(25)	MONAZITE	11- 556
4.140(75)	3.070(100)	3.260(90)	2.860(90)	3.490(50)	CHERALITE	8- 316
4.270(100)	3.000(85)	2.950(85)	3.480(70)	6.140(55)	DUMONTITE	12- 158
4.290(100)	2.920(80)	5.060(40)	2.090(30)	1.850(80)	VANDENBRANDEITE	4- 340
4.210(60)	2.920(100)	3.060(80)	3.520(60)	3.240(60)	KASOLITE	29- 788
4.120(60)	2.840(100)	3.480(80)	2.810(80)	1.858(80)	BRITHOLITE,HEATED	17- 724
4.160(100)	2.340(100)	3.190(80)	3.340(70)	1.911(50)	WIDENMANNITE	27- 281
4.170(100)	1.310(60)	1.300(60)	3.440(50)	2.580(50)	MOLDRANITE,HEATED	29-1371

4.090 - 3.900

3.980(80)	12.000(100)	5.980(90)	3.230(80)	3.180(80)	VANURALITE	23- 769
4.090(80)	9.920(100)	4.170(90)	3.160(90)	3.240(80)	METAVANURALITE	23- 770
4.070(90)	8.160(100)	2.990(100)	4.230(70)	5.110(60)	UNNAMED-(PB)	15- 496
4.080(60)	7.680(100)	3.950(80)	3.200(50)	8.180(40)	STRELKINITE	27- 822
3.960(70)	6.230(100)	3.140(80)	3.060(50)	3.520(40)	CURITE	14- 267
3.990(90)	5.830(80)	7.970(100)	3.130(80)	3.090(80)	RENARDITE	8- 328
3.920(30)	4.610(100)	4.300(70)	3.230(40)	2.640(25)	RUTHERFORDINE	11- 263
4.000(55)	4.140(30)	8.170(100)	3.510(14)	2.718(14)	META-AUTUNITE	14- 75
3.950(80)	4.080(60)	7.680(100)	3.200(50)	8.180(40)	STRELKINITE	27- 822
3.900(90)	3.510(60)	7.830(100)	3.190(50)	2.590(50)	BETAURANOPHANE	8- 301
4.020(18)	3.280(100)	2.840(78)	2.010(23)	2.788(17)	CLIFFORDITE	24-1209

4.020(100)	3.210(100)	2.510(80)	1.697(40)	1.850(30)	PETSCHECKITE,HEATED	29-1426
4.050(60)	3.200(100)	2.500(90)	1.830(50)	1.710(30)	BETAFITE,HEATED	18-1154
3.940(90)	2.990(80)	7.880(100)	2.910(90)	1.969(70)	URANOPHANE	8- 442
3.930(60)	2.990(60)	4.490(100)	2.450(60)	11.000(40)	SHARPITE	12- 164
4.090(90)	2.970(80)	8.180(100)	4.820(70)	6.100(60)	CUPROSKLODOWSKITE	8- 290
3.990(40)	2.890(100)	2.860(80)	3.160(60)	2.790(60)	BRITHOLITE,(LA)	13- 106
4.010(80)	2.490(40)	3.180(100)	1.838(30)	1.692(20)	LIANORATITE,HEATED	29-1435
3.990(60)	1.997(60)	7.930(80)	2.140(50)	3.580(40)	URANOPHANE-(BA)	-

3.890 - 3.750

3.870(20)	10.700(100)	2.950(50)	3.490(40)	2.620(30)	RAUVITE	8- 288
3.850(100)	8.410(80)	7.720(100)	3.130(80)	3.420(70)	ARSENURANYLITE	14- 268
3.890(60)	7.810(100)	3.760(70)	3.290(40)	2.150(40)	UNNAMED-(GA)	15- 609
3.890(60)	7.800(100)	3.210(80)	8.300(50)	1.990(50)	CALCURMOLITE	16- 145
3.870(70)	7.730(100)	6.160(90)	3.410(80)	3.130(70)	JOHANNITE	17- 530
3.830(60)	7.660(100)	13.100(90)	2.690(50)	2.210(50)	BAYLEYITE	4- 130
3.750(80)	5.540(60)	8.900(100)	4.420(60)	3.550(60)	METAHEINRICHITE	24- 128
3.868(100)	4.969(48)	2.601(23)	1.927(14)	3.143(12)	UO2(OH)2 (BETA)	24-1160
3.790(50)	4.700(35)	9.100(100)	4.800(35)	4.550(18)	METAZELLERITE	19- 258
3.760(70)	3.890(60)	7.810(100)	3.290(40)	2.150(40)	UNNAMED-(GA)	15- 609
3.830(85)	3.340(80)	9.100(100)	3.590(75)	5.640(70)	ABERNATHYITE	16- 386
3.790(90)	3.300(80)	8.590(100)	5.500(70)	4.350(70)	TROEGERITE	8- 326
3.780(100)	3.270(90)	9.090(100)	3.510(80)	5.530(70)	META-ANKOLITE	29-1061
3.800(100)	3.260(90)	9.020(100)	2.760(80)	2.160(80)	URAMPHITE	29- 121
3.810(80)	3.240(80)	7.630(100)	3.590(60)	3.350(60)	IANTHINITE	12- 272
3.760(50)	3.180(100)	7.530(80)	3.500(70)	2.039(50)	BILLIETITE	29- 208
3.870(70)	3.160(100)	1.830(80)	5.250(60)	3.470(60)	URANOSPHAERITE	8- 321
3.880(100)	3.080(100)	7.780(100)	2.976(80)	3.440(60)	BERGENITE	20- 154
3.870(70)	2.570(70)	1.795(100)	2.481(70)	1.708(70)	UO2(OH)2 (BETA)	9- 239

3.740 - 3.600

3.680(100)	13.000(100)	7.930(100)	5.670(100)	5.230(80)	ANDERSONITE	20-1092
3.639(40)	10.200(100)	8.620(80)	4.310(50)	2.868(35)	FURONGITE	29- 98
3.740(60)	9.820(100)	4.910(80)	3.197(60)	3.179(60)	SENGIERITE	8- 398
3.650(35)	9.660(100)	4.850(50)	5.590(35)	4.410(25)	ZELLERITE	19- 257
3.610(100)	9.080(90)	1.620(60)	1.530(60)	9.490(50)	PRZHEVALSKITE	29- 787
3.600(100)	8.340(80)	4.230(40)	4.270(35)	5.350(30)	META-URANOCIRCITE II	25-1468
3.740(35)	7.490(100)	3.210(80)	3.550(40)	3.160(30)	BECQUERELITE	29- 389
3.730(40)	7.480(100)	3.550(80)	3.200(80)	3.140(60)	BECQUERELITE	12- 176
3.730(30)	7.440(100)	3.200(35)	3.540(20)	2.566(10)	BECQUERELITE	13- 405
3.700(60)	7.400(100)	3.530(80)	3.190(80)	3.580(60)	COMPREIGNACITE	17- 167
3.700(80)	7.370(100)	3.220(100)	3.610(80)	3.160(80)	UO2(OH)2	28-1415
3.610(80)	7.370(100)	3.220(100)	3.700(80)	3.160(80)	UO2(OH)2	28-1415
3.670(25)	7.350(100)	3.220(50)	3.590(40)	3.160(30)	UO3.2H2O (BETA)	18-1436
3.660(15)	7.280(100)	5.080(70)	3.440(25)	3.510(12)	SCHOEPITE	13- 407
3.650(50)	7.120(100)	9.180(80)	4.280(80)	5.510(40)	URANOPILITE	8- 443
3.650(70)	5.760(100)	8.090(80)	3.080(80)	2.860(70)	GRIMSELITE	25- 679
3.730(100)	5.570(80)	8.860(100)	3.300(80)	3.570(70)	METAZEUNERITE	17- 146
3.730(80)	5.480(70)	8.930(100)	3.230(60)	1.658(50)	META-URANOCIRCITE	17- 758
3.610(90)	5.390(70)	8.550(100)	3.210(70)	4.250(60)	META-URANOCIRCITE II	17- 789
3.680(100)	5.350(90)	3.100(90)	4.730(80)	3.170(80)	SCHMITTERITE	25-1001
3.670(90)	4.390(80)	3.070(100)	3.150(80)	2.858(80)	RENARDITE	11- 215
3.660(55)	3.490(45)	7.340(100)	3.150(35)	2.858(15)	SODIUM-ZIPPEITE	29-1285
3.680(100)	3.480(80)	8.710(100)	3.230(80)	5.440(75)	METATORBERNITE	16- 404
3.620(100)	3.410(90)	10.000(80)	5.210(80)	4.970(80)	URANOSPINITE	29- 390
3.600(70)	3.344(70)	6.965(100)	3.489(70)	3.231(50)	MARGARITASITE	-
3.740(80)	3.290(80)	11.100(100)	2.938(70)	4.620(60)	XIANGJIANGITE	29-1401
3.630(90)	3.270(80)	8.420(100)	5.440(70)	3.550(70)	SODIUM URANOSPINITE	8- 446
3.730(65)	3.250(55)	8.920(100)	4.930(50)	3.490(50)	META-ANKOLITE	19-1008
3.660(50)	3.240(10)	7.350(100)	2.446(10)	3.210(4)	SCHOEPITE	13- 241
3.610(100)	3.170(75)	7.250(100)	1.985(40)	3.530(25)	VANOENDRIESSCHEITE	13- 117
3.740(60)	3.130(60)	4.160(100)	4.500(20)	3.500(20)	KOBEITE	11- 259
3.680(30)	3.070(100)	2.920(100)	2.590(40)	1.840(40)	SAMARSKITE,HEATED	4- 617
3.660(30)	2.980(100)	1.820(40)	1.720(40)	2.430(30)	EUXENITE,HEATED	5- 603
3.650(40)	2.950(40)	2.990(100)	2.600(30)	1.830(30)	EUXENITE,HEATED	9- 442
3.670(30)	2.910(100)	2.990(75)	1.574(30)	1.505(30)	AESCHYNITE	20-1401
3.670(100)	2.680(80)	1.570(80)	1.540(80)	3.230(70)	SODIUM META-AUTUNITE	29-1283
3.650(50)	2.540(30)	2.950(100)	2.510(30)	2.380(30)	ASHANITE	33- 660
3.610(85)	2.110(70)	8.470(100)	4.230(65)	5.370(45)	META-AUTUNITE	12- 423
3.660(90)	1.600(90)	8.530(100)	1.530(80)	9.250(70)	TROEGERITE-(P)	26- 887

3.590 - 3.500

3.500(80)	15.200(100)	7.600(100)	4.930(100)	0.000(0)	URANOSPATHITE	31- 587
3.590(60)	14.620(100)	7.620(100)	3.490(90)	5.030(80)	ARSENURANOSPATHITE	31- 586
3.530(100)	11.100(80)	5.550(50)	3.590(50)	1.603(40)	KAHLERITE	17- 145
3.580(45)	10.400(100)	5.190(50)	4.960(25)	4.480(20)	AUTUNITE	12- 418
3.580(90)	10.300(100)	4.940(90)	3.510(80)	6.610(40)	TORBERNITE	8- 360
3.510(80)	10.300(100)	4.940(90)	3.580(90)	6.610(40)	TORBERNITE	8- 360
3.500(100)	9.790(90)	5.000(80)	4.480(60)	3.310(60)	SALEEITE	29- 874
3.540(50)	9.620(35)	7.080(100)	3.440(35)	3.100(25)	ZINC-ZIPPEITE	29-1395
3.590(75)	9.100(100)	3.830(85)	3.340(80)	5.640(70)	ABERNATHYITE	16- 386
3.510(80)	9.090(100)	3.780(100)	3.270(90)	5.530(70)	META-ANKOLITE	29-1061
3.550(60)	8.900(100)	3.750(80)	5.540(60)	4.420(60)	METAHEINRICHITE	24- 128
3.570(70)	8.860(100)	3.730(100)	5.570(80)	3.300(80)	METAZEUNERITE	17- 146
3.590(100)	8.660(70)	2.980(50)	5.090(40)	3.500(30)	METALODEVITE	25-1239
3.590(100)	8.550(90)	4.290(60)	5.110(50)	2.150(50)	METAKAHLERITE	12- 576
3.560(10)	8.460(100)	4.220(20)	3.470(20)	3.000(10)	WYARTITE-(17A)	12- 636
3.550(70)	8.420(100)	3.630(90)	3.270(80)	5.440(70)	SODIUM URANOSPINITE	8- 446
3.520(60)	8.420(100)	4.190(80)	3.270(70)	3.000(60)	SKLODOWSKITE	29- 875

3.550(80)	8.390(100)	7.290(100)	6.680(60)	3.040(60)	GUILLEMINITE	18- 582
3.500(80)	8.230(100)	3.090(100)	3.220(90)	2.900(90)	MARTHOZITE	25- 320
3.510(14)	8.170(100)	4.000(55)	4.140(30)	2.718(14)	META-AUTUNITE	14- 75
3.530(70)	8.160(100)	4.820(90)	6.060(70)	3.290(40)	CUPROSKLODOWSKITE	19- 413
3.580(40)	7.930(80)	3.990(60)	1.997(60)	2.140(50)	URANOPHANE-(BA)	-
3.560(40)	7.910(100)	7.320(90)	3.280(60)	5.810(30)	UO3.H2O UNNAMED	15- 569
3.510(60)	7.830(100)	3.900(90)	3.190(50)	2.590(50)	BETAURANOPHANE	8- 301
3.590(60)	7.630(100)	3.810(80)	3.240(80)	3.350(60)	IANTHINITE	12- 272
3.550(40)	7.490(100)	3.210(80)	3.740(35)	3.160(30)	BECQUERELITE	29- 389
3.540(20)	7.440(100)	3.200(35)	3.730(30)	2.566(10)	BECQUERELITE	13- 405
3.580(60)	7.400(100)	3.530(80)	3.190(80)	3.700(60)	COMPREIGNACITE	17- 167
3.520(60)	7.370(100)	3.590(100)	3.240(80)	3.170(50)	SCHOEPITE	29-1376
3.590(40)	7.350(100)	3.220(50)	3.160(30)	3.670(25)	UO3.2H2O (BETA)	18-1436
3.510(12)	7.280(100)	5.080(70)	3.440(25)	3.660(15)	SCHOEPITE	13- 407
3.530(25)	7.250(100)	3.610(100)	3.170(75)	1.985(40)	VANDENORIESSCHEITE	13- 117
3.580(100)	7.200(80)	3.480(80)	3.110(60)	2.740(30)	MAGNESIUM-ZIPPEITE	29- 876
3.550(18)	7.200(100)	3.580(50)	3.180(50)	3.140(12)	FOURMARIERITE	13- 116
3.570(90)	7.120(100)	3.500(100)	3.140(100)	3.120(100)	RAMEAUITE	25- 631
3.550(70)	7.110(100)	5.570(90)	8.980(80)	3.300(70)	WEEKSITE	12- 462
3.560(35)	7.080(100)	3.520(70)	3.120(50)	3.480(20)	MASUYITE	13- 408
3.520(80)	7.080(100)	3.130(100)	3.490(90)	3.153(90)	AGRINIERITE	25- 630
3.530(50)	6.560(100)	3.120(70)	4.250(30)	3.250(30)	CARNOTITE	8- 317
3.520(40)	6.230(100)	3.140(80)	3.960(70)	3.060(50)	CURITE	14- 267
3.540(70)	6.010(100)	3.400(90)	2.910(70)	1.908(60)	BOLTWOODITE	29-1026
3.570(100)	5.080(60)	8.780(100)	4.300(60)	3.010(60)	METAKIRCHHEIMERITE	12- 586
3.580(90)	5.060(80)	10.200(100)	3.350(50)	6.800(40)	NOVACEKITE	8- 286
3.590(90)	5.040(80)	10.700(100)	3.390(70)	1.930(60)	ZEUNERITE	4- 90
3.570(100)	5.020(80)	10.000(100)	1.588(50)	3.350(40)	NOVACEKITE	17- 148
3.550(100)	4.720(85)	2.680(75)	1.834(65)	2.842(45)	THORITE	11- 419
3.500(20)	4.160(100)	3.740(60)	3.130(60)	4.500(20)	KOBEITE	11- 259
3.500(30)	3.590(100)	8.660(70)	2.980(60)	5.090(40)	METALOOEVITE	25-1239
3.590(50)	3.530(100)	11.100(80)	5.550(50)	1.603(40)	KAHLERITE	17- 145
3.560(100)	3.480(100)	7.140(90)	3.130(90)	2.620(80)	RICHETITE	25- 467
3.560(40)	3.450(100)	7.100(95)	3.100(65)	9.630(35)	NICKEL-ZIPPEITE	29- 944
3.530(100)	3.350(80)	10.000(100)	5.090(70)	1.600(70)	HEINRICHITE	29- 210
3.590(90)	3.340(80)	8.850(100)	5.100(70)	5.570(60)	META-URANOSPINITE	8- 319
3.570(100)	3.310(90)	8.650(100)	5.530(80)	3.000(50)	META-URANOSPINITE	18- 309
3.590(100)	3.240(80)	7.370(100)	3.520(60)	3.170(50)	SCHOEPITE	29-1376
3.540(100)	3.220(70)	10.900(100)	5.490(60)	5.030(40)	NOVACEKITE	17- 147
3.530(80)	3.210(80)	6.360(100)	4.220(60)	3.140(60)	CARNOTITE	11- 338
3.550(80)	3.200(80)	7.480(100)	3.140(60)	3.730(40)	BECQUERELITE	12- 176
3.530(80)	3.190(80)	7.400(100)	3.700(60)	3.580(60)	COMPREIGNACITE	17- 167
3.580(50)	3.180(50)	7.200(100)	3.550(18)	3.140(12)	FOURMARIERITE	13- 116
3.500(70)	3.180(100)	7.530(80)	3.760(50)	2.039(50)	BILLIETITE	29- 208
3.500(100)	3.140(100)	7.120(100)	3.120(100)	3.570(90)	RAMEAUITE	25- 631
3.590(45)	3.120(30)	7.210(100)	3.470(20)	1.963(12)	COBALT-ZIPPEITE	29- 520
3.590(45)	3.120(30)	7.210(100)	1.963(12)	2.491(11)	NICKEL-ZIPPEITE	29-1434
3.520(70)	3.120(50)	7.080(100)	3.560(35)	3.480(20)	MASUYITE	13- 408
3.500(90)	3.120(80)	7.060(100)	2.870(40)	2.650(40)	ZIPPEITE	29-1062
3.510(25)	3.090(100)	2.870(70)	3.300(50)	4.170(25)	MONAZITE	11- 556
3.510(40)	3.090(100)	3.470(80)	6.390(80)	3.130(60)	WOLSENDORFITE	12- 159
3.530(45)	2.920(100)	2.710(65)	2.627(40)	2.182(35)	ALLANITE	25- 169
3.520(60)	2.920(100)	3.060(80)	4.210(60)	3.240(60)	KASOLITE	29- 788
3.530(40)	2.900(100)	1.880(60)	4.650(40)	2.160(40)	COFFINITE-(Y)	17- 460
3.500(80)	2.670(80)	2.960(100)	1.630(60)	4.620(50)	ALLANITE,HEATED	9- 474
3.570(90)	2.140(60)	8.520(100)	4.290(50)	2.530(50)	METANOVACEKITE	17- 152
3.590(100)	1.610(70)	8.860(100)	2.540(60)	2.280(60)	METAKAHLERITE	17- 151

3.490 - 3.400

3.490(90)	14.620(100)	7.620(100)	5.030(80)	3.590(60)	ARSENURANOSPATHITE	31- 586
3.490(40)	10.700(100)	2.950(50)	2.620(30)	3.870(20)	RAUVITE	8- 288
3.470(40)	10.400(100)	3.080(80)	5.170(70)	3.400(50)	PHURALUMITE	33- 38
3.400(50)	10.400(100)	3.080(80)	5.170(70)	3.470(40)	PHURALUMITE	33- 38
3.470(10)	10.300(100)	5.190(30)	3.280(10)	7.600(5)	WYARTITE-(20A)	12- 635
3.410(90)	10.000(80)	3.620(100)	5.210(80)	4.970(80)	URANOSPINITE	29- 390
3.470(80)	9.690(100)	4.860(90)	2.188(60)	4.390(40)	SABUGALITE	5- 107
3.490(50)	8.920(100)	3.730(65)	3.250(55)	4.930(50)	META-ANKOLITE	19-1008
3.480(80)	8.710(100)	3.680(100)	3.230(80)	5.440(75)	METATORBERNITE	16- 404
3.460(100)	8.590(60)	4.890(100)	2.200(60)	4.250(30)	BASSETTITE	7- 288
3.470(20)	8.460(100)	4.220(20)	3.560(10)	3.000(10)	WYARTITE-(17A)	12- 636
3.430(80)	8.400(100)	4.180(80)	3.170(70)	4.240(60)	UPALITE	33- 37
3.440(60)	7.780(100)	3.880(100)	3.080(100)	2.976(80)	BERGENITE	20- 154
3.410(80)	7.730(100)	6.160(90)	3.870(70)	3.130(70)	JOHANNITE	17- 530
3.420(70)	7.720(100)	3.850(100)	8.410(80)	3.130(80)	ARSENURANYLITE	14- 268
3.490(45)	7.340(100)	3.660(55)	3.150(35)	2.858(15)	SODIUM-ZIPPEITE	29-1285
3.440(25)	7.280(100)	5.080(70)	3.660(15)	3.510(12)	SCHOEPITE	13- 407
3.470(20)	7.210(100)	3.590(45)	3.120(30)	1.963(12)	COBALT-ZIPPEITE	29- 520
3.480(100)	7.140(90)	3.560(100)	3.130(90)	2.620(80)	RICHETITE	25- 467
3.450(100)	7.100(95)	3.100(65)	3.560(40)	9.630(35)	NICKEL-ZIPPEITE	29- 944
3.490(90)	7.080(100)	3.130(100)	3.153(90)	3.520(80)	AGRINIERITE	25- 630
3.480(20)	7.080(100)	3.520(70)	3.120(50)	3.560(35)	MASUYITE	13- 408
3.440(35)	7.080(100)	3.540(50)	9.620(35)	3.100(25)	ZINC-ZIPPEITE	29-1395
3.489(70)	6.965(100)	3.600(70)	3.344(70)	3.231(50)	MARGARITASITE	-
3.490(80)	6.710(100)	2.920(100)	4.700(80)	3.370(80)	SODIUM BOLTWOODITE	29-1044
3.470(80)	6.390(80)	3.090(100)	3.130(60)	3.510(40)	WOLSENDORFITE	12- 159
3.490(18)	5.880(100)	3.390(30)	3.400(20)	4.230(12)	STUDTITE	16- 206
3.400(20)	5.880(100)	3.390(30)	3.490(18)	4.230(12)	STUDTITE	16- 206
3.450(80)	5.550(100)	7.740(90)	6.880(80)	3.230(80)	ROUBAULTITE	25- 318
3.406(100)	5.151(85)	3.434(32)	2.488(27)	2.857(26)	UO2(OH)2 (ALPHA)	25-1116
3.450(80)	5.110(100)	3.430(100)	2.857(60)	2.487(60)	UO3.0.8H2O	10- 309
3.480(100)	4.640(95)	2.640(95)	1.803(70)	2.789(45)	COFFINITE	11- 420
3.480(70)	4.270(100)	3.000(85)	2.950(85)	6.140(55)	DUMONTITE	12- 158

3.440(50)	4.170(100)	1.310(60)	1.300(60)	2.580(50)	MOLURANITE,HEATED	29-1371
3.490(80)	3.580(100)	7.200(80)	3.110(60)	2.740(30)	MAGNESIUM-ZIPPEITE	29- 876
3.490(90)	3.540(70)	6.010(100)	2.910(70)	1.908(60)	BOLTWOODOITE	29-1026
3.430(100)	3.450(80)	5.110(100)	2.857(60)	2.487(60)	UO3.0.8H2O	10- 309
3.434(32)	3.406(100)	5.151(85)	2.488(27)	2.857(26)	UO2(OH)2 (ALPHA)	25-1116
3.474(80)	3.366(60)	9.430(100)	2.197(60)	5.350(50)	THREADGOLDITE	33- 39
3.440(100)	3.350(100)	4.740(95)	6.040(35)	3.020(35)	BRANNERITE	12- 477
3.410(65)	3.280(100)	3.250(100)	4.230(65)	3.160(45)	PARSONSITE	12- 259
3.420(90)	3.180(80)	8.090(100)	4.100(50)	1.882(40)	JOLIOTITE	29-1378
3.470(60)	3.160(100)	1.830(80)	3.870(70)	5.250(60)	URANOSPHAERITE	8- 321
3.480(90)	3.130(90)	7.020(100)	1.960(60)	1.750(50)	ZIPPEITE	8- 138
3.430(50)	3.090(90)	1.680(60)	1.280(60)	1.990(40)	METACALCIOURANOITE	25-1451
3.490(50)	3.070(100)	3.260(90)	2.860(90)	4.140(75)	CHERALITE	8- 316
3.490(90)	3.000(80)	3.160(100)	3.088(70)	3.385(60)	MOCTEZUMITE	18- 707
3.450(20)	2.980(100)	3.050(70)	3.130(40)	5.540(20)	NIOBO-AESCHYNITE	29- 311
3.420(70)	2.850(60)	2.900(100)	3.070(50)	2.248(50)	DAVIDITE,HEATED	13- 505
3.400(100)	2.840(90)	1.740(60)	4.410(50)	1.696(50)	HALLIMONDITE	16- 706
3.480(80)	2.810(80)	2.840(100)	1.858(80)	4.120(60)	BRITHOLITE,HEATED	17- 724
3.450(100)	2.560(50)	1.770(50)	4.550(25)	2.150(25)	XENOTIME	11- 254
3.440(100)	2.560(60)	1.760(45)	4.540(25)	2.145(25)	XENOTIME	9- 377
3.410(70)	1.980(60)	3.090(100)	1.948(60)	1.908(60)	BAURANOITE	25-1469
3.420(100)	1.903(80)	2.460(70)	2.276(70)	3.320(60)	BRANNERITE,HEATED	8- 2
3.460(75)	1.730(40)	3.090(100)	6.910(35)	1.913(80)	WOLSENDORFITE	29- 786
3.450(50)	1.680(100)	3.220(80)	2.480(60)	1.042(60)	DAVIDITE,HEATED	8- 305

3.390 - 3.320

3.390(70)	10.700(100)	3.590(90)	5.640(80)	1.930(60)	ZEUNERITE	4- 90
3.350(50)	10.200(100)	3.580(90)	5.060(80)	6.800(40)	NOVACEKITE	8- 286
3.350(80)	10.000(100)	3.530(100)	5.090(70)	1.600(70)	HEINRICHITE	29- 210
3.350(40)	10.000(100)	3.570(100)	5.020(80)	1.588(50)	NOVACEKITE	17- 148
3.366(60)	9.430(100)	3.474(80)	2.197(60)	5.350(50)	THREADGOLDITE	33- 39
3.340(30)	9.300(100)	4.620(45)	4.470(40)	3.037(30)	HAIWEEITE	13- 118
3.340(80)	9.100(100)	3.830(85)	3.590(75)	5.640(70)	ABERNATHYITE	16- 386
3.340(80)	8.850(100)	3.590(90)	5.100(70)	5.570(60)	META-URANOSPINITE	8- 319
3.350(78)	8.420(100)	5.600(100)	16.800(70)	2.791(45)	UMOHOITE,17A	12- 778
3.390(50)	8.050(100)	3.100(80)	3.090(80)	2.878(70)	PHURCALITE	29- 391
3.350(60)	7.630(100)	3.810(80)	3.240(80)	3.590(60)	IANTHINITE	12- 272
3.344(70)	6.965(100)	3.600(70)	3.489(70)	3.231(50)	MARGARITASITE	-
3.370(80)	6.710(100)	2.920(100)	4.700(80)	3.490(80)	SODIUM BOLTWOODOITE	29-1044
3.340(90)	5.770(80)	3.170(100)	1.970(80)	1.860(60)	CLARKEITE	8- 315
3.320(55)	5.300(45)	3.380(100)	2.640(40)	2.000(25)	EKANITE	25- 677
3.380(80)	5.280(100)	3.310(100)	2.640(100)	7.360(80)	IRAQITE	29- 995
3.350(100)	4.740(95)	3.440(100)	6.040(35)	3.020(35)	BRANNERITE	12- 477
3.320(100)	4.480(90)	6.140(80)	2.690(70)	2.470(60)	SODDYITE	12- 180
3.340(70)	4.160(100)	2.340(100)	3.190(80)	1.911(50)	WIDENMANNITE	27- 281
3.320(60)	3.420(100)	1.903(80)	2.460(70)	2.276(70)	BRANNERITE,HEATED	8- 2
3.390(30)	3.400(20)	5.880(100)	3.490(18)	4.230(12)	STUDTITE	16- 206
3.380(100)	3.320(55)	5.300(45)	2.640(40)	2.000(25)	EKANITE	25- 677
3.380(60)	3.290(100)	1.700(80)	1.999(60)	2.980(50)	UMBOZERITE,HEATED	26-1384
3.370(90)	3.190(100)	11.000(90)	3.060(90)	5.530(80)	SEDOVITE	18-1425
3.385(60)	3.160(100)	3.490(90)	3.000(80)	3.038(70)	MOCTEZUMITE	18- 707
3.380(80)	3.120(70)	4.780(100)	2.620(70)	2.030(70)	DERRICKSITE	25- 319
3.380(100)	3.030(100)	4.570(90)	1.832(90)	1.160(90)	HAIWEEITE	17- 462
3.380(60)	3.020(100)	2.810(80)	2.130(80)	4.330(60)	NINGYOITE	12- 273
3.340(60)	2.970(100)	5.420(80)	5.890(60)	5.140(45)	DEMESAEKERITE	18- 692
3.320(30)	2.940(100)	4.470(85)	2.650(40)	6.400(35)	MCKELVEYITE	18- 901

3.310 - 3.250

3.300(20)	11.100(100)	5.560(40)	5.640(18)	4.590(14)	COCONINOITE	25- 16
3.290(80)	11.100(100)	3.740(80)	2.938(70)	4.620(60)	XIANGJIANGITE	29-1401
3.280(10)	10.300(100)	5.190(30)	3.470(10)	7.600(5)	WYARTITE-(20A)	12- 635
3.270(90)	9.090(100)	3.780(100)	3.510(80)	5.530(70)	META-ANKOLITE	29-1061
3.260(90)	9.020(100)	3.800(100)	2.760(80)	2.160(80)	URAMPHITE	29- 121
3.250(55)	8.920(100)	3.730(65)	4.930(50)	3.490(50)	META-ANKOLITE	19-1008
3.300(80)	8.860(100)	3.730(100)	5.570(80)	3.570(70)	METAZEUNERITE	17- 146
3.310(90)	8.650(100)	3.570(100)	5.530(80)	3.000(50)	META-URANOSPINITE	18- 309
3.300(80)	8.590(100)	3.790(90)	5.500(70)	4.350(70)	TROEGERITE	8- 326
3.270(70)	8.420(100)	4.190(80)	3.520(60)	3.000(60)	SKLODOWSKITE	29- 875
3.270(80)	8.420(100)	3.630(90)	5.440(70)	3.550(70)	SODIUM URANOSPINITE	8- 446
3.290(40)	8.160(100)	4.820(90)	6.060(70)	3.530(70)	CUPROSKLODOWSKITE	19- 413
3.280(60)	7.910(100)	7.320(90)	3.560(40)	5.810(30)	UO3.H2O UNNAMED	15- 569
3.290(40)	7.810(100)	3.760(70)	3.890(60)	2.150(40)	UNNAMED-(GA)	15- 609
3.300(70)	7.110(100)	5.570(90)	8.980(80)	3.550(70)	WEEKSITE	12- 462
3.250(30)	6.560(100)	3.120(70)	3.530(50)	4.250(30)	CARNOTITE	8- 317
3.260(60)	6.510(100)	4.220(80)	3.050(60)	5.190(40)	METATYUYAMUNITE	6- 287
3.302(25)	5.970(100)	2.890(40)	3.226(25)	3.181(25)	MOURITE	24-1359
3.250(100)	4.230(65)	3.280(100)	3.410(65)	3.160(45)	PARSONSITE	12- 259
3.310(60)	3.500(100)	9.790(90)	5.000(80)	4.480(60)	SALEEITE	29- 874
3.280(100)	3.250(100)	4.230(65)	3.410(65)	3.160(45)	PARSONSITE	12- 259
3.300(50)	3.090(100)	2.870(70)	4.170(25)	3.510(25)	MONAZITE	11- 556
3.250(50)	3.050(50)	3.110(100)	9.900(40)	2.720(40)	WALPURGITE	8- 324
3.250(100)	3.000(100)	7.770(100)	4.130(90)	6.520(80)	FRITZCHEITE	23-1249
3.260(90)	2.860(90)	3.070(100)	4.140(75)	3.490(50)	CHERALITE	8- 316
3.280(100)	2.840(78)	2.010(23)	4.020(18)	2.788(17)	CLIFFORDITE	24-1209
3.270(100)	2.840(80)	2.010(80)	2.755(70)	1.712(70)	CLIFFORDITE	25- 999
3.310(100)	2.640(100)	5.280(100)	7.360(80)	3.380(80)	IRAQITE	29- 995
3.250(100)	1.920(90)	6.200(100)	2.950(30)	2.190(80)	PSEUDO-AUTUNITE	18-1084
3.290(100)	1.700(80)	3.380(60)	1.999(60)	2.980(50)	UMBOZERITE,HEATED	26-1384

3.240 - 3.200

3.220(50)	14.100(25)	7.100(100)	3.180(25)	4.740(20)	UMOHOITE,14A	11- 375
3.230(80)	12.000(100)	5.980(90)	3.980(80)	3.180(80)	VANURALITE	23- 769
3.220(70)	10.900(100)	3.540(100)	5.490(60)	5.030(40)	NOVACEKITE	17- 147
3.200(50)	10.200(100)	5.020(90)	2.040(40)	6.620(30)	TYUYAMUNITE	6- 17
3.240(80)	9.920(100)	4.170(90)	3.160(90)	4.090(80)	METAVANURALITE	23- 770
3.200(40)	9.160(100)	4.590(70)	4.430(60)	8.070(30)	HAIWEEITE	22- 160
3.230(60)	8.930(100)	3.730(80)	5.480(70)	1.658(50)	META-URANOCIRCITE	17- 758
3.230(80)	8.710(100)	3.680(100)	3.480(80)	5.440(75)	METATORBERNITE	16- 404
3.210(70)	8.550(100)	3.610(90)	5.390(70)	4.250(60)	META-URANOCIRCITE II	17- 789
3.220(90)	8.230(100)	3.090(100)	2.900(90)	3.500(80)	MARTHOZITE	25- 320
3.200(50)	7.680(100)	3.950(80)	4.080(60)	8.180(40)	STRELKINITE	27- 822
3.240(80)	7.630(100)	3.810(80)	3.590(60)	3.350(60)	IANTHINITE	12- 272
3.200(80)	7.480(100)	3.550(80)	3.140(60)	3.730(40)	BECQUERELITE	12- 176
3.240(80)	7.370(100)	3.590(100)	3.520(60)	3.170(50)	SCHOEPITE	29-1376
3.240(10)	7.350(100)	3.660(50)	2.446(10)	3.210(4)	SCHOEPITE	13- 241
3.210(4)	7.350(100)	3.660(50)	3.240(10)	2.446(10)	SCHOEPITE	13- 241
3.231(50)	6.965(100)	3.600(70)	3.344(70)	3.489(70)	MARGARITASITE	-
3.210(80)	6.360(100)	3.530(80)	4.220(60)	3.140(60)	CARNOTITE	11- 338
3.226(25)	5.970(100)	2.890(40)	3.302(25)	3.181(25)	MOURITE	24-1359
3.230(80)	5.550(100)	7.740(90)	6.880(80)	3.450(80)	ROUBAULTITE	25- 318
3.230(100)	5.290(30)	3.130(25)	6.400(19)	2.974(19)	IRIGINITE	29-1372
3.230(40)	4.610(100)	4.300(70)	3.920(30)	2.640(25)	RUTHERFORDINE	11- 263
3.210(80)	3.890(60)	7.800(100)	8.300(50)	1.990(50)	CALCURMOLITE	16- 145
3.200(35)	3.730(30)	7.440(100)	3.540(20)	2.566(10)	BECQUERELITE	13- 405
3.220(100)	3.700(80)	7.370(100)	3.610(80)	3.160(80)	UO2(OH)2	28-1415
3.230(70)	3.670(100)	2.680(80)	1.570(80)	1.540(80)	SODIUM META-AUTUNITE	29-1283
3.220(50)	3.590(40)	7.350(100)	3.160(30)	3.670(25)	UO3.2H2O (BETA)	18-1436
3.210(80)	3.550(40)	7.490(100)	3.740(35)	3.160(30)	BECQUERELITE	29- 389
3.200(50)	3.150(40)	4.130(100)	12.200(30)	6.180(30)	UMOHOITE,12A	12- 693
3.240(100)	3.060(100)	1.970(100)	1.910(80)	1.706(80)	FERGUSONITE,BETA-(CE)	29- 402
3.230(30)	2.980(100)	2.920(90)	3.130(40)	1.561(30)	SAMARSKITE,HEATED	10- 398
3.240(60)	2.920(100)	3.060(80)	4.210(60)	3.520(60)	KASOLITE	29- 788
3.210(100)	2.620(55)	6.350(100)	4.280(50)	5.250(45)	IRIGINITE	18-1426
3.210(100)	2.510(80)	4.020(100)	1.697(40)	1.850(30)	PETSCHECKITE,HEATED	29-1426
3.200(100)	2.500(80)	4.050(60)	1.830(50)	1.710(30)	BETAFITE,HEATED	18-1154
3.220(80)	2.480(60)	1.680(100)	1.042(60)	3.450(50)	DAVIDITE,HEATED	8- 305
3.230(100)	2.110(80)	5.300(100)	1.970(80)	2.050(50)	VANURANYLITE	19-1417
3.210(100)	1.970(100)	1.650(100)	1.120(80)	1.044(80)	CALCIOURANOITE,HEATED	26-1003
3.230(100)	1.690(64)	1.980(58)	2.800(35)	1.284(26)	THORIANITE	4- 556

3.190 - 3.150

3.180(80)	12.000(100)	5.980(90)	3.980(80)	3.230(80)	VANURALITE	23- 769
3.190(100)	11.000(90)	3.370(90)	3.060(90)	5.530(80)	SEDOVITE	18-1425
3.160(90)	9.920(100)	4.170(90)	4.090(80)	3.240(80)	METAVANURALITE	23- 770
3.197(60)	9.820(100)	4.910(80)	3.740(60)	3.179(60)	SENGIERITE	8- 398
3.179(60)	9.820(100)	4.910(80)	3.740(60)	3.197(60)	SENGIERITE	8- 398
3.180(40)	9.260(100)	4.530(80)	4.410(50)	7.090(30)	HAIWEEITE	12- 721
3.170(70)	8.400(100)	4.180(80)	3.430(80)	4.240(60)	UPALITE	33- 37
3.180(80)	8.090(100)	3.420(90)	4.100(50)	1.882(40)	JOLIOTITE	29-1378
3.190(50)	7.830(100)	3.900(90)	3.510(60)	2.590(50)	BETAURANOPHANE	8- 301
3.180(100)	7.530(80)	3.500(70)	3.760(50)	2.039(50)	BILLIETITE	29- 208
3.160(30)	7.490(100)	3.210(80)	3.550(40)	3.740(35)	BECQUERELITE	29- 389
3.190(80)	7.400(100)	3.530(80)	3.700(60)	3.580(60)	COMPREIGNACITE	17- 167
3.170(50)	7.370(100)	3.590(100)	3.240(80)	3.520(60)	SCHOEPITE	29-1376
3.160(80)	7.370(100)	3.220(100)	3.700(80)	3.610(80)	UO2(OH)2	28-1415
3.160(30)	7.350(100)	3.220(50)	3.590(40)	3.670(25)	UO3.2H2O (BETA)	18-1436
3.150(35)	7.340(100)	3.660(55)	3.490(45)	2.858(15)	SODIUM-ZIPPEITE	29-1285
3.170(75)	7.250(100)	3.610(100)	1.985(40)	3.530(25)	VANDENDRIESSCHEITE	13- 117
3.180(50)	7.200(100)	3.580(50)	3.550(18)	3.140(12)	FOURMARIERITE	13- 116
3.180(25)	7.100(100)	3.220(50)	14.100(25)	4.740(20)	UMOHOITE,14A	11- 375
3.153(90)	7.080(100)	3.130(100)	3.490(90)	3.520(80)	AGRINIERITE	25- 630
3.181(25)	5.970(100)	2.890(40)	3.302(25)	3.226(25)	MOURITE	24-1359
3.190(80)	4.160(100)	2.340(100)	3.340(70)	1.911(50)	WIDENMANNITE	27- 281
3.150(40)	4.130(100)	3.200(50)	12.200(30)	6.180(30)	UMOHOITE,12A	12- 693
3.180(100)	4.010(80)	2.490(40)	1.838(30)	1.692(20)	LIANORATITE,HEATED	29-1435
3.170(80)	3.680(100)	3.350(90)	3.100(90)	4.730(80)	SCHMITTERITE	25-1001
3.160(100)	3.490(90)	3.000(80)	3.088(70)	3.385(60)	MOCTEZUMITE	18- 707
3.170(100)	3.340(90)	5.770(80)	1.970(80)	1.860(60)	CLARKEITE	8- 315
3.160(45)	3.280(100)	3.250(100)	4.230(65)	3.410(65)	PARSONSITE	12- 259
3.160(100)	3.090(100)	2.880(100)	7.960(80)	5.860(80)	PHOSPHURANULITE	19- 898
3.153(80)	3.070(100)	3.670(90)	4.390(80)	2.858(80)	RENARDITE	11- 215
3.150(50)	2.980(100)	1.700(90)	1.490(70)	1.550(50)	YTTROPYROCHLORE,HEATED	25-1015
3.160(60)	2.890(100)	2.860(80)	2.790(60)	3.990(40)	BRITHOLITE,(LA)	13- 106
3.170(70)	2.790(70)	2.900(100)	2.009(70)	1.913(70)	BELOVITE	17- 519
3.150(100)	1.930(49)	2.740(48)	1.649(47)	1.255(18)	URANINITE (UO2)	5- 550
3.160(100)	1.830(80)	3.870(70)	5.250(60)	3.470(60)	URANOSPHAERITE	8- 321
3.170(100)	1.730(85)	1.700(85)	1.632(40)	2.720(30)	THORUTITE,HEATED	14- 327

3.140 - 3.100

3.130(80)	7.970(100)	3.990(90)	5.830(80)	3.090(80)	RENARDITE	8- 328
3.130(70)	7.730(100)	6.160(90)	3.410(80)	3.870(70)	JOHANNITE	17- 530
3.130(80)	7.720(100)	3.850(100)	8.410(80)	3.420(70)	ARSENURANYLITE	14- 268
3.140(60)	7.480(100)	3.550(80)	3.200(80)	3.730(40)	BECQUERELITE	12- 176
3.120(30)	7.210(100)	3.590(45)	3.470(20)	1.963(12)	COBALT-ZIPPEITE	29- 520
3.120(30)	7.210(100)	3.590(45)	1.963(12)	2.491(11)	NICKEL-ZIPPEITE	29-1434
3.140(12)	7.200(100)	3.580(50)	3.180(50)	3.550(18)	FOURMARIERITE	13- 116
3.140(100)	7.120(100)	3.500(100)	3.120(100)	3.570(90)	RAMEAUITE	25- 631
3.120(100)	7.120(100)	3.500(100)	3.140(100)	3.570(90)	RAMEAUITE	25- 631
3.120(50)	7.080(100)	3.520(70)	3.560(35)	3.480(20)	MASUYITE	13- 408

3.100(25)	7.080(100)	3.540(50)	9.620(35)	3.440(35)	ZINC-ZIPPEITE	29-1395
3.120(80)	7.060(100)	3.500(90)	2.870(40)	2.650(40)	ZIPPEITE	29-1062
3.130(90)	7.020(100)	3.480(90)	1.960(60)	1.750(50)	ZIPPEITE	8- 138
3.100(60)	6.810(100)	8.680(90)	5.400(90)	4.550(60)	LIEBIGITE	11- 296
3.140(60)	6.360(100)	3.530(80)	3.210(80)	4.220(60)	CARNOTITE	11- 338
3.120(70)	4.780(100)	3.380(80)	2.620(70)	2.030(70)	OERKICKSITE	25- 319
3.133(80)	4.700(50)	9.000(100)	2.978(40)	1.850(40)	RANUNCULITE	33- 972
3.130(60)	4.160(100)	3.740(60)	4.500(20)	3.500(20)	KOBEITE	11- 259
3.140(80)	3.960(70)	6.230(100)	3.060(50)	3.520(40)	CURITE	14- 267
3.143(12)	3.868(100)	4.969(48)	2.601(23)	1.927(14)	UO2(OH)2 (BETA)	24-1160
3.100(90)	3.680(100)	5.350(90)	4.730(80)	3.170(80)	SCHMITTERITE	25-1001
3.110(60)	3.580(100)	7.200(80)	3.480(80)	2.740(30)	MAGNESIUM-ZIPPEITE	29- 876
3.130(90)	3.560(100)	3.480(100)	7.140(90)	2.620(80)	RICHETITE	25- 467
3.120(70)	3.530(50)	6.560(100)	4.250(30)	3.250(30)	CARNOTITE	8- 317
3.130(100)	3.490(90)	7.080(100)	3.153(90)	3.520(80)	AGRINIERITE	25- 630
3.100(65)	3.450(100)	7.100(95)	3.560(40)	9.630(35)	NICKEL-ZIPPEITE	29- 944
3.110(100)	3.250(50)	3.050(50)	9.900(40)	2.720(40)	WALPURGITE	8- 324
3.130(25)	3.230(100)	5.290(30)	6.400(19)	2.974(19)	IRIGINITE	29-1372
3.130(60)	3.090(100)	3.470(80)	6.390(80)	3.510(40)	WOLSENDORFITE	12- 159
3.100(80)	3.090(80)	8.050(100)	2.878(70)	3.390(50)	PHURCALITE	29- 391
3.130(40)	2.980(100)	3.050(70)	5.540(20)	3.450(20)	NIOBO-AESCHYNITE	29- 311
3.130(40)	2.980(100)	2.920(90)	3.230(30)	1.561(30)	SAMARSKITE,HEATED	10- 398
3.110(35)	2.980(100)	3.020(80)	2.698(30)	5.480(25)	AESCHYNITE	15- 864
3.120(100)	2.960(90)	1.900(50)	2.740(40)	1.855(30)	FERGUSONITE,HEATED	9- 443
3.120(100)	2.960(95)	1.900(75)	1.856(65)	2.734(50)	FERGUSONITE,BETA	23-1486
3.100(60)	2.960(100)	1.560(80)	1.820(70)	2.581(50)	PISEKITE,HEATED	25- 702
3.130(100)	2.930(90)	1.900(70)	1.641(70)	1.567(70)	FORMANITE,HEATED	26-1478
3.120(100)	2.870(70)	2.670(30)	2.280(10)	2.150(10)	TANTEUXENITE,HEATED	8- 293
3.130(80)	2.810(100)	2.750(90)	2.730(80)	3.090(50)	BRITHOLITE,(Y)	21- 173
3.140(100)	2.723(30)	1.918(25)	2.696(20)	1.926(20)	UNNAMED U3O7	15- 4
3.140(100)	2.720(30)	1.920(25)	2.696(20)	1.926(20)	URANINITE (U3O7)	15- 4
3.140(100)	1.924(50)	1.641(50)	2.721(45)	1.248(30)	URANINITE (U4O9)	20-1344
3.120(90)	1.920(90)	1.640(100)	1.247(80)	1.215(80)	URANINITE (UO2.25)	9- 206
3.120(100)	1.910(51)	1.630(44)	2.706(29)	1.241(15)	CERIANITE	4- 593

3.090 - 3.050

3.080(80)	10.300(100)	7.960(90)	2.870(80)	5.880(60)	KIVUITE	13- 419
3.090(80)	8.050(100)	3.100(80)	2.878(70)	3.390(50)	PHURCALITE	29- 391
3.090(80)	7.970(100)	3.990(90)	5.830(80)	3.130(80)	RENAROITE	8- 328
3.080(100)	7.780(100)	3.880(100)	2.976(80)	3.440(60)	BERGENITE	20- 154
3.050(60)	6.510(100)	4.220(80)	3.260(60)	5.190(40)	METATYUYAMUNITE	6- 287
3.060(50)	6.230(100)	3.140(80)	3.960(70)	3.520(40)	CURITE	14- 267
3.080(80)	5.760(100)	8.090(80)	3.650(70)	2.860(70)	GRIMSELITE	25- 679
3.080(80)	5.170(70)	10.400(100)	3.400(50)	3.470(40)	PHURALUMITE	33- 38
3.060(80)	4.210(60)	2.920(100)	3.520(60)	3.240(60)	KASOLITE	29- 788
3.070(100)	3.670(90)	4.390(80)	3.153(80)	2.858(80)	RENAROITE	11- 215
3.090(100)	3.470(80)	6.390(80)	3.130(60)	3.510(40)	WOLSENDORFITE	12- 159
3.090(100)	3.460(75)	1.730(40)	6.910(35)	1.913(80)	WOLSENDORFITE	29- 786
3.090(100)	3.410(70)	1.980(60)	1.948(60)	1.908(60)	BAURANOITE	25-1469
3.070(100)	3.260(90)	2.860(90)	4.140(75)	3.490(50)	CHERALITE	8- 316
3.090(100)	3.220(90)	8.230(100)	2.900(90)	3.500(80)	MARTHOZITE	25- 320
3.060(90)	3.190(100)	11.000(90)	3.370(90)	5.530(80)	SEDDVITE	18-1425
3.088(70)	3.160(100)	3.490(90)	3.000(80)	3.385(60)	MOCTEZUMITE	18- 707
3.050(70)	3.130(40)	2.980(100)	5.540(20)	3.450(20)	NIOBO-AESCHYNITE	29- 311
3.050(50)	3.110(100)	3.250(50)	9.900(40)	2.720(40)	WALPURGITE	8- 324
3.090(25)	3.020(100)	2.950(100)	5.500(20)	2.970(20)	AESCHYNITE,HEATED	18- 765
3.070(100)	2.920(100)	2.590(40)	1.840(40)	3.680(30)	SAMARSKITE,HEATED	4- 617
3.070(50)	2.900(100)	3.420(70)	2.850(60)	2.248(50)	DAVIDITE,HEATED	13- 505
3.090(100)	2.880(100)	3.160(100)	7.960(80)	5.860(80)	PHOSPHURANULITE	19- 898
3.090(100)	2.870(70)	3.300(50)	4.170(25)	3.510(25)	MONAZITE	11- 556
3.090(50)	2.810(100)	2.750(90)	2.730(80)	3.130(80)	BRITHOLITE,(Y)	21- 173
3.090(100)	2.690(50)	1.900(50)	1.620(40)	1.540(20)	URANINITE (UO2)	13- 225
3.070(100)	2.300(90)	4.990(100)	2.070(90)	4.590(80)	HAIWEEITE-(MG)	17- 463
3.060(100)	1.970(100)	3.240(100)	1.910(80)	1.706(80)	FERGUSONITE,BETA-(CE)	29- 402
3.080(80)	1.960(50)	2.860(100)	2.151(40)	1.738(40)	MONAZITE	29- 403
3.090(90)	1.680(60)	1.280(60)	3.430(50)	1.990(40)	METACALCIOURANOITE	25-1451

3.040 - 3.000

3.037(30)	9.300(100)	4.620(45)	4.470(40)	3.340(30)	HAIWEEITE	13- 118
3.010(60)	8.780(100)	3.570(100)	5.080(60)	4.300(60)	METAKIRCHHEIMERITE	12- 586
3.000(50)	8.650(100)	3.570(100)	3.310(90)	5.530(80)	META-URANOSPINITE	18- 309
3.000(10)	8.460(100)	4.220(20)	3.470(20)	3.560(10)	WYARTITE-(17A)	12- 636
3.000(60)	8.420(100)	4.190(80)	3.270(70)	3.520(60)	SKLODOWSKITE	29- 875
3.040(60)	8.390(100)	7.290(100)	3.550(80)	6.680(60)	GUILLEMINITE	18- 582
3.000(100)	7.770(100)	3.250(100)	4.130(90)	6.520(80)	FRITZCHEITE	23-1249
3.000(100)	5.200(60)	8.400(100)	4.260(60)	2.126(60)	FRANCEVILLITE	21- 381
3.030(100)	4.570(90)	3.380(100)	1.832(90)	1.160(90)	HAIWEEITE	17- 462
3.020(100)	4.400(80)	2.830(80)	2.150(80)	6.070(60)	RHABDOPHANE	12- 277
3.010(100)	4.100(80)	6.190(100)	5.130(60)	4.220(60)	CURIENITE	22- 402
3.020(35)	3.440(100)	3.350(100)	4.740(95)	6.040(35)	BRANNERITE	12- 477
3.000(80)	3.160(100)	3.490(90)	3.088(70)	3.385(60)	MOCTEZUMITE	18- 707
3.020(80)	3.110(35)	2.980(100)	2.698(30)	5.480(25)	AESCHYNITE	15- 864
3.020(100)	2.950(100)	3.090(25)	5.500(20)	2.970(20)	AESCHYNITE,HEATED	18- 765
3.000(85)	2.950(85)	4.270(100)	3.480(70)	6.140(55)	DUMONTITE	12- 158
3.020(80)	2.880(100)	2.840(80)	2.780(60)	2.960(55)	IIMORIITE	29-1388
3.020(100)	2.810(80)	2.130(80)	4.330(60)	3.380(60)	NINGYOITE	12- 273
3.020(100)	1.860(90)	1.580(90)	1.077(80)	1.017(80)	PLUMBOPYROCHLORE	25- 453
3.030(80)	1.760(80)	2.760(100)	1.940(60)	1.840(60)	BRITHOLITE	11- 459
3.010(100)	1.500(80)	1.740(70)	1.839(60)	1.782(60)	EUXENITE	14- 643

2.990 - 2.950

2.978(40)	9.000(100)	3.133(80)	4.700(50)	1.850(40)	RANUNCULITE	33- 972
2.970(80)	8.180(100)	4.090(90)	4.820(70)	6.100(60)	CUPROSKLODOWSKITE	8- 290
2.990(80)	7.880(100)	3.940(90)	2.910(80)	1.969(70)	URANOPHANE	8- 442
2.976(80)	7.780(100)	3.880(100)	3.080(100)	3.440(60)	BERGENITE	20- 154
2.950(80)	6.200(100)	3.250(100)	1.920(90)	2.190(80)	PSEUDO-AUTUNITE	18-1084
2.970(100)	5.420(80)	5.890(60)	3.340(60)	5.140(45)	DEMESAEKERITE	18- 692
2.990(60)	4.490(100)	3.930(60)	2.450(60)	11.000(40)	SHARPITE	12- 164
2.970(80)	4.440(100)	5.260(90)	2.590(70)	2.030(60)	VANDENBRANDEITE	8- 325
2.950(85)	4.270(100)	3.000(85)	3.480(70)	6.140(55)	DUMONTITE	12- 158
2.990(100)	4.070(90)	3.160(100)	4.230(70)	5.110(60)	UNNAMED-(PB)	15- 496
2.990(75)	3.670(30)	2.910(100)	1.574(30)	1.505(30)	AESCHYNITE	20-1401
2.990(100)	3.660(40)	2.950(40)	2.600(30)	1.830(30)	EUXENITE,HEATED	9- 442
2.950(100)	3.650(50)	2.540(30)	2.510(30)	2.380(30)	ASHANITE	33- 660
2.980(60)	3.590(100)	8.660(70)	5.090(40)	3.500(30)	METALODEVITE	25-1239
2.960(100)	3.500(80)	2.670(80)	1.630(60)	4.620(50)	ALLANITE,HEATED	9- 474
2.950(50)	3.490(40)	10.700(100)	2.620(30)	3.870(20)	RAUVITE	8- 288
2.980(50)	3.290(100)	1.700(80)	3.380(60)	1.999(60)	UMBOZERITE,HEATED	26-1384
2.974(19)	3.230(100)	5.290(30)	3.130(25)	6.400(19)	IRIGINITE	29-1372
2.950(100)	3.090(25)	3.020(100)	5.500(20)	2.970(20)	AESCHYNITE,HEATED	18- 765
2.980(100)	3.050(70)	3.130(40)	5.540(20)	3.450(20)	NIOBO-AESCHYNITE	29- 311
2.980(100)	3.020(80)	3.110(35)	2.698(30)	5.480(25)	AESCHYNITE	15- 864
2.970(20)	3.020(100)	2.950(100)	3.090(25)	5.500(20)	AESCHYNITE,HEATED	18- 765
2.950(40)	2.990(100)	3.660(40)	2.600(30)	1.830(30)	EUXENITE,HEATED	9- 442
2.980(100)	2.920(90)	3.130(40)	3.230(30)	1.561(30)	SAMARSKITE,HEATED	10- 398
2.960(55)	2.880(100)	2.840(80)	3.020(80)	2.780(60)	IIMORIITE	29-1388
2.960(90)	1.900(50)	3.120(100)	2.740(40)	1.855(30)	FERGUSONITE,HEATED	9- 443
2.960(95)	1.900(75)	3.120(100)	1.856(65)	2.734(50)	FERGUSONITE,BETA	23-1486
2.980(100)	1.820(40)	1.720(40)	3.660(30)	2.430(30)	EUXENITE,HEATED	5- 603
2.970(100)	1.820(80)	1.560(80)	1.190(80)	1.150(80)	SAMARSKITE,HEATED	2- 690
2.960(100)	1.810(45)	1.550(40)	1.179(20)	1.482(15)	BETAFITE,HEATED	13- 197
2.950(100)	1.710(100)	1.450(100)	1.190(50)	1.100(50)	SAMARSKITE	2- 717
2.980(100)	1.700(90)	1.490(70)	3.150(50)	1.550(50)	YTTROPYROCHLORE,HEATED	25-1015
2.960(100)	1.560(80)	1.820(70)	3.100(60)	2.581(50)	PISEKITE,HEATED	25- 702

2.940 - 2.900

2.938(70)	11.100(100)	3.740(80)	3.290(80)	4.620(60)	XIANGJIANGITE	29-1401
2.910(80)	8.760(100)	5.500(100)	7.310(90)	4.820(80)	SWARTZITE	4- 111
2.900(90)	8.230(100)	3.090(100)	3.220(90)	3.500(80)	MARTHOZITE	25- 320
2.910(80)	7.880(100)	3.940(90)	2.990(80)	1.969(70)	URANOPHANE	8- 442
2.910(70)	6.010(100)	3.400(90)	3.540(70)	1.908(60)	BOLTWOODITE	29-1026
2.920(80)	5.060(40)	4.290(100)	2.090(30)	1.850(80)	VANDENBRANDEITE	4- 340
2.920(100)	4.700(80)	6.710(100)	3.490(80)	3.370(80)	SODIUM BOLTWOODITE	29-1044
2.940(100)	4.600(70)	5.790(60)	1.701(50)	2.210(40)	UVANITE	8- 323
2.940(100)	4.470(85)	2.650(40)	6.400(35)	3.320(30)	MCKELVEYITE	18- 901
2.900(100)	3.420(70)	2.850(60)	3.070(50)	2.248(50)	DAVIDITE,HEATED	13- 505
2.900(100)	3.170(70)	2.790(70)	2.009(70)	1.913(70)	BELOVITE	17- 519
2.920(90)	3.130(40)	2.980(100)	3.230(30)	1.561(30)	SAMARSKITE,HEATED	10- 398
2.920(100)	3.060(80)	4.210(60)	3.520(60)	3.240(60)	KASOLITE	29- 788
2.910(100)	2.990(75)	3.670(30)	1.574(30)	1.505(30)	AESCHYNITE	20-1401
2.920(100)	2.710(65)	3.530(45)	2.627(40)	2.182(35)	ALLANITE	25- 169
2.920(100)	2.590(40)	3.070(100)	1.840(40)	3.680(30)	SAMARSKITE,HEATED	4- 617
2.930(90)	1.900(70)	3.130(100)	1.641(70)	1.567(70)	FORMANITE,HEATED	26-1478
2.900(100)	1.880(60)	4.650(40)	3.500(40)	2.160(40)	COFFINITE-(Y)	17- 460
2.940(100)	1.710(90)	2.240(80)	1.484(70)	5.900(60)	UVANITE	8- 322

2.890 - 2.850

2.870(80)	10.300(100)	7.960(90)	3.080(80)	5.880(60)	KIVUITE	13- 419
2.868(35)	10.200(100)	8.620(80)	4.310(50)	3.639(40)	FURONGITE	29- 98
2.878(70)	8.050(100)	3.100(80)	3.090(80)	3.390(50)	PHURCALITE	29- 391
2.858(15)	7.340(100)	3.660(55)	3.490(45)	3.150(35)	SODIUM-ZIPPEITE	29-1285
2.876(70)	7.260(100)	4.800(80)	8.480(70)	14.300(30)	SCHROECKINGERITE	8- 397
2.870(40)	7.060(100)	3.500(90)	3.120(80)	2.650(40)	ZIPPEITE	29-1062
2.880(60)	6.970(100)	4.210(90)	5.440(60)	5.870(50)	URANOPILITE	8- 131
2.860(70)	5.760(100)	8.090(80)	3.080(80)	3.650(70)	GRIMSELITE	25- 679
2.857(60)	5.110(100)	3.430(100)	3.450(80)	2.487(60)	UO3.0.8H2O	10- 309
2.857(26)	3.406(100)	5.151(85)	3.434(32)	2.488(27)	UO2(OH)2 (ALPHA)	25-1116
2.890(40)	3.302(25)	5.970(100)	3.226(25)	3.181(25)	MOURITE	24-1359
2.870(70)	3.300(50)	3.090(100)	4.170(25)	3.510(25)	MONAZITE	11- 556
2.880(100)	3.160(100)	3.090(100)	7.960(80)	5.860(80)	PHOSPHURANULITE	19- 898
2.860(80)	3.160(60)	2.890(100)	2.790(60)	3.990(40)	BRITHOLITE,(LA)	13- 106
2.860(100)	3.080(80)	1.960(50)	2.151(40)	1.738(40)	MONAZITE	29- 403
2.860(90)	3.070(100)	3.260(90)	4.140(75)	3.490(50)	CHERALITE	8- 316
2.858(80)	3.070(100)	3.670(90)	4.390(80)	3.153(80)	RENARDITE	11- 215
2.850(60)	2.900(100)	3.420(70)	3.070(50)	2.248(50)	DAVIDITE,HEATED	13- 505
2.890(100)	2.860(80)	3.160(60)	2.790(60)	3.990(40)	BRITHOLITE,(LA)	13- 106
2.880(100)	2.840(80)	3.020(80)	2.780(60)	2.960(55)	IIMORIITE	29-1388
2.870(70)	2.670(30)	3.120(100)	2.280(10)	2.150(10)	TANTEUXENITE,HEATED	8- 293
2.860(80)	1.700(100)	1.690(100)	1.440(90)	2.230(80)	DAVIDITE,HEATED	8- 291

2.840 - 2.800

2.842(45)	3.550(100)	4.720(85)	2.680(75)	1.834(65)	THORITE	11- 419
2.840(100)	3.480(80)	2.810(80)	1.858(80)	4.120(60)	BRITHOLITE,HEATED	17- 724
2.830(35)	3.230(100)	1.690(64)	1.980(58)	1.284(26)	THORIANITE	4- 556
2.840(80)	3.020(80)	2.880(100)	2.780(60)	2.960(55)	IIMORIITE	29-1388
2.830(80)	3.020(100)	4.400(80)	2.150(80)	6.070(60)	RHABDOPHANE	12- 277
2.810(80)	2.840(100)	3.480(80)	1.858(80)	4.120(60)	BRITHOLITE,HEATED	17- 724
2.810(100)	2.750(90)	2.730(80)	3.130(80)	3.090(50)	BRITHOLITE,(Y)	21- 173

2.810(80)	2.130(80)	3.020(100)	4.330(60)	3.380(60)	NINGYOITE	12- 273
2.840(78)	2.010(23)	3.280(100)	4.020(18)	2.788(17)	CLIFFORDITE	24-1209
2.840(80)	2.010(80)	3.270(100)	2.755(70)	1.712(70)	CLIFFORDITE	25- 999
2.840(90)	1.740(60)	3.400(100)	4.410(50)	1.696(50)	HALLIMONDITE	16- 706

2.790 - 2.750

2.760(80)	9.020(100)	3.800(100)	3.260(90)	2.160(80)	URAMPHITE	29- 121
2.791(45)	8.420(100)	5.600(100)	3.350(78)	16.800(70)	UMOHOITE,17A	12- 778
2.789(45)	3.480(100)	4.640(95)	2.640(95)	1.803(70)	COFFINITE	11- 420
2.788(17)	3.280(100)	2.840(78)	2.010(23)	4.020(18)	CLIFFOROITE	24-1209
2.755(70)	3.270(100)	2.840(80)	2.010(80)	1.712(70)	CLIFFORDITE	25- 999
2.760(100)	3.030(80)	1.760(80)	1.940(60)	1.840(60)	BRITHOLITE	11- 459
2.790(70)	2.900(100)	3.170(70)	2.009(70)	1.913(70)	BELOVITE	17- 519
2.790(60)	2.890(100)	2.860(80)	3.160(60)	3.990(40)	BRITHOLITE,(LA)	13- 106
2.780(60)	2.880(100)	2.840(80)	3.020(80)	2.960(55)	IIMORIITE	29-1388
2.750(90)	2.730(80)	2.810(100)	3.130(80)	3.090(50)	BRITHOLITE,(Y)	21- 173

2.740 - 2.700

2.718(14)	8.170(100)	4.000(55)	4.140(30)	3.510(14)	META-AUTUNITE	14- 75
2.740(30)	3.580(100)	7.200(80)	3.480(80)	3.110(60)	MAGNESIUM-ZIPPEITE	29- 876
2.710(65)	3.530(45)	2.920(100)	2.627(40)	2.182(35)	ALLANITE	25- 169
2.720(30)	3.170(100)	1.730(85)	1.700(85)	1.632(40)	THORUTITE,HEATED	14- 327
2.740(48)	3.160(100)	1.930(49)	1.649(47)	1.255(18)	URANINITE (UO2)	5- 550
2.721(45)	3.140(100)	1.924(50)	1.641(50)	1.248(30)	URANINITE (U4O9)	20-1344
2.740(40)	3.120(100)	2.960(90)	1.900(50)	1.855(30)	FERGUSONITE,HEATED	9- 443
2.734(50)	3.120(100)	2.960(95)	1.900(75)	1.856(65)	FERGUSONITE,BETA	23-1486
2.706(29)	3.120(100)	1.910(51)	1.630(44)	1.241(15)	CERIANITE	4- 593
2.720(40)	3.110(100)	3.250(50)	3.050(50)	9.900(40)	WALPURGITE	8- 324
2.730(80)	2.810(100)	2.750(90)	3.130(80)	3.090(50)	BRITHOLITE,(Y)	21- 173
2.720(30)	1.920(25)	3.140(100)	2.696(20)	1.926(20)	URANINITE (U307)	15- 4
2.723(30)	1.918(25)	3.140(100)	2.696(20)	1.926(20)	UNNAMED U307	15- 4

2.690 - 2.650

2.690(50)	7.660(100)	13.100(90)	3.830(60)	2.210(50)	BAYLEYITE	4- 130
2.650(40)	7.060(100)	3.500(90)	3.120(80)	2.870(40)	ZIPPEITE	29-1062
2.680(75)	3.550(100)	4.720(85)	1.834(65)	2.842(45)	THORITE	11- 419
2.690(70)	3.320(100)	4.480(90)	6.140(80)	2.470(60)	SODDYITE	12- 180
2.696(20)	3.140(100)	2.723(30)	1.918(25)	1.926(20)	UNNAMED U307	15- 4
2.696(20)	3.140(100)	2.720(30)	1.920(25)	1.926(20)	URANINITE (U307)	15- 4
2.670(30)	3.120(100)	2.870(70)	2.280(10)	2.150(10)	TANTEUXENITE,HEATED	8- 293
2.698(30)	2.980(100)	3.020(80)	3.110(35)	5.480(25)	AESCHYNITE	15- 864
2.670(80)	2.960(100)	3.500(80)	1.630(60)	4.620(50)	ALLANITE,HEATED	9- 474
2.650(40)	2.940(100)	4.470(85)	6.400(35)	3.320(30)	MCKELVEYITE	18- 901
2.690(50)	1.900(50)	3.090(100)	1.620(40)	1.540(20)	URANINITE (UO2)	13- 225
2.680(80)	1.570(80)	3.670(100)	1.540(80)	3.230(70)	SODIUM META-AUTUNITE	29-1283

2.640 - 2.580

2.620(30)	10.700(100)	2.950(50)	3.490(40)	3.870(20)	RAUVITE	8- 288
2.590(50)	7.830(100)	3.900(90)	3.510(60)	3.190(50)	BETAURANOPHANE	8- 301
2.620(55)	6.350(100)	3.210(100)	4.280(50)	5.250(45)	IRIGINITE	18-1426
2.640(100)	5.280(100)	3.310(100)	7.360(80)	3.380(80)	IRAQITE	29- 995
2.620(70)	4.780(100)	3.380(80)	3.120(70)	2.030(70)	DERRICKSITE	25- 319
2.640(25)	4.610(100)	4.300(70)	3.230(40)	3.920(30)	RUTHERFOROINE	11- 263
2.590(70)	4.440(100)	5.260(90)	2.970(80)	2.030(60)	VANDENBRANDEITE	8- 325
2.580(50)	4.170(100)	1.310(60)	1.300(60)	3.440(50)	MOLURANITE,HEATED	29-1371
2.601(23)	3.868(100)	4.969(48)	1.927(14)	3.143(12)	UO2(OH)2 (BETA)	24-1160
2.620(80)	3.560(100)	3.480(100)	7.140(90)	3.130(90)	RICHETITE	25- 467
2.640(95)	3.480(100)	4.640(95)	1.803(70)	2.789(45)	COFFINITE	11- 420
2.640(40)	3.380(100)	3.320(55)	5.300(45)	2.000(25)	EKANITE	25- 677
2.590(40)	3.070(100)	2.920(100)	1.840(40)	3.680(30)	SAMARSKITE,HEATED	4- 617
2.600(30)	2.990(100)	3.660(40)	2.950(40)	1.830(30)	EUXENITE,HEATED	9- 442
2.581(50)	2.960(100)	1.560(80)	1.820(70)	3.100(60)	PISEKITE,HEATED	25- 702
2.627(40)	2.920(100)	2.710(65)	3.530(45)	2.182(35)	ALLANITE	25- 169

2.570 - 2.510

2.540(60)	8.860(100)	3.590(100)	1.610(70)	2.280(60)	METAKAHLERITE	17- 151
2.530(50)	8.520(100)	3.570(90)	2.140(60)	4.290(50)	METANOVACEKITE	17- 152
2.566(10)	7.440(100)	3.200(35)	3.730(30)	3.540(20)	BECQUERELITE	13- 405
2.510(80)	4.020(100)	3.210(100)	1.697(40)	1.850(30)	PETSCHECKITE,HEATED	29-1426
2.540(30)	2.950(100)	3.650(50)	2.510(30)	2.380(30)	ASHANITE	33- 660
2.510(30)	2.950(100)	3.650(50)	2.540(30)	2.380(30)	ASHANITE	33- 660
2.570(70)	1.795(100)	3.870(70)	2.481(70)	1.708(70)	UO2(OH)2 (BETA)	9- 239
2.560(50)	1.770(50)	3.450(100)	4.550(25)	2.150(25)	XENOTIME	11- 254
2.560(60)	1.760(45)	3.440(100)	4.540(25)	2.145(25)	XENOTIME	9- 377

2.500 - 2.440

2.491(11)	7.210(100)	3.590(45)	3.120(30)	1.963(12)	NICKEL-ZIPPEITE	29-1434
2.446(10)	7.350(100)	3.660(50)	3.240(10)	3.210(4)	SCHOEPITE	13- 241
2.487(60)	5.110(100)	3.430(100)	3.450(80)	2.857(60)	UO3.0.8H2O	10- 309
2.450(60)	4.490(100)	3.930(60)	2.990(60)	11.000(40)	SHARPITE	12- 164
2.500(80)	4.050(60)	3.200(100)	1.830(50)	1.710(30)	BETAFITE,HEATED	18-1154
2.460(70)	3.420(100)	1.903(80)	2.276(70)	3.320(60)	BRANNERITE,HEATED	8- 2
2.488(27)	3.406(100)	5.151(85)	3.434(32)	2.857(26)	UO2(OH)2 (ALPHA)	25-1116
2.470(60)	3.320(100)	4.480(90)	6.140(80)	2.690(70)	SODDYITE	12- 180
2.490(40)	3.180(100)	4.010(80)	1.838(30)	1.692(20)	LIANORATITE,HEATED	29-1435
2.481(70)	1.795(100)	3.870(70)	2.570(70)	1.708(70)	UO2(OH)2 (BETA)	9- 239
2.480(60)	1.680(100)	3.220(80)	1.042(60)	3.450(50)	DAVIDITE,HEATED	8- 305

2.430 - 2.370

2.430(30)	2.980(100)	1.820(40)	1.720(40)	3.660(30)	EUXENITE,HEATED	5- 603
2.380(30)	2.950(100)	3.650(50)	2.540(30)	2.510(30)	ASHANITE	33- 660

2.360 - 2.300

2.300(90)	4.990(100)	3.070(100)	2.070(90)	4.590(80)	HAIWEEITE-(MG)	17- 463
2.340(100)	3.190(80)	4.160(100)	3.340(70)	1.911(50)	WIOENMANNITE	27- 281

2.290 - 2.230

2.280(60)	8.860(100)	3.590(100)	1.610(70)	2.540(60)	METAKAHLERITE	17- 151
2.276(70)	3.420(100)	1.903(80)	2.460(70)	3.320(60)	BRANNERITE,HEATED	8- 2
2.280(10)	3.120(100)	2.870(70)	2.670(30)	2.150(10)	TANTEUXENITE,HEATED	8- 293
2.240(80)	2.940(100)	1.710(90)	1.484(70)	5.900(60)	UVANITE	8- 322
2.248(50)	2.900(100)	3.420(70)	2.850(60)	3.070(50)	OAVIDITE,HEATED	13- 505
2.230(80)	1.700(100)	1.690(100)	1.440(90)	2.860(80)	DAVIDITE,HEATED	8- 291

2.220 - 2.160

2.188(60)	9.690(100)	4.860(90)	3.470(80)	4.390(40)	SABUGALITE	5- 107
2.197(60)	9.430(100)	3.474(80)	3.366(60)	5.350(50)	THREADGOLDITE	33- 39
2.160(80)	9.020(100)	3.800(100)	3.260(90)	2.760(80)	URAMPHITE	29- 121
2.210(50)	7.660(100)	13.100(90)	3.830(60)	2.690(50)	BAYLEYITE	4- 130
2.190(80)	6.200(100)	3.250(100)	1.920(90)	2.950(80)	PSEUDO-AUTUNITE	18-1084
2.160(50)	5.100(100)	2.040(100)	10.100(60)	1.462(60)	URANOCIRCITE	18- 199
2.200(60)	4.890(100)	3.460(100)	8.590(60)	4.250(30)	BASSETTITE	7- 288
2.210(40)	2.940(100)	4.600(70)	5.790(60)	1.701(50)	UVANITE	8- 323
2.182(35)	2.920(100)	2.710(65)	3.530(45)	2.627(40)	ALLANITE	25- 169
2.160(40)	2.900(100)	1.880(60)	4.650(40)	3.500(40)	COFFINITE-(Y)	17- 460

2.150 - 2.090

2.140(60)	8.520(100)	3.570(90)	4.290(50)	2.530(50)	METANOVACEKITE	17- 152
2.110(70)	8.470(100)	3.610(35)	4.230(65)	5.370(45)	META-AUTUNITE	12- 423
2.126(60)	8.400(100)	3.000(100)	5.200(60)	4.260(60)	FRANCEVILLITE	21- 381
2.140(50)	7.930(80)	3.990(60)	1.997(60)	3.580(40)	URANOPHANE-(BA)	-
2.150(40)	7.810(100)	3.760(70)	3.890(60)	3.290(40)	UNNAMED-(GA)	15- 609
2.110(80)	5.000(100)	3.230(100)	1.970(80)	2.050(50)	VANURANYLITE	19-1417
2.090(30)	4.290(100)	2.920(80)	5.060(40)	1.850(80)	VANDENBRANDEITE	4- 340
2.150(50)	3.590(100)	8.550(90)	4.290(60)	5.110(50)	METAKAHLERITE	12- 576
2.150(25)	3.450(100)	2.560(50)	1.770(50)	4.550(25)	XENOTIME	11- 254
2.145(25)	3.440(100)	2.560(60)	1.760(45)	4.540(25)	XENOTIME	9- 377
2.150(10)	3.120(100)	2.870(70)	2.670(30)	2.280(10)	TANTEUXENITE,HEATED	8- 293
2.150(80)	3.020(100)	4.400(80)	2.830(80)	6.070(60)	RHABDOPHANE	12- 277
2.130(80)	3.020(100)	2.810(80)	4.330(60)	3.380(60)	NINGYOITE	12- 273
2.151(40)	2.860(100)	3.080(80)	1.960(50)	1.738(40)	MONAZITE	29- 403

2.080 - 2.020

2.040(40)	10.200(100)	5.020(90)	3.200(50)	6.620(30)	TYUYAMUNITE	6- 17
2.040(100)	10.100(60)	5.100(100)	1.462(60)	2.160(50)	URANOCIRCITE	18- 199
2.050(50)	5.000(100)	3.230(100)	2.110(80)	1.970(80)	VANURANYLITE	19-1417
2.070(90)	4.990(100)	3.070(100)	2.300(90)	4.590(80)	HAIWEEITE-(MG)	17- 463
2.030(70)	4.780(100)	3.380(80)	3.120(70)	2.620(70)	DERRICKSITE	25- 319
2.030(60)	4.440(100)	9.260(90)	2.970(80)	2.590(70)	VANDENBRANDEITE	8- 325
2.039(50)	3.180(100)	7.530(80)	3.500(70)	3.760(50)	BILLIETITE	29- 208

2.010 - 1.940

1.997(60)	7.930(80)	3.990(60)	2.140(50)	3.580(40)	URANOPHANE-(BA)	-
1.969(70)	7.880(100)	3.940(90)	2.990(80)	2.910(80)	URANOPHANE	8- 442
1.990(50)	7.800(100)	3.210(80)	3.890(60)	8.300(50)	CALCURMOLITE	16- 145
1.985(40)	7.250(100)	3.610(100)	3.170(75)	3.530(25)	VANDENDRIESSCHEITE	13- 117
1.963(12)	7.210(100)	3.590(45)	3.120(30)	3.470(20)	COBALT-ZIPPEITE	29- 520
1.963(12)	7.210(100)	3.590(45)	3.120(30)	2.491(11)	NICKEL-ZIPPEITE	29-1434
1.960(60)	7.020(100)	3.480(90)	3.130(90)	1.750(50)	ZIPPEITE	8- 138
1.970(80)	5.000(100)	3.230(100)	2.110(80)	2.050(50)	VANURANYLITE	19-1417
2.000(25)	3.380(100)	3.320(55)	5.300(45)	2.640(40)	EKANITE	25- 677
1.999(60)	3.290(100)	1.700(80)	3.380(60)	2.980(50)	UMBOZERITE,HEATED	26-1384
2.010(23)	3.280(100)	2.840(78)	4.020(18)	2.788(17)	CLIFFORDITE	24-1209
2.010(80)	3.270(100)	2.840(80)	2.755(70)	1.712(70)	CLIFFORDITE	25- 999
1.970(100)	3.240(100)	3.060(100)	1.910(80)	1.706(80)	FERGUSONITE,BETA-(CE)	29- 402
1.980(58)	3.230(100)	1.690(64)	2.800(35)	1.284(26)	THORIANITE	4- 556
1.970(80)	3.170(100)	3.340(90)	5.770(80)	1.860(60)	CLARKEITE	8- 315
1.990(40)	3.090(90)	1.680(60)	1.280(60)	3.430(50)	METACALCIOURANOITE	25-1451
1.980(60)	3.090(100)	3.410(70)	1.948(60)	1.908(50)	BAURANOITE	25-1469
1.948(60)	3.090(100)	3.410(70)	1.980(60)	1.908(60)	BAURANOITE	25-1469
2.009(70)	2.900(100)	3.170(70)	2.790(70)	1.913(70)	BELOVITE	17- 519
1.960(50)	2.860(100)	3.080(80)	2.151(40)	1.738(40)	MONAZITE	29- 403
1.940(60)	2.760(100)	3.030(80)	1.760(80)	1.840(60)	BRITHOLITE	11- 459
1.970(100)	1.650(100)	3.210(100)	1.120(80)	1.044(80)	CALCIOURANOITE,HEATED	26-1003

1.930 - 1.860

1.930(60)	10.700(100)	3.590(90)	5.040(80)	3.390(70)	ZEUNERITE	4- 90
1.882(40)	8.090(100)	3.420(90)	3.180(80)	4.100(50)	JOLIOTITE	29-1378
1.920(90)	6.200(100)	3.250(100)	2.950(80)	2.190(80)	PSEUDO-AUTUNITE	18-1084
1.908(60)	6.010(100)	3.400(90)	3.540(70)	2.910(70)	BOLTWOODITE	29-1026
1.880(60)	4.650(40)	2.900(100)	3.500(40)	2.160(40)	COFFINITE-(Y)	17- 460
1.911(50)	4.160(100)	2.340(100)	3.190(80)	3.340(70)	WIDENMANNITE	27- 281

1.927(14)	3.868(100)	4.969(48)	2.601(23)	3.143(12)	UO2(OH)2 (BETA)	24-1160
1.910(80)	3.240(100)	3.060(100)	1.970(100)	1.706(80)	FERGUSONITE,BETA-(CE)	29- 402
1.860(60)	3.170(100)	3.340(90)	5.770(80)	1.970(80)	CLARKEITE	8- 315
1.926(20)	3.140(100)	2.723(30)	1.918(25)	2.696(20)	UNNAMED U307	15- 4
1.926(20)	3.140(100)	2.720(30)	1.920(25)	2.696(20)	URANINITE (U307)	15- 4
1.920(25)	3.140(100)	2.720(30)	2.696(20)	1.926(20)	URANINITE (U307)	15- 4
1.918(25)	3.140(100)	2.723(30)	2.696(20)	1.926(20)	UNNAMED U307	15- 4
1.900(70)	3.130(100)	2.930(90)	1.641(70)	1.567(70)	FORMANITE,HEATED	26-1478
1.900(50)	3.120(100)	2.960(90)	2.740(40)	1.855(30)	FERGUSONITE,HEATED	9- 443
1.900(75)	3.120(100)	2.960(95)	1.856(65)	2.734(50)	FERGUSONITE,BETA	23-1486
1.913(80)	3.090(100)	3.460(75)	1.730(40)	6.910(35)	WOLSENDORFITE	29- 786
1.908(60)	3.090(100)	3.410(70)	1.980(60)	1.948(60)	BAURANOITE	25-1469
1.900(50)	3.090(100)	2.690(50)	1.620(40)	1.540(20)	URANINITE (UO2)	13- 225
1.913(70)	2.900(100)	3.170(70)	2.790(70)	2.009(70)	BELOVITE	17- 519
1.930(49)	2.740(48)	3.160(100)	1.649(47)	1.255(18)	URANINITE (UO2)	5- 550
1.903(80)	2.460(70)	3.420(100)	2.276(70)	3.320(60)	BRANNERITE,HEATED	8- 2
1.924(50)	1.641(50)	3.140(100)	2.721(45)	1.248(30)	URANINITE (U409)	20-1344
1.920(90)	1.640(100)	3.120(90)	1.247(80)	1.215(80)	URANINITE (UO2.25)	9- 206
1.910(51)	1.630(44)	3.120(100)	2.706(29)	1.241(15)	CERIANITE	4- 593
1.860(90)	1.580(90)	3.020(100)	1.077(80)	1.017(80)	PLUMBOPYROCHLORE	25- 453

1.850 - 1.780

1.850(40)	9.000(100)	3.133(80)	4.700(50)	2.978(40)	RANUNCULITE	33- 972
1.850(80)	4.290(100)	2.920(80)	5.060(40)	2.090(30)	VANDENBRANDEITE	4- 340
1.850(30)	4.020(100)	3.210(100)	2.510(80)	1.697(40)	PETSCHECKITE,HEATED	29-1426
1.830(80)	3.870(70)	3.160(100)	5.250(60)	3.470(60)	URANOSPHAERITE	8- 321
1.795(100)	3.870(70)	2.570(70)	2.481(70)	1.708(70)	UO2(OH)2 (BETA)	9- 239
1.834(65)	3.550(100)	4.720(85)	2.680(75)	2.842(45)	THORITE	11- 419
1.803(70)	3.480(100)	4.640(95)	2.640(95)	2.789(45)	COFFINITE	11- 420
1.832(90)	3.380(100)	3.030(100)	4.570(90)	1.160(90)	HAIWEEITE	17- 462
1.830(50)	3.200(100)	2.500(80)	4.050(60)	1.710(30)	BETAFITE,HEATED	18-1154
1.838(30)	3.180(100)	4.010(80)	2.490(40)	1.692(20)	LIANDRATITE,HEATED	29-1435
1.856(65)	3.120(100)	2.960(95)	1.900(75)	2.734(50)	FERGUSONITE,BETA	23-1486
1.855(30)	3.120(100)	2.960(90)	1.900(50)	2.740(40)	FERGUSONITE,HEATED	9- 443
1.840(40)	3.070(100)	2.920(100)	2.590(40)	3.680(30)	SAMARSKITE,HEATED	4- 617
1.839(60)	3.010(100)	1.500(80)	1.740(70)	1.782(60)	EUXENITE	14- 643
1.782(60)	3.010(100)	1.500(80)	1.740(70)	1.839(60)	EUXENITE	14- 643
1.830(30)	2.990(100)	3.660(40)	2.950(40)	2.600(30)	EUXENITE,HEATED	9- 442
1.820(70)	2.960(100)	1.560(80)	3.100(60)	2.581(50)	PISEKITE,HEATED	25- 702
1.858(80)	2.840(100)	3.480(80)	2.810(80)	4.120(60)	BRITHOLITE,HEATED	17- 724
1.840(60)	2.760(100)	3.030(80)	1.760(80)	1.940(60)	BRITHOLITE	11- 459
1.820(40)	1.720(40)	2.980(100)	3.660(30)	2.430(30)	EUXENITE,HEATED	5- 603
1.820(80)	1.560(80)	2.970(100)	1.190(80)	1.150(80)	SAMARSKITE,HEATED	2- 690
1.810(45)	1.550(40)	2.960(100)	1.179(20)	1.482(15)	BETAFITE,HEATED	13- 197

1.770 - 1.680

1.750(50)	7.020(100)	3.480(90)	3.130(90)	1.960(60)	ZIPPEITE	8- 138
1.697(40)	4.020(100)	3.210(100)	2.510(80)	1.850(30)	PETSCHECKITE,HEATED	29-1426
1.770(50)	3.450(100)	2.560(50)	4.550(25)	2.150(25)	XENOTIME	11- 254
1.760(45)	3.440(100)	2.560(60)	4.540(25)	2.145(25)	XENOTIME	9- 377
1.740(60)	3.400(100)	2.840(90)	4.410(50)	1.696(50)	HALLIMONDITE	16- 706
1.696(50)	3.400(100)	2.840(90)	1.740(60)	4.410(50)	HALLIMONDITE	16- 706
1.700(80)	3.380(60)	3.290(100)	1.999(60)	2.980(50)	UMBOZERITE,HEATED	26-1384
1.712(70)	3.270(100)	2.840(80)	2.010(80)	2.755(70)	CLIFFORDITE	25- 999
1.706(80)	3.240(100)	3.060(100)	1.970(100)	1.910(80)	FERGUSONITE,BETA-(CE)	29- 402
1.680(100)	3.220(80)	2.480(60)	1.042(60)	3.450(50)	DAVIDITE,HEATED	8- 305
1.710(30)	3.200(100)	2.500(80)	4.050(60)	1.830(50)	BETAFITE,HEATED	18-1154
1.692(20)	3.180(100)	4.010(80)	2.490(40)	1.838(30)	LIANDRATITE,HEATED	29-1435
1.700(85)	3.170(100)	1.730(85)	1.632(40)	2.720(30)	THORUTITE,HEATED	14- 327
1.730(40)	3.090(100)	3.460(75)	6.910(35)	1.913(80)	WOLSENDORFITE	29- 786
1.740(70)	3.010(100)	1.500(80)	1.839(60)	1.782(60)	EUXENITE	14- 643
1.720(40)	2.980(100)	1.820(40)	3.660(30)	2.430(30)	EUXENITE,HEATED	5- 603
1.701(50)	2.940(100)	4.600(70)	5.790(60)	2.210(40)	UVANITE	8- 323
1.738(40)	2.860(100)	3.080(80)	1.960(50)	2.151(40)	MONAZITE	29- 403
1.760(80)	2.760(100)	3.030(80)	1.940(60)	1.840(60)	BRITHOLITE	11- 459
1.710(90)	2.240(80)	2.940(100)	1.484(70)	5.900(60)	UVANITE	8- 322
1.690(64)	1.980(58)	3.230(100)	2.800(35)	1.284(26)	THORIANITE	4- 556
1.708(70)	1.795(100)	3.870(70)	2.570(70)	2.481(70)	UO2(OH)2 (BETA)	9- 239
1.730(85)	1.700(85)	3.170(100)	1.632(40)	2.720(30)	THORUTITE,HEATED	14- 327
1.700(100)	1.690(100)	1.440(90)	2.860(80)	2.230(80)	DAVIDITE,HEATED	8- 291
1.700(90)	1.490(70)	2.980(100)	3.150(50)	1.550(50)	YTTROPYROCHLORE,HEATED	25-1015
1.710(100)	1.450(100)	2.950(100)	1.190(50)	1.100(50)	SAMARSKITE	2- 717
1.690(100)	1.440(90)	1.700(100)	2.860(80)	2.230(80)	DAVIDITE,HEATED	8- 291
1.680(60)	1.280(60)	3.090(90)	3.430(50)	1.990(40)	METACALCIOURANOITE	25-1451

1.670 - 1.580

1.600(70)	10.000(100)	3.530(100)	3.350(80)	5.090(70)	HEINRICHITE	29- 210
1.588(50)	10.000(100)	3.570(100)	5.020(80)	3.350(40)	NOVACEKITE	17- 148
1.658(50)	8.930(100)	3.730(80)	5.480(70)	3.230(60)	META-URANOCIRCITE	17- 758
1.610(70)	8.860(100)	3.590(100)	2.540(60)	2.280(60)	METAKAHLERITE	17- 151
1.600(90)	8.530(100)	3.660(90)	1.530(80)	9.250(70)	TROEGERITE-(P)	26- 887
1.620(60)	3.610(100)	9.080(90)	1.530(60)	9.490(50)	PRZHEVALSKITE	29- 787
1.603(40)	3.530(100)	11.100(80)	5.550(50)	3.590(50)	KAHLERITE	17- 145
1.650(100)	3.210(100)	1.970(100)	1.120(80)	1.044(80)	CALCIOURANOITE,HEATED	26-1003
1.632(40)	3.170(100)	1.730(85)	1.700(85)	2.720(30)	THORUTITE,HEATED	14- 327
1.649(47)	3.160(100)	1.930(49)	2.740(48)	1.255(18)	URANINITE (UO2)	5- 550
1.641(50)	3.140(100)	1.924(50)	2.721(45)	1.248(30)	URANINITE (U409)	20-1344

1.641(70)	3.130(100)	2.930(90)	1.900(70)	1.567(70)	FORMANITE,HEATED	26-1478
1.640(100)	3.120(90)	1.920(90)	1.247(80)	1.215(80)	URANINITE (UO2.25)	9- 206
1.630(44)	3.120(100)	1.910(51)	2.706(29)	1.241(15)	CERIANITE	4- 593
1.620(40)	3.090(100)	2.690(50)	1.900(50)	1.540(20)	URANINITE (UO2)	13- 225
1.580(90)	3.020(100)	1.860(90)	1.077(80)	1.017(80)	PLUMBOPYROCHLORE	25- 453
1.630(60)	2.960(100)	3.500(80)	2.670(80)	4.620(50)	ALLANITE,HEATED	9- 474

1.570 - 1.480

1.530(80)	8.530(100)	3.660(90)	1.600(90)	9.250(70)	TROEGERITE-(P)	26- 887
1.570(80)	3.670(100)	2.680(80)	1.540(80)	3.230(70)	SODIUM META-AUTUNITE	29-1283
1.540(80)	3.670(100)	2.680(80)	1.570(80)	3.230(70)	SODIUM META-AUTUNITE	29-1283
1.530(60)	3.610(100)	9.080(90)	1.620(60)	9.490(50)	PRZHEVALSKITE	29- 787
1.567(70)	3.130(100)	2.930(90)	1.900(70)	1.641(70)	FORMANITE,HEATED	26-1478
1.540(20)	3.090(100)	2.690(50)	1.900(50)	1.620(40)	URANINITE (UO2)	13- 225
1.561(30)	2.980(100)	2.920(90)	3.130(40)	3.230(30)	SAMARSKITE,HEATED	10- 398
1.550(50)	2.980(100)	1.700(90)	1.490(70)	3.150(50)	YTTROPYROCHLORE,HEATED	25-1015
1.490(70)	2.980(100)	1.700(90)	3.150(50)	1.550(50)	YTTROPYROCHLORE,HEATED	25-1015
1.560(80)	2.970(100)	1.820(80)	1.190(80)	1.150(80)	SAMARSKITE,HEATED	2- 690
1.550(40)	2.960(100)	1.810(45)	1.179(20)	1.482(15)	BETAFITE,HEATED	13- 197
1.482(15)	2.960(100)	1.810(45)	1.550(40)	1.179(20)	BETAFITE,HEATED	13- 197
1.484(70)	2.940(100)	1.710(90)	2.240(80)	5.900(60)	UVANITE	8- 322
1.574(30)	2.910(100)	2.990(75)	3.670(30)	1.505(30)	AESCHYNITE	20-1401
1.505(30)	2.910(100)	2.990(75)	3.670(30)	1.574(30)	AESCHYNITE	20-1401
1.560(80)	1.820(70)	2.960(100)	3.100(60)	2.581(50)	PISEKITE,HEATED	25- 702
1.500(80)	1.740(70)	3.010(100)	1.839(60)	1.782(60)	EUXENITE	14- 643

1.470 - 1.380

1.462(60)	5.100(100)	2.040(100)	10.100(60)	2.160(50)	URANOCIRCITE	18- 199
1.450(100)	2.950(100)	1.710(100)	1.190(50)	1.100(50)	SAMARSKITE	2- 717
1.440(90)	1.700(100)	1.690(100)	2.860(80)	2.230(80)	DAVIDITE,HEATED	8- 291

1.370 - 1.000

1.300(60)	4.170(100)	1.310(60)	3.440(50)	2.580(50)	MOLURANITE,HEATED	29-1371
1.160(90)	3.380(100)	3.030(100)	4.570(90)	1.832(90)	HAIWEEITE	17- 462
1.284(26)	3.230(100)	1.690(64)	1.980(58)	2.800(35)	THORIANITE	4- 556
1.120(80)	3.210(100)	1.970(100)	1.650(100)	1.044(80)	CALCIOURANOITE,HEATED	26-1003
1.044(80)	3.210(100)	1.970(100)	1.650(100)	1.120(80)	CALCIOURANOITE,HEATED	26-1003
1.255(18)	3.160(100)	1.930(49)	2.740(48)	1.649(47)	URANINITE (UO2)	5- 550
1.248(30)	3.140(100)	1.924(50)	1.641(50)	2.721(45)	URANINITE (U4O9)	20-1344
1.241(15)	3.120(100)	1.910(51)	1.630(44)	2.706(29)	CERIANITE	4- 593
1.280(60)	3.090(90)	1.680(60)	3.430(50)	1.990(40)	METACALCIOURANOITE	25-1451
1.077(80)	3.020(100)	1.860(90)	1.580(90)	1.017(80)	PLUMBOPYROCHLORE	25- 453
1.017(80)	3.020(100)	1.860(90)	1.580(90)	1.077(80)	PLUMBOPYROCHLORE	25- 453
1.190(80)	2.970(100)	1.820(80)	1.560(80)	1.150(80)	SAMARSKITE,HEATED	2- 690
1.150(80)	2.970(100)	1.820(80)	1.560(80)	1.190(80)	SAMARSKITE,HEATED	2- 690
1.179(20)	2.960(100)	1.810(45)	1.550(40)	1.482(15)	BETAFITE,HEATED	13- 197
1.190(50)	2.950(100)	1.710(100)	1.450(100)	1.100(50)	SAMARSKITE	2- 717
1.190(50)	2.950(100)	1.710(100)	1.450(100)	1.190(50)	SAMARSKITE	2- 717
1.042(60)	1.680(100)	3.220(80)	2.480(60)	3.450(50)	DAVIDITE,HEATED	8- 305
1.247(80)	1.640(100)	3.120(90)	1.920(90)	1.215(80)	URANINITE (UO2.25)	9- 206
1.215(80)	1.640(100)	3.120(90)	1.920(90)	1.247(80)	URANINITE (UO2.25)	9- 206
1.310(60)	1.300(60)	4.170(100)	3.440(50)	2.580(50)	MOLURANITE,HEATED	29-1371

THE FOLLOWING MINERALS HAVE NO RECORDED X-RAY PATTERN

COUSINITE
OEWINOTITE
EWALOITE
FERGHANITE
HUEGELITE
ISHIKAWAITE
LERMONTOVITE
MELANOCERITE
META-AUTUNITE II
META-URANOPILITE
METAVANOENORIESSCHEITE
ORTHOBRANNERITE
PLUMBOBETAFITE
PLUMBOMICROLITE
POLYCRASE
U3O8(OH)2
URANOMICROLITE
URANOPYROCHLORE
WALPURGITE-(P)
YTTROBETAFITE
YTTROCOLUMBITE
YTTROCRASITE
YTTROMICROLITE(HJELMITE)

Appendix 2

Optical data for uranium minerals

Appendix 2 tabulates most of the readily available optical data reported for uranium mineral species. Two primary sources of the data are those of Larsen and Berman[1] and Soboleva and Pudovkina.[2] Other references include Frondel,[3] Weeks and Thompson,[4] the data as cited in the *Powder diffraction file*[5] and original mineral descriptions. The first two sources are identified as LB and SP in the SOURCE column of the table. The other sources have not been specifically identified.

The entries in the table have been ordered on their indices of refraction to provide an aid to mineral identification. The index columns list entries only when specific data were reported. If a range in an index was reported, the minimum and maximum values are indicated. The order is based on either the $N(Y)$ index if the mineral is biaxial, ω if the mineral is uniaxial and N if the mineral is isotropic. Where one of these indices is not quoted the other indices are used. No distinction has been made for the optical character.

Several minerals are represented by multiple entries from different sources. The additional entries are necessary because of the different values reported. Some of the entries are obviously for a different species (e.g. carnotite 2.06, 2.08), but are retained because of insufficient data to justify discarding the information. Optical sign, $2V$ and colour are also included in the listing. The $2V$ includes a range when one has been reported. The codes *SM*, *MO* and *LG*, respectively, indicate small, moderate and large. The colour column also includes a range when necessary. The abbreviations used for colour are:

Colours	*Modifiers*
BK = black	DK = dark
BL = blue	EM = emerald
BR = brown	LM = lemon
CL = clear	LT = light
GR = green	OL = olive
O = orange	PA = pale
R = red	
TA = tan	
V = violet	
W = white	
Y = yellow	

N(X) MIN	N(X) MAX	N(Y) MIN	N(Y) MAX	N(Z) MIN	N(Z) MAX	SIGN	2V MIN	2V MAX	COLOR OR COLOR RANGE		MINERAL NAME	SOURCE
		1.490		1.500		-	30		Y		BAYLEYITE	
1.455		1.492		1.498		-	30		Y		BAYLEYITE	SP
		1.485-	1.501	1.540-	1.545	-	5	15	Y-GR		SCHROECKINGERITE	SP
1.494-	1.501	1.498-	1.503	1.532-	1.540	+	35	42	Y-GR		LIEBIGITE	SP
1.498		1.502		1.539-	1.542	+	40		Y	GR	LIEBIGITE	
1.499		1.503		1.538		+	42		GR		URANOTHALLITE	LB
1.502		1.508		1.525		+	15		Y		RABBITTITE	SP
1.488		1.510		1.521		-	0	69	LM-Y	PA-Y	URANOSPATHITE	SP
1.465		1.518		1.540		-	40		GR		SWARTZITE	
		1.520-	1.530	1.540-	1.547	+	0		GR		ANDERSONITE	
1.489-	1.495	1.542-	1.543	1.542-	1.544	-	16		Y	GR	SCHROECKINGERITE	
1.543				1.550					LM-Y		HAIWEEITE-(MG)	
1.541		1.547		1.564		+	60		EM-GR		VOGLITE	SP
1.548				1.556					LM-Y		HAIWEEITE	
1.545		1.555		1.680		+			LT-GR		STUDTITE	SP
1.536		1.559		1.697		+	30	40	LM-Y		ZELLERITE	
		1.564							Y		RANQUILITE	
1.543-	1.549	1.564-	1.567	1.570-	1.575	-	65		Y		FURONGITE	
1.541		1.568		1.570		-	32		Y	W	PSEUDO-AUTUNITE	
1.560		1.574		1.580		-	52	62	Y		BASSETTITE	LB
		1.569-	1.583			-			Y		HYDROGEN AUTUNITE	SP
1.554-	1.565	1.570-	1.582	1.571-	1.585	-	0	65	LM-Y	LT-Y	SALEEITE	SP
1.559		1.576		1.593		-			Y		XIANGJIANGITE	
1.570				1.584		-					UNNAMED-(U-SI-O)	
1.559		1.578				-			Y		SODIUM META-AUTUNITE	
		1.580				-			GR		META-ANKOLEITE	
		1.578-	1.586			-	0	25	Y	GR	AUTUNITE	
1.564		1.582		1.584		-	0	MO	LM-Y	LT-Y	SABUGALITE	SP
1.560		1.582		1.587		-	46		PA-Y		URANOSPINITE	LB
1.573		1.583		1.583		-	70		Y	GR	THREADGOLDITE	
1.574		1.583		1.588		-			Y		URANOCIRCITE	
1.560		1.586				-	0		Y		URANOSPINITE	LB
1.550		1.588		1.590		-	40		PA-Y		COCONINOITE	
				1.588			0		R		FRITZSCHEITE	SP
1.550-	1.590	1.570-	1.610	1.576-	1.606	-	0	45	Y-GR		AUTUNITE	SP
1.582		1.592		1.592		-	SM		GR		TORBERNITE	LB
1.550-	1.612	1.567-	1.618	1.572-	1.630	-	0	62	LM-Y	GR-BR	URANOSPINITE	SP
1.578-	1.592	1.590-	1.596			-	0	10	EM-GR		TORBERNITE	SP
1.572-	1.577	1.592-	1.597	1.612-	1.620	-	72	90	GR		JOHANNITE	SP
1.480		1.601				-	0		Y		GRIMSELITE	
1.596		1.603		1.606		-	60		Y		WEEKSITE	
1.580				1.627		-	SM		GR-Y		HYDROGEN URANOSPINITE	SP
1.536-	1.620	1.570-	1.637	1.573-	1.637	-	0	50	Y		NOVACHEKITE	
1.584		1.607				-	0	20	DK-GR		META-AUTUNITE (9A)	
1.570		1.608				-			Y		ABERNATHYITE	
1.586		1.602-	1.615			-	0		GR		ZEUNERITE	
1.603		1.610		1.617		-	90		OL-GR		BASSETTITE	
1.584		1.612				-	0		Y		TROEGERITE	
1.612		1.615		1.624		+	LG		Y		ZIPPEITE	LB
1.586		1.617				-	0		Y		SODIUM URANOSPINITE	
1.591		1.619		1.621		-	0	5	Y		META-URANOSPINITE	
1.604-	1.611	1.616-	1.623			-	0	47	Y		META-URANOCIRCITE	

1.576- 1.635	1.585- 1.654		-	SM		EM-GR		METAZEUNERITE	SP
	1.620		-	0		GR		METATORBERNITE	LB
1.620	1.621	1.630	+	MO		Y		ZIPPEITE	LB
1.596- 1.604		1.637- 1.651	-	SM		LM-Y		JOLIOTITE	
1.614- 1.624		1.618- 1.632	-	0	30	EM-GR		METATORBERNITE	SP
	1.623	1.625	+	0		GR		METATORBERNITE	LB
1.610	1.623	1.623	-	10	25	Y	LT-GR	URANOCIRCITE	SP
1.620- 1.624	1.623- 1.626	1.628- 1.634	+	52	60	LM-Y		URANOPILITE	SP
	1.626							METAZELLERITE	
1.582- 1.598	1.623- 1.632	1.627- 1.638	-	SM		LM-Y		TROEGERITE	SP
1.580- 1.582	1.627- 1.630	1.630	-	0		LM-Y		TROEGERITE	LB
1.610- 1.620	1.624- 1.635		-					META-AUTUNITE (8A)	
1.595	1.632		-	0		Y		METANOVACEKITE	
1.615	1.635	1.638	-	27	37	Y		METALODEVITE	
1.609	1.637		-			Y	GR	METAHEINRICHITE	
1.611- 1.613	1.635- 1.642	1.646- 1.657	-	89		LM-Y		SKLODOWSKITE	SP
	1.640					BR-GR	BR	NINGYOITE	
1.562- 1.574		1.702- 1.726	-			GR		LERMONTOVITE	SP
1.608	1.642		-	0	22			METAKAHLERITE	
1.613- 1.645		1.645- 1.672		LG		PA-Y	W	SODIUM BOLTWOODITE	
1.617	1.644		-	0	20			METAKIRCHHEIMERITE	
1.623- 1.635	1.643- 1.651		-	0		GR		METAZEUNERITE	
1.623- 1.635	1.643- 1.651		-	0		EM-GR		ZEUNERITE	SP
1.588- 1.695	1.580- 1.720	1.587- 1.770	-	0	20	LM-Y	BR	PHOSPHURANULITE	SP
1.616	1.654	1.655	-	0	5	Y		KIVUITE	
1.655	1.655	1.662	+	SM		GR		URANOCHALCITE	LB
1.570	1.660		-	0		GR	BK	MCKELVEYITE	
1.654	1.664- 1.667	1.664- 1.667	-	SM		EM-GR		CUPROSKLODOWSKITE	
1.654- 1.665	1.664- 1.667	1.680- 1.700	-			GR		CUPROSKLODOWSKITE	SP
1.642- 1.660	1.661- 1.670	1.667- 1.676	-	32	45	Y		URANOPHANE	SP
1.620- 1.633		1.720	+			Y-GR		SHARPITE	SP
1.645- 1.650	1.662- 1.685	1.699- 1.715	-	70	84	Y	GR-Y	SODDYITE	SP
1.658- 1.676	1.668- 1.690	1.685- 1.704	-	60	65	Y		BETA-URANOPHANE	SP
1.615- 1.725	1.650- 1.720	1.635- 1.779	-	LG		Y	O	ZIPPEITE	SP
1.660- 1.670	1.670- 1.700	1.680- 1.710	-	40	70	Y		BETA-URANOPHANE	
1.658	1.685	1.690	-	40	60	GR-Y		SCHROECKINGERITE	LB
1.660	1.690	1.698	-	45		Y		BERGENITE	
1.630	1.690	1.738	-	80		Y		SODIUM ZIPPEITE	
1.668- 1.670	1.695- 1.696	1.698- 1.703	-	LG		PA-Y		BOLTWOODITE	
1.669	1.710	1.710	-	SM		Y		PHOSPHURANULITE	
1.690	1.712	1.717	-	SM		PA-Y		UNNAMED-(CA-U-SI-O)	
1.690	1.714	1.735	-	89		LM-Y		SCHOEPITE	SP
1.655	1.716	1.768	-	LG		O	Y	ZIPPEITE	
1.691	1.720	1.720	-	0		LM-Y		PHOSPHURANYLITE	LB
1.700	1.720	1.735	-			Y		SCHOEPITE	
	1.726					BR	O-BR	CALCIOURANOITE	
1.690	1.730	1.749	-	68		Y		PHURCALITE	
1.715- 1.720	1.720- 1.750	1.800	+	53		Y		RUTHERFORDINE	SP
1.715- 1.721	1.735- 1.741	1.738- 1.745	-	45	LG	Y		RENARDITE	
1.739	1.749	1.752	-	30		Y	GR-Y	PRZHEVALSKITE	SP
1.720	1.750	1.820	-			Y		MAGNESIUM ZIPPEITE	
1.700	1.750	1.770	-			Y		PARASCHOEPITE	
1.705	1.760	1.770	-	40		LM-Y		PARASCHOEPITE	SP
1.680- 1.720	1.760	1.710- 1.760	-	SM		Y		URANOPILITE	SP
1.738	1.761	1.771- 1.778	-			Y		ARSENURANYLITE	
1.762	1.760- 1.763	1.765	+	LG		Y		DEWINDTITE	SP
1.730- 1.745	1.760- 1.777	1.820- 1.840	-	MO	LG	O	TA	NICKEL ZIPPEITE	
1.732- 1.750	1.750- 1.790	1.850	+	MO		O	Y	URANOCONITE	SP
	>1.770					Y		UNNAMED-(U-NB-O)	
1.720	1.770	1.810	-			Y		ZINC ZIPPEITE	
1.747	1.779	1.840	-	MO	LG	O	TA	COBALT ZIPPEITE	
	1.780- 1.785	1.795- 1.800	-	37		Y-GR	GR-BR	MARTHOZITE	
		1.783				Y		WALPURGITE	SP
1.765- 1.770	1.780- 1.792	1.782- 1.800		80	90	DK-GR	BK	VANDENBRANDEITE	SP
	>1.789					R-BR		SEDOVITE	
1.700	1.790	1.793	-			Y		EPI-IANTHINITE	SP
1.750	1.790	1.850	+	MO		LM-Y		URACONITE	LB
>1.790	1.798	1.802	-	10	15	Y		COMPREIGNACITE	
1.720	1.798	1.805	-			Y		GUILEMINITE	
1.730	1.800	1.805	-	37		Y		BILLIETITE	
1.700	1.800	1.820- 1.840	+			GR		ROUBAULTITE	
1.570	1.805	1.851	-	42		Y		TYUYAMUNITE	
	1.810					O-BR		UNNAMED-(PB)	
1.785	1.810	1.820	-	MO		Y		UNNAMED-(MINERAL X)	SP
1.725	1.815	1.825	-	32		Y-O		BECQUERELITE	
	1.810- 1.820					GR-Y		UNNAMED-(CA)	
1.797	1.818	1.820	-	10	14	Y		URANOPHANE-(BA)	
1.735	1.820	1.830	-	30		O-Y		BECQUERELITE	LB
1.730	1.820	1.930	+			Y		IRIGINITE	
1.770	1.816- 1.827	1.863	-			Y		CALCURMOLITE	
	1.830					BK		LIANORATITE	
1.660	1.831	1.915	-	65		DK-BL		UMOHOITE-(14A)	
	1.830- 1.835							YTTROPYROCHLORE	
1.680	1.835	1.865	-	45		Y		METATYUYAMUNITE	
1.725- 1.750	1.820- 1.870	1.830- 1.880	-	30		Y-O		BECQUERELITE	SP
1.770	1.850	1.890	-			GR		DERRICKSITE	
1.780	1.850	1.860	-	60		Y-O		VANDENDRIESSCHEITE	
1.650	1.850	1.900	-	44		Y		VANURALITE	

1.850		1.860	-					PARSONSITE	
1.790- 1.870	1.815- 1.900		-			CL	LM-Y	PARSONSITE	SP
1.850	1.860		-			BR		PARSONSITE	LB
1.750	1.870	1.860	-	30		Y		BECQUERELITE	LB
1.835		1.910	+			GR		DEMESMAEKERITE	
1.820		1.930				Y		IRIGINITE	SP
1.817	1.879	2.057	+	52		BR-Y		UVANITE	LB
1.850- 1.870	1.870- 1.890		+	LG		Y-O		DUMONTITE	SP
		1.880				P-R		RAUVITE	SP
1.674- 1.770	1.855- 1.907	1.880- 1.915	-	MO		Y		STRELKINITE	
	>1.884					O		VANDENDRIESSCHEITE	SP
1.863	1.885	1.890	-	50		R-O		FOURMARIERITE	
	1.880- 1.890		-			BL-BK		RAUVITE	
1.850- 1.900	1.870- 1.910	1.950	+	35	40	O	Y	KASOLITE	SP
1.670- 1.800	1.860- 1.930	1.895- 2.110	-	36	50	Y		TYUYAMUNITE	SP
1.785	1.895	1.915	-	50		R-O		MASUYITE	
1.674	1.900	1.920	-	LG		V-BK		IANTHINITE	LB
1.670- 1.777	1.870- 1.930	1.895- 1.970	-	48	55	Y		TYUYAMUNITE	
1.882		1.915- 1.939	+	80		Y		HALLIMONDITE	
1.803	1.905	1.945	-	63		Y		WIDENMANNITE	
1.750	1.895- 1.925	1.920- 1.950	-	39	44	Y		CARNOTITE	LB
1.685	1.910	1.930	-	58		V-BK		IANTHINITE	
1.897	1.911	1.932	-	81		R-BR		METACALCIOURANOITE	
1.911- 1.916		1.920- 1.932	-	81		R-BR		BAURANOITE	
1.850	1.920	1.945	-	LG		R	Y	FOURMARIERITE	SP
1.760- 1.770	1.920- 1.940	1.940- 1.970	-	37	39	Y-GR		SENGIERITE	SP
1.710	1.920- 1.950	1.950	-	SM		Y		VANURANYLITE	
	1.945	1.975	-	48				FRANCEVILLITE	
	1.950	1.970	-	32		O		RAMEAUITE	
	1.970- 1.980					GY		MOLURANITE	
1.871	1.975	2.005	-	52		Y-GR	CL	WALPURGITE	LB
1.959	1.981	2.060	+			R-O		URANOSPHAERITE	
1.955	1.985	2.050	+	LG		O-Y		URANOSPHAERITE	LB
1.871- 1.900	1.975- 2.000	2.050	-	52	66	Y		WALPURGITE	SP
	>2.000							BETAFITE	
	>2.000		-	66		Y		CURIENITE	
	>2.000					R-BR		PYROCHLORE	
	2.010	2.060	-	55		O		AGRINIERITE	
1.770	2.010	2.090	-	53		Y		CARNOTITE	
	2.000- 2.070		-	LG		BK		RICHETITE	SP
	>2.050	>2.110				PA-Y		SCHMITTERITE	
	2.050	2.080				R-O		WOLSENDORFITE	
	>2.060	>2.120				O-R		MASUYITE	SP
2.060		2.080	-	SM		Y		CARNOTITE	LB
2.050- 2.060	2.080- 2.110	2.120- 2.150	-	LG		R-BR		CURITE	SP
1.997	2.098	2.108	-	30	50	DK-BR	O-BR	CLARKEITE	LB
	>2.100							THORUTITE	
	>2.110					Y		CLIFFORDITE	
	>2.110		-			O		MOCTEZUMITE	
	2.200					BK		SAMARSKITE	
	2.240					BR-BK		EUXENITE	
	2.248					R-BR		POLYCRASE	
	2.300					BK		BRANNERITE	
	2.328					BK		ORTHOBRANNERITE	
2.310	2.350	2.400		70	75			ASHANITE	
1.830	2.490	2.700	-	45		Y		MARGARITASITE	

References

1. Larsen E. S. Jr. and Berman H. The microscopic determination of nonopaque minerals, 2nd edition. *Bull. U.S. geol Surv.* 848, 1934, 266 p.
2. Soboleva M. V. and Pudovkina I. A. *Mineraly urana: Spranvochnik (Uranium minerals: a reference book)* (Moscow: Gosgeoltekhizdat, 1957), 408 p. (Russian text); *Mineralog. Abstr.*, **14**, 1959–60, 13–14; U.S. Atomic Energy Commission Translation Series 4487, 1961, 433 p.
3. Frondel C. Systematic mineralogy of uranium and thorium. *Bull. U.S. geol. Surv.* 1064, 1958, 400 p.
4. Weeks A. D. and Thompson M. E. Identification and occurrence of uranium and vanadium minerals from the Colorado Plateaus. *Bull. U.S. geol. Surv.* 1009B, 1954, 13–62.
5. *Powder diffraction file 1980* (Swarthmore, Pa.: Joint Committee on Powder Diffraction Standards, International Centre for Diffraction Data, 1980).

Time, crustal evolution and generation of uranium deposits

R. W. Hutchinson
Formerly Department of Geology, University of Western Ontario, London, Canada
(now Department of Geology, Colorado School of Mines, Golden, Colorado, U.S.A.)

J. D. Blackwell
Formerly Department of Geology, University of Western Ontario, London, Canada
(now Cominco, Ltd., Vancouver, British Columbia, Canada)

In the 35 years following the awakening of interest in uranium and its uses major deposits of the element have been identified in several distinctly different geological environments. Numerous geological descriptions of these major types of uranium deposits have been provided, as well as many discussions and interpretations of the processes that are involved in their genesis. It is not so well recognized, however, that these deposits and genetic processes have undergone time-dependent evolutionary changes from Archaean to Caenozoic time. The purpose of this paper is to review briefly the descriptive geology of these deposits and the current views concerning their origin, and particularly to outline the evolutionary changes that have controlled their distribution in space and through time. Especially emphasized are the evolutionary changes in source of uranium, uranium transport mechanisms and depositional processes that have shaped the different major types of uranium deposits throughout the geological record.

Classification of uranium deposits

The classification of major uranium deposits followed in this paper is slightly revised from that of McMillan[60,61] and involves a genetic division into igneous, metamorphic-anatectic, detrital and hydrogenic groups (Table 1). The igneous group includes deposits associated with alkali syenitic and granitic suites and complex zoned pegmatites; the metamorphic-anatectic group encompasses pegmatite and skarn deposits; palaeo-placer ores are the only examples of detrital deposits; the hydrogenic group encompasses deposits formed by precipitation from aqueous solutions, irrespective of whether these are marine or continental, hot and ascending or cold and descending, and includes a wide range of deposits and their generative processes, ranging from clearly syngenetic ores, such as those in black shales, to epigenetic ores, such as sandstone-hosted, unconformity-related and vein deposits.

Like any other, this classification is arbitrary and involves some overlap among the four groups. Moreover, it is genetic and therefore open to interpretation and to controversy. Nevertheless, it is simple, is based on the relationships of the various deposits to their host rocks and is consistent with current usage. It does not include some deposits, such as carbonatites, supergene cappings, duricrusts and enrichments in lignites and karsts of restricted occurrence and minor economic significance.

Geochemistry of uranium

As background for this paper it is appropriate to briefly review some fundamental aspects of uranium geochemistry that are important in ore formation. For detailed information, however, the reader is referred, in particular, to Langmuir[56] and Rich and co-workers.[74]

The two common oxidation states of uranium are U^{6+} (uranyl) and U^{4+} (uranous). Uranyl minerals occur in oxidized environments, tend to be bright yellow, red, orange or green in colour and are common in oxidized portions of uranium orebodies. Some common uranyl minerals include autunite, tyuyamunite, torbernite and uranophane. Uranous minerals occur in reduced environments, tend to be black or brown in colour and are variably metamict owing to natural radiation disordering. Important uranous minerals include uraninite, pitchblende (which is a variably crystalline, partially oxidized variant of uraninite) and coffinite.

Uranous complexes tend to be insoluble at low temperatures and at pH 4.5–7. At temperatures above 150°C uranous transport may become dominant. Depending on ligand concentrations, uranous fluoride, phosphate, sulphate and especially hydroxide compounds are important species under these conditions, but uranous carbonate complexes are not. Uranyl species are soluble over a wide range of conditions. In 'normal' groundwater, at temperatures of 25°C, uranyl fluoride complexes are dominant at pH <4, uranyl phosphates at pH 4–7.5 and uranyl di- and tricarbonate complexes at pH >7.5. Uranyl silicate complexes are probably insignificant, and at temperatures near 100°C uranyl hydroxides predominate, whereas uranyl carbonate complexes dissociate.[56]

Isomorphous substitution of uranous (U^{4+}), thorium (Th^{4+}) and some rare-earth element ions occurs as a result of similar valences and ionic radii. This is especially common at higher temperatures, occurring in common accessory minerals in felsic igneous rocks, such as zircon, monazite, allanite, uranothorite and pyrochlore. In high-temperature igneous-affiliated deposits the Th:U ratio usually exceeds 1 and commonly approaches the crustal ratio of 3.5–4.0. In metamorphic-anatectic pegmatites and skarns the ratio is commonly 1.0, though variations are observed, probably owing to the variety of processes and source rocks involved in remobilization. Because of the high solubility of uranyl compounds in oxygenated, groundwater-type systems, and the relative insolubility of Th and REE ions under similar conditions, uranium is effectively partitioned from Th and REE, resulting in subsequent deposition of hydrogenic minerals with a low thorium content and a Th:U ratio of less than 1. Sandstone-type, vein and unconformity-related deposits therefore have considerably lower Th content than granitic-hosted deposits of the igneous group. This selective uranium enrichment and separation from Th and REE provides a valuable guide to genetic evaluation and classification of uranium deposits.

The deposition of insoluble and hence preservable uranous minerals from aqueous solutions requires a process of reduction or adsorption. Important mechanisms that may reduce uranyl to uranous ionic species, causing deposition, include addition to the solution of H_2S or HS^- from sulphide minerals, degradation of organic matter or natural gas, the oxidation of ferrous to ferric iron in sulphide or reduced iron silicate minerals in adjoining rocks with concomitant reduction of U^{6+} to U^{4+} in the solution, and possibly methane or carbon dioxide reduction by the action of decaying organic matter or oxidation of graphite. These precipitating mechanisms are involved at hydrostatic redox fronts in sedimentary basins and in basement country rock where clay or ferrous iron rich units or carbonaceous matter rich rocks are present. Some minerals have a strong adsorptive capacity for uranium: these include the smectites, kandites and illites, goethite, hematite, rutile, ilmenite, leucoxene and zeolites, as well as organic compounds. Uranium precipitation can also be accomplished by bacterial fixation, rapid pressure loss accompanied by CO_2 boiling and rapid

Table 1 Classification of important uranium deposits. After McMillan[61]

Genetic type/ association	Chemical associations	Comments	Examples
IGNEOUS			
Alkali syenite or granite	U,Th,P,Zr,S,REE	Refractory minerals, uraninite or uranothorite associated with dykes and apophyses or layered intrusions	Ilímaussaq, Greenland Baker Lake, Canada
METAMORPHIC–ANATECTIC			
Pegmatite	U,Th,REE,Mo	'Simple' type, not zoned, no Ta,Be,Li,Ce, etc.; developed within high-grade metamorphic rocks; pegmatites discontinuous and frequently stratiform	Rössing, Namibia Bancroft, Canada
DETRITAL			
Palaeo-placer	U,Ti,Au,Zr,C,S	Pyritic quartz-pebble conglomerate in fluvial channel deposits, uraninite–brannerite as matrix grains; age, restriction 2900–2200 m.y.	Elliot Lake, Canada Witwatersrand, R.S.A.
HYDROGENIC			
Shales	U,Pb,Ag,Zn,Ni,Co, P,C,As	Euxenic black shale; pyritic, chert-rich; syngenetic to diagenetic metal enrichment	Ranstad, Sweden Black Sea
Volcanic rocks	U,F,P,REE,Mo,Pb, Cu,S	Associated with felsic or alkalic pyroclastic volcanism and associated volcaniclastic rocks, in subaerial environment; syngenetic to epigenetic, related to exhalative activity	Rexspar, Makkovik, Canada Lazio, Novazza, Italy
Sandstone			
Tabular	U,V,Pb,Cu,Se, Mo,C,S	Flat-lying, controlled by palaeo-stream channels, in lithic to arkosic arenites; associated with organic-rich rocks; epigenetic	Grants, U.S.A. Oklo, Gabon
Stack	U,V,Pb,Cu,Se, Mo,C,S	Similar to tabular deposits; occur at impermeable buttress-like barrier (fault or diapir); epigenetic	Mikouloungou, Gabon Bolzano, Italy
Roll-front	U,V,Pb,Cu,Se, Mo,C,S	Shallow-dipping, developed at hydrostatic redox fronts between impermeable shale beds; epigenetic	Shirley Basin and Texas Coast Plain, U.S.A.
Unconformity-related	U,Ni,Co,As,Au	Developed within palaeosol at unconformity between mid-Proterozoic quartz arenite and lower Proterozoic metasedimentary rocks; mineralization closely associated with graphitic zones, clay-rich fault breccias; epigenetic, disconformable	Athabasca Region, Canada East Alligator River, Australia
Veins	U,Ni,Co,As,Ag, Bi,Se,Pb,Cu	Fracture-fillings in fault zones, breccias; as tabular forms of variable vertical extent; wallrock alteration (hematite, chlorite, quartz); multiphase paragenesis; epigenetic	Uranium City, Canada Massif Central, France Schwartzwalder, U.S.A.

temperature or pressure decreases that result in saturation of the solution.

Crustal cycling of uranium

The average crustal abundance of uranium is approximately 2.6 ppm.[26] Oceanic crust averages 0.5 ppm, continental crust 3.0 ppm, oceanic water 1.0 ppb and fresh water 0.1 ppb, and oceanic pelagic sediments range from 1.0 to 3.0 ppm. Fresh sea-floor basalt ranges from 0.02 to 0.08 ppm and, where altered, from 0.1 to 0.2 ppm up to a maximum of 4.0 ppm.[2] Uranium in sea-floor basalt and ultramafic rocks increases systematically away from the mid-oceanic ridges apparently as a result of secondary enrichment and alteration by hydrothermal convection of weakly uraniferous sea water containing 1.0 ppb uranium in sodium and potassium chloride rich brines.[2] The enrichment in these rocks is in fractures, pillow margins and along contacts between flow breccias and sedimentary strata. The sea-floor sediment of layer 1 contains 2.0–3.0 ppm U—a concentration level that probably reflects an equilibrium between pelagic detritus and sea water.

Anatexis of subducted oceanic lithosphere generates relatively uraniferous magmas. Continental andesites range from 0.5 to 1.0 ppm uranium, whereas island-arc andesites range from 0.2 to 0.4 ppm. Enrichment in continental andesites is probably due to continental crustal contamination.[31] Fractionation of andesitic magmas can separate uranium, alkaline-earth elements and volatile-rich components, producing comagmatic granitic rocks with uranium contents of 2–5 ppm.

Common uranium-enriched intrusive rocks include peralkaline granites with 5–30 ppm, *S*-type granites and felsic volcanic rock of bimodal tholeiitic suites with 3.5–20 ppm. These igneous rocks tend to be late to post-orogenic and of high-level emplacement, characteristically in continental rift environments. Their petrogenesis is believed to be due to partial melting of water-rich pre-existing rocks—probably sediments. The resultant magmas, in addition to uranium, are relatively enriched in alkali-, alkaline-earth and halogen elements, as well as CO_2 and water.

Subsequent chemical weathering releases labile uranium from those minerals which are readily broken down under oxidizing conditions, such as mica, hornblende, uraninite and plagioclase, as well as from volcanic glass. Zircon, monazite and sphene, though commonly uraniferous, are refractory and tend to remain as detrital grains. Uranium leached from weathered rocks subsequently follows various paths: most enters the hydrological cycle and ultimately returns to the ocean. A minor portion, however, penetrates crustal rocks in groundwaters, where it is precipitated by various mechanisms to form uraniferous deposits.

Uranium deposits through geological time

There is a distinct progression through geological time in the

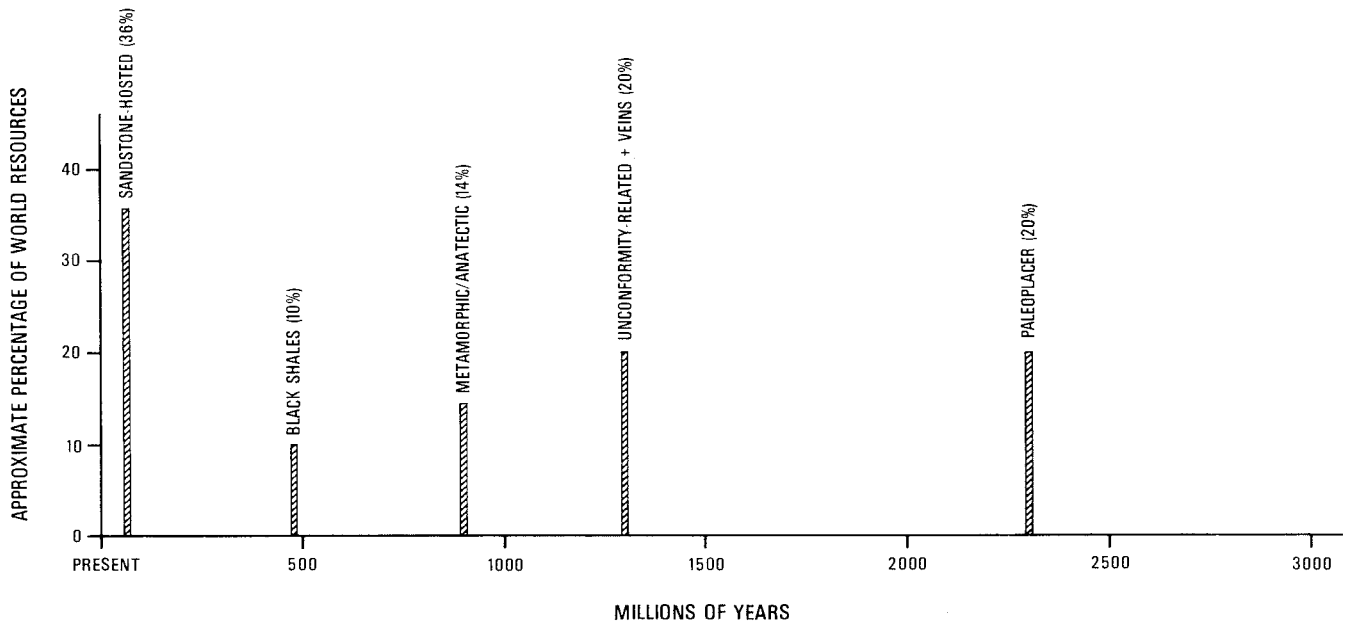

Fig. 1 Approximate global uranium reserves in major deposit types compared with age in formation (data from various sources; various minor deposits excluded)

ages and timing of first appearance of the major uranium-producing types of deposits (Fig. 1). Thus, each major type of deposit has its own distinctive geological setting and characteristics, and predominates during a distinct epoch; the palaeo-placer conglomerates in earliest Proterozoic time, the unconformity-related type in middle Proterozoic time, the anatectic pegmatites in late Proterozoic time, the marine black shales in early Palaeozoic time and the sandstone type in late Palaeozoic through Tertiary time. Most of the major types of deposit are represented in Precambrian rocks (Table 2). With the important exception of the palaeo-placer type, these deposits are replicated in Phanerozoic rocks whenever their favourable supracrustal environments reappear during the several orogenic cycles that accompany Phanerozoic plate tectonic interactions. The geological time scale utilized in this paper is indicated in Fig. 2.

Table 2 Comparison of Proterozoic and Phanerozoic uranium deposit types

Deposit type	Proterozoic examples	Phanerozoic examples
Detrital/placer	Elliot Lake, Canada/Witwatersrand, South Africa	None known
Sandstone-hosted		
Tabular	Oklo, Mounana, Gabon; Amer Lake, Canada	Grants, U.S.A.
Stack	Mikouloungou, Gabon	Bolzano, Italy; Karoo, South Africa; Shirley Basin, U.S.A.
Roll-front	None known	Shirley Basin, U.S.A.
Black shales	Wollaston Fold Belt, Canada	Ranstad, Sweden; Chattanooga Formation, U.S.A.
Anatectic pegmatites	Bancroft, Canada; Rössing, Namibia	Grandfather Mountains, U.S.A.
Veins	Uranium City, Canada	Schwartzwalder, U.S.A.; Massif Central, France
Unconformity-related	Athabasca Basin, Canada; East Alligator River, Australia	Possibly the Pitch and Pryor Mountains, U.S.A.
Volcanic-hosted	Makkovik, Canada; South Alligator River, Australia	Rexspar, Canada; McDermitt, U.S.A.; Lazio, Italy

Precambrian uranium deposits

Archaean

A negative, but nevertheless important, worldwide characteristic of uranium geology is that Archaean supracrustal rocks greater than 2500 m.y. in age are essentially devoid of uranium deposits, and even of rocks containing geochemically anomalous uranium contents. In general, supracrustal sequences, such as those of the Malene in west Greenland, which is more than 3000 m.y. in age and has remarkable lithological similarities to younger supracrustal successions, are U-deficient, containing only 0.2–1.5 ppm U.[59] The oldest significantly uraniferous rocks known are late Archaean granitic rocks of the Kenoran type at 2500 m.y. These batholithic granitic bodies frequently contain uranium concentrations in the 0.5–2.5 ppm U range and some have satellitic pegmatites that contain the uranous minerals uraninite, pyrochlore, allanite and monazite.[79] The Kenoran orogeny, though inconsequential for formation of commercially viable uranium deposits, is important because it represents the first major cycling of uranium into the sialic crust.

Early Proterozoic

Early Proterozoic time was characterized throughout the world by the initial deposition of layered supracrustal sequences composed predominantly of basal subaerial quartz-pebble conglomerate, shallow to deep water marine carbonate and clastic sedimentary rocks, iron formation and mafic volcanic or intrusive rocks. The depositional environments ranged from subaerial (fluvial) to marine, and the pre-depositional land surface was extensively peneplaned and chemically weathered,

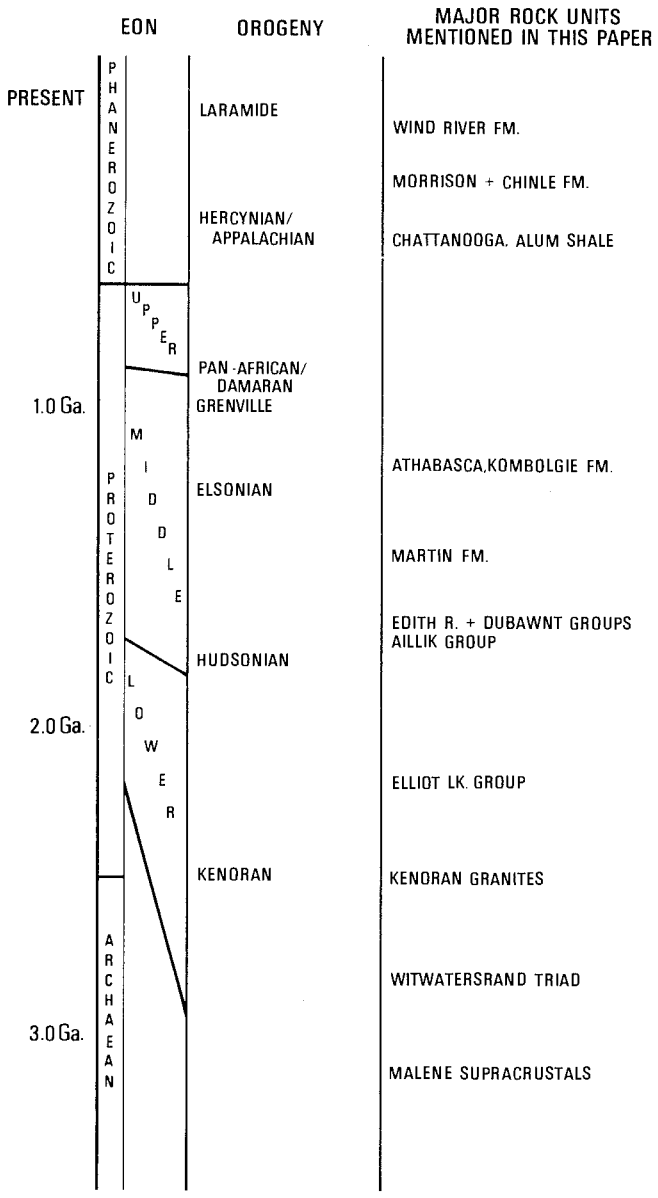

Fig. 2 Time-scale divisions utilized in this paper, orogenies and major rock units referred to in text

as evidenced by thick sericite–quartz palaeosols.[81]

The most important uranium ores are within basal quartz-pebble conglomerates with a pyritic matrix. Ages of deposition range from 2500 to 2100 m.y. for the Elliot Lake Group, Canada, to 2900 m.y. for the Dominion Reef System of the Witwatersrand Triad in South Africa. Sedimentation was diachronous and it is important that deposition of these rocks predated the transition of the earth's atmosphere from oxygen-deficient and reducing to oxygen-rich and oxidizing.[12, 13, 82] Common rock types, in addition to the pyritic quartz-pebble conglomerate, include quartz arenite and shale in thick- to thin-bedded units. Rounded pyrite clasts are ubiquitous in most of the rock types. Sedimentary features include cross-beds, scour and channel-fills, ripple and flaser bedding. Depositional environment was predominantly fluvial, with subordinate deltaic to shallow marine facies. Highest uranium content correlates positively with conglomeratic channel-fill bodies, with abundant detrital pyrite and with close packing of all clasts.[88] Detrital minerals, in addition to quartz and pyrite, include uraninite, uranothorite, zircon, monazite, gold, ilmenite, rutile and brannerite. Subordinate carbonaceous matter is commonly present, occurring as laminar masses and bedding-plane crusts of thucholite and kerogen in laminar siltstone or arenite beds. The uranium content is widely variable from 0.1% U_3O_8 at Elliot Lake, Ontario, Canada, to 0.02% U_3O_8 in the South African ores, where uranium is a by-product of gold mining. The ultimate source of the detrital uraninite is considered to have been late Archaean granitic rocks.[75]

These conglomerates and associated deposits are global in distribution. Examples include the Elliot Lake, Montgomery Lake and Sakami Lake Groups in Canada,[77, 78, 81] the Dominion Reef and Witwatersrand Systems in South Africa,[72] the Moeda Formation in Minas Gerais, Brazil, and the Serro de Corrego Formation in the Jacobina Range, Bahia, Brazil,[43] the Tarkwaian System of Ghana and the Nullagine and Green Hole Formation in Australia.[77] The Elliot Lake deposits are interesting because they are among the youngest pyritic quartz-pebble conglomerates known, and contain thucholite and mixed brannerite–rutile and ilmenite minerals, which occur downdip from the uraninite ore[88]—a feature strongly suggestive of the transport of some uranium in solution, in addition to transport of the detrital grains in suspension.

Early Proterozoic sedimentary rocks deposited after the atmosphere inverted to oxidizing conditions at about 2100 to 2200 m.y. display evidence of increasing chemical weathering of subaerial surfaces, and include the earliest true subaerial red bed strata; the quartz arenites of the Gordon Lake and Bar River Formations at the top of the Cobalt Group at Elliot Lake, Ontario, Canada,[78] or those of the Transvaal Supergroup in South Africa[77] are examples. These continental red beds comprise ferruginous lithic and arkosic arenite, siltstone and shale. The important worldwide Superior-type hematitic iron formations[50] also occur just above or within these fluvial to marine littoral sequences. Also present within these sequences are extensive thick carbonate strata and foetid pyritic black shale, both containing abundant stromatolites. Various sedimentary rocks of this age contain uranium. These include, first, extensive low-grade occurrences in marine black shale, ranging up to 150 ppm U, that also contain geochemically anomalous amounts of Mo, Pb, Ni, Co and As, and, second, important deposits hosted in arkosic arenite, such as Oklo, Mounana and Mikouloungou in the Francevillian Basin of Gabon,[22, 35] the Lianshanguan deposit in China[29] and the the occurrences at Amer Lake, Canada.[17] These arenite-hosted deposits resemble the Phanerozoic sandstone-hosted ores in their lithostratigraphic setting in sandstone units between shale interbeds, their significant hematite, carbonate and silica alteration, their common but not ubiquitous association with kerogen and their location adjacent to and updip from an impervious barrier, usually a fault contact. Moreover, their minor-element assemblage includes Cu, Pb, Ag, Mo, Au and V. No orebodies similar to the roll fronts in Phanerozoic rocks have, however, been documented.

About 1800 m.y. large-scale orogenic activity affected extensive cratonic blocks, forming regions of high-grade metamorphic rocks that underwent intense deformation and granitic plutonism. This represents a second major cycling of uranium into the sialic crust. In Canada this terrain constitutes the Churchill structural province, but similar terrains are present in Greenland, Scandinavia, the Soviet Union, Australia, China and Africa.[24, 34] This orogeny affected the older, Lower Proterozoic and Archaean rocks and led to extensive development of gneiss domes, tectonic interleaving and co-metamorphism of Archaean and Proterozoic strata, inverted metamorphic gradients and extensive anatexis. Large sections of basal Proterozoic strata apparently underwent partial melting, resulting in broad amphibolite-facies metamorphic terrains characterized by abundant *lit-par-lit* gneiss. Uranium-rich pegmatites with up to 5000 ppm U are common, particularly where the

original protoliths were early Proterozoic uraniferous shale and arenite. Examples include occurrences in the Wollaston Fold Belt, Canada,[87] and the eastern half of the Pine Creek Geosyncline, Australia.[66] These are, however, generally insufficiently rich to support mining, and anatectic pegmatite deposits of this age are not important world producers.

Uraniferous vein deposits, as in the Beaverlodge area, Saskatchewan and Port Radium, Northwest Territories, Canada, appear to be related to late orogenic fractures within these Proterozoic metamorphic terrains. These deposits are pitchblende–quartz–carbonate veins, commonly associated with a distinctive assemblage of Ni–Co–As–Ag–Bi–Pb–Se–S minerals. The minable veins in many instances are vertically extensive, occurring at fault intersections or along fault plane irregularities, localization being controlled by rock competency and associated wallrocks, many of which are graphitic metasedimentary or amphibolitic units. Wallrock alteration minerals include hematite, quartz, chlorite, dolomite or siderite and, rarely, albite. The mineral paragenesis is complex, commonly involving multiple generations of pitchblende–quartz–hematite and then arsenide–sulphide and carbonate mineral precipitation. Fluid inclusion studies indicate that formational temperatures ranged from 440 to 80°C.[86] A metamorphic genetic fluid is favoured by some writers[89] for these deposits.

Late-orogenic 'Rapakivi-like' granitic, syenitic and leucogabbroic plutons, as well as frequently preserved subaerial volcanic complexes characterized by rhyolitic, latitic to trachytic rocks, were generated late in the 1800 m.y. orogeny. Examples include rocks of the Edith River Group in northwestern Australia, the Aillik Group and intrusive rocks in Labrador in eastern Canada, and the Dubawnt Group and its associated intrusive suite in the Northwest Territories, Canada. These magmatic suites are characterized by a high content of U, Th, Zr, REE, F, H_2O and CO_2. They are thought to be related to post-orogenic tensional relaxation accompanied by late-stage intrusion of highly differentiated melts formed by anatexis at the base of the continental crust.

Uranium occurrences in the intrusive rocks include uraniferous bostonite dykes (syenite aplites), such as those at Yathkyed Lakes, Canada, ranging from 250 to 500 ppm U,[17] uraniferous zircon-, thorite- and uranothorite-rich dykes and sills adjacent to syenite/leucogabbro bodies or stocks, and lopoliths of porphyritic granite and syenite slightly enriched in uranium. Uraninite–fluorite–galena–quartz veins occur in roof pendants and contact aureoles of these intrusions.[17] Uranium occurrences in the extrusive rocks are associated with ash flow tuffs and intercalated volcaniclastic rocks. The mineralization is tabular, generally conformable and believed to have been contemporaneous with deposition of the enclosing rocks. It consists of uraninite–coffinite–brannerite associated with anomalous amounts of Th, Zr, Ti, REE, Ba, F and P. Similar mineralization has been found in exposed vent breccias. Examples include deposits at Kaipokok, in the Aillik Group of coastal Labrador,[37] occurrences in the Dubawnt Group, Northwest Territories, Canada,[17] and in the Edith River Group of the South Alligator River area, Northern Territory, Australia.[67]

Middle Proterozoic

Middle Proterozoic rocks of 1800 to 900 m.y. in age are characterized by thick marine biogenic and chemical carbonate strata, evaporites, fine-grained clastic sedimentary rocks, and extensive, thick subaerial tholeiitic basalts, and quartz arenite and conglomerate. Ophiolitic and calc-alkaline volcanic rocks are absent in sequences of this age.[39,48]

The most important uranium deposits in rocks of this age are those of the unconformity-related type. These deposits are found principally in the East Alligator River area, N.T., Australia,[45] and the Athabasca Region, Saskatchewan, Canada.[47] They are located at or within a few tens of metres of a major unconformity where relatively flat-lying, unmetamorphosed, kaolin-cemented Middle Proterozoic quartz arenite overlies deformed older Early Proterozoic metasedimentary rocks. The pre-arenite palaeo-surface is commonly marked by a thick illitic-kaolinitic-hematitic regolith up to 30 m thick. Mineralized zones are characterized by alteration to phyllosilicate minerals, including kaolinite, illite, dickite and septechlorite, zones of repeated brecciation owing to fault reactivation or solution collapse, irregular bodies of variably reduced or oxidized rock and multiple generations of pitchblende deposition. Ore minerals include uraninite and coffinite, commonly associated with Ni–Co–As minerals. Indicated temperatures of formation are 260 to 60°C.[20] The deposits are all exceptionally high-grade, ranging from 0.5 to 3% U_3O_8. The overlying quartz arenites are commonly 1650 to 1300 m.y. old,[5] whereas measured U–Pb ages of mineralization range from 1650 to 1200 m.y., with still younger ages recorded in remobilized or second generation pitchblende.[21,30] The oldest ages are obtained from high-grade pitchblende within the regolith where this is developed on early Proterozoic graphitic metapelitic or calc-silicate rocks, whereas much younger pitchblende is present in the immediately overlying Middle Proterozoic quartz arenite. There are two current genetic explanations for these deposits: one proposes formation via the passage along the unconformity of uranium-charged 'diagenetic-hydrothermal' groundwaters, which deposited uranium adjacent to reducing rocks in the subsurface[47,92] and the second considers these deposits to have formed before arenite deposition through supergene enrichment processes that accompanied intense weathering of the Aphebian palaeo-surface.[21,55,61] In the latter case the younger pitchblende within the arenite is explained as a later, upward remobilization from the older, deeper deposit.

Late Proterozoic

Late Proterozoic rocks from 900 to 570 m.y. old, though similar in lithology and setting to those of Middle Proterozoic age, contain few uranium deposits. Thick, subaerially deposited arenite of this age is common. Examples are those of the Adelaide System in Australia, the Borden Basin on Baffin Island, Northwest Territories, Canada,[52] or the Thule Basin in Greenland,[23] which are virtually identical to Middle Proterozoic sequences that contain the unconformity-type uranium deposits. Yet no uranium occurrences are known within rocks of this age. A possible significant exception may be the Roxby Downs Cu–Au–U deposit in South Australia, for which no data are yet available. Late Proterozoic redistribution of uranium from and around pre-existing uranium deposits of the unconformity and vein types is well documented in the East Alligator River area, N.T., Australia,[46] and the Athabasca region, Saskatchewan, Canada,[47] which strongly suggests that conditions were favourable for uranium transport in solution. Yet the lack of new uranium deposits within lithologically favourable, unmetamorphosed rocks of this age remains an enigma.

Metamorphic terrains related to the 900 to 1000 m.y. Grenville, Damaran and Svecokarelian[24,34] orogenies contain important anatectic-pegmatitic uranium deposits. Like those formed in the late Proterozoic orogeny about 1800 m.y. ago, these orogenies and deposits represent a third major cycling of uranium into the sialic crust by metamorphic reworking of older uraniferous supracrustal rocks, and generation of uraniferous granitic melts. Pegmatites of this age in places constitute important uranium reserves, as in the Bancroft district, Ontario, Canada,[79] and at Rössing, Namibia.[6] Minable pegmatites occur as tabular, steeply dipping, anastomosing dyke

complexes, characterized by homogeneous internal structure and a simple quartz–microcline–albite–zircon–uraninite–magnetite mineral assemblage. Rare-earth element, CO_2, F and sulphate concentrations may be high, but such elements as beryllium, lithium and caesium, which are common in zoned, rare-element pegmatites, are absent.[9] Grades range from 0.08 to 0.1% U_3O_8 and 0.1 to 1% ThO_2. The uranium deposits at Lagao Real, Bahia, Brazil,[32,36] are uraniferous metamorphic albitites related to alkali metasomatism accompanying Pan African aged (800–700 m.y.) thrusting and metamorphism. Mineralization is the result of fluid circulation in Archaean and Early Proterozoic rocks accompanying this orogeny.[32]

Phanerozoic uranium deposits

Palaeozoic

Early Palaeozoic rocks, 650 to 345 m.y. old, are widely variable in lithofacies, and represent markedly different tectono-stratigraphic depositional environments. They include obducted ophiolitic crustal sequences, volcanic island arc, fore-arc trench and back-arc basin successions, and thick sections of shelf-deposited carbonate and clastic sedimentary rocks. Large volumes of continental subaerial rocks, including arenaceous clastic sedimentary and volcanic rocks, are generally rare and restricted to Cambrian and Devonian strata.

Few important uranium deposits are associated with rocks of this age. Most notable are the euxenic black shales, such as the Alum Shale of Sweden,[7] and the Chattanooga Shale of the mid-continent, U.S.A.[14] Deposits of this type constitute unmined, very large-tonnage, but low-grade, resources with 150–450 ppm U associated with siliceous, pyritic black shale. Ages are from Cambrian to Devonian. The uraniferous strata range up to several tens of metres in thickness and many tens of kilometres in lateral extent. The uranium content varies inversely with the clastic sedimentary component of the rock, so clastic sediment-poor but chert-rich units have the highest content. The uranium was probably incorporated into the shale during deposition, possibly fixed by reducing bacteria, organo-metallic compounds or by adsorption on clay minerals.

Minor uranium occurs in the Devonian Old Red Sandstone in the British Isles.[70] It is restricted to reduced, pyritic organic matter rich layers, and the occurrences are tabular, thin and erratic in both uranium content and distribution. The uranium content is directly correlative with local reduced lenses rich in plant debris.

Late Palaeozoic sequences, 345 to 220 m.y. old, contain extensive, shallow marine carbonate and evaporite as well as subaerial arenite, coal and shale, some deep-water clastic sedimentary rocks and late orogenic felsic volcanic and plutonic rocks. This was a time of formation of important uranium deposits, particularly in southern and eastern Europe.[83] Here Hercynian plutonism was closely related to the generation of numerous 'hydrothermal' veins in the Bohemian, Armorican and Central Massifs, and in the Iberian Penisula.[15,84] Hercynian plutonism represents yet another recycling of uranium into the sialic crust, albeit on a smaller more restricted scale than the earlier Precambrian cycles. The veins are pitchblende-bearing and also contain quartz, fluorite, Pb–Cu–Fe sulphides and minor arsenopyrite and bismuthinite. The veins are tabular, extend only to shallow depths, and are restricted to fault breccias, fault intersections and areas of intense alteration, both within the plutons and adjacent country rock. The altered wallrocks exhibit silica depletion, alkali metasomatism with generation of episyenitic composition, and pervasive hematization. Indicated temperatures of the ore fluids range from 150 to 350°C. The host granitic rocks are *S*-type, considered to have been derived from partial melting of Precambrian rock during Acadian to Hercynian orogenies.[15,57,84] Ore formation is considered to have resulted from a combination of volatile-rich anatectic melt development and evolved metamorphic fluids.

Permo-Carboniferous rocks in Europe, North America, South Africa and Australia contain sandstone- and volcanic-hosted uranium deposits. Sandstone-hosted deposits commonly, though not always, occur in arkosic to lithic arenite with interbedded shale, deposited under subaerial fluvial and lacustrine conditions in post-Hercynian basins. The deposits contain pitchblende and coffinite, with associated pyrite, galena, chalcocite and molybdenite, and form restricted, greenish-grey sandstone lenses that contain abundant plant detritus and kerogen. Examples are the Deer Lake Basin, Newfoundland, Canada,[51] Bolzano in Italy[62] and Lodève in France.[84] Volcanic-hosted uranium occurrences are associated with Mississippian and Permian subaerial dacitic to rhyolitic ash flow tuff, flows and volcaniclastic sedimentary rocks. The uranium minerals include pitchblende and brannerite, with associated fluorite, quartz, barite, molybdenite, sphalerite and galena. Favourable host rocks are coarse breccias, agglomerate and interflow sedimentary strata, uranium mineralization forming irregular, stratiform lenses adjacent to fault zones and disconformities. Examples include the Rexspar deposit, British Columbia, Canada,[71] the Maureen and Ben Lomond deposits, Queensland, Australia,[3,69] and Novazza, northern Italy.[18]

Mesozoic and Caenozoic

Mesozoic and Caenozoic rocks include a variety of supracrustal and plutonic types similar to most Palaeozoic suites. Of particular interest for uranium deposits are the thick intermontane and rift-associated red bed clastic sedimentary sequences of the American Cordillera, Japan and the Middle East, the Laramide intrusions of the Cordillera and the subaerial, felsic volcanic rocks in the western United States.

Mesozoic and Tertiary continental red bed arenites host some of the world's most important uranium deposits. The host rocks include lithic arenite and volcaniclastic rock, shale and subordinate felsic tuff, deposited in fluvial and lacustrine environments. These rocks were laid down in post-orogenic intermontane basins and intracratonic rifts. Three sub-types of sandstone-hosted deposits are recognized. Peneconcordant or tabular sub-types (Fig. 3(*a*)) are flat-lying, tabular bodies that frequently occupy organic trash-filled palaeo-stream channels. They form large orebodies and, in addition to pitchblende and coffinite, contain geochemically anomalous amounts of V, Ca, Se, Cu and Pb. Examples include the deposits of the Grants district, New Mexico, U.S.A., in the Jurassic Morrison Formation,[41,64] as well as others on the Colorado Plateau of the western United States,[1] the Blizzard deposit in Eocene beds of south-central British Columbia, Canada,[11,68] and Tono mine in Miocene strata in Japan.[54] The origin of these deposits is ascribed to *in-situ* leaching of uranium by oxygenated groundwaters from detrital minerals and volcanic glass in the arenite host, followed by groundwater transport downdip along palaeo-stream channels, and precipitation where reducing conditions envelop pockets of decaying organic matter in the rocks. Deposits of the stack sub-type (Fig. 3(*b*)) are similar to tabular deposits, but are stacked *en échelon* within interbedded sandstone–shale sequences near an impermeable, buttress-like structure such as a fault zone or a salt diapir. Examples include *some* of the Gulf Coast deposits in the Tertiary rocks of Texas,[28] some in the Jurassic Morrison Formation in the Grants district, New Mexico, and those of the Uravan district, also in the Morrison Formation in Colorado. Deposits of the roll-front sub-type are shallow-dipping, ribbon-like orebodies, crescent-shaped in cross-section, that occur within sandstone beds between shale layers. The mineralization is localized at the boundary between oxidized (updip) and

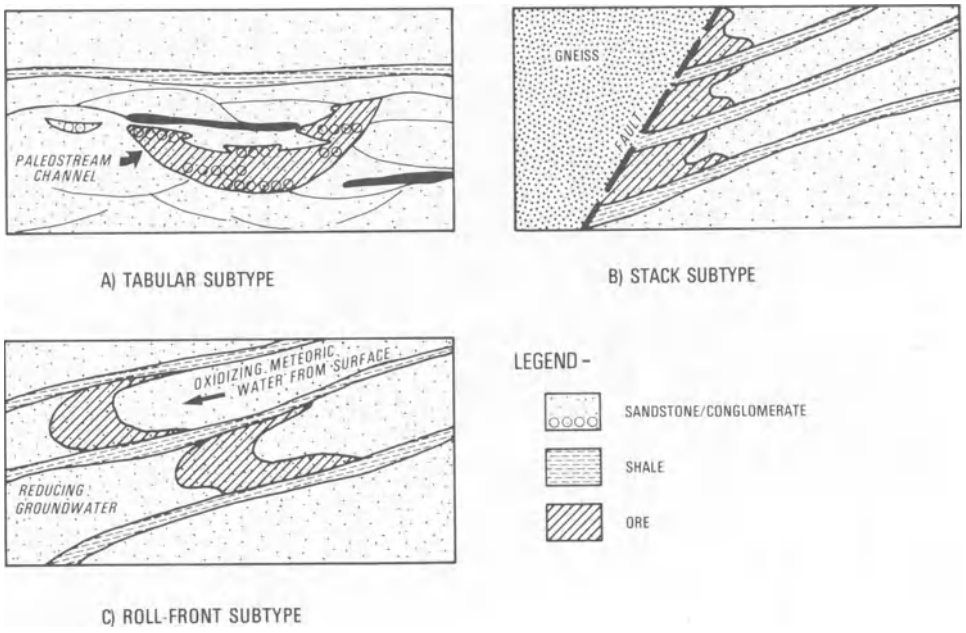

Fig. 3 Sandstone-type uranium deposits

reduced (downdip) sandstone, and consists of pitchblende and coffinite, with associated pyrite, hematite and calcite, and geochemically anomalous amounts of V, Ni, Co, As, Ag, Cu, Se and Mo. Organic matter is ubiquitous in the rocks. Roll-front deposits (Fig. 3(*c*)) are attributed to the leaching of uranium *in situ* from volcanic glass and detrital minerals in the sandstone, and its downdip transport by oxidized groundwater flow.[1] Uranium precipitation occurs at a redox front developed through hydrostatic equilibrium between the moving oxygenated, uraniferous groundwater and deeper reduced formational waters. Examples include the many deposits in the Tertiary Wind River Formation of the Wyoming intermontane basins,[19,44,73] in Tertiary strata of the Gulf Coastal Plain in Texas[33] and in the Triassic Chinle and Jurassic Morrison Formations near Moab, Utah and Uravan, Colorado, respectively,[63] all in the United States.

Coeval with much of the sandstone deposition in the western United States was extensive Laramide felsic plutonism at about 30 m.y. and prolonged, post-orogenic subaerial, but felsic-dominated bimodal volcanism. These igneous suites represent still another important and most recent recycling of uranium into the sialic crust. Detritus from these suites is a significant component in the Tertiary and younger arenites, which host many sandstone-type uranium deposits, and detrital uraniferous minerals and volcanic glass probably are the source of labile uranium available in the rocks themselves for redistribution and concentration into these deposits. In addition, extrusive and associated intrusive rocks are locally important uranium hosts. Tertiary rhyolitic centres, such as the McDermitt Caldera in Oregon, U.S.A., contain important low-grade ($<0.1\%$ U_3O_8) uranium occurrences. The uranium occurs in large, flat-lying tabular bodies of altered volcaniclastic rock and ash flows that flank the caldera. The mineralization is accompanied by silicification and development of smectite-rich phyllosilicate alteration, and carries geochemically anomalous amounts of Hg, Be and F. The altered and mineralized zones flank late-stage radial faults formed during caldera resurgence, and probably resulted from fumarolic discharge during cooling of the volcanic pile and volatile degassing.[80,85,90] Other examples of comparable deposits include Sierra de Peña Blanca in Mexico[25,40] and Spor Mountain in Utah.[8,58]

Two small but high-grade deposits in the western United States are possibly young examples of the unconformity-related type. Disseminated pitchblende mineralization at Pitch mine, Colorado, is hosted in folded and brecciated Mississippian dolomite, shale, sandstone and coal, which is in fault contact with Precambrian gneiss.[65] The Precambrian gneiss is anomalously enriched in uranium, and a Mesozoic or Caenozoic age of mineralization in the Mississippian host rocks, formed by downward percolation of uraniferous groundwater from the adjacent Precambrian terrain, is inferred.[27,50] Mineralization in the Pryor Mountains region, Montana, is hosted in karsts developed with the Mississippian Madison limestone[76] and consists of uraninite–tyuyamunite grading up to 7% U_3O_8 associated with clay minerals and silicified collapse breccias.[53] A Caenozoic age of mineralization, under conditions similar to those of Pitch mine, is favoured.

Interpretation and discussion

In general, major uranium accumulations occur in rocks of Lower and Middle Proterozoic, Permo-Carboniferous, Jurassic–Triassic and Tertiary ages, but are noticeably absent from Archaean rocks. Except for the marine black carbonaceous shales, there is a marked paucity of uranium occurrences of any kind within marine Phanerozoic sequences, particularly in mid-ocean ridge tholeiitic, and volcanic arc calc-alkaline igneous suites and their associated marine epiclastic rocks. There are strong lithologic and tectonic affiliations of uranium with major episodes of crustal tholeiitic to alkaline igneous activity in continental extensional settings. These were accompanied by uplift, development of profound subaerial unconformities marked by peneplanation and intense chemical weathering of pre-existing terrains, and deposition of clastic red bed arenite. There is a strong suggestion in the geological record that uranium underwent periodic, successive, cycles of enrichment that accompanied orogenic magmatism. During these cycles syngenetic, primary deposits of the igneous and metamorphic-anatectic groups were formed. Subsequently, during erosional degradation of these terrains, new secondary uranium deposits of the detrital and hydrogenic groups were formed in post-orogenic basins. These deposits reflect the evolutionary stages in the development of various uranium transporting, complexing and precipitating mechanisms.

Archaean supracrustal rocks are lacking in uranium occurrences, except for minor occurrences associated with late Archaean granitic rocks. Their absence within Archaean supracrustal rocks may appear enigmatic in view of the reducing nature of the Archaean atmosphere–hydrosphere and the many

reduced iron formations and massive base-metal sulphide deposits[50] in these rocks. All of these depositional environments should have precipitated any uranium present from the generative hydrothermal systems. Conversely, however, these systems were themselves strongly reduced,[49] precluding significant aqueous solution transport of uranium with common complexing agents. Thus, it is likely that uranium was simply not mobilized in and transported by these systems under Archaean supracrustal conditions. Another important contributing factor may be the lack of an earlier, pre-enriched protolith or source rock, insofar as the late Archaean orogeny represents the first cycling of uranium into the crust. It is unlikely that the earth's crust and mantle had undergone significant fractionation with respect to uranium prior to the late Archaean orogeny. The generation of weakly uraniferous granites in late Archaean time may mark the initial establishment of a thick sialic crust through development of large volumes of felsic magmas by partial melting of water-rich Archaean supracrustal rocks.[48,91]

Early Proterozoic rocks, deposited before oxygenation of the earth's atmosphere about 2200 m.y. ago, which host the detrital uraninite–gold–pyrite quartz-pebble conglomerate deposits, are global in distribution, constituting a 600 m.y. diachronous lithostratigraphic marker at the base of the Proterozoic succession. Their unique lithology of rounded, clastic uraninite, gold and pyrite grains in a compositionally mature conglomerate bespeaks special depositional conditions and provenance. The uraninite and quartz clasts are considered to have been derived from denudation of adjacent late Archaean granitic terrain. Preservation during weathering and detrital transport of both pyrite and uraninite are ascribed to the reducing nature of the Early Proterozoic atmosphere. The pyrite and gold clasts are classically considered to have been derived by weathering from pyritic lode gold sources in adjacent Archaean supracrustal greenstone belts. This view is conjectural, no definite proof having been presented.

As a possible alternative it is suggested that gold and pyrite may be endogenous to these Proterozoic sequences rather than exogenous. They may have been derived internally from reworking of original auriferous pyritic chert strata in a shallow, periodically regressive–transgressive, littoral fluviodeltaic depositional environment. The original auriferous pyritic strata may have formed in these Early Proterozoic sequences by exhalative hydrothermal discharge into the depository. This fumarolic activity may have been spatially and genetically associated with the thick, mafic intrusive–extrusive activity that so commonly accompanied this distinctive Early Proterozoic sedimentation, and also with the tensional rift faulting that controlled basin morphology.[10,72] There is indirect, circumstantial evidence to support this possibility. Minor, thin auriferous pyritic strata are mined in the Witwatersrand deposits, along with the much more important 'conglomerate' and 'hydrocarbon reefs'. In addition, a magnetite-rich, Algoman-type iron formation, which is probably exhalative,[42,50] forms the 'contorted bed'—an important stratigraphic marker in the Hospital Hill Series of the Witwatersrand System. This hypothesis also would aid in explaining the coarse, but mature and well-rounded, nature of many pyrite clasts: although preserved during reducing weathering conditions, detrital pyrite is brittle and would not probably survive prolonged fluvial transport to form these clasts. Local endogenous auriferous pyrite beds may represent a more probable source, and could have been 'detritalized' in the high-energy depositional environment described above.

With the gradual shift to increased oxygenation of the earth's atmosphere and hydrosphere, the detrital palaeo-conglomerate deposits became 'extinct' as a result of termination of the conditions essential to their generation and preservation. As was mentioned above, the Elliot Lake deposits of Ontario, Canada, are among the youngest of this type and they contain mixed brannerite–leucoxene downdip from the detrital uraninite ores, as well as thucholite in poorly developed algal mats. These minerals and relationships suggest some secondary, post-depositional solution transport of uranyl complexes in formational waters, possibly during sediment diagenesis and burial, which formed second-generation uranium minerals where suitable detrital collector grains were present. Although the overall detrital origin of these ores is not in dispute, it seems probable that burial diagenesis of the slightly younger Canadian ores spanned the period of atmospheric shift from reducing to oxidizing conditions, thus imparting some hydrogenic characteristics to the mainly detrital deposits.

Early Proterozoic rocks deposited after the atmospheric-hydrospheric change from reducing to oxidizing conditions reflect the major change from uranium deposits of the detrital group to those of the hydrogenic group, as well as the development of uranium reservoirs in oxygenated sea water, the appearance of new complexing and transporting agents, and the increasing importance in uranium precipitation of both inorganic and organic reductants, and of adsorbing clay and Fe–Ti hydroxide minerals. The presence of uraniferous black shale in shallow- to deep-water marine carbonate and clastic sections marks the development of the oceanic reservoirs, the elevated uranium content of which was presumably maintained by increased concentration of uranyl-complexing bicarbonate and sulphate ions. These shales also suggest that sea-water composition toward the end of Early Proterozoic time was similar to that of the present, particularly with respect to carbonate compensation depths controlled by water depth, Eh, pH and microbial activity.

Sandstone-hosted uranium deposits formed toward the end of Early Proterozoic time exhibit host rock and geochemical associations similar to those in Permo-Carboniferous, Mesozoic and Tertiary sandstones. An important difference is the absence in Proterozoic deposits of the roll-front sub-type on any scale. Roll-front deposits apparently represent dynamic, hydrologic redox fronts, locally enriched in uranium, that are migrating in subsurface groundwaters through porous continental sandstones. Perhaps their absence in older strata is simply due to the great age of these rocks, which has permitted ultimate stabilization and fixation by reduction of migratory uranium. Although roll fronts may have developed in Proterozoic sandstones, they have subsequently been stabilized, or modified through time by renewed hydrogenic remobilization into their present configurations. Like the other sandstone-hosted blanket and stack sub-types in Phanerozoic rocks, they represent remnants or variants somehow preserved by 'insulation' from renewed hydrological remobilization. This may be due to reduced permeability of their host rocks or some other barrier to groundwater flow, to simple lack of groundwater supply, or to the local abundance of carbonaceous matter, pyrite or clay minerals that fix the uranium in reduced uranous form.

The 1800 m.y. orogenic event at the end of Early Proterozoic time was the second recycling of uranium into the sialic crust. This involved generation of uranium-enriched granitic and syenitic intrusive and associated volcanic rocks, and the development of uraniferous anatectic pegmatites in related high metamorphic grade gneissic terrains. In comparison with the 2500 m.y. old Archaean granitic rocks, which introduced relatively minor quantities of uranium into the upper crust, this second major recycling introduced much larger amounts, probably by reworking older preconcentrations in Early Proterozoic arenite and black shale. It is important in this regard that all known exposures of Early Proterozoic supracrustal rock contain occurrences of uranium mineralization.

The numerous Early to Middle Proterozoic uranium occurrences in subaerial alkalic volcanic rocks are the oldest of this type. They are similar to others in Permo-Carboniferous and Tertiary rocks. All are related to post-orogenic, intracratonic rift-associated igneous activity. These occurrences are currently attributed to volcanogenic exhalative activity,[17,61,83] but there are significant problems with this interpretation. First, the host volcanic rocks are subaerial and commonly oxidized, with intense hematitic and argillic alteration owing to the passage of groundwaters. Secondly, the occurrences are strata-bound but not stratiform. They may represent some form of hydrogenic enrichment in which uranium was leached and transported within the volcanic sequence and precipitated at reducing sites of fumarolic discharge.

Early to Middle Proterozoic uranium veins, such as those at Uranium City, Saskatchewan, and Port Radium, N.W.T., Canada, have been among the world's most important producing vein-type deposits. Current genetic hypotheses strongly favour deposition from an evolved metamorphic fluid. Again, however, there are problems in this interpretation. First, the stratigraphic succession in each area records several depositional hiatuses, with several periods of subaerial, continental sedimentation and subaerial weathering in rocks younger than those that host the veins, but roughly coeval with the age of initial mineralization. Examples are the Martin and Athabasca Formations in the Uranium City area, Saskatchewan, Canada. Secondly, it is questionable whether metamorphic fluids would have been sufficiently alkaline and oxygenated to transport uranyl compounds, particularly the favoured bicarbonate complexes. If not, uranous complexes, transported at low pH and elevated temperatures, are implicated. Yet these reduced fluids are incompatible with the prominent hematization of the wallrocks. Alternatively, these deposits may be of hydrogenic supergene origin, formed by downward percolation of oxidized, uraniferous groundwater during the pre-Martin and pre-Athabascan weathering hiatuses. Precipitation occurred by reduction near graphitic and pyritic metasedimentary rocks and amphibolites.

Middle Proterozoic rocks contain the important unconformity-related uranium deposits. It is interesting that these are essentially restricted to a profound, deeply weathered unconformity surface of this age. Similar unconformities of younger age are not known to host deposits of this type, with a few rare exceptions—such as the Caenozoic age deposits in the Pryor Mountains, Wyoming, and Pitch mine, Colorado. A simple hydrogenic supergene origin is favoured. The minor- and trace-element assemblage is compatible with that of other hydrogenic deposits, such as the sandstone-hosted types. Repeated post-depositional resolution and precipitation probably account for the younger radiometric ages of remobilized mineralization in the overlying quartz arenite.[21] Phyllosilicate and other uranium-adsorbing minerals were probably important in concentrating uranium.[38,56] The regolith beneath the quartz arenites, such as the Kombolgie Formation in Australia, the Athabasca, Thelon and Hornby Bay Formations in Saskatchewan and the Northwest Territories in Canada, are unique both in extent and degree of development. This regolith probably represents a prolonged period of lateritization, thus accounting for these well-developed palaeosols.[21]

The abrupt changes in depositional environments, styles and tectonic setting of Middle and Late Proterozoic rocks and their associated uranium deposits are significant evidence of extensive changes in supracrustal processes. Calc-alkaline volcanic and ophiolitic oceanic crustal suites are lacking in strata of this age.[39,48,50] Rock sequences are dominated by shallow marine to fluvial arenaceous clastic and carbonate sedimentary strata, and subaerial tholeiitic basalt and related shallow intrusions, all deposited in passively subsiding, rift-controlled basins. Orogenic belts of this age are rare. It is likely that this period of earth history was characterized by rift tectonics, stable cratons undergoing intense chemical weathering and peneplanation. Although the exact mechanisms are not understood, the apparent absence of compression-generated, subduction-related sequences and obducted ophiolites, together with the dominance of rift-controlled and stable platform sedimentary sequences, supports the theory that the Middle to Upper Proterozoic was a period of global expansion.[48,50] In addition to the important and distinctive unconformity-related uranium deposits, clastic-hosted copper and massive lead–zinc–silver sulphide deposits are best developed and distinctive in rocks of this age, whereas marine volcanic-hosted lode gold and massive base-metal sulphide deposits are lacking.[48,50] These relationships can also be attributed to widespread tensional tectonics.

Metamorphic gneissic terrains related to widespread late Proterozoic orogenesis about 1000 to 700 m.y. ago contain numerous uraniferous anatectic pegmatites and granitic stocks. This orogeny marks the third recycling of uranium into the sialic crust and, as in its predecessors, uranium redistribution and concentration resulted from partial melting during orogenesis of pre-existing, uraniferous supracrustal rocks. Consequently, the most important deposits of the igneous and metamorphic-anatectic groups, such as those of Bancroft, Ontario, Canada, Rössing, Namibia, or Lagao Real, Brazil, are in rocks formed during this third orogenic recycling of uranium.

Lower Palaeozoic stratigraphy and palaeontology reveal two features that were probably important in concentrating uranium in rocks of this age—an abundance of marine carbonate rocks and rapid proliferation and diversification of life forms. The former, combined with continual addition of uranium into the oceanic reservoir by continental drainage, suggests that the ocean during this time contained abundant uranium, probably as uranyl sodic bicarbonate compounds. The worldwide occurrence of uraniferous black shale of this age[4] probably reflects this condition. Biochemical transport and reduction are important causes of uranium concentration and precipitation, and the restriction of these black shales to anaerobic organic oozes deposited in moderate to deep water and isolated basins probably reflects the profusion of biological activity in the near-surface phototropic zones of the early Palaeozoic seas. Conversely, the paucity of pre-Devonian terrestrial life severely restricted uranium precipitation owing to biogenic activity in pre-Devonian continental clastic sedimentary rocks.

Upper Palaeozoic rocks provide evidence of a fourth recycling of uranium into the sialic crust during the Taconian and Hercynian orogenies. Hercynian veins and volcanic-hosted deposits are directly related to this event. Permo-Carboniferous sandstone-hosted deposits were formed during post-Hercynian denudation and weathering of the uranium-enriched, late orogenic Hercynian plutonic and extrusive suites. Uranium deposition occurred in the fluvial, continental clastic sedimentary rocks deposited at this time, and precipitation was in structural traps and organic-rich strata. With the notable exception of the unconformity-related type, the uranium deposits, tectonics and stratigraphy all are similar to those that followed the Early Proterozoic 1800 m.y. orogeny and constitute a repetition of these conditions, though on a reduced scale of both time and space.

Mesozoic and Caenozoic strata, especially in the western United States, contain many important sandstone-hosted uranium deposits of blanket, stack and roll-front sub-types, with fewer volcanic-hosted types. As may be expected, the dynamic, migrating roll-front sub-type predominates in the youngest Tertiary rocks of the Wyoming basins, where final fixation of the migrating uranium is yet to be attained. In con-

trast, the more stabilized blanket and stack sub-types are more abundant in older Mesozoic rocks of the Colorado Plateau. The latter were generated periodically during Mesozoic time following successive local uplifts, such as the Antler, Uncompaghre, and Zuni, again followed by denudation, weathering, continental clastic sedimentation and uraniferous groundwater flow. The Laramide orogeny and uplift, about 30 m.y. ago, also generated alkalic and felsic intrusive and extrusive rocks. It represents yet another, though more local and most recent, recycling of uranium into the sialic crust. It ultimately shed important uraniferous clastic detritus into the post-orogenic intermontane basin that contains the epigenetic roll-front sub-type deposits. In post-Laramide Caenozoic rocks extreme uranium mobility is evident even today by metastable to actively migrating uranium deposits, such as those in the Latium region, Italy, and some of the Wyoming roll-front sub-types.

Summary and conclusions

Two broad processes, orogenesis accompanied by granitic plutonism and surficial weathering, have combined through geological time in varying manner and degree to form the world's major uranium deposits. Orogenesis together with accompanying granitic plutonism and anatexis of pre-existing rocks has produced primary, though economically less important, granitic, syenitic, related volcanic and pegmatitic uranium deposits of the igneous and metamorphic-anatectic groups. Variations among these deposits are due to various metasomatic or crystallization differentiation processes. Weathering has produced larger, economically more important, secondary deposits of the detrital and hydrogenic groups, by surficial degradation of sialic crust followed by uranium transport and precipitation under widely varying conditions. Uranium deposits fall into both syn-depositional and diagenetic to epigenetic categories: those of the igneous, metamorphic-anatectic and detrital groups, as well as the marine black shales of the hydrogenic group, were formed essentially coevally with their host rocks, but the others of the hydrogenic group are diagenetic-epigenetic, formed after deposition of their host rocks.

Uranium deposits exhibit marked evolutionary changes in geological setting and characteristics through geological time. Palaeo-placer conglomerate deposits are restricted to earliest Proterozoic rocks, deposits of the unconformity-related type are associated principally with Middle Proterozoic strata, anatectic pegmatites are most important in late Proterozoic gneissic terrains, the uraniferous marine black shales are widespread in the Lower Palaeozoic succession, and sandstone-hosted deposits are most common in Mesozoic and Caenozoic rocks. The changes that resulted in the development of these different types of deposit can be usefully summarized by considering the particular evolutionary changes that occurred through time in the fundamental aspects of deposit genesis, including sources, mobilization, transport and deposition of uranium.

Geochemical abundance data indicate that uranium is enriched in ensialic environments, particularly in felsic and alkalic granitic and syenitic igneous rocks and in shales. These rocks are sometimes sufficiently enriched to be minable. Normally, however, they constitute important sub-marginal grade but pre-enriched sources of uranium for both of the broad generative processes. Significantly uranium-enriched felsic igneous or metamorphic rocks and shales are rare in Archaean rocks, and apparently had not evolved at that time. Absence of these source rocks is one important factor in explaining the lack of any significant uranium deposits.

Each of three successive, major, worldwide Precambrian orogenies about 2500, 1800 and 1000 m.y. ago recycled uranium and thorium by magmatic-anatectic reworking of rocks of its predecessors and their erosional products. Consequently, the abundance and uranium content of these source rocks has increased through time, and the best deposits of the igneous and anatectic-metamorphic groups occur in rocks formed by the third orogeny about 1000 m.y. ago. Still younger, Phanerozoic orogenies have generated similar uraniferous rocks and deposits, but these are smaller and less important, though diverse, widespread and of local economic significance.

Important uranium-mobilizing processes were plutonic and dominated by high-temperature fluids for the primary deposits of the igneous and anatectic-metamorphic groups. Each major orogeny, Precambrian and Phanerozoic, was followed by a period of uplift, erosion and weathering. These released and thereby mobilized uranium by surficial low-temperature aqueous processes from these pre-enriched source rocks for subsequent transport to form secondary successor deposits of the detrital and hydrogenic groups.

Uranium transport for deposits of the igneous and metamorphic-anatectic groups involved high-temperature differentiates or fluids related to relatively oxidized silicate melts, and uranium probably moved as uranous hydroxide, fluoride or phosphate complexes. Hydrothermal uranium transport appears to have been relatively unimportant throughout time, probably because of the predominantly reduced nature of these fluids. Uranium transport prior to oxygenation of the atmosphere at about 2200 m.y. was accomplished by aqueous suspension of detrital grains in surface runoff waters, along with thorium and titanium minerals, pyrite and gold. During all subsequent weathering periods uranium was transported essentially free of thorium, in solution in oxygenated groundwaters, as uranyl carbonate, fluoride and phosphate complexes. In Middle Palaeozoic time land-based plants had become sufficiently established that organometallic complexes may have been locally important uranium complexing agents. Transporting fluids were both oxygenated surface runoff waters and oxygenated groundwaters, which carried hexavalent uranium to localized sites of reduction and deposition within watershed sub-strata, as well as ultimately to the sea.

Uranium-depositing processes in igneous and metamorphic-anatectic deposits involve precipitation from a melt, probably by changes in pH, oxygen or carbon dioxide partial pressure, or complexing anion activity. Concentration of uranium into late-stage igneous and anatectic differentiates is well documented, but was apparently not sufficiently effective to produce deposits with uranium concentrations in excess of 0.1% U_3O_8 over minable widths. Before the atmospheric-hydrospheric change to oxidizing conditions, uranium deposition was in clastic detrital form in littoral and fluviodeltaic environments. Deposition was by physical separation, depending on size and specific gravity of suspended grains where the flow velocity of surficial runoff waters suddenly decreased. Palaeo-placer deposits, concentrated in this manner, were subject to physical limitations on heavy mineral enrichment, and concentrations rarely exceed 0.12% U_3O_8 over minable widths.

After the establishment of global oxidizing conditions the processes that deposited uranium from solution in oxidizing groundwaters involved fluid reduction. Moreover, this was also a highly effective concentrating mechanism—more so than earlier depositional processes—and resulted in richer deposits grading up to several per cent U_3O_8. This was probably due both to prolonged weathering, which generated uraniferous groundwater, and highly effective, strongly reducing environments. Following orogenesis at 1800 m.y. oxidizing groundwaters moved in porous, clastic continental sediments along or near the underlying basal, major subaerial unconformity surface. Deposition of uranium was by inorganic precipitation at the reduced groundwater-table, by graphitic or pyritic rocks

in the subsurface, or by adsorption on to clay minerals or iron–titanium hydroxides. The resulting deposits formed just below or above this palaeo-surface and comprise the unique and economically important unconformity-related hydrogenic deposits. Hydrogenic vein deposits, characteristic of the Middle Proterozoic and also late Palaeozoic rocks, were similarly precipitated; though smaller, they have greater vertical extent relative to the unconformity. Deposition by reduction of oxygenated uraniferous groundwater has persisted until the present, with an important change in Middle Palaeozoic time to buried terrestrial organic detritus that increasingly took the place of inorganic reductants as the prime precipitating agent.

Since the establishment of global oxidizing conditions waters draining the continents have carried uranium into the ocean, where precipitation occurred by organic reduction, primarily in euxenic basins. The resulting black shale occurrences rarely exceed 0.05% U_3O_8. Where oxygenated, uraniferous groundwaters flowed through continental clastic sediments, local reducing conditions due to a high content of buried organic matter, or to the standing groundwater-table resulted in uranium deposition to form the various sub-types of sandstone-hosted deposits.

Acknowledgement

The writers acknowledge the assistance of Dr. L. Curtis of Toronto, Canada, and Dr. R. W. Hodder of the Geology Department at the University of Western Ontario, London, Canada. Dr. Curtis has contributed helpful comments and information concerning several of the deposit types discussed here, and Dr. Hodder provided constructive criticism of an earlier draft of the paper. The National Science and Engineering Research Council of Canada provided funds to R.W.H. that supported the study: this financial aid is gratefully acknowledged.

References

1. Adler H. H. Concepts of uranium-ore formation in reducing environments in sandstones and other sediments. In *Formation of uranium deposits* (Vienna: IAEA, 1974), 141–68.
2. Aumento F. Distribution and evolution of uranium in the oceanic lithosphere. *Phil. Trans. R. Soc. Lond.*, **A291**, 1979, 423–31.
3. Bain J. H. C. Uranium mineralization associated with late Palaeozoic acid magmatism in northeast Queensland. *BMR J. Aust. Geol. Geophys.*, **2**, 1977, 137–47.
4. Bell R. T. Uranium in black shales—a review. In *Short course in uranium deposits: their mineralogy and origin* Kimberley M. M. ed. (Toronto: The University Press for Mineralogical Association of Canada, 1978), 307–29.
5. Bell K. A review of the geochronology of the Precambrian of Saskatchewan—some clues to uranium mineralization. *Mineralog. Mag.*, **44**, 1981, 371–8.
6. Berning J. *et al.* The Rössing uranium deposit, South West Africa. *Econ. Geol.*, **71**, 1976, 351–68.
7. Bjørlykke K. Depositional history and geochemical composition of Lower Palaeozoic epicontinental sediments from the Oslo region. *Norg. geol. Unders.* no. 305, 1974, 81 p.
8. Burt D. M. and Sheridan M. F. A model for the formation of uranium lithophile element deposits in fluorine-enriched volcanic rocks. *Open-file Rep. U.S. Dep. Energy* GJBX-225(80), 1980.
9. Cameron E. N. *et al. Internal structure of granitic pegmatites* (Lancaster, Pa: Economic Geology Publishing Co., 1949), 115 p. (*Econ. Geol. Monogr.* 2)
10. Card K. D. and Hutchinson R. W. The Sudbury structure: its regional geological setting. In *New developments in Sudbury geology* Guy-Bray J. V. ed. *Spec. Pap. geol. Ass. Can.* no. 10, 1972, 67–78.
11. Christopher P. A. and Kalnins T. Exploration for basal type uranium deposits in B.C. *Western Miner*, April 1977, 75–9.
12. Cloud P. A working model of the primitive earth. *Am. J. Sci.*, **272**, 1972, 537–48.
13. Cloud P. Major features of crustal evolution. *Trans. Proc. geol. Soc. S. Afr. Annexure*, **79**, 1976, 33 p.
14. Conant L. C. and Swanson V. E. Chattanooga Shale and related rocks of central Tennessee and nearby areas. *Prof. Pap. U.S. geol. Surv.* 357, 1961, 91 p.
15. Cuney M. Geologic environment, mineralogy, and fluid inclusions of the Bois Noir–Limouzat uranium vein, Forez, France. *Econ. Geol.*, **73**, 1978, 1567–610.
16. Curtis L. Uranium in volcanic and volcaniclastic rocks—examples from Canada, Australia, and Italy. In *Uranium in volcanic and volcaniclastic rocks* Goodell P. C. and Waters A. C. eds. *AAPG Studies in Geology* no. 13, 1981, 37–53.
17. Curtis L. and Miller A. R. Uranium geology in the Amer–Dubawnt–Yathkyed–Baker Lakes region, Keewatin District, N.W.T., Canada. In *Uranium in the Pine Creek geosyncline* Ferguson J. and Goleby A. B. eds (Vienna: IAEA, 1980), 595–616.
18. D'Agnolo M. Novazza uranium deposits (Bergamasque Alps). In *IAEA summer school proceedings* (Vienna: IAEA, 1969), 237–54.
19. Dahl A. R. and Hagmaier J. L. Genesis and characteristics of the southern Powder River Basin uranium deposits, Wyoming, U.S.A. Reference 1, 201–18.
20. Dahlkamp F. J. and Tan E. H. Geology and mineralogy of the Key Lake U-Ni deposits, northern Saskatchewan, Canada. In *Geology, mining and extractive processing of uranium* Jones M. J. ed. (London: IMM, 1977), 145–57.
21. Dahlkamp F. J. Geologic appraisal of the Key Lake U-Ni deposits, northern Saskatchewan. *Econ. Geol.*, **73**, 1978, 1430–49.
22. Dahlkamp F. J. Typology and geographic/geotectonic distribution of uranium deposits. In *Energy resources* Burollet P. F. and Ziegler V. eds (Paris: Edition Technip, 1980), 499–536. *(26th Int. geol. Congr., Colloque C2)*
23. Dawes P. R. Field investigations in the Precambrian terrain of the Thule District, North-West Greenland. *Gronlands geol. Unders., Rep. of Activities 1978*, no. 95, 1979, 14–22.
24. Dearnley R. Orogenic fold-belts and a hypothesis of earth evolution. *Phys. Chem. Earth*, **7**, 1966, 1–114.
25. DeVoto R. H. Uranium in Phanerozoic sandstone and volcanic rocks. Reference 4, 293–306.
26. Dyck W. The mobility and concentration of uranium and its decay products in temperate surficial environments. Reference 4, 57–100.
27. Dupree J. A. and Maslyn R. M. Paleokarst controls on localization of uranium at Pitch Mine, Sawatch Range, Colorado. *AAPG Bull.*, **63**, 1979, 826. (Abstract)
28. Eargle D. H. and Weeks A. M. D. Geologic relations among uranium deposits, South Texas, Coastal Plain Region, U.S.A. In *Ores in sediments* Amstutz G. C. and Bernard A. J. eds (Berlin, etc.: Springer-Verlag, 1973), 101–13.
29. Fei Q. and Shaeokang H. Present exploration status of the Lianshanguan uranium deposit, northeast China. Reference 17, 655–61.
30. Ferguson J. and Rowntree J. C. Vein-type uranium deposits in Proterozoic rocks. Reference 22, 485–96.
31. Fyfe W. S. The geochemical cycle of uranium. *Phil. Trans. R. Soc. Lond.*, **A291**, 1979, 433–45.
32. Fyfe W. S. *et al.* Uranium mobilization into overthrust Archaean basement, Bahia, Brazil. In *GAC-MAC joint annual meeting, programme with abstracts* (Waterloo, Ont.: Geological Association of Canada, 1982), 51.
33. Galloway W. E. *et al.* Catahoula Formation of the Texas Coastal Plain: depositional systems, composition, structural development, ground-water flow history, and uranium distribution. *Rep. Invest. Texas Bur. Econ. Geol.* no. 87, 1977, 59 p.
34. Gastil G. The distribution of mineral dates in time and space. *Am. J. Sci.*, **258**, 1960, 1–35.
35. Gauthier-Lafaye F. *et al.* Le gisement d'Oklo et ses reacteurs de fission naturels. Reference 17, 663–73.
36. Geisel E. *et al.* O distrito uranifero de Lagao Real, Bahia. *An. XXXI Congr. Bras. Geol.*, **3**, 1980, 1499–510.
37. Ghandi S. S. Geological setting and genetic aspects of uranium occurrences in the Kaipokok Bay–Big River area, Labrador. *Econ. Geol.*, **73**, 1978, 1492–522.
38. Giblin A. M. The role of clay adsorption in genesis of uranium ores. Reference 17, 521–9.
39. Glikson A. Y. The missing Precambrian crust. *Geology*, **7**, 1979,

449–54.
40. Goodell P. and Carraway K. Geology of Sierra Peña Blanca Region, Chihuahua, Mexico. *AAPG Bull.*, **65**, 1981, 760–1. (Abstract)
41. Granger H. C. *et al.* Sandstone-type uranium deposits at Ambrosia Lake, New Mexico—an interim report. *Econ. Geol.*, **56**, 1961, 1179–210.
42. Gross G. A. Principal types of iron-formation and derived ores. *Trans. Can. Inst. Min. Metall.*, **69**, 1966, 41–4.
43. Gross W. H. Evidence for a modified placer origin for auriferous conglomerates, Canavieiras mine, Jacobina, Brazil. *Econ. Geol.*, **63**, 1968, 271–6.
44. Harshman E. N. Uranium rolls in the United States. *Mountain Geol.*, **9**, 1972, 135–41.
45. Hegge M. R. *et al.* Geologic setting of the East Alligator uranium deposits and prospects. Reference 17, 259–72.
46. Hills J. H. and Richards J. R. Pitchblende and galena ages in the Alligator Rivers region, Northern Territory, Australia. *Mineral. Deposita*, **11**, 1976, 133–54.
47. Hoeve J. *et al.* Athabasca basin unconformity-type uranium deposits: a special class of sandstone-type deposits? Reference 17, 575–94.
48. Hutchinson R. W. Massive base metal sulphide deposits as guides to tectonic evolution. In *The continental crust and its mineral deposits* Strangway D. W. ed. *Spec. Pap. geol. Ass. Can.* 20, 1980, 659–84.
49. Hutchinson R. W. Fyfe W. S. and Kerrich R. Deep fluid penetration and ore deposition. *Minerals Sci. Engng*, **12**, 1980, 107–20.
50. Hutchinson R. W. Mineral deposits as guides to supracrustal evolution. In *Evolution of the Earth* O'Donnell R. J. and Fyfe W. S. eds. *Geodynamics Series* 5, 1981, 120–40.
51. Hyde R. S. Uranium deposits in the Carboniferous Deer Lake Basin, western Newfoundland. Programme meeting CIM Geology Division, Saskatoon, Saskatchewan, 1981.
52. Jackson G. D. and Iannelli T. R. Rift-related cyclic sedimentation in the Neohelikian Borden Basin, northern Baffin island. In *Proterozoic basins of Canada* Campbell F. H. A. ed. *Pap. geol. Surv. Can.* 81-10, 1981, 269–302.
53. Jarrard L. D. Some occurrences of uranium and thorium in Montana, with sections on prospecting for radioactive minerals. *Misc. Contr. Montana Bur. Mines Geol.* no. 15, 1957, 90 p.
54. Katayama N. Kubo K. and Hirono S. Genesis of uranium deposits of the Tono mine, Japan. Reference 1, 437–52.
55. Knipping H. D. The concepts of supergene versus hypogene emplacement of uranium at Rabbit Lake, Saskatchewan, Canada. Reference 1, 531–49.
56. Langmuir D. Uranium solution-mineral equilibria at low temperatures with applications to sedimentary ore deposits. *Geochim. cosmochim. Acta*, **42**, 1978, 547–69.
57. Leroy J. The Margnac and Fanay uranium deposits of the La Crouzille district (western Massif Central, France): geologic and fluid inclusion studies. *Econ. Geol.*, **73**, 1978, 1611–34.
58. Lindsay D. A. Volcanism and uranium mineralization at Spor Mountain, Utah. Reference 16, 89–98.
59. McLennan S. M. and Taylor S. R. Th and U in sedimentary rocks: crustal evolution and sedimentary recycling. *Nature, Lond.*, **285**, 1980, 621–4.
60. McMillan R. H. Uranium in Canada. *Bull. Can. Petrol. Geol.*, **25**, 1977, 1222–49.
61. McMillan R. H. Genetic aspects and classification of important Canadian uranium deposits. Reference 4, 187–204.
62. Mittempergher M. Genetic characteristics of uranium deposits associated with Permian standstones in the Italian Alps. Reference 1, 299–311.
63. Motica J. E. Geology and uranium–vanadium deposits in the Uravan mineral belt, Southwestern Colorado. In *Ore deposits of the United States 1933–1967* Ridge J. D. ed. (New York: AIME, 1968), 805–13.
64. Nash J. T. Uranium deposits in the Jackpile Sandstone, New Mexico. *Econ. Geol.*, **63**, 1968, 737–50.
65. Nash J. T. Geology, petrology, and chemistry of the Leadville Dolomite: host for uranium at the Pitch Mine, Saguache County, Colorado. *Open File Rep. U.S. geol. Surv.* 79-1566, 1979, 54 p.
66. Needham R. S. Crick I. H. and Stuart-Smith P. G. Regional geology of the Pine Creek Geosyncline. Reference 17, 1–22.
67. Needham R. S. Ferguson J. and Prichard C.E. *Excursion guide for the international uranium symposium on the Pine Creek Geosyncline, N.T., Australia* (Sydney: The Symposium, 1979), 37 p.
68. Norcen Energy Resources Limited. *Royal Commission on Inquiry into uranium mining: phase 1, overview* 1979, 11 p.
69. O'Rourke P. J. Maureen uranium fluorite molybdenum prospect, Georgetown. In *Economic geology of Australia and Papua New Guinea 1. Metals* Knight C. L. ed. (Parkville: Australasian Institute of Mining and Metallurgy, 1975), 764–9. (*Monogr. Series* no. 5)
70. OECD Nuclear Agency and IAEA. *World uranium potential* (Paris: OECD, 1978), 170 p.
71. Preto V. A. Setting and genesis of uranium mineralisation at Rexspar. *CIM Bull.*, **71**, Dec. 1978, 82–8.
72. Pretorius D. A. The nature of the Witwatersrand gold–uranium deposits. In *Handbook of strata-bound and stratiform ore deposits, volume 7* Wolf K. H. ed. (Amsterdam: Elsevier, 1976), 29–88.
73. Rackley R. I. Environment of Wyoming Tertiary uranium deposits. *Mountain Geol.*, **9**, 1972, 143–57.
74. Rich R. A. Holland H. D. and Petersen U. *Hydrothermal uranium deposits* (Amsterdam: Elsevier, 1977), 264 p.
75. Richardson K. A. Killeen P. G. and Charbonneau B. W. Results of a reconnaissance type airborne gamma-ray spectrometer survey of the Blind River–Elliot Lake area. *Pap. geol. Surv. Can.* 75-1A, 1975, 133–5.
76. Roberts A. E. Stratigraphy of the Madison Group near Livingston, Montana, and discussion of karst and solution-breccia features. *Prof. Pap. U.S. geol. Surv.* 526-B, 1966, 23 p.
77. Robertson D. S. Basal Proterozoic units as fossil time markers and their use in uranium prospection. Reference 1, 495–512.
78. Robertson J. A. The Blind River uranium deposits: the ores and their setting. *Misc. Pap. Ontario Ministry nat. Res.* 65, 1976, 45 p.
79. Robertson J. A. Uranium deposits in Ontario. Reference 4, 229–80.
80. Roper M. W. and Wallace A. B. Geology of the Aurora uranium prospect, Malheur County, Oregon. Reference 16, 81–8.
81. Roscoe S. M. Huronian rocks and uraniferous conglomerates in the Canadian Shield. *Pap. geol. Surv. Can.* 68-40, 1969, 205 p.
82. Roscoe S. M. The Huronian Supergroup, a palaeoaphebian succession showing evidence of atmospheric evolution. *Spec. Pap. Geol. Ass. Can.* no. 12, 1973, 31–47.
83. Ruzicka V. Geological comparison between east European and Canadian uranium deposits. *Pap. geol. Surv. Can.* 70-48, 1971, 196 p.
84. Ruzicka V. Phanerozoic uranium deposits and occurrences in Europe and eastern North America. Reference 4, 217–28.
85. Rytuba J. J. and Conrad W. K. Petrochemical characteristics of volcanic rocks associated with uranium deposits in the McDermitt Caldera Complex. Reference 16, 63–72.
86. Sassano G. P. Fritz P. and Morton R. D. Paragenesis and isotopic composition of some gangue minerals from the uranium deposits of Eldorado, Saskatchewan. *Can. J. Earth Sci.*, **9**, 1972, 141–57.
87. Sibbald T. I. I. Munday R. J. C. and Lewry J. F. The geological setting of uranium mineralization in northern Saskatchewan. In *Uranium in Saskatchewan* Dunn C. E. ed. *Spec Publ. Sask. geol. Soc.* no. 3, 1977, 51–98.
88. Theis N. J. Mineralogy and setting of Elliot Lake deposits. Reference 4, 331–8.
89. Tremblay L. P. Geologic setting of the Beaverlodge-type of vein-uranium deposit and its comparison to that of the unconformity-type. Reference 4, 431–56.
90. Wallace A. B. and Roper M. W. Geology and uranium deposits along the northeastern margin, McDermitt Caldera Complex, Oregon. Reference 16, 73–9.
91. West G. F. Formation of continental crust. Reference 48, 117–48.
92. Ypma P. J. M. and Fuzikawa K. Fluid inclusion and oxygen isotope studies of the Nabarlek and Jabiluka uranium deposits, Northern Territory, Australia. Reference 17, 375–95.

Uranium exploration

Richard H. De Voto
Colorado School of Mines, Golden, Colorado, U.S.A.

This paper is a review of the methodology and technology that are currently being used in varying degrees in uranium exploration activities worldwide. Since uranium is ubiquitous and occurs in trace amounts (0.2–5 ppm) in virtually all rocks of the crust of the earth (Table 1), exploration for uranium is essentially the search of geologic environments in which geologic processes have produced unusual concentrations of uranium. Since the level of concentration of uranium of economic interest is dependent on the present and future price of uranium, it is appropriate here to review briefly the economic realities of uranium-fueled power generation.

Table 1 Average uranium contents, ppm

Crustal abundance	2	Granite	4
Sea water, ppb	3	Shale	3.2
Basalt	0.5	Sandstone	2.2
Andesite	2	Limestone	1.3

All natural occurrences of uranium, with the exception of one known occurrence in Gabon, where a natural fission reaction (the 'Okla phenomenon') has occurred in Proterozoic rocks, contain the three isotopes of uranium in the following relative abundances:

^{238}U 99.28 wt%
^{235}U 0.71 wt%
^{234}U 0.0054 wt%

The ^{235}U isotope, which constitutes only 0.71% of any uranium occurrence, fissions naturally and is the principal fuel in conventional burner reactors (power plants). The ^{238}U isotope, which constitutes the bulk (99.3%) of any uranium occurrence, can be transformed into a useful fuel, the ^{239}Pu

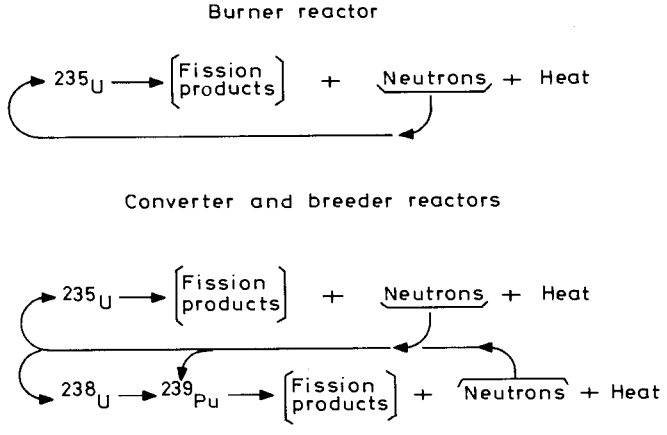

Fig. 1 Nuclear reactor schematic

isotope, which does not occur in nature, by bombardment of the ^{238}U with high-energy neutrons generated in the ^{235}U fission reaction in converter or breeder reactors (Fig. 1). Thus, through increased sophistication of engineering nuclear power plants and their political acceptance, it is possible to increase some five- to fifty-fold (Table 2) the energy obtained from the same pound of uranium.[18,28]

Present-day economic factors display a rough economic equivalency for newly constructed electricity-generating facilities (power plants) between \$12/bbl for oil, \$25/t for coal, and \$80–100/lb U_3O_8, even with the relatively resource-inefficient burner (^{235}U only) reactor. Thus, at current (1983) uranium prices of approximately \$20/lb U_3O_8, there exists a significant economic incentive (in a free market economy) for most new electricity-generating facilities in the world to be nuclear power plants, all other factors (political, environmental, etc.) being equal. In other words, even at today's prices, and certainly more so as the labour- and transportation-intensive coal prices and international cartel- and politics-susceptible oil prices increase, the price of uranium will respond to achieve its own balance within the framework of uranium supply and demand.

Table 2 Cumulative uranium requirements for market economy countries to A.D. 2050[28]

Reactor type or system	Natural uranium, t × 10^6	
	Low nuclear growth	High nuclear growth
Light-water—no Pu recycle	38	60
Light-water—Pu recycle	25	43
Light-water—thorium breeder	23	44
Thorium cycle CANDU	17	30
Fast breeder	10	15
Liquid fuel thorium breeder	9	16
Liquid fuel + fast breeder	5	10

The price of uranium has a significant effect on the uranium resources available to man. Fig. 2 graphically displays the general relationship between the price of uranium and the grade of a large near-surface deposit of uranium-bearing rock that may be economically viable as a uranium resource. The figure is a generalized statement in that the minimum economic grade level for any market price depends on (1) the size and geometry of a uranium deposit, (2) the depth and mining characteristics of the deposit, (3) the chemistry and extractive characteristics of the ore and (4) other factors of capital and operating costs. Fig. 2 does display, however, the general fact that as the price

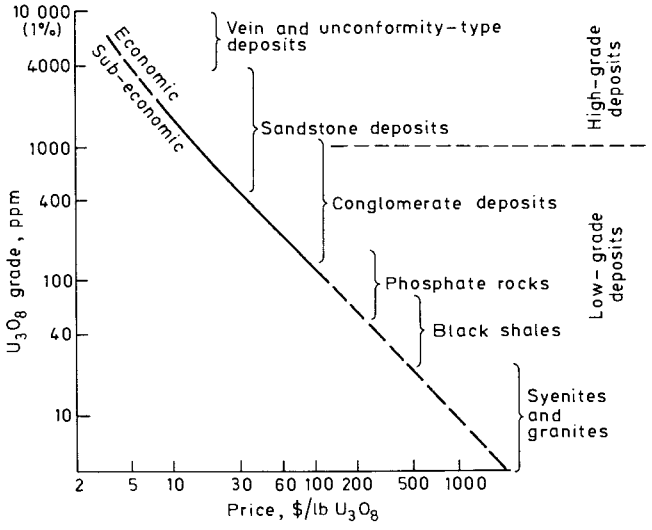

Fig. 2 Uranium grade versus price and different types of uranium resources

of uranium rose from \$6/lb U_3O_8 to the \$40/lb U_3O_8 range from 1973 to 1976, the minimum economic grade decreased from the 0.20–0.30 U_3O_8 range to the 400–500 ppm U_3O_8 range. With this price-dependent decrease in minimum economic grade, several types of geologic resources of low-grade uranium became economically viable. The discovery and development of the vast high-grade unconformity-type deposits in Australia and Canada have effectively reduced exploration for and development of the lower-grade resources.

Principal uranium-concentrating geologic environments

The first and fundamental step in any uranium exploration programme is the development of an integrated geologic and geochemical analysis and understanding of the genesis of the potential uranium accumulations under investigation. The U.S. Department of Energy has recently attempted to categorize uranium occurrences into general classes to facilitate the recognition of favourable uranium-concentrating geologic environments.[15, 17, 29] Whereas there are a myriad of uranium-concentrating geologic environments, there are but a few that have, to date, been important in the development of most of the world's known uranium reserves, historically produced or economically viable at today's prices. The general aspects of these most important geologic environments and the geologic and geochemical factors that are important in controlling the uranium occurrences are described elsewhere in this volume.

The bulk of the world's uranium has been produced historically from (1) lower Proterozoic uraninite placer deposits in quartz-pebble conglomerates, (2) epigenetic uranium deposits in sandstones located in many cases at, or near, groundwater oxidation–reduction interfaces and (3) hydrothermal vein uranium deposits. These three distinctly different geologic environments provided most of the uranium that was produced from the 1940s to the early 1970s and they continue to be important exploration targets in the search for new uranium deposits.

Exploration for economic uranium deposits has expanded to many geologic environments that have been generally overlooked in the past. Most notable among these are (1) granitic uranium deposits, (2) alkalic igneous-hydrothermal uranium deposits, (3) altered acidic or alkalic volcanic ash, ash flow or volcaniclastic uranium deposits, (4) unconformity-related uranium deposits and (5) calcrete uranium deposits in desert groundwater environments.

These and other relatively underevaluated geologic environments received substantial exploration attention in the 1970s and results of this cycle of exploration indicate that significant uranium deposits have been discovered in each.

The expanded search for economically viable uranium resources and the improved market and technology factors have caused exploration and development efforts to advance far beyond pre-1970 levels. Low-grade uranium resources that have been long known and ignored, such as uraniferous, black, organic-rich shales and marine phosphorites, are being developed for uranium production. *In-situ* solution-mining activities have permitted economic exploitation of uranium deposits that heretofore have been uneconomic because of their small size, low grade or depth. Exploration drilling and development activities for unknown uranium deposits have expanded to greater depths.

Exploration technology

A tabulation of techniques used in uranium exploration would include most techniques that are employed in the search for oil, gas and all other mineral commodities, as well as some unique to uranium. The emphasis here will be to review those techniques of widespread use or emerging usefulness in uranium exploration.

Exploration techniques are generally reviewed or tabulated according to discipline—for example, geology, remote sensing, geophysics, geochemistry, geobotany and exploration drilling. As such, a long and complete list of exploration tools or techniques can be elaborated. The approach here is to stress cost-effective techniques at the expense of those of limited value and to review their usefulness in exploration programmes that evolve from reconnaissance programmes to more local or detailed programmes.

Reconnaissance exploration techniques

Exploration techniques of widespread use in reconnaissance uranium exploration programmes include (1) geologic mapping, basin analysis and search for favourable geologic environments, (2) remote-sensing data analysis and synthesis, (3) gamma-ray spectrometry (airborne and ground) and (4) hydrogeochemical and stream and lake sediment sampling.

Depending on the nature and scope of the exploration programme, the above-described reconnaissance steps are often conducted simultaneously in a first phase of exploration and their results are integrated and analysed to select local favourable areas for more detailed exploration techniques in a second phase of exploration. In other cases the reconnaissance steps are conducted more or less sequentially, so the area and scope of subsequent steps are determined by the results of the previous steps. Thus, gamma-ray spectrometry need not be flown or conducted on the ground over the entire area, but only in the restricted areas of favourable geologic environments resulting from step 1.

Geologic mapping

Geologic mapping on a reconnaissance basis is essentially the compilation of all available, existing geologic mapping or initial mapping by means of the use of remote sensing imagery, principally aerial photographs, with reconnaissance field checking. The purpose of such reconnaissance geologic mapping in a uranium exploration programme is to locate and delineate geologic environments potentially favourable for uranium occurrences. Thus, the above review of the principal uranium-concentrating geologic environments serves essentially to describe the favourable geologic environments that should be evaluated in each area of reconnaissance geologic mapping. For sedimentary basins basin-wide stratigraphic analysis of the stratigraphic units and their alteration patterns may help to focus subsequent exploration efforts on the favourable area within the basin.[11]

Remote sensing data

Readily available remote sensing data, such as Landsat and ERTS imagery and aerial black and white and colour photography, are inexpensively and logically utilized to assist in the reconnaissance geologic mapping and delineation of favourable geologic environments. The combined use of medium-altitude ($\simeq 1:62\,000$) black and white photography and low-altitude ($\simeq 1:12\,000$) colour photography has been effective in uranium exploration efforts when going from the small-scale reconnaissance mapping to the larger-scale more detailed mapping.[10] Colour infrared, multi-band spectral and radar data have had limited application in uranium exploration, though recent expansion of the wavelength of multi-band spectral data has been shown to increase its utility in mapping clay-mineral alteration patterns and soil and rock types.[20]

Gamma-ray spectrometry

Most of the known large uranium districts in the world have been discovered radiometrically by airborne or ground 'gross count' radiometric surveys where the high-energy gamma radiation from radioactive decay of the ^{238}U series (^{214}Bi), the

^{232}Th series (^{208}Tl) and the ^{40}K has been measured as a total gamma radioactivity.[22] As such, radiometric surveys have been the primary exploration tool for prospectors and geologists alike for many years. More sophisticated (and expensive) instruments, gamma-ray spectrometers, which have greater sensitivity than earlier instruments and also selectively measure the gammas derived from each of the uranium series (^{214}Bi), thorium series (^{208}Tl) and ^{40}K, are in widespread use today.

Thus, the gamma-ray spectrometer has received widespread use in airborne and ground radiometric surveys in reconnaissance and detailed phases of uranium exploration programmes. Reconnaissance spectrometry surveys on widely spaced flight lines are useful in assisting geologic mapping, as well as in the delineation of generally favourable areas of occurrences of radioactive anomalies.

The ultimate limitation on gamma-ray surveys is that they are essentially two-dimensional. Gamma-rays only penetrate 6 in to 1 ft of soil or rock and are attenuated or absorbed by air, water, vegetation and snow. As exploration activities for uranium resources investigate deeper subsurface environments, airborne and surface gamma-ray surveys become less useful (borehole gamma-ray logging, however, is standard practice). Nevertheless, a surface radioactivity anomaly is still a good starting point for subsurface exploration.

A lesser limitation on gamma-ray surveys is that the gamma radioactivity anomaly (spectrometrically) is due to the anomalous content of ^{214}Bi, a daughter in the decay chain of ^{238}U. Thus, the uranium may be geochemically separated from the ^{214}Bi. The separation should, however, not be extreme and the ^{214}Bi detection offers an indirect 'pathfinder' to the parent ^{238}U.

Hydrogeochemical and stream and lake sediment surveys

Most of the known, large uranium districts in the world could have been discovered by uranium in ground- or surface water or uranium in stream or lake sediment surveys. These surveys are extremely useful in both reconnaissance and more local exploration programmes in that they commonly yield anomalies that are broader and, therefore, more readily detectable than the smaller uranium (radioactivity) anomaly itself and they, particularly groundwater hydrogeochemical surveys, can provide a meaningful investigation into subsurface environments.[5]

Hydrogeochemical surveys are of varying usefulness, depending on rainfall, runoff and background characteristics. Surface hydrogeochemical surveys are not as meaningful and useful in areas or times of high rainfall and runoff as in arid areas or times, because of dilution of any significant anomalous uranium content in the water. Groundwater hydrogeochemical surveys are not subject to these climatic variations and, hence, are more uniformly useful. Different host rocks, however, have different background levels of uranium content (the Wind River Formation (Eocene) in the Wyoming Basins commonly has a background level of 1–5 ppb uranium in groundwater, whereas the White River Formation (Oligocene) has a 10–20 ppb uranium background level), so the groundwater hydrogeochemical data should be interpreted carefully.

Stream and lake sediment surveys generally do not provide meaningful information of subsurface environments, but insofar as surface drainages are efficient collectors of soil constituents, these surveys can be used effectively, on reconnaissance and local bases, to systematically sample the uranium content variations of the bedrock terrain over large areas and in any kind of vegetative and soil cover. The remarkable example of the discovery of the Key Lake uranium–nickel deposit beneath more than 200 ft of glacial drift in northern Saskatchewan by lake sediment sampling down-ice from the deposit[27] illustrates the utility of these sediment sampling surveys.

Detailed exploration techniques

Detailed exploration techniques are applied generally on favourable 'target' areas that have been delineated by the reconnaissance or more regional exploration techniques. Exploration techniques used commonly in various combinations in local or detailed programmes include (1) detailed geologic and alteration mapping, (2) detailed hydrogeochemical surveys, (3) detailed radiometric surveys, (4) radon and helium soil-gas surveys, (5) soil and rock geochemical surveys, (6) subsurface stratigraphic analysis, (7) non-radiometric geophysical surveys, (8) geobotany and biogeochemistry and (9) exploration drilling and logging.

The geology of the area of detailed exploration and the nature of the potentially favourable geologic environments determine the relative utility and sequence of use of these and other detailed exploration techniques. All of these techniques are not used uniformly on all types of geologic targets. Some of their principal uses are emphasized here.

Detailed geologic and alteration mapping

Many genetic types of uranium deposits are associated with host rock alteration.[1] Thus, alteration mapping commonly is an extremely useful exploration technique in many geologic environments. For example, the oxidation–reduction interface, the locus of many epigenetic uranium deposits in sandstones, is often readily discernible on the outcrop or in drill samples owing to the oxidation alteration of many indigenous constituents of the rocks; pyrite is altered to limonite or hematite or leached, carbonaceous debris is destroyed, iron–magnesium silicate minerals and feldspars may be altered or destroyed and clay mineralogy may change.[13,16] These alteration evidences may be mapped lithologically, and they may also be detected indirectly by magnetic susceptibility (iron mineral alteration) or IP (pyrite or clay mineral alteration) logging in boreholes.

Detailed hydrogeochemical surveys

Hydrogeochemical surveys are effectively used in detailed exploration programmes as well as in a reconnaissance mode. Careful analysis of the uranium, radon and helium content of

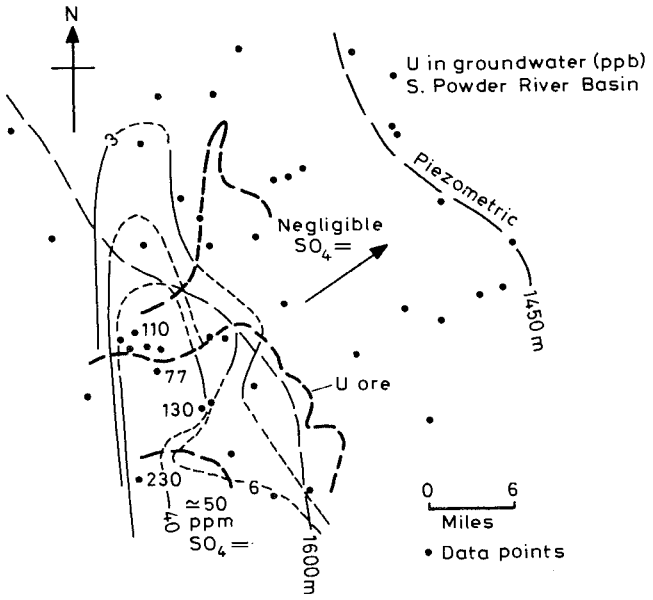

Fig. 3 Uranium content of shallow groundwaters in southern Powder River Basin, Wyoming. Thick dashed lines indicate some oxidation–reduction interfaces along which much of uranium ore occurs. All data points outside 3 ppb contour contain ≤2 ppb uranium. Arrow depicts current groundwater flow as determined by piezometric data[9]

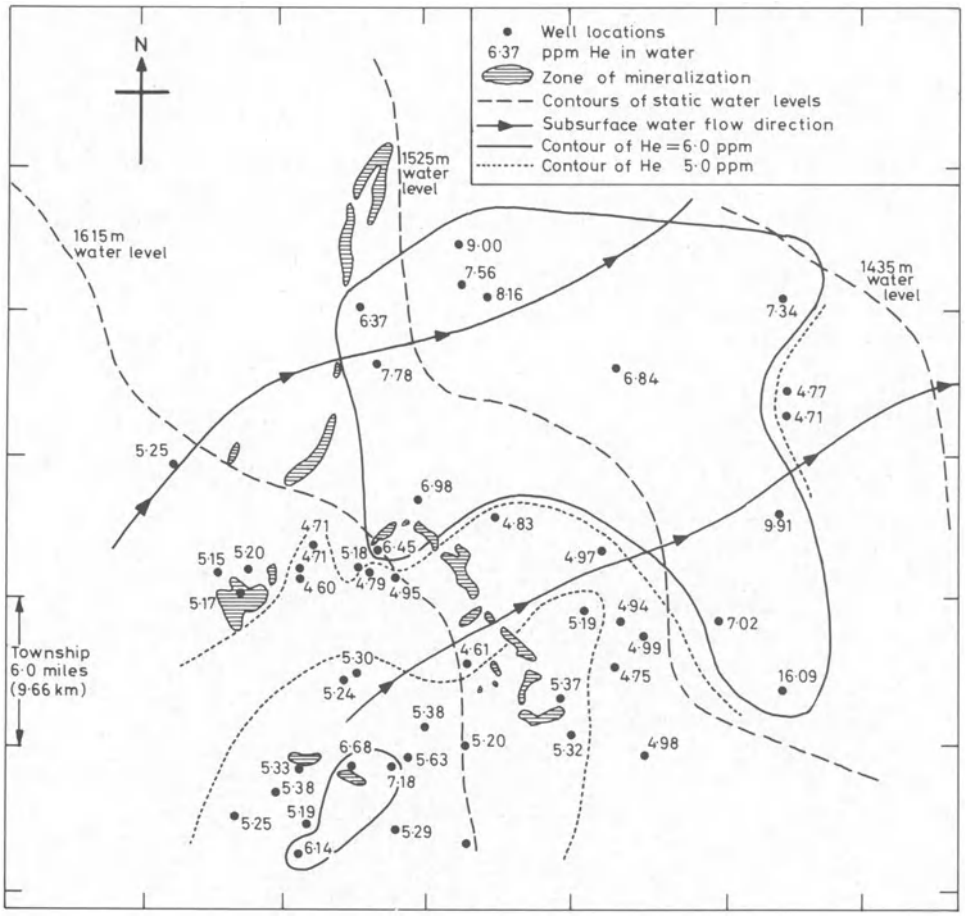

Fig. 4 Helium concentration measured in trapped air in equilibrium with water samples collected from water wells in southern Powder River Basin, Wyoming[9]

groundwaters, as well as other chemical parameters, such as the pH, Eh, alkalinity, SO_4^-, HCO_3^- and Cl^-, and an understanding of the groundwater hydrology permit maximum utilization of groundwater hydrogeochemical surveys in detailed exploration for uranium deposits.[6,25] The example of the southern Powder River Basin, Wyoming, is illustrative in this regard. Fig. 3 shows the uranium content in shallow groundwater within the Wind River and Ft. Union strata with respect to the uranium ore deposits of the southern Powder River Basin. Interpretation of the uranium data is imprecise because the groundwater samples are from several sandstone aquifers within a mudstone–sandstone sequence. A general pattern exists, however, that shows (1) $\leqslant 2$ ppb uranium and negligible SO_4^{--} in groundwater in the area of reduced, unaltered sandstone in the down-groundwater direction from the oxidation–reduction interfaces at which the uranium ore occurs; (2) >2 ppb and up to 230 ppb uranium and $\simeq 50$ ppm SO_4^{--} in groundwater up the groundwater gradient from the uranium deposits in the oxidized, altered portions of the sandstones; and (3) that the geologic mechanism of uranium and SO_4^{--} travelling in solution in the oxidized interior and being efficiently withdrawn from the groundwater by precipitation of uraninite and pyrite at the oxidation–reduction interface was detected by the hydrogeochemical survey.

In this case the geologic analysis of the uranium and SO_4^{--} groundwater data should have resulted in exploration efforts being concentrated at the transition zone from high to low uranium contents—not within the area of high uranium content.

The helium content of the groundwater within the same area is shown in Fig. 4. The helium pattern generally shows an area of anomalous helium content in groundwater ($\geqslant 6.0$ ppm) offset down the groundwater gradient from the uranium deposits. Insofar as helium is generated in the radioactive decay of uranium and its daughters, helium formed at the sites of the uranium deposits is apparently moving in the groundwater as it moves to the northeast. The schematic cross-section of Fig. 5 shows a possible reason, related to the cross-aquifer flow of groundwater in recharge and discharge areas, for the offset of the detectable area of anomalous helium derived from the uranium ore deposits in the shallow groundwaters. Thus, a uranium and helium groundwater hydrogeochemical survey, combined with analysis of the hydrology of this area, would have provided excellent data for focusing on prospective areas for exploration drilling in a detailed exploration programme.

Even more significant is the suggestion (Fig. 6) that helium migrates vertically from its progenerator uranium accumulation

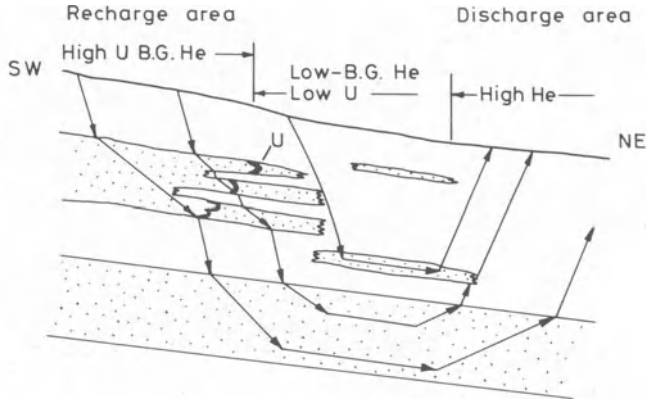

Fig. 5 Groundwater flow paths in relation to helium and uranium content in groundwater samples and uranium ore deposits, southern Powder River Basin[9]

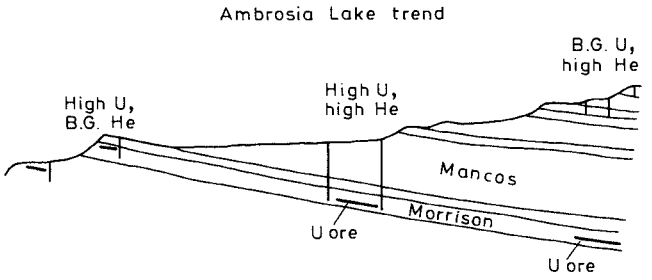

Fig. 6 Schematic geologic cross-section of uranium and helium content of groundwater with respect to aquifers of water samples and uranium ore deposits, Grants–Ambrosia Lake district (note high helium content of groundwaters from aquifers thousands of feet above ore deposit at right end of diagram[9])

through thousands of feet of overlying shale, coal and sandstone and is detectable as anomalous helium concentrations in groundwater in aquifers stratigraphically distant from the uranium host rock. If this is indeed the case, the implications for the usefulness of helium in groundwater surveys in both reconnaissance and detailed exploration programmes are far greater than are currently being exploited in most uranium exploration programmes. Certainly, these studies suggest that groundwaters should systematically be collected, if necessary by packer isolation of the potential host aquifer, so that the helium distribution in groundwaters can be used in conjunction with hydrologic data in exploration for uranium.

Complete analyses of the groundwater chemistry and computer calculation of saturation indices for uranium minerals and other indicator species have been demonstrated to be a potentially powerful tool in uranium exploration in areas where abundant groundwater samples are available.[6,23]

Detailed radiometric surveys

Detailed radiometric surveys are useful in detailed exploration programmes where the distribution of outcrop radioactivity with respect to lithologies and alteration patterns may have significance to the favourable geologic environment under exploration. For example, outcrop radioactivity along hematite-stained, brecciated vein structures would have important significance in exploring for a vein-type hydrothermal uranium deposit, whereas outcrop radioactivity surveys may not be of much value in exploring for deeply buried epigenetic uranium deposits in sandstones. Detailed radiometric surveys have been useful in the Athabasca Basin of northern Saskatchewan in the detection of radioactive boulders in glacial drift. By use of glacial geomorphology and reconstruction of ice movement directions these radioactive boulders have been traced to their source bedrock material and discoveries of uranium deposits have been made.[14,27]

Thus, detailed radiometric surveys should be used selectively according to the geologic terrain and the nature of the favourable geologic environment under exporation. Needless to say, in the exploration for uranium in near-surface environments radiometric surveys can still be an effective and inexpensive tool to the explorationist.

Radon and helium soil-gas surveys

Radon and helium soil-gas surveys may be useful in detailed or semi-regional exploration programmes by virtue of the fact that both are inert gases derived from the radioactive decay of uranium and its daughters. As such, the gases may migrate away from a buried uranium deposit to yield anomalous concentrations of radon and/or helium in soil gas. Thus, a buried uranium deposit may be remotely detectable indirectly by detection of anomalous radon and/or helium concentrations in soil gas.

The first generation of sophistication of radon and helium soil-gas surveys—that of collection of a soil-gas sample in the field at an instant and analysis of its radon or helium content—has had highly variable usefulness.[25] As in all soil-gas exploration surveys, commonly meteorologic variations and diurnal thermal and plant respiratory effects cause greater variations in trace gas content of the soil gas than does the ore deposit induced anomaly. Therefore, the utility of radon and helium soil-gas surveys has been greatly enhanced and will be more so in the future through the development and use of 'accumulator' measurements, whereby the amount of radon or helium that reaches the soil or soil-gas over a period of time (a month or two) is measured.

Cumulative radon in soil-gas measurements, by means of alpha-particle detection with photosensitive film or alpha electrometers placed in the soil for a period of time, have received widespread use in detailed exploration programmes. A fundamental limitation on the usefulness of radon soil-gas surveys, however, is the 3.8-day half-life of ^{222}Rn, the long-lived radon daughter in the ^{238}U decay series. This relatively short half-life means that radon derived from a buried uranium deposit must migrate to the soil within 20 days or so in order to be detectable as an anomaly. With this time limitation it is not likely that a radon soil-gas anomaly would be present in detectable levels above a uranium deposit buried more than several hundred feet, unless open faults or fractures facilitated radon movement to the surface from the deposit. Nevertheless, cumulative radon in soil-gas surveys provide an important detailed exploration tool in expanding the explorationist's view into the subsurface. Excellent examples of the use of cumulative radon in soil-gas surveys in detailed exploration programmes are provided in the example of the discovery of the buried uranium deposit at Spokane Mountain, Washington,[21] and in the uranium vein exploration in the Front Range of Colorado.[10]

Helium soil-gas surveying is in its infancy, but early work is indicating that its utility may be far greater than radon soil-gas surveying.[8,9] Helium does not suffer the short half-life limitation of radon in that it is not a radioactive material itself and, therefore, does not decay away. Helium derived from a buried uranium deposit can therefore travel a greater distance from the deposit, such as from a deeper deposit, and be detectable as anomalous helium in soil-gas (or groundwater). The relatively high level of helium content in the atmosphere (5.2 ppm), however, makes a helium anomaly in soil-gas difficult to detect in a non-cumulative survey. Meteorologic and diurnal plant respiratory effects are such that the non-cumulative helium soil-gas measurements must be corrected for variations in the major gas content—an expensive step at best. The development of cumulative helium collection systems should extend by orders of magnitude the usefulness of helium soil-gas surveys in exploration programmes for buried uranium deposits. Soil moisture may serve as a partial accumulator of helium, and collection and analysis of helium in soil moisture may provide a useful means of implementing helium in soil-gas surveys. In any case, soil-gas surveys will be of expanding use to the explorationist in his efforts to understand and unravel the distribution of uranium in subsurface environments.

Soil and rock geochemical surveys

Soil and rock geochemical surveys may be usefully conducted in detailed exploration programmes where the uranium or other associated trace-metal content of the bedrock or soil of an area may be a useful guide to a buried uranium deposit.[5,21] For example, uranium-, or copper- or molybdenum-in-soil geochemical surveys may be of value in detailed exploration programmes in the search for uranium vein deposits in terrain where uranium vein accumulations occur in association with copper and molybdenum sulphides.

In the search for epigenetic uranium deposits in sandstones, however, other than deposits at the ground surface, such soil or rock geochemical surveys have negligible value. Of possible future value, however, is the search for anomalies of solid daughter products of the gaseous ^{222}Rn (and, therefore, the ^{238}U decay series), such as ^{210}Po, ^{210}Pb, ^{206}Pb or $^{206}Pb/^{208}Pb$, in soil geochemical surveys in any geologic environment that might have a subsurface uranium deposit as a possible source for upward migration of radon and subsequent generation of its solid daughters in the soil. Thus, soil and rock geochemical surveys should be used selectively according to the geologic terrain and the nature of the favourable geologic environment being explored.

Subsurface stratigraphic analysis

Subsurface stratigraphic analysis may be an extremely effective tool in regional or sub-regional exploration programmes in sedimentary basins in the search for epigenetic uranium deposits in sandstones or for Proterozoic uraniferous quartz-pebble conglomerates. Obviously, the availability of subsurface data is an important factor in the utility of these analyses. As in all geologic analyses, subsurface data should be integrated with all other available data, particularly outcrop data, as they essentially represent extension of geologic mapping into subsurface environments.

Detailed subsurface stratigraphic analysis is an integral part of any exploration drilling programme. The lithologic data obtained from drill-holes should be fully utilized and integrated to map the subsurface rock, alteration and mineralization patterns.[11]

Non-radiometric geophysical surveys

Non-radiometric geophysical surveys are receiving greater utilization in uranium exploration activities as exploration expands into deeper subsurface environments and as the understanding of the geologic controls on the favourable uranium-concentrating environments increases.[26] Non-radiometric geophysical surveys of selective use in uranium exploration include gravity, magnetic, electrical (electromagnetic, resistivity and IP) and seismic surveys. The uses of each of these non-radiometric geophysical techniques are similar to those in exploration programmes for other mineral commodities (Table 3).

Thus, the different non-radiometric geophysical techniques should be selectively used as appropriate to solve specific geologic problems or to provide particular information to assist in the understanding of the geology of an area.

Excellent examples of recent uses of non-radiometric geophysical surveys are provided by the experiences in the Athabasca Basin of northern Saskatchewan, where airborne magnetometer and electromagnetic surveys and ground electromagnetic surveys have been conducted routinely in attempts to map fault offsets within the basement or of the unconformity at the base of the Athabasca sandstone and to detect conductive shear zones and/or graphitic schist units within the basement terrain. Such surveys, on drilling, have led directly to discoveries of several uranium deposits in the eastern Athabasca Basin.[4,7,14] Similarly, airborne and ground magnetometer surveys were found to be useful in the delineation of favourable geologic conditions and induced polarization surveys in indicating sulphide minerals within the newly discovered uranium deposit at Spokane Mountain, Washington.[21]

Table 3

Non-radiometric geophysical techniques	Geologic uses (mapping)
Gravity surveys	Geologic structures, regional and local; buried channels, local
Magnetic surveys	Geologic structures, regional and local; alteration of magnetic minerals, local
Electrical surveys	
Electromagnetic	Graphitic conductors, pyrite concentrations, buried channels, fault structures
Resistivity	Buried channels, fault, vein structures
IP	Sulphide minerals, clay mineralogy changes
Seismic surveys	Geologic structures, regional and local; facies changes; buried channels, local; unconformity mapping

Geobotany and biogeochemistry

The use of geobotany in uranium exploration has generally not been extensive. In expanded utilization of remote-sensing imagery and multi-band spectral data, detection of distressed vegetation or of certain vegetation types that prefer particular soil and/or bedrock conditions may provide for more extensive use of geobotany in geologic and alteration mapping in uranium exploration programmes.

Biogeochemistry can be of significant use in detailed exploration programmes and may provide a means of effectively sampling several tens of feet below the ground surface. The vegetation may contain significantly anomalous levels of uranium or other trace elements associated with uranium deposits and, by virtue of the depth penetration of their root system, may provide a depth penetration of investigation that soil geochemical surveys do not yield. Suggestions of anomalous uranium contents in eucalyptus trees in the vicinity of uranium deposits of the East Alligator Rivers district, Northern Territory, Australia,[2] and in pine trees near vein uranium deposits of the Front Range, Colorado,[10] have been observed. The analysis of the uranium content of the humic content in soils has also proved to be an effective exploration technique in certain areas.[21]

Exploration drilling and logging

Exploration drilling and logging is not only the ultimate test of any uranium exploration effort but is in itself an extremely important exploration technique in that it provides invaluable direct information concerning the subsurface geology. As an exploration technique, therefore, exploration drilling and logging are extensions of geologic mapping into subsurface environments. Fig. 7 displays how an exploration drilling and logging programme can be used to define the subsurface geology so that subsequent drilling is focused on favourable geologic environments.

Logging of exploration drill-holes is itself an extremely useful exploration technique.[24] Borehole logging should include, at a minimum, systematic lithologic and alteration logging, gamma-ray logging and spontaneous potential–resistivity logging.

In specific circumstances magnetic susceptibility (alteration of magnetic minerals), IP (clay and sulphide mineral changes) and gamma-ray spectrometry logging may be warranted and useful. Delayed neutron logging has been developed that permits direct measurement of uranium in the borehole—an expensive logging technique of particular value in development activities.

Conclusions

Exploration for uranium is essentially the search for geologic environments in which geologic processes have produced unusual concentrations of uranium. Favourable geologic environments in which significant economically viable uranium deposits occur include the following: (1) lower Proterozoic uraninite placer deposits in quartz-pebble conglomerates; (2)

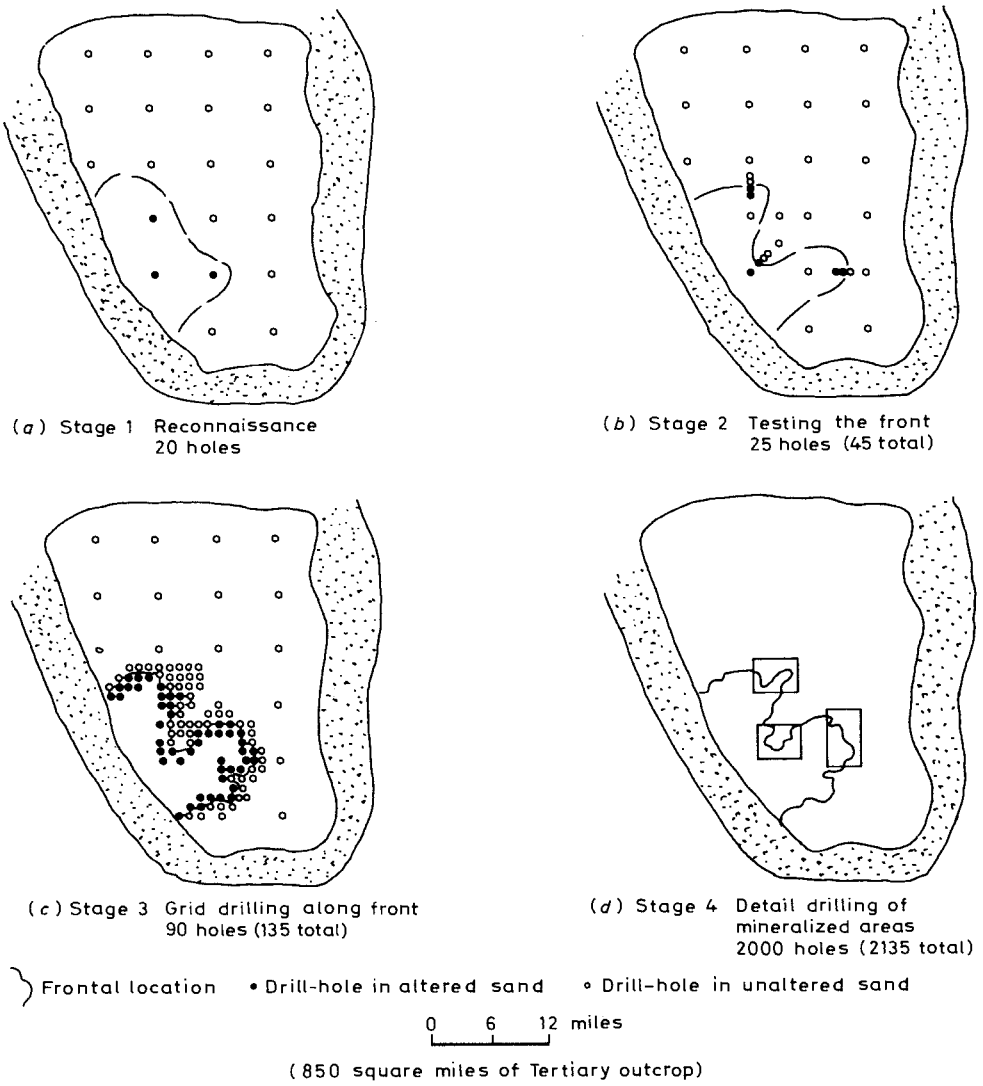

Fig. 7 Drilling sequence (generalized) for uranium in hypothetical Tertiary basin in Wyoming[3]

epigenetic uranium deposits in sandstones in most cases located at or near groundwater oxidation interfaces; (3) hydrothermal vein uranium deposits; (4) granitic uranium deposits; (5) alkalic igneous-hydrothermal uranium deposits; (6) altered acidic or alkalic volcanic ash, ash flow or volcaniclastic uranium deposits; (7) unconformity-related uranium deposits; (8) calcrete uranium deposits in desert groundwater environments; and (9) black, uraniferous organic-rich shales.

Exploration activities worldwide today are principally concentrated in the search for outcrop radioactivity and anomalies in favourable geologic environments and subsurface exploration in favourable geologic environments with known uranium mineralization.

Improved market and technology factors in the 1970s permitted exploration and development activities to expand to include lower-grade uranium resources, greater depths and smaller uranium deposits. Exploration techniques of widespread use in reconnaissance uranium exploration programmes include geologic mapping and search for favourable geologic environments, remote sensing data analysis and synthesis, gamma-ray spectrometry (airborne and ground) and hydrogeochemical and stream and lake sediment sampling.

Detailed exploration techniques that are generally applied to favourable 'target' areas delineated by the reconnaissance exploration include (1) detailed geologic and alteration mapping, (2) detailed hydrogeochemical surveys, (3) detailed radiometric surveys, (4) radon and helium soil-gas surveys, (5) soil and rock geochemical surveys, (6) subsurface stratigraphic analysis, (7) non-radiometric geophysical surveys, (8) geobotany and biogeochemical surveys and (9) exploration drilling and logging.

References

1. Adams S. S. *et al.* Interpretation and postdepositional processes related to the formation and destruction of the Jackpile–Paguate uranium deposit, northwest New Mexico. *Econ. Geol.*, **73**, 1978, 1635–54.

2. Armstrong C. W. and Brewster N. E. A comparison of exploration techniques in Saskatchewan and the Northern Territory. In *Uranium in the Pine Creek Geosyncline* Ferguson J. and Goleby A. B. eds (Vienna: IAEA, 1980), 733–42.

3. Boberg W. W. Exploration for uranium in Wyoming. *Earth Sci. Bull.*, **8**, 1975, 1–12.

4. Brummer J. J. *et al.* McClean uranium deposits, Saskatchewan. In *Uranium field excursion guidebook, Saskatchewan, September 1981* CIM Geology Division (Montreal: Canadian Institute of Mining and Metallurgy, 1981), 43–64.

5. Cameron E. M. and Hornbrook E. H. W. Current approaches to geochemical reconnaissance for uranium in the Canadian Shield. In *Exploration for uranium ore deposits* (Vienna: IAEA, 1976), 241–66.

6. Chatham J. R. Wanty R. B. and Langmuir D. Groundwater prospecting for sandstone-type uranium deposits; the merits of mineral-solution equilibria versus single element tracer methods; final report. *Rep. U.S. Dep. Energy* GJO 79-360-E, 1981, 197 p.

7. Clarke P. J. and Fogwill W. D. Geology of the Asamera Dawn Lake uranium deposits, Athabasca Basin, northern Saskatchewan. Reference 4, 19–36.
8. DeVoto R. H. *Uranium geology and exploration. Lecture notes and references* (Golden, Colo.: The School of Mines, 1978), 396 p.
9. DeVoto R. H. *et al.* Use of helium in uranium exploration, Grants district. *Mem. New Mex. Bur. Mines* 38, 1980, 368–79.
10. Fisher J. C. Remote sensing applied to exploration for vein-type uranium deposits, Front Range, Colorado. Ph.D. thesis, Colorado School of Mines, 1976.
11. Galloway W. E. Kreitler C. W. and McGowen J. H. eds. *Depositional and ground-water flow systems in the exploration for uranium: a research colloquium* (Austin: University of Texas Bureau of Economic Geology, 1979), 267 p.
12. Hanrahan E. J. Williamson R. H. and Bown R. W. United States uranium requirements. *Rep. U.S. Energy Res. Dev. Adm.* GJO-108(76), 1976, 51–65.
13. Harshman E. N. Distribution of elements in some roll-type uranium deposits. In *Formation of uranium ore deposits* (Vienna: IAEA, 1974), 169–83.
14. Heine T. The Rabbit Lake deposit and Collins Bay deposits. Reference 4, 87–102.
15. Jones C. A. A classification of uranium deposits in sedimentary host rocks. In *NURE uranium geology symposium* (Grand Junction, Colo.: Bendix Engineering Corporation, 1978), 23–8.
16. Langen R. E. and Kidwell A. L. Geology and geochemistry of the Highland uranium deposit, Converse County, Wyoming. *Earth Sci. Bull.*, **6**, Dec. 1973, 41–8.
17. Mathews G. W. A classification of uranium deposits in and related to plutonic igneous rock. Reference 15, 15–21.
18. Morse J. G. Nuclear power: issues and outlook. *Colo. Sch. Mines Mineral Ind. Bull.*, **19**, no. 6, Nov. 1976, 10 p.
19. Patterson J. A. Uranium market activities. *Rep. U.S. Energy Res. Dev. Adm.* GJO-108(75), 31–49; *Energy Abstr.*, **3**, 1977, 104.
20. Raines G. L. Offield T. W. and Santos E. S. Remote-sensing and subsurface definition of facies and structure related to uranium deposits, Powder River Basin, Wyoming. *Econ. Geol.*, **73**, 1978, 1706–23.
21. Robbins D. A. Applied geology in the discovery of the Spokane Mountain uranium deposit, Washington. *Econ. Geol.*, **73**, 1978, 1523–38.
22. Rowntree J. C. and Mosher D. V. Case history of the discovery of the Jabiluka uranium deposits, East Alligator River region, Northern Territory of Australia. Reference 5, 551–73.
23. Runnells D. D. *et al.* Applications of computer modeling to the genesis, exploration, and in-situ mining of uranium and vanadium deposits. *Mem. New Mex. Bur. Mines* 38, 1980, 355–67.
24. Scott J. H. and Daniels J. J. Non-radiometric borehole geophysical detection of geochemical haloes surrounding sedimentary uranium deposits. Reference 5, 379–90.
25. Smith A. Y. Barretto P. M. C. and Pournis S. Radon methods in uranium exploration. Reference 5, 185–211.
26. Smith B. *et al.* A case for "other" geophysical methods in exploration for uranium deposits. Reference 5, 337–51.
27. Tan B. Geochemical case history in the Key Lake area. In *Uranium in Saskatchewan* Dunn C. E. ed. *Spec. Publ. Saskatchewan geol. Soc.* no. 3, 1977, 323–30.
28. Tape G. F. The next twenty years—IAEA's role. *IAEA Bull.*, **19**, no. 4 1977, 49–54.
29. Young R. G. An overview of uranium in sedimentary rocks. Reference 15, 59–65.

Geochemistry of uranium in the hydrographic network

Bernard Soyer
Section de Géochimie, COGEMA, Paris, France

In France regional geochemistry is based on the sampling of the elements of the hydrographic network, water and stream-sediment sampling always being carried out. Uranium contents are determined in both elements of the hydrographic network—liquid and solid. For regional surveys hydrogeochemistry is best suited for elements that produce very soluble complexes—for example, uranium. At this stage no other elements are assayed, uranium being its own best tracer in water.

Hydrogeochemistry

Uranium solubility

Uranium is a strong oxiphile element, occurring as the tetravalent ion U^{4+} and the hexavalent ion U^{6+} (uranyl ion). Oxidation of the former is possible over a wide pH range by alteration of the primary sources of uranium, oxygen being supplied by air dissolved in water. Uranium is then separated from all the naturally radioactive products of disintegration.

The uranyl ion is extremely mobile, forming complexes with several anions (CO_3^{2-}, SO_4^{2-}, PO_4^{2-}, F^-), uranyl carbonates and sulphates, and also hydroxides and organic complexes. For the uranyl carbonate complexes bicarbonates $(UO_2(CO_3)_2)^{2-}$ and tricarbonates $(UO_2(CO_3)_3)^{4-}$ prevail at pH values greater than 4.5. For the uranyl sulphate complexes the bisulphates $(UO_2(SO_4)_2)^{2-}$ and trisulphates $(UO_2(SO_4)_3)^{4-}$ are stable at pH 4, whereas humic and fulvic complexes arise at close to neutral pH values.

Precipitation occurs as a result of the reduction of the hexavalent ion to a tretravalent ion with modification of pH, pressure, temperature, etc. Uranium is fixed by clay minerals, iron and manganese hydroxides, phosphates and organic matter.

Sampling

The advantage of sampling water over other materials is based on its homogeneity, which ensures a representative sampling of the environment. Water is always taken in the clearest flowing part of the stream as far away as possible from the banks. Water is stored in a soft polyethylene bag, which is sealed. Analyses are made as quickly as possible, but the use of the polyethylene bag ensures negligible changes in uranium content with time, which is not always true of rigid polyethylene bottles.

Uranium analysis

The water sample is analysed after a short decantation period (24 h). After the dissolved content of the water has been concentrated on a strip of chromatographic paper, uranium is isolated and assayed by fluorimetry. It is especially important not to acidify the water to avoid precipitation of organic material and leaching of suspended particles. Filtering of the water is not recommended—to avoid fixation of uranium on the filter paper. Thus, every effort should be made to obtain the clearest possible sample.

In regional prospecting pH measurements are not very satisfactory, but conductivity measurements do indicate the degree of water salinity.

Two types of assays are carried out on the water sample. *Dissolved uranium* is the form of analysis that is most widely used by geochemists. The inconvenience of this method lies in the low levels, usually expressed in ppb, and the poor contrast between anomalous and background values. Of primary importance is the *uranium content in the dry residue*: variations in the uranium content in water as a result of fluctuating water levels are virtually eliminated by this method.

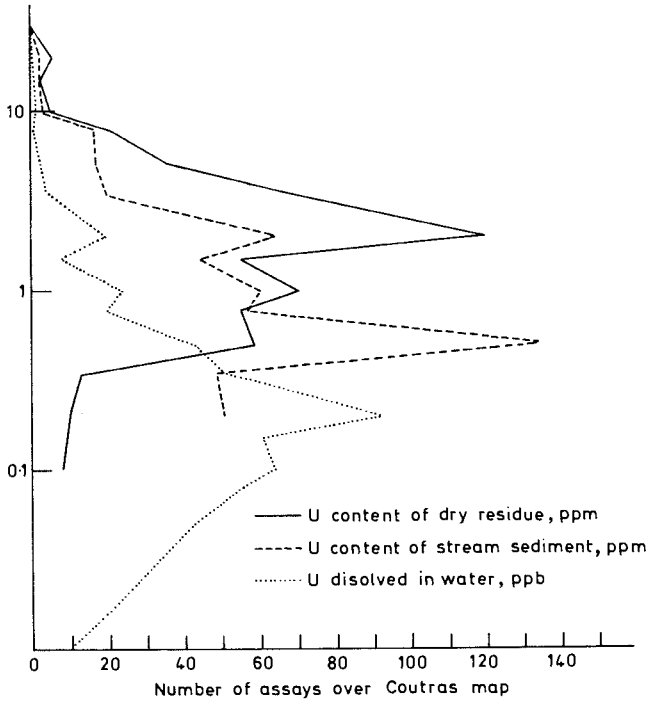

Fig. 1 Comparison of uranium content in dissolved water and dry residue, Coutras, France

Comparison at Coutras, France (Fig. 1) of frequency curves of uranium content dissolved in water and that of the dry residue and in the stream sediment reveals different results. The first peaks indicate background value. It is interesting that for uranium dissolved in water and stream sediment uranium content they represent a significant proportion of the assays in comparison with the anomalous values. For the uranium content in the dry residue, however, background values are denoted by a series of assays between 0.5 and 1.5 ppm. The anomaly is not only marked by a sharp peak but by an anomalous background (2 ppm) that progressively declines, despite many analyses of higher values (66 at 3.5 ppm and 36 at 5 ppm).

As is shown for the Goulor River, Coutras, the uranium content in the dry residue is not specific to the location of the mineralization but extends over a wide area, which is not so for other types of assay.

Hydrogeochemistry and prospecting

Even though the considerable mobility of uranium is a good regional pathfinder, it is appropriate to conduct detailed sampling, the grid being a function of relief, geology and, of course, type of drainage. In sedimentary terrain sampling is carried out at a density of 1/km^2, whereas in crystalline terrain the density must be much greater.

A study with widely spaced sampling would only give indi-

cations of regional geochemistry that could be obtained just as easily with stream or lake sediment samples.

An orebody can produce an anomalous trend of several kilometres in sedimentary terrain, but rarely more (at Coutras, the anomalous aureole is smaller). In crystalline terrain, such as the orebodies in La Crouzille, France, the anomalies are always very close to the mineralization. A sudden increase in the uranium content of water is undetectable unless dense sampling is used.

The use of hydrogeochemical prospecting is often criticised because of the lack of reproducibility of sample values. It is true that background and anomalous values are inconsistent, changing with the seasons and the passage of time in line with water-level variations and the environment in general. These variations are more pronounced for levels of uranium dissolved in water than for those expressed in the dry residue. It is possible to obtain consistent and representative values by sampling from basin to basin.

The absolute value of a sample is not always the most interesting feature: in hydrogeochemistry it is the increase of value along a line of drainage that is most significant.

An anomaly corresponds to an increase in uranium values and an increase in water flow: normally, values would decrease as a result of progressive dilution. The importance of the anomaly may change over the year, but the anomaly is denoted by the persistent increase downstream.

Coutras orebody

The discovery of the Coutras orebody was mainly due to the geochemistry of waters and stream sediments, this example illustrating the value of this method and also its limitations.

The orebody, of Middle to Upper Eocene age, is located in the Jean Vincent and Le Fieu formations of interbedded sequences of sandstones and shale. The average grade is low (1‰), but very extensive.

Mineralization occurs in several areas, each with a different geochemical response. On the right-hand bank of the Dronne River, from Chamadelle to La Barde, the mineralization is 30 m thick and sub-outcropping. The geochemical response (see Figs. 3 and 4) is very clear, especially in the dry residue. The example from the Goulor (Fig. 2), a small river draining part of the mineralized formations, is outstanding.

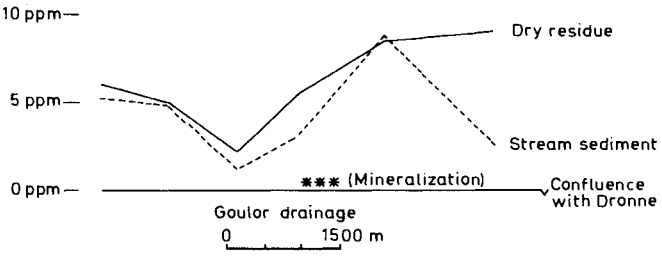

Fig. 2 Halo indicated by dry residue results in Goulor River, Coutras, France

After a progressive decline in uranium values both in stream sediments and dry residues, owing to background changes, the content again increases. The dry residue continues to increase, indicating an anomaly of interest at the position of known mineralization, whereas the stream sediment decreases sharply.

The sector west of Coutras gave better results from dry residues than stream sediments, coinciding with an extension of the orebody. On the other hand, the extension of the orebody located near Le Fieu is not at all evident from the geochemical survey, apart from one high value of the dry residue of a sample taken from a creek on the left-hand bank of the Dronne River (dry residue, 19 ppm; stream sediment, 5.1 ppm).

Only these values measured in water provide evidence of mineralization to the south of the Dronne River, corresponding with a deep mineralization (30–100 m below surface) untouched by the hydrographic network. In this case groundwater geochemistry, though difficult to interpret, would be the appropriate tool for a blind detailed study.

Limitations of hydrogeochemistry

In flat-lying areas with deeply dissected drainage (e.g. the Paris Basin) anomalies occur within particular aquifers and the problem of hydrogeological interpretation is not necessarily easy to solve.

In mountainous terrain, especially with carbonates (the Alps and Pyrenees) water is not always reliable. Cold water has a high capacity to dissolve carbon dioxide, which increases the leaching potential of the water. Uranium values are therefore frequently higher than normal, but no real significance can be presumed.

Detailed hydrogeochemistry

Hydrogeochemistry is infrequently used for detailed prospecting, but it can be effective. Two types of detailed survey are in use in France. Sample density is increased where background values rise significantly along a line of drainage: complimentary sampling of stream sediment and water is carried out every 200 m, or even every 100 m, to locate precisely the anomalous source area. This high-density sampling procedure is reliable and led to the discovery of a number of showings in Coutras.

Detailed study of all sites of groundwater discharge at the surface (springs and seepages) constitutes a good technique. Such a study was conducted in La Crouzille in France along mines and known showings to test the potential of the method.

In addition to the usual analyses (dissolved uranium in water, uranium content of dry residues and stream sediments), sampling also includes radon, since its short half-life (3.8 days) limits its possible displacement from its source. For radon sampling a hypodermic syringe (30 cm^3) is used to collect the water at the site of discharge and the sample is inserted into a vacuum-sealed test-tube.

The La Crouzille study was a good test of the method. The bedrock of the area is homogeneous (Saint Sylvestre leucogranite) and 2150 samples were taken within a 95-km^2 area (23 samples/km^2). Altogether the results are positive as each known mineralization was associated with geochemical anomalies. The real difficulty lies in the concordance of results for different types of analysis.

At Montmassacrot (Fig. 5) the mineralized formations trend WSW–ENE and dip 60–80° to the north. They consist of very brecciated seams of disseminated pitchblende and coffinite (average grade, 0.8‰). Radon clearly indicates the mineralization with anomalous values close to the ore deposit. There is a good correlation between these results and those of the dry residual uranium content.

At La Borderie (Fig. 6) the formations are similar (subvertical or dipping 70° to the north), but with a less brecciated seam. The mineralization occurs as coffinite (grade, 2.8‰), mostly concentrated in the intersection of tectonic trends.

Geochemistry on slopes

Hydrogeochemistry does not end with the study of the flow load, liquid and solid: one must consider what feeds that flow. This essential phase at the detailed prospecting stage, especially around an anomaly, must therefore include a slope study. This can be conducted by hydrogeochemistry if springs and seepages are abundant (see above). In the absence of water a soil survey must be undertaken on the slopes, close to the anomalous area.

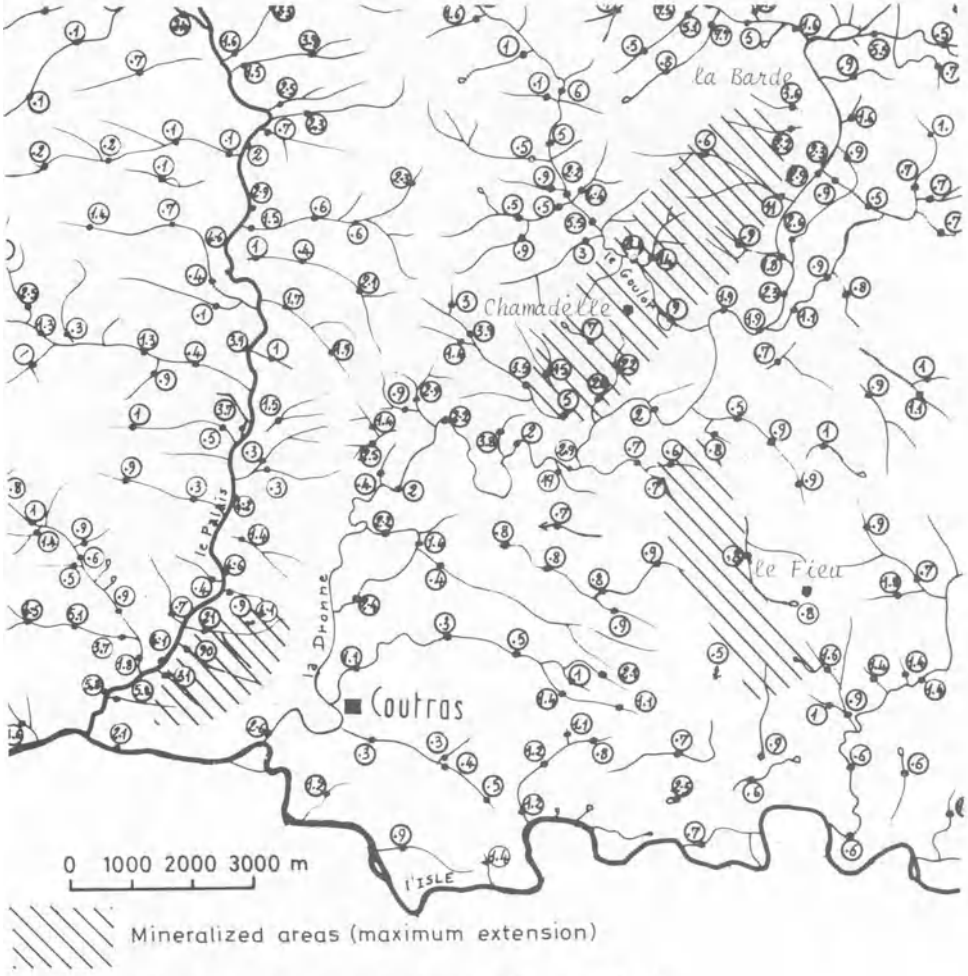

Fig. 3 U content (ppm) of dry residue in vicinity of Coutras orebody

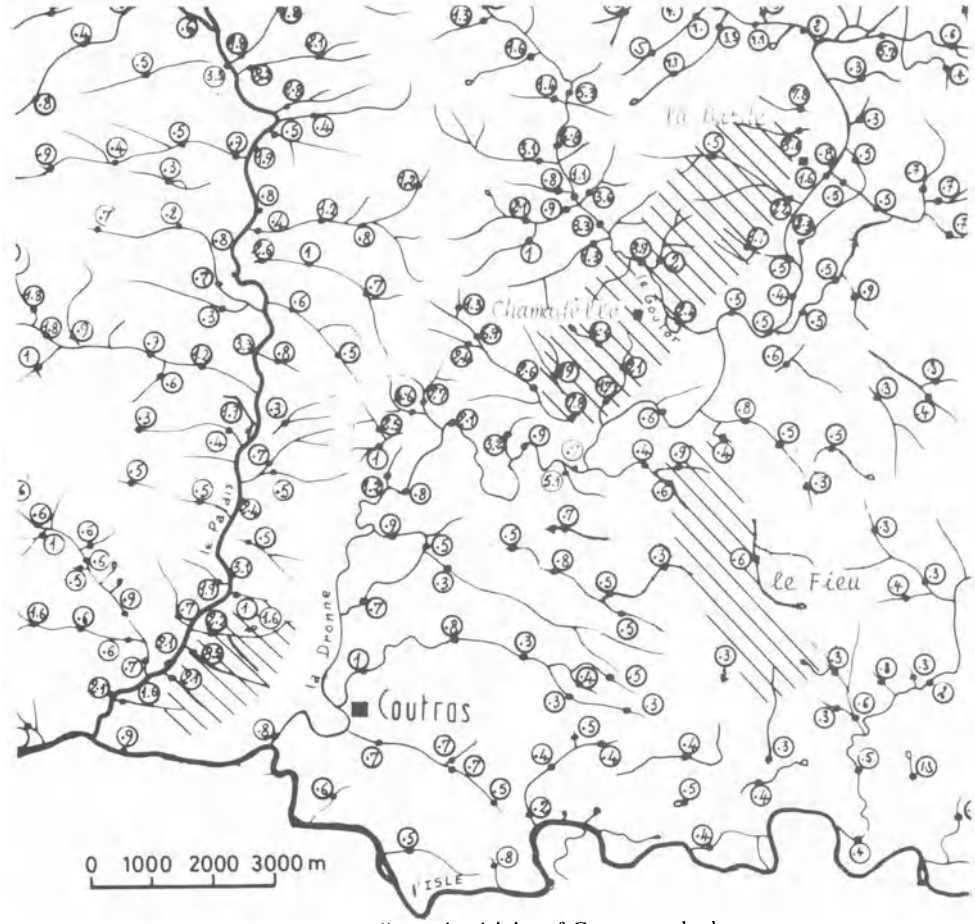

Fig. 4 U content (ppm) of stream sediment in vicinity of Coutras orebody

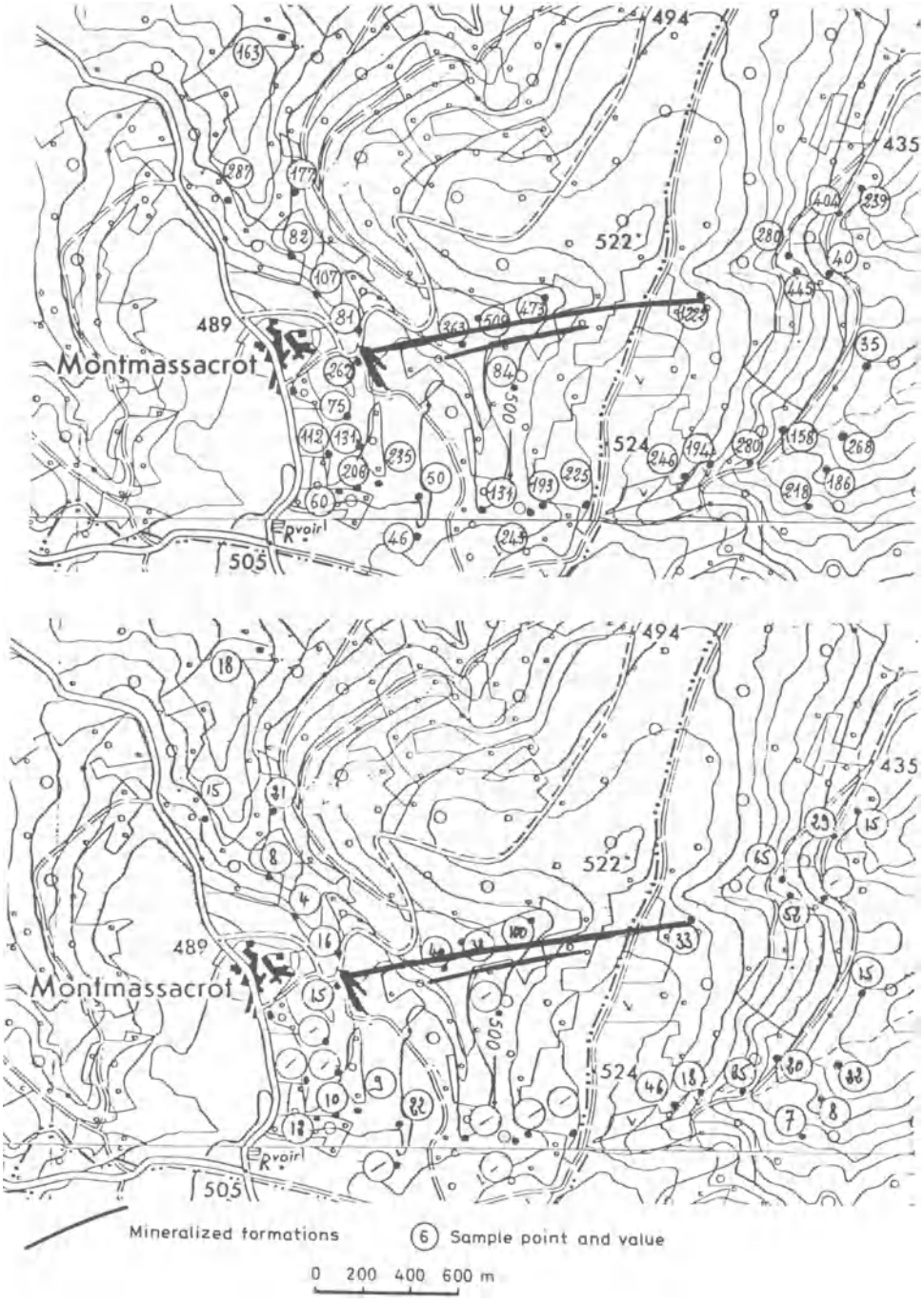

Fig. 5 Ra results in emanations (*top*) and U content (ppm) in dry residue

In this case, it can be helpful to use the decay products of uranium to focus on the source and to understand the arrangement of the anomalies in the hydrographic network.

Stream sediments

Stream sediment sampling is a common method that provides values high enough to be expressed in ppm. The contents of the stream sediment are consistent because they are not affected by meteorological fluctuations.

Sampling

For uranium the sample is usually taken from the flowing part of the stream, thereby yielding a sample that is sufficiently rich in clay or silt but with negligible organic content. Analyses are carried out on the -100-μm fraction. A weak HNO_3 acid attack is used to extract the uranium. The dissolved uranium is measured by fluorimetry after chromatographic separation.

The interpretation of the assays may not always be reliable because of variation in the constituents of the sediments in the stream. Stream sediments themselves may be leached or they may represent a rock that has already been leached to the point at which uranium is no longer accessible to the stream sediments. That is so for certain sedimentary environments in which values are too weak to enable the variation in uranium content to be assessed.

Importance of complementary water and stream sediment sampling

Only by sampling both water and stream sediment can a complete geochemical prospecting study be achieved.

In crystalline terrain conductivity varies within very narrow limits, without regard to the dissolved materials, even measured in the dry residue. It is therefore useful to sample stream sediments, the water being poorly mineralized. In addition, rapid lithological changes can obliterate the variation in the uranium content in water.

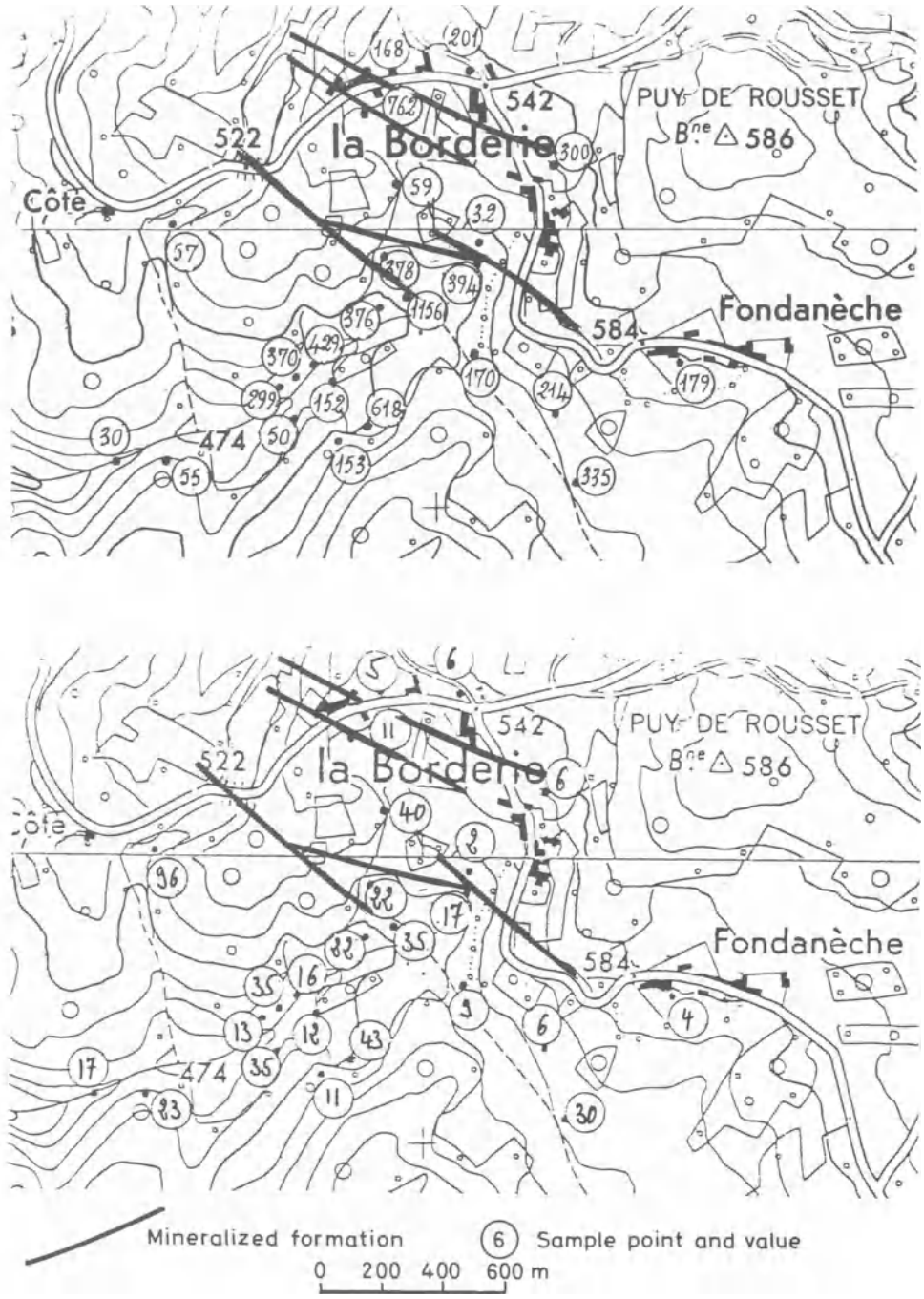

Fig. 6 Ra results in emanations (*top*) and U content (ppm) in dry residue

In sedimentary terrain the contrary is true. Stream sediments are themselves easily leached, the extreme case being that of limestones, where uranium is readily leached. Thus, uranium will be present in water rather than in stream sediments. In this environment uranium content varies in accordance with conductivity, even though there may be fluctuations of the local water-table. Uranium content in the dry residue of a water sample constitutes the best method of analysing water for uranium.

Commonly, if the sampling is sufficiently detailed there is a certain concordance between the uranium content in water, the dry residue and the stream sediment. Nevertheless, the anomalies in sedimentary terrain are more evident in the dry residue, whereas in crystalline terrain stream sediment sampling provides the best results.

Detailed geochemistry in regions of heavily leached soils

The Mikouloungou ore deposit in Gabon is a significant example of the potential use of soil geochemistry, despite intensive leaching. The uranium content of the soils developed on the Congolian sedimentary formations (Francevillian) is very low. This area is not favourable for such a study as precipitation is marked and the lateritic soils can be very thick (10 m and more).

A classic stream sediment survey was at the origin of the selection of the Mikouloungou area for a detailed soil geochemistry programme. A 200 m × 200 m grid was therefore laid out over a large area.

Geological setting

The Mikouloungou ore deposit is situated on a WNW–ESE fault of more than 7 km in length. This important tectonic feature is at the foot of a great escarpment that borders the Ogoué plain.

The mineralization is distributed in preferential beds and is always located in proximity to the fault, which is steeply

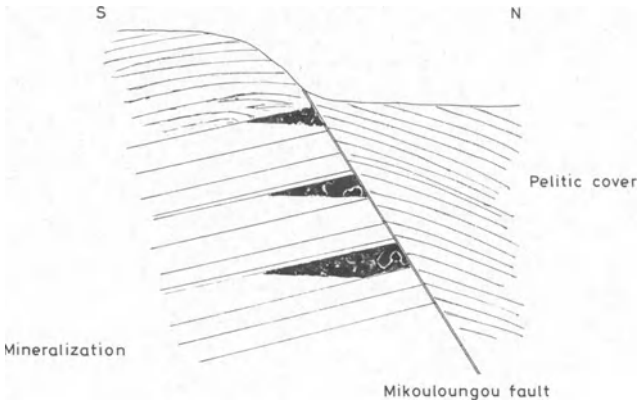

Fig. 7 Mineralization setting at Mikouloungou, Gabon

dipping (70°). The mineralization occurs in geometrical traps produced by several transverse displacements, forming a monocline and dipping gently (5–10°) and consistently to the south. The mineralization has a significant average thickness (approximately 2 m) and a rather high average grade (3.5‰), but distributed as pockets along the fault (Fig. 7).

In addition, owing to the tectonic deformation, the mineralized pockets occur at different levels from surface to significant depth, and with a pelitic cover.

Geochemical results

The anomalies that indicate the presence of the mineralized fault vary in intensity and extension.

In the western part (*A*, *B*, *C*, *D* and *E* in Fig. 8) the geochemical anomalies are well marked. The 2 ppm contour encircles extended surfaces. On the other hand, the eastern points (*F*, *G*, *H* and *I*) related to the same fault are not so well indicated by geochemistry. This is explained not by the change in soil thickness but by a different type of response at these mineralized points: the western part corresponds to anomalies in residual soil and the mineralization is sub-outcropping; the eastern part is far from the surface and the geochemical response is that of a leakage anomaly.

Thus, two kinds of soil anomalies—directly lying on the mineralization or indicating the presence of an anomaly at depth—are possible in regions of heavy leaching. The anomalous threshold is very low (1 or 2 ppm), but still reliable.

Use of radium in detailed soil geochemical exploration

Because of its weak mobility in relation to uranium, it is particularly useful to determine the radium content in the soil during detailed prospecting. The contrary geochemical behaviour of radium and uranium (mobility in reducing conditions, immobility in oxidizing conditions) may be used to interpret specific anomalies (swamps, stream beds, etc.).

Radium solubility

The reduced mobility of radium in comparison with uranium is explained by the solubility difference between the two elements, which occur in nature as sulphates and carbonates: at 18°C radium sulphate = 1.410^{-3} g/l; uranyl sulphate = 205 g/l; radium carbonate is insoluble; and uranyl carbonate = 60 g/l. With the acidity and alkalinity of water, however, radium solubility changes. The radium content of water also depends on the salt concentration of certain elements—mainly alkaline chloride (radium replaces sodium). Radium precipitates with complexes of barium (SO_4Ba) and with calcium carbonates (travertine). Radium is also fixed by clay, organic matter, iron and manganese hydroxides.

Application to soil geochemistry

Lagadaillère (Forez, France) is a significant example of the use of radium in focusing exploration over an uraniferous mineralization.

A siliceous vein that cuts through granite with a pitchblende mineralization forms small lenticulations unevenly distributed throughout the gangue. This setting lies in the middle of a slope 230 m from a stream. Soil sampling (at the limits of the *A* and *B* horizons) with a 20 m × 20 m grid was carried out and samples were analysed for mobile uranium and radium. Uranium results (Fig. 9) present the highest anomalies in the stream bed, but no important value was found close to the vein, with the exception of a small value related to a small thalweg that cuts the slope. Radium, however, remains very close to the vein. The

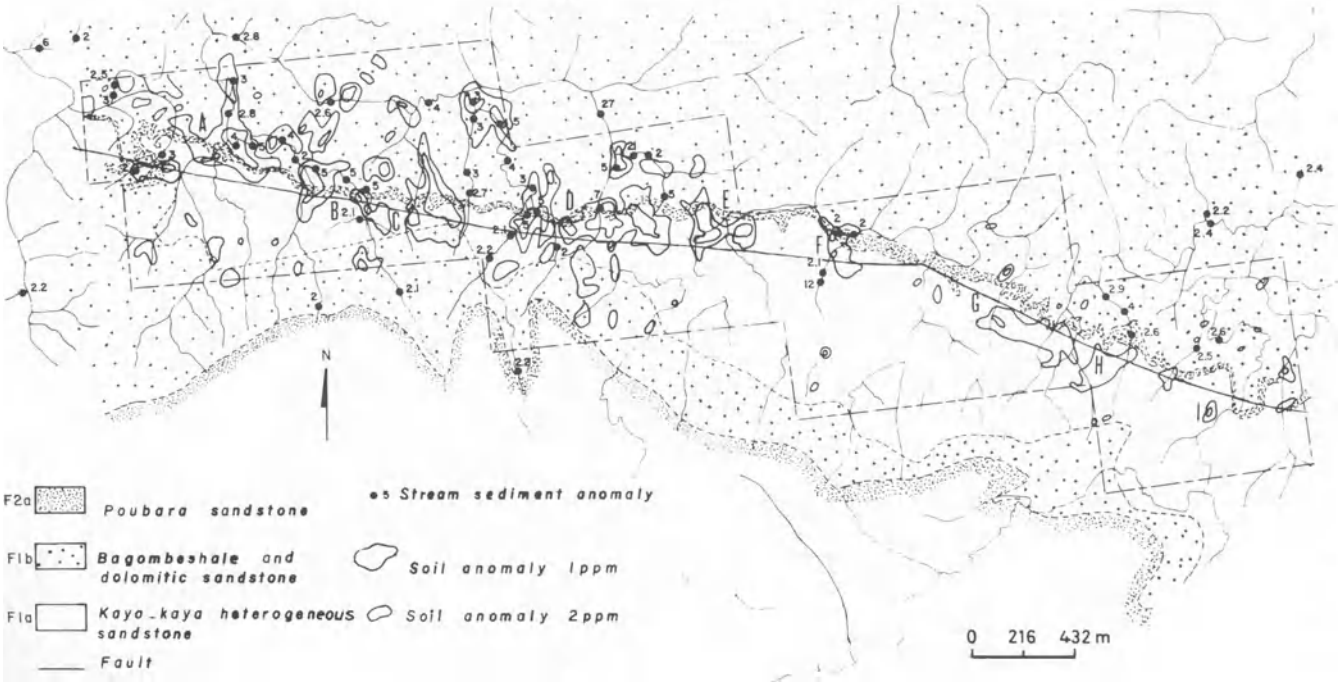

Fig. 8 U soil geochemistry at Mikouloungou, Gabon

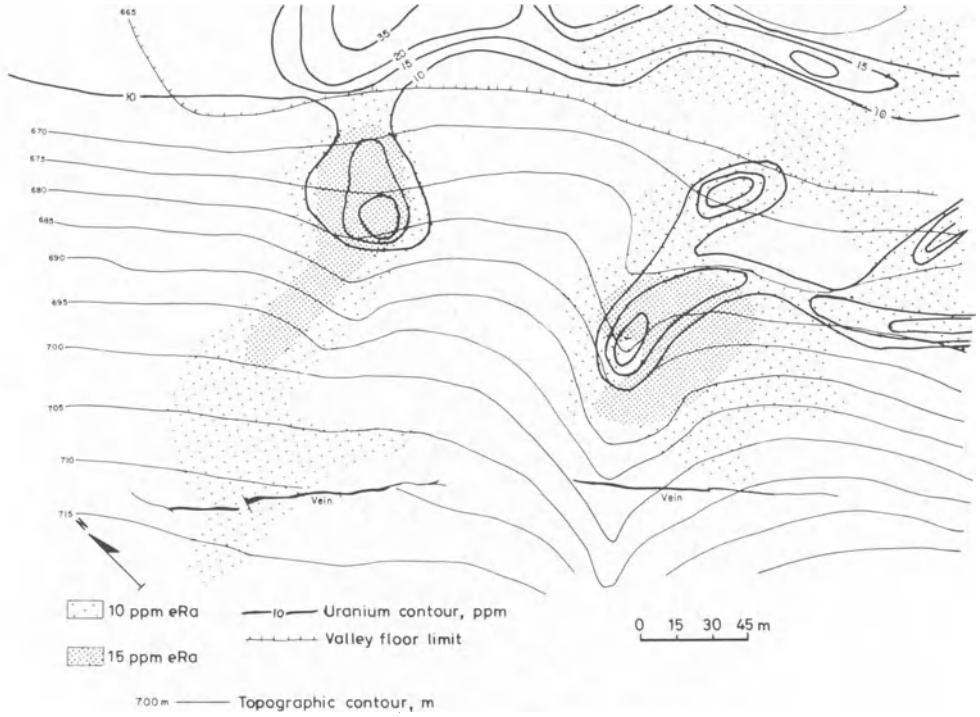

Fig. 9 U and Ra dispersion in soil, Lagadaillère, France

10 ppm contour starts from the vein and reaches the edge of the stream bed.

This example illustrates the different behaviour of the two elements according to topography and environment. Uranium is rapidly removed from the slope in a well-drained area and trapped in the valley floor, where organics are normally more abundant and conditions frequently more reducing. The leaching of radium towards the base of the slope is difficult as the soil is an oxidizing environment in which radium is rather immobile. For this reason radium remains close to its source—the pitchblende vein (Fig. 10).

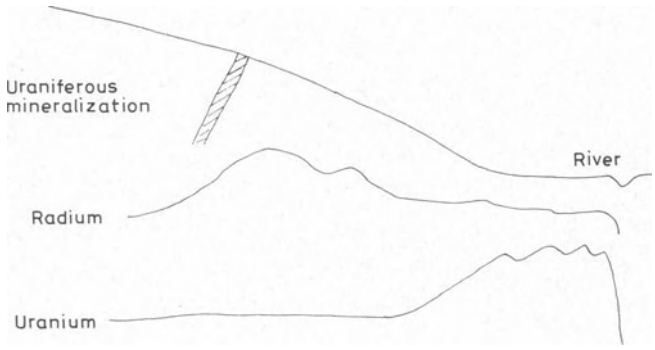

Fig. 10 U and Ra migration on slope, Lagadaillère, France

Lagadaillère illustrates a classic situation where the uranium anomaly is restricted to the valley floor with no relation to the position on the slope of the uraniferous mineralization. The judicious use of radium soil geochemistry establishes the relationship.

Conclusions

The hydrographic network provides an appropriate tool for uranium prospecting under the following conditions: water and stream sediment samples must be taken at the same location and assays in water must include uranium content in the dry residue, which appears to be the most suitable and reliable value.

Depending on the terrain under investigation, water (in sedimentary areas) or stream sediment (in crystalline areas) will be of major significance. In practice, there will be fluctuations in the same sense, but not of the same magnitude.

For regional reconnaissance uranium is its own best indicator, being readily oxidized to the hexavalent state and then remaining very mobile under oxidizing conditions. For detailed prospecting uranium and its decay products are interesting for assay purposes. The low mobility of radon and radium from their source makes them good tracers. To date, experience in France shows the results for radon always to have been better in water and for radium in soils.

Other decay elements have been tested—with contradictory results and low reliability—but, no doubt, they will be added to the range of tools available to the geochemist in the search for uranium in the future.

Bibliography

1. Beus A. A. and Grigorian S. V. *Geochemical exploration methods for mineral deposits* (Wilmette, Ill.: Applied Publishing, 1977), 287 p.
2. Blanchot A. and Clergue I. Utilisation des méthodes de prospection géochimiques en AOF. *Rev. Ind. minér.*, 1956, no. spécial IM, 310–4.
3. Boyle R. W. and Garrett R. G. Geochemical prospecting—a review of its status and future. *Earth Sci. Rev.*, **6**, 1970, 51–75.
4. Boyle R. W. *et al.* Hydrogeochemical methods—application in the Canadian Shield. *CIM Bull.*, **64**, Nov. 1971, 60–71.
5. Cadigan R. A. and Felmlee J. K. Radioactive springs geochemical data related to uranium exploration. *J. geochem. Explor.*, **8**, 1977, 381–95.
6. Cameron E. M. and Ballantyne S. B. Reconnaissance-level geochemical and radiometric exploration data from the vincinity of the Rabbit Lake uranium deposits. *CIM Bull.*, **70**, May 1977, 76–85.
7. Cameron E. M. and Hornbrook E. H. W. Current approaches to geochemical reconnaissance for uranium in the Canadian Shield. In *Exploration for uranium ore deposits* (Vienna: IAEA, 1976), 241–66.
8. Chamberlain J. A. Hydrogeochemistry of uranium in the Bancroft–Haliburton Region, Ontario. *Bull. geol. Surv. Can.* 118, 1964, 19 p.
9. Chork C. Y. Seasonal, sampling and analytical variations in stream sediment surveys. *J. geochem. Explor.*, **7**, 1977, 31–47.
10. Dall'Aglio M. and Tonani F. Archiviazione e trattamento dei dati idrogeochimici. *Studi Ric. Div. geominer. Ital*, **3**, 1960.
11. Dall'Aglio M. and Tonani F. L'analisi chimica dele acque naturali come mezzo di indagine geochimica. *Studi Ric. Div. geominer. Ital.*, **3**, 1960.

12. Dall'Aglio M. Comparison between hydrogeochemical and stream-sediment methods in prospecting for mercury. *Geochemical exploration* (Toronto: CIM, 1970), 126–31. (*CIM Spec. vol.* 11)
13. Dall'Aglio M. A study of the circulation of uranium in the supergene environment in the Italian Alpine range. *Geochim. cosmochim. Acta*, **35**, 1971, 47–59.
14. Dall'Aglio M. and Gigli C. Storage and automatic processing of hydrogeochemical data. In *Rep. 24th Int. geol. Congr., Canada, 1972*, Sect 16, 1972, 49–57.
15. Durham C. C. and Cameron E. M. A hydrogeochemical survey for uranium in the northern part of the Bear Province, Northwest Territories. *Pap. geol. Surv. Can.* 75-10, 1975, 331–2.
16. Dyck W. Geochemical studies in the surficial environment of the Beaverlodge area, Saskatchewan. *Pap. geol. Surv. Can.* 74-32, 1974, 30 p.
17. Dyck W. Geochemistry applied to uranium exploration. *Pap. geol. Surv. Can.* 75–26, 1975, 33–47.
18. Dyck W. Application of hydrogeochemistry to the search for uranium. In *Geophysics and geochemistry in the search for metallic ores* Hood P. J. ed. *Econ. Geol. Rep. geol. Surv. Can.* 31, 1979, 489–510.
19. Dyck W. *et al.* Well water trace element reconnaissance, Eastern Maritime Canada. *J. geochem. Explor.*, **6**, 1976, 139–62.
20. Dyck W. Pelchat J. C. and Meilleur G. A. Equipment and procedures for the collection and determination of dissolved gases in natural waters. *Pap. geol. Surv. Can.* 75-34, 1976, 12 p.
21. Fix P. F. Hydrogeochemical exploration for uranium. *Prof. Pap. U.S. geol. Surv.* 300, 1956, 667–71.
22. Fleischer R. L. and Delany A. C. Determination of suspended and dissolved uranium in water. *Analyt. Chem.*, **48**, 1976, 642–5.
23. Geffroy J. and Sarcia J. A. Quelques remarques relatives à la géochimie des filons épithermaux à pechblende. *Bull. Soc. géol. France*, 6e Sér., **8**, 1958, 531–6.
24. Granier C. Mise en évidence de structures minéralisées par prospection microchimique tactique. *Chron. Mines d'outre Mer*, **26**, 1958, 350–1.
25. Granier C. L. La terminologie des méthodes de prospection géochimiques. *Bull. Soc. fr. Minér. Cristallogr.*, **85**, 1962, 11–4.
26. Granier C. L. Informations données par les méthodes de prospection géophysique et géochimique. In *Colloque de géophysique minière, Nov. 1971.* (B.R.G.M.)
27. Granier C. L. *Introduction à la prospection géochimique des gîtes métallifères* (Paris: Masson, 1973), 143 p.
28. Grimbert A. La prospection hydrogéochimique dans la recherche des gîtes uranifères. *Conf. CEA* no. 7, 1956, 4 p.
29. Grimbert A. Applications des techniques géochimiques de prospection à la recherche et à l'étude des gîtes uranifères en France Métropolitaine. In *Symposium de exploración geoquímica, 20th Int. geol. Congr., Mexico, 1956*, vol. 3, 1960, 655–69.
30. Grimbert A. and Obellianne J. M. Essais de prospection géochimique de l'uranium en pays aride. *Rapport CEA* 2219, 1962, 48 p.
31. Hawkes H. E. The downstream dilution of stream sediment anomalies. *J. geochem. Explor.*, **6**, 1976, 345–58.
32. Haglund D. S. Friedman G. M. and Miller D. S. The effect of fresh water on the redistribution of uranium in carbonate sediments. *J. sedim. Petrol.*, **39**, 1969, 1283–96.
33. Hawkes H. E. and Webb J. S. *Geochemistry in mineral exploration* (New York: Harper and Row, 1962), 415 p.
34. Hoag R. B. Jr and Webber G. R. Hydrogeochemical exploration and sources of anomalous waters. *J. geochem. Explor.*, **5**, 1976, 39–57.
35. Hunt E. C. The examination of natural waters for uranium in Derbyshire. *Sci. Rep. DSIR* NCL/AE 538, 1958.
36. Illsley C. T. Preliminary report on hydrogeochemical exploration in the Mt. Spokane area, Washington. *Open-File Rep. U.S. AEC* MFC no. 7233, 1957, 19 p.
37. Illsley C. T. Hydrogeochemical reconnaissance for uranium in the Stanley area, south-central Idaho. *Rep. U.S. AEC* RME-140, 1961, 21 p.
38. Jurain G. Sur la teneur en uranium d'eaux thermales du Sud des Vosges. *C.R. Séanc. Acad. Sci. Paris*, **241**, 1955, 1482–5.
39. Jurain G. Remarques sur la teneur en uranium des eaux des Vosges méridionales. *C.R. Séanc. Acad. Sci. Paris*, **245**, 1957, 1071–4.
40. Jurain G. Signification géochimique des anomalies de teneur en radon des eaux des massifs cristallins et cristallophylliens. *C.R. somm. Soc. géol. France*, **14**, 1958, 348–50.
41. Jurain G. Moyens et résultats d'étude de la radioactivité due au radon dans les eaux naturelles. *Geochim. cosmochim. Acta*, **20**, 1960, 51–82.
42. Jurain G. Sur la possibilité d'utiliser le dosage du radon des eaux souterraines dans la prospection des gîtes uranifères. *C.R. Séanc. Acad. Sci. Paris*, **252**, 1961, 3090–2.
43. Jurain G. Contribution à la connaissance géochimique des familles de l'uranium–radium et du thorium dans les Vosges méridionales. Application de certains résultats en prospection des gisements d'uranium. *Rapport CEA* no. 2154, 1962, 349 p.
44. Krajnov S. R. L'utilisation des cours d'eaux alimentés par des eaux souterraines pour la prospection hydrogéochimique des gîtes minéraux. *Razv. Okhr. Nedr. SSSR*, 1958, 42–6.
45. Langmuir D. and Applin K. Refinement of the thermodynamic properties of uranium minerals and dissolved species, with application to the chemistry of groundwaters in sandstone-type uranium deposits. *Circ. U.S. geol. Surv.* 753, 1977, 57–60.
46. Levinson A. A. *Introduction to exploration geochemistry* (Calgary, Alberta: Applied Publishing, 1974), 612 p.
47. Lovering T. S. Work of the geochemical exploration section of the U.S. Geological Survey. *Trans. Am. Inst. Min. Engrs*, **202**, 1955, 963–6.
48. Lovering T. S. Prospection et recherche de l'uranium. Les travaux de prospection du Geological Survey, USA. In *Congrès du centenaire de la Société de l'Industrie Minérale* (Saint Etienne: The Society, 1956), 291–303.
49. Martin J. Fixation et transport de l'uranium par les substances humiques. *Rapport CEA* no. 2141, CEN-FAR, 1962, 79 p.
50. Nichol I. Garrett R. G. and Webb J. S. The role of some statistical and mathematical methods in the interpretation of regional geochemical data. *Econ. Geol.*, **64**, 1969, 204–20.
51. Ostle D. Coleman R. F. and Ball T. K. Neutron activation analysis as an aid to geochemical prospecting for uranium. In *Uranium prospecting handbook* Bowie S. H. U. Davis M. and Ostle D. eds (London: IMM, 1972), 95–107.
52. Ranchin G. La géochimie de l'uranium et la différenciation granitique dans la province uranifère du Nord-Limousin. *Rapport CEA* 4034, 1971, 394 p.
53. Rose A. W. and Keith M. L. Reconnaissance geochemical techniques for detecting uranium deposits in sandstones of northeastern Pennsylvania. *J. geochem. Explor.*, **6**, 1976, 119–37.
54. Routhier P. *Les gisements métallifères, volume 2* (Paris: Masson, 1963), 962–82.
55. Ridgley J. L. and Wenrich-Verbeek K. J. Scatter diagrams and correlations of uranium in surface water versus discharge, conductivity, and pH at various locations throughout the United States. *Open-File Rep. U.S. geol. Surv.* 79-581, 1978, 331 p.
56. Smith A. Y. and Lynch J. J. Field and laboratory methods used by the Geological Survey of Canada in geochemical surveys: no. 11. Uranium in soil, stream sediment and water. *Pap. geol. Surv. Can.* 69-40, 1969, 9 p.
57. Webb J. S. Observations on geochemical exploration in tropical terrain. Reference 29, vol. 1, 1960, 143–73.

Uranium deposits of the world, excluding Europe

Robert G. Young
Consulting Geologist, Grand Junction, Colorado, U.S.A.

Description of types of deposits

This paper is an overview of the diverse types of uranium deposits that are recognized in the world, exclusive of Europe, and presents brief descriptions of selected deposits of each major type. Descriptions of geology, mineralogy, genesis and economics of each type of deposit precede summaries of selected occurrences of most types. The locations of described deposits are shown in Fig. 1.

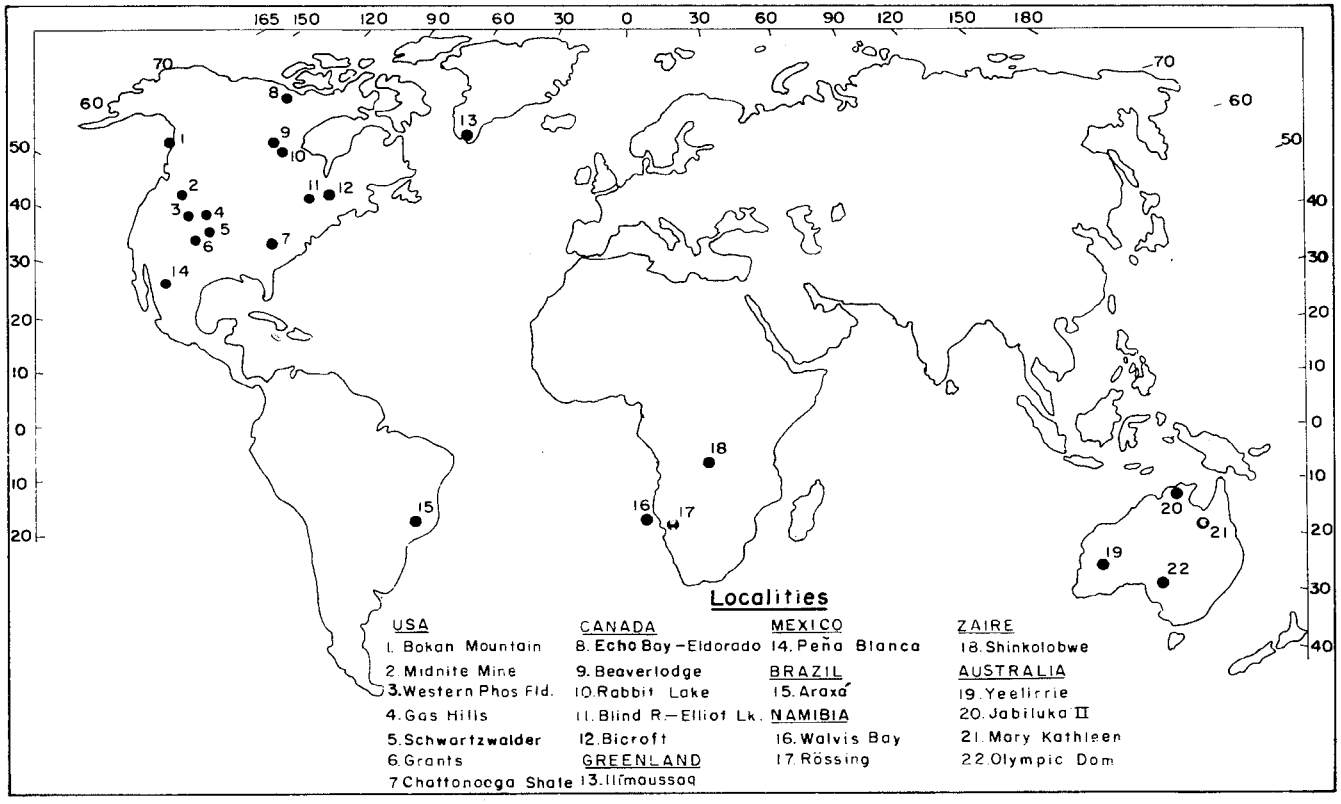

Fig. 1 Location of uranium occurrences described

Uranium is a lithophile element that is enriched in the earth's upper crust, where it has an abundance of about 2 ppm.[25,42] It is enriched in acid igneous rocks, such as granites, to about 4 ppm (occasionally to 20 ppm), whereas basic igneous rocks average 1 ppm. Uranium is known to have formed economic deposits in a great variety of igneous, metamorphic and sedimentary rocks, ranging in age from late Archaean to Holocene. Because of this ubiquitous nature and its habit of forming concentrations in diverse geologic environments, uranium deposits of one or more types are present in nearly every country.

One problem that is created by such a plethora of deposits is the difficulty of placing them in a rigid classification scheme. Many classifications have been proposed, but that used here (Table 1) is modified from that of Dahlkamp[30] and is based on the presumed time relationship of host rock to uranium emplacement. A few of the types of occurrences that are described here are not characterized by currently economic deposits, but they do represent potentially enormous uranium resources. The relative importance of major types of occurrences in relation to current reserves is shown in Fig. 2.

Sedimentary deposits

One of the major categories of uranium occurrences is that of sedimentary deposits. Such deposits are considered secondary occurrences in that they owe their existence to exogenic processes, but in these types the uranium was deposited at the same time as the enclosing sediments. They formed as a consequence of erosion of previous uranium deposits under both oxidizing and reducing conditions. Some formed in late Archaean–early Proterozoic time (2800–2200 m.y. ago) when a non-oxidizing atmosphere favoured mechanical weathering and led to the formation of placer deposits with detrital uranium.[64,93,94] Many other sedimentary uranium deposits formed after the development of an oxidizing atmosphere in mid to late Proterozoic time about 2200 m.y. ago.[103,112,113] From that time chemically liberated uranium has moved in aqueous solution to numerous lithochemical environments in which it has formed secondary concentrations. Sites of reconcentration include (1) the sea, where it has accumulated in muds, organic oozes and phosphates or has remained in solution in brines, (2) terrestrial sediments in intercratonic and intermontane basins, (3) littoral clastic sediments and (4) the weathering crust surface.

Quartz-pebble conglomerates

Quartz-pebble (Oligomictic) conglomerate uranium deposits

Table 1 Classification of uranium deposits

Mode of origin	Host rock/type deposit	Example
Sedimentary	Quartz-pebble conglomerate	Blind River–Elliot Lake (Canada)
	Black shales	Chattanooga Shale (U.S.A.)
	Muds	Walvis Bay (Namibia)
	Phosphorites	Western U.S.A.
	Bauxites	Arkansas (U.S.A.)
	Placers	Southeastern U.S.A.
	Brines	Sea water
Effusive	Silicic volcanics	Peña Blanca (Mexico)
	Mafic volcanics	Olympic Dam (Australia)
Intrusive	Peralkaline nepheline syenites	Ilímaussaq (Greenland)
	Carbonatites	Araxá (Brazil)
	Anatectics	Rössing (Namibia)
	Pegmatitic alkalitic granites	Bokan Mountain (U.S.A.)
	Granites	Spokane Mountain (U.S.A.)
	Pegmatites	Bancroft (Canada)
	Hydrothermal veins	Schwartzwalder (U.S.A.)
		Shinkolobwe (Zaire)
Metasomatic	Contact	Mary Kathleen (Australia)
	Sodic	Ukranian Shield (U.S.S.R.)
Metamorphic	Phyllites	Forstau (Austria)
	Schists	Portugal
Uncertain (vein-like)	Unconformity-related	Rabbit Lake (Canada)
		Jabiluka II (Australia)
	Vein-like in metamorphics	Beaverlodge (Canada)
		Echo Bay–Eldorado (Canada)
	Vein-like in sediments	Orphan mine (U.S.A.)
Epigenetic	Sandstones	
	Peneconcordant	Grants (U.S.A.)
	Roll-type	Gas Hills (U.S.A.)
	Stack	Franceville Basin (Gabon)
	Calcretes	Yeelirrie (Australia)
	Lignites, coals and carboniferous shales	Williston Basin (U.S.A.)
	Limestones	Todilto LS (U.S.A.)
	Epigenetic phosphates	Baukoma (Zaire)

occur in quartz-pebble conglomerates with a quartzite matrix and abundant pyrite. They contain probable detrital primary uranium minerals (uranite, brannerite, thucholite and uranothorite), and in some districts gold is an accessory. Economic concentrations are apparently restricted to the late Archaean–early Proterozoic (2800–2200 m.y. ago), but other uraniferous pebble conglomerates occur at various horizons in Precambrian shields throughout the world. The economic occurrences represent approximately 15.5% of known uranium reserves.

The origin of these deposits is controversial. They appear to be controlled not only by their proximity to unconformities (i.e. immediately above the post-Archaean unconformity) but also by hydrodynamic processes responsible for the packing density of the quartz pebbles, the abundance of pyrite and its predecessors, and its proximity to a uranium-rich Archaean source terrain. Many of the conglomerates were deposited in fluvial channels, but others appear to have been laid down in lacustrine, littoral marine and deltaic environments. Whether the uranium and other metals in the conglomerates are syngenetic (placer), hydrothermal or redistributed has not been completely resolved, but most recent literature[80, 92, 97] supports a detrital or placer origin. If they are true placers, these Precambrian uranium-bearing conglomerates are unique. The ore minerals, uraninite, brannerite, thucholite, etc., are rarely seen in Upper Proterozoic and Phanerozoic placers because of their instability during weathering and transport in an oxidizing environment.

	SHORT TONS U_3O_8	%
Pebble Conglomerate	380 000	15.54
Volcanic	380 000	15.54
Plutonic — Metamorphic	298 000	12.20
Veinlike	596 000	24.40
Sandstone	700 000	28.64
Other	90 000	3.67

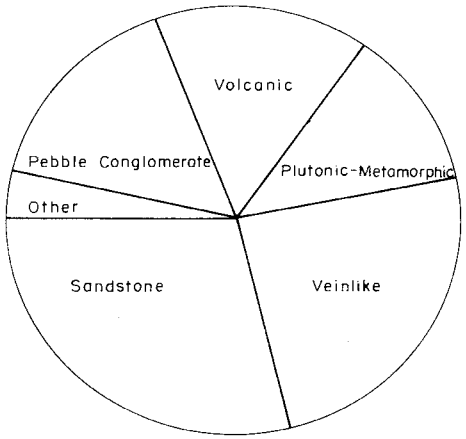

Fig. 2 Distribution of Western world uranium reserves ($30/lb) by host

Their preservation is presumably an indication of an anaerobic environment during late Archaean–early Proterozoic time.

Precambrian quartz-pebble conglomerates are low-grade uranium resources in which uranium may be just a by-product of gold mining with a grade as low as 0.01% U_3O_8, or it may be the major ore mineral with grades from 0.10 to 0.15% U_3O_8. Individual deposits range in size from 5000 to 150000 ton U_3O_8.

Classic quartz-pebble conglomerate districts are the Blind River–Elliot Lake district, Canada, and the Witwatersrand, South Africa. Similar deposits are known in Australia, Brazil, Finland, Algeria, India, the U.S.S.R. and the U.S.A.

Black shales

Uraniferous black shales are of marine origin and, in addition to colour, are characterized by high sapropelic organic content, abundant pyrite or marcasite in thin lenses, nodules or disseminated particles, and the paucity of calcium and magnesium carbonates. The shales also contain small quantities of such other metals as Mn, Ti, V, Cu, Cr, Mo, P and REE. Most of these metals are dispersed in the shale, but phosphate may also occur as nodules or phosphate-rich layers.[124]

Uraniferous shales are generally relatively thin, widespread units interbedded with other shales, limestones, phosphorites, cherts or bentonites. Some are members of cyclic units that consist of shale, sandstone and limestone, but others are siliceous and may be lateral equivalents of siliceous volcanic rocks. Most black shales are evenly laminated and dense, breaking with conchoidal fracture when fresh.

All black shales contain more uranium than the average sedimentary rock, but to be classified as a uraniferous black shale they must contain more than 0.005% U_3O_8. Uranium content differs from bed to bed, but the grade of a particular bed is remarkably uniform and predictable over large areas. Uranium content seems to be highest in closely laminated beds or those that are the finest grained, and also increases with increase in organic matter. Phosphate nodules are commonly richer in uranium than surrounding shale, but there are exceptions. No uranium minerals have been identified from the shales. It is probably adsorbed in organic or phosphatic molecules or absorbed by clays.

Uraniferous black shales are believed to have been deposited very slowly on or adjacent to tectonically stable continental platforms. Some of the richest and thickest deposits seem to have formed near platform margins. Pre-orogenic stability appears to be a requisite. The uranium seems to have accumulated syngenetically with the sediment. The marine waters may have been greatly enriched in soluble uranium by nearby volcanism or by intense weathering of granitic source terrain under oxidizing conditions. The uranium may have been extracted from the sea water (under reducing conditions), by organic matter, phosphate minerals, pyrite or colloidal clay.

Uranium deposits are typically several feet thick and cover tens, hundreds or thousands of square kilometres. Uranium content ranges from less than 0.001% to more than 0.05% U_3O_8; but, because of the immense volume of black shales, uranium resources are very large. The only near-economic deposit (Ranstad, Sweden) averages about 0.035% U_3O_8[75] and has potentially recoverable resources of about 300000 ton U_3O_8. Other uraniferous shales have almost an order of magnitude less uranium. Problems common to the development of these deposits are the difficult and costly metallurgy and the enormous environmental impact. Most of the deposits can be mined only by large open-pit operations that must be conducted in moderately populated areas.

All the larger and higher-grade uraniferous black shales are of Palaeozoic age, but some of the smaller deposits in Canada are Precambrian and some in the U.S.A. are of Mesozoic and Caenozoic age. The best known black shales are the Cambrian Külm Shale of Sweden and the Devonian–Mississippian Chattanooga Shale of the U.S.A. Similar shales are present in Brazil, Canada, France, Norway, Portugal, the U.S.S.R. and West Germany.

Muds

Many of the world's large anaerobic water bodies contain relatively thin deposits of Recent mud with a uranium content nearly an order of magnitude larger than that in average marine sediments. The muds range in thickness from 1 to 15 m and consist of planktonic ooze, sapropel and clay. Uranium averages about 25 ppm and most of it seems to be bound to planktonic matter (coccoliths and diatoms). Like black shales, uraniferous muds represent a very large uranium resource—perhaps 10000000–20000000 ton U_3O_8—but exploitation problems are enormous.

The two largest deposits of uraniferous muds are in the Black Sea (Turkey and U.S.S.R.)[33] and in the Walvis Bay area, South Africa.[78] Similar deposits are known from the Caspian and Baltic Seas and some Norwegian fjords. It thus appears that restricted environments with a trend to euxenic conditions favour uranium accumulation.

Phosphorites

Sedimentary marine phosphorites are composed principally of phosphatic minerals, and many contain significant amounts of disseminated uranium. These phosphorites have been classified as either miogeosynclinal or platform types. Four additional types that are low in uranium and of little economic importance are residual phosphorites, phosphatized rock, river pebble deposits and guano.

Phosphorites that are richest and thickest and contain the most uranium are the miogeosynclinal type deposited on the outer parts of continental shelves where upwelling of deep marine waters has occurred. These waters were saturated with respect to phosphate and were probably the source of the phosphate in the phosphorites. These phosphorites are commonly present in thick miogeosynclinal sequences, where they are associated with carbonates, black shale, chert, carbonaceous mudstone and minor amounts of mudstone.[74] The Phosphoria Formation of the western U.S.A. is an example.

Platform phosphorites are generally nodular, rather than bedded, and are associated with sandstone, limestone and glauconite. Most are low in uranium, but an exception is the Bone Valley Formation of the southeastern U.S.A. This unit has been reworked and enriched by re-exposure to sea water during a subsequent transgression. These phosphorites differ from shelf phosphorites in that they are near-shore sub-tidal and shoreline deposits, and they change facies oceanward to carbonate sediments.

All marine phosphorites consist mostly of microcrystalline apatite (carbonate fluorapatite) in the form of laminae, pellets, oolites, nodules and skeletal or shell debris. Uranium, considered syngenetic, may be present in carbonate fluorapatite as a substitute for calcium. Uranium in sea water was probably incorporated during or shortly after precipitation, and it is usually disseminated rather uniformly throughout a given bed or horizon. Primary uranium minerals are rarely present, but secondary uranium minerals (tyuyamunite, autunite, torbernite) have been identified in a few localities.

Because most of the world's phosphate resources are marine phosphorites, the uranium content of phosphate products is relatively uniform, ranging from 60 to 130 ppm. The phosphate product from the principal phosphate-producing fields of central and southern Florida (U.S.A.), Morocco, Idaho and Utah (U.S.A.), the Western Sahara, Mexico, Jordan, eastern Florida (U.S.A.), Peru and Iraq has a relatively uniform concentration of 100–120 ppm uranium. Other major phos-

phate-producing areas (North Carolina, Wyoming, Montana, other Florida districts, U.S.A., Australia, Tunisia and Algeria) have a concentration of 60–90 ppm uranium. DeVoto and Stevens[38] estimated that uranium in the 292 727 000 000 ton of the Western world's total estimated recoverable phosphate product is 29 532 000 ton. The U.S.A. has the bulk of these phosphate deposits (223 342 000 000 ton recoverable) with an estimated recoverable resource of 22 459 000 ton uranium. Other countries with sizable resources of uranium in phosphate are Morocco (4 950 000 ton uranium), Western Sahara (555 000 ton uranium), Mexico (415 000 ton uranium) and Jordan (360 000 ton uranium).

Bauxites

It has long been known that most bauxites are moderately radioactive. Assays of bauxite samples from throughout the world show ranges of concentration for the three radioactive elements present—thorium (8–132 ppm), uranium (3–27 ppm) and potassium (0–0.3%).[1] Approximate median values are thorium, 42 ppm; uranium, 8 ppm; and potassium, 0.1%. In general, bauxites developed on mafic igneous rocks are lowest in uranium (averages 4.2 ppm). Those formed on other rock types are higher—shales, 10.5 ppm; carbonates, 12.9 ppm; and acid igneous, 15.9 ppm. There are also indications that Th and U concentrations may reflect the grade of the bauxite ore.

Experiments indicate that much of the thorium and uranium is contained in resistate minerals, such as zircon, and that very little uranium is carried over into commercial alumina and aluminium metal.

In the aluminium industry the most widely used method for the extraction of alumina (Al_2O_3) from bauxite is the Bayer process, in which aluminium and silica are leached from bauxite under pressure with hot caustic soda. The residue is 'red mud', a silt-like mixture of iron oxides, titanium dioxide, silica, caustic and many impurities. Roughly one ton of insoluble residue of red mud is produced for each ton of alumina. The liquors, following appropriate treatment to recover alumina, are recycled. In view of its high solubility in nature, it seems that most of the uranium must also be leached and possibly build up in the leach liquors. Small mills are now recovering this uranium, but analyses of red muds show uranium contents that vary from 12 to 40 ppm uranium, which suggest that it is not all leached.

Present annual world production of bauxite is about 70 000 000 ton, which results in the production of 35 000 000 ton of red mud. Many plants throughout the world have been operating for 40 years or more, and the resulting red mud wastes may exceed 1 000 000 000 ton. Assuming an average of 10 ppm uranium in this mud, the volume of uranium is very large. The bulk of the radioactive bauxites are in Brazil, Cameroon, Surinam and the U.S.A.

Placers

Placer deposits are concentrations of heavy minerals that form in high-energy fluvial and littoral environments. Here currents and waves selectively concentrate high-density mineral grains and winnow out finer and lighter material. Placer minerals are generally dense and resistant to weathering, solution, abrasion and impact. In radioactive placers most radioactivity is from thorium-bearing minerals (i.e. monazite, zircon, thorite and euxenite). These minerals are generally more resistant than uranium to weathering and destruction during transport. Modern placers[32] show a total absence of uraninite, but trace amounts of uranium occur as minor constituents in monazite, xenotime and thorite. Conversely, ancient placers (quartz-pebble conglomerates) commonly contain uraninite and, in places, brannerite.

Radioactive placers consist of minerals derived from the weathering of silicic and alkalic igneous and metamorphic rocks. They are on and peripheral to shields or regions of strongly deformed and intruded rocks. Two types of placers can be recognized on the basis of depositional environment—stream and beach.

Stream placers, because they occur in mountainous high-energy environments, are ephemeral deposits formed close to their source areas. Seldom are they preserved by lithification. Stream placers are known in North Carolina, South Carolina and Idaho in the U.S.A., British Columbia in Canada, India and Japan.

Beach (littoral) placers are generally deposited near base level and are more susceptible to burial and preservation. Thus, they are more common in the geologic record. Included in this group are placers that form either as beaches or various types of bars (longshore, baymouth, shoal, etc.). Unlike stream placers, beach placers may form tens or hundreds of kilometres from their source areas. The greater the distance of transport the greater are the attrition and reduction in grade by abrasion and solution. Generally, only the most resistant minerals (monazite and zircon) survive. The most radioactive placers are those in Upper Cretaceous beach sandstones in the western U.S.A. and those in Holocene sediments in China, Egypt, India, Brazil, Korea, Malagasy Republic, Taiwan and Alaska, and Georgia and Florida in the U.S.A.

Placers are a low- or very low-grade uranium resource and many of their sometimes uraniferous minerals, such as monazite and zircon, are refractory and difficult to process. The low grade and refractory nature tend to make placers unattractive; but, on the other hand, the volume of individual placers may be millions of cubic metres and they may contain hundreds of thousands of tons of heavy mineral concentrate. Uranium may be recovered as a by- or co-product from large placers if they also contain economic concentrations of such minerals as ilmenite, rutile, cassiterite or gold.

Brines

All natural waters, such as surface water, groundwater, hot springs, oilfield brines, sea water and mine and mill waters, contain uranium. None of these is a 'deposit' in the usual sense, because they are not concentrations of crystalline minerals in rocks. Typical values for fresh surface and groundwaters are in the range 0.05–10 ppb uranium.[101] Such values are too low to constitute an economic source of uranium at present. Sea water and mine and mill waters are most likely to yield uranium economically, but some saline and playa lakes may also be profitable on a small scale. Fresh water from some mining districts may contain several hundred to several thousand ppm U. Mine waters of this type have been processed in the Grants mineral belt, U.S.A. Leach solutions at some copper mines and mills average as much as 10 ppm U.[131] At Bingham Canyon copper mine, Utah, by-product uranium is recovered. Sea water contains about 3 ppb U and is present in enormous volume. Pilot plants for its extraction from sea water have been built in Japan. Saline and playa lakes, common to hot dry climates, attain their high salt concentrations through evaporation. Most have concentrations of 5–10 ppb U,[63] but their volume is relatively small.

Effusive igneous deposits

In many localities anomalously high concentrations of uranium of probable hydrothermal origin have been noted in, or associated with, volcanic rocks. Volcanic rocks serve as hosts for important uranium deposits in several countries. Uranium is most commonly associated with highly silicic types of volcanic rocks, but peralkaline and peraluminous variants also can be uraniferous. Some deposits in Australia bear some relation to basaltic eruptives. It is estimated that about 15.5% of the

Western world's reasonably assured uranium reserves are found in volcanic rocks.

Silicic volcanics

It is generally recognized that alkaline rock provinces are anomalously enriched in uranium and other trace elements, such as F, Mo, Be, Li and Hg. Uraniferous alkaline volcanic rocks occur in taphrogenic zones that may flank orogenically uplifted areas or may represent foundered rift systems. Effusive activity within taphrogenes can produce a comagmatic sequence of alkaline volcanic rocks and their associated sediments, constituting a volcanogenic system.

Dewey and Bird,[39] in their model for the subduction of an oceanic plate beneath a continental plate, described the mechanisms and distribution of structural elements and associated rock types resulting from mountain building and subsequent relaxation tectonics. They concluded that igneous rocks become more alkaline and more differentiated with increasing distance on to the continent from the subduction zone. Deep-seated magmas arise from the melted zone of the subducting plate, and the deeper the magma the more time it will have for differentiation.

For a magma to differentiate sufficiently to concentrate elements necessary for the deposition of uranium it must remain undisturbed for considerable time at a relatively shallow depth in an environment such as that of a taphrogene. Any premature release of pressure may permit the escape of volatiles and preclude uranium mineralization.

A great variety of deposit forms and structural settings are found in volcanic uranium deposits[84] and, commonly, several types of deposits occur in the same district. Uranium deposits are associated with rhyolitic plugs and domes at several localities in the western U.S.A.[26, 29, 107, 122] Deposits at Marysvale, Utah, occur in faults cutting hypabyssal intrusives and outflow tuff, probably above an unexposed intrusive.[29] Similar deposits were reported from China and the U.S.S.R.[69] Deposits may occur in volcaniclastic sediments filling caldera moats (McDermitt Caldera, U.S.A.), filling grabens (central Italy) or filling palaeo-valleys. Some uranium deposits occur in, or are associated with, ignimbrites, agglomerates, ash flow tuffs and other outflow (extra-caldera) rocks at Rexspar, Canada, Peña Blanca, Mexico, Maureen, Australia, and Thomas Range, U.S.A.

Most writers have proposed a magmatic source for the principal elements of these deposits (U, F, Be, Hg, Th, Mo, etc.), also postulating elevated temperatures. Solutions with the same elements could, however, be produced by diagenetic or mildly hydrothermal alteration of volcanic sediments. Localization of uranium in some deposits appears to be controlled by carbonaceous material (Maureen, Australia; Anderson mine, U.S.A.), but in others the controls are not understood.

Mineralization style in volcanogenic rocks is variable. Where porosity and permeability changes are rapid, reduction in temperature and pressure may be sufficient to reduce hexavalent uranium and form pitchblende. Where porosity and permeability changes are less abrupt, cooling of the silica-rich uranium-enriched fluids may produce uranosilicates.

Silicic volcanogenic uranium deposits range in size from a few tons to several thousands of tons U_3O_8, and ore grades vary from 0.05 to 0.30% U_3O_8. Reasonably assured reserves for silicic host rocks in the Western world are probably of the order of 5000–10 000 ton U_3O_8.

Mafic volcanics

Mafic volcanic rocks appear to be relatively poor hosts for uranium deposits, but a few occurrences have been described. Most important is that in the McDermitt district of the U.S.A., where mafic flows in a caldera moat contain 8.5 ton at an average grade of 0.05% U_3O_8.[102] In this deposit fine-grained pitchblende and coffinite are associated with abundant pyrite and leucoxene.

It has been suggested that the large Cu–U deposit at Olympic Dam (Roxby Downs), Australia, is in some way related to alteration of associated basaltic flows, but this has not been fully documented.

Intrusive igneous deposits

High concentrations of uranium (>10 ppm) occur in many types of intrusive igneous rocks. Generally, the uranium content of large igneous bodies does not exceed 20 ppm, but the most differentiated components of these bodies may show extreme enrichment of uranium with respect to the mean value for the entire body.[86] Uranium, along with other incompatible elements, generally enters into the silicate melt and late-stage magmatic fluid or gas phases rather than into the liquidus minerals. In granites the highest uranium concentrations are most commonly in pegmatitic or aplitic portions of plutons. Studies by Rosholt and co-workers[104] and Bohse *et al.*[15] indicated that magmas that have retained their volatiles also have retained uranium, so rocks with high bulk-rock volatile content should have high uranium concentrations in late differentiates. Intrusive igneous and associated metamorphic rocks are host to approximately 12.2% of the Western world's reasonably assured $30/lb resources.

Peralkaline nepheline syenites

Peralkaline nepheline syenites are alkaline rocks characterized by a chemical composition with a $Na_2O + H_2O/Al_2O_3$ molecular ratio greater than 1.2. Rocks with this composition are termed 'agpaitic' by petrologists. Agpaitic nepheline syenites with unusually high concentrations of U, Th, Nb, Zr and REE occur in many localities: most notable are those of Ilímaussaq, Greenland, Pocas de Caldas, Brazil, Lovozero, U.S.S.R., and Pillanesberg, South Africa. Lesser known examples occur in India and Bolivia and elsewhere in Brazil. These rocks contain very little of the Western world's reasonably assured $30/lb U_3O_8 resources, but they may contain as much as 70 000 ton of the $50/lb U_3O_8 resources.

Carbonatites

Carbonatites have been designated as a separate class of igneous rocks because of their unusual composition. They are characterized by an abundance of incompatible elements (U, Nb, etc.) and a large proportion of carbonate minerals, such as calcite, dolomite, ankerite and other rock-forming carbonates.

There are more than 300 known carbonatites, but most cover less than 20 km^2 in area.[87] They have been reported from all continents except Antarctica and commonly show a tendency to cluster into belts or provinces. Some of the more important carbonatite provinces are the East African Rift Zone, the Monteregian province of eastern Canada, the South Atlantic occurrences of southern Brazil, Paraguay, Angola and Namibia, the Finland–Kola Peninsula provinces, southern Peninsular India and the Colorado Rocky Mountain Province in the U.S.A. Other carbonatites are found in Bolivia, Ecuador, Sweden, the Canary Islands, Germany, Greenland, Canada and the U.S.A.

Most carbonatites contain insufficient uranium to constitute a minable uranium deposit, but some are mined for other minerals and uranium is recovered as a co- or by-product. Valuable elements contained in, or associated with, carbonatites include Cu (Palabora, South Africa), REE (Mountain Pass, U.S.A., and Araxá, Brazil), Nb (Araxá, others in Brazil, Africa, Canada and the U.S.A.), Th (Wet Mountains, U.S.A.), Ta (U.S.S.R.) and V (Magnet Cove, U.S.A.).

Non-refractory primary uranium minerals are rare, but uranothorianite has been reported from Palabora[46] and uraninite from Lake Nipissing, Ontario, Canada.[48] Most carbonatite uranium-bearing minerals are refractory phases. Uranium occurs as a minor or trace element in zircon, apatite, baddeleyite, perovskite, monazite, pyrochlore minerals, goyazite, bastnaesite, allanite, anatase, rutile, etc. The secondary mineral autunite occurs in soil covering the Araxá carbonatite.[24]

The average uranium content of carbonatite is about 57 ppm, thorium is about 649 ppm and the Th/U ratio is 11.4.[49] The spread of values is large for both U (0.05–400 ppm) and Th (0.1–2500 ppm), however, as was shown by Nishimori and Powell.[87] It is estimated that carbonatites contain at least 150 000 ton recoverable U_3O_8, most of it in the reasonably assured $50/lb category.

Anatectics

Uranium released from sedimentary and igneous rocks by ultrametamorphic processes may become concentrated in anatectically derived quartzo-feldspathic melts. Liquidus crystallization of such uranium-enriched melts produces anatectic uranium concentrations in pegmatites, alaskites and, occasionally, aplites. Alkali feldspars and quartz are the major mineral components, but small amounts of biotite and altered ferromagnesian minerals are generally present. Muscovite is a common accessory mineral and trace amounts of garnet occur. Anatectic uranium concentrations are found in structurally complex, highly metamorphosed and migmatized terrains formed in deep metazonal and catazonal regions of mobile belts. They are characterized by steeply plunging, tight isoclinal folds.

Euhedral to subhedral primary uranium minerals, primarily uraninite and uranothorite, are finely disseminated throughout anatectic alaskites and pegmatites, but quartz-rich zones and pods may contain localized concentrations of uranium minerals. Secondary uranium minerals may be present in either the palingenetic rocks or host rocks.

Anatectic uranium occurrences are tabular to lenticular quartzo-feldspathic bodies that generally show sharp contacts with the host rocks. Dyke-like pegmatites and alaskites are most generally concordant to foliation, but locally may be discordant along axial folds. The size and grade of anatectic uranium occurrences depend on such factors as uranium content of source rocks, degree of cementation in the palingenetic melt and extent of uranium retention during subsequent crystallization. They range from small sub-economic occurrences to very large low-grade deposits. Grades range from about 0.01 to 0.20% U_3O_8, and the size of deposits ranges from a few to as much as 150 000 ton U_3O_8.

The largest and only currently economic deposit is the Rössing deposit in Namibia, but smaller deposits exist, such as those at Crocker Well, South Australia, Serido Province, Brazil, Saskatchewan and Manitoba Provinces, Canada, Travancore, India, Kenema, Sierra Leone, Wheeler Basin, U.S.A., and localities in Zimbabwe.

Pegmatitic alkalitic granites

Pegmatitic alkalitic (peralkaline) granites are distinct both geologically and chemically from calc-alkaline granites and granodiorites. They generally are holocrystalline and leuco- to mesocratic and consist of 25–40% quartz, about 50% alkali feldspar (microcline, perthite, or late forming albite) and 10–25% accessories (pyroxenes, amphiboles, etc.).

The origin of pegmatitic alkalic granites is somewhat in question. Some writers believe that they are derived from the mantle,[127] but others[7,17] contended that they form through anatexis of lower crustal material. Murphy *et al.*[83] suggested that they can be explained by a combination of genetic models, along with such factors as tectonic setting, crustal contamination and volatile segregations.

Uraniferous peralkaline granites are known in Scotland and in the ring complexes of Niger and Nigeria, but the only such granite with a history of uranium production is the albite–riebeckite granite at Bokan Mountain, Alaska. All these occurrences are characterized by (1) the strongly peralkaline nature of the host granite—a result of extreme chemical differentiation; (2) the concentration of incompatible elements (U, Th, Nb, Zr, Be, Li, etc.) in the volatile stage from the parent magma; (3) high oxygen fugacity, as shown by high Fe^{3+}/Fe^{2+} ratios and normative acmite; (4) reinjection of late-stage fluids either as a deuteric or metasomatic event; (5) additional enrichment of the volatile phase in the form of pegmatites; (6) hydrothermal reinjection of fluids into the host rock along faults; and (7) pervasive albitization of the pluton.

Uranium may occur as deuteric or autometasomatic concentrations in the albitized granite, syngenetic emplacements in pegmatite, epigenetic hydrothermal replacement veins or as epigenetic deposits in the adjacent country rocks. Primary uranium minerals are uranothorite, uranian thorianite and coffinite. Associated minerals include calcite, fluorite, pyrite, galena, hematite, quartz and clays. Grades of uranium mineralization range from 0.01 to 1.00% or more U_3O_8. Peralkaline granites host only a few hundred tons of the Western world's reasonably assured and estimated additional uranium resources.

Granites

In a series of granitic rocks the greatest uranium concentrations generally are in the youngest, most highly differentiated rock unit. Many granites have a bulk concentration of more than 10 ppm, but entire granite plutons with more than 20 ppm are rare.[86] The best examples of uranium-rich granites are the Hercynian massifs of France, but granites and quartz monzonites with 2–15 ppm U are known in Canada (Johan Beetz, Quebec), Australia (Elizabeth Creek, Queensland), the U.S.S.R. (Ognitsk, East Sayan), Ireland (Donegal) and the U.S.A. (Conway, New Hampshire; Granite Mountains, Wyoming; Mount Spokane and Midnite mine, Washington; Bingham Canyon, Utah).

Most high-uranium granites are post-orogenic, epizonal plutons that have not lost their uranium-bearing aqueous fluids during an orogenic episode. Because the uranium content of these granites is uniformly low, it is unlikely that any large syngenetic orebodies exist. In some areas, however, where other metals are present in sufficient quantity the disseminated U may be recovered as a by-product (Bingham copper mine, U.S.A.).

In some localities weathering of uranium-bearing granites may produce concentrations of secondary uranium minerals in vein-like bodies along and adjacent to major fracture systems within the parent pluton. Associated minerals may include sphalerite, pyrite, galena, chalcopyrite, fluorite, limonite and quartz. Fracture and joint systems may be expansion features related to pluton deroofing. Shear intersections are particularly favourable sites for deposition of secondary uranium minerals, so ore zones are generally lenticular to pod-shaped. Deposits are generally small, but may be high-grade: an example is the Daybreak mine, Washington, U.S.A., where uranium occurs as meta-autunite crystals along fractures, microfractures and cleavage traces in pegmatitic and alaskitic phases of a Cretaceous porphyritic quartz monzonite. Similar deposits occur in the Lachaux district of France.

In other areas uranium liberated by weathering from uranium-bearing granites has migrated into low- to medium-grade metamorphic rocks surrounding shallow-seated plutons.

Because potential host rocks must be capable of reducing hexavalent uranium in aqueous solution, ideal host lithologies are carbonaceous slates, graphitic schists and calc-silicate rocks. Uranium transportation may be a continuous process. Pitchblende and coffinite are the principal uranium minerals, but secondary uranium minerals may occur in the near-surface portions of the deposit. Gangue is variably abundant in the form of quartz, carbonates and fluorite. Examples of this type of occurrence are Spokane Mountain, U.S.A., Nisa, Portugal, and Mina Fe, Spain. Average uranium contents vary from 0.05 to 0.3%. Thickness of ore zones ranges from a few centimetres to metres or tens of metres, and lengths range from tens to hundreds of metres. They may extend vertically to depths of 100 to 200 m. Granitic deposits contain about 30000 ton of reasonably assured $30/lb uranium, but they contain much larger amounts of reasonably assured $50/lb uranium.

Pegmatites

Pegmatitic and aplitic uranium occurrences form from 'pegmatitic' fluids produced by saturation during late-stage magmatic evolution. Uranium, because it does not readily enter into common rock-forming minerals during orthomagmatic crystallization, becomes progressively concentrated in residual melts. Such pegmatitic fluids may become still more concentrated in a second boiling of the magma. For this reason pegmatitic phases of a comagmatic sequence are generally enriched in uranium relative to the main body of a given pluton.

Uraniferous pegmatites differ from non-uraniferous pegmatites primarily in their uranium content, which can be attributed to original uranium content of the parent magma, extent of uranium removal prior to saturation, and degree of concentration in the pegmatitic fluid. Other differences are in their contents of F, Nb, Ta, REE, primary hematite, sodic amphibole and/or sodic pyroxene. In general, the more complex the chemistry the more likely it is that a pegmatite will contain radioactive elements.[2] Uraniferous pegmatites are also characterized by temporal, spatial and probably genetic association with plutons with an anomalously high uranium content. They commonly occur within or at the margins of such plutons, but they may be injected into country rock. In general, their size, number and complexity decrease with increasing distance from the parent pluton.[79]

Pegmatitic uranium concentrations occur in areas of extreme crustal mobility. They occur most frequently in intercratonic mobile belt terrains associated with deep epizonal to mesozonal plutons produced from crustal materials. They are characteristically Precambrian or Devonian–Carboniferous and occur in high-grade metamorphic rocks as well as granitic intrusives. Because of their occurrence in high-grade metamorphic rocks, some writers have classified such pegmatites as ultra-metamorphic or anatectic.

Uraniferous pegmatites are generally granitic, consisting mostly of alkali feldspars and quartz with mica and a few sodic amphiboles and/or pyroxenes. Common accessory minerals are fluorite, topaz, hematite, zircon, garnet and apatite. Uranium and uranium-bearing minerals (uraninite, allanite, uranothorianite, brannerite) are disseminated throughout the dykes, but quartz-segregation blobs may contain higher concentrations. Much of the uranium is tied up in accessory minerals, such as apatite and zircon, but some may be present within or on the surfaces of rock-forming minerals.

Most uraniferous pegmatites occur as tabular discordant dykes, but some are elongate pods. Some are structurally simple, but others are zoned. Regardless of type, radioactive pegmatite minerals rarely occur in sufficient quantities to constitute an economic source of uranium or thorium. Grades range from a trace to more than 0.37% U_3O_8, but average about 0.01%.

Several hundred tons of complex oxide minerals has been produced from pegmatites in Malagasy. In recent years there has been exploration for uranium in both zoned and unzoned pegmatites in Canada. Most important are the unzoned red pegmatites in the Bancroft, Ontario, area, but there are also important unzoned white pegmatites and some zoned pegmatites in other parts of Canada.[65] It is estimated that Bancroft reserves are of the order of 2000 ton U_3O_8 averaging 0.11%.[18] Other uraniferous pegmatites are known in Argentina, Australia, Brazil, Ethiopia, Finland, India, Norway, Sri Lanka, Sweden, the U.S.S.R. and the U.S.A. Total reasonably assured $30/lb resources do not exceed a few thousand tons.

Hydrothermal veins

Hydrothermal (classical) uranium vein deposits are those with predominant structural control that are generally spatially and probably genetically related to uraniferous plutonic hypabyssal and/or pegmatitic bodies. Such deposits occupy relatively simple fault and fracture zones, some extending to depths of 300–500 m in a variety of host rocks, but display many mineralogical and geochemical similarities. Some veins occur in metamorphic rocks, such as in the Beaverlodge and Great Bear Lake districts of Canada, Schwartzwalder mine, U.S.A., Pribram and Freiberg districts of eastern Europe and Shinkolobwe mine, Zaire. Others occur within the parent pluton (intragranitic), such as the well-known deposits in France, Spain and Portugal.

Hydrothermal solutions responsible for these veins are generated during the final stages of magmatic differentiation. Continued magmatic evolution causes progressive increase in volatiles and, ultimately, a separate, very hydrous phase that may contain a wide variety of dissolved constituents. High oxygen fugacity causes oxidation of uranium, but not vanadium, bringing about an effective fractionation of the two elements. When hydrothermal solutions are released from the magma chamber it is by way of permeable channelways, such as fault and fracture zones that have been active for long periods. Such systems are of considerable length and depth and provide the most favourable sites of deposition. Here reductants for the hexavalent uranium are generally absent, but the mechanically induced decrease in oxygen fugacity of the system as the temperature, pressure and pH of the hydrothermal fluid change with upward migration into dilatant zones may result in reduction.[79]

Two types of vein deposits are recognized: (1) monometallic veins of pitchblende and (2) polymetallic veins of U with (Co, Ni, Bi, Ag) or (Ni, Co and Cu). Both types of deposits generally occur in brecciated veins and vein systems, and multiple stages of brecciation are common. The breccias normally consist of fragments of the enclosing wallrock. Quartz, both massive and cryptocrystalline, composes the bulk of the vein material. Associated minerals include Fe, Zn and Pb sulphides, barite, purple fluorite and carbonate minerals. (Cu, Ni, Ag and Bi) or (Ni, Co and Cu) enrichments are present in some veins as the result of telescoping of multiple primary mineralizations.[30] The major uranium mineral is uraninite, which may occur as finely disseminated euhedra, intergranular coatings, fracture fillings or as a replacement product. Ore-grade concentrations are intermittent along the veins, but grade tends to be highest along zones of maximum dilatancy. Grades of these deposits range from less than 0.10% to more than 1.0% U_3O_8. Hydrothermal vein deposits contain about 50000 ton of the Western world's reasonably assured $30/lb uranium resources.

Metasomatic deposits

Contact-metasomatic occurrences

Contact-metasomatic uranium occurrences form by replace-

ment reactions between magmatic emanations and pre-existing rocks during the late stages of magmatic evolution. Most commonly, metasomatism occurs as a halo in older metamorphic and igneous rocks intruded by the magma, but in places it occurs in outer zones of the pluton and in cataclastic rocks of shear zones bordering the pluton.

Some uranium and part or all of the uranium-transporting fluids that form contact-metasomatic deposits may be derived from the host rock, but uranium can also be introduced into the host rock as magmatic emanations. Berezina and co-workers[13] recognized a systematic increase in uranium content from the outer portions toward the centre of a 'metasomatizing column'. Uranium becomes progressively more concentrated along microfractures, cleavages and crystal defects, especially in ferromagnesian minerals. Distances of uranium transport in metasomatizing fluids and the sites of deposition are primarily governed by the temperature gradient and the effective porosity, permeability and composition of the host rock.

There seem to be two major types of metasomatic uranium occurrences: (1) carbonate-metasomatic and (2) alkaline or sodic-metasomatic (albititic), characterized by pervasive albitization of host rocks. Carbonate-metasomatic uranium deposits are normally found in middle- to high-rank dynamically metamorphosed rocks adjacent to silicic uraniferous plutonic and/or pegmatitic rocks in mobile belt terrains. The high-rank host rocks may indicate a deep-seated environment for evolution of the magma that would enable uraniferous fluids to permeate the country rock rather than escape along fractures. Common host rocks include ferruginous quartzites (taconite), iron ore, mafic and calc-silicate schist, gneisses and impure marbles. Primary uranium and uranium-bearing minerals (usually uraninite and thorianite) are finely disseminated in the host rocks, and some uranium may be within rock-forming minerals. Uraninite is the dominant uranium mineral, but uranium may occur in monazite, zircon, aegirine, riebeckite and biotite. Albitization, carbonatization and chloritization are the most common forms of alteration in these occurrences. Size and grade of the pod-shaped orebodies vary greatly. Most ore is low-grade, but secondary enrichment may make them economically viable. The most important occurrence is Mary Kathleen, Australia, but other deposits are known at many localities in Brazil, Canada and the U.S.S.R.

Contact-metasomatic uranium deposits contain only a few thousand tons of the Western world's reasonably assured $30 uranium resources. Grades range up to about 0.15% U_3O_8, but associated metals, such as REE, tend to make them more economic.

Sodic-metasomatic occurrences

The sodic-metasomatic (albititic) uranium occurrences are largely confined to the Ukranian Shield of the U.S.S.R.,[59] but similar occurrences may be found in association with the mantled gneiss domes of North America. Uraniferous sodic-metasomatic deposits occur in tectonic-metasomatic zones developed along large faults in ultra-metamorphic rock terrains. The faults are associated with fold structures of the basement and with exo-contacts of major (hundreds to thousands of km^2) abyssal granitoid massifs.[59] The uraniferous albitites replace interlayered granites, gneisses and pegmatites (migmatites?) near the fault contacts, as well as cataclastites and mylonites at the fault contacts. Most albitites have cataclastic textures that have been inherited largely from epidote–chlorite cataclastites formed prior to the sodic metasomatism. The ore minerals (uranotitanate, nenadkevite, brannerite, pitchblende, coffinite, uranophane, beta-uranophane and others) are evenly distributed in the albitites, where they impregnate and partly replace the fine-grained matrix and form discontinuous seams of micro-breccia. Orebodies are both vein type and disseminated. Both the uranium deposits and the host rocks have a similar age (~1800–2000 m.y.). They formed at shallow depth and are considered medium-temperature hydrothermal.

Vein-like type deposits

Much of the world's currently minable uranium is found in vein-like deposits of uncertain origin. They consist of three general types of unequal importance. Most important are unconformity-related deposits and vein-like deposits in metamorphic rocks. Least important and probably of different origin are vein-like deposits in sedimentary rocks. The origin of all three types is a matter of much conjecture. Major unsolved genetic questions are the source of the uranium and its mode of transport, the source of the mineralizing solutions, the nature and role of reductants and the control exerted on uranium deposition by structural and lithologic features of the host rocks. Unconformity-related deposits and vein-like deposits in metamorphics commonly occur in brecciated and foliated metamorphic rocks in stable Precambrian Shield areas. They contain about 24.4% of the Western world's reasonably assured $30 uranium resources.

Deposits of all three types are associated with faults and/or shear zones, but unconformity-related deposits are also closely associated with major regional unconformities where coarse terrestrial clastics overlie metamorphosed basement rocks. Unconformity-related deposits and vein-like deposits in metamorphic rocks are all of Precambrian age, whereas vein-like deposits in sedimentary rocks are found only in strata of Palaeozoic and Mesozoic age.

Unconformity-related deposits

Unconformity-related deposits are large moderately high-grade deposits consisting of epigenetic concentrations of primary uranium minerals in veins and strata-bound deposits spatially associated with major regional Middle Proterozoic unconformities. In Northern Territory, Australia, they are associated with the pre-Carpentarian unconformity and in northern Saskatchewan, Canada, with the Palaeohelikian unconformity.

Most unconformity-related deposits occur near the erosional edge of terrestrial units that overlie the unconformities. These terrestrial units are mostly unmetamorphosed Middle Proterozoic buff to red orthoquartzitic to feldspathic fluvial sandstones that may contain lenses of polymictic conglomerate near the unconformable contact and lenses of shale and siltstone higher in the sequence.

Metamorphosed sedimentary and igneous rocks of Early Proterozoic age underlie the unconformities and host most of the uranium deposits. Grade of metamorphism and degree of structural complexity of the host rocks show no correlation with uranium content, but most such uranium deposits are confined to, or are concentrated below, reducing horizons within metasedimentary host rocks. Graphite- and chlorite-bearing schists are the most common host lithologies. Quartzites, sericite schists, chloritic gneisses, calc-silicate rocks and marbles are present, but generally contain less uranium.

Uranium occurs as concentrations of pitchblende with some coffinite in veinlets along faults, in brecciated zones and in satellite structures associated with the major structure. These minerals may occur also as fine disseminations in selected horizons in the host rocks. Secondary uranium minerals are locally abundant, especially in near-surface portions of deposits. Small amounts of quartz and carbonates are the gangue minerals. Associated minerals vary in type and abundance and determine whether a deposit is classified as monometallic or polymetallic. The latter may contain a wide variety of associated minerals, including sulphides. Hematitization and chloritization are the most common forms of alteration

present. Hematitization generally precedes uranium mineralization, and higher-grade uranium concentrations commonly coincide with the most intense alteration.

Mineralization straddles the unconformity in some deposits, but is mostly restricted to the metamorphic rocks. Most occur at the erosional edge or a short distance in front of it. Ojakangas[89] discussed the probability of their presence underneath the terrestrial sediments. The uranium deposits vary in size and shape, their geometry depending on whether lithology or structure is the dominant factor in localization. They rarely extend more than 100 m below the unconformity, and they may extend horizontally for considerable distances. Structurally controlled deposits tend to be elongate, whereas those which are stratigraphically controlled are commonly amoeboid. Grades range from 0.01% to more than 50.0% U_3O_8.

The origin of these deposits is unknown, but any genetic hypothesis must explain (1) their presence in or near sequences of metamorphic rocks formed from marginal marine sedimentary units, (2) their proximity to Archaean granite–gneiss complexes with reactivated migmatite fringes, (3) ore occurrences in repeatedly faulted and chloritized zones and (4) their proximity to Middle Palaeozoic unconformities.[62]

Unconformity-related deposits are known only from Northern Territory, Australia (Rum Jungle, South Alligator Valley and Alligator River regions), and Saskatchewan, Canada (Athabasca Basin). They include many of the world's largest and richest deposits, such as Koongara, Ranger I, Ranger II and Jabiluka II in Australia and Rabbit Lake, Key Lake and Midwest Lake in Canada.

Vein-like deposits in metamorphic rocks

Vein-like deposits in metamorphic rocks also occur in Precambrian Shield areas, but they differ from unconformity-related uranium deposits in that they are not associated with major regional unconformities, the geometries of orebodies are different and they extend to greater depths. Vein-like deposits are closely associated with steeply dipping, brecciated major fault systems. Uranium minerals (pitchblende with some coffinite and brannerite) occur as open fracture fillings and as fine disseminations adjacent to the fractures in Proterozoic meta-igneous and metasedimentary rocks. Common associated minerals are chlorite, hematite and pyrite.

These uranium deposits are generally elongate and steeply dipping. They have very long strike lengths in comparison with their thickness, and they may extend to depths of several hundreds of metres. Some deposits are in anastamosing vein systems associated with cymoid structures related to the major fault systems. Other deposits may occur as individual veins or as a series of complex anastamosing veins and veinlets with a width up to 50 m. The long, deep major fractures may have been active over long periods of time[9] and may have served as passageways for hypogene or supergene mineralizing solutions.

Favourable host rocks are carbonaceous slates, chloritized schists and gneisses, graphitic units, metacarbonates and metavolcanics. All these rocks are characterized by retrogressive chloritization that predates uranium mineralization. Hematite haloes are common around ore, and carbonatization and chloritization are also normal features of the deposits. Both monometallic and polymetallic types of deposits are recognized.[6] Pitchblende is the principal uranium mineral in both types of deposits, and Ag, Ni, Cu and Co form accessory minerals (sulphides and arsenides) in the polymetallic deposits. Mineral assemblages, wallrock alteration types and mineral formation temperatures suggest that these deposits form from medium- to low-temperature hydrothermal solutions.

Vein-like deposits in sedimentary rocks

Vein-like deposits of uranium in sedimentary rocks are epigenetic deposits in brecciated, tabular bodies and pipe-like structures orientated transverse to stratification in Palaeozoic and Mesozoic rocks.[58] They occur in areas of thick sedimentary sequences and of moderate structural deformation.

Pipe-like structures are generally cone-shaped, and they become progressively narrower with depth. They range up to a hundred metres or more in diameter, but rarely attain a depth of more than 200 or 300 m. They consist of an inner core of brecciated downdropped blocks surrounded by a steep inward-dipping circular fault system. They occur at intersections of fracture systems in structurally stable areas and are underlain by massive carbonate and/or evaporite units. The pipe-like structures may terminate in these carbonates or evaporites, suggesting that they are produced by solution collapse. They may have acquired their uranium from remobilization of uranium in uranium-bearing strata cut by the pipe-like structure. Other suggested origins are cryptovolcanic explosions or pipe-drilling by gases from an underlying magma.

The types of rocks that comprise a collapse structure depend on the types of rock that are cut by the structure, the amount of underlying material removed by solution and rock units overlying the structure at the time of development. Blocks of sandstone, siltstone, shale and carbonates may be found in the collapse. Sandstone and some siltstones are the common uranium hosts. Well-known pipe-like bodies include Woodrow Pipe, New Mexico, Orphan mine, Arizona, and Temple Mountain, Utah, all in the U.S.A.

Tabular vein-like deposits may be associated with regional fractures, shear systems and/or growth faults. Breccia fragments within these deposits are generally limited to blocks of the host rock.[51]

Pitchblende is the dominant uranium mineral in all these vein-like deposits in sedimentary rocks. It occurs as small veinlets along fractures within and surrounding the structures and as finely disseminated crystals in porous breccia fragments within the structures. Pitchblende concentrations may be distributed zonally within the ore, and in some deposits may be concentrated in the upper levels of the structure. Associated minerals may include sulphides and sulpharsenides. Calcite and quartz are the most common gangue. Types of alteration include bleaching of red sediments, silicification, carbonatization and argillization.

Vein-like deposits in sedimentary rocks are generally quite small and relatively low-grade, ranging from a few to several hundred tons of U_3O_8 at grades of 0.05–0.25% U_3O_8. They represent less than 1000 ton of the Western world's reasonably assured $30 uranium resources.

Epigenetic uranium deposits

Epigenetic uranium deposits are similar to sedimentary uranium deposits in that they occur in sedimentary rocks and they owe their existence to exogenic processes. They differ, however, in that the sediments formed prior to introduction of uranium. Epigenetic deposits form by precipitation of uranium from solutions moving through previously deposited sediment or pre-existing rocks. Uranium-bearing solutions include hydrothermal solutions, connate and meteoric waters. Uranium in these oxidized groundwaters may be reduced and precipitated by organic matter in sandstone, limestone, lignite, coal and carbonaceous shale. Evaporites may contain secondary uranium minerals that precipitate on the outcrop or in pore spaces, solution cavities and fractures within the oxidized zone.

The largest and highest-grade epigenetic deposits are those in sandstone, but other types are important in a few areas. Epigenetic uranium deposits contain about 32% of the Western world's reasonably assured $30 uranium resources.

Sandstone

Sandstone-type uranium deposits occur primarily in sandstone, but may be found in silty and conglomeratic rocks as well. The host rock may be quartzose, feldspathic to arkosic, and tuffaceous to volcaniclastic. The most common hosts are medium- to coarse-grained, poorly sorted, quartzose and arkosic fluvial sandstones. The normally red or brown host sandstones are typically reduced (bleached) to grey, green or tan in the vicinity of uranium deposits. Most sandstones also contain iron sulphides that, together with the bleaching, reflect the reducing environment required for deposition and preservation of epigenetic uranium.

Host sandstones are of fluvial, lacustrine, eolian, deltaic, paludal and marginal marine origin, but deposits in fluvial sandstones are most common. Finch[45] calculated that, of 4600 sandstone deposits other than vein-like, 97% are in continental, 2% are in mixed continental and marine and 1% are in marine (marginal marine) rocks. Fluvial sandstones are most favourable because they are interbedded with mudstones and they commonly contain disseminated plant debris. Eolian sandstones are poor hosts because they lack mudstone partings and plant debris. Marginal marine sandstones are fair hosts because they may contain organic matter and are interbedded with carbonaceous marine, deltaic and lagoonal muds. Mudstones and shaly interbeds are important because they impede or stop groundwater movement.

Organic material in the sandstone and interbeds commonly acts as a reducing agent. A reducing environment is necessary to precipitate hexavalent uranium from solution to form insoluble tetravalent uranium (when vanadium is present it can cause uranium to precipitate in an oxidizing environment). The reductant may be a complex organic acid or it may be H_2S produced or introduced from one or more of these sources: anaerobic destruction of organic material in the sediment, oil and gas, or oxidation of pyrite. Most epigenetic uranium deposits in continental sandstones are Devonian or younger because of the absence of land plants prior to that period. Occurrences in marine sandstones as old as Precambrian are possible because of the earlier presence of marine organisms.

Uranium in epigenetic sandstone deposits is believed to have come from such varied sources as weathering of granitic rocks, siliceous tuffs or other uraniferous rocks in the source area for the sandstone; devitrification of tuffaceous sediment in or interbedded with the sandstone; hydrothermal solutions from nearby magmas; and recycling and redistribution of earlier-formed uranium deposits.

Three types of epigenetic uranium deposits in sandstone are recognized on the basis of their relationship to bedding or structure—peneconcordant, roll-type and tecto-lithologic (stack). Uraninite and coffinite are typical minerals of unoxidized portions of all three types of sandstone uranium deposits. They replace organic material, coat mineral grains and fill interstices in the host rock. Oxidation produces such secondary minerals as tyuyamunite, carnotite and uranophane. Cu, V, Cr, Mo and Se are common accessory elements in both economic and subeconomic occurrences. Grades in sandstone deposits range from less than 0.01 to more than 1.0% U_3O_8. Deposits range in size up to 45 000 ton U_3O_8. Most of the U.S.A., Argentina and Niger production is from sandstone uranium deposits. About 28.6% of the Western world's reasonably assured $30 resources is in sandstone deposits.

Peneconcordant deposits

Peneconcordant uranium deposits are those that generally lie parallel to bedding in nearly flat-lying sandstones, but in detail they are locally discordant. In cross-section they may be tabular, lenticular or irregular; in plan they are equidimensional to amoeboid (blanket-like) or elongate in one direction (trend). Thicknesses range up to 10 m and lengths may reach several thousands of metres.

Dominant ore minerals in the reduced zone are pitchblende and coffinite and, in some deposits, associated primary vanadium oxides—for example, montroseite. In oxidized zones the important uranium minerals are the uranyl vanadates (carnotite, tyuyamunite or francevillite). Accessory elements include Mo, Se and Cu. Average uranium content ranges from 0.01 to 0.40% U_3O_8.

Peneconcordant uranium deposits occur primarily in Permo-Carboniferous, Triassic, Jurassic and Tertiary sediments. Principal ore districts are the Colorado Plateau and Grants Mineral Belt, U.S.A., Agadès region, Niger, sub-Andean zone, Argentina, and Lake Frome, Australia. Lesser deposits occur in Algeria, Brazil, China, Egypt, Gabon, India, Italy, Japan, Mexico, New Zealand, Pakistan, Spain, Turkey, the U.S.S.R. and other areas in the U.S.A.

Roll-type deposits

Roll-type uranium occurrences were first noted in mines on the Colorado Plateau, but they are best developed in the Wyoming, U.S.A., deposits. In vertical section these deposits are *C*- or *S*-shaped and cut sharply across bedding. They form at the boundary between altered and unaltered sandstone. This boundary or 'solution front' is the result of oxidizing uraniferous groundwater moving progressively through a body of reduced (unaltered) sandstone bounded by shale partings.[8, 128] The roll front, which represents the farthest downdip or outer penetration front of the oxidizing waters, may extend in sinuous fashion across a broad front or may be elongate in one direction. In some areas rolls are closely associated with or gradational into stratiform peneconcordant ore deposits.

Roll-type orebodies are generally crescent-shaped in vertical section, the sharp concave margin facing the alteration. The highest-grade ore generally occurs near the contact with the altered sandstone, and the grade diminishes away from the alteration. Low-grade mineralization (protore) may extend for up to 100 m away from the roll front in unaltered rock. Modifications of the crescent shape are common and may produce *S*-shapes, compound crescents and other forms. Crescent horns are commonly elongated and are generally confined by less permeable strata above and below. Orebodies are elongate parallel to the roll front. They may be as much as 30 m wide and 2 km long and may be up to 10 m thick. Many deposits are less than 5 m wide and 3 m thick. The main ore minerals are pitchblende and coffinite. Selenium may be enriched on the convex side and molybdenum and calcite on the concave side. Grade of mineralization ranges from 0.01 to >0.50% U_3O_8.

Roll-type uranium deposits occur in intracratonic sedimentary basins in the U.S.A. Best known are those in Tertiary strata of Wyoming (Powder River, Shirley and Wind River basins) and the Texas Gulf Coast. Smaller deposits are present in Jurassic rocks of the Colorado Plateau.

Stack deposits

The term 'stack deposit' was first used to describe uranium ore deposits associated with peneconcordant deposits in the Grants Mineral Belt, New Mexico. Stack deposits are also called 'tecto-lithologic', 'redistributed' or 'post-fault' ore because they represent uranium that was mobilized from earlier peneconcordant or roll-type occurrences and redeposited in near-vertical bodies. The geometry of stack deposits commonly is controlled by faults or fractures that post-date the formation of the other uranium deposits. Stack deposits generally have greater thicknesses than the associated peneconcordant or roll-type deposits, but their shape is irregular.

In most cases red sandstone with hematite staining is closely

associated with stack deposits, which indicates that oxidized groundwater invaded the environment and redistributed the uranium. It is now concentrated as pitchblende and some coffinite along permeable fault zones with linguiform impregnation of the adjacent sandstone. Uranyl vanadates may be present in the oxidized zone. Thicknesses of ore range from a few tens of centimetres to more than 10 m. Lateral dimensions may be 100 m or more. Grades average from 0.10 to 0.40% U_3O_8.

The best-known deposits are those in the Precambrian Franceville Basin, Gabon, and in the Jurassic of the Grants Mineral Belt, U.S.A. Other occurrences are in the Miocene–Pliocene of Pakistan, the Miocene of Japan, the Permian of Europe, the Karoo Formation of South Africa and the Proterozoic of Canada.

Calcretes

Calcrete, dolocrete and gypcrete uranium deposits in arid Western Australia and the Namib Desert of Namibia contain uranium derived by weathering of granitoid rocks and transported laterally as uranyl carbonate complex ions in vadose and phreatic waters within the regolith.[22,23] Carnotite, the only uranium mineral present in most deposits, is deposited with authigenic carbonate (occasionally gypcrete or dolocrete) in trunk subsurface drainages and calcrete deltas. Mineralization occurs in areas of constricted flow or where waters are forced close to the surface. Carnotite is precipitated in, adjacent to, and commonly just below a valley calcrete mass, close to the water-table and in an oxidizing environment. It fills cavities and fractures in the calcrete and gypcrete and associated sediments.

Calcrete host rocks are crudely lenticular masses of alluvium and soil cemented by calcium or calcium–magnesium carbonates into masses that are up to tens of metres thick, several hundred metres to a few kilometres wide, and tens of kilometres long in the axial portions of palaeo or modern drainages in arid regions. In Australia these 'valley calcretes' cement and replace detritus derived primarily from the kaolinitic portions of lateritized granitic rocks. The calcretes are fine-grained to earthy, but are highly permeable because of shrinkage cracks and collapse structures, particularly within mound-like masses. In Namibia the uraniferous valley calcrete cements coarse to fine alluvium, and in areas near the ocean they are commonly overlain by gypcrete that can also contain uranium.

Because of their ephemeral nature there are no known uraniferous calcretes older than about 300 000 years.[23] The known deposits contain, however, about 2.4% of the Western world's reasonably assured $30 uranium resources. The largest and best-known are those at Yeelirrie, Western Australia (believed to contain about 50 000 ton U_3O_8), and Langer Heinrich, Namibia. Other occurrences are in these countries as well as in Angola, Botswana, Mauritania and Somalia.

Lignites, coals and carbonaceous shales

Lignite, coal and non-marine carbonaceous shale are among the least uraniferous sediments when deposited, but they may become sufficiently enriched locally by later processes to constitute a low-grade resource. Among the coaly rocks, high-ash lignite and sub-bituminous coal are the best hosts. Most beds of uraniferous coaly rocks are relatively thin, ranging from a few centimetres to a metre or more. The mineralized zone in the host rock is also thin, ranging from 1 to 25 cm. Thin beds may be completely mineralized, but in thicker units only the top is mineralized. Identifiable uranium minerals are sparse or absent. The uranium is probably present in organic ionic compounds similar to humic acids (uranyl humates). Some secondary minerals (meta-autunite and meta-tyuyamunite) may occur in higher-grade deposits.

Most uraniferous coaly rocks were deposited in structural basins, and many are interstratified with acid tuffs or tuffaceous sedimentary rocks. Others are within the drainage basin of rocks known to contain uranium (granite, uraniferous sandstone, etc.). Uraniferous coaly rocks appear to have been mineralized by uranium-bearing groundwaters that leached uranium from overlying tuffs or tuffaceous sediments and transported it to the reducing environment created by plant debris of the host rocks. Some uranium may have been leached from vein occurrences or marine black shale.

Uranium in uraniferous coaly rocks ranges from 0.005 to as much as 0.8% U_3O_8. Deposits range in size from less than 1 km^2 to more than 250 km^2 and contain from 100 to 10 000 ton U_3O_8. They are low-grade, relatively small and localized and most can be upgraded by burning or retorting. Most of the uranium remains in the ash along with small amounts of Ti, Ni, Co, Mo, Sn, V and REE. These deposits do not represent a sizable portion of the Western world's reasonably assured $30 resources. Best known of the uraniferous coals are those of the Williston Basin.[34]

Limestones

Limestone is not a favourable host for syngenetic uranium deposits. Both tetravalent and hexavalent uranium are highly soluble in the presence of concentrations of carbonate or bicarbonate ions; thus, in carbonate-forming environments most uranium will remain in solution. If any syngenetic uranium is present, it will be associated with such impurities as heavy mineral resistates, marine apatite, fluorite and some kinds of organic material.[12] The only favourable carbonate rocks are those which are capable of serving as hosts for epigenetic uranium. There are three types of epigenetic uranium deposits in limestone—peneconcordant, efflorescent and karstic. Most important are the *peneconcordant deposits*—tabular, lenticular or irregular masses concordant with gross sedimentary structures of the host rock. Best examples are the Todilto Limestone, U.S.A., and the Buda Limestone, Mexico. Others are known in Canada and the U.S.A.

Efflorescent deposits are unimportant powdery encrustations formed on rock surfaces by evaporation of uranium-bearing waters. Minerals such as tyuyamunite, carnotite and uranophane occur in cavities, on fractures and on exposed rock surfaces.

Karstic deposits are those in which secondary uranium minerals occur in large caverns, cave breccias and in bedded cave-fill deposits of clay and silt in karstified limestone. Best known of these deposits are Tyuya-Muyum, U.S.S.R., and Pryor Mountains, U.S.A. Tyuyamunite is the principal uranium mineral at both localities. These deposits are also of minor importance and contribute little to the $30 uranium resources.

Epigenetic phosphates

Most uraniferous phosphates are classified as syngenetic types because they acquired their uranium at the time of deposition. One exception appears to be the occurrence at Baukoma, Zaire, where uranium occurs in an Eocene phosphatic clay beneath a shallow lake. The phosphatic clay, with an average content of 3000 ppm uranium, rests on a limestone and in places on a sandstone that overlies the limestone.[70]

Tetravalent uranium replaces calcium in the apatite structure. Hexavalent minerals (autunite, meta-autunite and torbernite) are also present. Reserves are estimated at 10 000 ton uranium. The origin of this occurrence is uncertain, so an exploration model for this type deposit has not been constructed.

Examples of important types of deposits

Quartz-pebble conglomerates

Blind River–Elliot Lake district, Ontario, Canada

The Blind River–Elliot Lake district is on the north shore of Lake Huron, about 400 km northwest of Toronto. Uranium occurs here in lowermost Proterozoic fluvial conglomerates at the base of the Huronian Supergroup. The Huronian consists of a thick sequence of quartzite, conglomerate, argillite, arkose and siltstone. Deposition of the supergroup (Fig. 3) was cyclic, each cycle beginning with a conglomerate. The Matinenda Formation, at the base of the sequence, contains the oldest Huronian conglomerates, the ore-bearing quartz-pebble conglomerates. The lower part of the Matinenda consists of greenish arkose and conglomerate. The upper part is grey quartzite, and it is overlain by grey argillite of the McKim Formation. The two formations constitute a fining-upward transgressive sequence that onlaps Archaean basement rocks progressively toward the north.

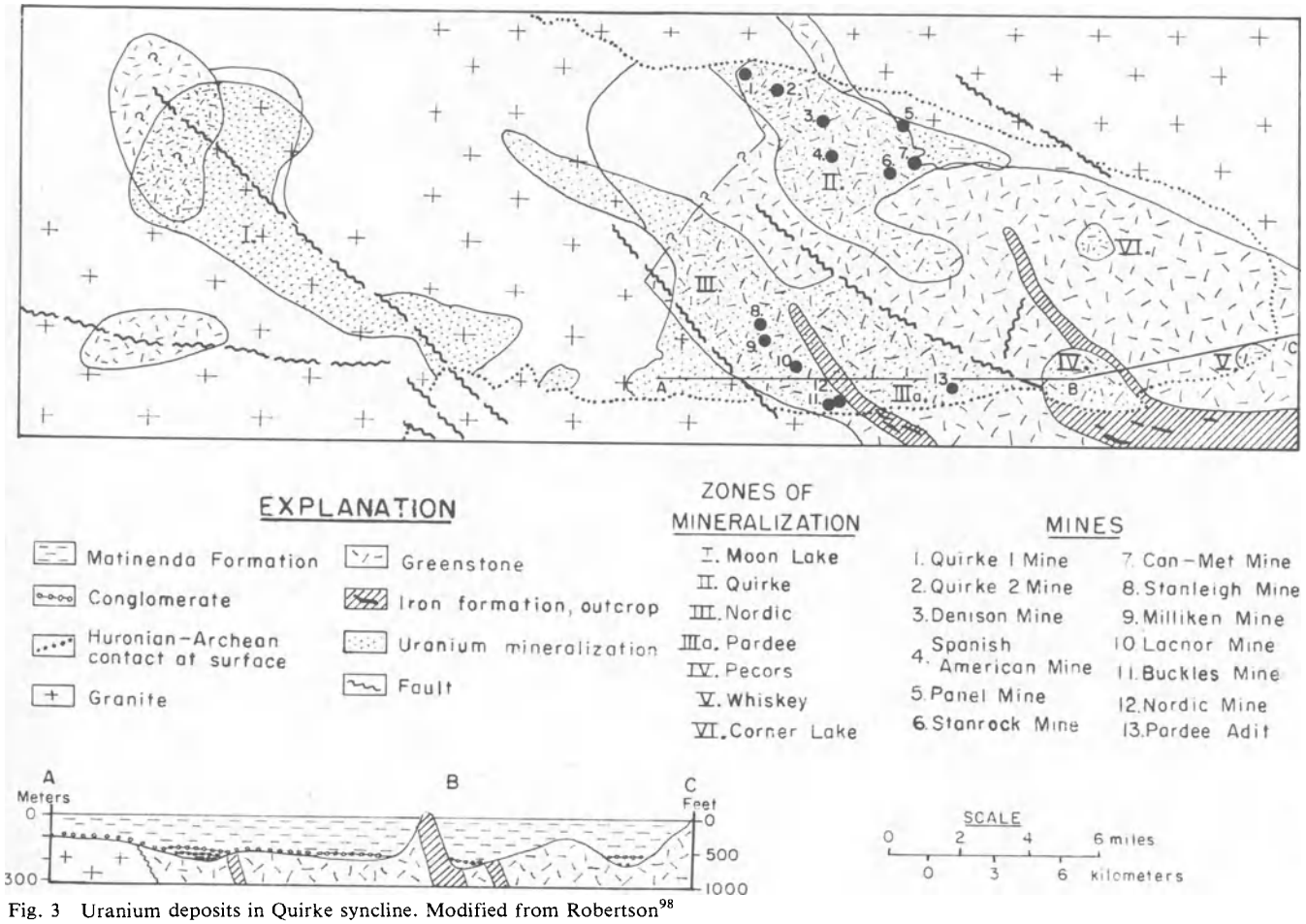

Fig. 3 Uranium deposits in Quirke syncline. Modified from Robertson[98]

The Matinenda ranges in thickness from zero to about 213 m in the south, but thickness varies because of basement irregularities. Ore-bearing conglomerates are generally at or near the base of the Matinenda, but may be as much as 45 m above the base. The pebble conglomerates are lenticular and range from a few centimetres to 6 m in thickness. Large-scale trough cross bedding is the most prominent sedimentary structure. It is probable that the conglomerates were deposited in anastamosing or braided stream channels, lateral migration coalescing the channels into broad thin sheets or reefs.[97] Cross bedding and pebble orientation indicate a northwest source; but, locally, currents were influenced by basement topography. Uraniferous conglomerates are best developed above old valleys on the basement surface that are underlain by greenstone. The courses of some palaeostreams may have been controlled by tholeiitic basalt flows that occur locally in the Matinenda.

Typical ore-bearing conglomerates consist of well-rounded, well-sorted quartz pebbles in a matrix of abraded quartz, feldspar, sericite and pyrite grains. Pyrite content ranges from 10 to 12% and occurs as rounded to subhedral grains or in massive form. Rarely does it replace or fill fractures in the quartz pebbles. Arnold[5] postulated that the pyrite was formed by sulphidization of detrital magnetite, and he reported grains with cores rich in leucoxene, believed to have formed from ilmenite exsolved from the original magnetite. The ore minerals (brannerite, uraninite and monazite) are in the matrix. Thucholite is present both in ore and as post-ore secondary material in fractures. Gummite (soddyite and uranophane), uranothorite and coffinite have also been reported. A great variety of minerals, especially heavy minerals, have been described from the conglomerates, but their quantity is very small.[32]

Brannerite occurs typically as ovoid, reddish-brown to black grains, which suggests that it is detrital.[36] Ferris and Rudd[44] stated that brannerite is a low-temperature diagenetic mineral formed when uranium replaced iron in decomposing ilmenite. They also believed that the released iron combined with volcanic sulphur to form the pyrite in the matrix.[16,96]

Uraninite generally occurs as black subhedral to rounded grains about 1 mm in diameter. Again the rounding indicates a detrital origin. Derry[36] noted that the 5–6% ThO_2 content of the uraninite is more typical of pegmatitic uraninite than hydrothermal types, thus supporting a detrital origin, but J. Patchett[97] suggested that uraninite may have resulted from leaching of brannerite by hydrothermal solutions. Carbon sometimes partly replaces uraninite and fills microfractures in

uraninite grains. Some uranium appears to have dissolved locally and reprecipitated as pitchblende with carbonaceous material (thucholite).

The origin of the Blind River–Elliot Lake uranium minerals is uncertain and controversial, but most workers favour a detrital beginning. McDowell[72] suggested that the source area was an area of low-grade uraniferous pegmatites and late Precambrian pitchblende occurrences some 210–400 km to the northwest. Robertson[98] favoured a source in bodies of red quartz monzonite and associated pegmatites (eroded) that occur in Archaean terrain just north of the Elliot Lake area. These monzonites contain anomalously high concentrations of uranium and are readily detected by airborne gamma-spectrometry surveys.[31,95]

The uranium deposits occur in three different southeast-striking channel systems or zones of mineralization controlled by topography.[36] They are, from west to east, the Moon Lake, Quirke and Nordic zones. The Quirke ore zone is 13 000 m long and 1800–5500 m wide, whereas the Nordic zone is 19 500 m long and 1400–8000 m wide. In the Quirke zone some eight orebodies or reefs are known. They range in thickness from 1.8 to 6 m and are separated by 3.6–30 m of quartzite. In the Nordic zone three or four reefs that vary in thickness from 1.5 to 3 m are being exploited.

Grade of ore is generally higher where conglomerate thickness and degree of pebble packing (least matrix) are greatest. Locally, conglomerate beds may contain as much as 1.0% U, but in mining widths of 2.7–9 m the average grade is 0.1–0.15% U_3O_8. Between 1955 and 1973 the Blind River–Elliot Lake district produced uranium valued as $1500 000 000 from ore averaging 0.10% U_3O_8. Robertson[98] estimated that identified and partly identified uranium resources in the district were at least 400 000 ton recoverable U_3O_8. Other geologists place the figure nearer 300 000 ton.

Black shales

Chattanooga Shale, eastern U.S.A.

The Devonian–Mississippian Chattanooga Shale of Kentucky, Alabama and central Tennessee is a massive, siliceous, pyritic shale lying unconformably on the Ordovician Leipers Limestone.[60] It averages about 9 m in thickness and is divisible into two members—the Dowelltown Member at the base and the Gassaway Member at the top. The Dowelltown is about 4.5 m thick and carries low uranium values (28 ppm in the lower 1.5-m 'A' unit and 11 ppm in the upper 3-m 'B' unit). The Gassaway is also about 4.5 m thick and is divided into three units. The lower ('C') unit is about 2 m thick, the middle ('D') unit is about 1 m thick and the upper ('E') unit varies from 1.5 to 2.5 m in thickness. The uranium content of the Gassaway ranges from 55 to 70 ppm and is generally greatest in the 'E' unit, which also contains phosphate nodules in its upper part in some areas.[82]

Carbonized plant material is abundant in the Chattanooga. It consists mostly of macerated and unidentifiable fragments that constitute about 20% of the shale by weight. The remains are those of land plants that drifted into the sea and indigenous planktonic marine algae. Oil yield by pyrolitic destruction of organic matter in the Gassaway Member is as much as 8 gal/ton.[27]

The Chattanooga shales were deposited at the southern end of a shallow sea, bordered on the southeast, south and west by a stable, nearly peneplained lowland formed on carbonates. Uranium was probably deposited syngenetically with the clay, silt and organic material that constitute the shale. The uranium is more or less evenly distributed throughout the shale, and was probably adsorbed from sea water on plant debris and clay particles.[123]

The Chattanooga constitutes a very large low-grade uranium resource.[124] The richer black shales of the Gassaway Member underlie an area of 10 000 km^2 and contain an estimated 30 000 000 ton U_3O_8 plus large amounts of V, Mo, petroleum and other potentially valuable by-products.

Muds

Walvis Bay area, Namibia

The Walvis Bay area, as used here, refers to an area of some 40 000 km^2 off the coast of Namibia between latitudes 19°S and 25°30′S. Water depths in this area range from 40 to 160 m. Investigations have revealed four depositional 'basins', the largest lying between 21° and 24°S.[78] Diatomaceous mud covers an area of about 19 000 km^2 within the basins and reaches a maximum thickness of 15 m. The diatomaceous ooze is underlain in most places by a layer of shells that, in turn, rests on hard grey siltstone, uncompacted silt, grey medium-grained sandstone, viscous grey clay, fine breccia or calcarenite.

The mud, dated as Eocene, is relatively homogeneous with an average solid content of 7% by weight in the upper part and 23% by weight in the lower part of the unit. It is greenish-grey to dark grey and emits H_2S odour. The mud is very fine-grained, 70–80% by weight of the grains being smaller than 6.3 μm and 15–25% between 6.3 and 20 μm. Most of the mud consists of disc-shaped diatoms, but some foraminifera, ostracods, pteropods, gastropods, lamellibranchs and a few shark teeth are present.

Uranium, which seems to occur in an amorphous state, has not been directly correlated with organic content. It occurs both in the mud and the underlying sediments. It varies in concentration from 7 to 70 ppm (average, ~21 ppm). Other average metal contents include Mo (112 ppm) and V (112 ppm). Based on the average of 21 ppm, it is estimated that the 19 000 km^2 of diatomaceous sediments contain 4 000 000–5 000 000 ton U_3O_8.

Phosphates

Western U.S.A. phosphate field

Phosphates in the western U.S.A. phosphate field occur in the Permian Phosphoria Formation in an area of 350 000 km^2 in southeastern Idaho, northeastern Utah, western Wyoming and southwestern Montana. The Phosphoria consists of two transgressive–regressive marine cycles, each cycle composed of a lower carbonaceous phosphatic shale member overlain by a chert or carbonate member. The phosphatic shale member is a complex of black carbonaceous shales, pelletal phosphorites and phosphatic shales. Phosphorite and mudstone are the lithologic end-members of the phosphatic shales. The lower phosphorite–chert couplet (Meade Peak Phosphatic Shale Member and Rex Chert Member) is thickest in southeast Idaho, where it ranges up to 396 m. The upper couplet (Retort Phosphatic Shale Member and Tosi Chert Member) is thickest in northwestern Wyoming and southwestern Montana, where it may be as much as 91 m thick.[74] Most of the phosphorite mining has been in the thick lower phosphatic shale member. Eastward in Wyoming the phosphatic shale and chert members change facies to carbonate rocks that, in turn, change facies still farther east in Wyoming to evaporites and red beds.

The phosphorites consist of carbonate–fluorapatite mixed with varying amounts of quartz silt, clay minerals, calcite, dolomite, chert and carbonaceous matter. Most of the phosphate occurs as pellets with amounts of oolites, intraclasts, scales, phosphatic shells and replaced skeletal grains. The pellets are cemented with dolomite, calcite, phosphate or, rarely, chert. Some phosphorite beds are composed of phosphate mud. There is a general decrease in size and abundance of intraclast fragments and an increase in carbonaceous content in the phosphorite beds toward the west. These characteristics, plus the close association of phosphorites with cherts and

carbonaceous shales and their shoreward facies change to carbonate rocks, suggest that the Phosphoria accumulated on a moderately shallow shelf edge with prolific planktonic life or in an anoxic basin with restricted circulation.

Where fresh and unweathered, phosphorite beds are hard and dark brown or black, and interbedded mudstones are pyritic. Weathered phosphorites are friable and brown to grey, and they are commonly enriched in phosphate and depleted in uranium. Phosphatic shale members are most phosphatic at both top and bottom or at the bottom only. In southeast Idaho the Meade Peak averages 11–12% P_2O_5, but beds 1–3 m thick near the base and at the top assay 25–33% P_2O_5. Nearly all phosphorites and phosphatic beds contain U, but content varies from 0.001 to 0.65%. Uranium content generally increases with increase in P_2O_5, and both uranium and P_2O_5 increase westward. McKelvey and Carswell[73] determined that phosphate beds of minable thickness (1 m +) that contain more than 31% P_2O_5 generally contain 0.01–0.02% U. It is estimated that this phosphate field has reserves of 202 324 000 000 ton of recoverable phosphate product (about 30% P_2O_5) containing 20 783 000 ton U.

Brines

Uranium in sea water

Uranium concentration in sea water ranges from 1 to 4 ppb,[101] except in inland seas, such as the Caspian Sea, where uranium content ranges from 3 to 10 ppb. The total amount dissolved in the oceans is estimated at 5000 000 000 ton uranium.[131] Research on extraction has been conducted by several countries, including Japan, the United Kingdom, the U.S.A. and West Germany.

Methods considered for uranium extraction include desalination-uranium plants, pumped-water plants, tidal-powered plants and masses of floating logs. Although all these methods can recover uranium from sea water, a profitable method of recovery has yet to be devised. The major difficulty with most processes is the problem of ensuring large and constant volumes of untreated sea water and to prevent processed water from being recycled through the plant. Llewelyn[66] estimated that to obtain 1000 ton uranium per year would require the processing of one trillion ton of sea water.

Silicic volcanics

Sierra Peña Blanca district, Chihuahua, Mexico

The Peña Blanca uranium district is about 50 km northeast of Chihuahua, Mexico, on the east side of a large Basin and Range horst block and near the eastern edge of the Caenozoic Sierra Madre Occidental volcanic province. The bulk of the uranium deposits, which total about 5000 ton of reasonably assured U_3O_8 resource, occur in extracaldera ash-flow tuffs overlying Cretaceous limestones.[50] The source of the tuffs is unknown, but some appear to be related to a large caldera south of Chihuahua. Other tuffs appear to have a western source.

The volcanic sequence at Peña Blanca consists of about 200 m of limestone conglomerate and welded, unwelded and epiclastic tuffs. The volcanics were laid down on a surface of considerable relief. A Cretaceous rudistid reef complex was being exhumed with the formation of local limestone conglomerates prior to deposition of the oldest volcanics.

Uranium occurs in at least five different environments in the district.

(1) Mineralized step faults in welded members: jointing or faulting of the brittle massive ignimbrite provided pathways for solutions and sites for precipitation. Deposits average 300–500 ton U_3O_8 at grades of 0.30–0.40% U_3O_8. Examples are Nopal nos. 1, 3 and 5 deposits.

(2) Mineralization within the more porous and permeable units, such as lapilli tuff: porosity was provided by pumice and lithic fragments.

(3) Mineralization in altered vitrophyre at the base of a welded tuff: larger lower-grade deposits, such as the Margaritas, are of this type. It is about 2 km long, 100–200 m wide and several metres thick, and it contains about 4000 ton U_3O_8 at an average grade of 0.20%. Uranium occurs mostly as uranophane with some carnotite and autunite. Alteration is characterized by the formation of hematite and montmorillonite. The position of this deposit adjacent to a slightly petroliferous rudistid reef complex suggests possible palaeo-hydrologic and organic-reductant influences on mineralizing fluids.

(4) Mineralization of a pumice zone below an ignimbrite, as at Margaritas.

(5) Mineralization in underlying rudistid limestones: uranium occurs in faults, solution cavities, palaeo-karsts and other zones in fetid limestone beneath volcanics at Domatilla mine.

Mafic volcanics

Olympic Dam, South Australia

An important discovery of uranium, apparently related in part to mafic volcanic rocks, is the very large Cu–U orebody in probable Proterozoic rocks at Olympic Dam (Roxby Downs), South Australia. This blind orebody, covered by 350 m of unmineralized rock,[84] was discovered by utilizing the concept that continental basaltic rocks release Cu during alteration.[54]

Uranium occurs here in hematitic granitic breccia or arkose about 800 m thick overlain by more than 100 m of hematite-sericite-altered volcanic rocks and 100 m of shale. Pitchblende, brannerite and davidite occur with chalcopyrite, cobaltite and gold. REE are also abundant. Gangue is hematite, barite, fluorite, magnetite, quartz and sericite.[108]

The origin of this deposit, and a similar one at Mt. Painter 250 km to the east,[133] is not fully understood, but may be related in some way to submarine volcanism.[84] The thick breccia and conglomerate units are also a key element, probably indicating active faulting along platform boundaries. Hydrothermal solutions moving up the flanks of a shallow marine basin from a nearby intrusive source created a sulphidic environment where they encountered the granitic debris. Uranium, concentrated here with Cu, combined with Ti liberated by sulphidization of Fe–Ti oxides in the arkose to form brannerite and davidite.

The orebody is about 1.5 km by 0.5 km and up to 170 m thick. It contains thick zones of 0.05–0.10% U_3O_8 in 1–2% Cu, and early estimates[132] are that it contains about 600 000 ton U_3O_8 and 11 000 000 ton Cu. Patterson and Pitman[91] gave an estimate of 375 000 ton U_3O_8.

Peralkaline nepheline syenites

Ilímaussaq, Greenland

At Ilímaussaq at the southern tip of Greenland uranium occurs within a large peralkaline syenite intruded into lavas, intraflow sandstones and the Julianehaab granite about 1020 m.y. ago.[19] In its later stages the intrusion crystallized by accreting crystals under an impervious roof (foyaite and naujaite zone) at the same time as a layered mass (kakortokite zone) accumulated near the base of the magma chamber. Finally, a lujavrite formed in between.[43] The lujavrite commonly contains 200–300 ppm Th, but numerous xenoliths and dykes make U–Th values highly erratic. Local zones exceed 1000 ppm U and 5000 ppm Th, but minable zones in excess of 400 ppm are thin and the ore is refractory.[15] The principal ore mineral is the rare mineral steenstrupine, which contains 0.2–1.5 wt% U and 2.0–7.5 wt% Th.[119] Other radioactive minerals, such as eudialyte and monazite, are also present. It is estimated that the

Ilímaussaq deposit contains about 35 000 ton U_3O_8 reasonably assured resource at $50/lb.[88]

Carbonatites

Araxá, Brazil

The best-known and probably most important uranium-bearing carbonatite in Brazil is Araxá, located north of Pocos de Caldas in Minas Gerais. The Araxá pipe is an intrusion of biotite–carbonatite that strongly domes the intruded Precambrian Araxá Group. Uranium and thorium are associated with pyrochlore and apatite in a highly decomposed mass of carbonatite. The roughly circular pipe is about 4.7 km in diameter and is almost completely surrounded by fenitized quartzite. The carbonatite consists largely of magnesian calcite with oxides of iron, titanium and apatite. Lesser components include pyrite, sphene, barite, ilmenite, zircon and monazite.[77] The entire carbonate mass, except for one outcrop, is covered by a weathered mantle up to 300 m thick. The mantle is composed of manganese and iron oxides, phosphate, barite, pyrochlore and monazite. Pyrochlore occurs in the residual crust and as disseminations and stockworks in fresh rock, but the richest material is in a centralized body just below the weathered mantle. This is one of the largest niobium deposits in the world (300 000 000 ton easily accessible ore). Phosphate is associated with the pyrochlore and is concentrated in the weathering mantle. Uranium is present in small amounts throughout the carbonatite. The niobium deposit contains from 0.023 to 0.05% U_3O_8, the phosphate deposit contains about 0.01% U_3O_8, REE concentrations average about 0.03% U_3O_8 and the weathering mantle averages about 0.01% U_3O_8. It is estimated that the entire deposit contains 139 700 t U_3O_8 and 1 323 000 t ThO_2.[71]

Anatectics

Rössing deposit, Namibia

The Rössing deposit is a large low-grade uranium occurrence on the southwestern flank of a large domal structure in the central part of the late Precambrian Damaran orogenic belt in Namibia (Fig. 4). Uranium minerals occur in syntectic alaskites within steeply dipping isoclinal folds of the migmatized Khan and Rössing Formations. These formations consist of highly metamorphosed and migmatized pyroxene and hornblende gneisses, amphibolites, schists and marbles. Three stages of dynamothermal metamorphism and accompanying deformation have affected the host rocks. A younger thermal event is recognized adjacent to the alaskite.[129]

Syntectic alaskites range from small secretionary lenses to large intrusive and replacement bodies. They show concordant, discordant and replacement relations with the folded metasediments. The alaskites were emplaced along shears, fractures, bedding planes and axial planes of isoclinal folds. The alaskites are mostly pegmatitic, but hypidiomorphic-granular textures are common. They consist of quartz, microcline and microcline–perthite together with accessory amounts of zircon, fluorite, molybdenite, apatite, biotite and sphene.

Uraninite, the dominant ore mineral, occurs as small euhedra poikilitically enclosed in quartz and feldspar and as finely disseminated euhedra interstitial to and along microfractures in major rock-forming minerals. Secondary uranium minerals, mostly beta-uranophane, are concentrated in the upper part of the deposit and constitute nearly 40% of the ore. They formed as replacements of uraninite or as films along microfractures as the result of upgrading in the unusual Namib Desert climate, where nightly fogs form small amounts of moisture.[14]

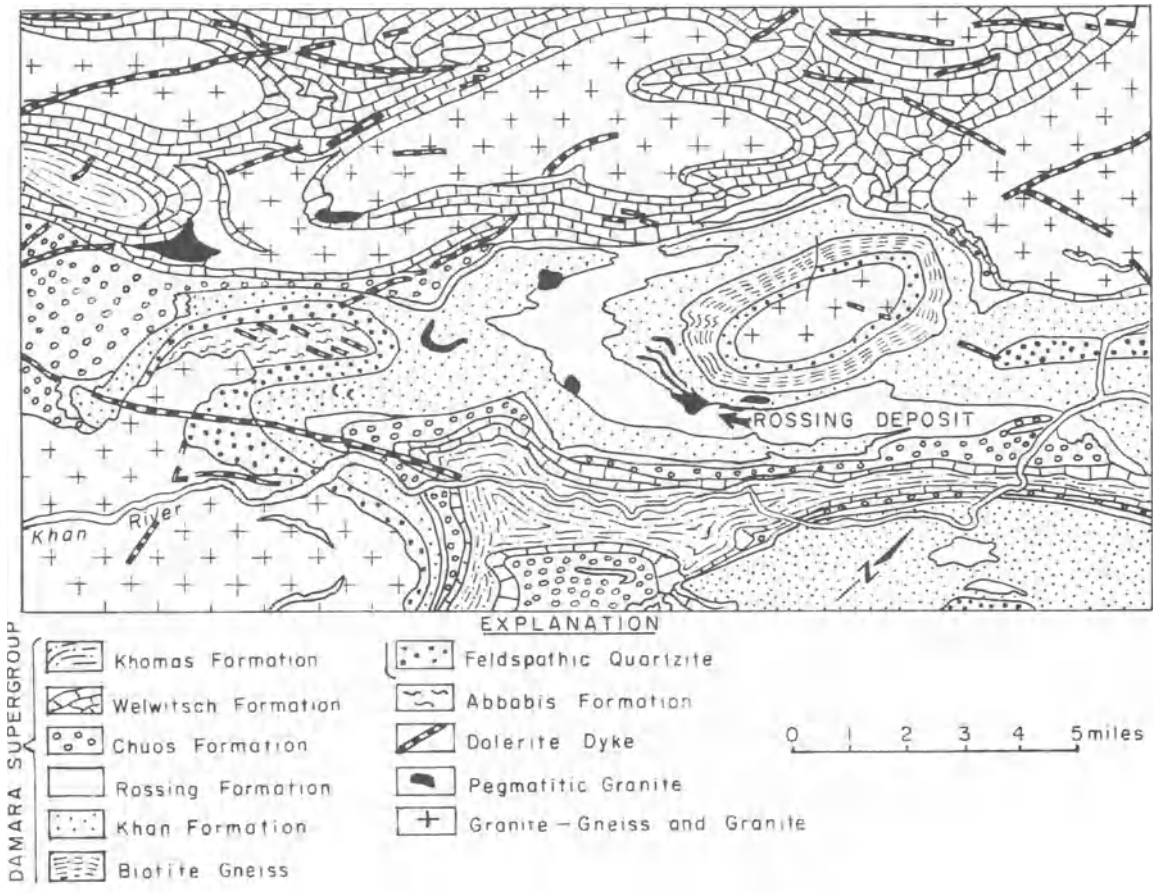

Fig. 4 Setting of Rössing uranium deposit. Modified from Smith[117]

Rössing is the largest known anatectic or ultra-metamorphic deposit, containing about 150 000 ton U_3O_8 at an average grade of 0.035% U_3O_8.

Peralkaline granites

Bokan Mountain, Alaska, U.S.A.

The Bokan Mountain uranium occurrence is associated with the late Cretaceous to early Tertiary Bokan Mountain granite pluton on Prince of Wales Island in southernmost Alaska. The granite is an epizonal, circular ring-dyke complex intruded into eugeosynclinal metasediments and a Devonian(?) plutonic sequence.[125] Its epizonal nature is shown by contact effects, roof pendants and associated hypabyssal intrusives. The lack of internal structures, discordance with structures in the metasediments and extensive alkali metasomatism suggest that it is a postorogenic intrusive.

The border zone of the 6.5-km^2 complex is a riebeckite granite pegmatite/aplite up to 13 m thick. Next inward is an aegirine granite porphyry shell about 180 m thick that grades inward into a 15-m thick transition zone in which riebeckite is the dominant ferromagnesian mineral. Ring dykes of riebeckite aplite porphyry were injected into these marginal zones. Interior portions of the complex consist of banded or massive riebeckite-bearing granites cut by aplitic plugs and ring dykes.

The uranium–thorium mineralization is localized in highly albitized shear zones as vein-like or irregular pipe-shaped bodies formed by concentrations of uranium-bearing microveinlets. The ore zones occur within or on top of syenitic masses and show intense albitization, chloritization and hematitization. MacKevett[68] and Staatz[121] also reported minor syngenetic concentrations within the magma body and in the pegmatites. They considered the veins and pipe-like bodies to be postmagmatic hydrothermal.

Uranothorite and thorian uraninite are the main ore minerals, but coffinite, brannerite and pigmentary materials are also present. Accessory minerals include calcite, fluorite, quartz, sulphides and tourmaline. U/Th ratios range from 10 to 100 in ore, but are less than 10 outside ore. The Ross-Adams mine produced about 1000 ton U_3O_8 at a grade of about 1.00% U_3O_8 between 1957 and 1971.

Granites

Midnite mine, Washington, U.S.A.

At Midnite mine, about 64 km northwest of Spokane, Washington, uranium occurs in a roof pendant of the late Precambrian Togo Formation, adjacent to a late Cretaceous quartz monzonite. The Togo consists of steeply dipping, low-grade metamorphosed black shales (metapelites) with lenses of calcareous material. It contains up to 2% iron sulphides and ubiquitous graphite. The monzonite is composed of large feldspar phenocrysts in a groundmass of quartz, potash feldspar, plagioclase and biotite. Accessory minerals are muscovite, sphene, zircon, apatite and fluorite.

The average uranium content of the intrusive is about 12 ppm. Primary uranium minerals (pitchblende and coffinite) are concentrated along small step faults and shears in the metasediments.[10] Uranium minerals occur as replacements, disseminations along foliation planes and fracture fillings. Orebodies are roughly tabular, have nearly horizontal upper surfaces and are bordered on one or more sides by unmineralized monzonite. Dimensions range up to 380 m long, 210 m wide and 50 m thick.[85] Midnite mine has produced about 6000 ton U_3O_8 at a grade of 0.21% U_3O_8 since 1957.[84]

Pegmatites

Bicroft mine, Bancroft district, Ontario, Canada

Bicroft mine near Bancroft, Ontario, is within the Cardiff plutonic complex, consisting of two gneissic granites and a gneissic syenite intruded into late Precambrian metasediments. The Bicroft pegmatites occur at the contact between the Centre Lake granite and the metasediments. The uranium-bearing pegmatites are in paragneisses and para-amphibolites adjacent to the granite. Four types of pegmatites are recognized here (pyroxene, pyroxene granite, granite and quartz-rich pegmatites), but uranium is largely restricted to the quartz-rich pegmatites.

Ore minerals are uraninite, uranothorianite, allanite, pyrochlore and betafite in a gangue of smoky quartz with accessory zircon, molybdenite, amphibole and anatase. Minor calcite and fluorite are present. Unzoned pegmatites have U_3O_8 contents of 0.024–0.117% in widths of 1–4 m.[111] Reserves for Bicroft are unknown, but for the entire Bancroft area they are 2200 ton U_3O_8 at a grade of about 0.13%.

Hydrothermal veins

Schwartzwalder mine, Colorado, U.S.A.

An example of veins with simple mineralogy is the *Schwartzwalder mine*, 25 km west of Denver, Colorado. Host rocks for this deposit are metasediments of the late Precambrian Idaho Springs Formation—a complex of sandstone, shale, carbonates and mafic intrusives.[114] Large breccia-reef fault zones formed during late Precambrian cataclastic deformation were reactivated about 50–70 m.y. ago. Structures hosting the uranium are subsidiary to the major structures (Fig. 5).

Uranium occurs in flat or horsetail veins with low dip in the hanging-wall of the major Illinois vein, but they steepen near the major faults.[90] Mineralized portions of faults are continuous for more than 900 m vertically, but strike lengths are less than 200 m.[37] Brittle metasediments are the favoured hosts.

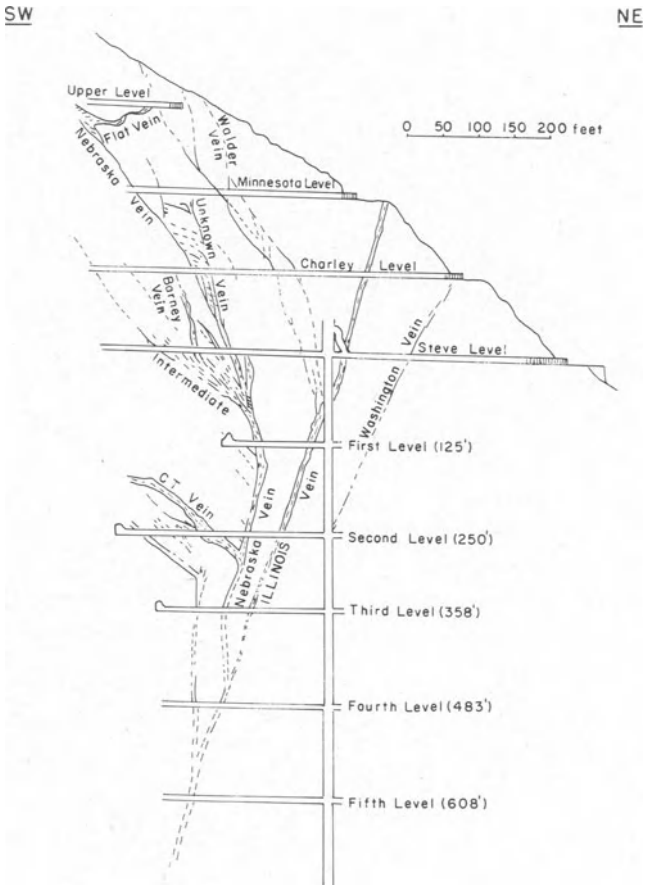

Fig. 5 Cross-section, Schwartzwalder mine. Modified from Downs and Bird[41]

Pitchblende and coffinite along with jordesite and adularia were formed during the main mineralization. A later base-metal stage added chalcopyrite, chalcocite, ankerite, pyrite and marcasite. Chloritization and sericitization are the main types of alteration. The Schwartzwalder has produced about 5500 ton U_3O_8 and has an equal amount of reserves.[90]

Shinkolobwe deposit, Zaire

An example of veins with complex mineralogy is the mined-out uranium deposit at *Shinkolobwe*, Zaire, at the northwest end of the African Copperbelt. It occurs in a faulted transported fold in metamorphosed dolomitic shales of the middle Proterozoic Mine Series of the Roan Group.[21] Uraninite and uranophane mineralization (about 620 m.y. ago) was followed by several later mineralizations in which pyrite, molybdenite, monazite, selenium, Co–Ni sulphides and selenides and copper minerals were formed. It is believed that this orebody was formed by redistribution of metals originally deposited in marine sedimentary rocks.[47] The uranium, originally weathered from granites and deposited in the marine sediments, was in low concentrations (50–100 ppm), but was remobilized during the post-tectonic metamorphism and 'dammed' under a large nappe to form the Shinkolobwe deposit.

Contact metasomatics

Mary Kathleen deposit, Queensland, Australia

The Mary Kathleen uranium deposit[35,53] is in metamorphosed and metasomatized nearshore clastic and carbonate sediments of the lower to middle Corella Formation in northeastern Queensland, Australia. The uppermost unit of the Corella is a breccia-conglomerate formed as a cobble beach. This unit hosted most of the ore at Mary Kathleen.

The Corella metasediments occupy a broad syncline bordered on the east by the post-orogenic Mount Burstall granite. This differentiated pluton has an unusually high uranium content (1–12 ppm) and late-stage pegmatites extend westward to within 3 km of the Mary Kathleen orebody. A large north-trending eastward-dipping shear zone, extending through the metasediments toward the granite, may have served as a channelway for metasomatizing fluids from the granite.

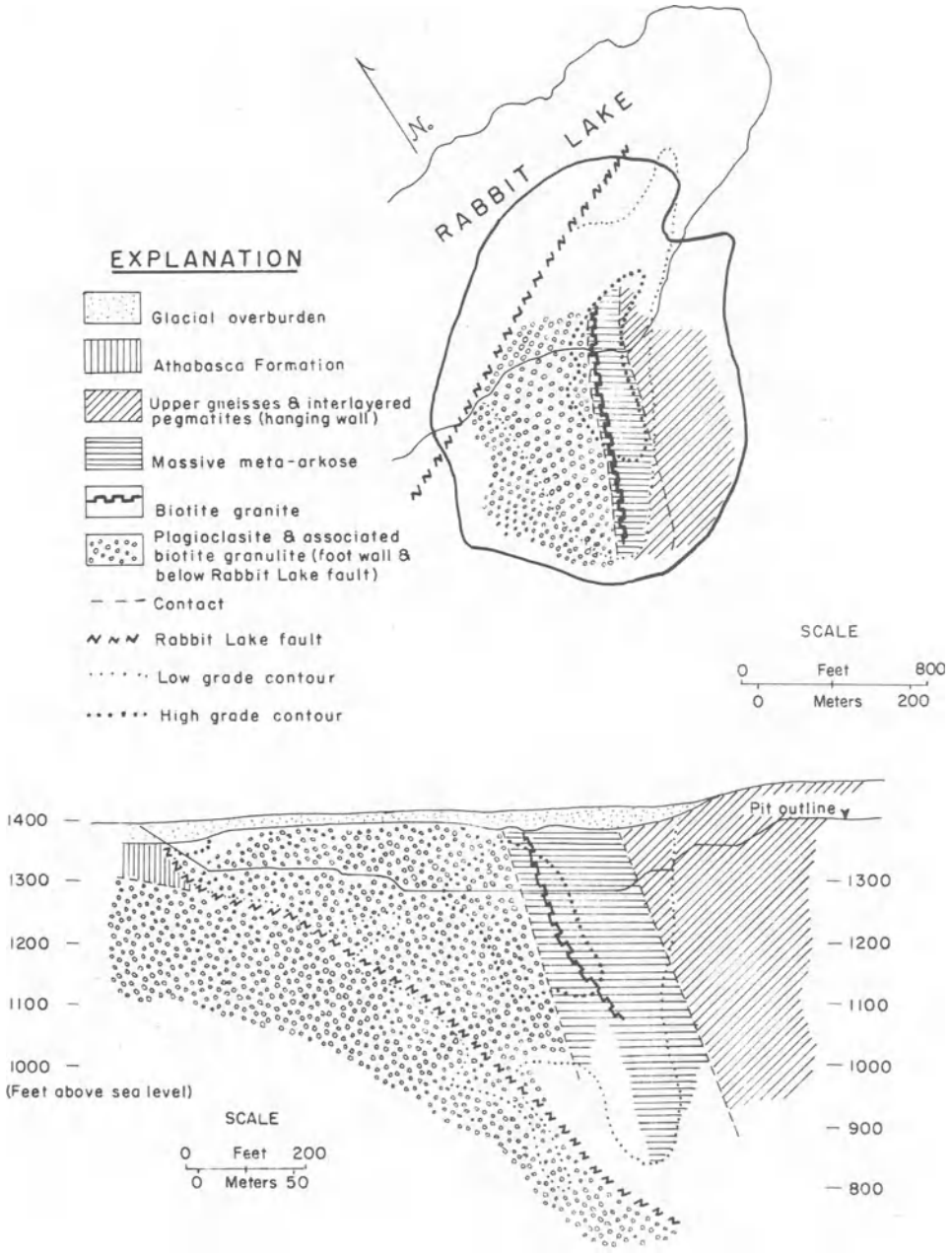

Fig. 6 Map and section, Rabbit Lake orebody, showing lithology. After Sibbald[115]

The orebody, totally within the garnet-rich breccia conglomerate near the axis of the syncline, consisted of 40% garnet, 35% allanite, 10% apatite and 15% 'other', including stillwellite, albite and scapolite.[130] Uranium occurs chiefly as uraninite within allanite and stillwellite. The adjacent beds were variously enriched in REE, Th, B, P, S and Fe. Production at Mary Kathleen was about 12 000 ton U_3O_8 at an average grade of 0.14% U_3O_8, 0.02% ThO_2 and 3.6% REE.

Vein-like types

Unconformity-related

Rabbit Lake, northern Saskatchewan, Canada The Rabbit Lake occurrence in northern Saskatchewan is an example of a monometallic unconformity-related uranium deposit.[57,61,65,75,76] It is in Aphebian metasediments of the Wollaston fold belt, along the eastern erosional edge of the unconformably overlying Helikean Athabasca Formation. The metasediments include meta-arkose, biotite paragneiss, calc-silicate rocks and marble. The Athabasca is a series of red to brown quartz sandstones and conglomerates.

The Rabbit Lake deposit, the upper surface of which is only 15 m below the plane of the unconformity, is in a steeply dipping, highly chloritized breccia zone in the metasediments (Fig. 6). Breccia fragments are cemented by dolomite, calcite and quartz. Massive and sooty pitchblende occur in veinlets and as fracture fillings and are associated with minor galena, sphalerite, pyrite, marcasite and chalcopyrite. At depth the breccia zone is terminated by a low-angle thrust that placed the Aphebian metasediments above the Athabasca sediments locally. Chloritic alteration is pervasive and zonal around the ore. Two stages of mineralization are recognized—deposition of massive pitchblende preceding chloritization and deposition of sooty pitchblende and coffinite following an intervening red alteration and leaching stage. The deposit is dated at 1100 m.y., whereas the Athabasca is dated at ≃1350 m.y. This deposit is reported to contain about 21 000 ton U_3O_8 at a grade of 10–15% U_3O_8.

Jabiluka II, Northern Territory, Australia The Jabiluka II uranium deposit[40,81,105,116] is a polymetallic unconformity-related occurrence. This uranium–gold deposit is in the East Alligator River district, Northern Territory. It occurs in brecciated metasedimentary rocks beneath the unconformably overlying Middle Proterozoic Kombolgie Sandstone. The metasediments (Cahill Formation) consist of pyritic quartz–chlorite–graphite schist, chlorite–graphite schist and some calc-silicate rocks (Fig. 7). They have been folded into an open asymmetric syncline. Near Jabiluka II a thrust fault truncates the sub-Kombolgie unconformity and has placed the Kombolgie in fault contact with the Cahill.

Pitchblende, the principal uranium mineral, coats breccia fragments and forms veinlets up to 2 mm wide. Native gold, which assays 0.44 oz/ton, is associated with the pitchblende in part of the deposit. Associated minerals are pyrite, chalcopyrite and hematite. Ore is generally confined to extensively chloritized and brecciated zones and is most concentrated within and below graphite schists. Ore reserves at Jabiluka II are believed to be about 224 000 ton U_3O_8 at a grade of 0.45% U_3O_8.

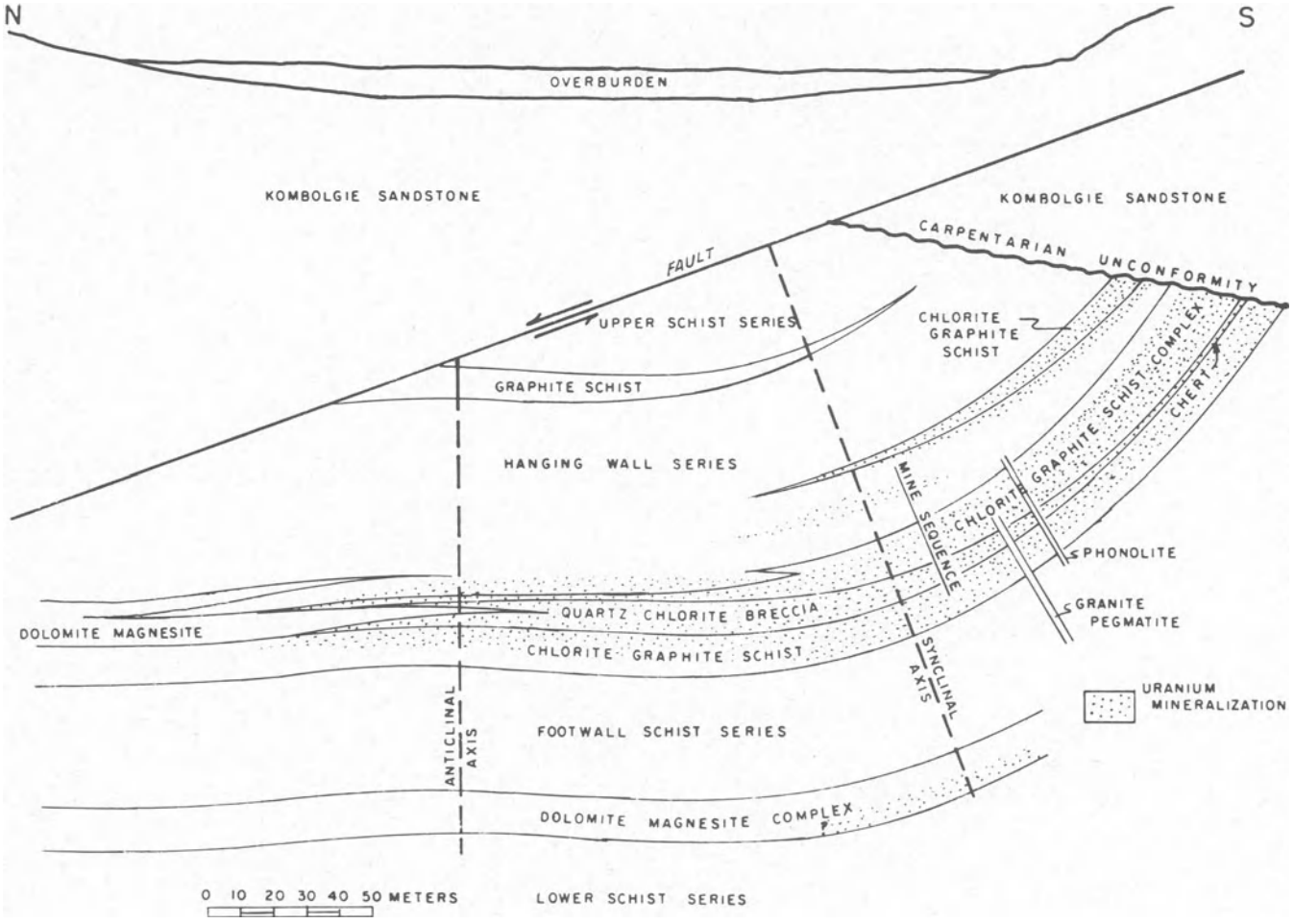

Fig. 7 Cross-section, Jabiluka II deposit. After Rowntree and Mosher[105]

Vein-like deposits in metamorphic rocks

Beaverlodge area, northern Saskatchewan, Canada
The Beaverlodge area in northern Saskatchewan is characterized by monometallic vein-like uranium deposits in metamorphic rocks.[11,67,110,126] Underlying this area is metamorphosed and granitized gneiss of the Lower Huronian Tazin Group. The gneiss is unconformably overlain by continental red beds of the Middle Huronian Martin Formation.

Pitchblende and calcite occur in veins and multiple-vein systems in the Tazin, and some pitchblende occurs in the overlying Martin. Uranium-bearing veins have a strike length of more than 4500 m and they extend to a depth of more than 1645 m. The pitchblende occurs as vein fillings in shears, fractures and brecciated zones within 100 m of the St. Louis Fault. It is also disseminated in rocks adjacent to the veins. Initial pitchblende deposition (1780 m.y. ago) was followed by a thermal event that remobilized and redeposited the uranium about 1140 m.y. ago.

Echo Bay–Eldorado mine, Northwest Territories, Canada
The Echo Bay and Eldorado uranium–silver mines in northern Canada are polymetallic vein-like deposits in metamorphic rocks.[99,100,106] The two mines are in a vein system containing U, Ag, Ni and Cu. The veins occur in roof pendants of Aphebian sedimentary and volcanic rocks (Echo Bay Group) within a Hudsonian granitic intrusive. The margins of the pendants were thermally metamorphosed, but the centres are little metamorphosed. Mineralization occurs in green and red banded andesitic tuffs in the pendant centres. Ore occurs in three steeply dipping veins that average 0.5 m in thickness, 1500 m in length and more than 400 m in depth. Veins contain pitchblende, native silver, native bismuth with small amounts of base-metal sulphides and Co–Ni arsenides. Veins are surrounded by a halo of feldspatization, hematitization, chloritization and carbonatization.

Epigenetic types

Sandstones

Peneconcordant deposits The largest concentration of high-grade uranium in peneconcordant deposits is in the *Grants Mineral Belt* near Grants, New Mexico.[28,52,56,109,134] The uranium hosts are massive green to reddish-brown arkosic fluvial sandstones in the Westwater Canyon and Brushy Basin Members of the late Jurassic Morrison Formation (Fig 8). These sandstones have thin mudstone partings and contain much woody trash. In the Ambrosia Lake portion of the Belt the mineralized trend is as much as 2.5 km wide and more than 6 km long.

Individual peneconcordant deposits are tabular bodies generally elongate parallel to palaeo-drainage and clusters of orebodies show the same alignment. Orebodies range from 0.5 to 9 m in thickness, 20 to 240 m in width and 100 m to 2 km in length. Ore boundaries are generally sharp. Bedding planes commonly form the lower boundaries of orebodies, but the upper boundaries may be gradational. Ore tends to concentrate parallel to intraformational disconformities, along mudstone contacts and coincident with subtle low-amplitude synclinal folds. In some cases ore terminates against sharply curved surfaces (rolls).

Coffinite is the principal uranium mineral, but organo-uranium complexes and uraninite are also present. They coat sand grains black and fill interstices. In places masses of jordesite and vanadium and manganese minerals occur marginal to ore. Secondary uranium minerals are not common, but they include phosphates, silicates and hydrous oxides. Alteration consists of bleaching from red to green or grey, kaolinitization of feldspars and formation of calcite haloes. Production plus reserves in the Grants Mineral Belt total about 221 300 ton U_3O_8 at a grade of 0.15% U_3O_8.

Roll-type deposits In the *Gas Hills district of Wyoming* roll-

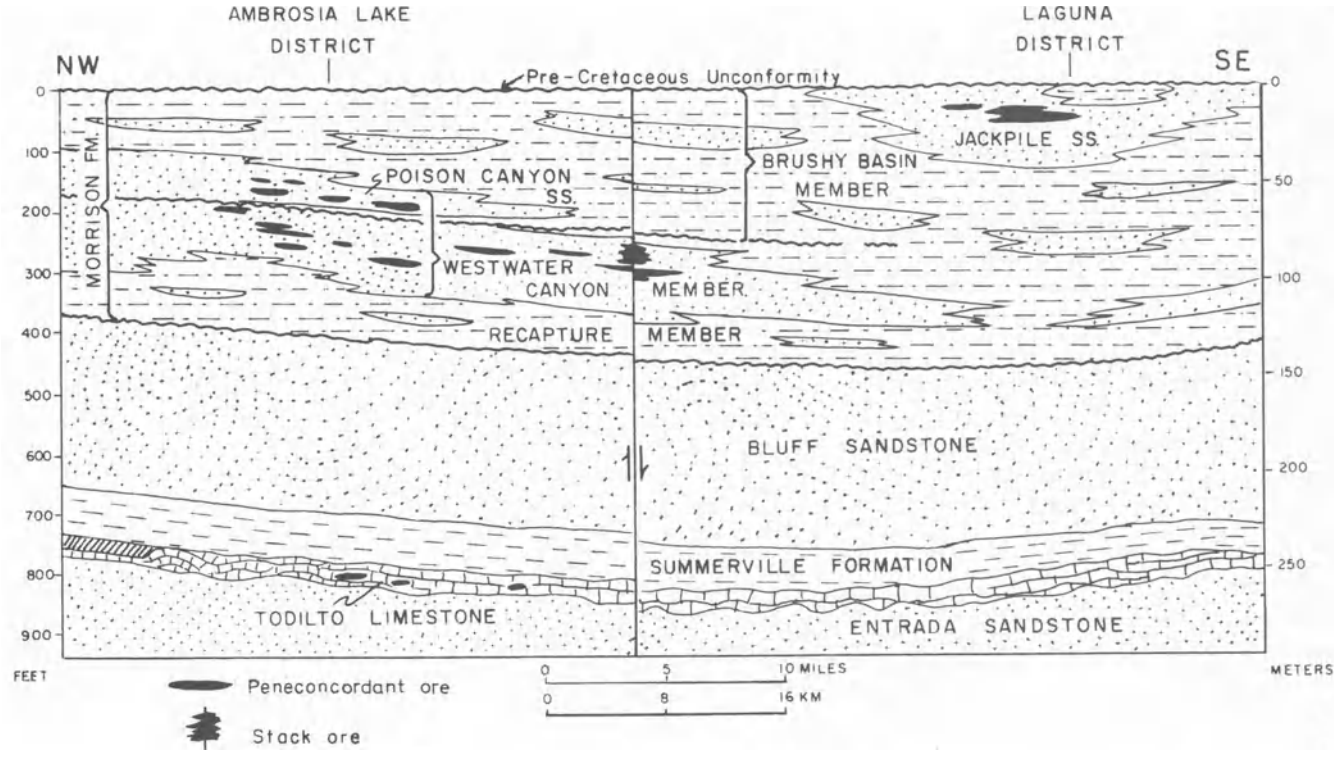

Fig. 8 Cross-section, Grants Mineral Belt. Modified from Hilpert[55]

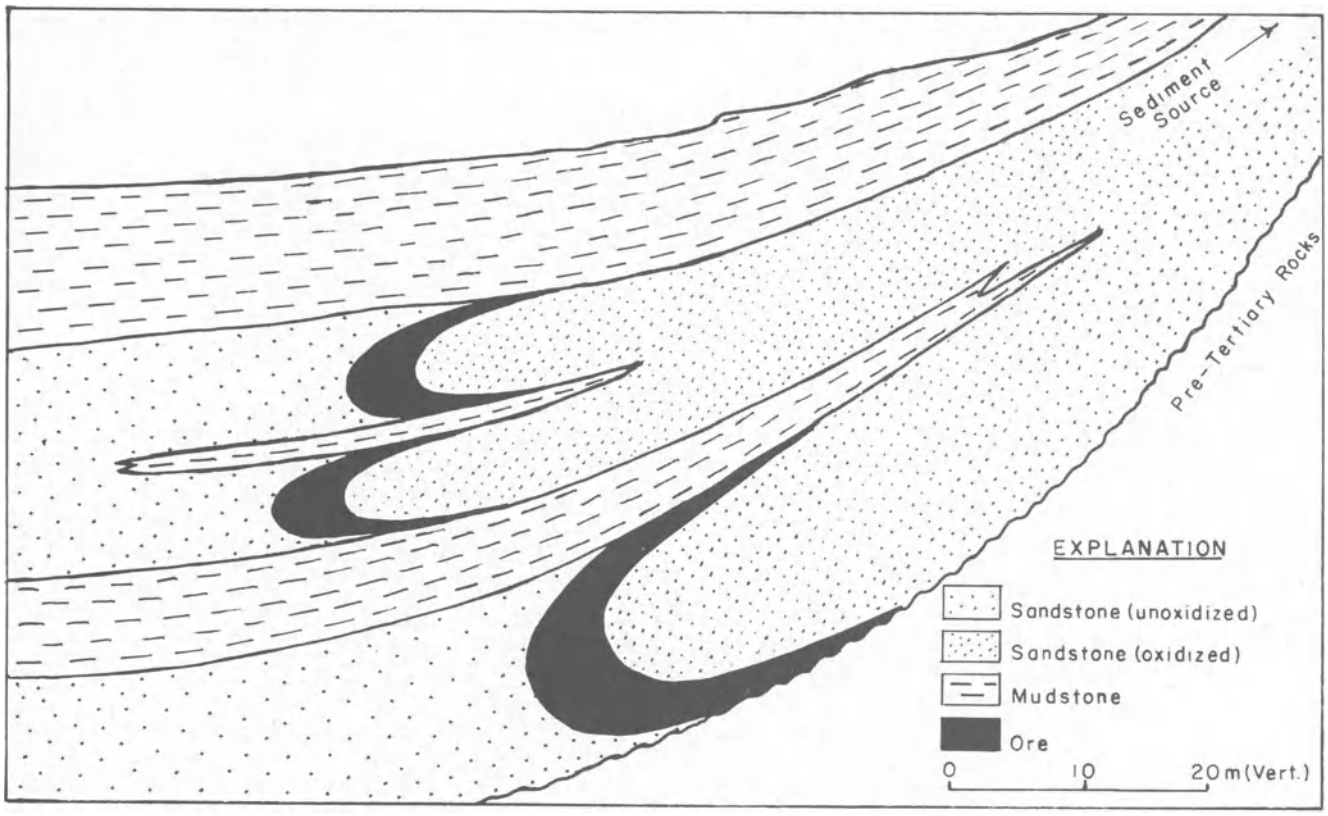

Fig. 9 Schematic diagram of roll-type uranium occurrences in Wyoming Basins

type uranium deposits occur in the upper part of the Eocene Wind River Formation.[3,4,118] The Wind River is a 90- to 245-m thick unit of cross-bedded arkosic fluvial sandstone with interbeds of mudstone, carbonaceous shale and conglomerate.

Roll-type orebodies, found below the water-table, vary from 0.3 to 8.0 m in thickness. Rolls are tongue-shaped in plan and concentric *C*-shaped in vertical section (Fig. 9). Solution fronts have been traced for several kilometres and individual orebodies extend for 1000 m or more. The thickness of the individual sandstone bed that contains the solution-front controls the ore thickness.

Ore-bearing zones have much coaly material and carbonized wood. The ore consists of uraninite and coffinite, which occur as black coatings on grains and as interstitial fillings. They are accompanied by Se, Mo and As enrichment. Oxidized zones (above the water-table) contain uranium phosphates, silicates and hydrous oxides. It is estimated that the Gas Hills district will ultimately produce about 75 000 ton U_3O_8.

Calcrete deposits

The most important uraniferous calcrete deposit is *Yeelirrie, Western Australia*.[20,23] Yeelirrie is an area of interior drainage, deep valley fills, abundant evaporite lakes and clay pans in an arid region. Valley calcretes are typically elongate masses of carbonate-cemented alluvium deposited parallel to subsurface valley drainage courses, but some form delta-like deposits that fringe salt lakes.

Uranium from weathered granites and vanadium derived from greenstones are present in the groundwater and valley-fill sediments. Uranium, vanadium and potassium concentrate downstream by evaporation and combine in the oxidizing environment to form carnotite, which fills cavities and fractures in the calcrete. Carnotite also forms in a clay–quartz unit beneath the calcrete. Resources at Yeelirrie are estimated at 47 000 ton U_3O_8 at grades of 0.05–0.10%.

References

1. Adams J. A. S. and Richardson K. A. Thorium, uranium and zirconium concentrations in bauxite. *Econ. Geol.*, **55**, 1960, 1653–75.
2. Adams J. W. Arengi J. T. and Parrish I. S. Uranium- and thorium-bearing pegmatites of the United States. *Open-File Rep. U.S. Dep. Energy* GJBX-166-80, 1980, 454 p.
3. Anderson D. C. Uranium deposits of the Gas Hills. *Contr. Geol. Wyoming Univ.*, **8**, 1968, 93–103.
4. Armstong F. C. Geologic factors controlling uranium resources in the Gas Hills District, Wyoming. *Wyoming geol. Ass. Guidebook, 22nd ann. Field Conf.*, 1970, 31–4.
5. Arnold R. G. A preliminary account of the mineralogy and genesis of the uraniferous conglomerate of the Blind River, Ontario. M.A.Sc. thesis, University of Toronto, 1954.
6. Badham J. P. N. Orogenesis and metallogenesis with reference to the silver–nickel, cobalt arsenide ore association. In *Metallogeny and plate tectonics* Strong D. F. ed. *Spec. Pap. geol. Ass. Can.* 14, 1976, 560–71.
7. Bailey D. K. Crustal warping—a possible tectonic control of alkaline magmatism. *J. geophys. Res.*, **69**, 1964, 1103–11.
8. Bailey R. V. Applied geology in the Shirley Basin uranium district, Wyoming. *Contr. Geol. Wyoming Univ.*, **4**, 1965, 27–35.
9. Bain J. H. C. Uranium mineralization associated with late Palaeozoic acid magmatism in northeast Queensland. *BMR J. Aust. Geol. Geophys.*, **2**, 1977, 137–47.
10. Barrington J. and Kerr P. F. Uranium mineralization at the Midnite Mine, Spokane, Washington. *Econ. Geol.*, **56**, 1961, 241–58.
11. Beck L. S. Genesis of uranium in the Athabasca region and its significance in exploration. *CIM Bull.*, **63**, May 1970, 367–77.
12. Bell K. G. Uranium in carbonate rocks. *Prof. Pap. U.S. geol. Surv.* 474-A, 1963, 29 p.
13. Berezina L. A. Goleva R. V. and Zheleznova E. I. Content and distribution of uranium in minerals from an ultrametamorphic complex and from uraniferous sodium metasomatites. *Geochem. Int.*, **13**, no. 6 1976, 41–50; *Geokhimiya*, no. 11 1976, 1673–82.
14. Berning J. *et al.* The Rössing uranium deposits, South West Africa. *Econ. Geol.*, **71**, 1976, 351–68.
15. Bohse H. *et al.* On the behaviour of uranium during crystallization

of magmas—with special emphasis on alkaline magmas. In *Formation of uranium ore deposits* (Vienna: IAEA, 1974), 49–60.
16. Bottrill T. J. Uraniferous conglomerates of the Canadian Shield. *Pap. geol. Surv. Can.* 71-1A, 1971, 77–82.
17. Bowden P. Origin of the younger granites of northern Nigeria. *Contr. Mineral. Petrol.*, **25**, 1970, 153–62.
18. Bowie S. H. U. Some geological concepts for consideration in the search for uranium provinces and major uranium deposits. In *Uranium exploration geology* (Vienna: IAEA, 1970), 285–300.
19. Bridgewater D. Isotopic age determinations from South Greenland and their geological setting. *Bull. Groenl. geol. Unders.* 53, 1965, 56 p.
20. Butt C. R. M. Horowitz R. C. and Mann A. W. Uranium occurrences in calcretes and associated sediments in Western Australia. *CSIRO Rep.* no. FP-16, 1977, 67 p.
21. Cahen L. Igneous activity and mineralisation episodes in the evolution of the Kibaride and Katangide orogenic belts of central Africa. In *African magmatism and tectonics* Clifford T. N. and Gass I. G. eds (Darien, Conn.: Hafner, 1970), 97–117.
22. Carlisle D. Possible variations on the calcrete–gypcrete uranium model. *Open File Rep. U.S. Dep. Energy* GJBX-53-80, 1980, 38 p.
23. Carlisle D. *et al. The distribution of calcretes and gypcretes in southwestern United States and their uranium favorability; based on a study of deposits in Western Australia and South West Africa (Namibia)* (Los Angeles: University of California, 1978), 274 p.
24. Castro L. O. A pesquisa de urânio em Araxá. *Soc. Bras. Geol., XXII Congr.*, 1968, 93–6.
25. Clark S. P. Jr Peterman Z. E. and Heier K. G. Abundances of uranium, thorium and potassium. *Mem. geol. Soc. Am.* 97, 1966, 521–41.
26. Cohenour R. E. Geology and uranium occurrences near Lakeview, Oregon. *Rep. U.S. atom. Energy Comm.* RME-2070, 1960, 33 p.
27. Conant L. C. and Swanson V. E. Chattanooga Shale and related rocks of cental Tennessee and nearby areas. *Prof. Pap. U.S. geol. Surv.* 357, 1961, 91 p.
28. Corbett R. G. The geology and mineralogy of Section 22 Mine, Ambrosia Lake uranium district, New Mexico. Ph.D. Dissertation, University of Michigan, 1963.
29. Cunningham C. G. and Steven T. A. Postulated model of uranium occurrence in the central mining area, Marysvale district, west-central Utah. *Open-File Rep. U.S. geol. Surv.* 78-1093, 1978, 20 p.
30. Dahlkamp F. J. Typology and geographic/geotectonic distribution of uranium deposits. In *Energy resources* Burollet P. F. and Ziegler V. eds (Paris: Edition Technip, 1980), 499–536. *(26th Int. Geol. Congr., Colloque C2)*
31. Darnley A. G. and Grasty R. L. Airborne radiometric survey of the Elliot Lake area. *Open-File Rep. geol. Surv. Can.* no. 75, 1971.
32. Davidson C. F. On the occurrence of uranium in ancient conglomerates. *Econ. Geol.*, **52**, 1957, 668–93.
33. Degens E. T. Khoo F. and Michaelis W. Uranium anomaly in Black Sea sediments. *Nature, Lond.*, **269**, 1977, 566–9.
34. Denson N. M. and Gill J. R. Uranium-bearing lignite and its relation to volcanic tuffs in eastern Montana and North and South Dakota. *Prof. Pap. U.S. geol. Surv.* 300, 1956, 413–8.
35. Derrick G. M. Metasomatic history and origin of uranium mineralization at Mary Kathleen, northwest Queensland. *BMR J. Aust. Geol. Geophys.*, **2**, 1977, 123–30.
36. Derry D. R. Evidence of the origin of the Blind River uranium deposits. *Econ. Geol.*, **55**, 1960, 906–27.
37. De Voto R. H. and Paschis J. A. Geology of uranium vein deposits (including Schwartzwalder mine) in Proterozoic metamorphic rocks, Front Range, Colorado. In *Uranium in the Pine Creek Geosyncline* Ferguson J. and Goleby A. B. eds (Vienna: IAEA, 1980), 683–92.
38. DeVoto R. H. and Stevens D. N. Uraniferous phosphate resources and technology and economics of uranium recovery from phosphate resources, United States and Free World, volume 1. *Open-File Rep. U.S. Dep. Energy* GJBX-110(79), 1979, 724 p.
39. Dewey J. F. and Bird J. M. Mountain belts and the new global tectonics. *J. geophys. Res.*, **75**, 1970, 2625–47.
40. Dodson R. G. *et al.* Uranium mineralization in the Rum Jungle–Alligator Rivers Province, Northern Territory, Australia. Reference 15, 551–67.
41. Downs G. R. and Bird A. G. The Schwartzwalder uranium mine, Jefferson County, Colorado. *Mountain Geol.*, **2**, 1965, 183–91.
42. Dybek J. Zur Geochemie und Lagerstättenkunde des Urans. *Rohstoffe*, pt 1 1962, 163 p.
43. Ferguson J. Geology of the Ilímaussaq alkaline Intrusion, South Greenland, *Meddr Grønland*, **172**, no. 4 1964, 82 p.
44. Ferris C. S. and Rudd C. W. Brannerite: its occurrences and recognition by microprobe. *Colo. Sch. Mines Q.*, **66**, Oct. 1971, 35 p.
45. Finch W. I. Geology of epigenetic uranium deposits in sandstone in the United States. *Prof. Pap. U.S. geol. Surv.* 538, 1967, 121 p.
46. Forster I. F. Paragenetical ore mineralogy of the Loolekop–Phalaborwa Carbonatite Complex, eastern Transvaal. *Trans. Proc. geol. Soc. S. Afr.*, **61**, 1958, 359–65.
47. Garlick W. G. The syngenetic theory. In *The geology of the Northern Rhodesian Copperbelt* Mendelsohn F. ed. (London: Macdonald, 1961), 146–65.
48. Gill J. E. and Owens O. E. Columbium–uranium deposits at North Bay, Ontario. *Trans. Can. Inst. Min. Metall.*, **60**, 1957, 244–50.
49. Gold D. P. The average and typical chemical composition of carbonatites. In *I.M.A. volume—International Mineralogical Association 4th general meeting* (New Delhi: Mineralogical Society of India, 1966 [1967]), 83–91.
50. Goodell P. C. Trentham R. C. and Carraway K. Geologic setting of the Peña Blanca uranium deposits, Chihuahua, Mexico. In *Formation of uranium ores by diagenesis of volcanic sediments* Henry C. D. *et al.* eds *Open-File Rep. U.S. Dep. Energy* GJBX-22(79), 1978, 38 p.
51. Gornitz V. and Kerr P. F. Uranium mineralization and alteration, Orphan Mine, Grand Canyon, Arizona. *Econ. Geol.*, **65**, 1970, 751–68.
52. Granger H. C. Mineralogy. In *Geology and technology of the Grants uranium region. Mem. New Mex. Bur. Mines Min. Res.* 15, 1963, 21–37.
53. Hawkins B. W. Mary Kathleen uranium deposit. In *Economic geology of Australia and Papua New Guinea 1. Metals* Knight C. L. ed. (Parkville, Victoria: Australasian Institute of Mining and Metallurgy, 1975), 398–402. (*Monogr. Series* no. 5)
54. Haynes D. W. Geological technology in mineral resource exploration. In *Mineral resources of Australia* Kelsall D. F. and Woodcock J. T. eds (Parkville, Victoria: Australian Academy of Technological Sciences, 1979), 73–95. *(Third Invitation Symposium)*
55. Hilpert L. S. Regional and local stratigraphy of uranium-bearing rocks. *Mem. New Mex. Bur. Min. Res.* 15, 1963, 6–18.
56. Hilpert L. S. Uranium resources of northwestern New Mexico. *Prof. Pap. U.S. geol. Surv.* 603, 1969, 166 p.
57. Hoeve J. and Sibbald T. I. I. The Rabbit Lake uranium mine. In *Uranium in Saskatchewan* Dunn C. E. ed. *Spec. Publ. Saskatchewan geol. Soc.* 3, 1976, 331–54.
58. Jones C. A. A classification of uranium deposits in sedimentary rocks. In *Preliminary classification of uranium deposits* Mickle D. G. ed. *Open-File Rep. U.S. Dep. Energy* GJBX-63 (78), 1978, 1–15.
59. Kalyaev G. I. Mode of albitite distribution in zones of the Ukrainian Shield. In *Albitized uranium deposits* Arashov A. transl. *Open-File Rep. U.S. Dep. Energy* GJBX-193(80), 1980, 13 p.
60. Kehn T. M. Uranium in the Chattanooga shale, Youngs Bend area, Eastern Highland Rim, Tennessee. *Rep. U.S. geol. Surv.* TEI-528-A, 1955, 60 p.
61. Knipping H. D. The concepts of supergene versus hypogene emplacement of uranium at Rabbit Lake, Saskatchewan, Canada. Reference 15, 531–49.
62. Langford F. F. A supergene origin for vein-type uranium ores in the light of the Western Australian calcrete–carnotite deposits. *Econ. Geol.*, **69**, 1974, 516–26.
63. Lawrence Livermore Laboratory. Preliminary report on the Walker River Basin study (California/Nevada). *Open-File Rep. U.S. Dep. Energy* GJBX-44(76), 1976, 14 p.
64. Liebenberg W. R. The occurrence and origin of gold and radioactive minerals in the Witwatersrand System, the Dominion Reef, the Ventersdorp Contact Reef and the Black Reef. *Trans. Proc. geol. Soc. S. Afr.*, **58**, 1955, 101–254.
65. Little H. W. Distribution of types of uranium deposits and favourable environments for uranium exploration. Reference 18, 35–48.
66. Llewelyn G. I. W. Recovery of uranium from sea-water. In *Uranium ore processing* (Vienna: IAEA, 1976), 205–21.
67. MacDonald B. C. and Kermeen J. S. The geology of Beaverlodge. *Can. Min. J.*, **77**, June 1956, 80–3; 156.
68. MacKevett E. M. Jr. Geology and ore deposits of the Bokan

Mountain uranium–thorium area, southeastern Alaska. *Bull. U.S. geol. Surv.* 1154, 1963, 125 p.
69. Malan R. C. Volcanogenic uranium–molybdenum deposits in Russia and China. Paper presented at U.S. Department of Energy uranium seminar, 1980, 17 p.
70. Mannweiler U. and Haftka F. J. On-line analysis speeds uranium ore assays in Central African Empire. *World Min.*, **31**, May 1978, 56–7.
71. Marciel A. E. and Cruz P. R. Perfil analitico do urânio. *Bolm Dep. nac. Prod. min., Rio de J.* 27, 1973, 70 p.
72. McDowell J. P. The sedimentary petrology of the Mississagi quartzite in the Blind River area. *Geol. Circ. Ontario Dep. Mines* no. 6, 1957, 31 p.
73. McKelvey V. E. and Carswell L. D. Uranium in the Phosphoria formation. *Prof. Pap. U.S. geol. Surv.* 300, 1956, 483–7.
74. McKelvey V. E. Swanson R. W. and Sheldon R. P. The Permian phosphorite deposits of western United States. In *Origine des gisements de phosphates de chaux. C.R. XIX Int. Geol. Congr., Algiers 1952*, sect. 11, fasc. 11, 1953, 45–64.
75. McMillan R. H. Metallogenesis of Canadian uranium deposits: a review. In *Geology, mining and extractive processing of uranium* Jones M. J. ed. (London: IMM, 1977), 43–55.
76. McMillan R. H. Uranium in Canada. *Bull. Can. Petrol. Geol.*, **25**, 1977, 1222–49.
77. McNeil M. *Brazil's uranium/thorium deposits: geological reserves potential* (San Francisco: Miller Freeman Publications, 1979), 126 p.
78. Meyer K. Uran-Prospektion vor Südwestafrica. *Erzmetall*, **26**, 1973, 313–7.
79. Mickle D. G. and Mathews G. W. eds. Geologic characteristics of environments favorable for uranium deposits. *Open-File Rep. U.S. Dep. Energy* GJBX-67-78, 1978, 250 p.
80. Minter W. E. L. Detrital gold, uranium and pyrite concentrations related to sedimentology in the Precambrian Vaal Reef placer, Witwatersrand, South Africa. *Econ. Geol.*, **71**, 1976, 157–76.
81. Morton R. D. The western and northern Australian U deposits—exploration guides or exploration deterrents for Saskatchewan? In *Uranium in Saskatchewan* Dunn C. E. ed. *Spec. Publ. Saskatchewan geol. Soc.* 3, 1976, 211–54.
82. Mountain States Research and Development and PRC Toups Corporation. Engineering assessment and feasibility study of Chattanooga Shale as a future source of uranium. *Open-File Rep. U.S. Dep. Energy* GJBX-4-79, 1978, 262 p.
83. Murphy M. *et al.* Uranium in alkaline rocks. *Open-File Rep. U.S. Dep. Energy* GJBX-78(78), 1978, 185 p.
84. Nash J. T. Geology and genesis of major world hardrock uranium deposits; an overview. *Open-File Rep. U.S. geol. Surv.* 81-0166, 1981, 129 p.
85. Nash J. T. and Lehrman N. J. Geology of the Midnite uranium mine, Stevens County, Washington—a preliminary report. *Open-File Rep. U.S. geol. Surv.* 75-402, 1975, 36 p.
86. Nishimori R. K. *et al.* Uranium deposits in granitic rocks. *Open-File Rep. U.S. Dep. Energy R&D Adm.* GJBX-13(77), 1977, 298 p.
87. Nishimori R. K. and Powell J. D. Uranium in carbonatites, USA. *Open-File Rep. U.S. Dep. Energy* GJBX-147-80, 1980, 180 p.
88. OECD Nuclear Agency and IAEA. *World uranium potential* (Paris: OECD, 1978), 170 p.
89. Ojakangas R. W. Criteria for Alligator River type uranium deposits in the United States. In *NURE uranium geology symposium* (Grand Junction, Colo.: Bendix Field Engineering Corporation, 1978), 193–210.
90. Paschis J. A. Mining and geologic developments at Cotter Corporation's Schwartzwalder uranium mine, Jefferson County, Colorado. In *Papers presented at the National Western Mining Conference* (Denver, Colo.: Mining Yearbook, 1979), 123–8.
91. Patterson J. A. and Pitman R. K. Foreign uranium outlook. Paper presented at U.S. Department of Energy uranium industry seminar, 1981, 19 p.
92. Pretorius D. A. The depositional environment of the Witwatersrand goldfields: a chronological review of speculations and observations. *Minerals Sci. Engng*, **7**, 1975, 18–47.
93. Ramdohr P. Neue Beobachtungen an Erzen des Witwatersrands in Südafrika und ihre genetische Bedeutung. *Abh. dt. Akad. Wiss. Berlin, Kl. math. naturw.*, no. 5 1954, 43 p.
94. Ramdohr P. New observations on the ores of the Witwatersrand in South Africa and their genetic significance. *Trans. Proc. geol. Soc. S. Afr.*, **61**, 1958, Annex., 173 p.
95. Richardson K. A. Killeen P. G. and Charbonneau B. W. Results of a reconnaissance type airborne gamma-ray spectrometer survey of the Blind River–Elliot Lake area, Ontario. *Pap. geol. Surv. Can.* 75-1A, 1975, 133–5.
96. Robertson J. A. A review of recently acquired geological data, Blind River–Elliot Lake area. In *Huronian stratigraphy and sedimentation. Spec. Pap. geol. Ass. Can.* no. 12, 1973, 169–98.
97. Robertson J. A. The Blind River uranium deposits: the ores and their setting. *Misc. Pap. Ontario Div. Mines* 65, 1976, 45 p.
98. Robertson J. A. Uranium deposits in Ontario. In *Short course in uranium deposits: their mineralogy and origin* Kimberley M. M. ed. (Toronto: The University Press for Mineralogical Association of Canada, 1978), 229–80.
99. Robinson B. W. and Morton R. D. The geology and geochronology of the Echo Bay area, Northwest Territories, Canada. *Can. J. Earth Sci.*, **9**, 1972, 158–71.
100. Robinson B. W. and Ohmoto H. Mineralogy, fluid inclusions, and stable isotopes of the Echo Bay U–Ni–Ag–Cu deposits, Northwest Territories, Canada. *Econ. Geol.*, **68**, 1973, 635–56.
101. Pertlik F. *et al.* Uranium. In *Handbook of geochemistry, II-5* Wedepohl K. H. ed. (Berlin: Springer-Verlag, 1969), 50 p.
102. Roper M. W. and Wallace A. B. Geology of Aurora uranium prospect, Malheur County, Oregon. In *Uranium in volcanic and volcaniclastic rocks* Goodell P. C. and Waters A. C. eds *AAPG Studies in Geology* no. 13, 1981, 81–8.
103. Roscoe S. M. Huronian rocks and uraniferous conglomerates in the Canadian Shield. *Pap. geol. Surv. Can.* 68-40, 2969, 205 p.
104. Rosholt J. N. Prijana and Noble D. C. Mobility of uranium and thorium in glassy and crystallized silicic volcanic rocks. *Econ. Geol.*, **66**, 1971, 1061–9.
105. Rowntree J. C. and Mosher D. V. Jabiluka uranium deposits. Reference 53, 321–6.
106. Ruzicka V. Geological comparison between East European and Canadian uranium deposits. *Pap. geol. Surv. Can.* 70-48, 1971, 196 p.
107. Rytuba J. J. and Glanzman R. K. Relation of mercury, uranium and lithium deposits to the MacDermitt caldera complex, Nevada–Oregon. In *Papers on mineral deposits of western North America: volume II* Ridge J. D. ed. *Rep. Nevada Bur. Mines Geol.* 33, 1979, 109–17.
108. SADME. Diamond drill core display—Olympic Dam prospect. Report South Australia Department of Mines and Energy, 1979, 2 p.
109. Santos E. S. Relation of ore deposits to the stratigraphy of host rocks in the Ambrosia Lake area. *Mem. New Mex. Bur. Mines miner. Res.* 15, 1963, 53–9.
110. Sassano G. P. Fritz P. and Morton R. D. Paragenesis and isotopic composition of some gangue minerals from the uranium deposits of Eldorado, Saskatchewan. *Can. J. Earth Sci.*, **9**, 1972, 141–57.
111. Satterly J. Radioactive mineral occurrences in the Bancroft area. *Ann. Rep. Ontario Dep. Mines 1956*, **65**, no. 6 1957, 181 p.
112. Schidlowski M. Archaean atmosphere and evolution of the terrestrial oxygen budget. In *The early history of the earth* Windley B. F. ed. (New York: Wiley, 1976), 525–35.
113. Schopf J. W. The evolution of the earliest cells. *Scient. Am.*, **239**, Sept. 1978, 84–102.
114. Sheridan D. M. Maxwell C. H. and Albee A. L. Geology and uranium deposits of the Ralston Buttes district, Jefferson County, Colorado. *Prof. Pap. U.S. geol. Surv.* 520, 1967, 121 p.
115. Sibbald T. I. I. Uranium metallogenetic studies; I, Rabbit Lake. In *Summary of investigations 1977* Christopher J. E. *et al.* eds *Summ. Invest. Sask. geol. Surv.*, 1977, 111–23.
116. Smart P. G. *et al.* Geology and geophysics of the Alligator Rivers region. Reference 53, 285–301.
117. Smith D. A. M. The geology of the area around the Khan and Swakop Rivers in South West Africa. *Mem. geol. Surv. S. Afr. South West Africa Ser.* 3, 1965, 113 p.
118. Soister P. E. Stratigraphy of the Wind River Formation in south-central Wind River Basin, Wyoming. *Prof. Pap. U.S. geol. Surv.* 594-A, 1968, 50 p.
119. Sørensen H. On the occurrence of steenstrupine in the Ilímaussaq massif, southwest Greenland. *Meddr Grønland*, **167**, no. 1 1962, 251 p.
120. Sørensen H. Low-grade uranium deposits in agpaitic nepheline syenites, South Greenland. Reference 18, 151–9.
121. Staatz M. H. I and L uranium and thorium vein system, Bokan Mountain, southeastern Alaska. *Econ. Geol.*, **73**, 1978, 512–23.

122. Staatz M. H. and Carr W. J. Geology and mineral deposits of the Thomas and Dugway Ranges, Juab and Tooele Counties, Utah. *Prof. Pap. U.S. geol. Surv.* 415, 1964, 188 p.
123. Swanson V. E. Oil yield and uranium content of black shales. *Prof. Pap. U.S. geol. Surv.* 356-A, 1960, 1–44.
124. Swanson V. E. Geology and geochemistry of uranium in marine black shales, a review. *Prof. Pap. U.S. geol. Surv.* 356-C, 1961, 67–112.
125. Thompson T. B. Lyttle T. and Pierson J. R. Genesis of the Bokan Mountain, Alaska, uranium–thorium deposit. *Open-File Rep. U.S. Dep. Energy* GJBX-38(80), 1980, 232 p.
126. Tremblay L. P. Uranium subprovinces and types of uranium deposits in the Precambrian rocks of Saskatchewan. *Pap. geol. Surv. Can.* 78-1A, 1978, 427–35.
127. Tuttle O. F. and Bowen N. L. Origin of granite in the light of experimental studies in the system $NaAlSi_3O_8KA1Si_3O_3$–SiO_2–H_2O. *Mem. geol. Soc. Am.* 74, 1958, 153 p.
128. Vickers R. C. Alteration of sandstone as a guide to uranium deposits and their origin, northern Black Hills, South Dakota. *Econ. Geol.*, **52**, 1957, 599–611.
129. von Backström J. W. and Jacob R. E. Uranium in South Africa and South West Africa (Namibia). *Phil. Trans. R. Soc. Lond.*, **A291**, 1979, 307–19.
130. Whittle A. W. G. Contact mineralization phenomena of the Mary Kathleen uranium deposit. *Neues Yb. Mineralogie*, **94**, 1960, 798–830.
131. Woodmansee W. C. Uranium. In *Mineral facts and problems: 1975 edition. Bull. U.S. Bur Mines* 667, 1976, 1177–200.
132. Western gets BP Australia to finance Roxby Downs. *World Min.*, **32**, Sept. 1979, 128.
133. Youles I. P. Mount Painter uranium deposits. Reference 53, 505–8.
134. Young R. G. Uranium deposits of the southern San Juan mineral belt, Mexico. *Rep. U.S. AEC* TM-170, 1960, 48 p.

Uranium deposits in Europe

Valery Ziegler
Jacques Dardel
Direction de l'Approvisionnement en Matières Nucléaires, Commissariat à l'Energie Atomique, Paris, France

Outline of geological structure of Europe

The purpose of this section is to review briefly the major geotectonic features of the European continent and their associations in order to present a consistent geological background for the distribution of the different uranium districts in this part of the world. More detailed descriptions may be found in the list of references to this paper, on which the present authors have drawn extensively.

As is well known, Hercynian-Alpine Europe is enclosed between the Fenno-Scandinavian Precambrian Shield to the north, the Russian Precambrian Shield to the east and the African Shield to the south. The Fenno-Scandinavian (or Baltic) Shield is formed of (*a*) an Archaean core (Saamo–Karelian) for most of Finland, apart from the southwest, (*b*) a Lower Proterozoic unit (Sveco-Fennian) that extends from this Archaean unit southwards to southwest Sweden and (*c*) a Middle Proterozoic unit (Sveco-Norwegian), almost entirely rejuvenated by the Gothian and later Precambrian orogenies.

To the west this shield is bordered by the Caledonian orogen, which extends from the north of Norway through Scotland and the north of England to Ireland. This orogen is incomplete: as a result of continental drift it was split conformably to the general trend into a European part and a northeast Greenland part. There is evidence of the Caledonian orogeny within the Hercynian and Alpine sections, but such considerations are beyond the scope of this paper.

Between the Precambrian–Caledonian area, the Alpino-Carpathian front and Africa occurs the most characteristic central Western European geotectonic unit—the Hercynian (Variscan) orogen. Nevertheless, the area occupied by this orogen does not represent the total original Hercynian space, numerous Hercynian fragments being set within the Alpine orogen.

Since 1927 (Kossmatt[21]—from Poland to Ireland) and 1942 (Lotze[27]—the Iberian section) several attempts have been made to subdivide the Hercynian orogen into successive geotectonic zones that represent the different structural units of the Hercynian geosyncline. For our purpose we have merely individualized its most central zone (inner zone), corresponding to the area of maximum orogenic, metamorphic and plutonic activity. In central Western Europe it is commonly recognized as the 'Moldanubian zone' and in the Iberian peninsula as the 'Galician–Castillian' zone. Julivert and co-workers[20] merged it with Lotze's Lusitanian–Alcudian zone adjacent to its southern limit into a single Central Iberian zone.

The outer zone is generally subdivided into a Saxo–Thuringian zone, followed by the Rheno-Hercynian zone, etc., but as that does not appear to be essential here they were not differentiated in our geostructural sketch map (Fig. 1).

The Alpine orogen occupies a large area of Europe—the whole of Italy and Switzerland, a major part of Austria, the whole of Hungary, Yugoslavia, Greece, a major part of Rumania and Bulgaria, Turkey and, at the opposite side, the northern, eastern and southern parts of the Iberian peninsula. Nevertheless, as was stated above, this space incorporates numerous and often large fragments of the Hercynian orogen—for example, the Bergamask Alps in Italy, the Pannon Basin in Hungary, the Romanian Transylvanian Basin and the Rhodope Massif in Yugoslavia, Greece and Bulgaria.

In addition, although not a component of the European continent, Greenland is nevertheless a province of Denmark and contains all the uranium resources of that country. This large island, apart from its northern fringe (Innuitian Belt) and northeastern margin (Caledonian Belt), is built up of Precambrian rocks. Nearly four-fifths of its surface is covered by a glacier, the thickness of which is locally 3000 m. The uranium is restricted to the southwestern extremity, formed of Lower Proterozoic rocks bordering, to the north, an Archaean block. This zone underwent important magmatic reactivation between 1300 and 1030 m.y. along an ENE general trend, giving rise to the Gardar magmatic province, which is characterized by alkaline intrusions.

Distribution of main European uraniferous districts and their relation to geology

Uranium mineralization is present in all these different geological provinces, but its economic importance and the geological types of occurrence vary considerably from one geostructural unit to the next.

Southern Greenland is known to contain a huge natural stock of uranium in low-grade material from which extraction is difficult and recovery poor (the so-called refractory ores). It is related to alkaline intrusion.

The Precambrian European province proper contains limited resources in vein-type deposits in northern Sweden and, again, a huge low-grade uranium natural stock in Cambrian black shales. Grades, under present market conditions, are not economic.

The Caledonian province contains no known economic deposit, but some granite-related and sandstone-bound uranium occurrences occur in Scotland and Ireland, and there is some promise for these.

The Hercynian region is by far the major economic uranium province. From the Iberian Meseta in the west to Lysa Gora to the east, with the exception of the Ardennes and the Harz Mountains, practically all the Hercynian outcropping massifs reveal uranium occurrences. The two major uranium districts (Western Massif Central, Vendée district, and the Western Bohemian Massif district), as well as all other significant uranium districts, however, occur within the Moldanubian zone, which corresponds to the inner unit of the Hercynian orogen or to the immediately adjacent outer zone.

Uranium deposits in this unit are of numerous geological types, but three are typical of the Hercynian orogen: (1) intragranitic deposits related to leucogranites, (2) deposits bound to the contact-metamorphic haloes of granite intrusives in Lower Palaeozoic shales (the so-called 'Iberian type') and (3) deposits bound to Permian cover rocks or Permian acid volcanics. Other types are veins in less differentiated granites, veins in metamorphic environments, sandstone-type deposits in Mesozoic or Caenozoic cover rocks in basin structures of the Hercynian space included in or adjacent to the Moldanubian zone (or its Iberian equivalent).

Less important is the Alpine region in regard to uranium

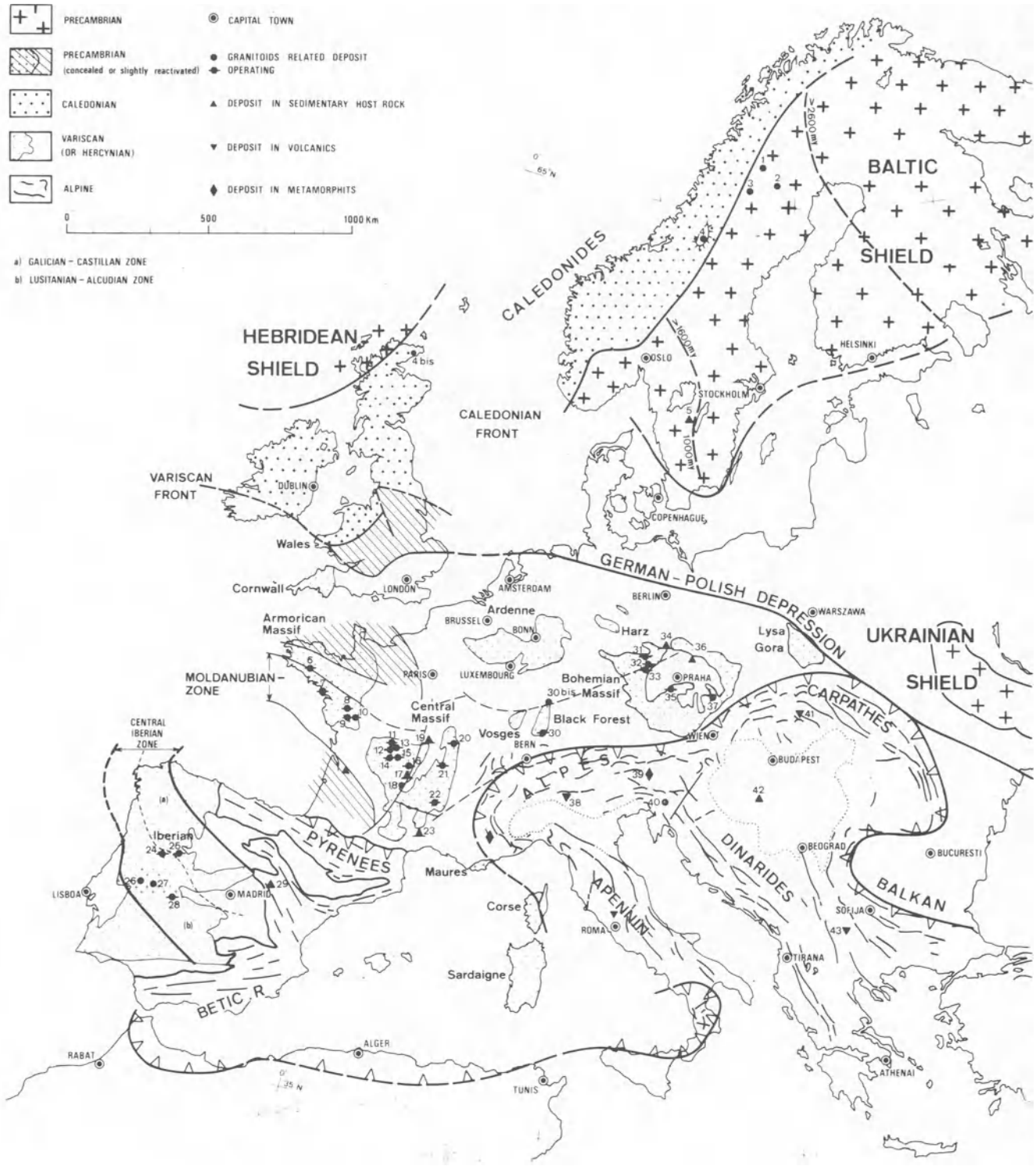

Fig. 1 Main uraniferous deposits in Europe: 1, Pleutajokk; 2, Ravaberget; 3, Duobblon; 4, Hotagen; 4 bis, Ousdale; 5, Ranstad; 6, Pontivy; 7, Pennaran; 8, Ecarpière-le-Chardon; 9, Beaurepaire; 10, La Chapelle Largeau—La Commanderie—La Dorgissière; 11, Le Bernardan; 12, Le Brugeaud; 13, Bellezane; 14, Margnac-Peny; 15, Fanay—Le Fraisse; 16, Hyverneresse; 17, St-Pierre du Cantal; 18, Bertholène; 19, Cerilly; 20, Grury; 21, Bois Noirs; 22, Le Cellier—Les Pierres Plantées; 23, Mas Lavayre; 24, Urgeiriça; 25, Fe; 26, Nisa; 27, Tarabau; 28, El Pedrigal; 29, Mazarete; 30, Menzenschwand; 30 bis, Mullenbach; 31, Aue; 32, Jachymov district; 33, Horni Slavkov; 34, Königstein; 35, Pribram district; 36, Hamr; 37, Rozna-Olsi; 38, Novazza; 39, Forstau; 40, Zirovski Vrh; 41, Huta—Mura; 42, Mecsek; 43, Zletovska Reka

resources, though some economic deposits have been identified in Western Europe and, apparently, some major deposits by European standards are or were mined in Eastern Europe (Hungary, Romania and Czechoslovakia). A striking feature is that, with few exceptions, they are bound to Permian sedimentary or volcano-sedimentary rocks covering Hercynian nuclei set within the Alpine orogen. Some examples of genuine Alpine mineralization are, nevertheless, encountered. A characteristic type of occurrence is related to Permian shales that have undergone greenschist metamorphism during the Alpine orogeny, as in the Italian Western Alps, Switzerland and Austria. Another is connected with Tertiary volcanics, as in Macedonia, or Pleistocene–Quaternary volcanics, as in Latium in Italy.

Uranium districts in the Precambrian

Gardar alkaline province, southwest Greenland

This area, located at the southwest tip of Greenland, pertains

to the Ketilidian structural Hudsonian (1800 m.y.) province, reactivated during the Gardar (1300–1030 m.y.) magmatic period and characterized by alkaline intrusions: the Ilímaussaq complex presents an elliptical horizontal section of 17 km × 10 km. Two genetic stages can be distinguished (Fig. 2): during the first an augitic syenite shell, a few hundred metres thick, was formed with an alkaline granite in the apical zone and in the second stage a stratoidal agpaitic suite developed inside the shell, represented from bottom to top by (*a*) thick, banded kakortokite rich in eudialyte (concealing huge zirconium resources), (*b*) green (aegirine) lujavrite, (*c*) black (arfvedsonite), fine-grained lujavrite, (*d*) eudialyte-rich naujaite and (*e*) sodalite foyaite.

There is no typical vertical age relationship between the different facies, the kakortokite containing roof-pendants of all other rocks. Lujavrite is probably the most recent, a coarse-grained block variety extending dyke intrusives in all the upper varieties of the agpaitic suite and even the wallrocks of the alkaline intrusion. Practically all the uranium and thorium is carried by steenstrupine. The green lujavrite contains some 60 ppm U and the fine-grained black variety averages 200 ppm U and contains a natural stock of uranium of the order of 200 000 t U.

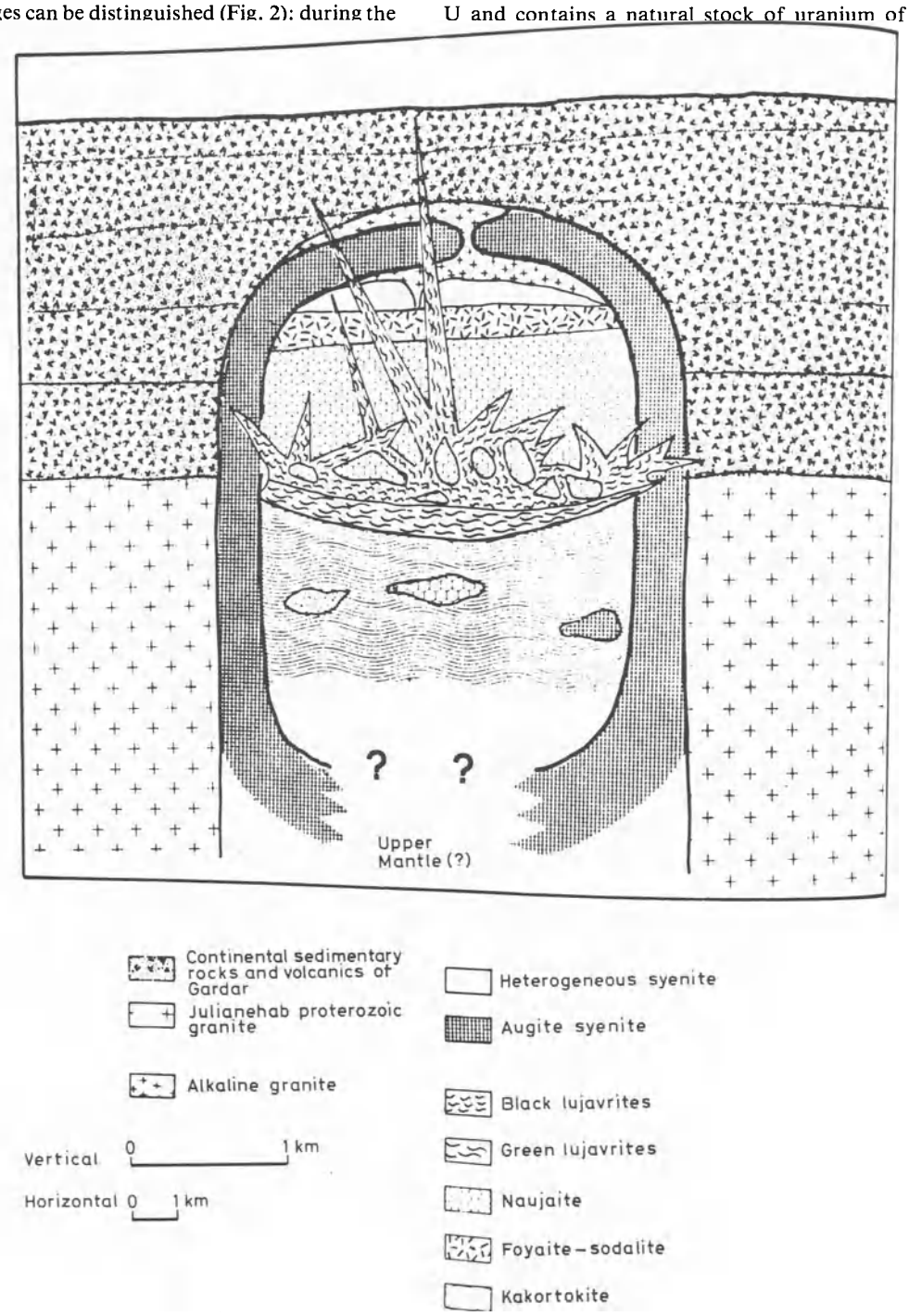

Besides the magmatic steenstrupine there is a second-generation variety contained in the coarse-grained black lujavrite variety, which, at the intersections with analcite veins and mainly with volcanic or gabbroic country rocks, fine-grained lujavrite, etc., is locally enriched in uranium up to 3000 ppm. It can form orebodies averaging 300–400 ppm U, the total known resources of this type being estimated at some 30 000 t U.

This type of deposit is characterized by a Th/U ratio of the order of 2.5, whereas in all other economic occurrences thorium occurs as a trace element.

Arjeplog–Arvidsjaur uranium district, northern Sweden
Located in the north of the Sveco-Fennian Lower Proterozoic unit, the district is built-up of continental-type pre-Svecofennian basement associated with younger greenstone belts and unconformably covered by aerial volcanics with widely developed acidic rocks, including ignimbrites.

To the south a basin with marine metasediments is developed. Both units have undergone the Svecofennian orogeny (approximately equivalent to the Hudsonian in the North American Shield).

Two types of economic, or potentially economic, uranium occurrences are known. The first, at Pleutajokk, is represented by veins or lenticular disseminations, preferentially in fractures of acid volcanics or acid intrusives of the early stage of the Svecofennian orogeny. The deposits are related to the latest phases of tectono-magmatic reactivation responsible for (*a*) large-scale sodium metasomatism developing metasomatic albitite, (*b*) brecciation of the metasomatites followed by irregularly scattered skarns associated with clinopyroxene, garnet, calcite, Pb–Zn, Cu–Fe sulphides and magnetite, and (*c*) the introduction of uranium mineralization—uraninite pitchblende(?) and uranotitanates. A similarity with Ukrainian deposits is commonly suggested. The age of the uraninites is 1750 ± 26 m.y. Known resources are of the order of 5000 t U, but the grade is rather low.

The second type of mineralization, at Duobblon, some 80 km south of Pleutajokk, is related to subaerial volcanics subsequent to the major orogenic phase. Uranium is bound to two rhyolite–ignimbrites horizons separated by a conglomeratic horizon. Unfortunately, the average U content is 200–300 ppm, individual samples varying from 20 to 3000 ppm. The orebodies are almost 1000 m long and 5–25 m thick. Mineralization is represented by uranotitanates, uranium-bearing micas and fine-grained pitchblende in microfractures. The main associated elements are Pb, V and Mo.

Uraniferous Alum shales, Billingen–Ranstad, Sweden
Quite often the black shales show a clear uranium enrichment, the Lower Palaeozoic shales containing millions of tonnes of uranium with average contents grading from some 10 to almost 100 ppm U. Their extraction cannot be envisaged with present technology for environmental and technical reasons and under present market conditions.

In the Västergotland and Närke provinces of Sweden, however, the Alum shales (average 70 ppm U) present a 2- to 3-m thick horizon (Fig. 3) enriched in uranium, probably by a diagenetic process, to an average of some 300 ppm U. These shales are of Middle and Upper Cambrian plus Tremadoc age, and have a thickness of several tens of metres.

The enriched horizon, characterized by *Peltura Scarobaeoides*, is enclosed at bottom and top by layers of hydrocarbides, locally called 'kolm', 4–5 m thick and containing up to 10 000 ppm U (generally, 3000 ppm U).

At one stage mining took place in the Närke province for the extraction of oil (content 4%), sulphur, lime, ammonia, etc. Elements associated with uranium are V (same content as U), W, Mo, Ni, Zn and Ca—but pyrite and melnikovite are the most abundant (6–7% S). The total amount of resources reported was 1 000 000 t U, but only 300 000 t U is considered as potentially recoverable.

Similar shales, but without the enriched horizon, occur elsewhere in the Baltic Shield.

Uranium districts of the Caledonian
To date, there are no proved economic resources within the Caledonian region, though in northern Scotland and the Orkneys further investigations of already identified occurrences could reveal economic interest.

The area of concern here is composed of Precambrian basement overlain by Lower Palaeozoic geosynclinal, strongly metamorphosed sediments that grade southwards to coarser terrigenous facies. The major orogenic phase took place in the Upper Silurian. After peneplanation the Caledonian orogen was overlain by the famous Devonian Old Red Sandstones (ORS).

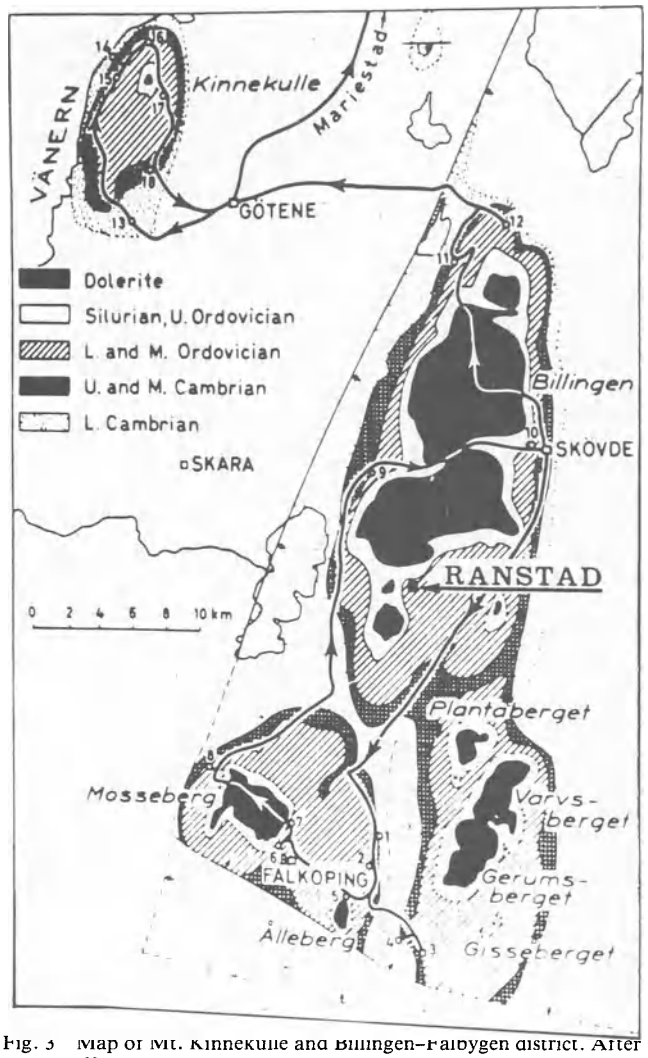

Fig. 3 Map of Mt. Kinnekulle and Billingen–Falbygen district. After Peterson[33]

Limited uraniferous concentrations have been discovered in association with granitoids in the Northern Highlands—in particular, in association with the Helmsdale granite—in discrete veins. Uranium often appears in supergene minerals in the hexavalent form.

Uneconomic uraninite mineralization (though with some high local contents) has also been reported in the Southern Uplands near Dalbeattie in a bismuth vein intersecting the contact zone of a granodiorite. In the lower part and at the bottom of the middle part of the ORS—in particular, in the extreme northeast of Scotland—resting on a metamorphic Precambrian basement intersected by Caledonian granitoids and syenites, are the main uraniferous occurrences in Britain. There appears to be a very strong correlation between uranium and the high content of the rock in phosphate or organic material. The concentrations vary between 200 and 300 ppm U in cumulative thicknesses of 10 or so m. Exceptionally, contents of up to 1000 ppm U have been found in a 10-m thick phosphatic horizon. These sandstones cover a total area of around 3000 km^2 and extend to the north into the Orkney Islands.

Uranium districts of the Hercynian

Uranium districts in leucogranites

The term leucogranite refers to highly differentiated granites, of crustal origin, with an average mineralogical composition of some 36% quartz, 27% orthoclase, 27% albite and 10% muscovite. In addition to their high potassium content, they present abnormally high contents of such lithophile elements as Be, Li, F, W, Sn, Th and U. The most representative area worldwide for this type of deposit is France, where the distribution of leucogranites is remarkable (Fig. 4). With a few exceptions they occur along linear belts. The outcropping masses form a belt that runs from the western tip of Brittany to the central western Massif Central, with some minor branches. Inferred leucogranites, concealed by the Mesozoic southern margin of the Paris Basin, extend along a line east of Brittany to the Vosges. East of the Sillon Houiller, in the Massif Central, leucogranites are less developed and apparently randomly scattered. The spatial connexion between uranium districts (other than those bound to Permian or Palaeogene cover rocks) and outcropping leucogranites is conspicuous, even in the eastern Massif Central.

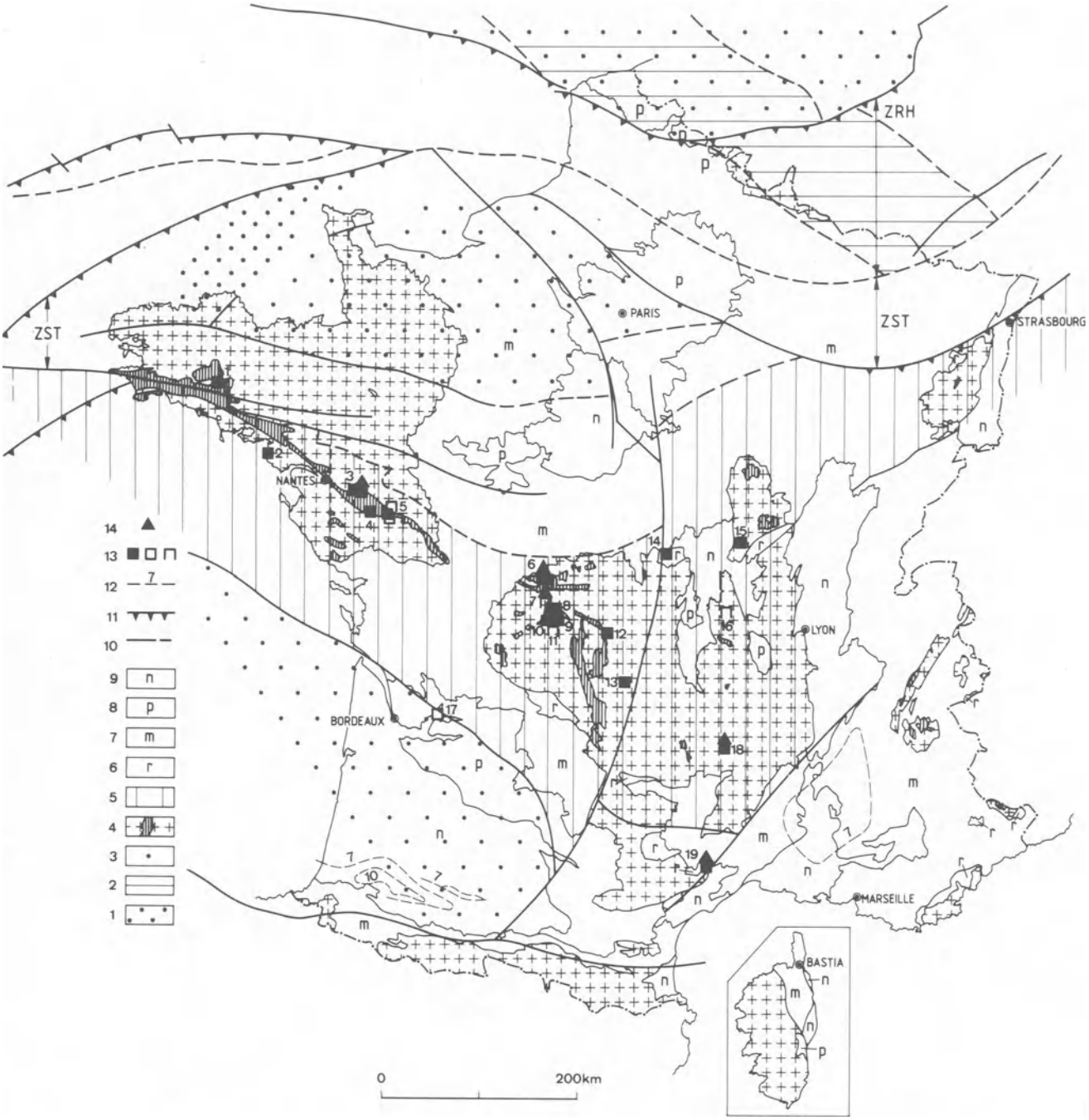

Fig. 4 Uranium deposits and concentrators in France: 1, Pontivy; 2, Pennaran; 3, Le Chardon, L'Ecarpière (Ecarpière); 4, Beaurepaire; 5, La Chapelle Largeau, La Commanderie, La Dorgissière; 6, Le Bernardan (Mailhac); 7, Le Brugeaud (Bessines); 8, Bellezane; 9, Fanay, Le Fraisse; 10, Margnac, Peny; 11, Henriette; 12, Hyverneresse; 13, St-Pierre du Cantal (Saint-Pierre); 14, Cerilly; 15, Grury; 16, Les Bois Noirs; 17, Coutras; 18, Le Cellier, Les Pierres Plantées (Le Cellier); 19, Mas Lavayre (St-Martin du Bosc).

Geological key: 1, Icartian basement (Early Proterozoic); 2, basement with Caledonian structure (Brabant–Ardennes area); 3, Cadomian (pre-Variscan) basement; 4, Variscan orogenic domain (with hatching: aluminous leucogranite); 5, Internal Variscan (or Moldanubian) zone; ZST Saxo-Thuringian zone, ZRH Rheno-Hercynian zone; 6, Permian; 7, Mesozoic; 8, Palaeogene; 9, Neogene and Quaternary; 10, fault; 11, thrust; 12, thickness, km, of sedimentary cover; 13, deposit being mined, under development, mined out; 14, operating uranium mill

La Crouzille–Limousin type district

Fig. 5 shows the general geological setting of the La Crouzille–Limousin district. The leucogranitic complex includes three units from west to east—the Brâme, St. Sylvestre and St. Goussaud granites.

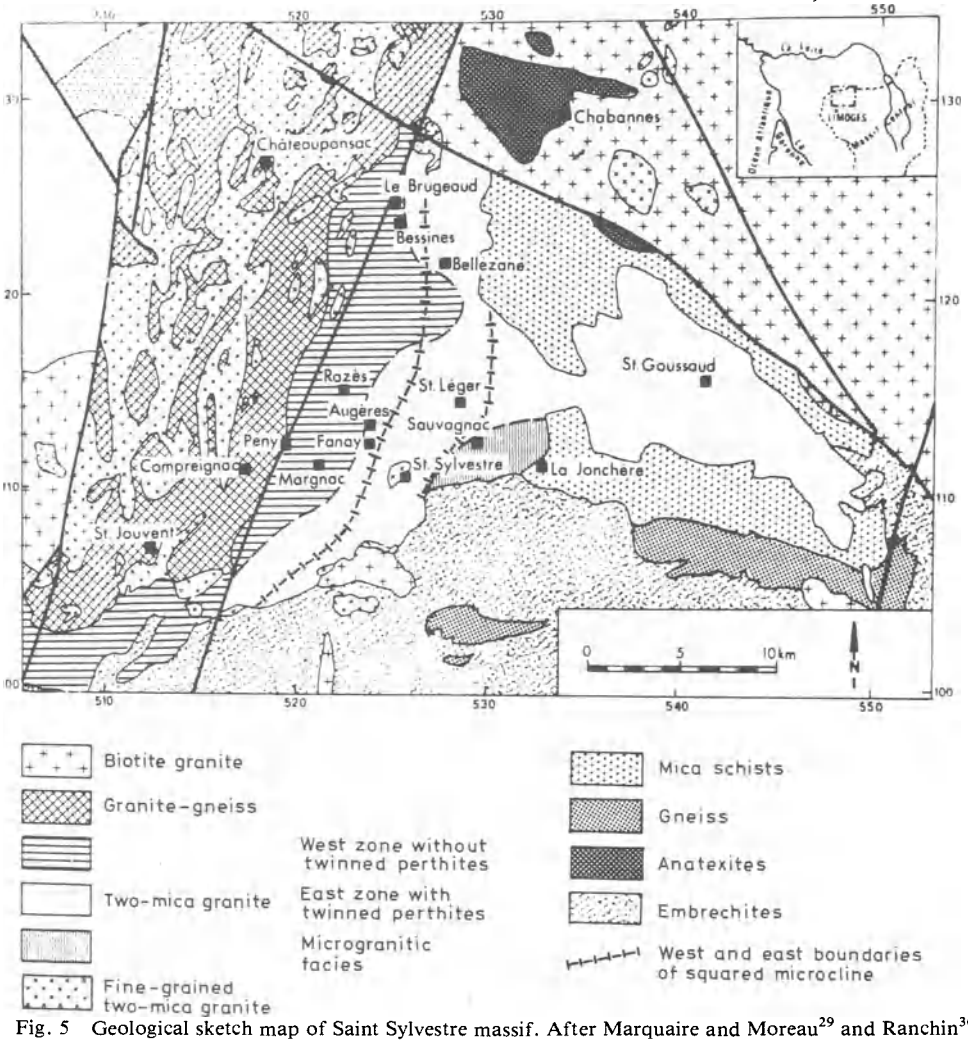

Fig. 5 Geological sketch map of Saint Sylvestre massif. After Marquaire and Moreau[29] and Ranchin[36]

This complex is partly intrusive in the monzogranite–granodiorite of the Guérêt complex (360–345 m.y.) (phase *P*1). There is disagreement with respect to the emplacement of the leucogranitic complex. On the one hand, according to Autran and Guillot,[4] and, quite independently, Moreau,[30] the Brâme unit, characterized by a planar texture, was emplaced first (during phase *P*2) under parautochthonous conditions. The St. Sylvestre and St. Goussaud units, of allochthonous or diapyric type, were intruded during phases *P*3 and *P*4 (320–300 m.y.). The contact zone between the Brâme and St. Sylvestre granites is underlain by numerous pegmatite and aplite bodies. On the other hand, Leroy[25] and, earlier, Chenevoy[13] and Ranchin,[36] considered that the whole leucogranite complex was intruded during phase *P*2 in parautochthonous conditions. But, during phases *P*3 and *P*4, further tectonic magmatic (intrusion of the fine-grained Châteauponsac granite in the Brâme unit) and deuteric processes have shaded off differentially the primary characteristics. In particular, through an incomplete isotopic homogenization they deduced an age of 315 m.y. for the St. Sylvestre leucogranite.

Leroy[25] considered the contact between the Brâme and St. Sylvestre granites as gradual. Unfortunately, a younger shear zone parting those two units obscures their relationships.

Lamprophyre and microgranite dykes intruded the St. Sylvestre granite at 285 m.y. and, at the same time, mica-episyenitization created further sites of concentration of uranium and led to the dissolution of quartz and muscovitization of other minerals. Another type of episyenitization, more strictly bound to diaclases and fissures, consists in the dissolution of quartz, the formation of albite and/or microcline and hematitization. The latter is not related to mineralization.

The main factors that control the mineralizing processes are listed below.

(*a*) The significantly high uranium contents of these leucogranites resulting from deuteric processes: this uranium occurs mainly as uraninite, which explains the abnormally low Th/U ratios. Table 1 shows these values within the three leucogranitic units.

Table 1

Leucogranite facies	U, ppm	Th, ppm	Th/U
La Brâme	8.70–14.88	?–12.67	?–0.86
Châteauponsac (fine-grained facies intrusive in Brâme)	18.24	8.71	0.41
St. Sylvestre	16.00–22.09	23.37–34.67	1.13–2.17
St. Goussaud	14.90–21.20	18.11–26.27	0.85–1.75

(*b*) This easily leachable uranium could have been remobilized during phases *P*3 and *P*4 processes. The thermal flow induced by the intrusion of lamprophyres and microgranites could have

produced convective systems in the aquifer as well as the rise of CO_2-rich fluids from the north–south fractures, thus increasing the dissolution of the uraninites of the granites by formation of uranyl carbonate.

(*c*) The depression occurring in the micaceous episyenites and in the brecciated rocks (porosity effect) is responsible for the release of CO_2 and the accompanying reduction of uranium from valency 6 to valency 4, thus resulting in the deposition of pitchblende, followed by that of pyrite and silica at temperatures of 345°C: contacts with lamprophyre dykes, involving an additional chemical factor, increase the rate of precipitation.

(*d*) Following the CO_2 release, the convective cells are restored and contribute to the first reworking of pitchblende, which is thus altered into coffinite with simultaneous crystallization of quartz, montmorillonitization of muscovite (at temperatures of 330–140°C), and deposition of fluorite, barite and calcite.

(*e*) The succeeding decrease in temperature interrupts the convective system and the primary history of the deposits ends.

(*f*) The further processes involve meteorological factors—erosion and weathering, with a climax during the Oligocene. They result in the production of orebodies that associate Permian primary uranium ores with reworked secondary low-temperature minerals.

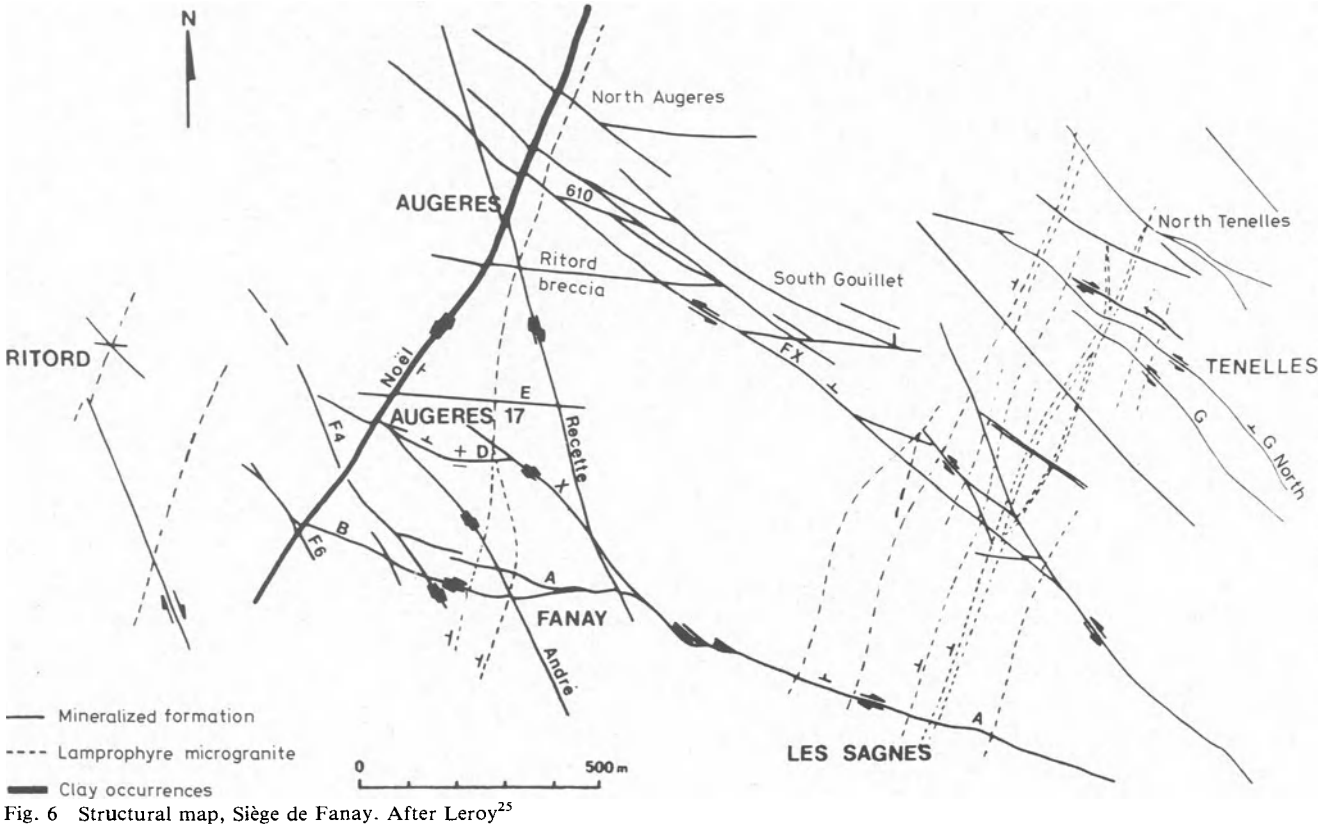

Fig. 6 Structural map, Siège de Fanay. After Leroy[25]

In the Limousin district all economic occurrences are restricted to the St. Sylvestre unit and, more precisely, to its western part corresponding to the less homogeneous zone where the pegmatites and aplites occur.

Uranium orebodies present two main morphological types. The classical vein-like linear bodies result in the association of east–west directions with the northwestern. The resulting trends vary from WNW to northwest (Fig. 6). Only the east–west sections present mica-episyenite alteration. The same is observed in vertical sections (Fig. 7). When intersecting or partly following lamprophyre dykes, veins often present conspicuous uranium enrichment. This was the case of the famous Henriette orebody, which was the first economic deposit in France. It produced 103 t U at an average grade of 31.2% U. The ore was extracted from a column 250 m high with an average length of 5 m and width of 0.40 m. Fig. 8 shows this exceptional morphology.

The other variety of orebody is represented by mica-episyenite bodies, usually developed at the intersections of east–west and north–south fractures. This brittle and vesicular rock forms extremely irregular three-dimensional bodies able to exceed significantly 100 m in height. Fig. 9 shows such a typical body of the Margnac deposit of the La Crouzille district. They are sometimes vertically interrupted (Fig. 10). The main uranium-bearing minerals are pitchblende and coffinite.

In both kinds of orebodies the deposition of pitchblende, associated with pyrite, is followed by a rapid precipitation of silica accompanied by hematitization. Then followed the deposition of marcasite and crystalline quartz, accompanied by a first reworking, producing coffinite. This stage ends with deposition of fluorite, barite and calcite. In general, the associated sulphides and gangue minerals are quantitatively insignificant.

Other uranium districts related to leucogranites

Other uranium districts assignable to this type are known in France. The most important, from the resources viewpoint, is that of Vendée. As Fig. 11 shows, deposits in that district present a less intragranitic position. The bulk of resources occurs in the granite in the vicinity of the contact. But mineralization also occurs in the metamorphic country rock, again close to the contact, recalling the Iberian type examined later in this paper. Less important in size, but economically very important, is the Creuse–North Limousin district. East of the Sillon Houiller uranium mineralization in mica-episyenites is mined in the Langogne area. One of the orebodies reveals remarkable development and shape (Fig. 12).

Outside France the Krunkelbach–Menzenschwand in the southern Black Forest of the Federal Republic of Germany belongs to this type.

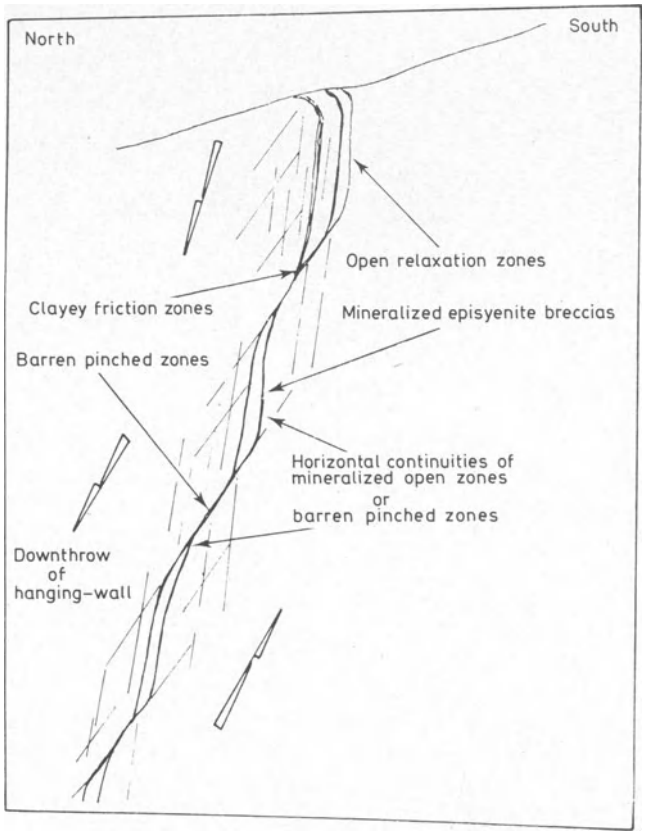

Fig. 7 Vertical cross-section of 'East–West' formation. After Gagnadre[18]

Uranium deposits in less differentiated granites

This type is much less represented in the European Hercynian belt. But the most important individual vein-type mine in Europe, the Bois Noirs–Limouzat in the area of the Massif Central called Montagne Bourbonnaise or Forez (France), belongs to this type.

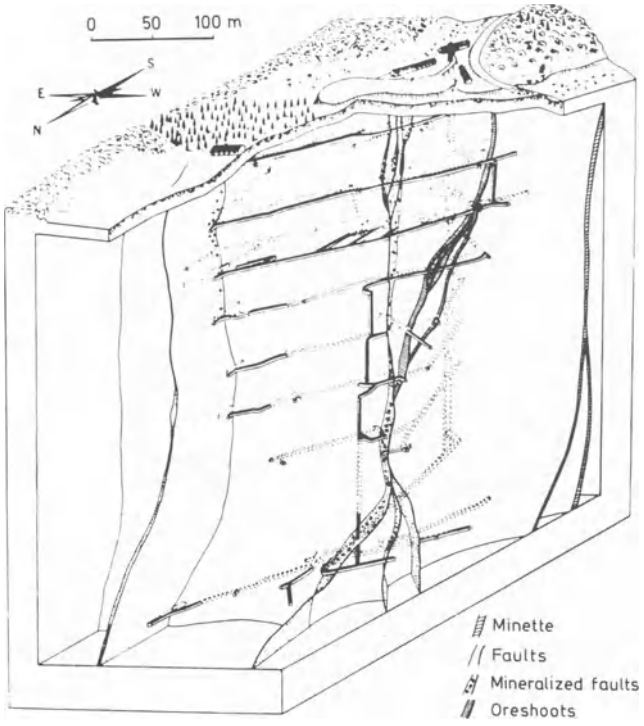

Fig. 8 Block diagram, Henriette mine. After Sarcia and Sarcia[39]

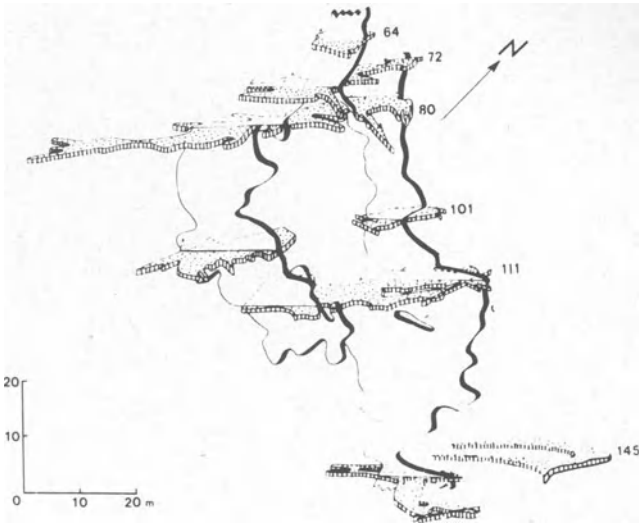

Fig. 9 Margnac Point 132: vertical and horizontal cross-sections of micaceous 'episyenite' oreshoot. After Leroy[25]

Bois Noirs–Limouzat deposit

The Lachaux–Bois Noirs granite is not characterized by any remarkable geostructural position, contrary to leucogranites in France, except that it also occurs in the Moldanubian zone of the Hercynian orogen. The country rock is a Precambrian (600–700 m.y.) metamorphic basement with 520 m.y. granitoids and unconformably overlain by a non-metamorphic Devono-Dinantian sequence of shales and sandstones capped by Upper Viséan rhyo-dacitic tuffs. This structure was invaded by three sets of granites between 335 and 300 m.y. ago—from south to north (Fig. 13) the typical syntectonic leucogranite of Vimont (300 m.y.), the equigranular Lachaux–Bois Noirs–Madeleine 'epileucogranites' and the large porphyroidal monzogranite of Mayet de Montagne–Arfeuilles.

The term 'epileucogranite' was used by Moreau[30] to qualify a variety of acid aluminous granites, poor in biotite, with sometimes muscovite and tourmaline. They occur in pre-existing metamorphic and granitic basements, exhibit no evidence of diapirism and present some chemical and petrographical zoning with increasing Si–Na–K and decreasing Ca–Fe–Mg contents. They may result from the percolation of magmatic fluids at temperatures below the solidus. Uranium deposits are limited to the Bois Noirs epileucogranite, but significant occurrences are known in that of Lachaux. Both are intersected by numerous lamprophyre and microgranite dykes 316 m.y. old.

Table 2

Rocks	U, ppm	Th, ppm	Th/U
Leucogranite of Vimont	8.4	11.6	0.7
Epileucogranites (Bois Noirs)	7.4–11.9	32–33	3–4
Monzogranites (Mayet de Montagne)	9.7	38.6	4
Upper Viséan rhyolites	6–7	40	4–6
Lower Viséan detrital shales	2–2.5	6–12	3–5

The uranium and thorium contents of the different Hercynian granites and of the pre-existing Palaeozoic rocks are given in Table 2.[30]

In comparison with similar data from Limousin the following remarks can be made: although the uranium contents of granites are significantly higher than normal, they remain well below those of Limousin; as the thorium contents are higher, the Th/U ratios are, in turn, significantly higher than the overall lithosphere average (with the exception of the Vimont

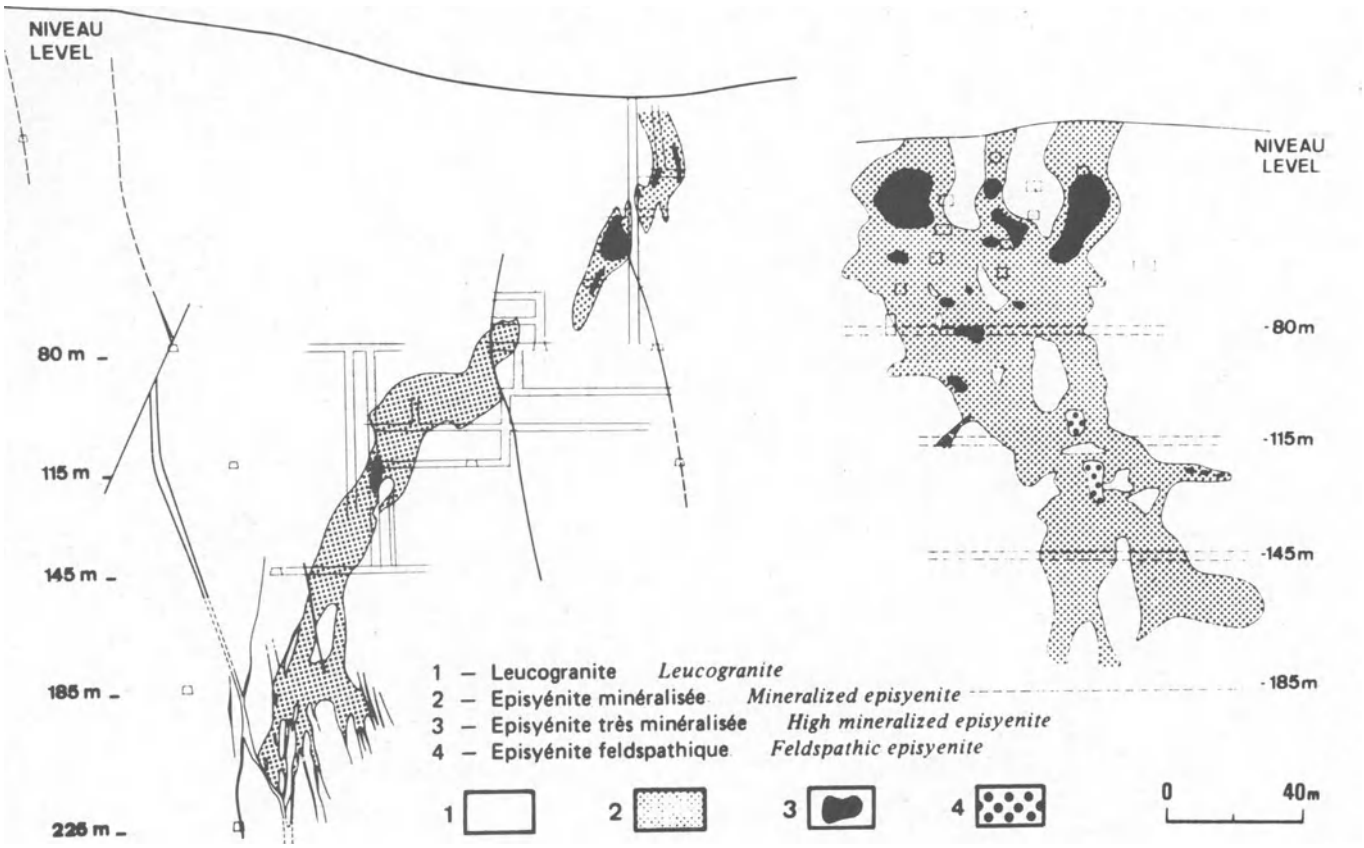

Fig. 10 Cross-sections of pipes of mineralized episyenite at Margnac 2 and point 132, Margnac. After Dardel *et al.*[32]

leucogranite); and similar values for uranium, but higher for thorium, are recorded for rhyolites, leading to higher Th/U ratios.

The bulk of the uranium in granites is contained in micas and heavy minerals. Uraninite (containing 3–15% Th) is the major uranium-bearing mineral.

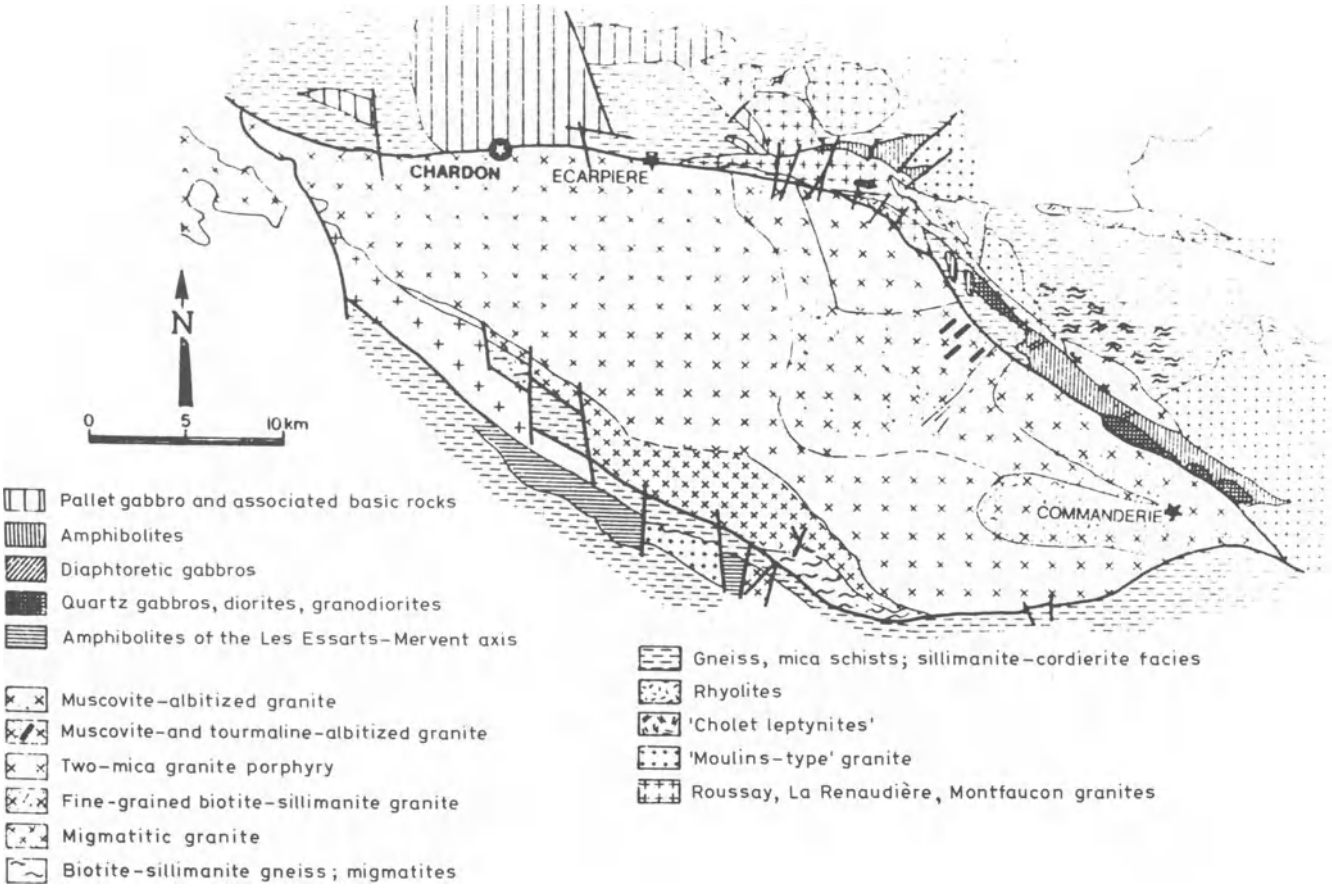

Fig. 11 Clisson-Mortagne massif with metamorphic aureole. After Cathelineau[12]

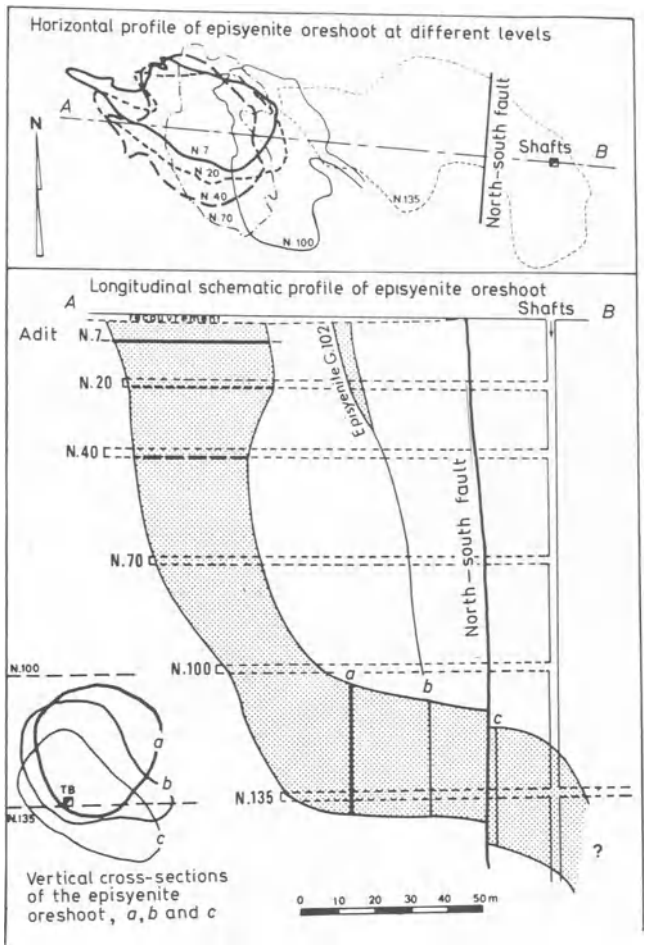

Fig. 12 Les Pierres Plantées (Lozère): morphology of main 'episyenite' oreshoot between surface and −135 level. After Cariou[10]

The Bois Noirs deposit, now exhausted, produced some 7000 t U. Its maximum extension was 1500 m and it was mined to a depth of 400 m and drilled down to 520 m. As Fig. 14 shows, the deposit is related to a fracture complex, with a general northwest trend and with development of a stockwork southeast of shaft *P*3 between the 'filon toit' (hanging-wall vein)–BN6 system, dipping 70° northeast, and the 'filon-mur' (footwall vein) system, dipping 65° northeast. The major trends within the stockwork are close to east–west.

Mineralization occurs (*a*) in east–west veinlets and veins varying from a few centimetres to a few metres in width: they occur together between levels 80 and 40 m and beyond up to the surface, forming a locally very rich stockwork, and (*b*) in the fractures of the 'filon-toit'–BN6 and 'filon-mur' systems, where mineralized veins show thicknesses from several metres to a few tens of metres carrying sooty pitchblende, hexavalent uranium minerals in a jasper and banded quartz gangue.

Although uranium predominates, the elemental and ore-mineral associations are very broadly represented here. In addition, gangue filling and, mainly, silica are very abundant.

Pitchblende, with some comb quartz, accompanied by pyrite, marcasite and löllingite, is introduced at the early stage. Then comes the bulk of hematitized jasper, brecciating the earlier pitchblende and partly reworking it as coffinite; galena, fluorite and then chalcopyrite accompany this stage. During further stages new generations of the same sulphides plus carbonates are introduced; later comes crystalline quartz with more sulphides, including bismuthinite (and native bismuth). During the final stages sooty pitchblende and hexavalent uranium minerals result from the alteration of primary ores.

It is interesting to stress the marked difference between veins of this type of deposit, characterized by the abundance of gangue material, mainly hematitized jasper, alternating with crystalline comb quartz, often smoky, and the orebodies associated with leucogranites where gangue material is very scarce and veins look simply like shear zones in the granite.

According to Cuney,[14] the Bois Noirs granite results from the anatexis of U- and Th-rich sediments under granulite-facies type conditions (800°C, weak partial water pressure, presence of CO_2). The alteration, enhanced by residual fluids of magma crystallization, of major and mainly accessory minerals, mobilized contained uranium. The uraniferous fluid phase then migrated and precipitated uranium contemporaneously with quartz–muscovite alteration. The thermal activity lasted from the intrusion of the granite (335 m.y.) until the intrusion of quartz porphyry (270 m.y.), inducing hydrothermal convective cells. The mixing of water, of probably meteoric origin, with the CO_2 from depth enhanced the dissolution of uraninite and its further transfer as uranyl carbonate, and east–west breccias were reopened and H_2S circulated in the fractures. The pressure drop resulted in CO_2 release and oxidation of sulphides, thus producing the reduction of uranyl carbonates and, subsequently, the deposition of pitchblende, pyrite and marcasite (between 77 and 100°C). Deposition of pitchblende still lasted some time with variations of temperature and composition of solutions. Pitchblende was then partly altered to coffinite. The later stages of weathering are attributable to the Oligocene tectonics with the formation of the *per descensum* supergene sooty pitchblende and coloured uranium minerals.

Other districts

As has already been mentioned, the type of deposit discussed here seems to present in Europe much less importance than that related to genuine leucogranites. Nevertheless, other districts, comparable with the Bois Noirs, are known in the Iberian Meseta, where they are often also related to the Iberian type of deposits described later.

The well-known Urgeiriça and the neighbouring Cunha Baixa deposits in the province of Beira Alta in Portugal are the most important (of the order of 1000 t U) of this type of deposits in the Iberian Peninsula. In Spain the Los Ratones deposit in the Caceres district is almost of the same magnitude; Villar de Peralonso in the Ciudad Rodrigo district is only half as large. The even smaller deposit of La Virgen, in the Andujar district, is characterized by a larger proportion of copper.

Uranium districts in perigranitic shales (Iberian type)

In Europe the privileged zone of occurrence of this type of deposits seems to be the outer zone immediately bordering the inner zone of the Hercynian orogen, characterized by maximum metamorphism and granitization. It is, in particular, the case in the Iberian Peninsula, where these deposits are scattered within sub-zone (*b*) of the Central Iberian zone of Fig. 1. In Bohemia, however, the Pribram and Jachymov districts belong to the Moldanubian zone, though being attributable to the same type of deposit.

Perigranitic deposits in Ciudad Rodrigo, Spain, and Nisa–Portalegre, Portugal, districts

This type of deposit is frequent in the Iberian Meseta (or Iberian Hercynian Massif), but assumes economic importance only in the Nisa–Portalegre district and mainly in that of Ciudad Rodrigo (Fig. 15). Deposits of this type are distributed in the exometamorphic contact haloes of Hercynian granites, intrusive in Lower Proterozoic shales, little or not modified by general metamorphism. Wherever such deposits have been identified the shales present, in some horizons, abundant evidence of organic material, generally transformed into graphite, at least within the contact-metamorphic haloes. The

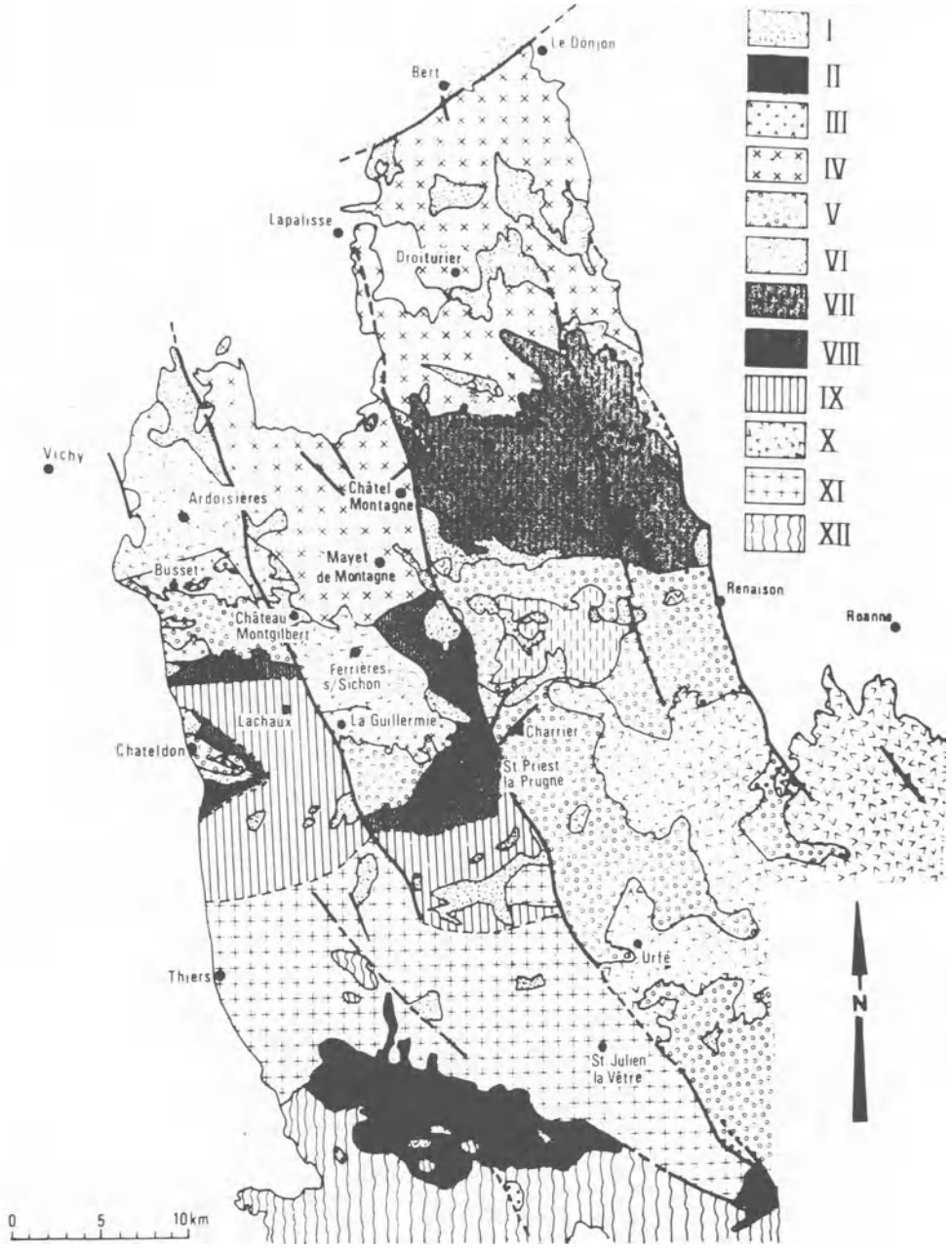

Fig. 13 Geological sketch map of Montagne Bourbonnaise. I, Permian sedimentary rocks; II, Vimont two-mica granite; III, Busset and La Guillermie granites; IV, Mayet–Arfeuilles–Droiturier granites; V, porphyritic microgranite cover; VI, fine-grained granites; VII, Madeleine granite; VIII, northern facies of Lachaux–Bois Noirs granite; IX, central facies of Lachaux–Bois Noirs granite; X, Devonian and Viséan sedimentary rocks; XI, St. Julien-la-Vêtre–south Bois Noirs granite; XII, metamorphic basement. Star (northwest of St. Priest la Prugne) is Bois Noirs–Limouzat deposit. After Cuney[14]

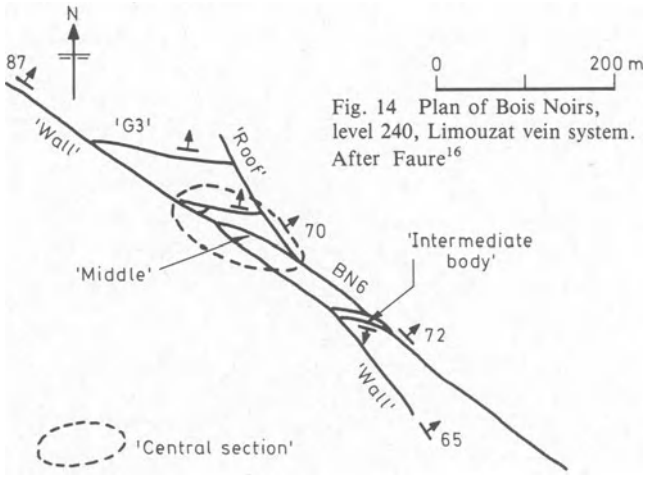

Fig. 14 Plan of Bois Noirs, level 240, Limouzat vein system. After Faure[16]

latter, of kilometre width, are formed of hornfels, with andalusite–cordierite schists carrying porphyroblastic concentrations of sericite and muscovite and, in places, chlorite, biotite, quartz and graphite.

Granites responsible for these haloes often contain intragranitic uranium vein-type deposits, economic or not, wherever uranium concentrations were identified within those haloes. It is, in particular, the case for the Villar de Peralonso (Ciudad Rodrigo district), Tarabau, Palheiros de Tolosa occurrences (Nisa district) and, of course, Urgeiriça and Cunha Baixa in the Beira Alta, where large low-grade uranium mineralization in shales is known in the southern contact area (Sinde–Azere). These deposits present three kinds of occurrence.

(*a*) In the immediate vicinity of the granite contact within a belt of some 1000–1500 m: the contact itself is quite often offset

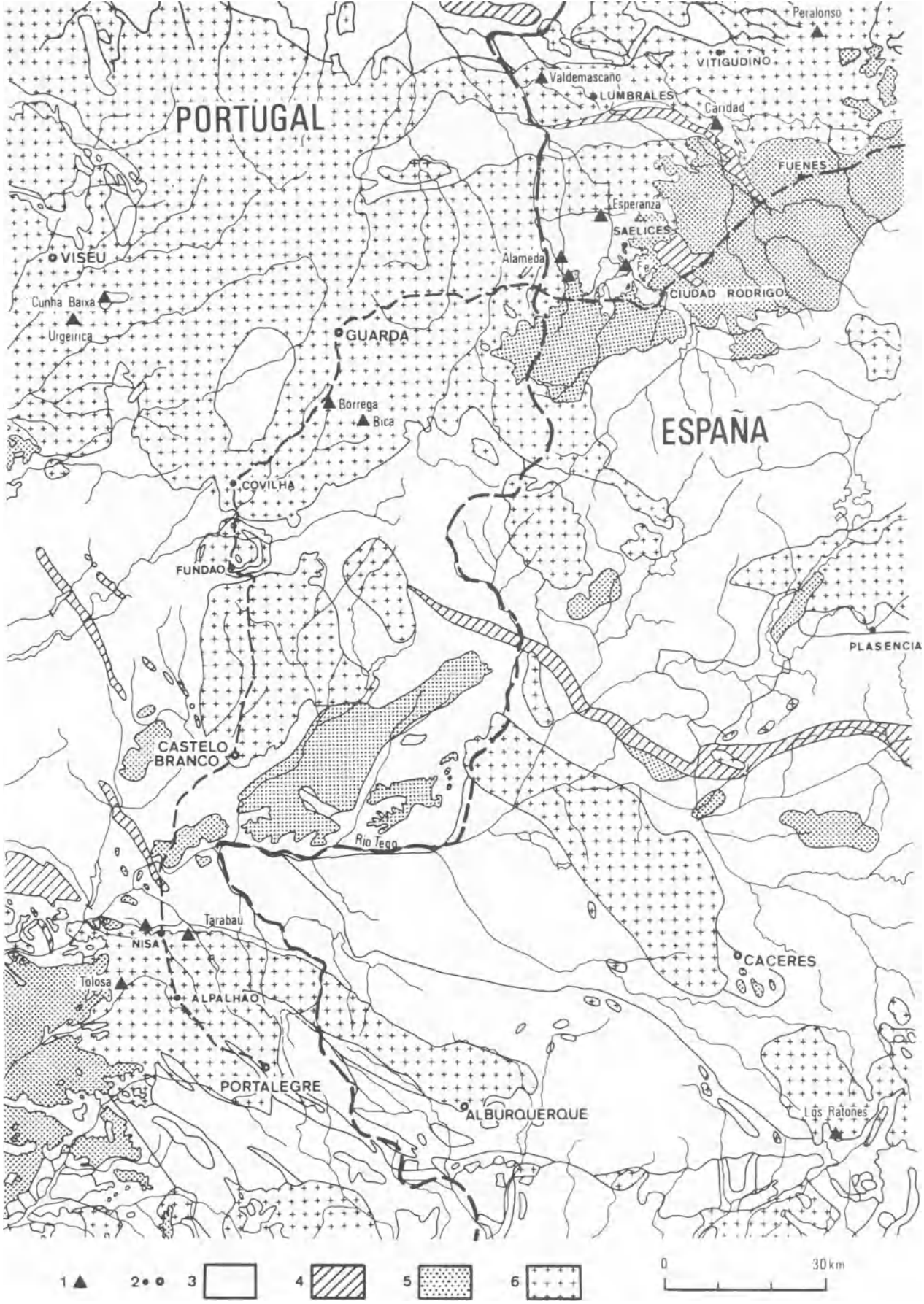

Fig. 15 Perigranitic deposits in Ciudad Rodrigo and Nisa–Portalegre districts. After Dardel *et al.*[32] (1, uranium deposit; 2, town; 3, Pre-Ordovician schist-greywacke; 4, Silurian–Ordovician formation; 5, Caenozoic and Quaternary cover; 6, granitoids)

by orthogonal faulting, so 'drawer-like' compartments of shales are 'pushed' within the granite, thus forming preferential sites of occurrence for uranium deposits. This is typical of the Alameda, Esperanza and Caridad deposits in the Ciudad Rodrigo district of Spain and Nisa in Portugal (Fig. 16).

(*b*) In roof-pendants of shales within the granite the orebodies acquire a vein-like morphology. This is particularly true of the Senhora das Fontes deposit, north of the Guarda district (Fig.

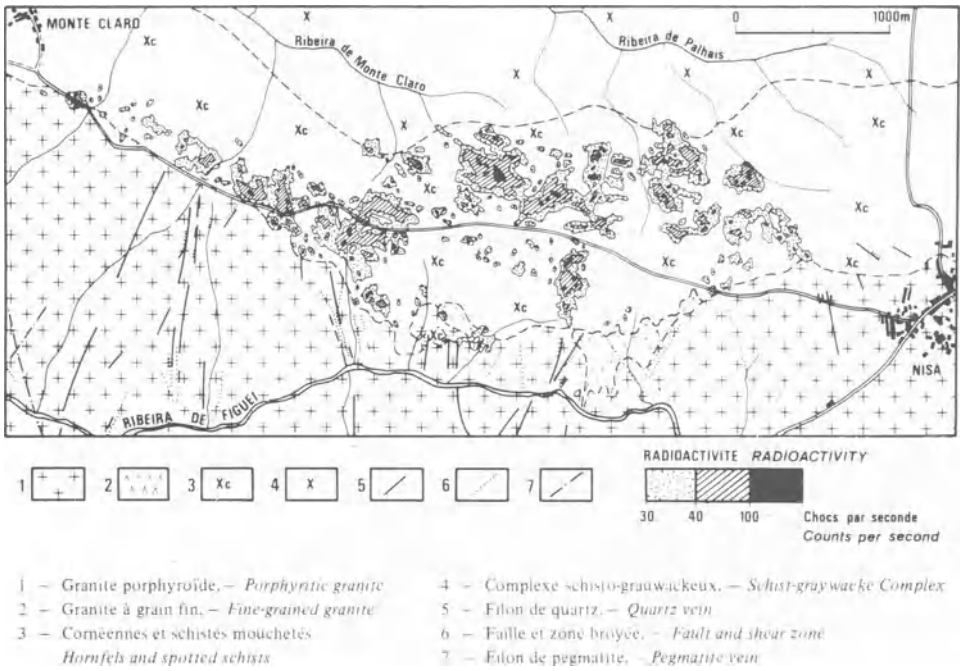

Fig. 16 Nisa deposit. After Dardel *et al.*[32]

15), which produced about 90 t U to some 100 m in depth.
(*c*) Between a set of granite outcrops, but at relatively important horizontal distances (several kilometres) from them, as at Fe, the best-known deposit in Spain (Fig. 17). It occurs, however, in an area where the reappearance of the hornfels facies could indicate the vicinity of granite in depth.

In all these deposits uranium mineralization impregnates fracture zones or any kind of heterogeneity in shales, offering enough permeability for preferential circulation of solutions. This, at least, can be observed above the water-table, but exploration below it was not developed sufficiently to provide reliable information. Present known minable resources lie

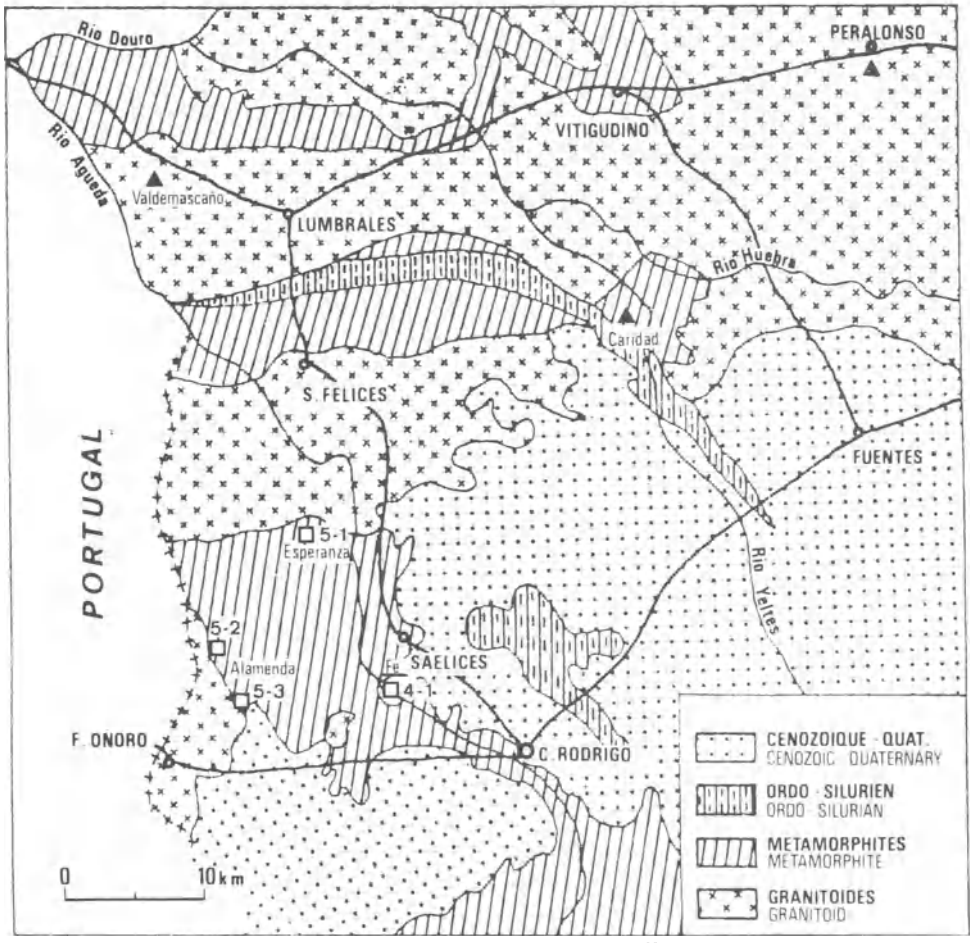

Fig. 17 Main uranium deposits of Salamanca. After Dardel *et al.*[32]

almost completely in the oxidation zone within a vertical range of some 15–25 m from surface.

In the Ciudad Rodrigo district, however, as well as in that of Nisa, some deeper drillings have reached levels between 100 and 200 m from the surface: few have intersected steep veinlets of pitchblende.

The bulk of the known resources in these deposits is formed of uranium hexavalent minerals—mainly autunite. Other supergene minerals are torbernite, ianthinite, kasolite, saleeite, sabugalite, coracite and gummites, but some pitchblende was identified in Fe (*D* zone) and Esperanza, and coffinite in those two as well as Caridad. Small amounts of sulphides (pyrite, galena, sphalerite, chalcopyrite and marcasite) were identified.

This type of deposit is generally characterized by rather low grades (of the order of 1000 ppm U or even less), but resources may be quite important.

In Nisa, where the horizontal extension is considerable (some 4000 m) the resources are of the order of 2000 t of uranium, but they are several times larger in the Ciudad Rodrigo district, where part occurs beneath Tertiary cover rocks.

The genesis of this type of deposit remains controversial, but the supergene theory has attracted more supporters. According to Fernandez Polo[17] and others, weathering and erosion of the neighbouring granites during the Caenozoic enhanced the leaching of uranium, further deposited in topographic lows and in the brecciated zones close to granites, and resulting in superficial concentrations, without significant extension in depth. More recently, Moreau[30] produced an interesting hypothesis in connexion with the Spokane deposit, Washington, U.S.A., which has quite similar characteristics. According to him, an enrichment of uranium in magmas occurred during the anatexis of the uranium-rich pre-existing sedimentary sequences (black shales, etc.). It was further concentrated in the residual fluid phase and later deposited (pressure release) in the heterogeneities of the contact, uranium being associated with such high-temperature minerals as molybdenite and arsenopyrite and also magnetite. Later on this primary mineralization was redistributed to yield the present orebodies.

Nevertheless, another effect of the granite intrusion may be evoked—that of the high-temperature isotherms rising as thermal domes in a 'cold' environment close to the surface. Such thermal domes could enhance in the intruded sediments, rich in surface waters, convective cells mobilizing uranium from such rocks as black shales and concentrating it in some privileged zones as fractures and other heterogeneities. It is possible to imagine that this effect can be superimposed on that developed by Moreau.[30]

The genetic model may have major significance for the identification of additional resources in these deposits. A very simple calculation shows that if pure pitchblende veinlets only 1 cm thick were repeated at 20-m intervals, the uranium content of the whole rock volume would average 1000 ppm, which is the grade of the oxidized ores presently mined. Therefore, the presently known resources could possibly be increased several times in depth. It therefore appears highly desirable to undertake major scientific research on this type of deposit.

Other occurrences

The most interesting European uranium districts that contain comparable deposits occur in Czechoslovakia. The most similar is that of Pribram (Fig. 1), where mineralization is located in the exocontact halo developed in Eocambrian shales metamorphosed into biotite, biotite–cordierite hornfels and andalusite–cordierite schists. In this area, however, fractures are discrete and, subsequently, uranium mineralization presents a steady continuity in depth and primary mineralization is widely developed. In addition, the paragenetic association, much more diversified here, includes three phases: first, carbonates, quartz, Co–Ni sulphides and sulpharsenides, sphalerite and galena; second, carbonates and pitchblende; and, third, calcite and some pyrite.

Minerals of the different phases may occur in separate veins or as a single orebody. There is no formal information available on the uranium resources of that district, but it is likely that they are important by European standards.

The Jachymov district (Fig. 1) is less typical as the country rock had already undergone a general metamorphism. Uranium deposits again occur within the exocontact zone, developed in the metasediments, around an 'autometamorphic' late Carboniferous or early Permian granite (probably submitted to an intense deuteric process). The orebodies are typically vein-like. The northeast veins contain the Ni–Co–Bi–Ag–U association. The northeast fractures present clay and quartz breccia fillings and at the intersections with the north–south fractures the five-metal association, plus Zn, again appears.

Uranium vein-type deposits in metamorphic environment without apparent connexion with granites

Tirschenreuth, Oberpfalz uranium district (east Bavaria, Federal Republic of Germany)

The type of deposit dealt with here was generally ignored until recently, but the uranium occurrences discovered and presently under active investigation in the northern part of eastern Bavaria are, in our opinion, assignable to this type. The Tirschenreuth, Oberpfalz district, lies in the Saxothuringian zone of the western margin of the Bohemian Massif, against the contact with the Moldanubian zone. The country rock assemblage is composed of late Precambrian and Cambrian formations from north to south (Fig. 18): (*a*) Cambrian flat-lying lustrous schists; (*b*) Precambrian biotite–sillimanite schists intruded by Assyntic granodiorite; (*c*) mica-schists; (*d*) cordierite–sillimanite gneiss interbedded with gneissic granitoids and amphibolites; (*e*) cordierite–silicate gneisses. Units (*c*), (*d*) and (*e*) are intruded by Moldanubian elongated granites with northwest axes perpendicular to the northeast general trend of the area. The early ENE sub-conformable fracture system is offset by a dense system of northwest fractures.

Two deposits were identified in unit (*b*)—Höhenstein, some 1.5 km north of Poppenreuth, and Wäldel, some 2 km north of Mähring. In turn, some 1.5 km north of Wäldel, across the Czechoslovak border, the Dylen and Slatina deposits occur in the same geological unit. The area dealt with here is the western extension of the Czechoslovak uranium district of Marianske–Lazne.

The Wäldel deposit contains two mineralized structures: one is a north–south shear zone and the other is related to a northwest quartz vein. Uranium mineralization is contained in pitchblende and coffinite, in close association with pyrite. Evidence of major reworking within the reduced zone was recorded. In the upper parts numerous hexavalent uranium minerals were identified. It seems that the Dylen deposit is also bound to a quartz vein.

In the Höhenstein deposit mineralization is related to fractures and, preferentially, to intersections of fractures. The main uranium-bearing mineral is pitchblende (with coffinite). Again, evidence of major reworking is recorded. It would be unwise at this stage to propose genetic assumptions regarding these deposits, more information and much more scientific research being required. As uranium mineralization is discovered in other districts of this eastern Bohemian Massif margin, and as reconnaissance programmes are still in progress, we are hopeful that a better knowledge of this interesting area will soon be acquired.

Uranium deposits in Stephanian sediments

Uranium deposits associated with sedimentary rocks in general

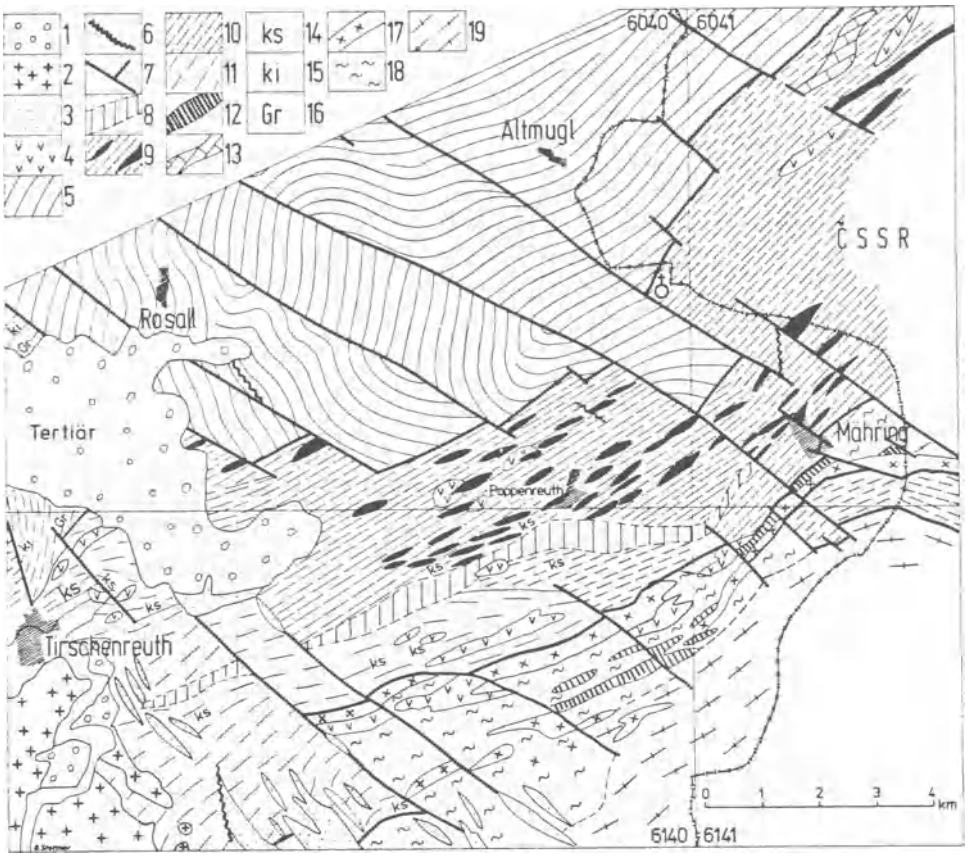

Fig. 18 Geological-tectonic map of Saxonian–Thuringian-Moldanubian border. 1, Tertiary; 2, granite of Falkenberger Massif; 3, 'Moldanubian' granite; 4, Redwizite; 5, Cambrian micaceous schists; 6, quartz vein; 7, fault; 8, diaphthorites II, phyllonites; 9, Assyntic granodiorite; 10, biotite and sillimanite Precambrian micaceous schists and biotite, muscovite and sillimanite schists; 11, muscovite and biotite gneiss; 12, amphibolites; 13, marbles; 14, hornfels; 15, siliceous metaschists; 16, graphitic rocks; 17, granitoid gneiss; 18, cordierite and sillimanite gneiss associated with diaphthorite gneiss; 19, cordierite and sillimanite gneiss. After Stettner[42]

are numerous and vary in terms of location, type and age of their surroundings. They are found in a number of places in Europe—for example, in the Ranstad, Sweden, Cambrian carbonaceous shales, in the Müllenbach, Germany, Stephanian sandstones and carbonaceous siltites, in the Lodève, France, Permian lutites and siltites and in the Permian to lower Tertiary sandstones in many other localities.

Müllenbach deposit, Baden-Würtemberg, Federal Republic of Germany

The Müllenbach deposit occurs in the small Triassic–Carboniferous basin of Oos-Salle (180 km^2) on the northern border of the Variscan Black Forest Massif. The following materials have been deposited on a granitic basement (Forbach two-mica granite, 293 ± 2 m.y.; Fig. 19).

During the Upper Carboniferous (Stephanian), more or less coarse light arkoses with conglomerates (granite, quartz and rhyolite pebbles), and finer-grained sediments (grey-blackish siltite, sandstones rich in carbonaceous material); the minimum thickness of the Stephanian is 250 m.

During the Permian, first, Autunian conformable red clays with some grey interbeds (a few tens of metres); then a thick rhyolitic unit (~ 150 m thick); and, finally, an unconformable

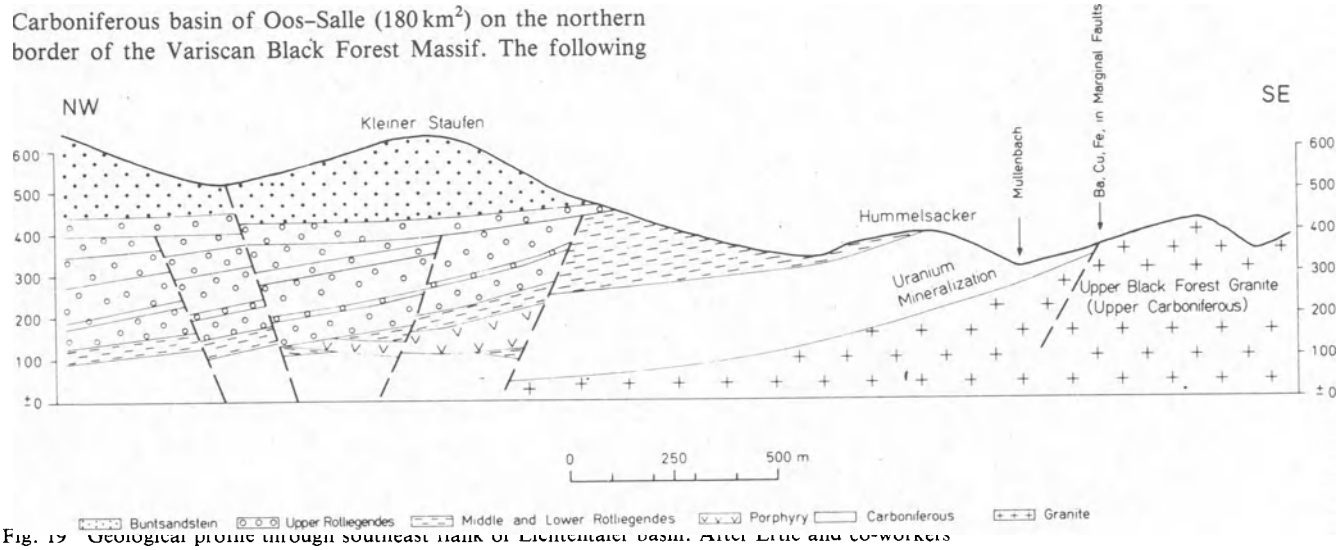

Fig. 19 Geological profile through southeast flank of Lichtentaler basin. After Ertle and co-workers

conglomeratic unit (rhyolite, including red clay brindles). During the Triassic, non-feldspathic sandstones.

The sedimentary cover reaches a thickness of some 2000 m in the centre of the basin and 125 m above the deposit. Uranium mineralization occurs mainly in the Stephanian, especially in carbonaceous siltites and argillaceous sandstone lenses with organic matter, at the contact between both layers. Mineralization occurs conformably or as scattered clusters, uranium being contained in pitchblende, coffinite, autunite, torbernite, heinrichite and uranophane.

Also worthy of mention is a deposit in carbonaceous shales of similar age at St. Hippolyte, Haut-Rhin, France.

Uranium deposits in Permian and Triassic sediments

Deposits of Lodève, Hérault, uraniferous district—Mas Lavayre and Mas d'Alary

Present-day reserves in the Lodève area amount to some 20 000 t of uranium contained in ores with an average content of 0.2%.

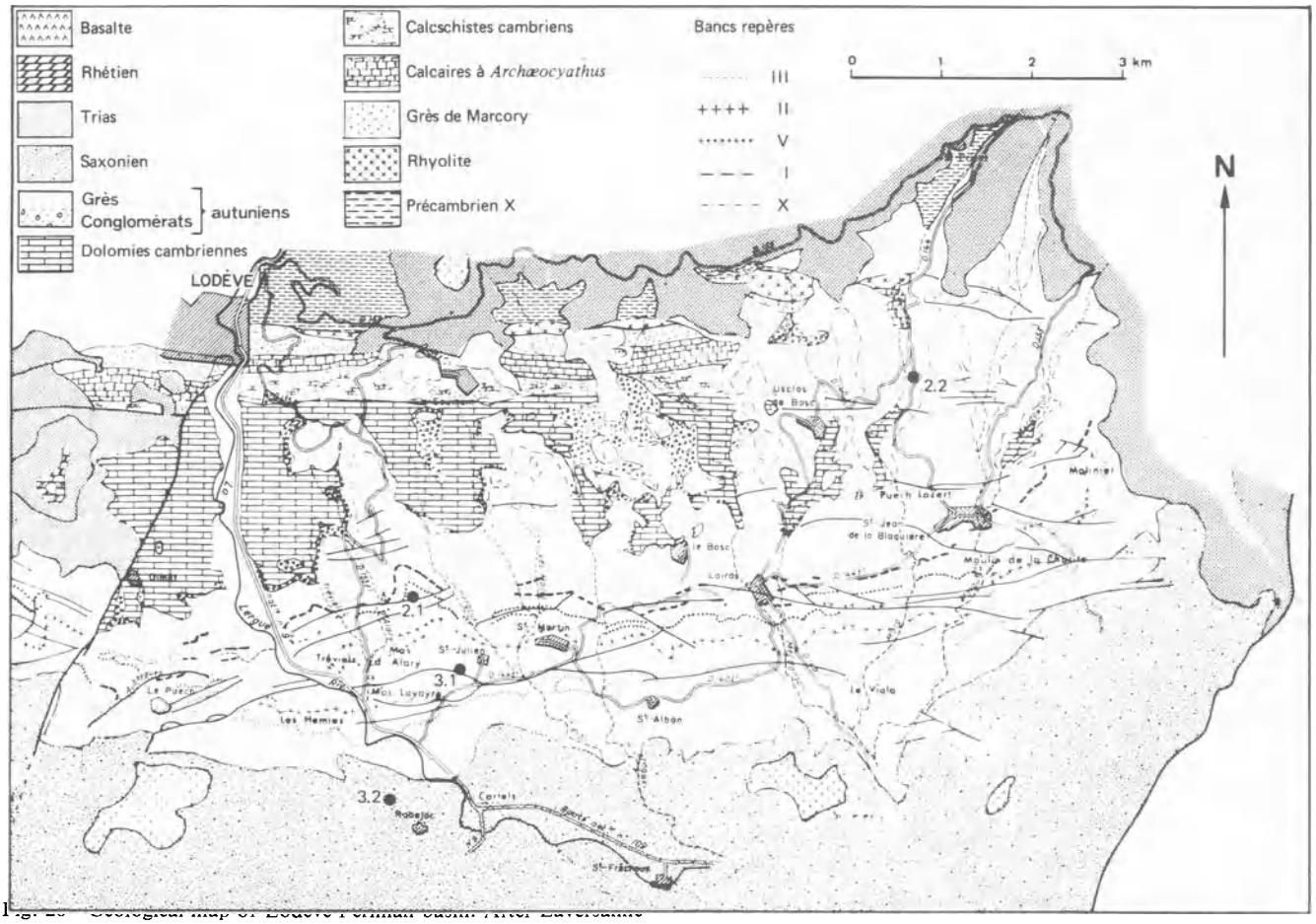

Fig. 20 Geological map of Lodève Permian basin. After Lavergne.

In this district the deposits occur in the Permian basin of Lodève in the folded north Pyrenean foreland on the eastern border of the Montagne Noire. The basin has an area of about 150 km^2 and is a diamond-shaped, southwest–northeast-trending depression, 26 km long, dominated by the 200–300 m high Jurassic limestone plateau (Figs. 20 and 21).

The Permian cover rests unconformably on a schistose Precambrian basement with rhyolitic tuff, sometimes overlain by Cambrian sandstones and dolomite. The Permian of Lodève, which is roughly 2000 m thick, is mainly composed of 600–700 m of Autunian sediments (lower third, grey; middle, grey and red; upper third, red) and 1300 m of slightly unconformable, entirely red, Saxonian sediments. With the exception of a few tens of metres of coarse sediments at their base (conglomerates and sandstones for the Autunian microconglomerates and sandstones for the Saxonian), the Permian sequences are composed of remarkably fine-grained deposits. The Autunian sequence in the Lodève basin is characterized by its specially fine grain (mostly arkosic siltites with carbonates), cyclic depositional features, lateral regularity and the presence of sulphates and boron. During Autunian time there was an abrupt evolution from an originally predominating saline environment to a flood plain with a few saline intercalations. The Autunian of the Lodève area is thus composed of unitary sequences (more than 70) a few metres thick (Fig. 22). Each of these includes (from bottom to top)[23,24] grey arkosic siltites, mostly tidal; dark bituminous laminites of lagoonal origin (relics of sulphates and rock salt), sometimes with cineritic levels; their evaporitic top is invaded by dolomite; green paludal argillites; and red argillaceous siltites from flood plains with sandstone-like fillings in channels.

The Saxonian sequence follows a red conglomerate, slightly unconformable with the Autunian; it is composed of a sandstone pelitic unit (about 100 m thick) followed by a thick monotonous unit of red argillaceous lutites.

In the Lodève basin the Permian age shows an equatorial climate with cycles of dry and wet seasons. The Permian pile underwent a strong diagenesis, characterized by a tight compaction accompanied by fracturation of the palaeo-reliefs and palaeo-channels, segregation of the alkaline elements (potassium in the grey facies, sodium in the red), disappearance of volcanic glass, crushing of some clays and presence of oil in the laminites. During a north–south tension phase the recurrent late Variscan wrench faults controlled the subsidence of the basin, which then developed into a semi-graben. The sediments were progressively tilted as they deposited (15–20°S).[38] Prior

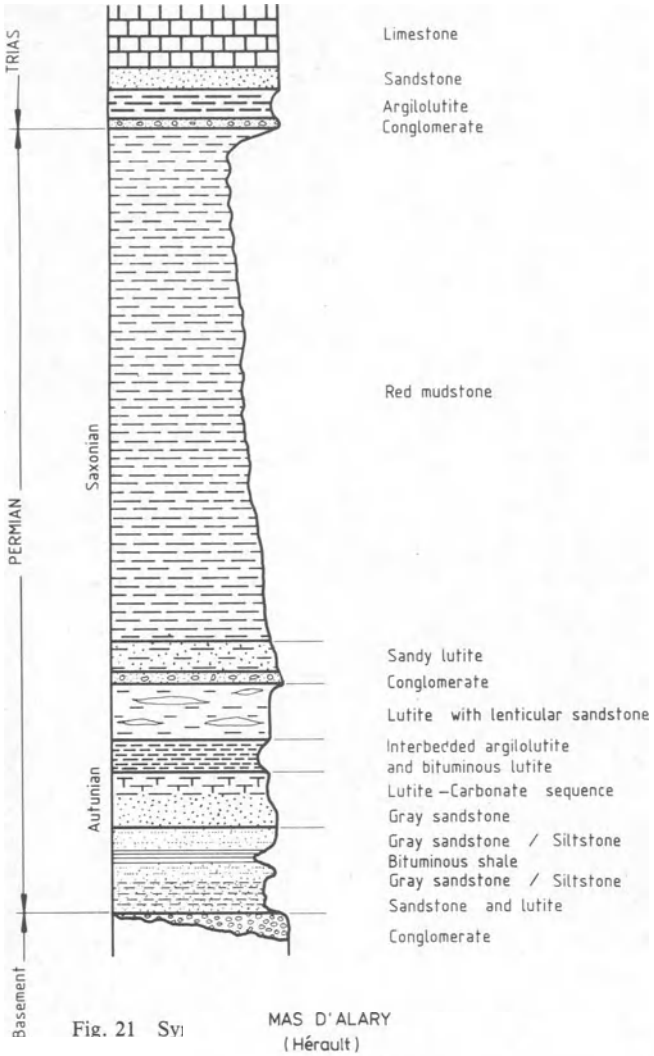

Fig. 21 Sy

to the deposition of Trias a number of tension periods reactivated the Permian faults. During the Eocene north–south compression produced thrust and transcurrent faults and folding along pre-existing discontinuities.

The major mineralization at Mas Lavayre occurs in the Autunian grey or grey and red alternating units. The uraniferous mineralization[23] is found in trap structures and drainage systems; in association with hydrocarbides apparently younger than the mineralization itself; and in the form of oxides (uraninite) or silicates (coffinite, complex silicates similar to clay minerals and zirconium silicates) invariably associated with titanium: zirconium is found at the bottom and molybdenum at the top of the sequence. Three types of mineralization were noted:[6] the early diagenetic mineralization (1% of reserves) in the form of large areas in the bituminous laminites of the red Autunian; the late diagenetic mineralization (10% of reserves) associated with molybdenum, which could result from the trapping of uranium contained in volcanic glass, montmorillonite, red sediments, in the vicinity of synsedimentary fractures, and in the bituminous laminites and grey arkosic siltites at the contact with nascent oil; and the epigenetic mineralization—the major and richest resources—related to pre-Triassic fracturing, which occurs as long thin belts, sometimes as accumulations, along the faults.

Deposits of Cerilly, Allier, uranium district

Present resources of the deposits around Cerilly (Lombre, Ainesse) amount to some 1500 t of uranium in ore averaging up to 1% U.

The Lombre deposit is located on the northern margin of the Massif Central, at the western border of the large Aumance basin (500 km^2) in the subordinate Permian basin of Cerilly (50 km^2) (Fig. 23).

The argillaceous fluviatile detrital sediments of the Cerilly basin rest on a granitic basement. They are cut by a marine sequence (Early Mesozoic) of the southern rim of the Paris

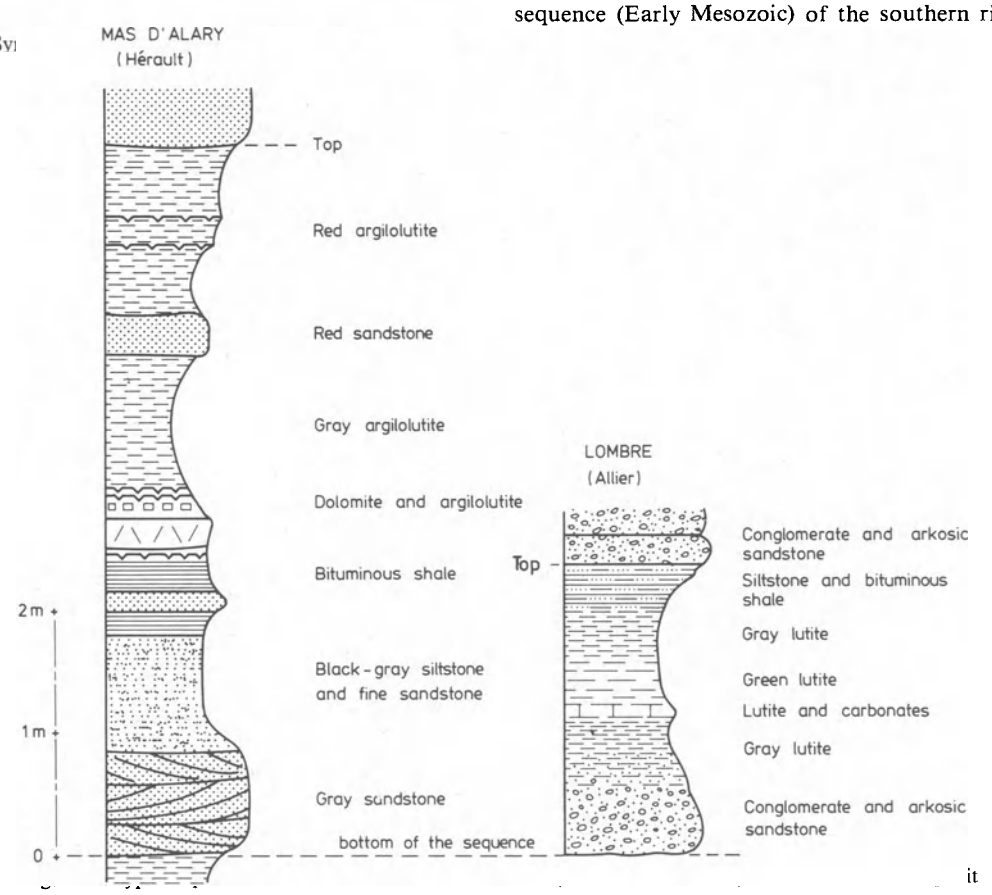

it

(COGEMA unpublished work)

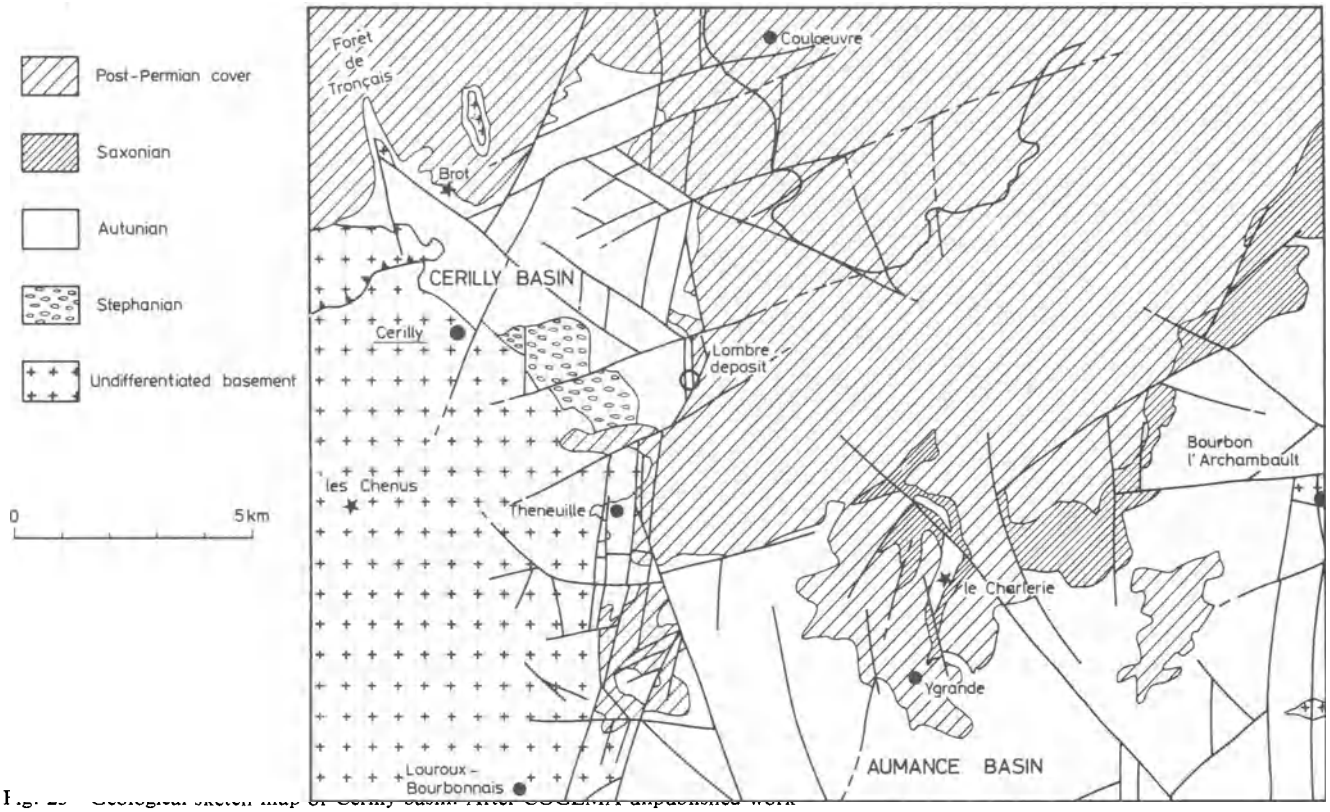

Basin (Fig. 24). At Cerilly, the Autunian reveals (from bottom to top):[9] a conglomerate with arkosic matrix (Mont conglomerate), 0–100 m thick; a grey Autunian (maximum thickness, 150 m) mostly composed of interbedding sandstones, siltites and clays, including two beds enriched in organic material; and an upper Autunian, composed of a unit with dominant red clay and ash-like kaolinitic sandstones.

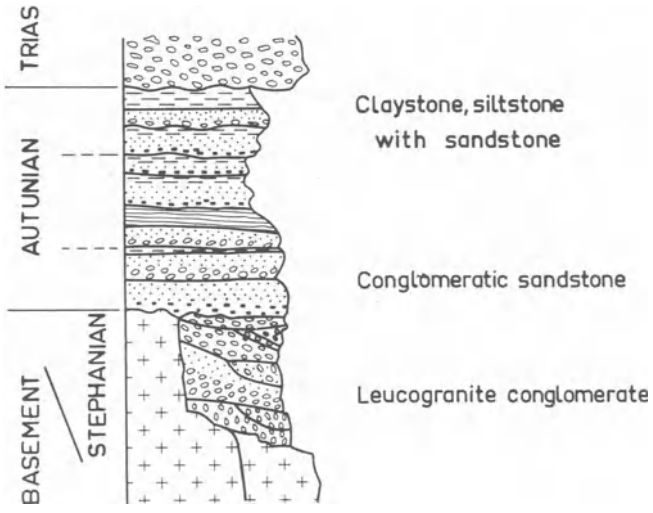

Fig. 24 Synthetic succession in Cerilly basin (Allier). After COGEMA unpublished work and Capus[9]

In the Cerilly basin Autunian sediments are immature and arkosic, but in the Aumance basin they are much more mature and are developing into lutites. The grey Autunian sediments, which carry the uranium mineralization of the Cerilly basin, arise from a torrential scattering type over the marginal swamps surrounding the edge of a larger basin (Aumance) during an active tectonic period (Fig. 25). The immature character of the sediments involves rapid transportation and weak mineral diagenesis. The palaeo-burial of these sediments is unlikely to be more than 200–300 m.[6]

The mineralization at Lombre occurs in lenticular orebodies associated with meandering fluviatile channels (Fig. 25). According to Brulhet *et al.*,[6] the loci of concentration occur along the banks (mainly on the convex banks where meander bars penetrate the silty surrounding environment enriched in organic materials) at the bottoms and tops of the channels. Mineralization occurs within fine-grained sediments with organic material, containing the channel system, but often extends into sandstones and conglomerates when enriched in iron sulphides and organic matter (synsedimentary or resulting from an early migration). The high grades are to be found in indentations of coarse sandstones into carbonated sediments and greenish lutites layers containing organic matter specks.

The fine-grained levels with organic matter are barren where they occur far from the fluviatile channels (a few tens of metres). The mineralization occurs as pitchblende and coffinite specks.

Other districts

In the European Permian sandstones other deposits occur in the Mecsek Mountains, Hungary, Zirovski Vrh, Yugoslavia, and Königstein, German Democratic Republic.

To date, only a small number of deposits are known in Europe in Triassic sandstones; the only notable prospect is located at Mazarate in the Guadalajara Province of Spain. Mineralization occurs in Lower Triassic red arkosic sandstones rich in volcanic debris and organic matter. Uranium appears as pitchblende and sooty pitchblende in reduced facies.

Uranium deposits in Cretaceous and Palaeogene sediments

Hamr deposit, Czechoslovakia

The Hamr deposit occurs in a Cretaceous basin of the Bohemian Massif, in Cenomanian sandstones of continental to epicontinental facies. Uraniferous mineralization occurs in coarse sandstones interfingered with siltites, covered with lutites, in local depressions and generally close to the unconformity. The

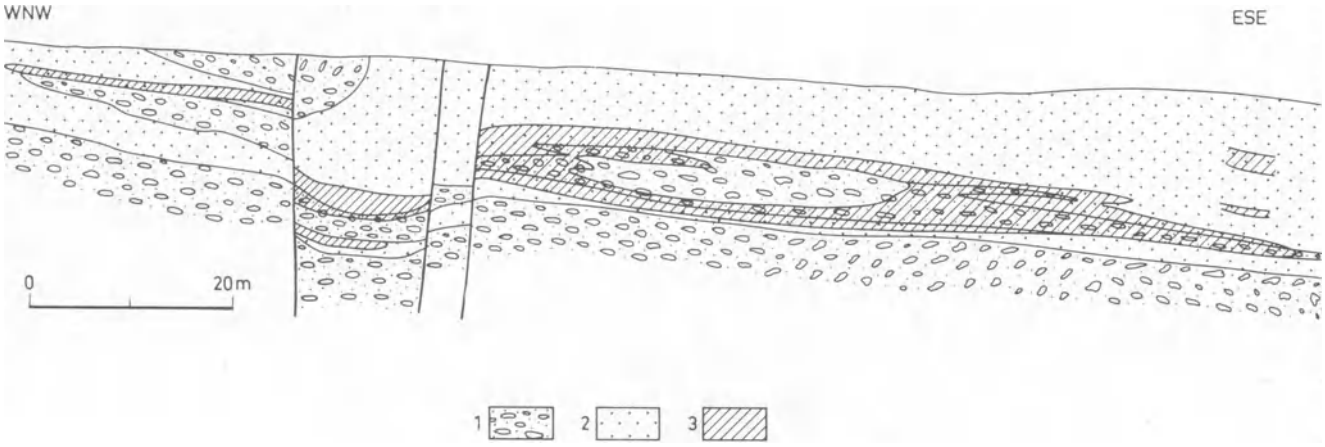

Fig. 25 Schematic cross-section of Lombre deposit (Allier). 1, Sandstone and conglomerate (fluviatile channel); 2, siltstone and finely laminated sandstone, lutite, sandstone tongues (lateral and paludal organic matter-rich sediments); 3, uranium ores. After Brulhet *et al.*[6]

average uranium content is as high as 0.2% and the main associated elements are titanium and, more notably, zirconium, which are more concentrated than uranium.

In the vicinity of the basaltic intrusives the boundaries of the deposits are locally parallel to them.

Saint-Pierre du Cantal deposit, Cantal, France

The deposit is located in sand lenses of a small Oligocene outlier. Present reserves are only 200 t, 1800 t of uranium having already been extracted at an average grade of 0.14% U. The Saint Pierre Oligocene outlier (3.5 km^2), preserved in a small rift valley trending NNW–SSE, rests on a peneplaned basement of metamorphic rocks and intrusive granites. The outlier is, on average, 20–30 m thick in the area of the deposit.[11] It is composed of a channel-shaped sandy member, additionally characterized by the occurrence of kaolinite and by considerable alkali leaching, and a silty argillaceous member, characterized by the stability of the inherited biotites and by the predominance of montmorillonite in a less leached and more alkali environment.

Both detrital members interfinger and progressively merge. They can be interpreted as fluviatile deposits of meanders over a flood plain. The uraniferous mineralization is totally controlled by sandy lenses of the channel-shaped member, two-thirds of the metal occurring in the lower sequence and the remainder in the upper. Uranium-bearing species are mainly phosphates and vanadates (francevillite-tyuyamunite, autunite, uranocircite); uranium is associated with selenium, arsenic, zinc and lead.

Coutras deposit, Gironde, France

In the north of the Aquitaine basin the Coutras deposit is located in Eocene argillaceous sandy sediments. Reserves amount to some 20 000 t U. This deposit, quite considerable in itself, is also particularly interesting in that it indicates that similar deposits may occur in formations that, to date, have seldom been prospected in Europe.

Uranium districts in the Alpine

At the present stage of reconnaissance at least, a striking feature of the Alpine orogen, from Western Europe to the Far East, is its paucity of uranium deposits and, with few exceptions (Siwaliks Formation in Pakistan, India, Bangladesh), almost all the Alpine uranium resources are located in Europe. Again, all the major deposits are found in Permian cover rocks that overlie Hercynian basement fragments. It is true that this setting does not occur east of Turkey in the Alpine Belt; in addition, the richest section of this belt in Europe is that of the Carpathian–Balkan region. We consider here as genuine Alpine uranium mineralization the deposits genetically related to the Alpine orogeny, that is uranium concentrations in metamorphic Permian sediments, in Alpine intrusives and in Tertiary and Pleistocene-Quaternary volcanics.

Uranium deposits related to Permian volcanosedimentary cover rocks

The best examples are those of the deposits of Novazza and Val Vedello in Italy.[43] Ruzicka[37] has described a deposit of this type in the Czechoslovakian West Carpathians—Spis–Gemer.

The volcanosedimentary Permian sequence overlies unconformably Middle Carboniferous graphitic shales. It contains basal conglomerates, sandstones and siltstones and is interbedded with tuffaceous horizons. The whole set was folded and faulted after ore deposition.

The volcanic activity was followed by pneumatolytic and hydrothermal processes. Mineralization occurs in tuffites, quartz porphyries and arkosic shales and is represented by pitchblende, molybdenite, chalcopyrite, tetrahedrite, galena, sphalerite, arsenopyrite, magnetite, ilmenite, hematite and supergene minerals. Surprisingly, according to Ruzicka,[37] there is no host-rock alteration.

Uranium districts related to Permian sedimentary cover rocks

A remarkable feature of European uranium geology is that, wherever continental or epicontinental Permian cover rocks are found, they contain uranium occurrences often of economic value. Apart from Italy,[43] many other areas can be mentioned.[28] Well known is the Yugoslav deposit of Georenja Vas–Zirovski Vrh in northern Slovenia.

The Permian here is in an unusual position, forming, together with the Permo-Carboniferous, an overthrusted pile of sheets lying on autochthonous Triassic carbonate rocks, subsequently folded and faulted. The deposit is in the Middle Permian so-called Groeden beds—sandstone, siltstone, clay and conglomerate. Their general colour is red, but in the lower parts grey and greenish facies occur, often with red intercalations. This last setting is characteristic of the mineralized section. The grey sandstone sequences are formed of three sedimentary cycles, uranium occurring in the upper, which starts with brecciated red conglomerate, resting on the red clastics of the top of the preceding cycle and followed by cross-bedded sandstones that contain organic matter and mineralization. Stratification is often obscured by tectonic cleavage of the rocks. The orebodies present very complicated '*S*' vertical sections resulting from the overthrusted emplacement of this sheet (Fig. 26). The foot- and hanging-walls of the orebodies are accompanied by red interfaces. In addition to this morphological complication, the distribution of the orebodies is very irregular. Mineralization is bound to three to five lenticular bands separated by interbeds of red slaty sandstone.

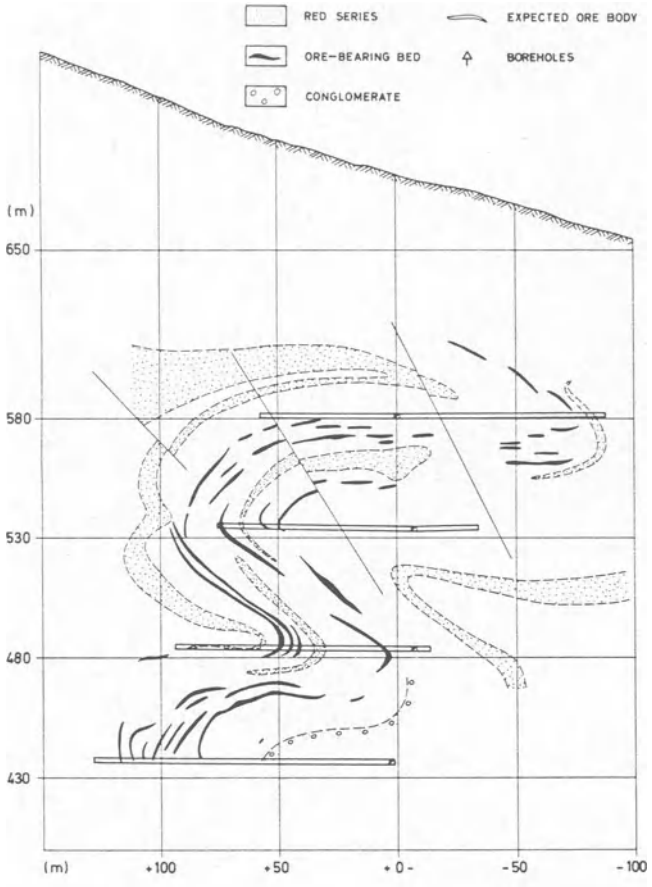

Fig. 26 Geological cross-section through Zirovski Vrh uranium deposit (recent interpretation). After Lukacs and Florjančič[28]

Fig. 26 Geological cross-section through Zirovski Vrh uranium deposit (recent interpretation). After Lukacs and Florjančič[28]

Uranium is contained mainly in pitchblende, impregnating the matrix of the sandstone with arsenopyrite, pyrite, galena, chalcopyrite and supergene minerals. There is a marked correlation between organic material and ore. The generally accepted genetic assumption is that uranium was primarily introduced in the sediments while they were being deposited or still lay in their original basin. It was redistributed later as a result of considerable tectonic deformation.

Deposits related to detrital Permian in the Alpine region of Europe are known in the Mecsek Mountains in the Pannonian Basin of Hungary and also in the southern and eastern Carpathians of Romania.

Uranium deposits related to Alpine granitoids

The single deposit of this type in the European Alpine occurs in an unspecified area of the Romanian Carpathians.[31] The area is built up of a pile of overthrust sheets on a crystalline basement partly covered by autochthonous Mesozoic carbonates. The lower sheet is formed of the same Mesozoic carbonates, followed by a Permian nappe of continental detrital Permian rocks interbedded with clay and rhyolitic volcanics. At the top occur two further sheets of crystalline rocks, the total thickness being 6000 m. The pile is intruded by an intermediate to acid volcanic complex followed by plugs of dioritic or alkaline granites (locally known as banatites) and, later, by lamprophyre, andesitic and quartz-porphyry dykes and sills.

Deposits of different elements are related in that area to magmatic activity—U, Mo, Bi, Cu, Pb, Zn and B. Uranium deposits occur as conformable lenticular orebodies made up of vein disseminations or stocks. Mineralization was preceded by strong alteration processes, including diopsidization, albitization, epidotization, zeolitization, chloritization, sericitization and silicification. The orebodies occur either in the metamorphic schists or in the Permian (and Werfenian ?) grey sandstone packs enclosed within red sandstones. There is no indication of the economic importance of the deposits.

Uranium deposits in epimetamorphic schists

Occurrences of this type were identified in the early 1950s in the Italian Western Alps and in the Savoy region of France. None has proved to be of economic value. More recently, the Forstau deposit in the Austrian Alps in the eastern margin of the famous 'tectonic window of the Hohe Tauern' was discovered.

Regional tectonic structure is extremely complicated: very roughly it can be represented as a huge pile of overthrust complexes of, from bottom to top, Helvetic nappes: non-metamorphic Trias; Lower Austro-Alpine nappes, the central zone of which contains the uranium-bearing Permian schists; Upper Austro-Alpine nappes (Triassic carbonates); super-Alpine nappes (Triassic special facies); and Dolomites (Julian Alps/ Triassic limestones and marls).

The Forstau deposit occurs within a narrow west–east belt of Permian schists, dipping 50–60°N and containing uranium anomalies along an extension of some 10 km. A 4-km section was explored by drilling and a 1000-m section by underground workings. Lenticular orebodies present horizontal extensions up to some 100 m and are contained in a belt 10–20 m thick. Unfortunately, the average grade is rather low (~ 700 ppm U); resources may exceed 1000–2000 t U.

The mineralized Permian varies from quartz schists to sericite (phengite) and chlorite schists. Mineralization, emphasized by hematitization, is formed of microscopic pitchblende, a titaniferous uranium mineral (uranium–titanium hydroxide (?)) with pyrite (and tetrahedrite (?)).

According to Petrascheck and co-workers,[34] the uranium mineralization could derive from an original preconcentration in Permian black shales subsequently remobilized during the Alpine metamorphism.

Owing to the persistence of reducing conditions the displacement from the original site to that of deposition may have been rather short and uranium reconcentrated in the shear zones and hinges of folds. According to M. Moreau (personal communication), these remobilizations and reconcentrations result from the pyrite–hematite buffer effect. Moreau compares this deposit with the Savoy occurrences, where the even stronger reducing conditions have more greatly limited the lengths of transfer.

Uranium deposits related to Tertiary and Pleistocene-Quaternary volcanics

The deposits linked to Pleistocene-Quaternary volcanics in Latium are not described here as they are dealt with elsewhere by Tedesco.[43]

Deposits related to the Tertiary volcanics are limited in the European Alps to the Macedonia area, where the main occurrence is that of Zletovska Reka in southeast Yugoslavia. This area is located in the northwest of the Rhodope Massif, which is a fragment of the cystalline metamorphic Hercynian basement. It underwent major volcanic activity from the Eocene, which developed in three phases.[35] The first phase was characterized by andesitic flows covering extensive areas, accompanied by pyroclastics (tuffs, breccias). The second phase produced dacitic ignimbrites and the third corresponds to the intrusion of green, partly propylitized, andesites and dacite, latite, dacite-andesites and even quartz monzonite. The area was submitted to strong faulting, to which the volcanic activity was related, with major trends NNW and ENE–EW with very steep dips.

Hydrothermal activity was controlled by the NNW trend in respect of sulphide deposits (mainly Zn–Pb), but the uranium deposits of Zletovska Reka were controlled by the ENE–EW system.

Alteration is intensely developed—propylitization, carbonitization, argillitization, chloritization, sericitization, silicification, alumitization and zeolitization.

Uranium mineralization is mainly pitchblende, occurring as veinlets and stains along fracture zones. It is accompanied by sphalerite and, sometimes, by pyrite and galena.

The deposit is of rather low grade—a few hundred ppm—and publicly stated resources are of several hundred tons of uranium.

Concluding remarks

In comparison with each of the major uranium provinces that of Europe is not insignificant (see De Vivo and Ippolito).[44] Some 35 years after the start of nuclear energy development entire European geological megastructures remain virtually unexplored—the Caledonian orogen and its cover rocks, the Fennoscandian Shield, Hercynian outcrops in Germany, Italy and their cover rocks, the Western Alpine orogen, etc. In recent years a considerable effort has been made, strongly supported in most member states by a European Economic Community subsidy system. Favourable results can therefore be expected within the next few years. Many types of deposits may be discovered and special attention should be devoted to the variants of vein-type deposits in general metamorphic environments. In spite of the fact that they are usually much more difficult to identify and define at our present stage of experience, they appear to be quite promising for the future.

Naturally, deposits related to fine- and coarse-grained detrital sediments may conceal large additional resources in Europe. Again, it appears that in our province the ore controls may considerably differ from the conventional controls that characterize the North American scene. In addition, economic concentrations are necessarily hidden by more or less thick barren rock or water cover. Even in better explored areas, such as France, new resources in such conditions can be foreseen. They are, nevertheless, almost inaccessible with present techniques. A tremendous effort in the field of uranium geology and exploration techniques is therefore necessary. Equally, significant progress in ore-treatment processes could rehabilitate not insignificant resources in the refractory or argillaceous ores that exist in Europe.

References

1. Adamek P. M. and Wilson M. R. The evolution of a uranium province in northern Sweden. *Phil. Trans. R. Soc. Lond.*, **A291**, 1979, 355–68.
2. Aubouin J. Propos sur les géosynclinaux. *Bull. Soc. géol. France, 7^e Sér.*, **3**, 1961, 629–702.
3. Autran A. L'évolution structurale du Protérozoïque aux distensions post-hercyniennes. In *Evolutions géologiques de la France* Autran A. and Dercourt J. eds. *Mém. BRGM* no. 107, 1980, 10–17. *(Colloquium C7, 26th Int. geol. Congr.)*
4. Autran A. and Guillot P. L. L'évolution orogénique et métamorphique du Limousin au Paléozoïque (Massif Central Français). *C.R. Séanc. Acad. Sci. Paris*, **D280**, 1975, 1649–52.
5. Bach A. Evolution dans les conditions d'affleurements de shales uranifères a matière organique. Thèse, E.N.S.G., Nancy, 1980.
6. Brulhet J. *et al.* Gisements d'uranium dans le Permien d'Europe (France, Italie, Suisse). *Sciences Terre*, **23**, no. 4 1979, 1–33. *(Excursion guide, 26th Int. geol. Congr.)*
7. Bültemann H. Die Uranvorkommen im ostbayerischen Grundgebirge Raum Mähring, Krs. Tirschenreuth/Opf. *Z. dt. geol. Ges.*, **130**, pt 2 1979, 575–96.
8. Capdevila R. Corretgé G. and Floor P. Les granitoïdes varisques de la Meseta Iberique. *Bull. Soc. géol. France, 7^e Sér.*, **15**, 1973, 209–28.
9. Capus G. Matières organiques et minéralisations uranifères: exemples des bassins permo-carbonifères de l'Aumance (Allier) et de Lodève (Hérault). Thèse, E.N.S.G., Nancy, 1979.
10. Cariou L. Les gites et indices uranifères des régions médianes et sud du Massif Central Français. In *Les minerais uranifères français, tome III* Roubault M. ed. (Paris: Presses Universitaires de France, 1964), 10–162.
11. Carre J. L. Les minéralisations uranifères des dépôts oligocènes de Saint-Pierre (Cantal—France) dans leur cadre géologique régional et local. Thèse, 3ème cycle, Nancy, 1979.
12. Cathelineau M. Les gisements d'uranium liés spatialement aux leucogranites sudarmoricains et à leur encaissant métamorphique: relations et intéractions entre les minéralisations et divers contextes géologiques et structuraux. Thèse, Nancy, 1981.
13. Chenevoy M. Contribution à l'étude des schistes cristallins de la partie nord-ouest du Massif Central français. *Mém. Serv. Carte géol. Fr.*, 1958, 428 p.
14. Cuney M. Geologic environment, mineralogy, and fluid inclusions of the Bois Noirs Limouzat uranium vein, Forez, France. *Econ. Geol.*, **73**, 1978, 1567–610.
15. Ertle H. J. Kneuper G. and Müller H. Sedimentary uranium occurrences in the Upper Carboniferous of the northern Black Forest. In *Recognition and evaluation of uraniferous provinces* (Vienna: IAEA, 1977), 217–27.
16. Faure J. Le gisement uranifère des Bois-Noirs (Loire): le piège structural. *Sciences Terre*, **13**, no. 3 1968, 235–56.
17. Fernandez Polo J. A. Genesis de los yacimientos uraniferos en metasedimentos de Salamanca (España). In *Uranium exploration geology* (Vienna: IAEA, 1970), 243–52.
18. Gagnadre A. Ensemble minier de Fanay. Internal report, Division de la Crouzille (COGEMA), 1976.
19. Geffroy J. and Sarcia J. A. La notion de "gîte épithermal uranifère" et les problèmes qu'elle pose. *Bull. Soc. géol. Fr., 6^e Sér.*, **8**, 1958, 173–90.
20. Julivert M. Martinez F. J. and Ribeiro A. The Iberian segment of the European Hercynien foldbelt. In *Geology of Europe* Cogné J. and Slansky M. eds. *Mém. BRGM* no. 108, 1980, 132–58. *(Colloquium C6, 26th Int. geol. Congr.)*
21. Kossmatt F. Gliederung des varistischen Gebirgebaues. *Abh. sächs. geol. Landesamts*, 1927, 1–39.
22. Landais P. and Connan J. Relation uranium-matière organique dans deux bassins permiens français: Lodève (Hérault) et Cerilly-Bourbon l'Archambault (Allier). *Bull. Centre Rech. Explor. Prod. Elf-Aquitaine* 4, 1980, 709–57.
23. Laversanne J. Sédimentation et minéralisation du Permien de Lodève, Hérault. Thèse, Université Paris Sud, 1976.
24. Laversanne J. Le Permien de Lodève (Massif Central français). Evolution des dépôts autuniens et exemples de minéralisations uranifères diagénétiques et postdiagénétiques par circulation de solutions exogènes. In *Concentrations métalliques et milieux confinés* Busson G. ed. *Sciences Terre*, **22**, no. 2 1978, 147–66.
25. Leroy J. Metallogénèse des gisements d'uranium de la division de La Crouzille (COGEMA-Nord Limousin—France). *Mém. Sciences Terre* no. 36, 1978, 276 p.
26. Lindroos H. and Smellie J. A stratabound uranium occurrence within middle Precambrian ignimbrites at Duobblon, northern Sweden. *Econ. Geol.*, **74**, 1979, 1118–30.
27. Lotze F. Die iberische Halbinsel. *Geol. Jb.*, **4B**, 1942, 245–57.
28. Lukacs E. and Florjančič A. P. Uranium ore deposits in the Permian sediments of northwest Yugoslavia. In *Formation of uranium ore deposits* (Vienna: IAEA, 1974), 313–29.
29. Marquaire Ch. and Moreau M. Esquisse géologique du Nord-Limousin et répartition des minéralisations uranifères. *Rapport CEA* R 3684, 1969, 7–40.
30. Moreau M. L'uranium et les granitoïdes: essai d'interprétation. In *Geology, mining and extractive processing of uranium* Jones M. J. ed. (London: IMM, 1977), 83–102.
31. Nitu G. Les conditions tectono-magmatiques de la formation des gisements d'uranium de Roumanie. Reference 28, 679–92.
32. Dardel J. *et al.* Gisements d'uranium dans les schistes péribatholitiques (type ibérique) et dans les leucogranites (type limousin) (Portugal, Espagne, France). *Sciences Terre*, **23**, no. 4 1979, 37–81. *(Excursion guide, 26th Int. geol. Congr.)*
33. Peterson A. Ranstad—a new uranium-processing plant. In *Processing of low-grade uranium ores* (Vienna: IAEA, 1967), 193–209.
34. Petrascheck W. E. Erkan E. and Siegl W. Type of uranium deposits in the Austrian Alps. Reference 30, 71–5.
35. Radusinović D. Zletovska Reka uranium deposit. Reference 28, 593–601.
36. Ranchin G. La géochimie de l'uranium et la différenciation

granitique dans la province uranifère du Nord-Limousin. *Mém. Sciences Terre* no. 19, 1971, 394 p.
37. Ruzicka V. Geological comparison between East European and Canadian uranium deposits. *Pap. geol. Surv. Can.* 70-48, 1971, 196 p.
38. Santouil G. Tectonique et microtectonique comparée de la distension permienne et de l'évolution post-triassique dans les bassins de Lodève, St. Affrique et Rodez (France SE). Thèse, 3ème cycle, Université de Monpellier, 1980.
39. Sarcia Jean A. and Sarcia Jacqueline A. Les gites d'uranium du Nord-Limousin. *Mém. Sciences Terre* no. 4, 1956, 239–306.
40. Sass J. H. *et al.* Heat flow and surface radioactivity at two sites in South Greenland. *J. geophys. Res.*, 77, 1972, 6435–44.
41. Sørensen H. *et al.* The uranium deposit at Kvanefjeld, the Ilímaussaq intrusion, South Greenland. *Rapp. Grønlands geol. Unders.* no. 60, 1974, 54 p.
42. Stettner G. Der Grenzbereich Saxothuringikum–Moldanubische Region im Raum Tirschenreuth–Mähring (Oberpfalz) und die Situation des Uran-führenden Prekambriums. *Z. dt. geol. Ges.*, **130**, pt 2 1979, 561–74.
43. Tedesco C. Uranium deposits in Italy. In *Uranium geochemistry, mineralogy, geology, exploration and resources* De Vivo B. *et al.* eds (London: IMM, 1984), 179–88.
44. De Vivo B. and Ippolito F. Uranium in the economics of energy. Reference 43, 162–6.

Uranium in the economics of energy*

B. De Vivo
Centro di Studio per la Geocronologia e la Geochimica delle Formazioni Recenti, CNR, Istituto di Geochimia, Rome, Italy

F. Ippolito
Istituto di Geologia e Paleontologia, Rome, Italy

Studies into the use of fissile elements and uranium for the production of atomic weapons in particular and of energy in general were initially kept a strict secret when research was begun during the second world war. Even after the war, until 1952, the U.S.A., which possessed almost all the scientific and technological information on the refining and uses of uranium, kept its knowledge even from its most loyal allies. The MacMahon Act forbade the U.S.A. from giving any help, which included the transfer of information and technology, to any other country.

American policy was rapidly changed, however, when the Russian thermonuclear explosion in 1953, preceded to a lesser degree by progress in work carried out in England, France and Scandinavia, showed clearly that the American monopoly had come to an end.

In December, 1953, President Eisenhower, in his historic speech at the United Nations, announced his 'Atoms for Peace' programme, and the UN became the promoter of the first world conference, held in Geneva in the summer of 1955, on the use of nuclear energy for peaceful purposes. From 8 to 20 August of that year 1700 delegates, 3000 observers and some 1000 journalists exchanged technical and economic information on all the problems connected with the use of nuclear energy in peace time, mainly for the production of electrical power. Thus, all the barriers that until then had existed in this field were broken down. Reserve was maintained, however, in two fields—those of military application and, among the Soviet bloc countries, the quantitative evaluation of uranium (and thorium) mineral resources.

As a result of this change in policy, the second UN Geneva conference, held in 1958, led to the creation of IAEA (International Atomic Energy Agency), which was intended to be a kind of 'uranium bank' with responsibility for the inspection of the safety of all nuclear plants in use in various countries to guarantee the use of uranium for 'peaceful' purposes. At the same time the 1958 Rome Treaty, signed by the six European countries that had previously combined to form the European Coal and Steel Community (ECSC), led to the establishment of the European Atomic Energy Community (EAEC).

Both the ECSC and the EAEC were later amalgamated in the vaster and more comprehensive European Economic Community (EEC), of which ten countries are now members. In the euphoria of the détente of the late 1950s, however, neither the IAEA nor the EAEC—Euratom—developed in the way that their founders had intended.

Among the various aims that were associated with the launching of the 'Atoms for Peace' programme the U.S.A. clearly intended not only to achieve an industrial and commercial exploitation, in a monopoly regime, of the technology stored up in the military field but also to control the industrial development of the other countries, though at that time there was not a high demand for nuclear energy, oil dominating the energy scene with a market price of about $2.00 a barrel. This state of affairs was abruptly turned upsidedown with the 1973 Arab–Israel crisis, when the price of oil began to soar, automatically rendering nuclear energy competitive.*

The American trend conflicted strongly with the interests of the other industrialized countries, however, since many of them had acquired, in a little more than a decade, the necessary technology and technicians to compete in the world markets with American industries.

This possibility of competing technologically with the U.S.A. meant that some of the countries, by carrying out national nuclear programmes, were not confined to a subordinate political role. This happened, though, where strong and farsighted politicians took the right decisions at the right time, whereas other industrialized countries are still paying for not selecting the 'nuclear' option during the 1960s after the euphoria of the preceding years, and they are forced to accept a subordinate economic and political role.

In that regard the case of Italy in emblematic. In 1963 that country already had three nuclear power plants, which indicated possession of an advanced nuclear technology. Nevertheless, because of refusing the 'nuclear' option, despite the lack of conventional sources of energy, Italy became an importer country, subject to heavy restrictions as regards its own industrial development.

In this regime of competition orders for the construction of nuclear power plants awarded to the U.S.A., which still maintains an important supremacy over other countries in terms of availability of uranium, advanced technology and enrichment plants, decreased from 85% in 1972 to 40% in 1976.

Time has shown quite clearly that the continuous oil crisis makes recourse to uranium more and more necessary, but the quantitative and qualitative expansion of nuclear power plants has led to greater reflection on the problems that surround nuclear energy. In this sense the anti-nuclear movement has not been completely negative as it has prevented attention from being focused exclusively on nuclear energy and has shown the importance of other energy sources—which are, however, integrative not alternative—such as solar and geothermic and a return to coal.

Reserves and resources

Uranium, relatively abundant in the earth's crust, being present on average at a concentration of 4 ppm, is also present in sea water at concentrations of the order of 0.003 ppm. Enormous resources of uranium are therefore available, ocean waters containing an amount equal to some thousand million tons. The effective available uranium resources are, however, estimated on the basis of deposits that contain higher concentrations from which uranium can be extracted at various costs, though not more than $130/kg. On this basis the 'reasonably assured' and 'additional estimated' uranium resources are shown in

*Since 1958, however, the results of a study carried out in Italy and sponsored by the World Bank (IBRD) were presented at the second Geneva conference. The study predicted the cost of nuclear-generated electricity becoming competitive with that of oil-generated electricity within a few years. Hence, on the basis of this study, Italy was granted a loan by the World Bank for the construction, by means of international tender, of a 150-MW nuclear power plant.

Tables 1 and 2 for different geographic areas. The data are expressed in physical (tons) and not energetic units as, for uranium, the 'calorific power' cannot be defined unequivocally.

Table 1 Reasonably assured resources, ton $\times 10^3$ U[1]

Cost range	<$80/kg U	$80–130/kg U	Total at <$130/kg U
Algeria	26	0	26
Argentina	25	5.3	30.3
Australia	294	23	317
Austria	0	0.3	0.3
Brazil	119.1	0	119.1
Canada	230	28	258
Central African Republic	18	0	18
Chile	0	0.02	0.02
Denmark	0	27	27
Finland	0	3.4	3.4
France	59.3	15.6	74.9
Gabon	19.4	2.2	21.6
Germany, Federal Republic of	1	4	5
Greece	1.4	4	5.4
India	32	0	32
Italy	0	2.4	2.4
Japan	7.7	0	7.7
Korea, Republic of	0.04	11	11.04
Mexico	2.9	0	2.9
Namibia	119	16	135
Niger	160	0	160
Portugal	6.7	1.5	8.2
Somalia	0	6.6	6.6
South Africa	247	109	356
Spain	12.5	3.9	16.4
Sweden	0	38	38
Turkey	2.5	2.1	4.6
U.S.A.	362	243	605
Zaire	1.8	0	1.8
Total (rounded)	1747	546	2293

Table 2 Estimated additional resources, ton $\times 10^3$ U[1]

Cost range	<$80/kg U	$80–130/kg U	Total at <$130/kg U
Argentina	3.8	9.6	13.4
Australia	264	21	285
Austria	0.7	1	1.7
Brazil	81.2	0	81.2
Canada	358	402	760
Chile	0	6.7	6.7
Denmark	0	16	16
Egypt	0	5	5
France	28.4	18.1	46.5
Gabon	0	9.9	9.9
Germany, Federal Republic of	1.5	7	8.5
Greece	2	5.3	7.3
India	0.9	24.2	25.1
Italy	0	2	2
Mexico	3.5	2.6	6.1
Namibia	30	23	53
Niger	53	0	53
Portugal	2.5	0	2.5
Somalia	0	3.4	3.4
South Africa	84	91	175
Spain	8.5	0	8.5
Sweden	0	44	44
United Kingdom	0	7.4	7.4
U.S.A.	681	416	1097
Zaire	1.7	0	1.7
Total (rounded)	1605	1115	2720

On the basis of these estimates Western countries (the resources of the U.S.S.R., China and Eastern Europe are not known) should be able to count on about 5 000 000 ton of uranium that can be extracted at costs of not more than $130/kg, of which about 3 300 000 ton is extractable at costs of less than $80/kg.

The OECD–IAEA estimates[1] agree with those which were presented at the World Energy Conference held in Munich in September, 1980, which indicated values of 2 200 000 ton for the 'reasonably assured' resources and global values of 4 000 000 ton for those resources which can be exploited economically.

One ton of completely fissioned uranium provides in energy terms about 2 Mtep (million tons equivalent petroleum), so the 5 000 000 ton of uranium at a low extraction cost would give, if used in light water reactors (energy yield = 0.5%), about 250 000 Mtep of thermic energy. That is equivalent to, in terms of quantity, known and estimated oil resources.

Table 1 shows that the U.S.A. and Canada alone possess approximately 36% of total world reserves, excluding China, the Soviet Union and Eastern Europe.

The entity of uranium resources, because of the very nature of the deposits, is, on the other hand, strictly linked to the cost of extraction. This is true, generally speaking, of all minerals, but is particularly relevant for uranium. If gradually higher extraction costs are accepted, larger quantities of low uranium concentration become available—for example, from materials such as schists and granites, where the uranium concentrations range from 80 to 10 ppm.

Besides the resources estimated at $130/kg there exist other uranium sources, generally with a lower content and at a higher extraction cost. These are either an extension of conventional uranium deposits cultivated at $130/kg or conventional deposits the extraction cost of which exceeds $130/kg because of their limited size, deep location or presence in remote areas. Examples of these additional uranium sources are the vast high-cost resources associated with the Elliot Lake deposits in Canada, the 5000–10 000 ton of uranium at costs of more than $130/kg in Italy, the 12 000 ton contained in granitic rocks at a cost of $130–$260/kg in Namibia, the 141 000 ton contained in the conglomerates and the 46 000 ton in the surface sediments in South Africa at a cost of $130–$260/kg and the vast quantities of uranium contained in the sandstones of Colorado, Wyoming and New Mexico.

Other additional uranium sources, associated with unconventional deposits or exploited as a by-product of other minerals (e.g. copper and gold), are those found in old mine dumps (gold mines in South Africa), phosphate rocks (Morocco, the U.S.A. and the U.S.S.R.), with a content ranging from 0.001 to 0.07%, in copper deposits, such as the 'porphyry coppers', in marine black shales with a content ranging from 0.001 to 0.008% (the U.S.A. and Sweden), in coal and lignite deposits with a content normally of 0.001%, exceptionally reaching 1% (the U.S.A.), in monazite deposits with 0.3% (India, Brazil, Australia and Malaysia), in igneous rocks, such as the alkaline intrusives distributed in various parts of the world, and, as has already been mentioned, in sea water.

September, 1980, World Energy Conference estimates gave additional figures of 13 000 000 ton of uranium present in minerals (schists) with a uranium content ranging from 25 to 80 ppm.

The importance of considering ore deposits with such high extraction costs is apparent when one compares the enormous amounts of energy produced by nuclear fuel with the amounts produced by conventional fuels. In fact, the energy content of a conventional fuel, like coal, oil or natural gas, is an intrinsic property of the same and is equal to the quantity of energy freed

during the combustion of a unit of weight of the fuel (calorific power). On the other hand, in the case of nuclear fuel, the energy produced depends not only on the amount of combustible material contained in the unit of weight but also on the particular characteristics of the process used to obtain the energy.

The characteristics of the reactor and the combustion cycle used bring about an important variation in the energy that is obtained from the unit of weight of the starting material. There exists a ratio of about 100 between a light water reactor with no recycling of the unburnt fissile and a fast reactor that completely recycles plutonium. Although the former exploits barely 0.5% of the potential energy contained in natural uranium, the latter can exploit from 40 to 60%.

Thus, the fast reactors yield, using only those uranium resources which are economically exploitable (in light water reactors) 25000 billion tep of thermic energy; if it is remembered that the use of fast reactors makes high-cost extraction deposits economically exploitable, and perhaps even sea water, it is clear how this kind of reactor is able to provide practically inexhaustible quantities of energy.

World uranium production (Western countries)

From 1943 to 1960 uranium production was mainly concerned with military aims. From 1960 to 1975 uranium production was kept at a stable level of about 20000 ton/year, increasing to about 44000 ton/year in 1981 (Table 3).

Of the above production, 70% is attributable to the main producer countries (the U.S.A., Canada and South Africa). As regards estimates for the coming decades, production will obviously be linked to market demand: the OECD–IAEA report[1] estimated a production of about 72000 ton/year in 1985 and about 70000 ton/year in 1990 (Table 4). Naturally, before such production levels can be reached the growth of the nuclear energy industry must become stable so that the mining companies enjoy the incentive necessary to make long-term investments in the finding and developing of new mineral deposits.

As regards the substitution of oil power plants by nuclear power plants, some important data follow concerning the principal European countries. The contribution of the primary sources to the production of electrical energy will be 75% in France in 1990, 40% in West Germany, more than 20% in Great Britain and less than 10% in Italy. The corresponding

Table 3 Uranium production, ton U[1]

Country	Pre 1977	1977	1978	1979	1980	1981 (planned)
Argentina	340	100	126	134	187	180
Australia	8159	356	516	705	1561	2600
Brazil	0	0	0	0	0	100
Canada	112180	5790	6800	6820	7150	8400
Finland	30	—	—	—	—	—
France	23133	2097	2183	2362	2634	2824
Gabon	8464	907	1022	1100	1033	1000
Germany, Federal Republic of	151	15	35	25	35	n.a.
Japan	38	3	2	2	5	3
Namibia	594	2340	2697	3840	4042	3939
Niger	6183	1609	2060	3620	4100	4500
Portugal	1932	95	98	114	82	107
South Africa	75332	3360	3961	4797	6146	6700
Spain	476	177	191	190	190	145
U.S.A.	209800	11500	14200	14400	16800	13500
Zaire	25600	0	0	0	0	0
Total	472237	28891	33891	38109	43965	43998

Table 4 Attainable production capabilities, ton U[1]

Country	1981	1982	1983	1984	1985	1986	1987	1988	1989	1990
Argentina	180	240	240	240	500	500	500	500	500	500
Australia	2600	4500	4500	4500	3800	6000	6000	5200	4700	4700
Brazil	100	n.d.	n.d.	n.d.	n.d.	n.d.	n.d.	n.d.	n.d.	n.d.
Canada	8400	9500	10800	14800	14700	14000	12900	12300	11500	10500
Central African Republic	0	1000	1000	1000	1000	1000	1000	1000	1000	1000
France	3706	3900	3900	3900	3900	4050	4050	4050	4050	4050
Gabon	1000	1200	1500	1500	1500	1500	1500	1500	1500	1500
Germany, Federal Republic of	40	40	40	?	?	?	?	?	?	?
India	200	200	200	200	200	200	200	200	200	200
Italy	—	—	—	—	—	—	170	170	170	170
Japan	30	30	9	9	9	9	9	9	9	9
Mexico	—	212	593	593	593	539	593	394	394	276
Namibia	3939	3923	3923	3923	3923	4154	4154	4154	4154	4154
Niger	4500	4500	5800	8000	10500	12000	12000	12000	12000	12000
Portugal	107	126	126	126	346	346	346	346	346	346
South Africa	6700	7200	7800	8200	8000	7900	7800	7800	7700	7600
Spain	145	110	110	110	382	670	797	882	967	1052
U.S.A.	17100	16900	19500	20500	23000	24700	23500	23000	22300	21800
Yugoslavia	—	100	100	100	220	220	220	220	220	370
Total	48747	53681	60141	67701	72573	77842	75685	73725	71710	70227

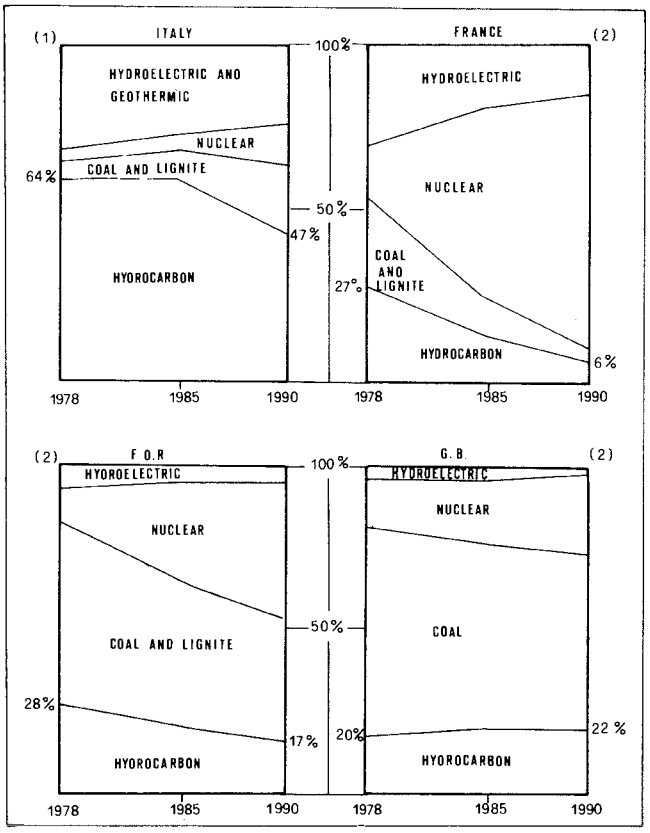

Fig. 1 Percentage contribution of primary sources to production of electric power. For France, FDR and UK data produced by ENEL on basis of Unipede CEE Committee (August–September, 1979) document following operative programmes indicated by these Community countries[6]

percentages for hydrocarbons (gas + oil) will be 6, 17, 22 and 47 (Fig. 1). In Belgium, by 1985, nuclear-generated electricity will reach 58% (by means of eight PWR plants), whereas hydrocarbon (gas + oil)-generated electricity will be only 17% and coal-generated 23%.*

It should also be borne in mind that in 1980 the cost of electric energy in Western Europe, taking 1 as the cost of a nuclear kilowatt, is about 1.7–1.8 for coal and more than 2.5 for oil.

Uranium market

Between 1950 and 1960 uranium transactions were carried out mainly for military purposes and at prices of the order of $10/lb U_3O_8. Between 1960 and 1972 the price of uranium dropped to $6/lb as a result of the reduced demand for uranium for military purposes and only limited demand for peaceful uses. The 1973 oil crisis caused the price of uranium to soar to $24/lb in 1974. The price of uranium continued to rise from 1974 to 1979, when it reached more than $40/lb. The sharp decline in the demand for uranium, owing to the well-known difficulties in carrying out nuclear programmes, has meant that during the last few years the price of uranium has fallen to less than $40/lb ($30/lb on the European market). The future uranium market will, of course, be influenced by a series of factors, such as orders for new reactors, stockpiling, uranium and plutonium recycling, increased production capacity and the appearance on the market of new producer countries.

Need for uranium

The most reliable estimates on the short- and medium-term need for uranium can be found in documents of the INFCE Working Groups. These estimates hypothesize that electro-

*PWR, pressurized water reactor; LWR, light water reactor; FBR, fast breeder reactor.

Table 5 Estimates of installed electro-nuclear power plants from 1985 to 2025 (GWe), excluding U.S.S.R., China and Eastern Europe[1]

Year	Low growth	High growth
1980	124	126
1985	232	258
1990	361	401
1995	451	562
2000	585	804
2005	725	1120
2010	880	1503
2015	1034	1928
2020	1180	2366
2025	1311	2794

nuclear power will increase from the present ≃ 130 GWe to 590 GWe (low growth) or 800 GWe (high growth) in the year 2000 and to 1300 GWe (low growth) or 2800 GWe (high growth) in the year 2025 (Table 5 and Fig. 2).

The significant divergence between low and high growth indicates the uncertainties that exist in forecasting the increase in energy consumption. This divergence becomes even more apparent when the two growth conditions refer to the medium–long term (from the year 2000 to 2025).

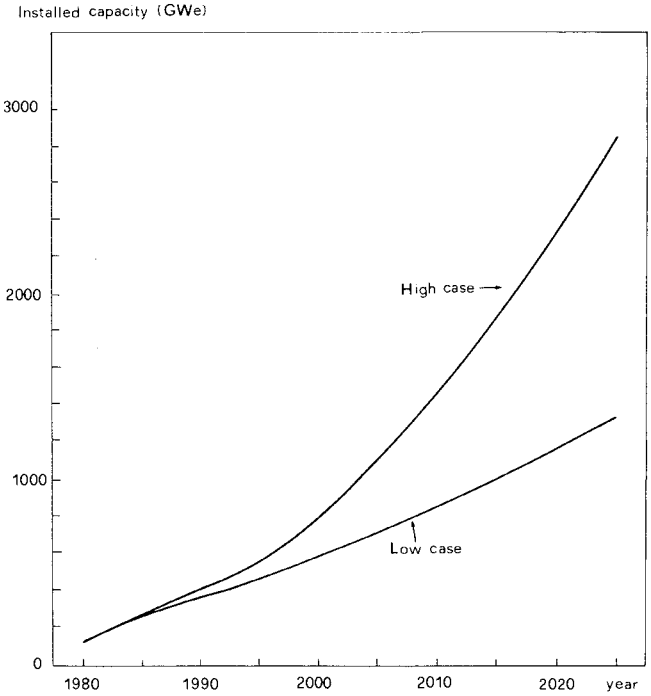

Fig. 2 World installed nuclear capacity (1980–2025), excluding the U.S.S.R., China and Eastern Europe[1]

The evolution in the demand for uranium in the period 1980–2025 obviously depends not only on the electro-nuclear capacity that will be installed but also on other factors, the most important of which is the type of reactor used (light water, heavy water or fast breeder).

The INFCE study hypothesizes various possible strategies (preserving for each one the hypothesis of a high and low growth in the demand for electricity) ranging from the use of open-cycle LWR alone to considerable penetrations of the FBR (3.6% in the year 2000; from 26 to 80% in the year 2025).

The results of this complex analysis show that the annual production of natural uranium in the year 2000 will range from

a minimum of 90000 to a maximum of 200000 ton/year, and in the year 2025 from a minimum of 50000 to a maximum of 600000 ton/year.

Another interesting result of the INFCE analysis is the cumulative need of natural uranium for the various strategies considered. This need ranges from 1 300000 to 2 200000 ton in the year 2000 and from 3500000 to 12000000 ton in the year 2025.

The minimum production and cumulative need values naturally refer to an extensive use of fast reactors; the maximum values to the use of open-cycle LWR reactors alone. These data, related to the economically exploitable uranium resources, show that no problems of uranium supply should exist before the year 2000; thereafter the choice of an adequate strategy (including, if possible, a non-marginal use of FBR) becomes fundamental in providing a satisfactory answer to the problems of fuel supply.

Nuclear proliferation

'Nuclear proliferation' indicates the spread of nuclear knowledge and technology that, though initially may be for the use of nuclear energy for peaceful purposes, can eventually enable many nations, even those of the Third World, to build their own nuclear weapons. The INFCE report dwelt mainly on this subject, but perhaps, in conclusion, the most *sensitive* points regarding the *proliferation* of the nuclear fuel cycle should be examined here.

The sensitive points with regard to the risks of illegal action to which a government may be subject have been listed by Simen:[5] unrefined fuel containing enriched uranium or plutonium; uranium enrichment; reactors; stockpiling of irradiated fuel; reprocessing, including stockpiling, of the plutonium produced and the production of mixed uranium and plutonium oxide fuels; waste disposal or disposal of the irradiated not reprocessed fuel.

The risk of transporting fuel was considered essentially as that of theft, but this would still be a violation of the internal rights of the country involved.

As far as the first point is concerned, unrefined fuel, obviously excluding any risks for the fuel containing natural uranium, is declared as unsuitable for weapons, even though insufficiently enriched for use in the existing nuclear power plants that use ordinary water; but highly enriched fuel used in some research reactors is considered as very sensitive.

Mixed oxide unrefined fuel, used both in thermic and in fast reactors, should also be considered as sensitive as it can contain up to 20% plutonium.

The material that is found in enrichment plants is to be considered as sensitive because of its possible illegal transfer to other plants capable of enriching it until the material becomes of weapon grade.

It should be noted, however, that plants that enrich the material for existing commercial reactors do not exceed an enrichment of 3–4% of fissile content, whereas weapon-grade enrichment is closer to 100%. It is also true, however, that the technological knowledge that is required for the setting up of a commercial plant can be profitably used for the construction of one for military aims and that the relative difficulties in time are reduced. As regards the kind of technology used, such as ultra-centrifugation, gaseous diffusion and chemical enrichment, from the proliferation risk standpoint the advantages and disadvantages of the various kinds balance.

Nuclear reactors as sources of proliferation pose one of the most significant points of the whole study, since it relates to one of the problems that brought into being the study itself. It is common knowledge that the U.S.A., in order to stem the proliferation of nuclear weapons, has taken as its target the development of fast reactors, because such technology activates the plutonium cycle, and, secondly, the reprocessing of irradiated fuel from which plutonium is obtained. It is just as well known that this aspect of American policy has caused much anti-American controversy in some European countries, which, having no or very few uranium resources, rightly see in the fast self-fertilizing reactors a chance to multiply by fifty- or sixty-fold the energy potential of the fuel cycle.

Pursuing the aim of energy-independence, or at least trying to loosen the oil vice, is undoubtedly respectable and worthy of international protection for the reasons of world balance mentioned above. Not so respectable is the goal of absolute supremacy of some countries in decisions regarding the export of technology and materials, especially to the world's 'hot' areas. Maintaining that from the proliferation standpoint the introduction of fast reactors does not present greater risks or the need for fewer safeguards compared with the thermic reactor cycle, INFCE had no intention of closing the dispute with an unfavourable judgement passed on the Americans, as has been stated: its purpose was only to reinforce the argument for the necessity of new anti-proliferation measures to be introduced with international agreements.

A possibility that many experts see, even though it is a long-term possibility, as may be the point of arrival of any agreements, is to oppose any possible negative effects of the spread of fast reactors with a stockpiling system of plutonium surplus in deposits put under international control—for example, of the IAEA. Indeed, the control of isolated plutonium (plutonium is found in this state once separated from the products of fission contained in the irradiated fuel) is the essential factor on which the most realistically conceivable international security system is based, according to INFCE, presupposing a recourse to fast reactors.

In fact, to safeguard reprocessing plants or plants where mixed oxide material with uranium or plutonium is produced would be much more difficult, whereas, because of the no more than slight danger, of little interest are the temporary deposits of irradiated fuel, where the deposited elements maintain high levels of radioactivity—so high, in fact, that any clandestine extraction of plutonium would be practically unfeasible.

Just as few threats, from the point of view of proliferation, are presented by the final deposits of radioactive wastes.

References

1. OECD/Nuclear Energy Agency and IAEA. *Uranium; resources, production and demand* (Paris: OECD, 1982), 213 p.
2. *11th World energy conference, Munich 1980. General reports* (London: Organizing Committee, 1980), 10 vols.
3. *International nuclear fuel cycle evaluation* (Vienna: IAEA, 1980), 8 vols.
4. *Energia Materie prime*, 1980 and 1981.
5. Simen F. INFCE e collaborazione nucleare mondiale. *Energia Materie prime*, **14**, 1980, 23–8.
6. Centaro G. and Pont E. Uno scenario energetico italiano al 2000. *Energia Materie prime*, **16**, 1980, 25–42.

Role of high heat production granites in uranium province formation

P. R. Simpson
Jane A. Plant
British Geological Survey, London, England

A genetic relationship has long been indicated between acid magmatism (granite intrusion, rhyolitic and tuff vulcanicity) and the formation of uranium provinces as a result of the high mean clarke values of uranium in acid igneous rocks (4 ppm)[1,2] and their relative abundance in uranium provinces. Studies of the occurrence and distribution of uranium in granites[3–8] and in acid volcanics[9] enable further progress to be made in understanding this association. It has been suggested,[6,10] for example, that major uranium provinces can be formed by mass transfer of radioelements entrained in acid magmas characterized by high heat production from subcontinental lithosphere to the upper crust during cratonization following orogenesis. Rapid uplift and displacement along deep faults, hot spring activity and circulating groundwater (as a result of high geothermal gradients characteristic of such tectonic settings) may then redistribute uranium into various types of hydrothermal ore deposits. These may be closely associated with granites and acid volcanics, and epigenetic uraniferous phosphatic hot spring deposits may also occur in diatremes related to basement-controlled faults.

Rapid subaerial erosion of uraniferous acid igneous rocks in newly formed and uplifted cratonic segments is likely to result in the generation of sedimentary deposits: for example, detrital uraniferous conglomerates may develop in outwash zones from geomorphologically young, glaciated, mineralized and mountainous terrain. Progressive reworking favours uranium enrichment relative to thorium in associated distal organic-rich low-energy environments. As the continental setting matures, the regime evolves into a red bed environment in which uranium is concentrated on basement unconformities and in discrete reduced facies of the basin infill and in later discordant, possibly hydrothermal, structures. Subsequent reworking by laterally migrating oxidized water generates higher-grade deposits, such as ore rolls.

Criteria for the recognition of high heat production acid intrusions indicative of uranium provinces have been developed[3,4] and the geochemical, geophysical and geological signatures of uraniferous granites in the Scottish Caledonides, which contain about 12 ppm U, are useful for the recognition of such granites in the identification of uranium provinces in the western U.S.A. and elsewhere with the use of indices or binary classification systems.[11] Indeed, comparison of data sets on a normalized basis with the mutually exclusive ranges established for different magma types in the Scottish Caledonides is also proving to be a powerful discriminator for Archaean and Early Proterozoic high heat production granites in the Kaapvaal Craton, South Africa.[12]

Such 'metalliferous' intrusions (in which uranium and associated metals are present in relatively high primary magmatic concentration, predominantly in silicate minerals) may form large-volume low-grade sources of uranium. Although uranium occurs in accessory minerals at the present level of erosion, such intrusions may represent the eroded root zones of mineralized plutonic/volcanic complexes, the uranium being leached during erosion and concentrated in adjacent sedimentary basins to form ore deposits. Moreover, metamictization of uraniferous accessory minerals, which is likely to be particularly important in old Precambrian intrusions, would also provide large-volume sources of uranium for leaching. It has been demonstrated that such intrusions emplaced at 2370 m.y. could be the indirect primary sources of uranium for Tertiary calcrete deposits.[13]

Uraniferous granites may also be 'mineralized' in the sense of Plant *et al.*[4] with secondary enrichment of uranium in ore minerals and other leachable sites and greater variation in the uranium content of the granite, but the relationship between granites, hydrothermal uranium mineralization and uranium provinces is more complex. In the Scottish Caledonides, for example, large quantities of uranium and Sn–Be–Li–K–Rb–Th–F are contained in the Cairngorm–Mount Battock late tectonic alkaline granite batholith, as indicated by regional geochemistry and associated lithogeochemistry.[4] Recorded occurrences of uranium or other mineralization associated with the batholith are very limited, however, in comparison with the

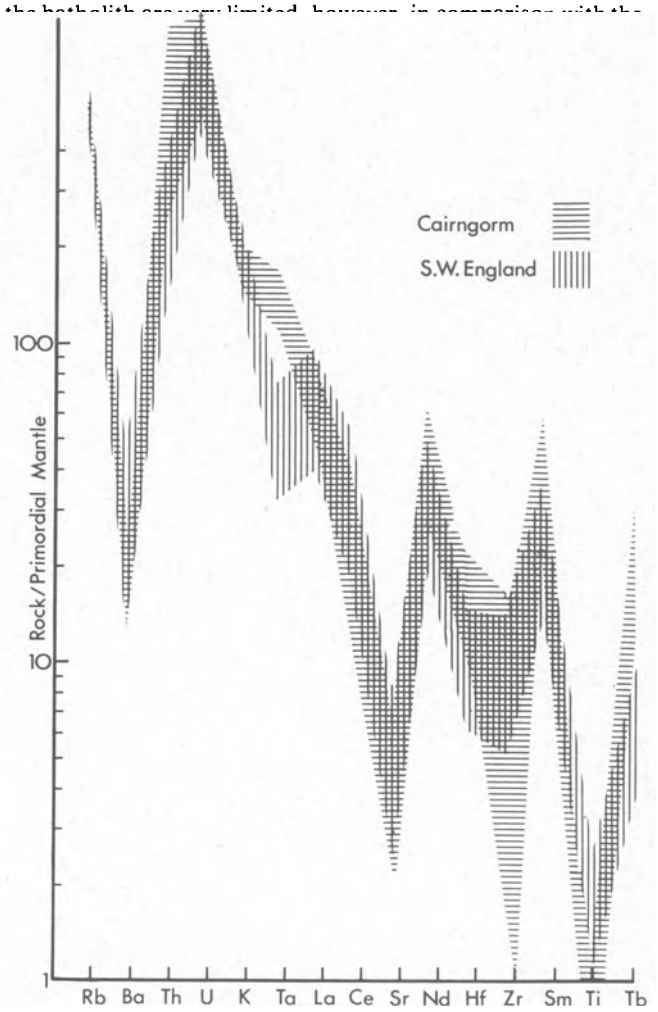

Fig. 1 Comparison of high heat production 'metalliferous' Cairngorm granite in Scottish Caledonides with samples from 'mineralized' Cornubian batholith of southwest England away from mineralization. Degree of geochemical evolution in the two batholiths is very similar with but minor differences, though Cairngorm has no significant mineralization and Cornubian batholith is the focus of a major metallogenic province

Hercynian province of southwest England. The Cornubian batholith, which has a chemical composition (particularly in terms of the contents of U, Sn and other metals) comparable with that of the Cairngorm–Mount Battock batholith[3] (Fig. 1), is associated with extensive mineralization, mainly of Sn, W and Cu[14,15] and an estimated 2000 ton of uranium ore has also been recovered.[16]

The distinction between 'metalliferous' granites with high primary magmatic contents of uranium and 'mineralized' granites in which uranium has been further concentrated into secondary mineral occurrences has been attributed to reaction of the granite magma with epizonal (metamorphic–formational–meteoric) water. According to the model of Simpson *et al.*,[3] mineralization initially involves high-temperature reaction with metamorphic and formational water evolving at lower temperatures into a hydrothermal circulation system with flow of meteoric water through fracture systems. Such a model suggests that the type of uraniferous mineralization associated with granites depends not only on the chemistry of the intrusions but also on the crustal setting in which they are emplaced, particularly lithology, metamorphic grade and fracture systems. It is suggested that characterization of 'mineralized' granites and their distinction from 'metalliferous' granites, their crustal setting—especially the role of regional fracturing in controlling granite emplacement and mineralization—and their geochemical and geophysical 'signature' can help in the design of exploration programmes by indicating the likely mode of concentration of uranium and associated mineralization in the basement and sedimentary cover sequence. The occurrence of 'mineralized' granite, for example, would indicate the likely presence of high-grade uranium vein and hydrothermal deposits in addition to sedimentary and roll-front deposits derived from uraniferous intrusions generally.

Models for mineralization associated with granites

Exploration for uranium or tin mineralization associated with granites is often based on the *I* and *S* models of granite genesis, and one example of this approach is the work of Wilson and Åkerblom[17] in Sweden. Although Cu–Mo porphyries are generally attributed to an igneous (*I*-type) origin at destructive plate margins, the mineralization being related to formational/meteoric water–magma interaction, the genesis of 'two-mica' tin and uranium granites is usually ascribed to crustal anatexis in areas of thickened sial in 'geosynclines'[18] or in arc–continent or continent–continent collisions.[19] The origin of tin and uranium mineralization in such granites has been attributed to palingenesis of wet sediments,[20] pitchblende vein mineralization resulting from downward percolation of solutions from the weathering zone.[20,21]. These are the sedimentary-protolith granites (*S*-type) of Chappel and White,[22] characterized by relatively low sodium with high potassium and alumina, a restricted range of composition of predominantly high SiO_2 lithologies, irregular elemental variation diagrams, high initial strontium isotope ratios, the absence of hornblende and the

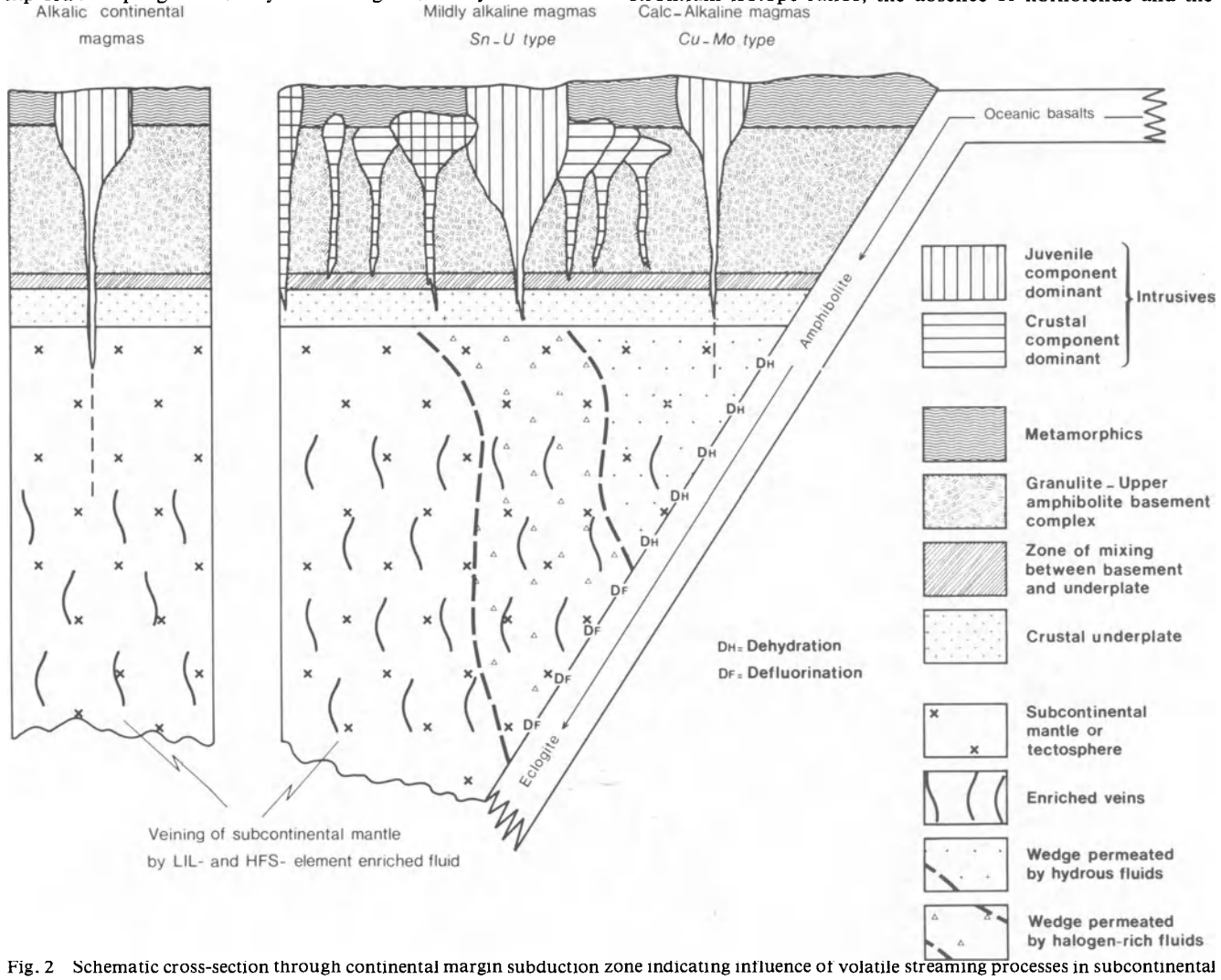

Fig. 2 Schematic cross-section through continental margin subduction zone indicating influence of volatile streaming processes in subcontinental mantle on nature and position of acid magmas where juvenile component is dominant. Formation of Sn–U-type high heat production magmas attributed to defluorination processes on downgoing slab, leading to scavenging of LIL and HFS elements from overlying mantle wedge and their preconcentration in the crustal underplate

presence of biotite and muscovite with accessory monazite and garnet rather than sphene—properties that are attributed to the sedimentary pile from which the granites formed by partial melting. More recently, Beckinsale,[23] in a discussion of the tin granites of southeast Asia, has added the criteria of ^{18}O enrichment and low ferric:ferrous iron ratios. Where *S*-type and *I*-type granites are found together, the former are expected to occur on the 'oceanic' side of the latter.

Other workers[3,4,10] use a different model for mineralization associated with granite intrusion. Following Mitchell and Garson,[24] they suggested that suites of metalliferous granites are related to subcrustal processes at destructive plate margins (Fig. 2) and that the granites are emplaced along deep faults at the end of the orogenic cycle. For granite magmas to rise in the crust they must be water-deficient[25] and mineralization is thought to occur initially as a result of hydration of the granite by host rock fluids at high (metamorphic) temperature. Reduction of silicate and primary accessory minerals will also commence at this stage, evolving into deuteric alteration of the granite magma and, as the magma cools and fissures, hydrothermal convection with flow of formational and, finally, meteoric water through fracture systems (Fig. 3). Fluid inclusion studies of the southwest England batholith, which identify early saline fluids containing B, S, Sn, Cu, Pb and W in the Dartmoor granite, low- to moderate-salinity fluids in the Sn–W–Cu mineralized Carnmenellis granite and pervasive low-temperature low-salinity fluids in the southwest England granites generally, are consistent with such a model. Sn (cassiterite) deposition occurs as the hydrothermal system begins to be established at temperatures in the range 450°C,[26] probably also accompanied by minor amounts of disseminated uraninite, whereas finer-grained pitchblende mineralization occurs later at lower temperatures (150°C or less) in well-developed vein systems. According to this model, such *S*-type characteristics as the high initial Sr ratios, ^{18}O enrichment and low ferric/ferrous ratios result from reaction between the granite and its host rocks. Independent studies[27,28] also indicate that the high boron content of the southwest England batholith is the result of metasomatic alteration of granite by host rock (greywacke, shale) fluids.

Studies of metamorphic aureoles provide support for such a model of mineralization and Yardley and Long[29] have shown in the Easky adamellite in Ireland that formation of a metamorphic aureole involved flow of H_2O from the host rocks into a water-undersaturated granite magma, giving rise to desilication (and the formation of corundum-bearing assemblages) and oxidation (resulting in alteration of garnet and biotite to magnetite) of the aureole. The formation of magnetite could account for the magnetic aureoles around such intrusions,[4,30] though their formation will depend on the buffering assemblage and they are likely to form only in a relatively anhydrous crustal setting. For the Ardara granite, Donegal, Atkin[31]

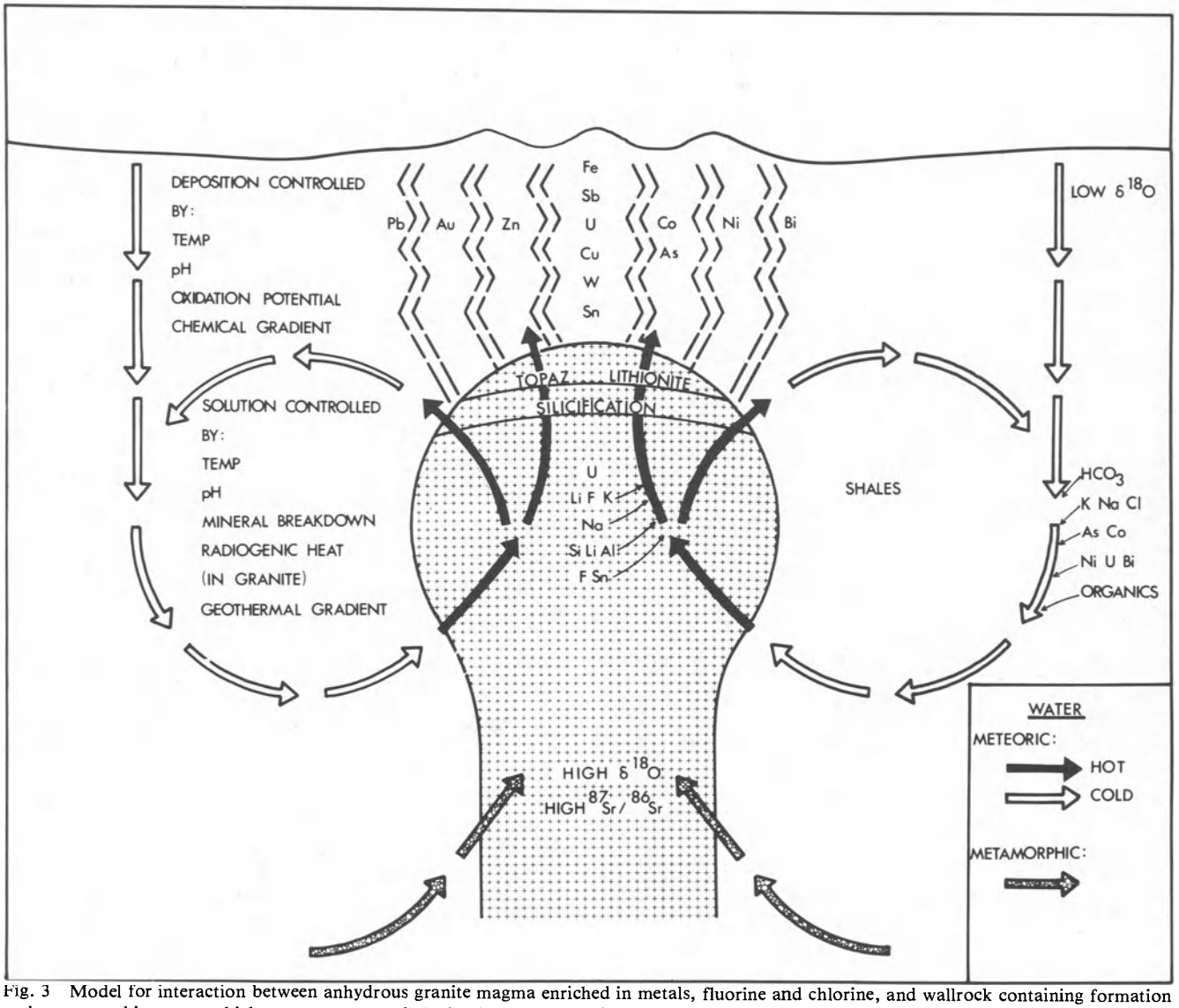

Fig. 3 Model for interaction between anhydrous granite magma enriched in metals, fluorine and chlorine, and wallrock containing formation and metamorphic water, which generates meteoric hydrothermal convective systems with vein-type mineralization

demonstrated that the iron ore mineral suite of the intrusion was a function of host rock lithology of the intrusion as a result of oxidation–reduction reactions.

This model for uranium mineralization associated with granites requires (1) a 'metalliferous' Sn–U mildly alkaline type or 'transitional' granite to rise to a level in the crust where it will create a thermal anomaly; (2) adequate water of suitable chemistry for hydration and reduction of primary silicates (thus rocks of low metamorphic grade and more pelitic composition, particularly graphitic shales, will favour mineralization); and (3) a well-developed fracture system, particularly for low-temperature mineral deposition.

This model is evaluated with particular reference to the British Caledonian and Hercynian granites. The geochemistry and crustal setting of the Cairngorm–Mount Battock 'metalliferous' granites are compared with the 'mineralized' Helmsdale granite and those of the southwest England Cornubian batholith. Factors (1) and (2) are the most important for the formation of high-temperature mineralization, such as cassiterite and uraninite, and factor (3) for lower-temperature deposits, such as those of pitchblende or Bi in vein-type mineralization.

Relationship between crustal setting, regional fracturing and mineralization

The late Caledonian 'metalliferous' granites, such as those of the Cairngorm–Mount Battock batholith, were emplaced in a continental crust composed mainly of Precambrian rocks previously metamorphosed at moderate to high metamorphic grades.[32,33] The lower 15–20 km have high seismic velocities and are thought to include granulites similar to those in the Lewisian basement of northwest Scotland.[34] In the west around Cairngorm the upper crustal layer consists of medium- to high-grade Moinian metasediments (northern and central Highlands) and in the east around Mount Battock of low- to high-grade Dalradian metasediments and metavolcanics (Grampian Highlands). Both of these assemblages had undergone repeated folding and metamorphism long before the emplacement of the late granites—the Moinian at or before 900 m.y. and again in early Caledonian time, the Dalradian during an early Caledonian event that reached its climax at 500–470 m.y.[35] In contrast, the southwest England batholith, which is also a late discordant intrusion of similar dimensions to the Cairngorm–Mount Battock batholith, was emplaced in Devonian and Carboniferous shales, limestones and thin sandstones, which had been metamorphosed only weakly prior to granite intrusion.

Most of the 'metalliferous' Caledonian granites in the Scottish Highlands are located on linear fractures that are independent of the local structure and that appear to be determined by faults in the lower crust giving access to fluids or melts of subcrustal origin. The Hercynian granites of southwest England have a comparable relationship with a WSW feature that is oblique to the east–west structural trend of the Upper Palaeozoic country rocks and which also represent a deep dislocation. A relationship between very large fractures in the lower crust and emplacement of 'metalliferous' granites is also recorded elsewhere, e.g. in the Peruvian batholith[36] and Proterozoic granites associated with uranium in the Canadian Shield,[6] which supports the deduction of Simpson *et al.*[3] that subcrustal sources contributed to the formation of the parent magmas.

Although major crustal fractures at depth may provide entry to the upper crust for 'metalliferous' granites, the later hydrothermal reworking of uranium and associated metals to form vein-type mineralization after emplacement requires the development of a mesh of fractures in the upper crust capable of transmitting large volumes of fluid through both the granites and their envelopes. The swarms of mineral lodes that occupy systematically arranged fissures in and around the granites of southwest England appear to have opened in response to a regional stress field.[37] In Scotland mineral lodes are very rare and even barren pegmatites and quartz veins are of restricted occurrence. The low water content of the metamorphic complexes through which the granites rose limited the volume of volatiles absorbed prior to consolidation and the semi-arid climate of Devonian times may have reduced the availability of meteoric water. Thus, although saussuritization of granite is seen locally along joints or faults and is associated with limited redistribution of uranium (giving rise to high values of U in water), the bulk of the metalliferous granites are fresh and carry uranium only in stable accessories.[3] It is worth noting that in the Cairngorm–Mount Battock batholith rotted and saussuritized granite recorded metalliferous occurrences and high values for U in water have been noted, mainly from the marginal parts of the granites; these occurrences are commonly located in lowland areas or valleys excavated by glacial and river erosion, whereas the fresh interior parts of the granites form upland massifs traversed by only a few deeply excavated valleys. It therefore seems possible that scavenging of uranium by water was restricted by (1) the limited amouts of formational or metamorphic water that could initiate hydration and expansion of the granite during consolidation; (2) the lack of meteoric water in an arid climate for hydrothermal circulation; and (3) the scarcity of major fractures at the contacts or in the interiors of the granites.

In these conditions the emplacement of uranium-rich granites at high crustal levels did not generate hydrothermal mineralization. These conditions were, however, suitable for remobilization of uranium by sedimentary processes, since the uranium-rich granites were eroded before and during the accumulation of Old Red Sandstone in internal basins. The organic-rich lacustrine Middle ORS sediments of the Orcadian basin, which was flanked on the south by the Cairngorm–Mount Battock batholith, has local syngenetic concentrations of uranium and of associated metals and shows higher values of uranium in water than those of other Highland formations.

Small quantities of epigenetic fault-controlled uranium mineralization occur in association with the Helmsdale Granite and overlying Ousdale Arkose[38] and in the Stromness region of Orkney. Although these deposits are small, they illustrate the distinction between magmatic processes that transported U from depth and high-level processes that generated ore deposits in near-surface environments.

Geochemical signatures of high heat production granites

Geochemical criteria for distinguishing between 'metalliferous' and 'mineralized' granites are discussed in relation to the 'metalliferous' Cairngorm–Mount Battock granite batholith and the 'mineralized' southwest England Cornubian batholith, which are both high heat production subalkaline Sn–U granites.

The chemistry of the two batholiths shows many similarities when data for portions of the Cornubian batholith away from centres of mineralization are compared with data for the Cairngorm–Mount Battock batholith. Paired-element plots for a wide range of LIL and HFS elements—for example, Zr/U (Fig. 4), Sr/U (Fig. 5), Sn/U and Sr/Rb (Fig. 6), Sr/K, Ba/K, Ba/Rb, K/Rb and Zr/Rb—show very good agreement, which suggests that these values represent primary magmatic concentrations of these elements with a similar degree of magmatic evolution. Detailed mapping of Dartmoor,[39] however, indicates much variability in grain size between different samples of granite, but the different textural varieties, when classified into six groups, bear no systematic geochemical relationship within or between groups[28] and the geochemical variations for all six groups, taken together, lie within the field previously

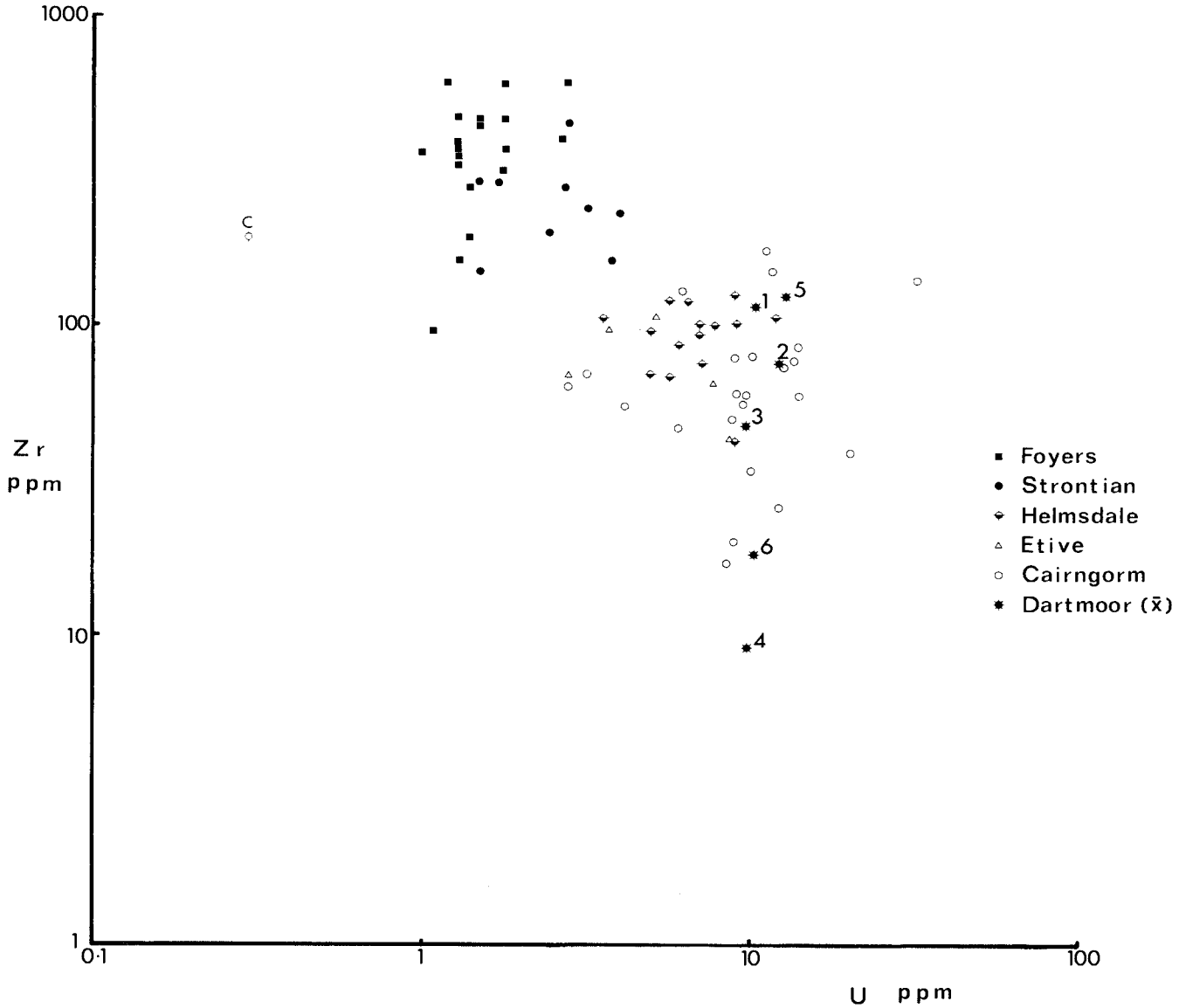

Fig. 4 Zirconium:uranium—Dartmoor data shown as mean values for each of six textural varieties shown in Fig. 7 (note similarity between Cairngorm and Dartmoor data; *C* indicates mean for Lewisian basement)

established for Cairngorm[4] (Fig. 7). Thus, there is no textural or geochemical evidence that the Cornubian batholith generated the associated ore deposits by progressive high-level magmatic fractionation.

Samples from Dartmoor are, however, notably enriched in Li, Sn and B in comparison with those from Cairngorm, as is indicated by Li/Sr, Sn/Zr, B/Si and B/Ga paired-element plots. It is suggested that this may be due to widespread pervasive high-temperature metamorphic and formational water–rock interaction, which probably occurred prior to vein-type mineralization (see also fluid inclusion evidence of Rankin and Alderton[26]).

Regional geochemical maps[40] and lithogeochemistry[28] suggest that secondary enrichment of Li and Sn has occurred within the granite, as was suggested previously for uranium by Simpson *et al.*[3] The enrichment in boron is not so readily explained. In the Caledonian uraniferous granites boron levels are generally below 10 ppm and the Cairngorm granite has only about 1 ppm—figures that are comparable with clarke values for boron in granite. Higher average values of up to 50 ppm B are, however, obtained from crustally derived granites. The boron content of the Dartmoor granite away from centres of mineralization ranges up to 900 ppm B, however, with a considerably higher mean and standard deviation than any of the Caledonian granites (Fig. 8). Detailed mineralogical studies[3,27] indicate that the boron in the southwest England granites is in secondary tourmaline: hence it is argued that the source of the boron in the Dartmoor granite is most probably the sedimentary rocks in the metamorphic aureole of the Cornubian batholith from which it was probably remobilized by thermal metamorphism and hydration of the granite.

Thus, the high and variable content of boron in 'mineralized' granites, such as the Cornubian batholith, provide evidence of granite host rock–fluid interaction that can thus be detected in samples that lack discrete mineralization.

In confirmation of these findings it should be noted that Li, Sn and B are all closely associated with the subsequent hydrothermal ore-forming events in the Cornubian batholith. Li in stream sediments shown on the *Wolfson atlas*[40] is in the range 200–400 ppm in the vicinity of hydrothermally altered and kaolinized granite. Sn has a widespread occurrence in vein-type mineralization and boron is the matrix of diatremes such as the Wheal Remfry breccia in the St Austell granite.[41]

It is therefore proposed that, on the basis of the studies of British Caledonian and Hercynian granites, in a search for vein-type hydrothermal mineralization in high heat production

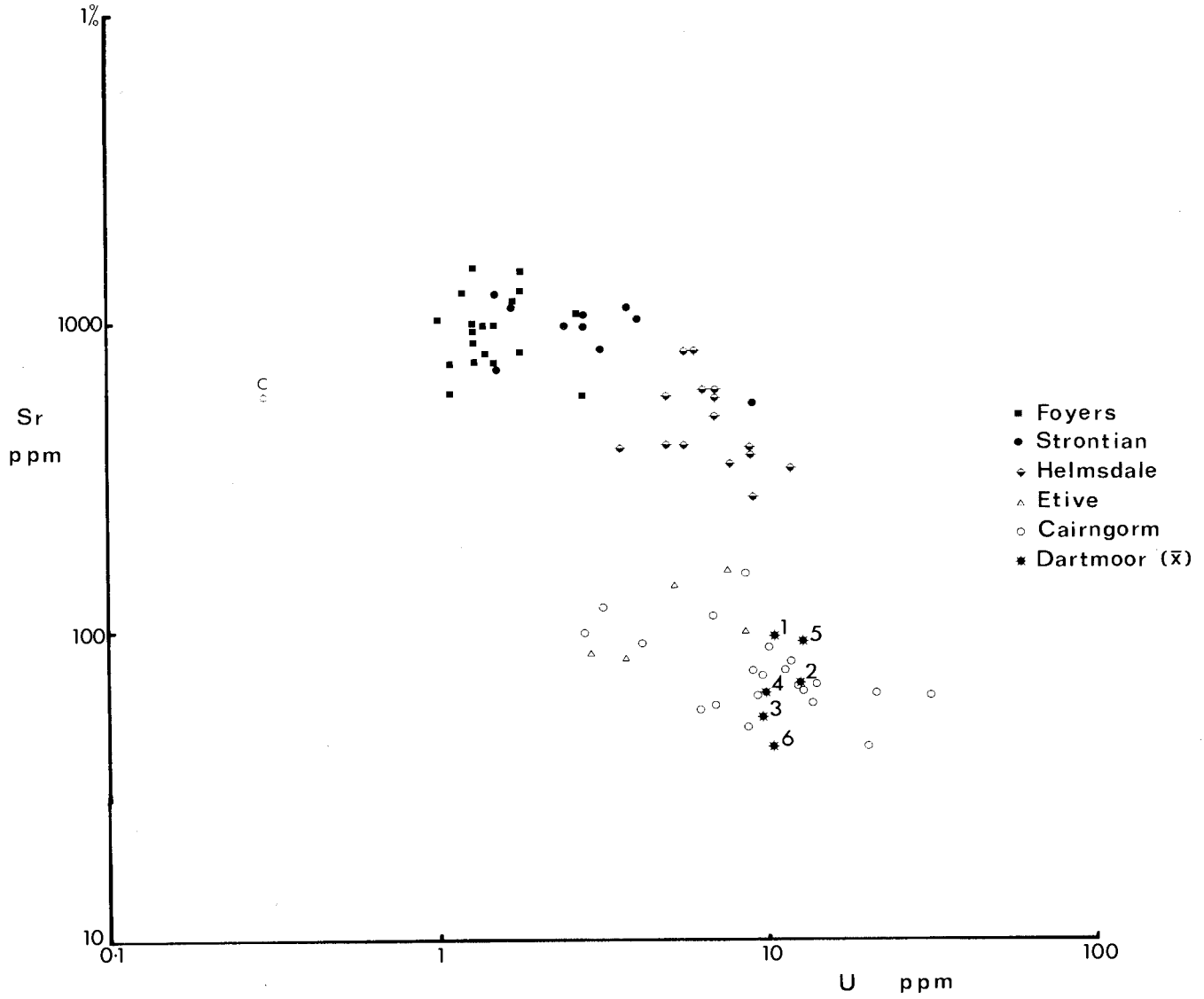

Fig. 5 Strontium : uranium—Dartmoor data shown as mean values for each of six textural varieties shown in Fig. 7 (note similarity between Cairngorm and Dartmoor data; *C* indicates mean for Lewisian basement)

Sn–U-type mildly alkaline granite a study be made of element pair diagrams—first, for element distributions mainly controlled by magmatic processes, such as Sr, Rb, K, Ba, Zr and U and, second, for Li, Sn and B (i.e. Li/Sr, Sn/Zr, B/Si or B/Ga), which record the pervasive metamorphic rock–water interaction event(s).

Geophysical signatures of high heat production granites

The geophysical criteria of large negative Bouguer gravity anomalies associated with large-amplitude aeromagnetic anomalies for 'metalliferous' granites, such as the Cairngorm–Mount Battock batholith in the Scottish Caledonides previously described by Plant *et al.*,[4] are discussed in relation to the 'mineralized' Cornubian batholith of southwest England, which also has a large negative gravity anomaly, thus indicating that both batholiths have similar dimensions and persist in depth to 12–15 km in the crust. The magnetic anomalies are very variable, however, since the anomaly at Cairngorm–Mount Battock is centred over the batholith, whereas the Cornubian batholith has no central anomaly but two linear anomalies along the northern contact zones of the Dartmoor and Bodmin granites.

Etive granite in the Scottish Caledonides has a large circular aeromagnetic anomaly centred over the aureole. If the presence of magnetic anomalies over aureoles indicates the presence of magnetite, however, there are three possibilities, according to Yardley:[42] (1) isochemical metamorphism of Fe^{2+} and Fe^{3+} original minerals, (2) oxidation of a relatively reduced precursor or (3) reduction of a relatively oxidized precursor.

Because the partial pressure of oxygen is so low in natural fluids options (2) and (3) would require extensive fluid circulation.

In the light of fluid inclusion data,[26] geochemical data, especially for boron, and the textural evidence cited, it is tentatively suggested that massive hydration of the Cornubian batholith has occurred together with reduction of magnetite to ilmenite, whereas Cairngorm–Mount Battock is unreacted and Etive has only partially reacted with resultant oxidation of the aureole. A large negative gravity anomaly over a granite that lacks a central aeromagnetic anomaly therefore probably indicates 'mineralized' granite.

It has been demonstrated above that, in the British Isles, uranium province formation depends on acid magmatism for the transfer of large amounts of uranium entrained within high heat production granite magmas from beneath the crust to a high level in the crust, and many aspects of uranium distribution associated with granites in the British Caledonian and Hercynian Provinces that have been outlined here can also be

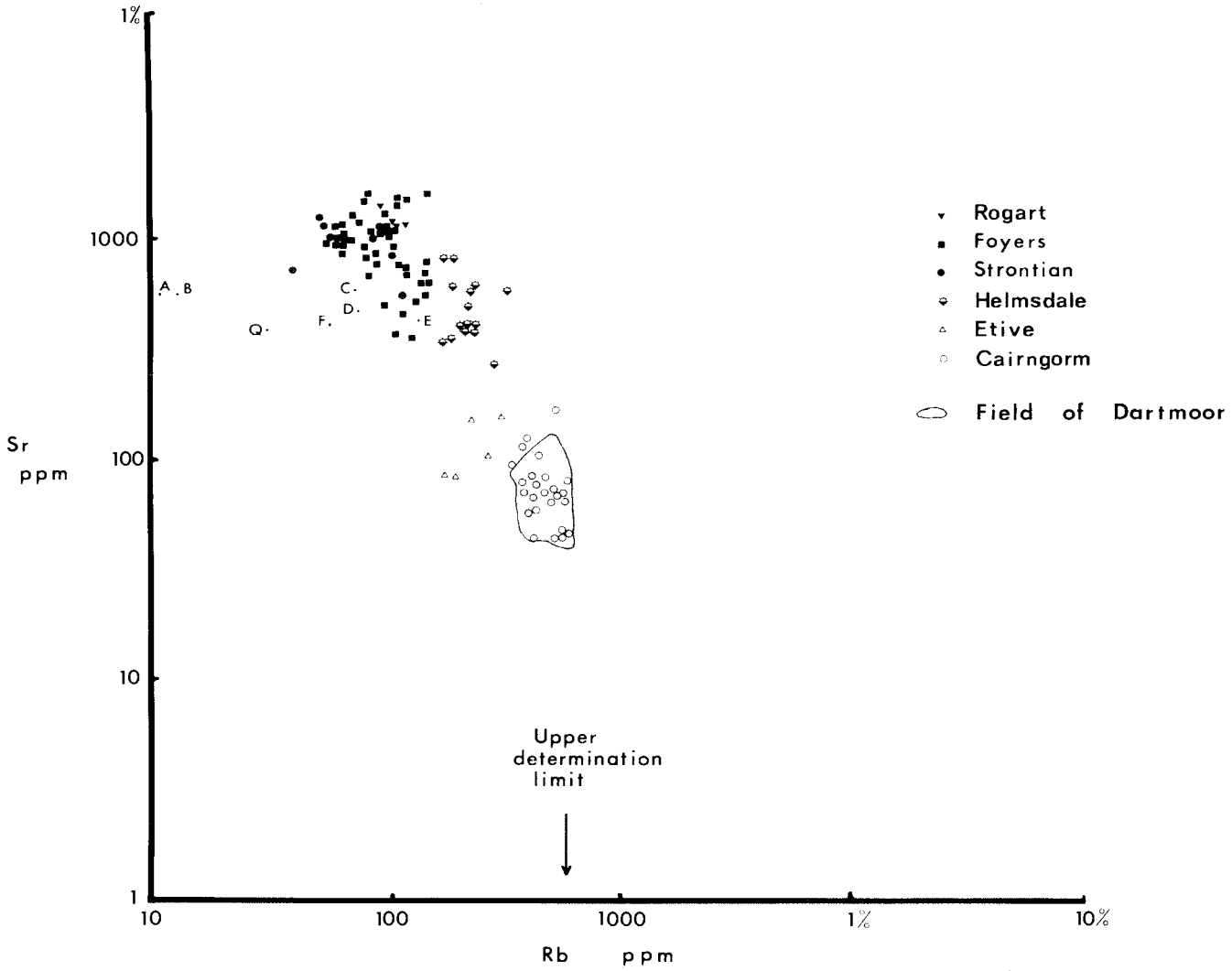

Fig. 6 Strontium:rubidium (note similarity between Cairngorm and field of Dartmoor; *A*, *B*, *C*, *D*, *E*, *F* and *Q* indicate means for Lewisian basement)

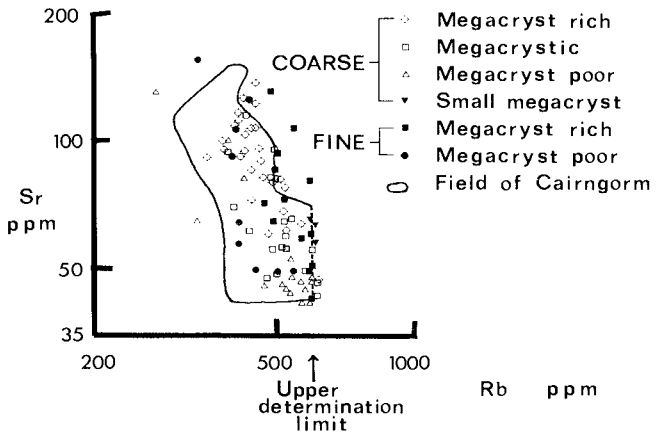

Fig. 7 Strontium:rubidium—six textural varieties of Dartmoor with field of Cairngorm data. Ranges are similar for both granites, but textural variation is unrelated to Sr:Rb content and not indicative of chemical fractionation between different textural varieties. It is therefore probable that they are the product of postmagmatic recrystallization in a hydrous and volatile-rich environment. It is important to note that such variation is absent from the Cairngorm granite, which is emplaced in an anhydrous high-grade metamorphic environment

recognized in other geological settings. For example, uranium mineralization at Helmsdale depends mainly on factor (3) in the model for mineralization described here (formation of a well-developed fracture system for low-temperature deposition). This also appears to be the case for uranium mineralization associated with granites elsewhere in the Caledonides.[7,8]

The South Mountain batholith of Nova Scotia,[43,44] which has many features in common with the 'mineralized' Cornubian batholith, has a large negative gravity anomaly but no aeromagnetic anomaly centred over the intrusion. Fracture-bound uranium mineralization occurs within the granite and tin mineralization is located at a site in the aureole of the granite where the regional metamorphic grade is low.[45]

An example of the application of the granite model described here to uranium province formation in the Archaean–Early Proterozoic is presented below to illustrate the potential of this approach for the general understanding of ore-forming processes and genetic modelling in mineral exploration.

Role of high heat production granites in Archaean–Early Proterozoic uranium provinces

Tilsley[46] pointed out that recognition of the correct geological controls of mineralization has important implications for the success of the mineral exploration industry, which is usually

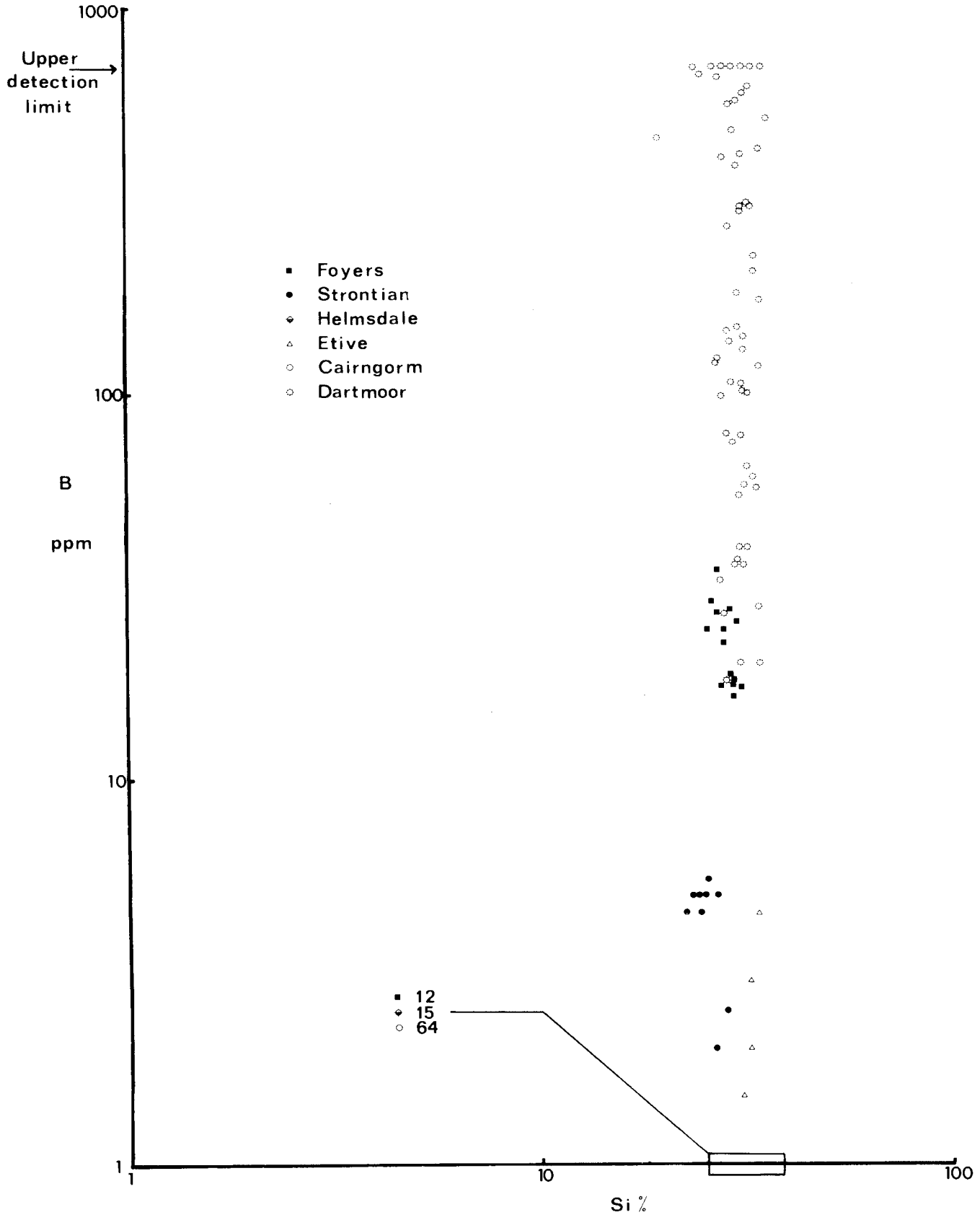

Fig. 8 Boron : silicon (note high and variable values of boron for Dartmoor relative to all Caledonian granites: only Caledonian granites with anomalous contents of boron are those such as Foyers, which is considered to have a significant crustal component. Anomalously high levels of boron in Dartmoor thought to have been introduced into the granite in variable amounts by formational and metamorphic water from the wallrock during and shortly after emplacement)

based on well-defined concepts and models. He also emphasized the time-bound character of uranium deposits through geological time, which were placed into four main categories—conglomerates, palaeo-surface-related vein-type, shales and sandstones. The major uranium deposits located in Archaean–Early Proterozoic conglomerates, though not exceptional in being confined to a particular period of the geological record, were, nevertheless, considered[46–50] to be evidence for reducing or anoxic atmospheric conditions during their formation. Following detailed mineralogical studies by Simpson and Bowles,[51,52] Windley and co-workers[12] have proposed that the Witwatersrand uraniferous conglomerates can be accounted for more readily by emplacement of high heat production granites some 3000 m.y. ago into thick crust (60–70 km) followed by their rapid uplift and erosion into voluminous clastic-filled basins. Nd–Sr relationships of these early Precambrian granitic rocks suggest derivation from the mantle. By analogy with comparable granites in the Phanerozoic these granites were probably highly uraniferous and could have been the principal control in the formation of the uranium provinces in the Archaean.

The Witwatersrand Basin is encircled by a series of domed inliers of granite greenstone basement. Viljoen and co-workers[53] suggested that the source of the gold is likely to be found in the greenstone belts. The uraninite was probably derived from granitic plutons located in Archaean greenstone belts and from granite plutons in high-grade gneisses that are common between greenstone belts (e.g. in the Rhodesian Craton), and granites in high-grade gneiss belts, such as the Limpopo mobile belt.

Whereas the greenstone belts have not been highly uplifted, the high-grade gneisses, which typically have indications of metamorphic recrystallization at 7–11 kb pressure, have been so uplifted that the whole of their upper crust has been eroded. Moreover, the synclinal-shaped greenstone belts in places overlie at their margins high-grade gneisses and geophysical studies suggest the belts to be underlain by gneissic basement.

The uranium and gold mineralization of the Witwatersrand deposits occurs in high-energy conglomerates in the lower Dominion Reef and in high-energy conglomerate and low-energy carbonaceous reefs of probable microbial mat origin in the Upper Witwatersrand. These Supergroups, together with the Ventersdorp Supergroup, are grouped together as the Witwatersrand Triad.[54] The deposits of the Witwatersrand Triad are constrained within the period 2800–2300 m.y. approximately by a Rb–Sr age of 2820 ± 55 m.y. for whole rock samples of an underlying granite[55] and a U–Pb zircon age of 2300 ± 100 m.y. for an interbedded quartz porphyry lava from the Ventersdorp Supergroup.[56] Uranium data for the granites are sparse and may be unreliable as indicators of primary magmatic concentrations owing to the age and complex geological history of the region. The limited number of epithermal neutron activation analyses, however, that is available for uranium in granites from Barberton Mountain Land indicates values in the range 0.5–1.08 ppm U for Ancient tonalitic gneisses of 3350 m.y. age and 1–14 ppm U on Homogeneous Hood granites of 3000 m.y. age.[57] This suggests that anomalously uraniferous granites were probably emplaced in the Kaapvaal Craton about 3000 m.y. ago.

A survey of granitic events in the Kaapvaal Craton by Hunter[58] indicates events at 3350, 3310, 3100, 3000, 2900, 2600–2700, 2600, 2300 and 2000 m.y. that vary widely in both major- and minor-element composition, though data for uranium are lacking. The 3000 m.y. granites quoted by Hunter[58] are from the Vryburg area, the Klerksdorp area and some Hood granites from the Barberton region. Both the Vryburg and Klerksdorp granites lie within a possible westerly source region for the uraninite concentrated in the Witwatersrand Basin, which has a U–Pb age of 3050 ± 50 m.y.[59]

In the present study selected whole rock geochemical data[58] for the granitic events of the Kaapvaal Craton are normalized to primordial mantle and compared with the geochemical data ranges previously established for 'barren' and 'metalliferous' granites in the Scottish Caledonides[10] (Fig. 9). The results indicate that there is an important change in the chemistry of the granites as a function of age of emplacement in the

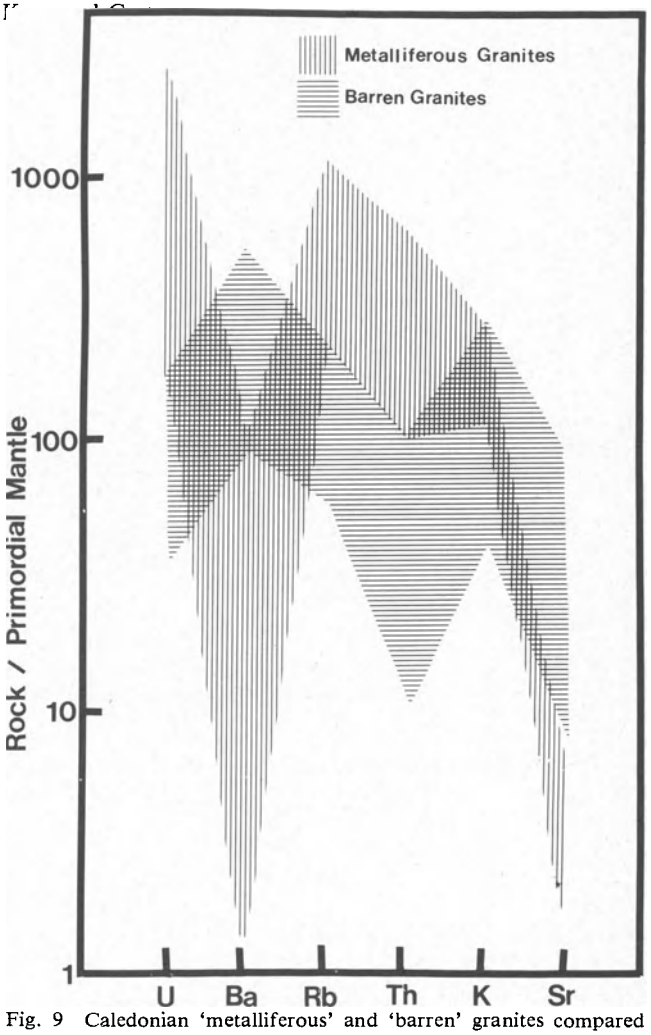

Fig. 9 Caledonian 'metalliferous' and 'barren' granites compared (note mutually exclusive ranges for all elements shown except K). Data from Howarth *et al.*[11]

Prior to 3100 m.y. all the granites are of the 'barren' type (Fig. 10). At 3100 m.y., however, there is a 'transitional'-type granitic event prior to the introduction of 'metalliferous'-type granites at 3000 m.y. All subsequent intrusions are also of this type, except for the 'barren'-type 2900 m.y. granitic event (Fig. 11). The 'metalliferous'-type plutons of 3000–2000 m.y. age differ from younger granites of similar type. They generally have lower levels of Sn, which may indicate chemical differences in the source area for the granites or high-level loss during hydrothermal reworking. These alternative possibilities can only be resolved by further study.

Nevertheless, it is possible to account in this way for the Kaapvaal Craton becoming a uranium province at 3000 m.y. as a result of a 'metalliferous', high heat production granitic event with granites containing an estimated 12 ppm uranium. The variation in magma type is well illustrated by plotting one of the criteria for the recognition of 'metalliferous' granites[49,50]—the Rb : Sr ratio—against age of intrusion (Fig. 12).

The well-defined hiatus in the ratio between <0.31 for 'barren' granites and >2 for 'metalliferous' granites supports the suggestion that there are primary differences in source

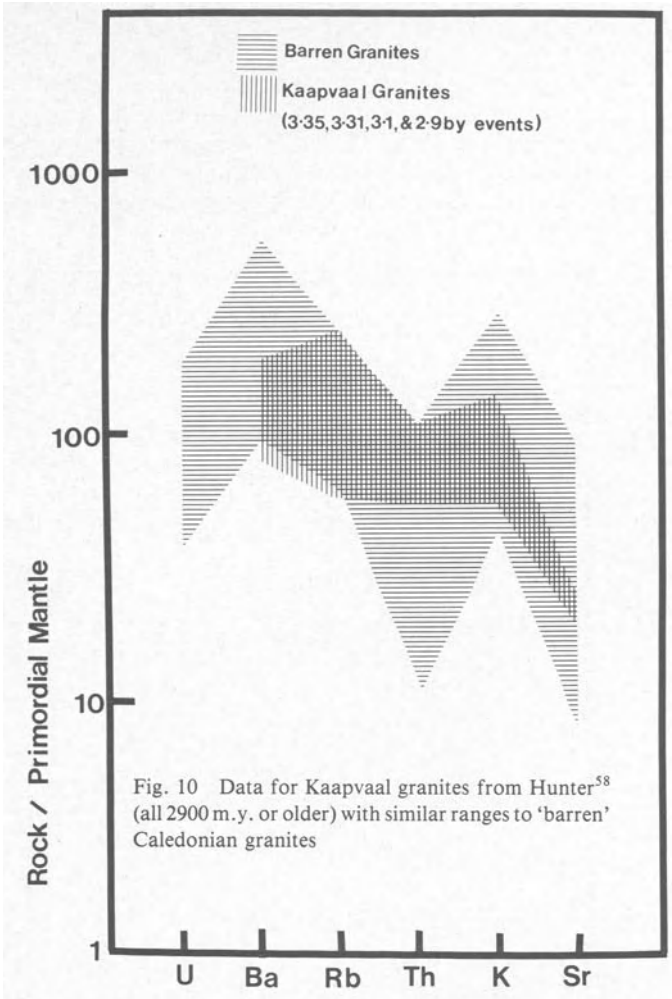

Fig. 10 Data for Kaapvaal granites from Hunter[58] (all 2900 m.y. or older) with similar ranges to 'barren' Caledonian granites

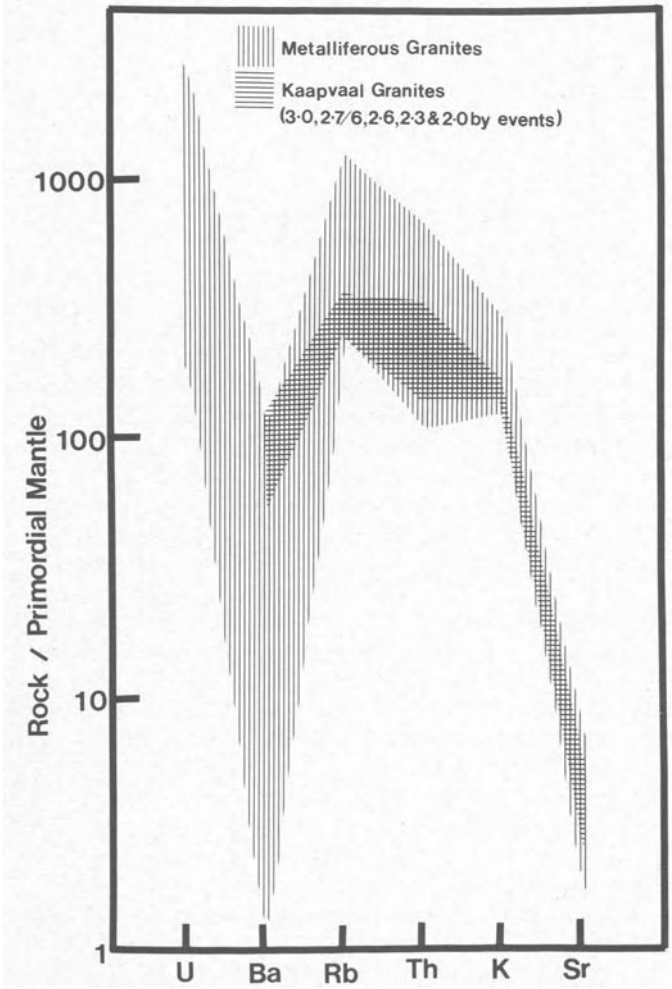

Fig. 11 Data for Kaapvaal granites from Hunter[58] (all 3000 m.y. or younger) with similar ranges to 'metalliferous' Caledonian granites

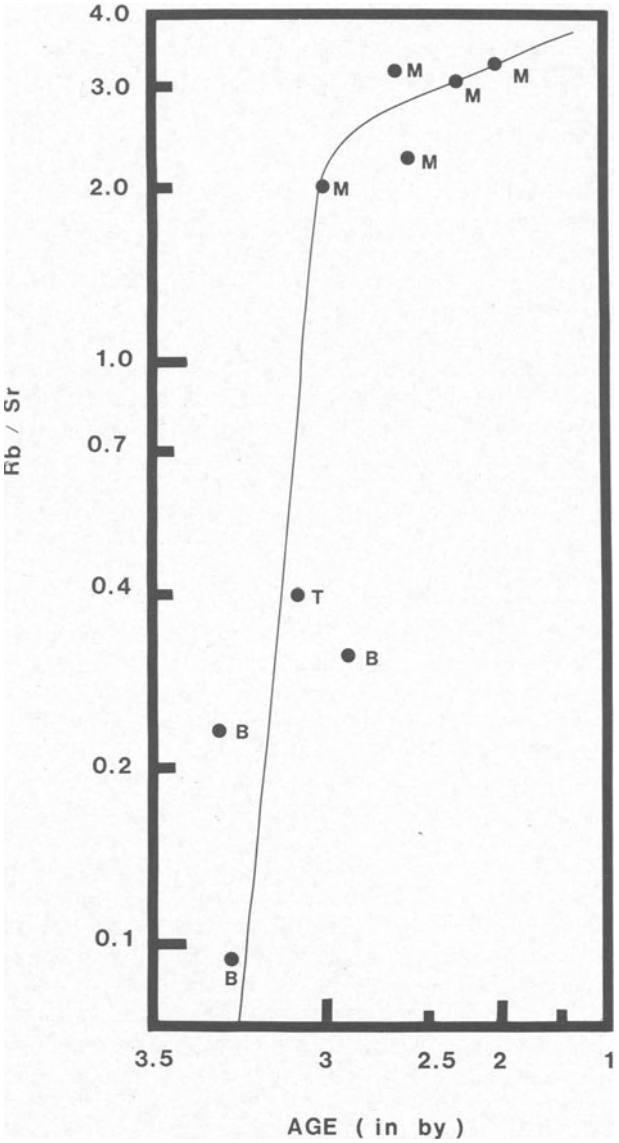

Fig. 12 Rb : Sr diagram constructed from Hunter's data[58] to indicate change from 'barren' (B) and 'transitional' (T) granites at about 3000 m.y. to 'metalliferous' (M) granites. Large gap in data suggests that barren and metalliferous granites originate in different source regions, as previously suggested for the Caledonian granites by Simpson *et al.*[3]

regions for these granites, as was previously suggested for the Scottish Caledonian granites,[3,4,5] where the 'barren' granites are thought to be crustally derived and the 'metalliferous' granites derived from metasomatized upper mantle/lower crust.

The predominance of uraninite-bearing placer deposits in the Archaean–Early Proterozoic was therefore partly attributed by Windley and co-workers[12] to high-temperature hydrothermal reworking of the source granites in a high heat flow regime, resulting in extensive redistribution of mobile elements, such as uranium, to form thorian uraninite mineralization in granite—associated with pegmatites (now removed by erosion) but evident from a study of the sediments.

In the Phanerozoic uranium oxide mineralization in granites tends to occur as a lower-temperature phase, such as low thorium pitchblende in veins, which is less resistant to weathering than euhedral thorian uraninite crystals and, hence,

unlikely to form detrital deposits. Thus, the absence of major economic placer concentrations of uraninite in younger sediments may also be a reflection, in part, of the reduced levels of thorian uraninite mineralization in a generally lower-temperature thermal regime.

The application of this model to exploration for new uraniferous deposits in deeply buried sediments emphasizes the importance of correctly identifying potential source granites, which may lack discrete mineralization at the present level of exposure but which could, nevertheless, be the source of major sedimentary deposits.

Conclusions

The *I*- and *S*-type model for high heat production 'metalliferous' and 'mineralized' granite genesis is not applicable for the Scottish Caledonides or the southwest England Cornubian batholith. On the other hand, the identification of 'metalliferous' granites on regional geochemical and geophysical maps and study of the crustal setting of granites with particular reference to lithology, metamorphism and fracture systems of the host rocks point to 'mineralized' granites that merit further exploration. The development of uranium mineralization associated with granites depends on magma emplacement in an adequately hydrous environment. Thus, the contrast in styles of mineralization between the Hercynian and Caledonian Provinces is thought to be related more to the nature of the crust of the Caledonides and Hercynides than to primary differences in granite magmatism. The model can also be successfully applied to understanding the genesis of uranium provinces ranging in age and location from the Archaean of southern Africa to the Hercynian of southwest England and probably elsewhere, thus enabling reliable exploration criteria to be established and targets identified.

Acknowledgement

This contribution is published by permission of the Director, British Geological Survey (NERC). *Jane Hurdley* is thanked for assistance with the illustrations and references.

References

1. Grutt E. W. Jr. Prospecting criteria for sandstone-type uranium deposits. In *Uranium prospecting handbook* Bowie S. H. U. Davis M. and Ostle D. eds (London: IMM, 1972), 47–78.
2. Malan R. C. *Summary report: distribution of uranium and thorium in the Precambrian of the western United States* (Grand Junction: USAEC, 1972).
3. Simpson P. R. *et al.* Uranium mineralization and granite magmatism in the British Isles. *Phil. Trans. R. Soc. Lond.*, **A291**, 1979, 385–412.
4. Plant J. A. *et al.* Signatures of metalliferous granites in the Scottish Caledonides. *Trans. Instn Min. Metall. (Sect. B: Appl. earth sci.)*, **89**, 1980, B198–210.
5. Plant J. A. *et al.* Metalliferous and mineralized Caledonian granites in relation to regional metamorphism and fracture systems in northern Scotland. *Trans. Instn Min. Metall. (Sect. B: Appl. earth sci.)*, **92**, 1983, B33–42.
6. Darnley A. G. The relationship between uranium distribution and some major crustal features in Canada. *Mineralog. Mag.*, **44**, 1981, 425–36.
7. O'Connor P. J. Radioelement geochemistry of Irish granites. *Mineralog. Mag.*, **44**, 1981, 485–95.
8. Steenfelt A. Uranium and selected trace elements in granites from the Caledonides of East Greenland. *Mineralog. Mag.*, **46**, 1982, 201–10.
9. Smellie J. A. T. The mineralogy and genesis of uranium in rhyolitic ignimbrites of Precambrian age from Duobblon, Sweden. *Mineralog. Mag.*, **46**, 1982, 187–99.
10. Watson J. V. and Plant J. A. The regional geochemistry of uranium as a guide to deposit formation. *Phil. Trans. R. Soc. Lond.*, **A291**, 1979, 321–38.
11. Howarth R. J. *et al.* Identification of uraniferous granitoids in the U.S.A. using stream sediment geochemical data. *Mineralog. Mag.*, **44**, 1981, 455–70.
12. Windley B. F. Simpson P. R. and Muir M. D. The role of atmospheric evolution in Precambrian metallogenesis. *Fortschritte der Mineralogie*, in press.
13. Stuckless J. S. Bunting J. A. and Nkomo I. T. U–Th–Pb systematics of some granitoids from the northeastern Yilgarn Block, Western Australia and implications for uranium source rock potential. *J. geol. Soc. Aust.*, **28**, 1981, 365–75.
14. Hosking K. F. G. Permo-Carboniferous and later primary mineralisation of Cornwall and south-west Devon. In *Present views of some aspects of the geology of Cornwall and Devon* Hosking K. F. G. and Shrimpton G. J. eds (Penzance: Royal Geological Society of Cornwall, 1964), 201–45.
15. Stemprok M. Burnol L. and Tischendorf G. eds. *MAWAM (Metallization Associated With Acid Magmatism) volume 3* (Prague: Geological Survey; Stuttgart: Schweizerbart, 1978), 446 p.
16. Dines H. G. *The metalliferous mining region of south-west England* (London: HMSO, 1956), 2 vols, 795 p. *(Mem. geol. Surv. Gt Br.)*
17. Wilson M. R. and Åkerblom G. V. Geological setting and geochemistry of uranium-rich granites in the Proterozoic of Sweden. *Mineralog. Mag.*, **46**, 1982, 233–45.
18. Tischendorf G. The metallogenetic basis of tin exploration in the Erzgebirge. *Trans. Instn Min. Metall. (Sect. B: Appl. earth sci.)*, **82**, 1973, B9–24.
19. Mitchell A. H. G. Southwest England granites: magmatism and tin mineralization in a post-collision tectonic setting. *Trans. Instn Min. Metall. (Sect. B: Appl. earth sci.)*, **83**, 1974, B95–7.
20. Moreau M. L'uranium et les granitoïdes: essai d'interprétation. In *Geology, mining and extractive processing of uranium* Jones M. J. ed. (London: IMM, 1976), 83–102.
21. Barbier M. J. Continental weathering as a possible origin of vein-type uranium deposits. *Mineral. Deposita*, **9**, 1974, 271–88.
22. Chappel B. W. and White A. J. R. Two contrasting granite types. *Pacific Geol.*, **8**, 1974, 173–4.
23. Beckinsale R. D. Granite magmatism in the tin belt of South-East Asia. In *Origin of granite batholiths: geochemical evidence* Atherton M. P. and Tarney J. eds (Orpington, Kent: Shiva Publishing, 1979), 34–44.
24. Mitchell A. H. G. and Garson M. S. Relationship of porphyry copper and circum-Pacific tin deposits to palaeo-Benioff zones. *Trans. Instn Min. Metall. (Sect. B: Appl. earth sci.)*, **81**, 1972, B10–25.
25. Brown G. C. and Fyfe W. S. The production of granitic melts during ultrametamorphism. *Contr. Mineral. Petrol.*, **28**, 1970, 310–8.
26. Rankin A. H. and Alderton D. H. M. Fluid inclusion evidence for the evolution of hydrothermal fluids in SW England: abstract. *J. geol. Soc. Lond.*, **139**, 1982, 96.
27. Lister C. J. Quartz-cored tourmaline from Cape Cornwall and other localities. *Proc. Ussher Soc.*, **4**, 1979, 402–18.
28. Simpson P. R. *et al.* Geochemical and geophysical criteria in the exploration for uraniferous granites: abstract. *Trans. Instn Min. Metall. (Sect. B: Appl. earth sci.)*, **89**, 1980, B196.
29. Yardley B. W. D. and Long C. B. Contact metamorphism and fluid movement around the Easky adamellite, Ox Mountains, Ireland. *Mineralog. Mag.*, **44**, 1981, 125–31.
30. Brown G. C. and Locke C. A. Space–time variations in the British Caledonian granites: some geophysical correlations. *Earth Planet. Sci. Lett.*, **45**, 1979, 69–79.
31. Atkin B. P. Oxide–sulphide–silicate mineral phase relations in some thermally metamorphosed granitic pelites from Co. Donegal, Eire. In *The Caledonides of the British Isles—reviewed* Harris A. L. Holland C. H. and Leake B. E. eds. *Spec. Publ. geol. Soc. Lond.* no. 8, 1979, 375–84.
32. Simpson P. R. *et al.* The role of metalliferous and mineralised uranium granites in the formation of uranium provinces. In *Uranium exploration techniques: proceedings of the symposium, Paris, June 1982* (Paris: NEA, 1982), 157–68.
33. Watson J. V. *et al.* Uranium provinces in relation to metamorphic grade and regional geochemistry. Reference 32, 235–48.
34. Bamford D. and Prodehl C. Explosion seismology and the continental crust–mantle boundary. *J. geol. Soc. Lond.*, **134**, 1977, 139–51.

35. Fettes D. J. A metamorphic map of the British and Irish Caledonides. Reference 31, 307–21.
36. Pitcher W. S. Comments on the geological environments of granites. Reference 23, 1–8.
37. Moore J. McM. A mechanical interpretation of the vein and dyke systems of the S.W. England orefield. *Mineral. Deposita*, **10**, 1975, 374–88.
38. Bowie S. H. U. Simpson P. R. and Rice C. M. Application of fission-track and neutron activation methods to geochemical exploration. In *Geochemical exploration 1972* Jones M. J. ed. (London: IMM, 1973), 359–72.
39. Hawkes J. Personal communication to Simpson P. R.
40. Webb J. S. *et al. The Wolfson geochemical atlas of England and Wales* (Oxford: Clarendon Press, 1978), 79 p.
41. Allman-Ward P. *et al.* An intrusive hydrothermal breccia body at Wheal Remfry in the western part of the St Austell Granite Pluton, Cornwall, England. In *Metallization associated with acid magmatism* Evans A. M. ed. (Chichester, etc.: Wiley-Interscience, 1982), 1–28. (*MAWAM Series* vol. 6)
42. Yardley B. W. D. Personal communication to Plant J. A.
43. Muecke G. K. and Clarke D. B. Geochemical evolution of the South Mountain Batholith, Nova Scotia: rare-earth-element evidence. *Can. Mineralogist*, **19**, 1981, 133–45.
44. Chatterjee A. K. Polymetallic tin mineralization related to acid magmatism, southwest Nova Scotia, Canada: abstract. *Trans. Instn Min. Metall. (Sect. B: Appl. earth sci.)*, **89**, 1980, B194.
45. Keppie J. D. Muecke G. K. and Chatterjee A. K. *Folio of the geological maps of Nova Scotia, 1:2 000 000 scale* (Halifax: Nova Scotia Department of Mines and Energy, 1979).
46. Tilsley J. E. General discussion on Theoretical and practical aspects of uranium geology. *Phil. Trans. R. Soc. Lond.*, **A291**, 1979, 447–51.
47. Liebenberg W. R. The occurrence and origin of gold and radioactive minerals in the Witwatersrand System, the Dominion Reef, the Ventersdorp Contact Reef and the Black Reef. *Trans. geol. Soc. S. Afr.*, **58**, 1955, 101–227.
48. Ramdohr P. New observations on the ores of the Witwatersrand in South Africa and their genetic significance. *Trans. geol. Soc. S. Afr.*, **61**, 1958, annexure, 50 p. + 61 plates.
49. Holland H. D. Model for the evolution of the earth's atmosphere. In *Petrologic studies: a volume to honour A. F. Buddington* (New York: Geological Society of America, 1962), 447–77.
50. Schidlowski M. Eichmann R. and Junge C. E. Precambrian sedimentary carbonates: carbon and oxygen isotope geochemistry and implications for the terrestrial oxygen budget. *Precamb. Res.*, **2**, 1975, 1–69.
51. Simpson P. R. and Bowles J. F. W. Uranium mineralization of the Witwatersrand and Dominion Reef systems. *Phil. Trans. R. Soc. Lond.*, **A286**, 1977, 527–48.
52. Simpson P. R. and Bowles J. F. W. Detrital uraninite and pyrite: are they evidence for a reducing atmosphere? In *Genesis of uranium- and gold-bearing Precambrian quartz-pebble conglomerates* Armstrong F. C. ed. *Prof. Pap. U.S. geol. Surv.* 1161, 1981, S1–S12.
53. Viljoen R. P. Saager R. and Viljoen M. J. Some thoughts on the origin and processes responsible for the concentration of gold in the early Precambrian of Southern Africa. *Mineral. Deposita*, **5**, 1970, 164–80.
54. Hamilton G. N. G. and Cooke H. B. S. *Geology for South African students, 4th edition* (Johannesburg: Central News Agency, 1960).
55. Allsop H. L. Rubidium–strontium ages from the Western Transvaal. *Nature, Lond.*, **204**, 1974, 361–3.
56. Button A. The Transvaal Supergroup in the Cratonic environment of Southern Africa. In *Precambrian of the southern hemisphere* Hunter D. R. ed. (Amsterdam, etc.: Elsevier, 1981), 527–34.
57. Erasmus C. S. and Watterson J. I. W. Epithermal-neutron-activation analysis for uranium in Barberton and Bushveld granites. *Natn. Inst. Metall.-Rep.* no. 1749, 1975, 4 p.
58. Hunter D. R. Geochemistry of granitic and associated rocks in the Kaapvaal Craton. *Inf. Circ. Univ. Witwatersrand Econ. Geol. Res. Unit* no. 81, 1973, 73 p.
59. Rundle C. C. and Snelling N. J. The geochronology of uraniferous minerals in the Witwatersrand triad; an interpretation of new and existing U–Pb age data on rocks and minerals from the Dominion Reef, Witwatersrand and Ventersdorp Supergroups. *Phil. Trans. R. Soc. Lond.*, **A286**, 1977, 567–83.

Uranium deposits in Italy

Claudio Tedesco
AGIP, Direzione Attività Uranifere, Rome, Italy

Uranium exploration: history and results

Uranium exploration in Italy was begun in the early 1950s by private companies, which evaluated known radioactive occurrences. In 1954 two state-owned organizations—the Comitato Nazionale Ricerche Nucleari (CNRN) and the Ente Nazionale Idrocarburi (ENI)—became active in the exploration field and, a few years later, were the sole operators.

Maximum exploration effort was apparent in the period 1958–60, the dramatic reduction in the 1960s following the depressed state of the uranium market. Since 1974 responsibility for uranium supply to meet national needs has rested with ENI, which continues to explore potential Italian uranium targets.

From the outset exploration activity has been focused on the crystalline and continental volcanosedimentary formations of the Alps, Sardinia and Calabria and the alkaline Quaternary volcanics of central Italy.[14] Uranium occurrences have been found in all these geological settings (Fig. 1), numerous mineralized showings and the Novazza and Val Vedello deposits occurring in the volcanosedimentary formations of the post-Hercynian basins of the Alpine range.

In the Western Alps these formations were metamorphosed in Alpine time and, consequently, the host mineralization was metamorphosed and redistributed—as, for example, at Preit, Cuneo. The results of the investigation of the Hercynian granitoids have proved to be of no significance: a few vein-like occurrences were discovered in the mylonites of the Monte Bianco massif and in the peribatholitic schists of southern Sardinia; minor occurrences related to recent continental coarse deposits overlying, or adjacent to, the granitoids have also been found in Calabria and Sardinia. Tabular, low-grade uranium mineralization controlled by the groundwater-table occurs in the Quaternary alkaline volcanoes of central Italy.[12]

Collio Basin

The Permian Collio Basin, located in the Lombardy Alps, is particularly important in terms of uranium geology, both the economic deposits that have so far been discovered in Italy (Novazza and Val Vedello) occurring in this basin. It is one of the several continental basins, filled mainly with acid volcanics and sediments derived from the erosion of metamorphic and volcanic formations, that formed at the edge of the Hercynian chain at the end of the orogenic event in the late Carboniferous.

The Collio formation outcrops over an area of 800 km^2; its original extension is not known, as it is bordered to the north and to the south by two major structural features (Fig. 2). The maximum thickness is about 1500 m. To the north the Collio formation is in tectonic contact with the crystalline basement as a result of reverse faulting. To the south the Permian formations are in tectonic contact with Mesozoic marine formations. Two structural highs limit the basin both to the east and to the west, where the younger (Upper Permian) Verrucano formation unconformably overlies the crystalline basement.

The general late Palaeozoic stratigraphy of the central Collio Basin[1] is outlined below (Fig. 3).

The first post-Hercynian sedimentary formation is the 'basal conglomerate', which comprises coarse- to medium-grained sediments typical of a high-energy environment; it overlies unconformably the basement gneisses, mica-schists and phyllites. The basal conglomerate is present only locally. The Collio formation overlies either the basal conglomerate or, directly, the basement and is composed of fluvial and lacustrine sediments, interbedded with volcanic deposits. Alluvial fan, marginal and lacustrine deposits are the prevailing sedimentary facies.

The alluvial fan deposits consist of polygenetic conglomerates with a clastic and/or tuffaceous matrix. The fragments are of volcanic and crystalline basement rocks. The marginal lacustrine deposits are coarse to fine micaceous grey to green sandstones and blackish silty sandstones. The offshore lacustrine deposits are varved terrigenous carbonate sediments and, occasionally, calcareous dolomites. Gypsum concretions may indicate a local evaporitic environment. Numerous volcanic units are interbedded with the sedimentary facies: acid volcanics predominate, the intermediate facies being uncommon. Lava flows, mud flows, tuffs and ash flows have been identified.

The 'Verrucano Lombardo' formation overlies, often unconformably, the Collio formation. Consisting of reddish conglomerates, sandstones and siltstones, its depositional environment evolves from that of high energy to a more mature environment that is indicative of the Triassic marine transgression.

The Collio formation has been affected by both Permian and Alpine structural deformation, the effect varying throughout the basin as a result of the lithostratigraphic changes and the distribution of tectonic events. Alpine folding is more developed within the plastic lacustrine facies, whereas rigid deformation prevails in the coarse, poorly stratified alluvial fan facies.

Novazza deposit

The Novazza uranium deposit, located in a Permian acid ignimbrite, lies on the western side of the Seriana Valley 2 km west of Gromo. It was discovered in 1959 by Somiren. Mineralization in Permian sandstones had previously been discovered in the Alps (see later). Study of such occurrences had shown that a part of the uranium minerals was disseminated in the clasts derived from volcanites, which led to the supposition that uranium mineralization might have existed in the Permian volcanics.[6,7] As a consequence, such formations had become a specific target for uranium exploration.

Surface anomalies located by the ground radiometric survey were examined by underground work and 1500 t U_3O_8 (average grade, 0.08%) has been proved.[16] Exploitation will depend on the uranium market and the solution of certain environmental problems.

Recent work by Bakos and co-workers[1] has led to a better understanding of the geology and controls of the deposit (see below).

Geology

The Novazza deposit is located near the southern border of the Collio Basin in one of the volcanic units of the lower Collio formation. In the area of the deposit the crystalline basement is composed of para-schists of low-grade metamorphic facies. These are unconformably overlain by a thick volcanosedimentary sequence that forms the lower portion of the Collio formation (Fig. 4). The lower sedimentary units (*S*1, *S*2 and *S*3, Fig. 4) are mainly coarse-grained basement-derived clastic deposits, typical of a high-energy environment. The upper units (*S*4 and *S*5) are mainly finer sediments indicative of evolution to a more mature lower-energy environment (the last is mostly made up of volcanic fragments). The thicknesses of all the sedimentary units vary markedly over short distances (Fig. 4).

The interbedded volcanic units are mostly acid ignimbrites. The lower units (*I*1 and *I*2, Fig. 4) are thin (maximum 20-m thickness) fine-grained vitroclastic hyalo-ignimbrites. The 'Abete unit' (*I*3 in Fig. 4) is a porphyritic ignimbrite 20–40 m thick. Its basal portion is mostly fine-grained, whereas

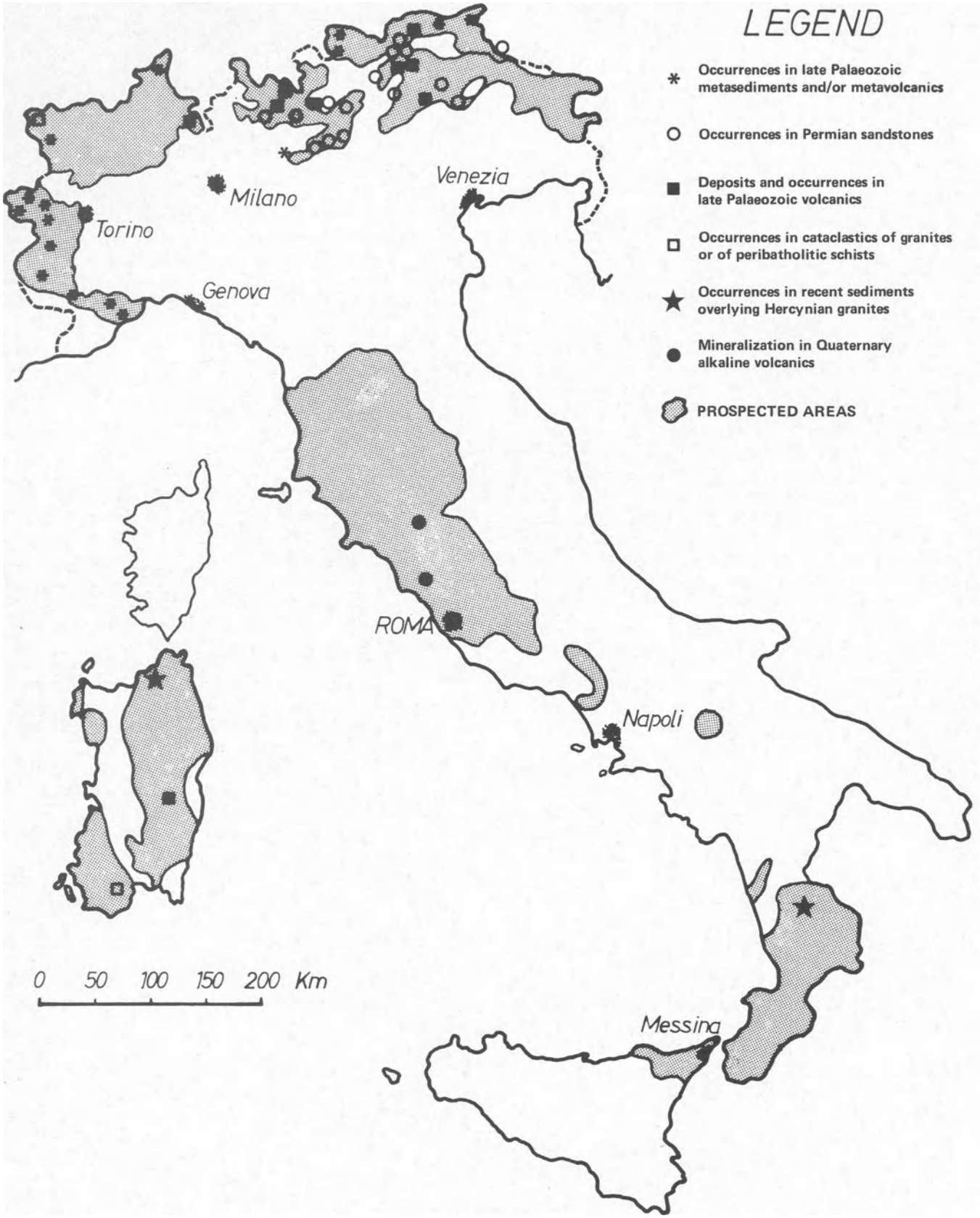

large pumices and glass shards are abundant in the upper portion.

The 'Novazza unit' (*I*4, Fig. 4) is a coarse-grained porphyritic single cooling unit composed of multiple ignimbrite flows. The average thickness is 40 m, but varies from 12 to 90 m. Lithic fragments are abundant in its lower portion. The unit is overlain by two volcanic complexes (*I*5 and *I*6, Fig. 4) made up of multiple aphanitic pyroclastic flows, coarse-grained ignimbrites, lithic and crystal tuffs, volcanic breccias and agglomerates and lava flows of intermediate (probably trachyandesitic) composition. The maximum aggregate thickness of these two complexes is 120 m.

Monogenetic and polygenetic breccia pipes related to east-trending faults cut the volcanic sequences: they are probably the vents of volcanic units that exist in a higher stratigraphic position in the Collio formation.

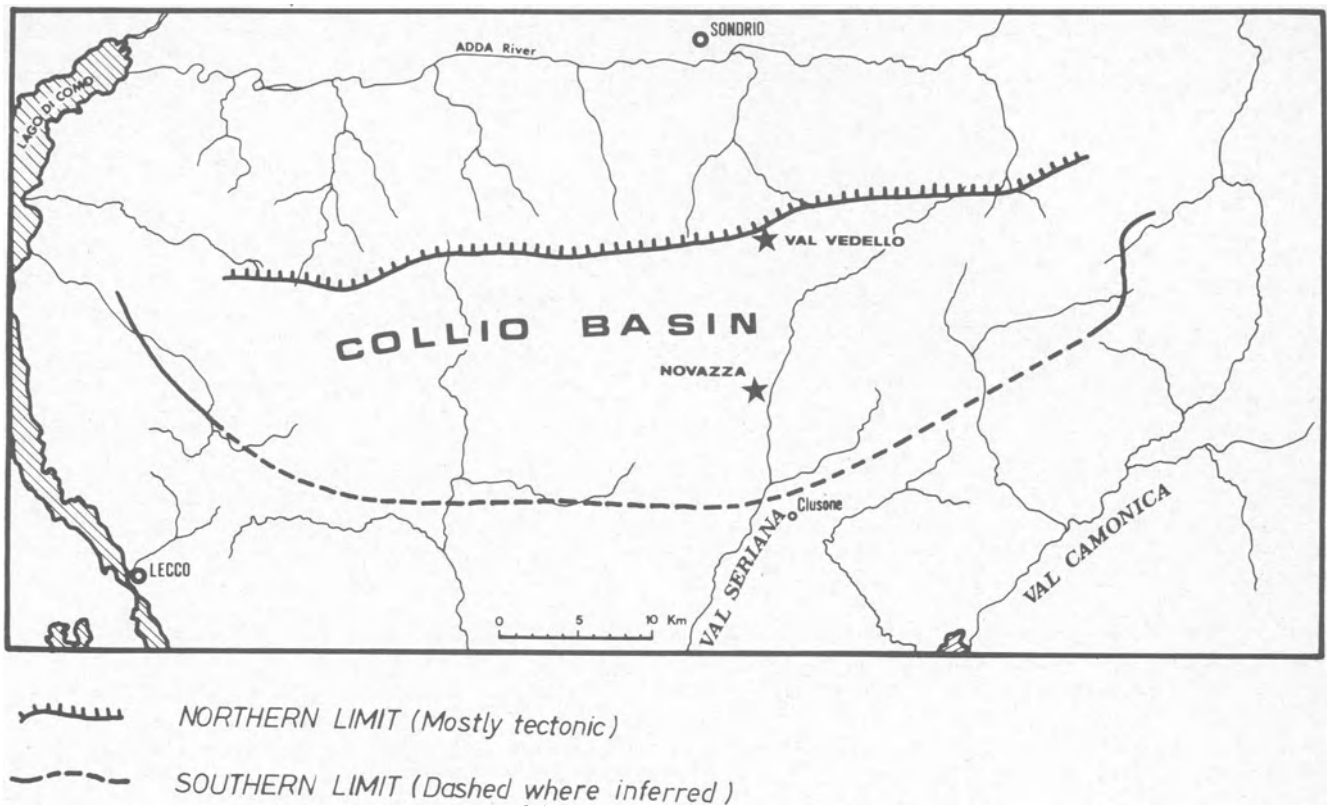

Tectonics

The volcanosedimentary sequence dips about 25°SW. This monoclinal tilt is the main Alpine structural feature of the Novazza deposit area; further to the south the Alpine Val Canale fault places the Permian formations in tectonic contact with the Mesozoic carbonate sequence. Within the ore deposit the important structural features are syndepositional faults.

A succession of three main pre-Alpine (Permian) deformation phases has been recognized.[1] Phase 1 is older than the *S*4 sedimentary units and is responsible for the thickness variability of the lower Collio units. Phase 2 comprises northwest-trending faults that are older than the *I*5 volcanic complex; they are responsible for the formation of the palaeo-structural highs in which the uranium mineralizations are, for the most part, confined (Fig. 4). Phase 3 comprises east-striking normal faults that were probably active after the deposition of units *I*6 and *S*5 (the above-mentioned volcanic pipes are related to this last tectonic phase). The distribution of the uranium mineralization is also related to this structural trend.

Polyphase syndepositional tectonism has strongly influenced the evolution of the lower Collio formation in the Novazza deposit area, affecting both the spatial distribution and the thickness of the various volcanosedimentary units and giving rise to palaeo-structural features to which the location of the uranium orebodies seems to be related.

Mineralization

The uranium mineralization forms east-striking, flat, elongate strato-concordant bodies that are hosted in acid ignimbrites affected by strong deuteric alteration and sulphide mineralization. The main features of the mineralization and of its geological setting are described below.[1]

The volcanics of the Novazza area are generally affected by more or less intense deuteric alteration, which results in a

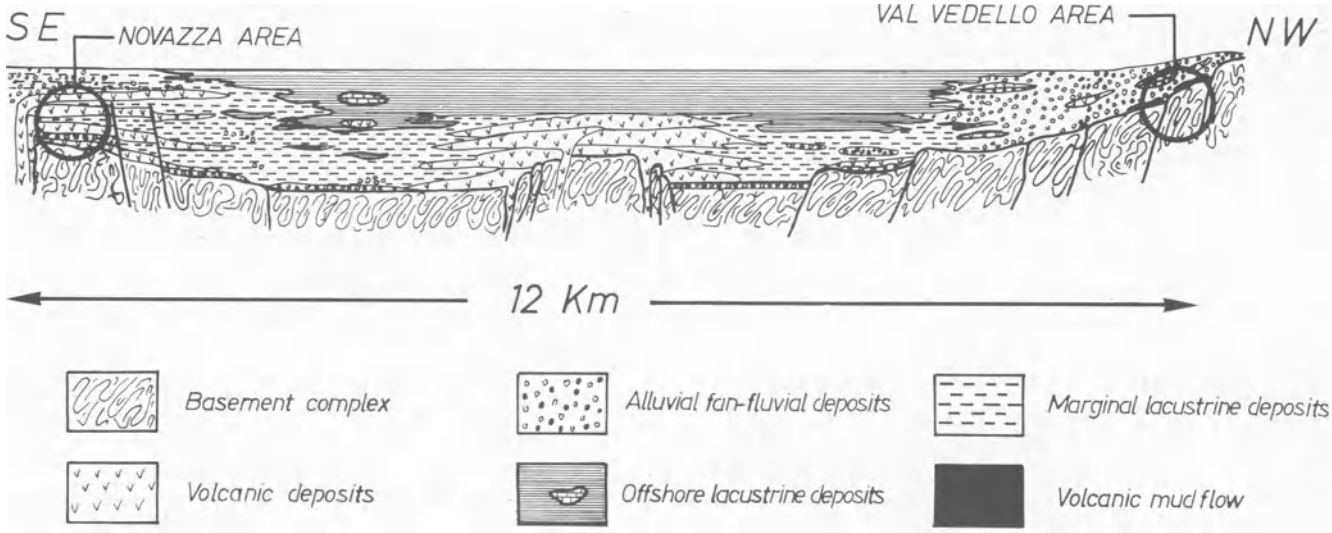

Fig. 3 Diagrammatic cross-section of central Collio basin showing major stratigraphic and structural relationships at end of Collio deposition. After Bakos and co-workers[1]

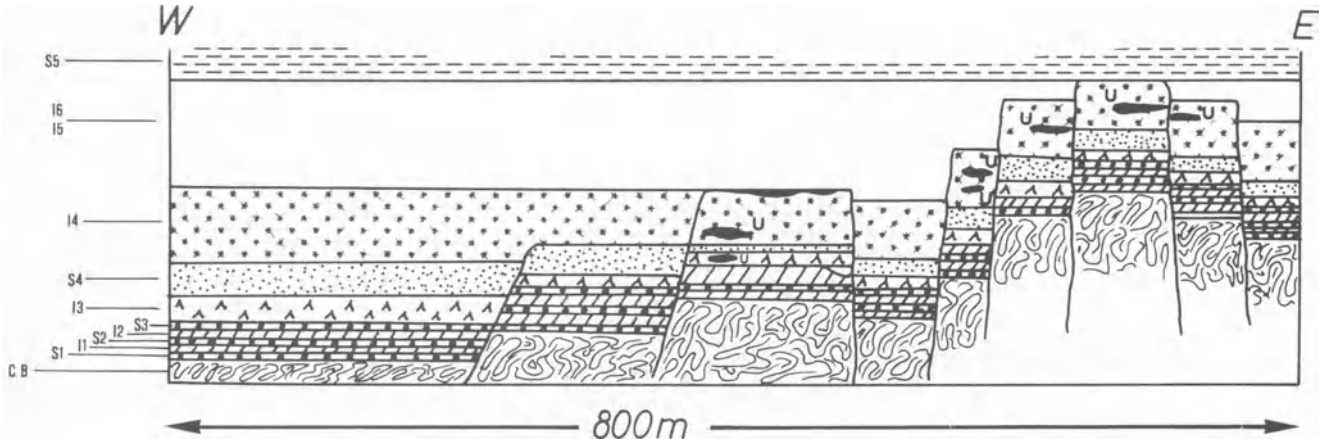

Fig. 4 Novazza area: palaeo-structural sketch shows syndepositional volcano-tectonic block-faulting and distribution of uranium mineralization (*CB*, crystalline basement; *S*1, sieve deposit; *I*1, hyalo-ignimbrite; *S*2, conglomerates and sandstones; *I*2, hyalo-ignimbrite; *S*3, conglomerates and sandstones; *I*3, porphyritic ignimbrite (Abete unit); *S*4, coarse- to fine-grained clastic sediments; *I*4, coarse-grained ignimbrite (Novazza unit); *I*5–*I*6, volcanic sequence of ignimbrites, volcanic agglomerates, lavas, lithic tuffs, volcanic breccias; *S*5, fine-grained sediments; *U*, uranium mineralization). After Bakos and co-workers[1]

quartz–albite–K-feldspar–sericite–tourmaline–pyrite–arsenopyrite association; finely disseminated chalcopyrite, sphalerite and other sulphides are also occasionally present.

Uranium mineralization occurs in the deuterically altered volcanics, and all the orebodies of economic interest lie within the *I*4 Novazza unit (minor mineralization is present in the *I*3 (Abete), *I*5 and *I*6 units). The uranium mineral is pitchblende, accompanied by a second generation of sulphides—mainly sphalerite, galena, tennantite and Mo sulphides. The pitchblende–sulphide mineralization is distributed as fine stockworks in the volcanic host rock and intersects the initial deuteric sulphide mineralization. At the larger scale the uranium sulphide mineralization forms strato-concordant, elongate, east-striking bodies up to 400 m long, 100 m wide and of a maximum thickness of 30 m (Fig. 5). Pyrite and sphalerite are the most abundant sulphides, but the zinc content is not economic.

The upper volcanic units (*I*5 and *I*6) and, in particular, the intermediate lavas have been subjected to occasional intense propylitic alteration, which has resulted in a carbonate–sericite–Fe,Mn oxides association. No uranium or sulphide mineralization is present in the propylitic rocks and even their geochemical uranium content is abnormally low.

The uranium deposit occurs mainly in structural highs of the *I*4 volcanic unit and appears to be related to the last east-striking Permian tectonic phase: the age of uranium deposition is, presumably, younger than the *I*6 volcanic complex, which has occasional mineralization, and is coincident with or younger than that of the third tectonic phase. No definite absolute age determinations are yet available.

The main ore deposit controls are lithogeochemical (acid volcanics, deuteric zones), stratigraphic (lower Collio formation, close to the basement) and structural (syndepositional faults, palaeo-structural highs).

The Novazza deposit may be classified as the 'acid volcanic type' of Dahlkamp.[8] It is considered to be of hydrothermal origin, and its genesis might be analogous to that of similar deposits in the U.S.S.R.[17] and China.[5]

Val Vedello deposit

The presence of radiometric anomalies in the Vedello Valley on the southern side of the Valtellina (Sondrio province, central Alps), was first noted by CNEN geologists in 1969.[13] Significant spectrometric anomalies were found in the area in 1975 by Agip during an experimental helicopter-borne survey; successive ground surveys outlined major uranium mineralization at an altitude of 2000 m above sea-level that is being evaluated by underground work. Some 4000 t U_3O_8 (average grade, 0.1%) has been proved.[2]

Study of the deposit continues and its nature is at present a topic of controversy: some Agip geologists do not agree with the views that are expressed below. The principal points at issue are those which concern the basal Collio palaeogeography and volcanism and their relationship with the formation of the uranium deposit.

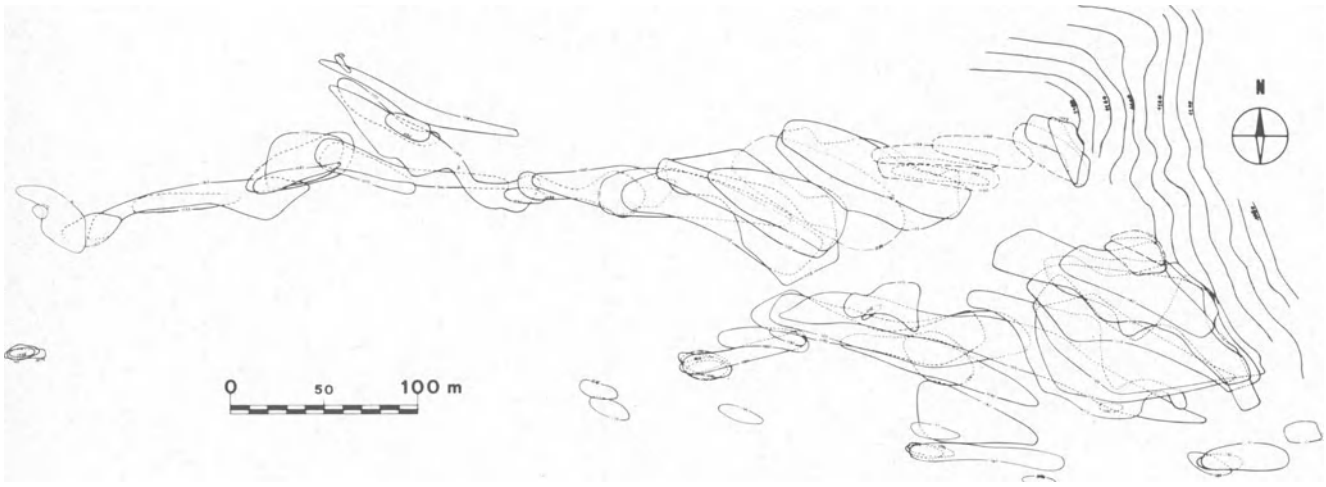

Fig. 5 Novazza deposit: horizontal sections of orebodies at different levels. From Ravagnani[16]

Geology

The Val Vedello deposit lies in the Orobic Alps about 10 km south of the Insubric line that divides the northern and southern Alpine regions. Its location is therefore intermediate between the zones of prevailing Alpine deformation and metamorphism to the north of the line and those in which Alpine metamorphism is almost absent and tectonism is weaker (Orobic Alps). The morphology of the area is very rough owing to glacial action and successive landslides.

The deposit is related to the tectonic contact between the crystalline basement, metamorphosed mostly in Hercynian time, and the post-Carboniferous clastic sequence. The 'Morbegno gneisses', mostly paragneisses of amphibolite facies locally transformed to greenschist facies, are the basement rocks of the area. In the ore deposit zone they are mainly albite–biotite–muscovite gneisses, with rare granate and staurolite; the greenschist facies is therefore dominant, with relicts of amphibolite facies. Deformation was intense and polyphase, the main metamorphic and tectonic phase being the pre-Carboniferous (Hercynian cycle).

The lower levels of the Collio formation, fanglomerates with boulders up to several metres in diameter, minor sandstone and tuff beds, outcrop in the Val Vedello deposit area. The clasts comprise heterogeneous basement rocks (gneisses, schists, phyllites) and volcanics (rhyolitic products and rare andesite lavas); the volcanism was probably penecontemporaneous with the sedimentation. The formation dips about 40°N in the ore deposit area. Large fragments of arenaceous shales, recognized as mud-flow or debris-flow deposits, consisting of basement-derived clasts, are locally present in tectonic contact between the basement and the Collio conglomerates. Arenaceous and argillaceous sediments (Carona schists, beyond the Val Vedello deposit area) were deposited above or alongside the conglomerates.

A typical situation of an active margin of a sedimentary basin, with high-energy gradients, synsedimentary tectonics and volcanism, may be recognized.

Tectonics

The Permian sequences were subjected to strong polyphase Alpine deformation, some phases being mostly plastic (folds), other mainly rigid. Obviously, such tectonics involved also the basement being superimposed on the older pre-Alpine deformation. Detailed structural studies[4] led to the recognition of the following succession of main deformation phases in the Val Vedello area (Fig. 6). Phase 1 involved tectonic contact between the Collio sediments and the Morbegno gneiss. Such a phase may tentatively be interpreted as a Permian synsedimentary event—possibly a normal basin border N60°E-trending fault, dipping 60°SE, rejuvenating an ancient basement fault. Mylonites related to such an event formed both at the Collio–basement contact and, within the two formations, up to several tens of metres from the contact. Phase 2 involved isoclinal recumbent folding with axial plane schistosity. Axial planes strike eastwards and dip to the north. Phase 3 comprises a north-striking normal fault dipping 50°E. The western block has been upthrown several hundred metres, mylonites being produced. This phase is clearly later than phases 1 and 2. Phase 4 comprises east-striking compressive rigid deformation that produced slaty cleavage of the sediments and numerous reverse faults (70°S) and uplifting the southern blocks 100–120 m. The spacing between the major faults is about 300–500 m. This phase is later that the others (Figs. 6 and 7).

Massive rock slides took place in the Quaternary postglacial age on the Vedello Valley slopes.

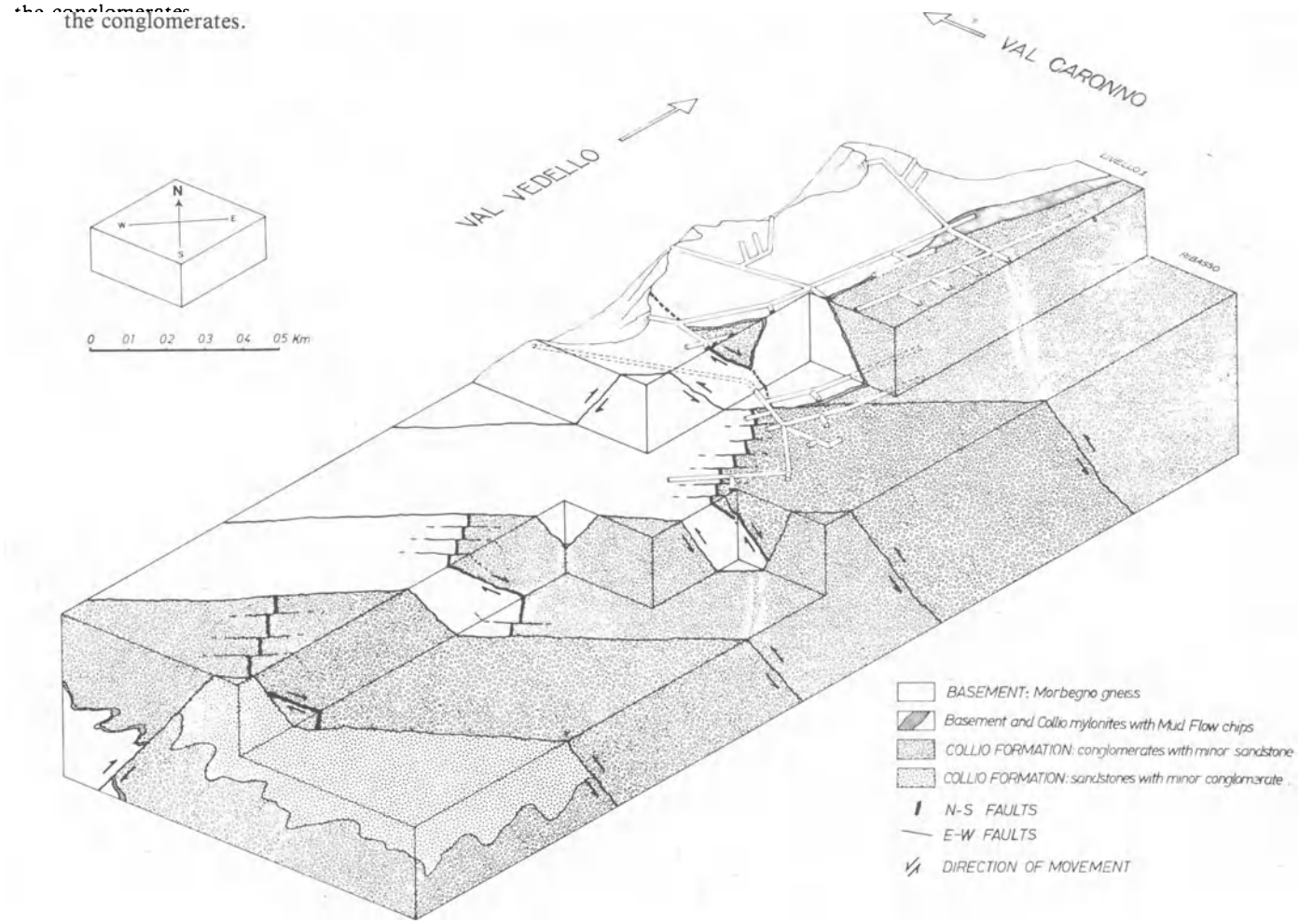

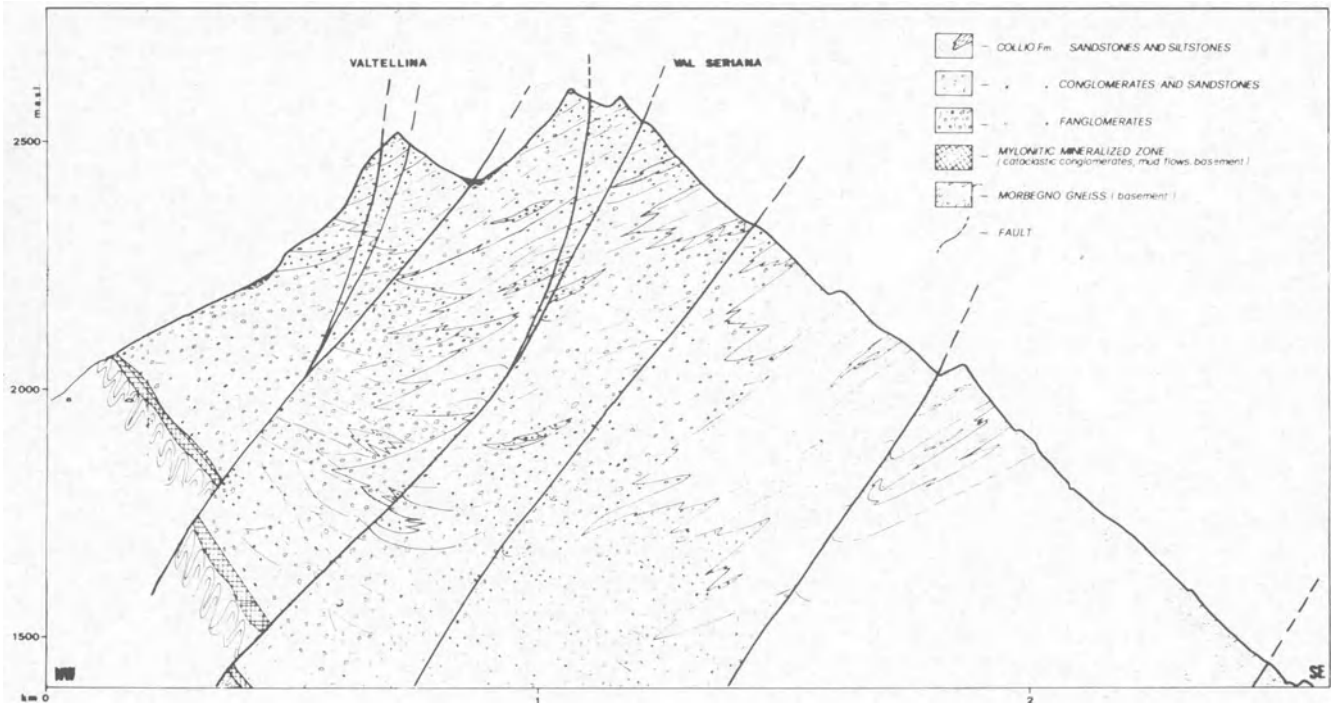

Fig. 7 Cross-section of Val Vedello deposit area. Uranium-bearing mylonitic contact is displayed by east-striking reverse faults. After Brancaleoni and co-workers[2]

Mineralization

The study of Cancelliere and Martinotti[4] resulted in a better understanding of the relationships between tectonic events and uranium mineralization. The Val Vedello uranium mineralization of economic grade is placed in well-defined structural positions related to phases 1 and 3.

The uranium ore related to the N60°E-striking fault of phase 1 is emplaced at the tectonic contact between the basement and the Collio formation and in the cataclastic zones of the two formations—to a maximum distance of 15 m from their contact (C. M. Pessina, personal communication). The uranium deposition was probably not much later than the Collio sedimentation and/or diagenesis, according to some absolute age determinations. The horizontal width of the mineralization varies between 600 m in outcrop to 200 m at the altitude of 1400 m. Its average thickness is 3–4 m.[2]

The mineralization related to the phase 3 north-striking fault is also emplaced at the contact between basement and Collio conglomerates; it forms parallel, 100 m wide, flat bodies elongate along the dip and separated by barren bands. The average thickness of the orebodies is 2 m (C. M. Pessina, personal communication). The probable age of uranium deposition is Alpine. Minor mineralization is related to the phase 4 east-striking faults close to their intersection with the mineralization described above.

Pitchblende, the main uranium mineral, is commonly associated with pyrite, chalcopyrite and rare galena, quartz and carbonates. The distribution of all these minerals is related to the cataclastic zones. Pitchblende is always accompanied by sulphides, but these may well not carry uranium (C. M. Pessina, personal communication).

In conclusion, uranium deposition is clearly related to two main structural events, both distinguished by widely spaced tension faults with wide vertical displacement. Two major controls on mineralization have been identified to date—structural (N and N60°E-trending faults) and lithogeochemical (contact between the basement and the Collio formation or its immediate surroundings). The deposit can tentatively be stated to be of the hydrothermal vein type, though some aspects are typical of the vein-like type.[8]

Uranium occurrences in Permian continental sandstones of the southern Alps

A number of 'sandstone-type' uranium occurrences have been found in the Permian continental sandstones of the southern Alps—the 'Collio' and 'Verrucano Lombardo' formations in the central Alps, the 'Val Gardena sandstones' in the Trentino–Alto Adige region and the eastern Alps (Fig. 1). These clastic fluvial deposits overlie either directly the pre-Hercynian crystalline basement or the post-orogenic volcanics and are overlain by epicontinental sediments.

The 'Val Gardena sandstones' formation was studied by Cadel.[3] The alluvial fan deposits prevail in the basal part of the formation; the braided stream deposits are by far the more abundant. The palaeo-climate was rather hot and arid and favoured the penecontemporaneous oxidation of a large part of the sequence (red sandstones). In places sediments accumulated sufficiently rapidly to prevent oxidation and unoxidized beds could be preserved (grey sandstones in the lower part of the sequence). The rock-forming material was mostly derived from volcanics and metamorphics.

The upper Collio–Verrucano sequence of the central Alps was described earlier.

Uranium occurrences in these clastic formations are widespread, the most important being located in the Rendena Valley area (western Trentino) and in the Seriana Valley (Lombardy). Uranium mineralization is tabular and peneconcordant with the sandstone beds; it is commonly associated with organic matter, the best occurrences being located in the grey beds close to the geochemical boundary with the red beds.

Uranium is mostly microcrystalline uraninite; pitchblende forms local tectonic or diagenetic remobilization. Pyrite is abundant; other sulphides are present but are quantitatively subordinate to uraninite. Uranium mineralization is related to high Pb, Cu, V, Zn and As geochemical values.[6]

The most promising uranium occurrences were investigated by Somiren in the Val Rendena area (1958–60) and Agip in Val Seriana (1976–78). Individual ore lenses proved to be small in size, variable in grade and fragmented by tectonics. Reserves total some 100 t of uranium. Genetically, the mineral-

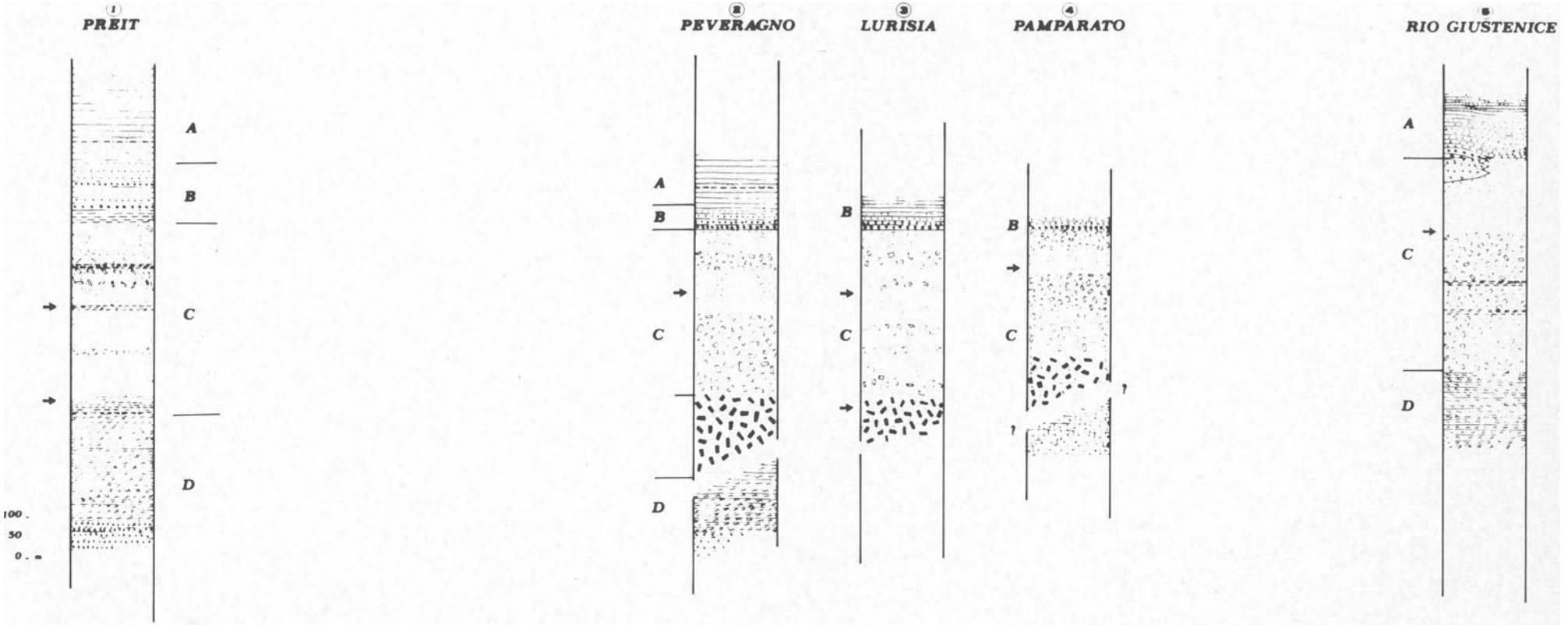

Fig. 8 Cottian and Maritime Alps (Permo-Carboniferous formations). After Prato[15]

ization may be ascribed to 'sandstone-type' epigenetic uranium deposits.

Uranium occurrences in Permian metamorphosed volcanosedimentary formations of western Alps

The most relevant uranium occurrences in the late Palaeozoic metamorphosed sequences of the western Alps are located in the 'Briancon zone' of the Cottian and Maritime Alps (Fig. 8). The host formation is a volcanosedimentary sequence of mostly acid ignimbrites, ash tuffs and argillaceous sandstones due to reworking of volcanic material; it was deposited in a continental environment in the Permian and metamorphosed to

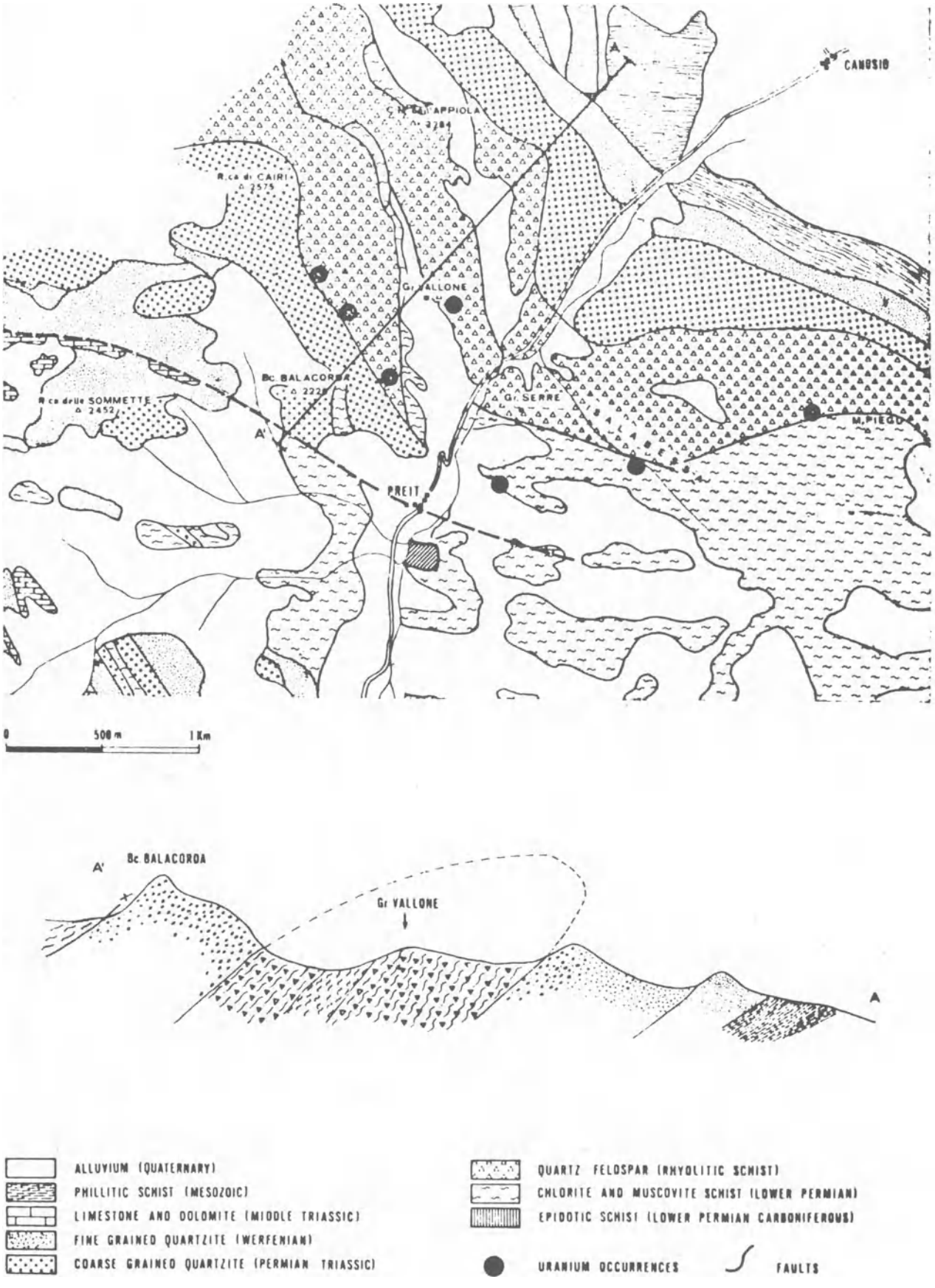

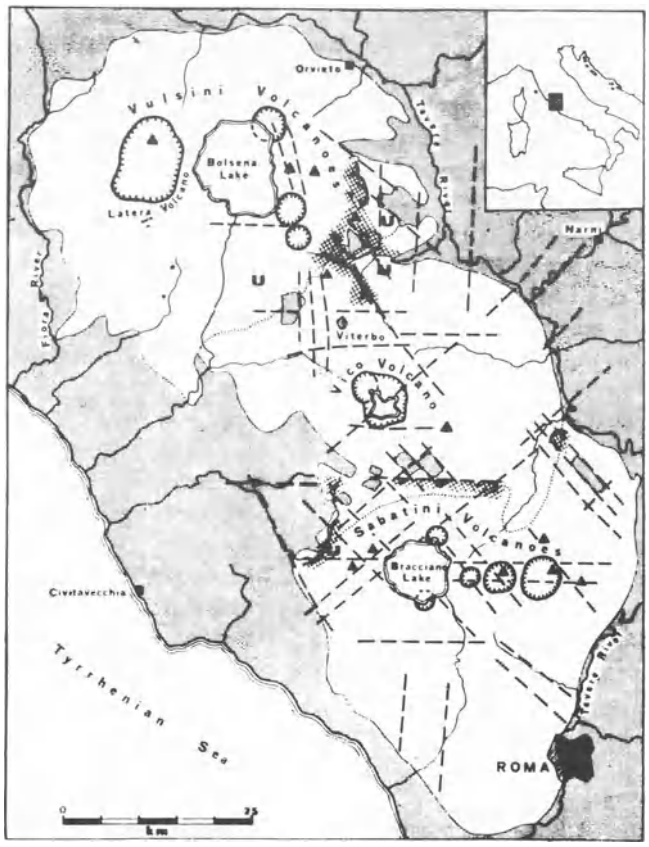

Fig. 10 Type and distribution of U and Th mineralization in Vulsini, Vico and Sabatini volcanic groups. Substratum formed mainly of Plio-Pleistocene clays and Cretaceous-Oligocene flysch. Relationships between faults and calderas, with solfataras (full black triangles) and perivolcanic kaolinic fields (full black lines with cross hatching where fields are buried) may be seen. After Locardi and Mittempergher[11]

greenschist facies in Alpine time.[15] The most significant uranium mineralization occurs in the Preit Valley near Cuneo. The Permian formation is tightly folded in the area (Fig. 9).

Radioactive anomalies were located in the Preit Valley in the year 1956 by CNEN geologists and exploration work underground was carried out by Somiren. A new campaign (15 500 m of drilling) was performed by Agip in the period 1978–80. Six strato-concordant lens-shaped orebodies have been delineated, their diameters varying from 50 to 150 m; the maximum thickness of each mineralized bed is 2 m and several superimposed lenses exist in a stratigraphic interval 5–10 m thick (A. De Bonis, personal communication). Present proven reserves are some 200 t U_3O_8; the average grade is *ca* 600 ppm.[9]

Prato has described the results of geological investigations in the area.[15] Tabular, lens-shaped bodies occur in apatite-rich quartz mica schists composed of alternating muscovite and quartz + feldspar beds interbedded with the acid metavolcanics; petrochemical analyses of the host rocks indicate a composition intermediate between feldspathic sandstones and argillites. The mineral association is pitchblende + pyrite + chalcopyrite + tetrahedrite + hematite, the first two being the most abundant. The uranium + sulphide mineralization is parallel both to the schistosity and to the younger tectonic deformations produced by the Alpine dynamo-metamorphism; in particular, pitchblende is confined to the apatite-rich micaceous beds. Apatite is clearly replaced by pitchblende.

The neoblastic quartz beds contain neither uranium nor sulphides; on the other hand, neoblastic fluorspar crystals are abundant. Fluorspar is also present in the quartz veins that cut the schistosity.

Geostatistical analysis of the distribution of the minor elements shows a Pb–Mo–Hg–U–P association; no association exists between U and organic matter. The organic carbon values were always very low.

Uranium was emplaced after apatite deposition, as the

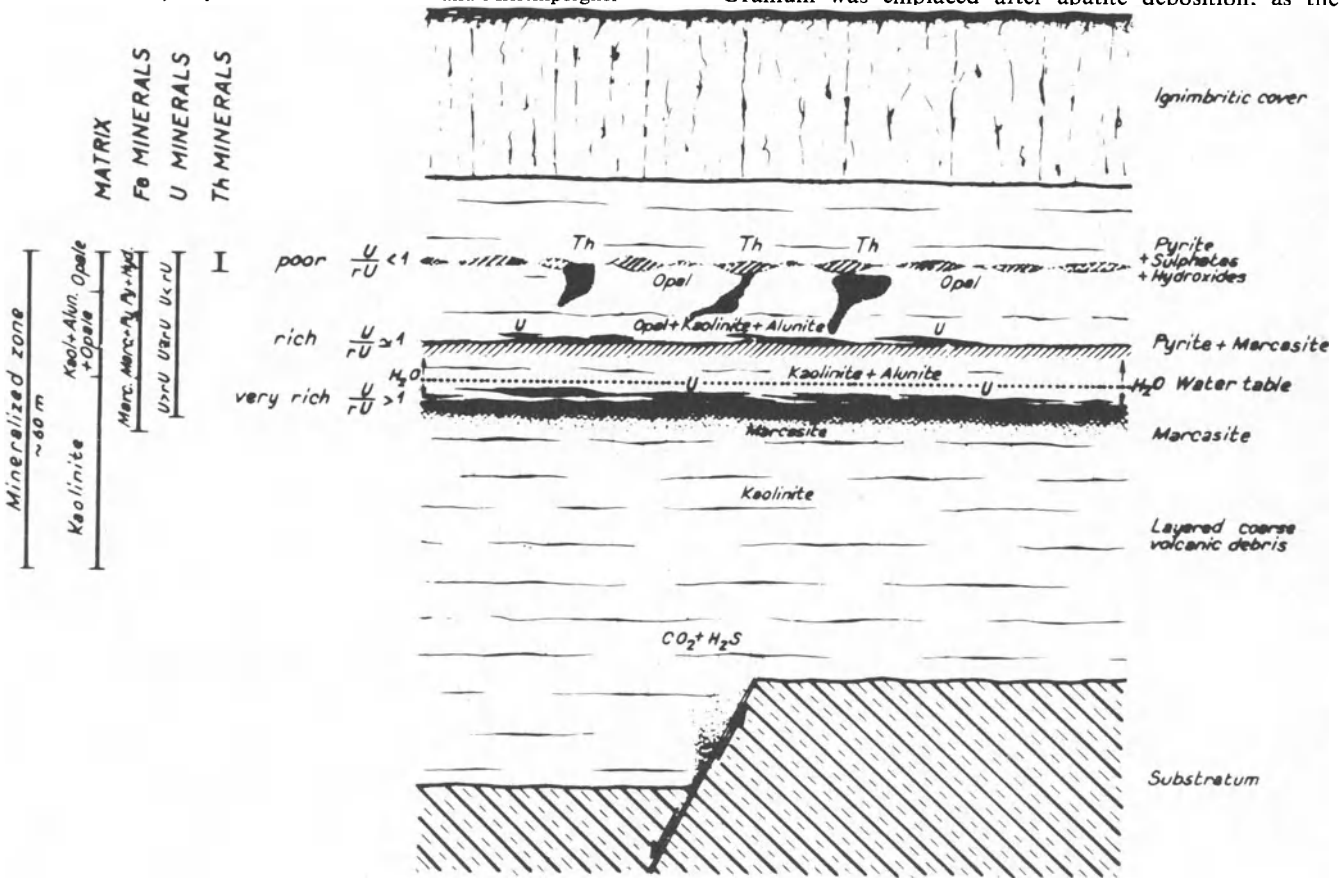

Fig. 11 Ore formation mechanism and typical uranium distribution in volcanic deposits of northern Latium. After Locardi and Mittempergher[11]

replacement phenomena show. On the other hand, the age of the mineralization is clearly pre-metamorphic. Absolute age determinations indicate a Permian age of deposition for the uranium minerals.

Uranium mineralization in Quaternary volcanics of northern Latium

Low-grade uranium deposits occur in the Quaternary alkaline volcanics of northern Latium (Fig. 10).[12] Thin stratiform peneconcordant uranium mineralization is found in reworked loose tuffaceous deposits and, locally, in diatomite layers.[10] Widespread kaolinization and pyrite–marcasite mineralization occur in the host volcanic beds.[11] Uranium mineralization is related to the supergene environment.

The uranium content of the alkaline volcanics of northern Latium is very high (20–70 ppm U). The mineralizing process is related to H_2S rising from the volcanic pile or from deep faults: uranium leached from the volcanics by meteoric waters is reduced and precipitated at the water level by H_2S dissolved in the groundwater. The process is still active (Fig. 11).

Aggregate sub-marginal resources in the area are in the range 5000–10 000 t U_3O_8 at a grade of a few hundred ppm.

References

1. Bakos F. Moratto S. and Veronese L. Considerazioni geominerarie preliminari sulle mineralizzazioni uranifere a solfuri di Novazza. Internal Report Agip SpA, 1981.
2. Brancaleoni G. P. Cosi M. and Pessina C. Uranium exploration Val Vedello Project 1980–1981. Preliminary report on operations from 1.10.1980 to 31.3.1981. Internal Report Agip SpA, 1981.
3. Cadel G. Sedimentologia delle Arenarie di Val Gardena dell'Alto Adige. Internal Report Agip SpA, 1977.
4. Cancelliere G. and Martinotti G. Rilievo geologico strutturale dell'area di Val Vedello. Internal Report Agip SpA, 1981.
5. Chen Zhaobo. 'Double mixing' genetic model of uranium deposits in volcanic rocks and the relationship between China's Mesozoic vein type uranium deposits and Pacific plate tectonics. Paper presented at 26th International Geological Congress, Paris, 1980.
6. D'Agnolo M. Manifestazioni uranifere connesse ad arenarie permiane nel Trentino Sud-occidentale. In *Atti del symposium internazionale sui giacimenti minerari delle Alpi, volume 2* (Trento: C.C.I.A.A., 1966), 253–78.
7. D'Agnolo M. Il giacimento uranifero di Novazza in Val Goglio (Bergamo). Reference 6, 289–317.
8. Dahlkamp F. J. Typology and geographic/geotectonic distribution of uranium deposits. In *Energy resources* Burollet P. F. and Ziegler V. eds (Paris: Edition Technip, 1980), 499–536. *(26th Int. Geol. Congr., Colloque C2)*
9. De Bonis A. Relazione tecnica relativa ai sondaggi del Preit. Internal Report Agip SpA, 1979.
10. Ferretti O. and Molin D. Concentrazioni di carnotite in un bacino diatomifero del Viterbese. *Rc. Soc. ital. Miner. Petrol.*, **27**, 1971, 149–65.
11. Locardi E. and Mittempergher M. Exhalative supergenic uranium, thorium and marcasite occurrences in Quaternary volcanites of Central Italy. *Bull. volcan.*, **35**, 1971, 173–84.
12. Locardi E. Mineralizzazioni ad Uranio in vulcaniti quaternarie del Lazio. *Boll. Soc. geol. ital.*, **92**, 1973, 541–66.
13. Mittempergher M. Mineralizzazioni uranifere della Valle del Belviso. *Notiz. CNEN*, **16**, 1970, 39–50; *Chem. Abstr.*, **76**, 1972, 143422.
14. Mittempergher M. Le ricerche per uranio in Italia: risultati conseguiti e prospettive. *Notiz. CNEN*, **18**, no. 4 1972, 25–39.
15. Prato R. Uranium occurrences in the Western Alps. Internal Report Agip SpA, 1980.
16. Ravagnani D. Il giacimento uranifero di Novazza. Internal Report Agip SpA, 1980.
17. Kazansky V. I. and Laverov N. P. Deposits of uranium. In *Ore deposits of the U.S.S.R., volume II* Smirnov V. I. ed. (London: Pitman, 1977), 349–424.

Name index

Abeledo M. E. J. de 68
Abeledo M. J. de 54, 67
Adamek P. M. 160
Adams J. A. S. 2, 20, 21, 22, 136
Adams J. W. 136
Adams S. S. 26, 37, 38, 40, 41, 42, 107
Adler H. H. 22, 99
Agrinier H. 67
Ahern J. L. 9, 11
Ahmed F. R. 70
Åkerblom G. V. 168, 177
Albee A. L. 11, 138
Alderton D. H. M. 171, 177
Alekseeva M. A. 59, 67
Allègre C. J. 5, 10, 11
Allman-Ward P. 178
Allsop H. L. 178
Altschuler Z. S. 22
Amstutz G. C. 99
Anderson C. A. F. 54, 67
Anderson D. C. 136
Anderson D. L. 9, 11
Anikina L. I. 62, 63, 67, 69
Appleman D. E. 60, 62, 67, 68, 70
Applin K. 116
Arashov A. 137
Arengi J. T. 136
Armstrong C. W. 107
Armstrong F. C. 136, 178
Arnold R. G. 128, 136
Arribas A. 46, 67
Atherton M. P. 177
Atkin B. P. 170, 177
Atkin D. 68
Aubouin J. 160
Aumento F. 99
Austin S. R. 38, 42
Autran A. 145, 160

Bach A. 160
Bachet B. 68
Backström J. W. von 139
Badham J. P. N. 136
Baer T. 42
Bailey D. K. 4, 10, 136
Bailey R. V. 136
Bain J. H. C. 99, 136
Bakos F. 179, 181, 188
Baldridge W. S. 11
Ball T. K. 116
Ballantyne S. B. 115
Bamford D. 177
Barbier M. J. 177
Barnes W. H. 70
Barretto P. M. C. 41, 108
Barrington J. 136
Bartel A. J. 42
Bastovanov M. 52, 68
Bayushkin I. M. 46, 67
Beauchemin Y. 42
Beck L. S. 136
Beckinsale R. D. 169, 177
Becquerel H. 1, 2
Begovich C. L. 42
Beintema J. 57, 58, 67
Bell K. 99
Bell K. G. 136
Bell R. T. 99
Belov N. V. 70
Belova L. N. 55, 67, 68
Bennett J. T. 5, 10
Bennett T. J. 10
Benyacar M. A. R. de 68
Benyacar M. R. de 67, 68
Berezina L. A. 124, 136
Bergeron M. B. 10
Berman H. 69, 86, 88
Bernard A. J. 99
Bernat M. 11
Berning J. 99, 136
Beus A. A. 115
Bhattacharyya B. K. 30, 41
Bignand C. 49, 68
Bird A. G. 132, 137
Bird J. M. 121, 137
Bjørlykke K. 99
Blackwell J. D. 89
Blanchot A. 115
Boberg W. W. 107
Boettcher A. L. 4, 10
Bohse H. 22, 121, 136
Borène J. 59, 60, 68
Bornhorst T. J. 10
Bosschart R. A. 30, 41
Botbol J. M. 35, 42
Bottrill T. J. 137
Bowden P. 137
Bowen N. L. 139
Bowie S. H. U. 22, 116, 137, 177, 178
Bowker A. H. 42
Bowles J. F. W. 175, 178
Bown R. W. 108
Boyd F. R. 10
Boyle R. W. 115
Brancaleoni G. P. 184, 188
Branche G. 59, 68
Brandenburg N. P. 62, 64, 65, 66, 68, 69
Brandstätter F. 68
Brewster N. E. 107
Bridgewater D. 137
Brindley G. W. 52, 68
Brophy G. P. 62, 68
Brown G. C. 177
Brulhet J. 157, 158, 160
Brummer J. J. 107
Buddington A. F. 178
Bültemann H. W. 55, 68, 160
Bunting J. A. 177
Burnol L. 177
Burollet P. F. 41, 99, 137, 188
Burt D. M. 99
Buryanova E. Z. 59, 68
Busson G. 160
Butt C. R. M. 137
Button A. 178

Cadel G. 184, 188
Cadigan R. A. 115
Cahen L. 137
Calas G. 8, 9
Callihan M. C. 42
Cameron E. M. 107, 115, 116
Cameron E. N. 99
Campbell F. H. A. 100
Campbell J. A. 41
Cancelliere G. 183, 184, 188
Capaldi G. 5, 6, 10
Capdevila R. 160
Capus G. 157, 160
Card K. D. 99
Cariou L. 149, 160
Carlisle D. 137
Carmichael I. S. E. 11
Carr W. J. 139
Carraway K. 100, 137
Carre J. L. 160
Carswell L. D. 130, 138
Carter S. R. 11
Casentini E. 22
Castro L. O. 137
Cathelineau M. 148, 160
Centaro G. 166
Cesbron F. 52, 58, 59, 60, 66, 68
Chaffee M. A. 42
Chamberlain J. A. 115
Chappel B. W. 168, 177
Charbonneau B. W. 100, 138
Chase C. G. 7, 9, 11
Chatham J. R. 41, 42, 107
Chatterjee A. K. 178
Chen Zhaobo 188
Chenevoy M. 145, 160
Chernikov A. A. 53, 68
Chevalier R. 48, 68
Chork C. Y. 115
Christ C. L. 49, 51, 64, 65, 68
Christopher J. E. 138
Christopher P. A. 99
Church S. E. 4, 9, 10
Civetta L. 11, 22
Clark J. R. 49, 51, 65, 68
Clark S. P. Jr. 137
Clarke D. B. 178
Clarke P. J. 108
Clarke R. S. Jr. 22
Clasen D. 46, 70
Clergue I. 115
Clifford T. N. 137
Cloud P. 99
Coda A. 68
Cogné J. 160
Cohen R. S. 11
Cohen-Addad C. 68
Cohenour R. E. 137
Coleman R. F. 116
Coleman R. G. 62, 65, 68
Conant L. C. 99, 137
Condomines M. 5, 8, 10, 11
Connan J. 160
Conrad W. K. 100
Cooke H. B. S. 178
Corbett R. G. 137
Cordfunke E. H. P. 63, 68
Corretgé G. 160
Cortini M. 4, 10, 11
Cosi M. 188
Crick I. H. 100

Cromer D. T. 70
Crookes *Sir* William 1
Cruz P. R. 138
Cunningham C. G. 137
Cuney M. 99, 149, 150, 160
Curie M. S. 1
Curie P. 1
Curtis L. 99
Czarnecki R. F. 33, 42

Dagbert M. 42
D'Agnolo M. 99, 188
Dahl A. R. 99
Dahlberg E. C. 42
Dahlkamp F. J. 26, 40, 41, 99, 117, 137, 182, 188
Dall'Aglio M. 19, 22, 115, 116
Dana E. S. 43
Daniels J. J. 108
Dardel J. 140, 148, 151, 152, 160
Darnley A. G. 137, 177
David M. 37, 42
Davidson C. F. 137
Davis M. 22, 116, 177
Dawes P. R. 99
de Abeledo M. E. J. *see* Abeledo M. E. J. de
Dearnley R. 99
de Benyacar M. A. R. *see* Benyacar M. A. R. de
De Bonis A. 188
Declercq J. P. 69
Degens E. T. 137
Delany A. C. 116
Deliens M. 50, 52, 53, 55, 65, 68, 69, 70, 71
Denson N. M. 137
Derrick G. M. 137
Dercourt J. 160
Derry D. R. 128, 137
De Vivo B. 10, 161, 162
De Voto R. H. 99, 101, 108, 137
Dewey J. F. 121, 137
Dines H. G. 177
Dodson R. G. 137
Doi K. 46, 69
Dongarra G. 18
Donnay G. 65, 68
Donnay J. D. H. 65, 68
Downs G. R. 132, 137
Dunn C. E. 100, 108, 137, 138
Dupré B. 11
Dupree J. A. 99
Durham C. C. 116
Dybek J. 137
Dyck W. 31, 32, 33, 41, 42, 99, 116

Eargle D. H. 99
Eichmann R. 178
Eisenhower D. D. 162
Emerson D. O. 53, 68
Epstein G. Yu. 62, 68
Erasmus C. S. 178
Erdman J. A. 42
Erkan E. 160
Erlank A. J. 4, 10
Ertl R. F. 53, 68
Ertl S. 53, 68
Ertle H. J. 154, 160
Evans A. M. 178
Evans H. T. Jr. 51, 57, 58, 60, 62, 67, 68, 70
Evans R. 10

Fairchild J. G. 58, 68
Faure G. 11
Faure J. 160
Fei Q. 99
Felmlee J. K. 115
Ferguson J. 42, 99, 100, 107, 137
Fernandez Polo J. A. 153, 160
Ferretti O. 188
Ferris C. S. 128, 137
Fettes D. J. 178
Finch W. I. 126, 137
Fischer R. P. 41
Fisher J. C. 108
Fix P. F. 116
Fleischer M. 43, 68
Fleischer R. L. 116
Floor P. 160
Florjančič A. P. 159, 160
Fogwill W. D. 108
Foreman D. W. Jr. 68
Forster I. F. 137
Fraser D. C. 41
Freeman R. W. 42
Friedman G. M. 116
Fritz P. 100, 138
Froideveaux R. 42
Frondel C. 43, 44, 46, 49, 50, 52, 55, 62, 63, 64, 65, 68, 86, 88
Fuchs L. H. 46, 68
Fuzikawa K. 100
Fyfe W. S. 99, 100, 177

Gagnadre A. 147, 160
Gaines R. V. 68
Gallagher M. J. 68
Galloni E. E. 67
Galloway W. E. 99, 108
Galy J. 66, 69
Garlick W. G. 137
Garrett R. G. 42, 115, 116
Garson M. S. 169, 177
Gasparini P. 1, 2, 22
Gasperin M. 48, 68, 69
Gass I. G. 137
Gast P. W. 4, 5, 10
Gastil G. 99
Gauthier-Lafaye F. 99
Gavrilova I. N. 68
Gebert E. 46, 68, 70
Geffroy J. 116, 160
Geisel E. 99
Gerasimovsky V. I. 43, 69
Gesell T. S. 22
Getseva R. V. 43, 69
Ghandi S. S. 99
Giblin A. M. 99
Gigli C. 116
Gill J. E. 137
Gill J. R. 137
Gillot P. Y. 10
Glanzman R. K. 138
Glikson A. Y. 99
Gold D. P. 137
Goldhaber M. B. 42
Goleby A. B. 42, 99, 107, 137
Goleva R. V. 136
Goodell P. C. 10, 99, 100, 137, 138
Gorman D. H. 54, 69
Gornitz V. 137
Granger H. C. 42, 100, 137
Granier C. 116
Grasty R. L. 137
Grigorian S. V. 115
Grimbert A. 116
Grønvold F. 45, 69
Gross E. B. 69
Gross G. A. 100
Gross W. H. 100
Gruner J. W. 70
Grutt E. W. Jr. 177
Guillenmin C. 64, 69
Guillot P. L. 145, 160
Guy-Bray J. V. 99

Haftka F. J. 138
Haglund D. S. 116
Hagmaier J. L. 99
Haines E. L. 10
Hamilton E. I. 10
Hamilton G. N. G. 178
Hamilton J. C. 42
Hanrahan E. J. 108
Harrach G. H. 42
Harris A. L. 177
Harshman E. N. 38, 42, 100, 108
Hawkes H. E. 35, 42, 116
Hawkes J. 178
Hawkesworth C. J. 9, 10
Hawkins B. W. 137
Haynes D. W. 137
Hegge M. R. 100
Heier K. G. 137
Heine T. 108
Heinrich E. W. 43, 69
Henry C. D. 137
Hermes O. D. 11
Herschel *Sir* William 22
Hills J. H. 100
Hilpert L. S. 135, 137
Hirono S. 100
Hoag R. B. Jr. 38, 42, 116
Hodder R. W. 99
Hoekstra H. R. 49, 69, 70
Hoeve J. 41, 42, 100, 137
Hogarth D. D. 48, 69
Holland C. H. 177
Holland H. D. 10, 41, 100, 178
Hollis J. D. 4, 10
Honea R. M. 53, 69
Hood P. J. 116
Hornbrook E. H. W. 107, 115
Horowitz R. C. 137
Hosking K. F. G. 177
Howarth R. J. 175, 177
Hunt E. C. 116

Hunter D. R. 175, 176, 178
Hurdley J. 177
Hutchinson R. W. 89, 99, 100
Hutton C. O. 69
Huynen A. M. 54, 69
Hyde E. K. 3
Hyde R. S. 100

Iannelli T. R. 100
Illsley C. T. 116
Il'menev Ye. S. 46, 67
Ippolito F. 161, 162
Ito J. 68

Jackson G. D. 100
Jacob R. E. 139
Jahn B. 11
Jaquet J. M. 42
Jarrard L. D. 100
Jeannin Y. 69
Jennings J. K. 41
Jones C. A. 108, 137
Jones M. J. 99, 138, 160, 177, 178
Jöreskog K. G. 37, 42
Journel A. G. 42
Julivert M. 140, 160
Junge C. E. 178
Jurain G. 116

Kaiman S. 70
Kalnins T. 99
Kalyaev G. I. 137
Kamhi S. R. 69
Kane V. E. 42
Katayama N. 100
Kazansky V. I. 188
Kehn T. M. 137
Keith M. L. 42, 116
Kelsall D. T. 137
Keppie J. D. 178
Kermeen J. S. 137
Kerr P. F. 62, 68, 136, 137
Khitarov N. I. 22
Khoo F. 137
Khosrawan-Sazedj F. 57, 69
Kidwell A. L. 108
Killeen P. G. 100, 138
Kimberley M. M. 69, 99, 138
King J. W. 42
Kirvokoneva G. K. 47, 69
Kiss J. 63, 69
Klaproth M. H. 18
Klohn M. L. 42
Klovan J. E. 37, 42
Kneuper G. 160
Knight C. L. 100, 137
Knipping H. D. 100, 137
Koch G. S. Jr. 37, 42
Kopchenova E. V. 47, 69
Kossmatt F. 140, 160
Kovba L. M. 52, 69
Krajnov S. R. 116
Krauskopf K. B. 18, 22
Kreitler C. W. 108
Krishnaswami S. 10
Krutetskaya O. V. 68
Kubo K. 100

Laborde A. 1
Landais P. 160
Langen R. E. 108
Langford F. F. 137
Langmuir D. 21, 22, 40, 41, 42, 59, 64, 69, 89, 100, 107, 116
Larsen A. C. 70
Larsen E. S. Jr. 69, 86, 88
Laverov N. P. 188
Laversanne J. 155, 156, 160
Lazenby P. G. 30, 41
Leake B. E. 177
Legros J. P. 69
Lehrman N. J. 138
Lepeltier C. 35, 42
Leroy J. 100, 145, 146, 147, 160
Leventhal J. S. 41
Levinson A. A. 30, 41, 116
Lewry J. F. 100
Liberman G. J. 42
Liebenberg W. R. 137, 178
Lindroos H. 160
Lindsay D. A. 100
Link R. F. 37, 42
Lipscomb W. N. 70
Lister C. J. 177
Little H. W. 137
Llewelyn G. I. W. 130, 137
Lloyd F. E. 4, 10
Locardi E. 9, 187, 188
Locke C. A. 177
Long C. B. 169, 177
Loopstra B. O. 51, 62, 63, 64, 65, 66, 68, 69, 70
Lotze F. 140, 160
Lovering T. S. 116
Lowder W. M. 22
Lukacs E. 159, 160
Lur'e E. A. 70
Lynch J. J. 116
Lyttle T. 139

McBurney T. C. 53, 69
McCammon R. B. 42
McCarthy G. J. 69
MacDonald B. C. 137
McDonald R. 10
McDowell J. P. 129, 138
McGowen J. H. 108
McKelvey V. E. 130, 138
MacKevett E. M. Jr. 132, 137
McLennan S. M. 100
McMillan R. H. 23, 40, 41, 89, 90, 100, 138
McNeil M. 138
Makarov Ye. S. 62, 63, 67, 69
Malan R. C. 138, 177
Mann A. W. 69, 137
Mannweiler U. 138
Marciel A. E. 138
Markgraf S. A. 67
Marquaire Ch. 145, 160
Martin J. 116
Martinez F. J. 160
Martinotti G. 183, 184, 188
Masaki N. 46, 69
Maslyn R. M. 99
Mathews G. W. 23, 26, 41, 108, 138
Maxwell C. H. 138
Meilleur G. A. 116
Mendelsohn F. 137
Menzies M. 4, 10
Mereiter K. 51, 52, 69
Meunier G. 66, 69
Meyer H. O. A. 10
Meyer K. 138
Meyrowitz R. 68, 71
Michaelis W. 137
Mickle D. G. 23, 41, 137, 138
Miller A. R. 99
Miller D. S. 116
Milton C. 65, 69
Minter W. E. L. 138
Mitchell A. H. G. 169, 177
Mitronova O. F. 21, 22
Mittempergher M. 100, 180, 187, 188
Moh G. H. 55, 68
Mokeeva V. I. 54, 69
Molin D. 188
Momme I. A. 70
Moore G. W. 22
Moore J. McM. 178
Morand P. 10
Moratto S. 188
Moreau M. 145, 147, 153, 159, 160, 177
Morin N. 59, 68
Morley L. W. 30, 41
Morosin B. 57, 69
Moroz I. Kh. 70
Morse J. G. 108
Morse R. H. 33, 42
Morton R. D. 69, 100, 138
Mosher D. V. 108, 134, 138
Motica J. E. 100
Mücke A. 69
Muecke G. K. 178
Muir M. D. 177
Müller H. 160
Munday R. J. C. 100
Murdoch J. 53, 69
Murphy M. 122, 138
Murthy V. R. 4, 10
Muto T. 47, 69

Naito K. 46, 69
Nash J. T. 41, 42, 100, 138
Naumov G. B. 21, 22
Needham R. S. 100
Nekrasova Z. A. 69
Nesbitt R. W. 10
Neumann E.-R. 10
Nichol I. 37, 42, 116
Nichols C. E. 23, 33, 41
Niinisto L. 63, 69
Nishimori R. K. 122, 138
Nitu G. 160
Nkomo I. T. 32, 42, 177
Noe-Spirlet M. R. 50, 69
Norry M. J. 4, 7, 9, 10

Obellianne J. M. 116
O'Connor P. J. 177
O'Donnell R. J. 100
Offield T. W. 108
Ohmoto H. 138
Ojakangas R. W. 125, 138
O'Nions R. K. 10, 11
Oosterbosch R. 68
Organova N. I. 68
O'Rourke P. J. 100
Osmond J. K. 22
Ostle D. 22, 116, 177
Ottonello G. 9
Outerbridge W. F. 53, 69
Oversby V. M. 5, 10
Owens O. E. 137
Owens R. B. 1

Pacer J. C. 42
Palacky G. J. 30, 41
Pankhurst R. J. 10
Parrish I. S. 136
Paschis J. A. 137, 138
Patchett J. 128
Paterson N. R. 30, 41
Patterson J. A. 108, 130, 138
Pece R. 10
Pelchat J. C. 116
Pemberton R. H. 30, 41
Pertlik F. 138
Pessina C. M. 184, 188
Peterman Z. E. 137
Petersen U. 10, 41, 100
Peterson A. 143, 160
Peterson F. 42
Peterson R. J. 41
Petrascheck W. E. 159, 160
Pickens W. R. 42
Pierrot R. 66, 68, 69
Pierson J. R. 139
Piret P. 50, 55, 57, 58, 60, 65, 68, 69, 71
Piret-Meunier J. 54, 69, 70
Pitcher W. S. 178
Pitman R. K. 130, 138
Plant J. A. 167, 172, 177
Pogorski L. A. 42
Pont E. 166
Pournis S. 108
Powell J. D. 122, 138
Prato R. 185, 186, 188
Preston H. 65, 68
Preto V. A. 100
Pretorius D. A. 100, 138
Price T. J. 42
Prichard C. E. 100
Prodehl C. 177
Protas J. 52, 64, 69, 70
Pudovkina I. A. 43, 47, 55, 70, 86, 88

Quirt G. S. 42

Rackley R. I. 25, 41, 100
Radusinović D. 160
Raines G. L. 108
Ramberg I. B. 10
Ramdohr P. 138, 178
Ramsey *Sir* W. 1
Ranchin G. 116, 145, 160
Rankin A. H. 171, 177
Ravagnani D. 182, 188
Renfro A. R. 41
Reyment R. A. 42
Reynolds R. L. 42
Ribeiro A. 160
Rice C. M. 178
Rich R. A. 10, 26, 41, 89, 100
Richards J. R. 100
Richardson K. A. 100, 136, 138
Richardson S. H. 10
Ridge J. D. 100, 138
Ridgley J. L. 116
Robbins D. A. 108
Roberts A. E. 100
Robertson D. S. 100
Robertson J. A. 100, 128, 129, 138
Robinson B. W. 138
Rogers J. J. W. 20, 22, 41
Rogers N. W. 10
Rogova V. P. 52, 70
Romberger S. B. 12
Röntgen W. K. 1
Roof R. B. Jr. 70
Roper M. W. 100, 138
Roscoe S. M. 100, 138
Rose A. W. 35, 41, 42, 116
Rose W. I. Jr. 10
Rosenzweig A. 54, 70
Rosholt J. N. 32, 42, 121, 138
Ross D. R. 68
Ross M. 57, 58, 62, 70
Roubault M. 160
Routhier P. 116
Rowntree J. C. 99, 108, 134, 138
Rudd C. W. 128, 137
Ruh R. 70
Rundle C. C. 178
Runnells D. D. 108
Rupnitskaya L. S. 62, 70
Rutherford E. 1, 2
Ruzicka V. 26, 41, 100, 138, 158, 161
Ryan R. R. 54, 70
Rye R. O. 42
Rytuba J. J. 100, 138

Saager R. 178
Sámsoni Z. 10
Santos E. S. 108, 138
Santouil G. 161
Saprykina T. V. 22
Sarcia J. A. 116, 147, 160, 161
Sass J. H. 142, 161
Sassano G. P. 100, 138
Satterly J. 138
Saucier A. E. 37, 42
Saveleva K. T. 43, 69
Scheetz B. E. 67
Schidlowski M. 138, 178
Schilling J.-G. 4, 10, 11
Schmidt G. C. 1
Schmidt-Collerus J. J. 37, 42
Schoep A. 49, 70
Schopf J. W. 138
Scott J. H. 108
Scott S. D. 26
Scott W. J. 41
Serezhkin V. 70
Sergeev A. S. 55, 70
Shaeokang H. 99
Shaner B. E. 46, 70
Shannon S. S. Jr. 31
Shashkin D. P. 54, 60, 68, 70
Shchipanova O. V. 70
Sheldon R. P. 138
Sheridan D. M. 138
Sheridan M. F. 99
Sherwood A. M. 70
Shitov V. A. 68
Shockey P. N. 41
Shrimpton G. J. 177
Sibbald T. I. I. 41, 42, 100, 133, 137, 138
Sidelnikova V. D. 68
Sidorenko G. A. 53, 70
Siegel S. 49, 51, 69, 70
Siegl W. 160
Simen F. 166
Simpson P. R. 167, 168, 170, 171, 175, 176, 177, 178
Sinclair A. J. 35, 42
Skvortsova K. V. 47, 70
Slansky M. 160
Smart P. G. 138
Smellie J. 160
Smellie J. A. T. 177
Smirnov V. I. 188
Smith A. Y. 108, 116
Smith B. 108
Smith D. A. M. 131, 138
Smith D. K. 10, 43
Smith D. K. Jr. 53, 54, 70
Smith R. B. 42
Snelling N. J. 178
Soboleva M. V. 43, 47, 55, 70, 86, 88
Sobry R. 50, 51, 52, 67, 69, 70
Soddy F. 1, 2
Soister P. E. 138
Somayajulu B. L. K. 10
Sørensen H. 138, 161
Soyer B. 109
Spector A. 30, 41
Spera F. J. 4, 10
Staatz M. H. 132, 138, 139
Steacy H. R. 70
Steenfelt A. 177
Stemprok M. 177
Stern T. W. 70
Stettner G. 154, 161
Steven T. A 137
Stevens D. N. 137
Stieff L. R. 46, 70
Stohl F. V. 53, 54, 67, 70
Stokova G. S. 68
Stradiot S. 49, 70
Strangway D. W. 100
Strong D. F. 136
Strunz H. 69
Stuart W. K. 70
Stuart-Smith P. G. 100

Stuckless J. S. 32, 41, 42, 177
Sun S.-S. 10, 11
Sutherland F. L. 4, 10
Swallow A. G. 62, 70
Swanson R. W. 138
Swanson V. E. 99, 137, 139
Szalay S. 10

Tan B. 108
Tan E. H. 99
Tape G. F. 108
Tarney J. 177
Tatsumoto M. 4, 9, 10, 11
Taylor J. C. 51, 52, 70
Tedesco C. 159, 161, 179
Tennant C. B. 42
Tera F. 10
Theis N. J. 100
Thomas R. L. 42
Thompson M. E. 71, 86, 88
Thompson T. B. 139
Thomson J. J. 1
Threadgold I. M. 53, 62, 70
Tilsley J. E. 41, 42, 173, 178
Tischendorf G. 177
Toivonen J. 69
Tonani F. 115
Toussaint J. 69
Tremblay L. P. 100, 139
Trentham R. C. 137
Turcotte D. L. 9, 11
Turekian K. K. 10
Turner-Peterson C. E. 42
Tuttle O. F. 139

Vaes J. F. 62, 70
Valkanen J. 69
Van der Putten N. 62, 70
Van Meerssche M. 54, 69, 70
Van Wambeke L. 55, 70
Verbeek T. 68, 69
Veronese L. 188
Vickers R. C. 139
Vijan P. N. 42
Viljoen M. J. 178
Viljoen R. P. 175, 178
Villari L. 10
Viste A. 70
Vochten R. 52, 70
Vollmer R. 4, 7, 9, 10
Von Backström J. W. *see* Backström J. W. von
Voultsidis V. 46, 70

Wadsley A. D. 70
Walenta K. 50, 53, 55, 63, 65, 70, 71
Wallace A. B. 100, 138
Wanty R. B. 28, 41, 42, 107
Wass S. Y. 10
Waters A. C. 10, 99, 138
Watson J. V. 177
Watterson J. I. W. 178
Wauters-Stoop D. 69
Weaver C. E. 21, 22
Webb J. S. 35, 42, 116, 178
Webber G. R. 38, 42, 116
Wedepohl K. E. 22, 41, 138
Weeks A. D. 71, 86, 88
Weeks A. M. D. 99
Wenrich-Verbeek K. J. 59, 71, 116
West G. F. 30, 41, 100
White A. J. R. 168, 177
White M. L. 42
Whittle A. W. G. 139
Williamson R. H. 108
Willis B. T. M. 45, 71
Wilson M. R. 160, 168, 177
Wilson P. W. 51, 70
Wimmenauer W. 55, 65, 71
Windley B. F. 138, 175, 176, 177
Wolf K. H. 100
Woodcock J. T. 137
Woodmansee W. C. 139
Wright H. D. 53, 68
Wyllie P. J. 4, 10

Yardley B. W. D. 169, 172, 177, 178
Youles I. P. 139
Young E. J. 55, 71
Young E. S. 22
Young R. G. 42, 108, 117, 139
Ypma P. J. M. 100

Zacharisen W. H. 51, 71
Zartman R. E. 10, 42
Zheleznova E. I. 136
Zhiltsova I. G. 70
Ziegler V. 41, 99, 137, 140, 188
Zolensky M. E. 57, 67, 71

Subject index

Abernathyite, chemical and structural classification of 56, 57, 58
Absite 47
Adelaide System, Australia 93
Aeschynite, chemical and structural classification of 49
Agadès deposits, Niger 126
Agrinierite, chemical and structural classification of 50, 52
Aillik Group, Labrador, Canada 93
Ainesse deposit, France 156
Alameda deposit, Spain 151
Allanite, chemical and structural classification of 49
Alligator Rivers deposits, Northern Territory, Australia 125
Alteration features in uraniferous sandstones 27–9
Alum shales, Sweden 94, 121, 143
Amer Lake deposits, Northwest Territories, Canada 92
Anderson mine, U.S.A. 121
Andersonite, chemical and structural classification of 64, 65
Antler uplift, western U.S.A. 98
Araxá uranium-bearing carbonatite, Brazil 121, 131
Ardara granite, Donegal, Ireland 169–70
Arjeplog–Arvidsjaur deposits, northern Sweden 143
Arsenuranospathite, chemical and structural classification of 56
Arsenuranylite, chemical and structural classification of 55
Ashanite, chemical and structural classification of 44
Athabasca Formation, Saskatchewan, Canada 41, 97, 134
Athabasca region deposits, Saskatchewan, Canada 26, 93, 105, 106, 125
'Atoms for Peace' programme 162
Autunite family, chemical and structural classification of 22, 55, 56, 57–8, 60, 65, 89

Bancroft district deposits, Ontario, Canada 93, 97, 123, 132
Barberton granites, South Africa 175
Bar River Formation, Elliot Lake, Ontario, Canada 92
Bassetite, chemical and structural classification of 56
Baukoma mineralization, Zaire 127
Bauranoite, chemical and structural classification of 50, 52
Bauxites, uranium deposits in 120
Bayleyite, chemical and structural classification of 64, 65
Beaverlodge deposit, Saskatchewan, Canada 26, 40, 93, 123, 135
Becquerelite, chemical and structural classification of 50, 52
Belovite, chemical and structural classification of 49
Ben Lomond deposit, Queensland, Australia 94
Bergen, Vogtland, Democratic Republic of Germany, mineralization in 55
Bergenite, chemical and structural classification of 55
Betafite, chemical and structural classification of 44
Betauranophane, chemical and structural classification of 53, 54
Bicroft mine, Bancroft district, Ontario, Canada 132
Billietite, chemical and structural classification of 50, 52
Billingen–Ranstad district, Sweden, uraniferous shales in 143
Bingham Canyon copper mine, Utah, U.S.A. 120, 122
Biogeochemistry, use of, in uranium exploration 33–4, 106
Black shales, uranium deposits in 91, 92, 94, 97, 98, 99, 107, 119, 121, 129, 163
Blind River–Elliot Lake deposits, Ontario, Canada 47, 119, 128–9
Blizzard deposit, British Columbia, Canada 94
Bois Noirs–Limouzat deposit, France 147–9
Bokan Mountain granite, Alaska, U.S.A. 122, 132
Boltwoodite, chemical and structural classification of 53, 54
Bolzano deposit, Italy 94
Bone Valley Formation, southeastern U.S.A. 119
Borden Basin, Northwest Territories, Canada 93
Brâme granite, France 145
Brannerite, chemical and structural classification of 43, 44, 47
'Briancon zone' 186
Brines, uranium deposits in 20, 90, 120, 130
Britholite, chemical and structural classification of 49
Brushy Basin Member, Morrison Formation, U.S.A. 135
Buda Limestone, Mexico 127
Burbankite, rare earth mineral 65

Cahill Formation, Northern Territory, Australia 134
Cairngorm–Mount Battock batholith, Scotland 167ff
Calciouranoite, chemical and structural classification of 50, 52
Calcretes, uranium deposits in 102, 107, 127, 136
Calcurmolite, chemical and structural classification of 62
Carbonaceous shales, uranium deposits in, *see* Lignites, coals and carbonaceous shales, uranium deposits in
Carbonatites, uranium deposits in 121–2, 131
Cardiff plutonic complex, Ontario, Canada 132
Caridad deposit, Spain 151, 153
Carlin black shale, Nevada, U.S.A. 25
Carmenellis granite, southwest England 169
Carnotite, chemical and structural classification of 22, 59, 60
Carona schists, Italy 183
Central Mineral District, Texas, U.S.A., exploration in 34
Centre Lake granite, Ontario, Canada 132
Cerianite, chemical and structural classification of 49
Cerilly (Allier) deposits, France 156–7
Châteauponsac granite, France 145
Chattanooga Shale, Tennessee, U.S.A. 26, 94, 119, 121, 129
Chemical and structural classification of uranium minerals, *see* Uranium minerals, chemical and structural classification of
Cheralite, chemical and structural classification of 49
Chinle Formation, Utah, U.S.A. 95
Ciudad Rodrigo deposits, Spain 149, 150, 151, 153
Clarkeite, chemical and structural classification of 50
Classification of uranium deposits 23ff, 89, 102, 117ff
Cliffordite, chemical and structural classification of 65, 66
Coals, uranium deposits in, *see* Lignites, coals and carbonaceous shales, uranium deposits in
Cobalt Group, Elliot Lake, Ontario, Canada 92
Cobalt zippeite, chemical and structural classification of 64
Coconinoite, chemical and structural classification of 55, 58, 62, 63
Coffinite, chemical and structural classification of 43, 44, 46–7, 89
Collio Formation, Italy 179, 180, 181, 182, 183, 184
Colorado Plateau deposits, U.S.A. 24, 40, 46, 53, 55, 59, 94, 98, 126, 163
Compreignacite, chemical and structural classification of 50, 52
Conway mineralization, New Hampshire, U.S.A. 122
Corella Formation, Queensland, Australia 133
Cornubian batholith, southwest England 168, 170
Cousinite, chemical and structural classification of 62
Coutras deposit, France 109, 110, 158
Creuse–North Limousin deposits, France 146
Crocker Well deposit, South Australia 122

Crustal evolution of uranium deposits 89ff
Crystal structure of uranium minerals, *see* Uranium minerals, chemical and structural classification of
Cunha Baixa deposit, Portugal 149, 150
Cuprosklodowskite, chemical and structural classification of 53, 54
Curienite, chemical and structural classification 59, 60
Curite, chemical and structural classification of 50, 51, 52

Dalbeattie mineralization, Scotland 143
Dartmoor granite, southwest England 169, 171
Davidite, chemical and structural classification of 44
Daybreak mine, Washington, U.S.A. 122
Deer Lake Basin deposit, Newfoundland, Canada 94
Demesmaekerite, chemical and structural classification of 66
Derricksite, chemical and structural classification of 66
Dewindtite, chemical and structural classification of 55, 56
Djalmaite, *see* Uranmicrolite, chemical and structural classification of
Dominion Reef System, South Africa 92
Donegal granite, Ireland 122
Dowelltown Member, Chattanooga Shale, eastern U.S.A. 129
Drilling and logging, use of, in uranium exploration 106
Dronne River mineralization, Coutras, France 110
Dubawnt Group, Northwest Territories, Canada 93
Dumontite, chemical and structural classification of 55, 56
Duobblon deposit, northern Sweden 143
Dylen deposit, Czechoslovakia 153

Easky adamellite, Ox Mountains, Ireland 169
East Alligator River deposits, Northern Territory, Australia 40, 93, 106
Echo Bay Group, Northwest Territories, Canada 135
Echo Bay mine, Northwest Territories, Canada 135
Edith River Group, Australia 93
Effusive igneous uranium deposits, *see under* Uranium deposits, types of
Ekanite, chemical and structural classification of 49
Eldorado mine, Northwest Territories, Canada 135
Elizabeth Creek mineralization, Queensland, Australia 122
Elliot Lake deposits, Ontario, Canada 63, 96 (*see also* Blind River–Elliot Lake deposits, Ontario, Canada)
Elliot Lake Group, Ontario, Canada 92
Ellsworthite, *see* Uranpyrochlore, chemical and structural classification of
El Sherana mine, Northern Territory, Australia 62
Energy, economics of, role of uranium in 162–6
Epigenetic uranium deposits, *see under* Uranium deposits, types of
Epi-ianthinite, classification of 49
Esperanza deposit, Spain 151, 153
Etive granite, Scotland 172
Etna volcanic area, distribution of uranium in 5, 8, 9
European Atomic Energy Community 162
Euxenite, chemical and structural classification of 44
Ewaldite, chemical and structural classification of 49, 65
Exogenous cycle of uranium 18–9, 20–1
Exploration, uranium, *see* Uranium exploration

FAMOUS volcanic area, distribution of uranium in 5, 8
Fe deposit, Spain 152, 153
Felder deposit, Texas, U.S.A. 38
Ferghanite, chemical and structural classification of 59
Fergusonite, chemical and structural classification of 49
Forbach granite, Federal Republic of Germany 154
Forstau deposit, Austria 159
Formanite, chemical and structural classification of 49
Ft. Union formation, Wyoming, U.S.A. 104
Fourmarierite, chemical and structural classification of 50, 52
Franceville deposit, Gabon 59, 127
Francevillite, chemical and structural classification of 59, 60
Freiberg district, Democratic Republic of Germany, hydrothermal veins in 123
Fritzcheite, chemical and structural classification of 56, 58, 59
Front Range deposits, Colorado, U.S.A. 105, 106
Furongite, chemical and structural classification of 55

Gardar alkaline province, southwest Greenland 141–2
Garfield mine, Colorado, U.S.A. 38
Gas Hills deposits, Wyoming, U.S.A. 38, 135–6
Gassaway Member, Chattanooga Shale, eastern U.S.A. 129
Gastunite, chemical and structural classification of 53
Generation of uranium deposits 89ff
Geochemical uranium exploration techniques 30–4, 35, 103, 105–6
Geochemistry of uranium 18ff, 89–90
Geologic uranium exploration techniques 27–9, 102, 103
Geophysical uranium exploration techniques 29–30, 102, 103
Georenja Vas–Zirovski Vrh deposit, Yugoslavia 158–9
Gordon Lake Formation, Elliot Lake, Ontario, Canada 92
Goulor River mineralization, Coutras, France 109, 110
Granite Mountains mineralization, Wyoming, U.S.A. 26, 122
Granites, uranium deposits in 32, 48, 53, 65, 91, 92, 94, 102, 107, 114–5, 122–3, 144–9, 163, 167–78
Granites, high heat production, role of, in uranium province formation 167–78
Grants deposits, New Mexico, U.S.A. 37, 38
Grants mineral belt, U.S.A. 94, 120, 126, 127, 135
Great Bear Lake mineralization, North West Territories, Canada 123
Green Hole Formation, Australia 92
Green River Formation, Wyoming, U.S.A. 65
Grimselite, chemical and structural classification of 65
Groeden beds, Yugoslavia 158
Guaymas Basin, Mexico 26
Guérêt complex, France 145
Guilleminite, chemical and structural classification of 66
'Gummite' minerals, chemical and structural classification of 46, 49–50

Hachettolite, *see* Uranpyrochlore, chemical and structural classification of
Haiweeite, chemical and structural classification of 53, 54
Haiweeite-(Mg), chemical and structural classification of 53
Half-lives, decay constants and modes of decay of ^{238}U, ^{235}U and ^{232}Th series 2–3
Hallimondite, chemical and structural classification of 55
Hamr deposit, Czechoslovakia 157–8
Happy Jack mine, Utah, U.S.A. 62
Hawaii volcanic area, distribution of uranium in 5, 7, 8, 9
Heinrichite, chemical and structural classification of 56
Helmsdale granite, Scotland 143, 170, 173
Henriette deposit, France 146
Hexavalent uranium minerals, chemical and structural classification

of 18ff, 49–66, 89–90
Hjelmite, *see* Yttromicrolite, chemical and structural classification of 44
Hohe Tauern mountains, Austria 159
Höhenstein deposit, Federal Republic of Germany 153
Hood granites, South Africa 175
Hornby Bay Formation, Canada 97
Hospital Hill Series, Witwatersrand System, South Africa 96
Huegelite, chemical and structural classification of 55
Huronian Supergroup, Canada 128
Hydrogen meta-autunite, chemical and structural classification of 56, 57, 58
Hydrogeochemistry, use of, in uranium exploration 23ff, 27, 30, 31–2, 34, 38–40, 41, 103–5, 109–16
Hydrothermal systems, transport and deposition of uranium in 12–17
Hydrothermal vein uranium deposits 62, 94, 102, 107, 123, 132–3

Ianthinite, chemical and structural classification of 44, 46, 49, 50, 64
Idaho Springs Formation, U.S.A. 132
Identification of uranium minerals 66–7
Ilmoriite, chemical and structural classification of 49
Ilímaussaq deposit, Greenland 121, 130–1, 142
INPUT surveys, use of, in uranium exploration 29, 30
International Atomic Energy Agency 162, 166
Intrusive igneous uranium deposits, *see under* Uranium deposits, types of
Iraqite, chemical and structural classification of 49
Iriginite, chemical and structural classification of 62
Ishikawaite, chemical and structural classification of 44

Jabiluka II deposit, Northern Territory, Australia 125, 134
Jachymov deposits, Czechoslovakia 65, 149, 153
Jean Vincent formation, Coutras, France 110
Johan Beetz mineralization, Quebec, Canada 122
Johannite, chemical and structural classification of 62, 63, 64
Joliotite, chemical and structural classification of 64, 65

Kaapvaal craton, South Africa 167
Kahlerite, chemical and structural classification of 56
Kaipokok deposits, Labrador, Canada 93
'Kaolin nests' 28
Karoo Formation, South Africa 127
Kasolite, chemical and structural classification of 53, 54
Kenema deposit, Sierra Leone 122
Kerguelen volcanic area, distribution of uranium in 7
Key Lake deposit, Saskatchewan, Canada 40, 41, 46, 103, 125
Khan Formation, Namibia 131
Kivuite, chemical and structural classification of 55
Klerksdorp granites, South Africa 175
Kobeite, chemical and structural classification of 44
Kobokobo pegmatite, Kivu, Zaire, mineralization in 55
Koenigstein deposits, German Democratic Republic 157
Kombolgie Sandstone, Northern Territory, Australia 134
Koongara deposit, Northern Territory, Australia 125
Krunkelbach–Menzenschwand deposit, Federal Republic of Germany 146
Külm Shale, Sweden 119

La Borderie mineralization, La Crouzille, France 110
Lachaux deposits, France 122
Lachaux–Bois Noirs granite, France 147
Lachaux–Bois Noirs–Madeleine epileuco-granite, France 147
La Crouzille–Limousin deposits, France 110, 145–6
Lagadailière mineralization, France 114–5
Lagao Real deposits, Bahia, Brazil 94, 97
Lahr, Baden, Federal Republic of Germany, mineralization at 55
Lake Frome deposits, South Australia 126
Lake Nipissing mineralization, Ontario, Canada 122
Langer Heinrich deposit, Namibia 127
Langmuir's saturation index 40
Langogne mineralization, France 146
La Petrazza lava, Stromboli volcanic area, distribution of uranium in 5
Large ion lithophile elements, *see* Mantle processes, uranium in
La Virgen deposit, Spain 149
'Lead paradox' 9
Le Fieu formation, Coutras, France 110
Leipers Limestone, eastern U.S.A. 129
Lermontovite, chemical and structural classification of 44, 47
Liandratite, chemical and structural classification of 44, 48–9
Lianshanguan deposit, China 92
Liebigite, chemical and structural classification of 64, 65
Lignites, coals and carbonaceous shales, uranium deposits in 55, 95, 127
LIL elements, *see* Mantle processes, uranium in
Limestones, uranium deposits in 127
Limousin deposits, France, *see* La Crouzille–Limousin deposits, France
Limpopo mobile belt 175
Llano area, Texas, U.S.A., exploration in 34
Lodève (Herault) deposits, France 94, 154, 155
Lodochnikite 47
Lombre deposit, France 156, 157
Los Ratones deposit, Spain 149
Lovozero deposit, U.S.S.R. 121

McDermitt Caldera, Oregon, U.S.A. 95, 121
Mckelveyite, chemical and structural classification of 65
McKim Formation, Ontario, Canada 128
MacMahon Act (U.S.A.) 162
Madison limestone, Montana, U.S.A. 95
Magnesium zippeite, chemical and structural classification of 64
Magnet Cove mineralization, U.S.A. 121
Malene, Greenland, supracrustal sequence, uranium-deficient 91
Mantle processes, uranium in 4–11
Mapping, geologic, use of, in uranium exploration 102, 103
Margaritasite, chemical and structural classification of 59, 60
Margnac deposit, France 52, 146
Marthozite, chemical and structural classification of 66
Martin Formation, Saskatchewan, Canada 97, 135
Mary Kathleen deposit, Queensland, Australia 124, 133–4
Marysvale deposits, Utah, U.S.A. 62, 121
Mas d'Alary mineralization, France 154
Mas Lavayre mineralization, France 155
Masuyite, chemical and structural classification of 50, 52
Matinenda Formation, Ontario, Canada 128
Maureen deposit, Queensland, Australia 94, 121
Mayet de Montagne–Arfeuilles monzogranite, France 147
Mazarate deposit, Spain 157
Meade Peak Phosphatic Shale Member, Phosphoria Formation, western U.S.A. 129, 130
Mecsek Mountains deposits, Hungary 157
Melanocerite, chemical and structural

classification of 49
Meta-ankoleite, chemical and structural classification of 56, 57
Meta-autunite family, chemical and structural classification of 52, 55, 56, 57–8
Metacalciouranoite, chemical and structural classification of 50, 52
Metaheinrichite, chemical and structural classification of 56
Metakahlerite, chemical and structural classification of 56
Metakirchheimerite, chemical and structural classification of 56
Metalodevite, chemical and structural classification of 56, 57
Metamorphic host rocks, uranium deposits in 26–7, 29, 93–4, 97, 98, 125, 135
Metanovacekite, chemical and structural classification of 56
Metaschoepite, chemical and structural classification of 49, 50
Metasomatic uranium deposits 123–4, 133–4
Metasomatism, mantle, *see* Mantle processes, uranium in
Metastudtite, chemical and structural classification of 50
Metatorbernite, chemical and structural classification of 52, 56, 57, 58
Metatyuyamunite, chemical and structural classification of 59
Meta-uranocircite, chemical and structural classification of 56, 57, 58
Meta-uranocircite II, chemical and structural classification of 56
Meta-uranopilite, chemical and structural classification of 63, 64
Meta-uranospinite, chemical and structural classification of 56
Metavandendriesscheite, chemical and structural classification of 50, 52
Metavanmeerscheite, chemical and structural classification of 55
Metavanuralite, chemical and structural classification of 59, 60
Metazellerite, chemical and structural classification of 64, 65
Metazeunerite, chemical and structural classification of 56
Midnite mine, Washington, U.S.A. 122, 132
Mid-oceanic ridge basalts, distribution of uranium in 6, 7, 9
Midwest Lake deposit, Canada 125
Mikouloungou deposits, Gabon 92, 113
Mina Fe mineralization, Spain 123
Minerals, uranium, *see* Uranium minerals
Mine Series, Roan Group, Zaire 133
Moab deposits, Utah, U.S.A. 95
Mobility, geochemical, of uranium 19–20
Moctezuma mineral deposit, Mexico 65
Moctezumite, chemical and structural classification of 65, 66
Moeda Formation, Minas Gerais, Brazil 92
Moluranite, chemical and structural classification of 44, 48, 62
Monazite, chemical and structural classification of 49
Montagne Bourbonnaise area, France, mineralization in 147–9
Mont conglomerate, Cerilly, France 157
Montgomery Lake Group, Canada 92
Montmassacrot mineralization, La Crouzille, France 110
Moon Lake ore zone, Ontario, Canada 129
MORB, *see* Mid-oceanic ridge basalts, distribution of uranium in
'Morbegno gneisses', Italy 183
Morrison Formation, southwestern U.S.A. 38, 94, 95, 135
Mounana mine, Gabon 59, 92
Mount Battock granite, Scotland, *see* Cairngorm–Mount Battock batholith, Scotland
Mount Burstall granite, Queensland, Australia 133
Mt. St. Helens volcanic area, distribution of uranium in 5, 8
Mourite, chemical and structural classification of 44, 47–8, 62
Muds, uranium deposits in 119, 129
Müllenbach deposit, Federal Republic of Germany 154–5
Musonoi deposits, Katanga 66

Närke province, Sweden, uraniferous shales in 143
Nickel zippeite, chemical and structural classification of 64
Ningyoite, chemical and structural classification of 47
Ningyo-toge mine, Tottori Prefecture, Japan 47
Niobo-aeschnyite, chemical and structural classification of 49
Nisa-Portalegre deposits, Portugal 123, 149, 150, 151, 153
Nordic ore zone, Ontario, Canada 129
Novacekite, chemical and structural classification of 56
Novazza deposit, Italy 94, 158, 179–82
Nyirangongo volcanic area, distribution of uranium in 4, 7, 8

Ognitsk mineralization, East Sayan, U.S.S.R. 122
Olympic Dam (Roxby Downs) deposit, Australia 93, 121, 130
Optical data for uranium minerals 86–8
Orphan mine, Arizona, U.S.A. 125
Orthobrannerite, chemical and structural classification of 44, 47
Oursinite, molecular formula of 67
Ousdale Arkose, Scotland 170

Palabora uranium-bearing carbonatite, South Africa 121, 122
Palangana uranium deposit, Texas, U.S.A. 38
Palheiros de Tolosa deposit, Portugal 150
Paraschoepite, chemical and structural classification of 49, 50
Parsonite, chemical and structural classification of 55
Pascoeite, chemical and structural classification of 62
Pedogeochemistry, use of, in uranium exploration 33, 105–6, 113–5
Pegmatites, uranium deposits in 43, 47, 48, 55, 59, 91, 92–3, 94, 96, 98, 123
Pegmatitic alkaline granites, uranium deposits in 91, 122, 132
Peltura scarobaeoides 143
Peña Blanca deposit, Chihuahua, Mexico 121, 130
Peneconcordant deposits 24–5, 40, 94, 97, 98, 126, 127, 135
Peralkaline nepheline syenites, uranium deposits in 121, 130–1
Petrogeochemistry, use of, in uranium exploration 32, 105–6
Petscheckite, chemical and structural classification of 44, 48–9
Phosphates, uranium deposits in 55, 127
Phosphoria Formation, western U.S.A. 129, 130
Phosphorites, uranium deposits in 119–20, 129–30
Phosphuranulite, chemical and structural classification of 55, 56
Phuralumite, chemical and structural classification of 55, 56
Phurcalite, chemical and structural classification of 55, 56
Pilanesberg deposit, South Africa 121
Pine Creek Geosyncline, Australia 93
Pisekite, chemical and structural classification of 44
Pitchblende, as variety of uraninite 46
Pitch mine, Colorado, U.S.A. 95, 97
Placer uranium deposits 20, 91, 98, 120
Pleutajokk deposit, northern Sweden 143
Plumbobetafite, chemical and structural classification of 44
Plumbomicrolite, chemical and structural classification of 44
Plumbopyrochlore, chemical and structural classification of 44
Pocas de Caldas deposit, Brazil 121
Polycrase, chemical and structural

classification of 44
Port Radium deposits, Northwest Territories, Canada 93, 97
Powder River Basin deposits, Wyoming, U.S.A. 104, 126
Preit Valley mineralization, Italy 187
Pribram deposits, Czechoslovakia 123, 149, 153
Prices, uranium 101–2, 165
Production, world, of uranium 164–5
Prospecting, uranium, *see* Uranium exploration
Pryor Mountains deposits, U.S.A. 95, 97, 127
Przhevalskite, chemical and structural classification of 56
Pseudo-autunite, chemical and structural classification of 55, 58

Quartz-pebble conglomerates, uranium deposits in 47, 91–2, 98, 102, 106, 117–9, 128–9
Quirke ore zone, Ontario, Canada 129

Rabbitite, chemical and structural classification of 65
Rabbit Lake deposit, Saskatchewan, Canada 40, 125, 134
Radioactivity as science, history of 1–3
Radiometric surveys, use of, in uranium exploration 29–30, 102–3, 105
Radium, use of, in detailed soil geochemical exploration 114–5
Rameauite, chemical and structural classification of 50, 52
Ranger 1 deposit, Northern Territory, Australia 26, 125
Ranger 2 deposit, Northern Territory, Australia 125
Ranquilite, chemical and structural classification of 53, 54
Ranstad deposits, Sweden 119, 143, 154
Ranunculite, chemical and structural classification of 56
Rauvite, chemical and structural classification of 59, 62
Renardite, chemical and structural classification of 55, 56
Reserves and resources of uranium 162–4
Resources of uranium, *see* Reserves and resources of uranium
Retort Phosphatic Shale Member, Phosphoria Formation, western U.S.A. 129
Rex Chert Member, Phosphoria Formation, western U.S.A. 129
Rexspar deposit, British Columbia, Canada 94, 121
Rhabdophane, chemical and structural classification of 47, 49, 65
Richetite, chemical and structural classification of 50
Rifle mine, Colorado, U.S.A. 38
Roan Group, Zaire 133
Rock sampling, *see* Petrogeochemistry, use of, in uranium exploration
Roll-type deposits 22, 25–6, 37–40, 62, 94–5, 96, 97, 98, 126, 135–6
Ross–Adams mine, Alaska, U.S.A. 132
Rössing deposit, Namibia 93, 97, 122, 131–2
Rössing Formation, Namibia 131
Roubaltite, chemical and structural classification of 50, 52
Roxby Downs deposit, South Australia 93, 121, 130
Rum Jungle deposit, Northern Territory, Australia 40, 125
Rutherfordine, chemical and structural classification of 64, 65

Sabugalite, chemical and structural classification of 56
St. Austell granite, southwest England 171
St. Goussaud granite, France 145
St. Hippolyte deposit, France 155
St. Louis Fault, Saskatchewan, Canada 135
Saint-Pierre du Cantal deposit, France 158
St. Sylvestre leucogranite, La Crouzille, France 110, 145, 146
Sakami Lake Group, Canada 92
Saleeite, chemical and structural classification of 56
Samarskite, chemical and structural classification of 44
Sandstones, uranium deposits in 22, 23–6, 27–9, 37–40, 46, 53, 55, 57, 59, 62, 91, 94–5, 96, 97–8, 102, 107, 126–7, 135–6, 163
San Juan Basin deposits, New Mexico, U.S.A. 39
Savoy deposits, France 159
Sayrite, molecular formula of 67
Schmitterite, chemical and structural classification of 65, 66
Schoepite, chemical and structural classification of 49, 50, 51, 62, 65
Schroeckingerite, chemical and structural classification of 63, 64, 65
Schwartzwalder deposit, Colorado, U.S.A. 40, 132–3
Sedimentary host rocks, uranium deposits in 23–6, 43, 92, 125, 153–8 (*see also* Sandstones, uranium deposits in)
Sedimentary uranium deposits, *see under* Uranium deposits, types of
Sedovite, chemical and structural classification of 44, 47–8, 62
Sengierite, chemical and structural classification of 59, 60
Senhora das Fontes deposit, Portugal 151–2
Serro de Corrego Formation, Bahia, Brazil 92
Shales, uranium deposits in, *see* Black shales, uranium deposits in; Lignites, coals and carbonaceous shales, uranium deposits in
Sharpite, chemical and structural classification of 64, 65
Shinkolobwe mine, Zaire 52, 65, 123, 133
Shirley Basin deposits, Wyoming, U.S.A. 126
Sierra de Peña Blanca deposit, Mexico 95
Sinde-Azere contact area, Portugal, large low-grade mineralization at 150
Siwaliks Formation, Pakistan, India, Bangladesh 158
Sklodowskite, chemical and structural classification of 53, 54
Slatina deposit, Czechoslovakia 153
Soddyite, chemical and structural classification of 53, 54–5
Sodium boltwoodite, chemical and structural classification of 53
Sodium meta-autunite, chemical and structural classification of 56
Sodium uranospinite, chemical and structural classification of 56
Sodium zippeite, chemical and structural classification of 62, 64
Soil sampling, *see* Pedogeochemistry, use of, in uranium exploration
South Alligator River deposits, Northern Territory, Australia 93, 125
South Mountain batholith, Nova Scotia, Canada 173
Spis–Gemer deposit, Czechoslovakia 158
Spokane Mountain deposit, Washington, U.S.A. 105, 106, 122, 123, 153
Spor Mountain deposits, Utah 95
Stack deposits 94, 96, 97, 98, 126–7
Stream sediment geochemistry, use of, in uranium exploration 30, 32–3, 35, 103, 112–3
Strelkinite, chemical and structural classification of 59
Streuberg, Democratic Republic of Germany, bergenite in dumps at 55
Stromboli volcanic area, distribution of uranium in 5, 8, 9
Stromness deposits, Scotland 170
Studtite, chemical and structural classification of 50
Supergene environment, uranium in, geochemical behaviour of 18–22
Swartzite, chemical and structural classification of 65

Tanteuxenite, chemical and structural classification of 44
Tarabau deposit, Portugal 150
Tarkwaian System, Ghana 92

Tazin Group, Saskatchewan, Canada 135
Temple Mountain mineralization, Utah, U.S.A. 125
Tetravalent uranium minerals, chemical and structural classification of 43–9, 89–90
Texas Gulf Coast deposits, U.S.A. 25, 27, 34, 39
Thelon Formation, Canada 97
Thomas Range deposits, U.S.A. 121
Thorianite, chemical and structural classification of 49
Thorite, chemical and structural classification of 49
^{232}Th series, half-lives, decay constants and modes of decay of 3
Thorutite, chemical and structural classification of 44, 47
Threadgoldite, chemical and structural classification of 56, 57, 58
Thule Basin, Greenland 93
Time-dependent evolutionary changes in uranium deposits 89ff
Tirschenreuth (Oberpfalz) deposits, Federal Republic of Germany 153
Todilto Limestone, U.S.A. 127
Togo Formation, Washington, U.S.A. 132
Tono mine, Japan 94
Torbernite, chemical and structural classification of 56, 89
Tosi Chert Member, Phosphoria Formation, western U.S.A. 129
Transport and deposition of uranium in hydrothermal systems 12–17
Transvaal Supergroup, South Africa 92
Travancore deposits, India 122
Triangulite, molecular formula of 67
Trinidade volcanic area, distribution of uranium in 7
Tristan volcanic area, distribution of uranium in 7
Trögerite, chemical and structural classification of 56, 58
Trögerite-(P), *see* Hydrogen meta-autunite, chemical and structural classification of
Tyuyamunite, chemical and structural classification of 22, 59, 89
Tyuya-Muyum deposit, U.S.S.R. 127

Umbozerite, chemical and structural classification of 49
Umohoite, chemical and structural classification of 62
Uncompaghre uplift, western U.S.A. 98
Unconformity-related uranium deposits 29, 93, 95, 97, 98–9, 102, 106, 107, 124–5, 134
Upalite, chemical and structural classification of 55
Uramphite, chemical and structural classification of 56
Uranium City deposits, Saskatchewan, Canada 97
Uranium deposits, types of
  effusive igneous 4ff, 94, 95, 97, 98, 102, 107, 121, 130
  epigenetic 125–7, 135–6
    in calcretes 102, 107, 127, 136
    in lignites, coals and carbonaceous shales 55, 95, 127
    in limestones 127
    in phosphates 55, 127
    in sandstones 22, 23–6, 27–9, 46, 53, 55, 57, 59, 62, 91, 94–5, 96, 97–8, 102, 107, 126–7, 135–6, 163, 184–6
      peneconcordant 24–5, 40, 94, 97, 98, 126, 127, 135
      roll-type 22, 25–6, 37–40, 62, 94–5, 96, 97, 98, 126, 135–6
      stack 94, 96, 97, 98, 126–7
  intrusive igneous 90, 93, 107, 121–3, 163
    in anatectics 93, 122, 131–2
    in carbonatites 121–2, 131
    in granites 32, 48, 53, 65, 91, 92, 94, 102, 107, 114–5, 122–3, 163, 167–78
    hydrothermal veins 62, 94, 102, 107, 123, 132–3
    in pegmatites 43, 47, 48, 55, 59, 91, 92–3, 94, 96, 98, 123
    in pegmatitic alkaline granites 91, 122, 132
    in peralkaline nepheline syenites 121, 130–1
  in metamorphic host rocks 26–7, 29, 93–4, 97, 98, 125, 135
  metasomatic 123–4, 133–4
  sedimentary 91, 117–20
    in bauxites 120
    in black shales 91, 92, 94, 97, 98, 99, 107, 119, 121, 129, 163
    in brines 20, 90, 120, 130
    in muds 119, 129
    in phosphorites 119–20, 129–30
    placer 20, 91, 98, 120
    in quartz-pebble conglomerates 47, 91–2, 98, 102, 106, 117–9, 128–9
  in sedimentary host rocks 23–6, 43, 92, 125 (*see also* Sandstones, uranium deposits in)
  unconformity-related 29, 93, 95, 97, 98–9, 102, 106, 107, 124–5, 134
  vein-type 93, 97, 99, 102, 106, 124, 125, 134–5
  geologic model for 40–1
Uranium exploration 23–42, 101–8
  detailed 103–7
  models for 37–41
    geochemical 37–40
    geologic 40–1
  reconnaissance 102–3
  techniques used in 27–37, 102–6
    drilling and logging 106
    geochemical 30–4, 35, 103, 105–6
      biogeochemistry 33–4, 106
      hydrogeochemistry 23ff, 27, 30, 31–2, 34, 38–40, 41, 103–5
      pedogeochemistry 33, 105–6
      petrogeochemistry 32, 105–6
      stream sediment geochemistry 30, 32–3, 35, 103
    geologic 27–9, 102, 103
    geophysical 29–30, 102, 103
      INPUT surveys 29, 30
      radiometric surveys 29–30, 102–3, 105
Uranium minerals
  chemical and structural classification of 43–66
  alkali and alkaline-earth uranyl oxide hydrates 50–2
    agrinierite 50, 52
    bauranoite 50, 52
    becquerelite 50, 52
    billietite 50, 52
    calciouranoite 50, 52
    clarkeite 50
    compreignacite 50, 52
    curite 50, 51, 52
    fourmarierite 50, 52
    masuyite 50, 52
    metacalciouranoite 50, 52
    metavandendriesscheite 50, 52
    rameauite 50, 52
    richetite 50
    roubaltite 50, 52
    uranosphaerite 50
    vandenbrandeite 50
    vandendriesscheite 50, 52
    wolsendorfite 50, 52
  brannerite 43, 47
  coffinite 43, 46–7, 89
  lermontovite 47
  liandratite 48–9
  ningyoite 47
  orthobrannerite 47
  petscheckite 48–9
  uraninite 44, 46, 52, 64, 89
  uranium columbites 47, 48
  uranium molybdates 47–8
  uranium niobates 44
  uranium pyrochlores 48
  uranium tantalates 44
  uranium titanates 44
  uranyl arsenates 55–8
    arsenuranylite 55
    autunite family 22, 55, 56, 57–8, 60, 65, 89
    hallimondite 55
    huegelite 55
    meta-autunite family 52, 55, 56, 57–8
    walpurgite 55, 58
  uranyl carbonates 63–5
    andersonite 64, 65
    bayleyite 64, 65
    grimselite 65
    joliotite 64, 65
    liebigite 64, 65
    mckelveyite 65
    metazellerite 64, 65
    rabbitite 65
    rutherfordine 64, 65

schroeckingerite 63, 64, 65
sharpite 64, 65
swartzite 65
voglite 65
widenmannite 65
wyartite 44, 65
zellerite 64, 65
uranyl molybdates 62
calcurmolite 62
cousinite 62
iriginite 62
moluranite 44, 48, 62
mourite 44, 47–8, 62
sedovite 44, 47–8, 62
umohoite 62
uranyl oxide hydrates 49–50
ianthinite 44, 46, 49, 50, 64
metastudtite 50
metaschoepite 49, 50
paraschoepite 49, 50
schoepite 49, 50, 51, 62, 65
studtite 50
uranyl phosphates 55–58
autunite family 22, 55, 56, 57–8, 60, 65
bergenite 55
coconinoite 55, 58, 62, 63
dewindtite 55, 56
dumontite 55, 56
furongite 55
kivuite 55
metavanmeerscheite 55
meta-autunite family 52, 55, 56, 57–8
parsonite 55
phosphuranulite 55, 56
phuralumite 55, 56
phurcalite 55, 56
pseudo-autunite 55, 58
renardite 55, 56
upalite 55
vanmeerscheite 55
walpurgite-(P) 55
uranyl selenates 65–6
demesmaekerite 66
derricksite 66
guilleminite 66
marthozite 66
uranyl silicates 52–4
betauranophane 53, 54
boltwoodite 53, 54
cuprosklodowskite 53, 54
haiweeite 53, 54
haiweeite-(Mg) 53
kasolite 53, 54
sklodowskite 53, 54
soddyite 53, 54–5
sodium boltwoodite 53
uranophane 52, 53, 54, 55
weeksite 53, 54
uranyl sulphates 62–3
cobalt zippeite 64
johannite 62, 63, 64
magnesium zippeite 64
meta-uranopilite 63, 64
nickel zippeite 64
sodium zippeite 62, 64
uranopilite 62, 63, 64
zinc zippeite 64
zippeite 62, 64
uranyl tellurates 65–6
cliffordite 65, 66
moctezumite 65, 66
schmitterite 65, 66
uranyl vanadates 58–62
carnotite 22, 59, 60
curienite 59, 60
ferghanite 59
francevillite 59, 60
fritzscheite 56, 58, 59
margaritasite 59, 60
metatyuyamunite 59
metavanuralite 59, 60
rauvite 59, 62
sengierite 59, 60
strelkinite 59
tyuyamunite 22, 59
uvanite 59, 62
vanuralite 59, 60
vanuranylite 59
identification of 66–7
optical data for 86–8
X-ray data for 71–85
^{235}U series, half-lives, decay constants and modes of decay of 3
^{238}U series, half-lives, decay constants and modes of decay of 2
Uraninite, chemical and structural classification of 43, 44–6, 52, 64, 89
Uranmicrolite, chemical and structural classification of 44, 48
Uranocircite, chemical and structural classification of 56
Uranophane, chemical and structural classification of 52, 53, 54, 55, 89
Uranopilite, chemical and structural classification of 62, 63, 64
Uranosilite, molecular formula of 67
Uranosphaerite, chemical and structural classification of 50
Uranospathite, chemical and structural classification of 56
Uranospinite, chemical and structural classification of 56
Uranpyrochlore, chemical and structural classification of 44
Uravan deposits, Colorado, U.S.A. 24, 38, 94
Urgeiriça deposit, Portugal 149, 150
Ursilite, chemical and structural classification of 53, 54
Uvanite, chemical and structural classification of 59, 62

Val Canale fault, Italy 181
Val Vedello deposit, Italy 158, 179, 182–4
'Val Gardena sandstones', Italy 184
Val Rendena deposits, Italy 184–6
Val Seriana deposits, Italy 184–6
Vandenbrandeite, chemical and structural classification of 50
Vandendriesscheite, chemical and structural classification of 50, 52
Vanmeerscheite, chemical and structural classification of 55
Vanuralite, chemical and structural classification of 59, 60
Vanuranylite, chemical and structural classification of 59
Västergotland province, Sweden, uraniferous shales in 143
Vein-type uranium deposits 93, 97, 99, 102, 106, 124, 125, 134–5, 153
geologic model for 40–1
Vendée deposits, France 146
Ventersdorp Supergroup, South Africa 175
'Verrucano Lombardo' formation, Italy 179, 184
Vesuvius volcanic area, distribution of uranium in 5, 8, 9
Villar de Peralonso deposit, Spain 149, 150
Vimont leucogranite, France 147
Voglite, chemical and structural classification of 65
Volcanic area, distribution of uranium in, *see* Mantle processes, uranium in
Vulcano, Vulcanello and Lipari volcanic area, distribution of uranium in 5, 8
Vryburg granites, South Africa 175

Wäldel deposit, Federal Republic of Germany 153
Walpurgite, chemical and structural classification of 55, 58
Walpurgite-(P), chemical and structural classification of 55
Walvis Bay uraniferous muds, Namibia 119, 129
Water sampling, *see* Hydrogeochemistry, use of, in uranium exploration
Weeksite, chemical and structural classification of 53, 54
Westwater Canyon Member, Morrison Formation, U.S.A. 135
Wet Mountains mineralization, U.S.A. 121
Wheal Remfry mineralization, southwest England 171
Wheeler Basin deposits, U.S.A. 122
White River Formation, U.S.A. 103
Widenmannite, chemical and structural classification of 65
Williston Basin mineralization, U.S.A. 127
Wind River Formation, Wyoming, U.S.A. 95, 103, 104, 126, 136
Witwatersrand deposits, South Africa 96, 119, 175
Witwatersrand Triad, South Africa 92, 175
Wollaston fold belt, Canada 93, 134
Wolsendorfite, chemical and structural classification of 50, 52
Woodrow Pipe, New Mexico, U.S.A. 125
Wyartite, chemical and structural

classification of 44, 65
Wyoming basin deposits, U.S.A. 22, 25, 95, 97, 103, 104, 126, 136

Xiangjiangite, chemical and structural classification of 56
X-ray data for uranium minerals 71–85

Yeelirrie deposit, Western Australia 127, 136
Yttrobetafite, chemical and structural classification of 44
Yttrocolumbite, chemical and structural classification of 44
Yttrocrasite, chemical and structural classification of 44
Yttromicrolite, chemical and structural classification of 44
Yttropyrochlore, chemical and structural classification of 44

Zellerite, chemical and structural classification of 64, 65
Zeunerite, chemical and structural classification of 56
Zinc zippeite, chemical and structural classification of 64
Zippeite, chemical and structural classification of 62, 64
Zirovski Vrh deposits, Yugoslavia 157
Zletovska Reka deposit, Yugoslavia 159
Zuni uplift, western U.S.A. 98